MONASH University

Extending Alkali Metal Mediated Magnesiation from Nitrogen to Phosphorus: Synthesis, Structure and Synergy

A thesis submitted for the degree of *Doctor of Philosophy* at Monash University in 2021. Faculty of Science

Michael Stevens

BSci(Hons) Monash University Australia

School of Chemistry

Monash University

February 2021

Declaration

This thesis is an original work of my research and contains no material which has been accepted for the award of any other degree or diploma at any university or equivalent institution and that, to the best of my knowledge and belief, this thesis contains no material previously published or written by another person, except where due reference is made in the text of the thesis.

Signature:

Print name: Michael Stevens

Date: 19/02/2021

Publications during enrolment

Atom Efficient Magnesiation of N-Substituted Alkyl Indoles with a Mixed Sodium-Magnesium Base.

Stevens, M. A., Blair, V. L.

European Journal of Inorganic Chemistry, 2018, 2018 (1), 74-79.

Contrasting Synergistic Heterobimetallic (Na–Mg) and Homometallic (Na or Mg) Bases in Metallation Reactions of Dialkylphenylphosphines and Dialkylanilines: Lateral versus Ring Selectivities

Stevens, M. A., Hashim, F.H., Gwee, E.S.H., Izgorodina, E.I., Mulvey, R.E., Blair, V.L.

Chemistry - A European Journal, 2018, 24, 15669 - 15677

Synthesis, Structure, and Solution Studies of Lithiated Allylic Phosphines and Phosphine Oxides

Eren, Nimrod M., Orr, Samantha A., Thompson, Christopher D., Border, Emily C., Stevens, Michael A., Blair, Victoria L.

Organometallics, 2020, 39, *11*, 2080-2090.

Contents

Acknowledgements

I wish to acknowledge the people of the Kulin Nations, on whose ancestral lands this research project was conducted. I pay my respects to their Elders, past, present and emerging. Sovereignty has never been ceded. I am mindful that within and without the buildings, the Land always was and always will be, Aboriginal land.

I would like to thank my supervisor Dr Victoria Blair, for always been supportive and helpful throughout the last four years, and encouraging me to try my hardest and persevere with what was at times quite challenging chemistry. Your feedback and guidance over the years has been most appreciated, in both a professional and personal sense.

I'd like to thank Prof Phil Andrews, for all his advice and thoughts along the way. You always offered a unique perspective, and I value your contribution to my development as a scientist.

To Kirralee - your company in the lab throughout the years has made the journey way more bearable. Your friendship both inside and outside the lab will always be appreciated.

To Megan - it's been great sharing this journey with you as we both started together, as well as been great office buddies. I wish you all the best in your future career, and I hope we can keep in touch.

Life doesn't pause when you're completing a PhD, and my life and direction vastly changed throughout the process. To top it off, 2020 was without doubt one of the most difficult years of my life - attempting to finish a PhD during a global pandemic and during Melbourne lockdown was no mean feat. Throughout the uncertainty and challenges of 2020, I was glad to have a group of close friends who were sharing this journey. Darcy, Sam, Sammy, Daniel and Lauren - I don't think I could have finished this PhD without you. I hope you realise how much I value your friendship, and how important you all are to me.

To Caite - your help and encouragement over the last couple of years helped me get to where I am now. Your encouragement to always aim high, and put myself out there has helped me get to the next step in my career, and I will always appreciate it.

I'd like to thank all the past and present members of the Andrews and Blair comrades - your company and support over the years has been greatly appreciated. In particular, I'd like to thank Dr Melissa Werrett for being such a positive role model and a great example - I aspire to as helpful and kind as you in all my future roles.

I wouldn't have been able to complete this PhD without the technical support within Monash University Chemistry. I'm particularly thankful for Dr Craig Forsyth, Dr Boujemma Moubaraki, Dr Alasdair Mckay and Scott Blundell for all their help with X-ray crystallography, NMR and mass spectroscopy.

I'd also like to thank Dr David Turner, who helped me get onto the career and path I am following today. He gave me a chance in my third year of undergraduate to do a research project, when I may not have had the requisite marks. This research project inspired me to work harder and helped get me to where I am now. Furthermore, as Graduate Coordinator throughout my PhD, you have always been a friendly and kind mentor for advice.

Finally, I'd like to acknowledgement my parents, for all their love and support over the years of my university degrees.

This research was supported by an Australian Government Research Training Program (RTP) Scholarship. This research was supported by a Monash University Graduate Research Completion Award.

Abstract

The primary aim of this research project was to explore the reactivity of the sodium magnesiate base [(TMEDA)Na(TMP)(CH_2SiMe_3)Mg(TMP)] **1** with a range of functionalised aromatic compounds through Alkali Metal Mediated *Magnesiation* (AMM*M*).

Looking to gain insight into the solution state structure of the sodium magnesiate [(TMEDA)Na(TMP)(CH_2SiMe_3)Mg(TMP)], ^{1}H-DOSY studies were conducted, which revealed the base retained its solid state structure in solution. Looking to further expand the range of known alkali metal magnesiates, a series of lithium, potassium and rubidium magnesiates were synthesised, and comprehensively characterised in the solution and solid state.

Next we explored the reactivity of the sodium magnesiate **1** with *N,N*- and *P,P*-dialkyl substituted anilines and phenylphosphines resulting in predominately *meta*- or lateral magnesiation. Some of these magnesiations occurred in the presence of ethyl- groups, which we have shown are not tolerated by monometallic reagents, instead undergoing *beta*-elimination to generate ethene gas. The results of this chapter are supported by calculated C-H acidities, as well as DFT calculations comparing the stability of all regioisomers. This work was then extended to the *N,N*-dimethylnapthylamine and *P,P*-dimethylnapthylphosphine, where the unprecedented selective 6-magnesiation (for amine) or lateral-magnesiation (for phosphine) was observed.

The reactivity of the sodium magnesiate **1** is further explored against a variety of *N*-heterocyclic indoles and 7-azaindoles. This study resulted in primarily α- magnesiation occurring. Differing metallated base architectures were observed dependent on the identity of the directing group, with methyl- and ethyl- groups favouring the more atom efficient disodium tetraindol-2-ylmagnesiates. In the case of the bulkyl silyl protecting group triisopropylsilyl-1H-indole, β- magnesiation was observed. The use of these metallated

species in *in situ* iodolysis reactions has been explored, and in Pd-catalysed cross coupling reactions.

This study was further extended from *N*-heterocyclic indoles to *P*-heterocyclic phosphindoles. The reactivity of **2** against *P*-heterocycles was found to be oxidation state dependent - phosphorus (III) phosphindoles underwent α-magnesiation, whereas the corresponding phosphorus (V) phosphindole oxides were di-magnesiated at the α- and *ortho*-positions. These metallated phosphorus (V) complexes were found to be NMR silent radical species, which has not been encountered before in Alkali Metal Mediated *Magnesiation*.

1 Introduction

A key aspect of synthetic chemistry is the regio- and chemo-selective functionalisation of organic molecules. The deprotonative metallation reaction (the conversion of an inert C-H bond to a reactive C-M bond) is one of the pre-eminent methods to generate reactive carbonucleophiles. The requirement for highly reactive species to perform these reactions leads to the use of organometallic compounds, where strongly electropositive metals combine with organic reagents to form highly polarised, highly reactive carbon-metal bonds (or in some cases nitrogen-metal bonds). Organometallic alkyl- and aryl-lithium compounds (RLi, R = Me, *n*Bu, *t*Bu, Ph, etc.) and lithium secondary amides (the "utility amides" lithium diisopropylamide (LDA), lithium 1,1,1,3,3,3-hexamethyldisilazide (LiHMDS) and lithium 2,2,6,6-tetramethylpiperidide (LiTMP)) are some of the most widely used reagents for deprotometallation (see Figure 1.1).[1] Despite their highly reactive nature, often resulting in pyrophoricity, these reagents find substantial usage in both academic and industrial laboratories worldwide. Their relative ease of use, combined with the commercial availability of stable hydrocarbon solutions of organolithiums make them a powerful tool in the synthetic chemists arsenal.

Alkyllithium reagents give rise to another important class, that of the sterically-hindered lithium 'utility amides'.[1] The deprotonation of acidic amines such as diisopropylamine (DA) and 2,2,6,6-tetramethylpiperidine (TMP(H)) with *n*BuLi allows the generation of lithium amides. These lithium secondary amides feature complementary high Brønsted

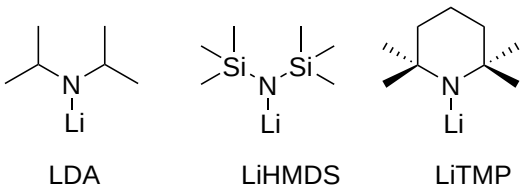

Figure 1.1: The lithium utility amides; lithium diisopropylamide (LDA), lithium hexamethyldisilazide (LiHMDS) and lithium tetramethylpiperidide (LiTMP).

basicity as well as poor nucleophilicity. They are often the reagent of choice, particularly with more sensitive heterocycles where problems arise from the high nucleophilicity of alkyllithiums. The lithiation of pyridine heterocycles is problematic with alkyl-lithium reagents - resulting in nucleophilic addition rather then deprotonation. For example, treatment of pyridines bearing a directing group in the 2- position with *n*BuLi results in the nucleophilic addition product, whereas the secondary amides LDA or LiTMP result in lithiation *ortho*- to the directing group functionality (see Scheme 1.1).[2,3]

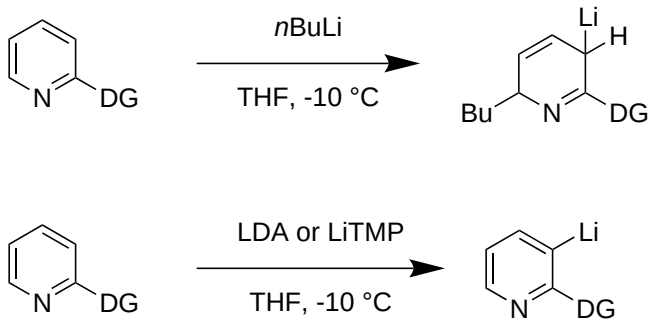

Scheme 1.1: Comparison of the reactivity of *n*BuLi and the lithium secondary amides with 2-methoxypyridine

Another key class of organometallic reagents in a synthetic chemists arsenal are organo-magnesium species, most prominently the Grignard reagent (of the form RMgX). Since discovery by Victor Grignard at the beginning of the 20th century (for which he received the 1912 Nobel Prize), Grignard reagents are ubiquitous in organic synthesis as a tool for carbon-carbon bond formation. Grignard reagents are easily prepared, feature good stability and their high reactivity make them useful on both the academic laboratory scale as well as in industrial synthesis. As an example, the industrial production of Tamoxifen, a selective estrogen receptor modulator used for the treatment of breast cancer, makes use of phenylmagnesium bromide (see Scheme 1.2).[4] Tamoxifen is considered an essential medicine by the World Health Organisation.[5]

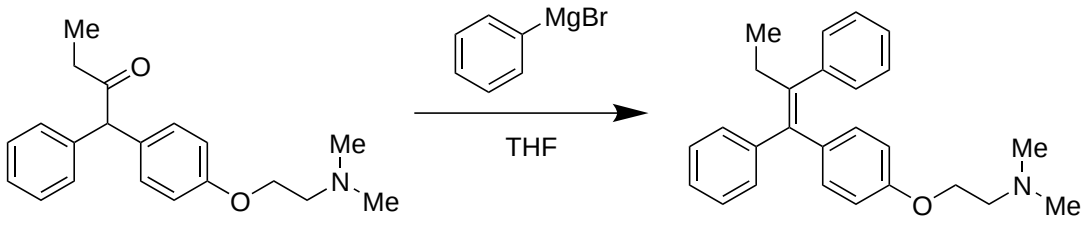

Scheme 1.2: A key step of the industrial synthesis of the breast cancer drug Tamoxifen

Determination of the solution state of Grignard reagents is particularly challenging due to the presence of multiple chemical species at thermodynamic equilibrium.[6] While initially thought to be of the form RMgX, pioneering work by Schlenk father and son led to the discovery of the Schlenk equilibrium (see Scheme 1.3).

Basic Schlenk Equilibrium

$$2\,\mathrm{RMgX} \rightleftharpoons \mathrm{MgR_2} + \mathrm{MgX_2}$$

Advanced Schlenk Equilibrium

$$\text{oligomers} \rightleftharpoons (\mathrm{RMgX})_2 \rightleftharpoons 2\mathrm{RMgX} \rightleftharpoons \mathrm{R_2Mg \cdot MgX_2} \rightleftharpoons \mathrm{R_2Mg + MgX_2}$$

Scheme 1.3: Schlenk equilibrium for Grignard reagents in ethereal solvents

More recently, it has become evident that the halide groups in RMgX and MgX_2 tend to form bridges between magnesium atoms, leading to a range of dimers and other oligomeric species present in solution. A comprehensive understanding of the solution state structure is complex, as the equilibrium "*depends on the nature of R, the nature of X, the properties of the coordinating solvent, concentration and temperature*".[7]

1.1 Structural chemistry in organometallic chemistry

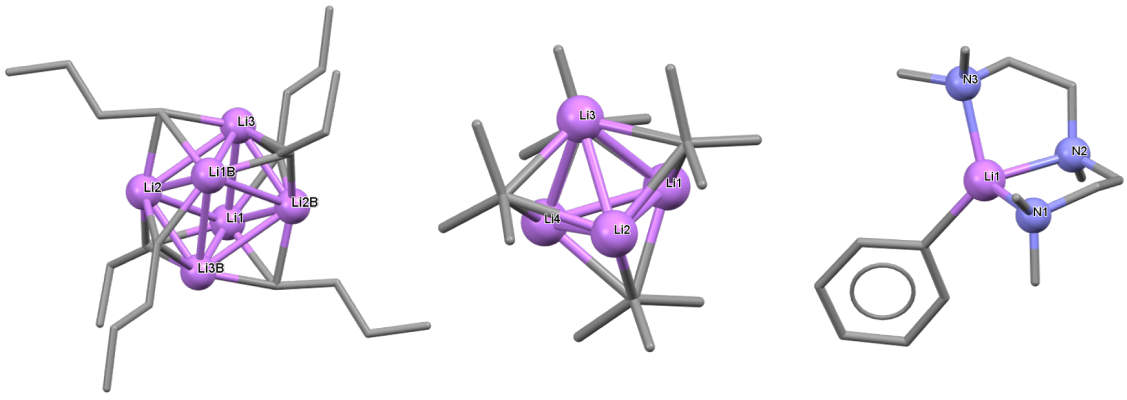

[*n*BuLi]$_6$ [*t*BuLi]$_4$ [(PMDETA)PhLi]

Figure 1.2: Solid state structures of three organolithium complexes

While organolithium chemistry is often represented as R−Li or R_2N−Li, implying a simple monomeric aggregate, it is rarely the case. The knowledge of organolithium aggregate

structures is fundamental to understanding their reactivity profile.[8] Alkyl-lithiums often favour oligomeric structures in the solid state, such as hexamers (for example, $[n\text{BuLi}]_6$, $[i\text{PrLi}]_6$) or tetramers (for example, $[\text{MeLi}]_4$, $[t\text{BuLi}]_4$).[9] The addition of coordinating solvents or neutral Lewis bases can deaggregate these structures, to dimers or even monomers ([PhLi(PMDETA)], see Figure 1.2).[10] As a general rule, lower aggregate states tend to produce more reactive organometallic species.

The bulky lithium secondary amides tend to be used in etheral solvents, which leads to smaller aggregates, generally dimers or monomers.[11–13] Interestingly, LDA exists as an infinite polymeric structure in the solid state when crystallised from non-coordinating *n*-hexane (see Figure 1.3).[14]

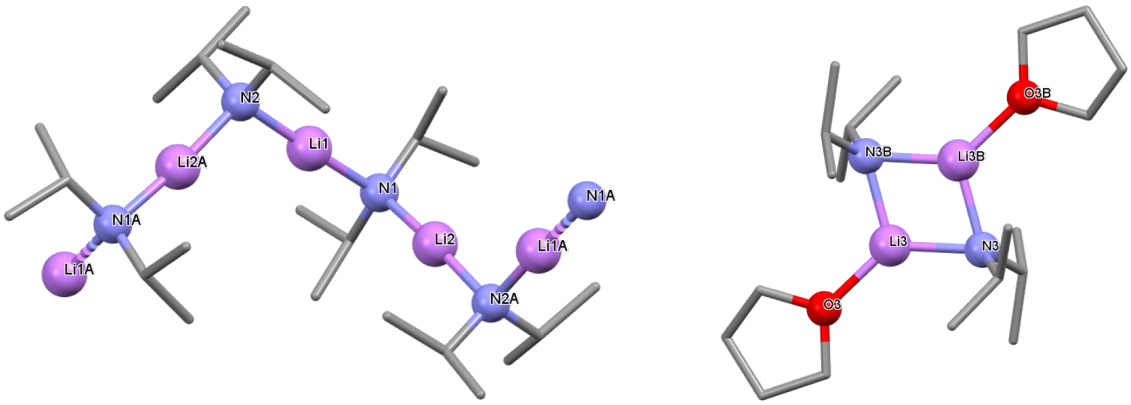

$[\text{LDA}]_\infty$ $[\text{LDA.THF}]_2$

Figure 1.3: Solid state structure of unsolvated LDA (left) and $[\text{LDA} \cdot \text{THF}]_2$ dimer (right)

Lithium TMP, another important lithium secondary amide, exists in hydrocarbon solutions to be an equilibrium between the cyclic-trimer and -tetramer. In 1983, studies by Lappert and co-workers revealed the solid state structure to be the cyclic-tetramer.[15] Following on from this, Collum and Lucht published detailed ^{6}Li and ^{15}N NMR solution studies which revealed that both the cyclic-tetramer and a cyclic-trimer exists in solution.[16] Hevia and Mulvey *et al.* were able to crystallise the cyclic-trimer, where they found crystallisation temperature the main determining factor of which isomer crystallised (- 35 ° C resulted in predominately the cyclic trimer, whereas 5 ° or 25 ° C resulted in the cyclic tetramer).[17] Further NMR spectroscopic studies including ^{1}H DOSY NMR (Diffusion

ordered spectroscopy) were conducted, which showed a similar temperature dependence between the two oligomers in solution.

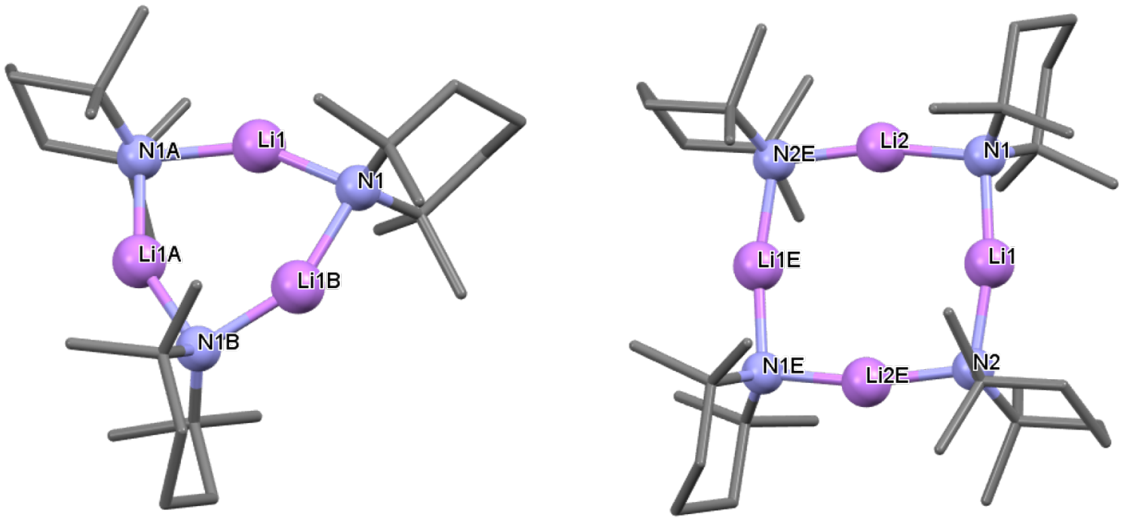

Figure 1.4: Solid state structure of unsolvated LiTMP, showing the cyclic-trimer (left) and cyclic-tetramer (right)

Similarly to LDA, LiTMP tends to exist as either disolvated monomers or various dimeric structures depending on the nature of the coordinating solvents (see Figure 1.5).[18,19] Interestingly, the open dimeric species (right of Figure 1.5) is thought to be an essential aspect of the reactivity of [(TMEDA)Li_2(TMP)$_2$].

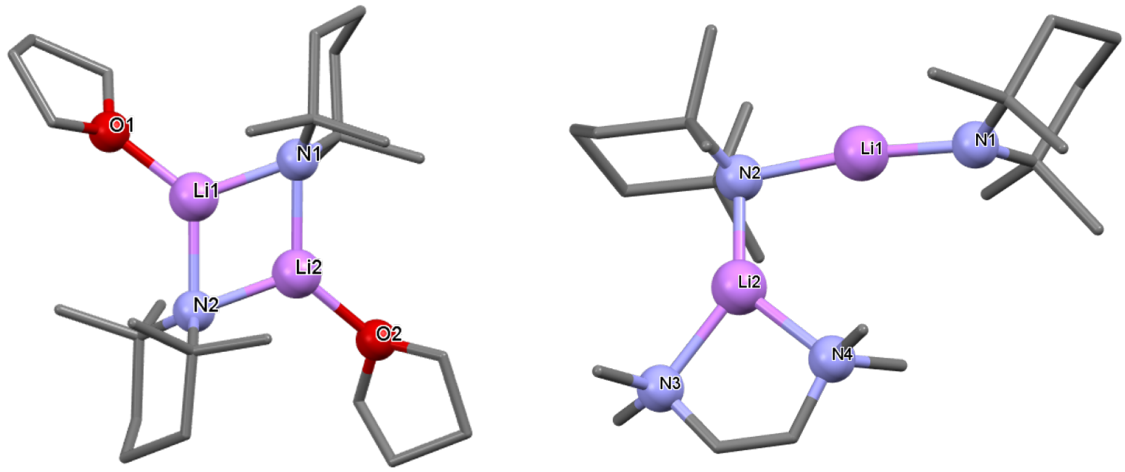

Figure 1.5: Solid state structure of dimeric LiTMP (left) and the open dimeric structure (right)

Determination of both the solid and solution state structures of organolithium reagents is key to understanding their associated reactivity. Lewis basic donor solvents (TMEDA,

THF, etc.) are often considered essential for the desired reactivity of many organolithium reagents, and this can be related back to the deaggregation to smaller oligomers these solvents cause.

1.2 The development of Mixed Metal Chemistry

One common theme amongst the organolithium chemistry discussed so far is the general requirement for sub-ambient temperatures to increase the functional group tolerance as well increasing the stability of the lithio-intermediates. This increased energy usage associated with cryogenic cooling is applicable on the research laboratory scale, but has the potential to add substantial cost to any process on the industrial scale. For instance, figures used within the Chemical Development department at GlaxoSmithKline suggest that performing reactions at temperatures below -40 ° C results in an additional cost of at least £250 000 per annum per batch tonne process.[20]

This has led numerous research groups across the world to generate new metallating reagents which can solve aspects of these challenges. This has led to new classes of organometallic reagents have been developed which incorporate multiple metal species. The reactivity of these multi-metallic bases is synergic in origin, and are able to afford new reactivity not previously seen with the mono-metallic components.

Early examples of these mixed metal systems include 'ate' complexes pioneered by Wittig (which took the form 'RLi.RM', where M was a heavier alkali metal). More recently, ate complexes are commonly of the form 'R_3MLi' or 'R_4MLi_2'. The composition of these reagents is through the combination of an organolithium compound 'LiR' and an organometallic divalent metal 'MR_2' (such as magnesium or zinc).

Another prominent example of a mixed metal base is the Lochmann-Schlosser superbase (commonly abbreviated as LIC-KOR), a bimetallic mixture of *n*BuLi with potassium tert-butoxide. The exact composition of this superbase remains elusive, but recent evidence from the metallation of benzene and toluene suggests that it exists as a mixed organo-

lithium/potassium compound. The LIC-KOR reagent offers unique reactivity compared to both its individual components and conventional reagents. This can be seen in the case of reacting LIC-KOR with toluene, where exclusive benzylic metallation is observed (see Scheme 1.4). However, the LIC-KOR superbase often reacts with poor regioselectivity, as is the case when attempting to dimetalate the aromatic naphthalene. This reaction results in a mixture of all ten disubstituted isomers.

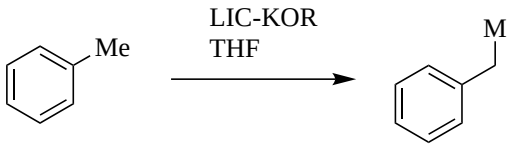

Scheme 1.4: Exclusive benzylic metallation of toluene with LIC-KOR reagent, where M represents the mixed organolithium/potassium metalating reagent.

Another prominent example of the potential use of the LICKOR superbase is in the synthesis of Ibuprofen (see Scheme 1.5). The initial synthesis requires six steps, whereas the use of the LICKOR superbase can cut this down to three steps,[21] which can all be done in 'one-pot' synthesis without isolating each individual step.

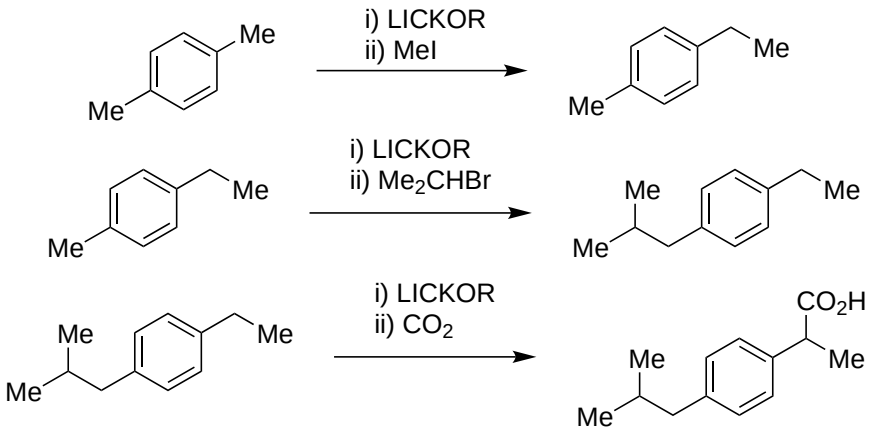

Scheme 1.5: One-pot synthesis of ibuprofen by sequential metallations with the LIC-KOR superbase

Another superbase formed from the addition of *n*BuLi to a metal alkoxide is [*n*BuLi−$Me_2N(CH_2)_2OLi$] (BuLi−LiDMAE). This reagent, formed from the addition of two equivalents of *n*BuLi to *N,N*-dimethylaminoethanol, offers up new regioselectivity in the metallation of 2-functionalised pyridines (see Scheme 1.6). Similarly to LDA (and

LiTMP), nucleophilic addition across the azomethine bonds is avoided, however unique C-6 lithiation is observed, which can be trapped with a variety of electrophiles to produce 2,6-substituted pyridines.[2,3,22,23]

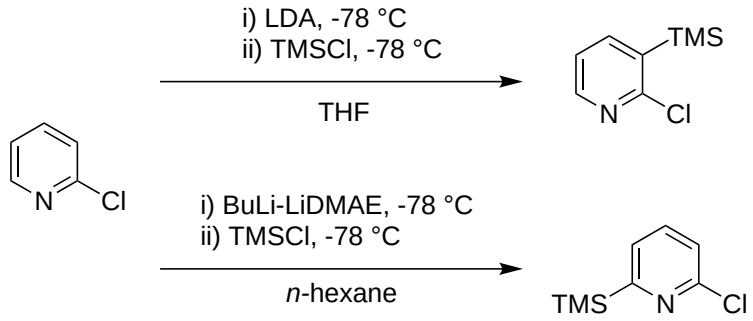

Scheme 1.6: Comparison of the regioselectivity of LDA (top) and *n*BuLi-LiDMAE (bottom)

This reactivity can be explained when considering the mechanism behind this reaction (see Scheme 1.7). The observed regioselectivity relates to the way the base 'docks' the C6-H in close proximity to the basic *n*BuLi.[22]

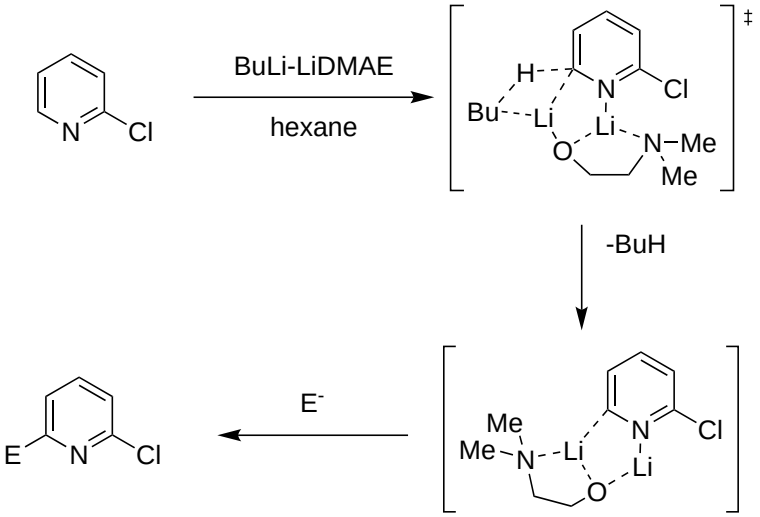

Scheme 1.7: Mechanism of the reaction of *n*BuLi-LiDMAE with 2-chloropyridine

Mongin and coworkers have developed a wide range of lithium-ate complexes, combining lithium with a variety of secondary metals to form a bi-metallic contact ion-pair system. Prominent examples include the use of zinc,[24–26] cadmium[25] or copper[27] (see Scheme 1.8 for the reaction of a lithium cadmate with anisole). Other examples exist of indium,[25] cobalt,[28] iron,[29] and magnesium.[30,31] Highlighting the importance of structural chemistry

in the understanding of how these multi-component systems react, recent DOSY (Diffusion-ordered spectroscopy) NMR experiments have confirmed that rather than a traditional contact ion-pair lithium cadmate, Li(TMP) and $Cd(TMP)_2$ exist as separate entities and the reaction proceeds via a lithiation followed by transmetallation.[32] It is clear from this result that the exact structural nature and reactivity path of these reagents is not known.

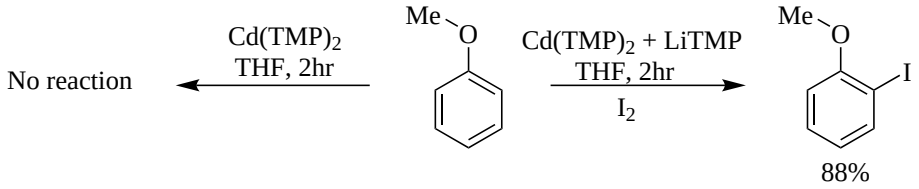

Scheme 1.8: Use of a lithium cadmate for the metallation of anisole.

Uchiyama and coworkers have published extensively in s-block metal 'ate' chemistry. In 2004 they reported the lithium aluminate [iBu$_3$Al(TMP)Li], and its use as a chemoselective deprotonating reagent.[33] Deprotonative aluminium occurred in the presence of carbonyl and cyano groups, and eliminated benzyne formation in halogenated aromatics (see Scheme 1.9 for two examples). They have published extensively on aluminium,[33,34] copper,[35,36] and a variety of other metal pairings.[26,37]

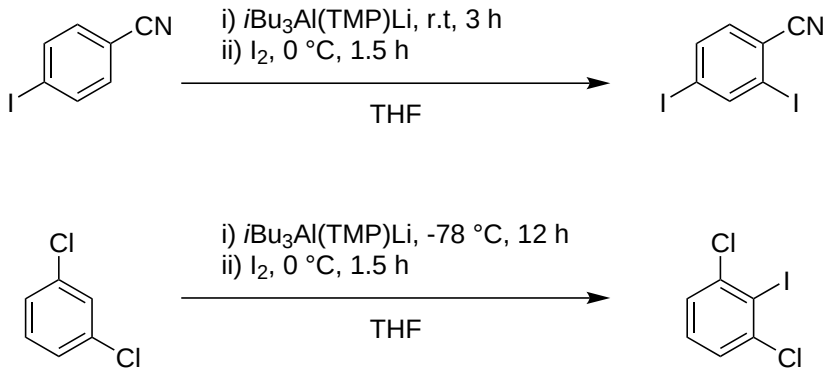

Scheme 1.9: Use of a lithium aluminate for the metallation of aromatics containing sensitive functional groups

Another class of bi-metallic reagents are those based on Grignard reagents. Knochel developed Turbo-Grignard reagents, formed by the addition of a stoichiometric quantity of LiCl to a Grignard reagent (RMgCl, where R = iPr or sBu).[38] These reagents allow metal-halogen exchanges to proceed at a higher rate compared to the MgRX or MgR_2 species. Highlighting their increasing popularity, Turbo-Grignard reagents are employed

in a number of natural product and pharmaceuticals synthesis (see Scheme 1.10 for two examples).[39]

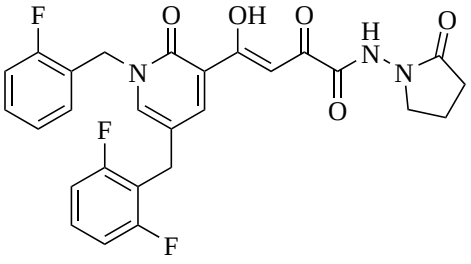

Anti-HIV Active Integrade Inhibitor

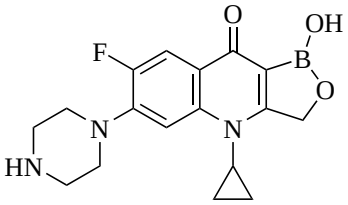

Fluoroquinolone

Scheme 1.10: Two examples of complex organic molecules utilising Turbo-Grignard reagents on a large scale.

Hauser bases were initially prepared in 1947 and had the general formula R_2NMgX or $(R_2N)_2Mg$.[40] Unfortunately these reagents had low solubility in common organic solvents, requiring a large excess of the metallating reagent. This area was further developed with the introduction of the Knochel-Hauser base, which is a mixed lithium/magnesium amide base [(TMP)MgCl.LiCl].[41] The introduction of LiCl leads to a highly reactive, THF soluble reagent. The Knochel-Hauser base has been successfully used in functionalising a wide variety of molecules, and is tolerant of nitriles, esters, halogens and aryl ketones. (TMP)MgCl · LiCl has been used for the 4-functionlisation of 2-chloropyrimidines (see Scheme 1.11).

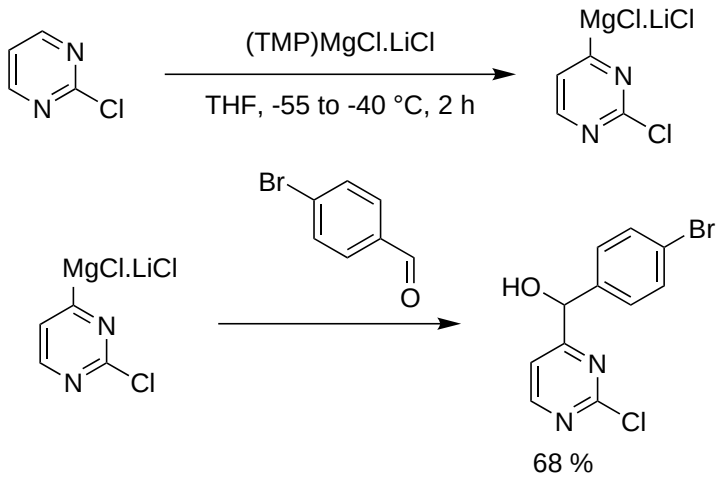

Scheme 1.11: Reaction of the Knochel-Hauser base (TMP)MgCl · LiCl with 2-chloropyrimidine

The Mulvey group in 2008 confirmed the solid state structure of the Knochel-Hauser base (TMP)MgCl · LiCl, revealing a monomeric species with coordinating solvent THF molecules (see Figure 1.6).[42] Highlighting the increasing prevalence of these new Grignard-based reagents, they are both commercially available from Aldrich.

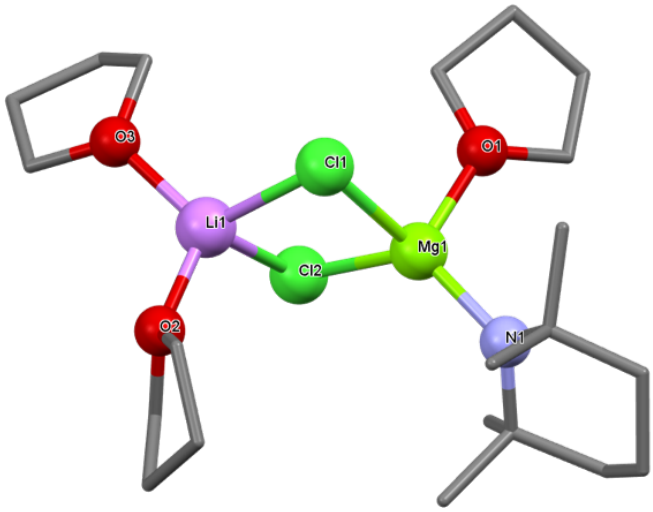

Figure 1.6: Molecular structure of the Knochel-Hauser base $[(THF)_2Li(Cl_2)Mg(THF)TMP]$.

The Knochel group has recently begun developing metallation chemistry in continuous flow reactors.[43–49] This often leads to increased yields and more desirable reaction conditions, and in some cases reactivity that cannot be conducted on a batch scale. For example, the magnesiation of 2,3-dichloro-5-(trifluoromethyl)pyridine with the Knochel-Hauser base TMPMgCl · LiCl proceeds smoothly at room temperature in flow (compared to -40 ° C in batch), with complete conversion in 30 seconds (compared to 2 hours in batch, see Scheme 1.12). This magnesiated intermediate can subsequently be quenched with iodine, to give the corresponding 2,3-dichloro-5-trifluoro-6-iodopyridine in a high yield of 73 % (compared to only 56 % yield in batch).[43]

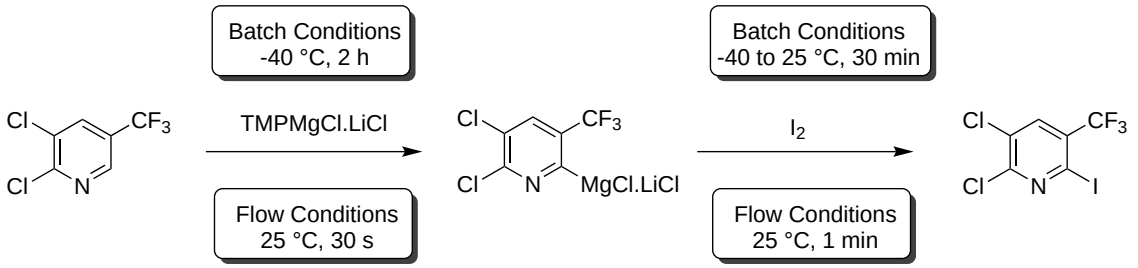

Scheme 1.12: Comparison of the batch and flow conditions for the metallation of 2,3-dichloro-5-(trifluoromethyl)pyridine with TMPMgCl · LiCl

1.3 Alkali Metal Mediated *Metallation* (AMM*M*)

Another major development in mixed metal chemistry is the unique reactivity obtained from alkali metals coupled with less polar, less reactive subordinate metals such as magnesium,[50,51] zinc,[52] aluminium[53] or manganese,[54] coined *Alkali Metal Mediated Metallation.*[55–57] The structural chemistry of these reagents was pioneered by the Mulvey group, isolating both starting bases and the metallated intermediates for X-ray crystallographic studies. More recently, solution state ^{1}H-DOSY studies have complemented these structural and reactivity studies. This differs from most previously mentioned mixed metal reagents, where little to no structural data is available on either the reagents themselves or the metallated species.

The earliest examples of these Mulvey-type bases were lithium or sodium magnesiates which formed inverse-crown structures affording di-metallations of substrates. These are so called 'inverse crowns' as they are typically an eight-membered cationic ring of alternating amide bridged metal cations. An example of this is the sodium magnesiate $[Na_4Mg_2(TMP)_6(nBu)_2]$, which was used to *ortho-meta'* dimagnesiate toluene (see Scheme 1.13).[58] The authors found in this study that the identity of the alkyl group of the base had an effect on the observed reactivity, with the bulkier CH_2SiMe_3 alkyl chain resulting in the selective *meta-meta'* dimagnesiation.

While attempting to isolate the mixed metal intermediate prior to the deprotonation step, stoichiometric quantities of the bidentate diamine TMEDA was added in the absence of

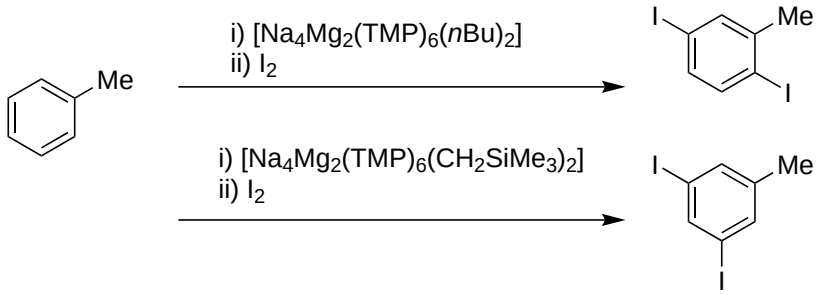

Scheme 1.13: Effect of the basic alkyl group on the regioselective dimetallation of toluene

toluene.[59] The authors were able to structurally characterise the isolated crystals as the bis-amido monoalkyl magnesiate [(TMEDA)Na(nBu)(TMP)Mg(TMP)], rather than the expected inverse-crown complex (see Figure 1.7 for the crystal structure).

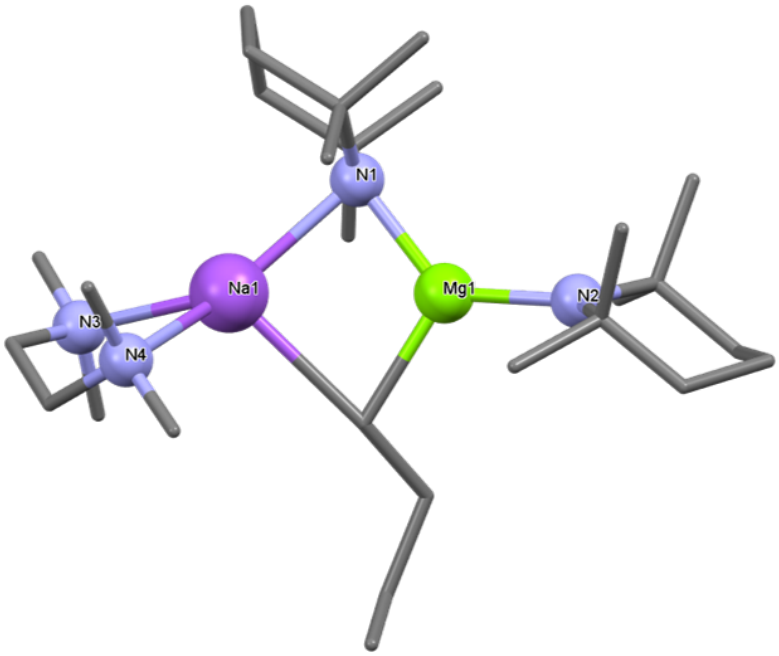

Figure 1.7: The isolated bis-amido monoalkyl magnesiate [(TMEDA)Na(nBu)(TMP)Mg(TMP)]. Hydrogen atoms omitted for clarity.

Anisole, an important scaffold in pharmaceutical synthesis, is able to be metallated in the *ortho* position using conventional metallation reagents (as would be expected due to directed *ortho* metallation).[60–63] The sodium magnesiate base $[Na_4Mg_2(TMP)_6(nBu)_2]$ reacts with anisole to form the *ortho-meta'* (D*om*M) dimetallated species, which allows access to 2,5-disubstituted anisole when quenched with I_2 (see Scheme 1.14).[64]

The reaction of the same base with *N,N*-dimethylaniline and *N,N*-diisopropylaniline results

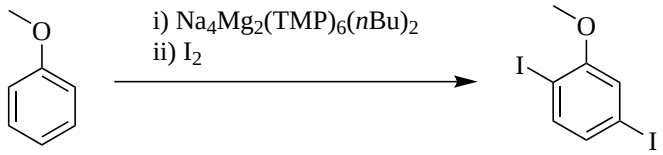

Scheme 1.14: *Ortho-meta*' dimetallation of anisole using $[Na_4Mg_2(TMP)_6(nBu)_2]$

in the selective 3,5-magnesiation (or *meta-meta'* magnesiation, see Scheme 1.15). Both these metallated species have been characterised crystallographically, and it is seen that the formation of an inverse crown base system allows the magnesium to be in close proximity to the deprotonation site while sodium is able to electrostatically interact with the deprotonation site (see Figure 1.8). It is clear that the structures are examples of magnesiation, as evidenced by the magnesium carbon bond length of 2.216(2) Å (compared to the sodium carbon bond length of 2.699(2) Å).[64]

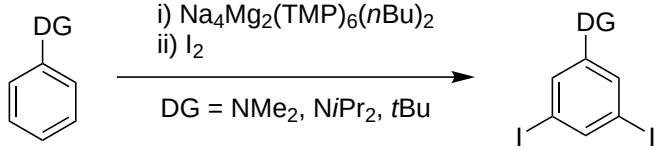

Scheme 1.15: *Meta-meta*' dimetallation of N,N-dimethylaniline, N,N-diisopropylaniline and tert-butylbenzene using $[Na_4Mg_2(TMP)_6(nBu)_2]$

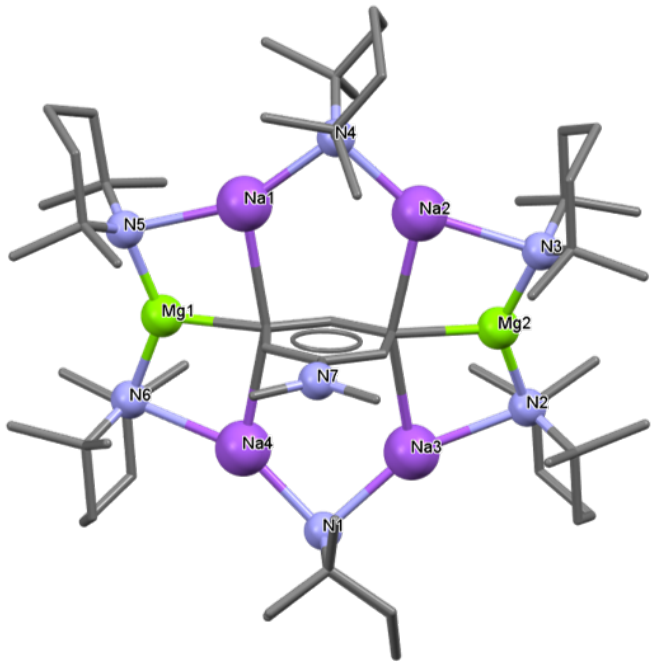

Figure 1.8: Crystal structure of the *meta-meta'* dimagnesiated compound $[Na_4Mg_2(TMP)_6(C_6H_3NMe_2)]$. Hydrogen atoms omitted for clarity.

This directed *meta-meta'* metallation (DmmM) overrides the conventional directed ortho metallation effect observed in anilines. In both D*om*M and D*mm*M, the observed reactivity is heavily influenced by both electronic and steric effects.[64] The nature of the directing group on the arenes determined the reaction speed, with stronger directing groups proceeding more rapidly and at lower temperatures when compared to those with weak directing groups. Furthermore, the spatial nature of the directing group can redirect the metallation to the *meta-meta'* position.[64]

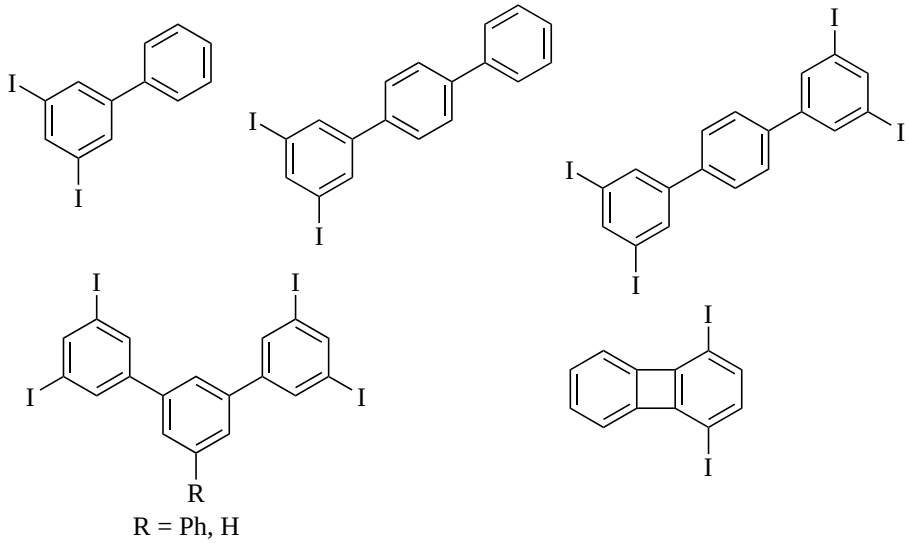

Figure 1.9: A selection of the multi-iodoarenes accessible through the use of the sodium magnesiate $[Na_4Mg_2(TMP)_6(nBu)_2]$

When this inverse-crown based base was utilised in the metallations of polyaryl systems, a new series of previously inaccessible multi-iodoarenes were established (see Figure 1.9).[65] These substrates are difficult to metallate with conventional s-block organometallics (such as *n*-butyl lithium, which requires activation with TMEDA), as they lack a directing group to guide the metallation, or to act as a strong acidifying group. Access to these iodo-substituted substrates is of interest, as they can then be further utilised in transition metal catalysed cross-coupling reactions allowing access to a vast range of possible substitutions (see Scheme 1.16 for an example cross-coupling reaction).

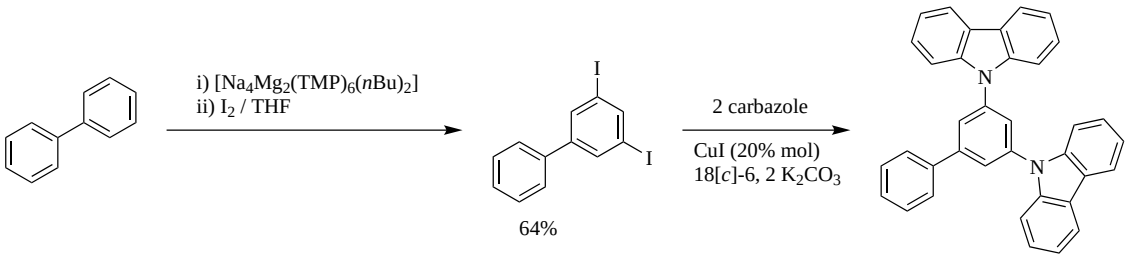

Scheme 1.16: *Meta-meta*' dimagnesiation of biphenyl followed by iodolysis and copper catalysed cross coupling with carbazole

1.4 Reactivity of the sodium magnesiate [(TMEDA)Na(TMP)(CH_2SiMe_3)Mg(TMP)]

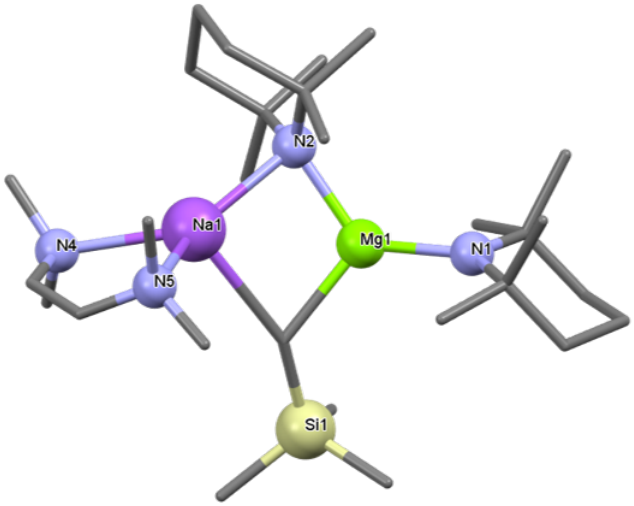

Figure 1.10: The sodium magnesiate [(TMEDA)Na(TMP)(CH_2SiMe_3)Mg(TMP)]

Of particular relevance to the contents of this thesis is the sodium magnesiate [(TMEDA)Na(TMP)(CH_2SiMe_3)Mg(TMP)] **1** (see Figure 1.10). It has only been briefly explored in the literature, where it has been utilised in the deprotometallation of furan, tetrahydrofuran, thiophene and tetrahydrothiophene.[66–69]

The cyclic ether tetrahydrofuran (THF) has always been troublesome for an organometallic chemist.[70] While incredibly useful due to higher solubilities of organometallic species, and increased reaction kinetics (in comparison to nonpolar hydrocarbon solvents),[71] it is sensitive to decomposition.[70,72–74] Many reactive organometallic species deprotonate at the α- carbon adjacent to the oxygen heteroatom, inducing spontaneous

ether cleavage via reverse [3 + 2] cycloaddition to form ethene and the corresponding metal enolate.[75] The sodium magnesiate [(TMEDA)Na(TMP)(CH_2SiMe_3)Mg(TMP)] induces ether cleavage of stoichiometric THF.[68] Remarkably, all the components of this decomposition are captured by the components of the base **1**, and stable enough to be crystallographically characterised as [$Na_2Mg_2(TMP)_4O$] and [$\{$(TMEDA)Na$(TMP)_2\}_2\{1,4-[Mg(TMP)]_2-C_4H_4\}$] (see Scheme 1.17). In comparison, the sodium zincate [(TMEDA)Na(TMP)(CH_2SiMe_3)Zn(CH_2SiMe_3)] is able to perform an α-zincation, without inducing cyclic ether cleavage.[76]

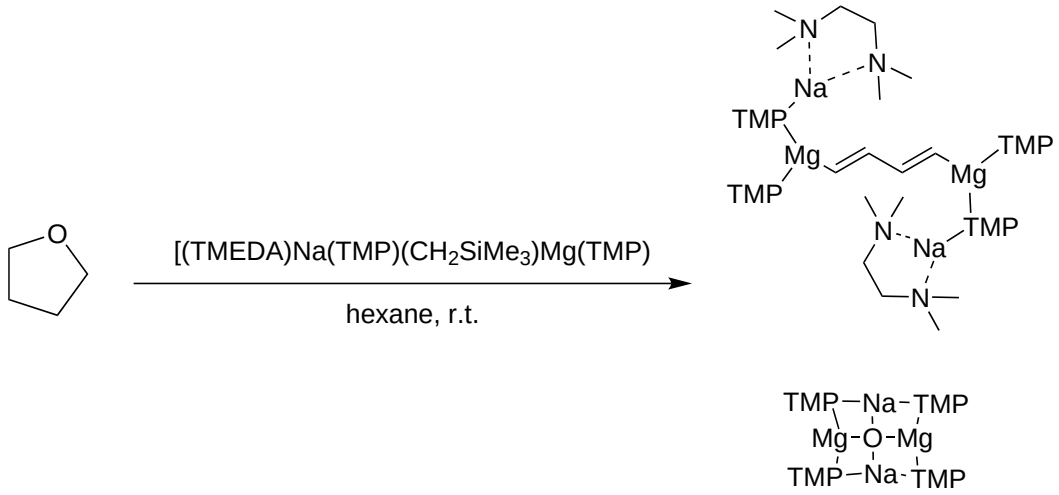

Scheme 1.17: Reaction of the sodium magnesiate **1** with tetrahydrofuran

Two differing reactivity profiles are observed when the sodium magnesiate **1** is reacted with tetrahydrothiophene and thiophene. In the case of tetrahydrothiophene, **1** shows alkyl-basicity, losing its alkyl group to afford the bis amido α- magnesiated complex [(TMEDA)Na(TMP)($\alpha-C_4H_7S$)Mg(TMP)] (seen on the left of Figure 1.11). When **1** is reacted with thiophene, it exhibits tri-basicity, losing both its alkyl and two amido basic groups to afford the α- magnesiated complex [(TMEDA)Na($\alpha-C_4H_3S)_3$Mg(TMEDA)] (seen on the right of Figure 1.11).

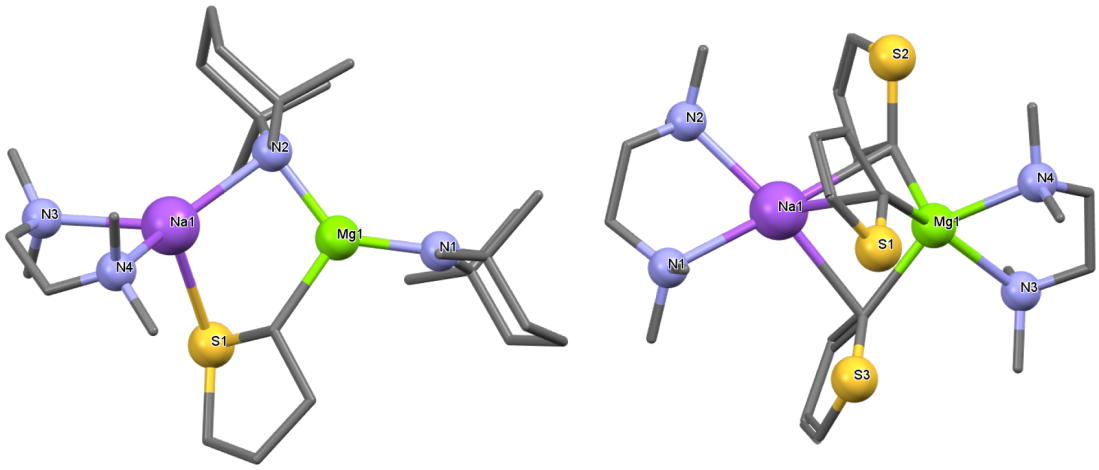

Figure 1.11: Comparison of the reactivity of the sodium magnesiate **1** with tetrahydrothiophene (left) and thiophene (right)

When the sodium magnesiate **1** is used in the magnesiation of furan, it once again shows dual basicity, however the unexpected dodecasodium hexamagnesiate ate complex $[\{(TMEDA)_3Na_6Mg_3(CH_2SiMe_3)(2,5-C_4H_3))(2-C_4H_3O)_5\}_2]$ is isolated. This complex contains ten alpha-deprotonated and six twofold α,α' deprotonated furan ligands.

1.5 Project aims and objectives

This thesis has a particular focus on expanding the reactivity of the sodium magnesiate base [(TMEDA)Na(TMP)(CH_2SiMe_3)Mg(TMP)] **1** against a variety of nitrogen- and phosphorus- based systems. When compared to the breadth of knowledge on s-block metal amides, it is evident that the analogous phosphorus compounds have been largely ignored. The analogous nitrogen systems will also be explored (where previously unstudied), to allow the development of fundamental concepts in s-block chemistry.

Chapter two focuses on the synthesis and extended characterisation of a series of Group 1 metal magnesiates. The magnesiates synthesised are characterised in the solid state by Single-crystal X-ray diffraction, and their solution state behaviour is explored using NMR spectroscopy in d_{12}-cyclohexane, including ^{1}H-DOSY and ^{1}H$-^1$H-NOESY NMR spectroscopy.

Chapter three focuses on the reactivity of the sodium magnesiate **1** against a variety of *N,N*- and *P,P*-dialkyl substituted anilines and phenylphosphines. This study features both analysis of crystalline metallated intermediates, as well as electrophile quenching studies. The regioselectivities observed are explored computationally with pKa calculations, and further developed with calculations comparing the relative energies of differing isomers. This work is then extended to changing the aryl- substituent to napthyl-based systems.

Chapter four focuses on the use of sodium magnesiates for the functionalisation of *N*-heterocycles. A range of differing base architectures is observed, as well as differing regioselectivities. The usage of these magnesiated species in *in situ* iodolysis reactions is conducted, as well as in some cases Pd-catalysed cross-coupling reactions.

Chapter five explores the reactivity of the sodium magnesiate **1** with *P*-heterocyclic compounds. This leads to the discovery of unique redox-state induced polymetallations, as well as the generation of stable radical species. This chapter features X-ray characterisation of metallated intermediates, NMR and EPR spectroscopic studies as well as electrophile studies.

2 Investigation into the solution state structure and stability of mixed metal magnesiate bases

Bimetallic base formulations are finding increasing synthetic utility in both academia and industrial settings,[39] offering unique reactivity and chemistry that can be interpreted in terms of synergistic effects. The coupling of an alkali metal with a lower polarity metal such as magnesium,[77] zinc,[52] aluminium[33] or gallium[78] have emerged as powerful metallation tools for the regioselective funtionalisation of weakly acidic molecules.

Our group has been particularly interested in heteroleptic alkali metal mediated *magnesiation*. The earliest example of a lithium magnesiate was prepared by Wittig in 1951, where he combined equimolar quantities of phenyllithium and diphenylmagnesium to form Ph_3LiMg.[79] The chemistry of lithium magnesiates was pioneered by Wittig,[80,81] and has more recently been extended by the Davies[82] and Mongin[30,31] groups via *in situ* reaction mixtures. These lithium magnesiate reagents tend to be of the form "R_3MgLi" or "R_4MgLi_2", formed by the combination of an organolithium compound 'LiR' with an organometallic divalent magnesium compound "MgR_2". Various Lewis donors are often used within these mixtures to aid solubility and reactivity.

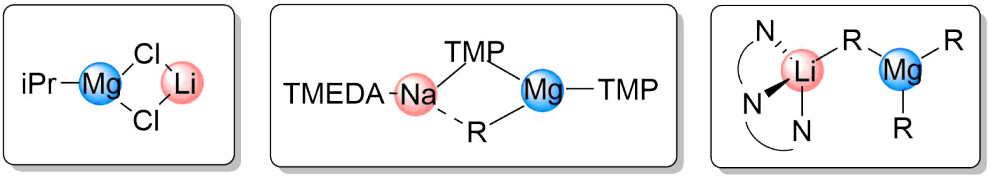

Knochel Turbo-Grignard | Mulvey-type heteroleptic sodium magnesiate | Hevia homoleptic lithium magnesiate

Figure 2.1: Chemdraw representation of the structures of typical alkali metal magnesiates

Mongin and co-workers have pioneered numerous bimetallic 'ate' formations for the metallation of functionalised arenes, predominately focusing on lithium coupled with a more electropositive metal such as magnesium,[30,31] zinc[24–26] or copper.[27] These metallating

reagents consist typically of a mixed alkyl or amido lithium species with either a divalent metal salt of a dialkyl/amido metallic species.

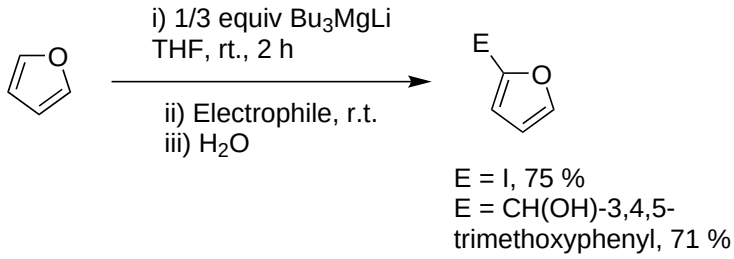

Scheme 2.1: Reaction of the lithium magnesiate Bu_3MgLi with furan[31]

The homoleptic lithium magnesiate Bu_3MgLi proved to be an efficient metallator of aromatic substrates such as furan (Scheme 2.1).[31] The higher order dilithium tetrabutyl-magnesiate $(Bu_4)MgLi_2$ was also used, and found to be more efficient at metallating furans. When moving to another aromatic substrate, thiophene, Mongin and co-workers found that the addition of the Lewis donor TMEDA to Bu_3MgLi resulted in much higher yields of the deprotonated substrate, presumably through the complexation of TMEDA to the lithum ion of of the magnesiate (Scheme 2.2).[30]

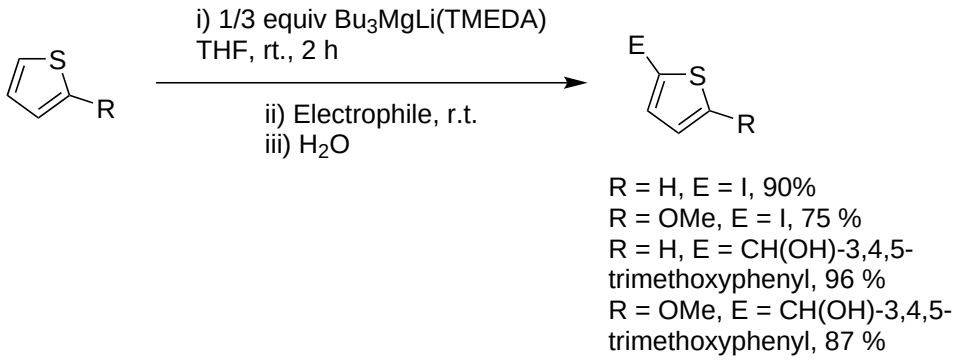

Scheme 2.2: Reaction of the lithium magnesiate $Bu_3MgLi(TMEDA)$ with thiophene[30]

The Hevia group has expanded the structural characterisation of lithium magnesiates, predominately focussing on homoleptic basic alkyl components.[83,84] These studies have highlighted an array of structural motifs upon changing both the alkyl component and the Lewis donor, with oxygen donors (THF and dioxane) favouring polymeric compositions in contrast to discrete monomeric units obtained with nitrogen Lewis donors (TMEDA and PMDETA) (see Scheme 2.3).

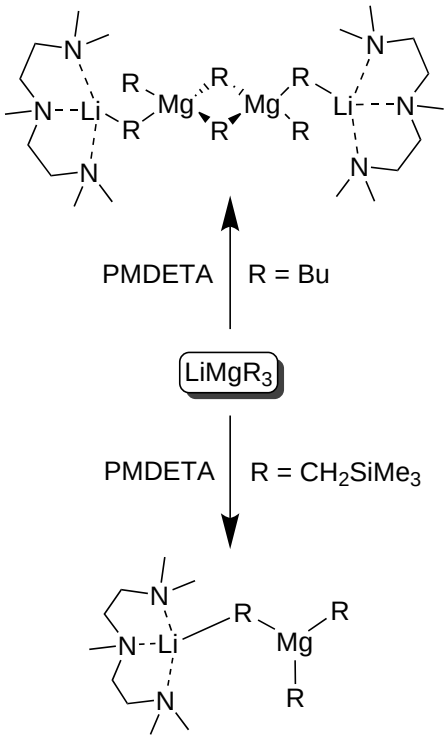

Scheme 2.3: Structural comparison of homoleptic lithium magnesiates when changing the alkyl component

Potassium magnesiates have only briefly been explored in the literature. The earliest example was the use of three equivalents of TMP(H) being added to a stoichiometric mixture of *n*BuK and $n\text{Bu}_2\text{Mg}$ suspended in *n*-hexane. The authors proposed this formed an *in situ* mixture of K(TMP)/Mg(TMP)_2. When a large excess of either benzene or toluene was added, the new complexes $[(\text{TMP})_{12}\text{K}_6\text{Mg}_6(\text{C}_6\text{H}_5)_6]$ and $[(\text{TMP})_{12}\text{K}_6\text{Mg}_6(\text{C}_6\text{H}_4\text{CH}_3)_6]$ were formed in high yields.[85] While the authors postulated the formation of an amido potassium magnesiate, based on the solubilisation of the reaction mixture, no analysis was done on the reaction mixture pre-metallation of the arene solvents.

Another example of a potassium magnesiate was in the direct magnesiation of bis(benzene)chromium.[86] When an equimolar mixture of potassium HMDS and magnesium bis(HMDS) were employed, no metallation occurred, but coordination of the bis(benzene)chromium to the potassium cation occurred, and formation of an anionic $[\text{Mg(HMDS)}_3]^-$ fragment. When the authors moved to the more basic TMP(H) amide, they instead found mono-metallation to exclusively occur (in comparison to organolithium reagents, where predominately di-metallation occurs). When the synergic base mixture of

benzylpotassium, dibutylmagnesium, TMP(H) and TMEDA (in a 1:1:3:1 mixture) were employed in a 4-fold molar excess with bis(benzene)chromium, the mono-magnesiated complex [(TMEDA)K(TMP){Cr(C_6H_5)(C_6H_6)}Mg(TMP)] was afforded (see Scheme 2.4).

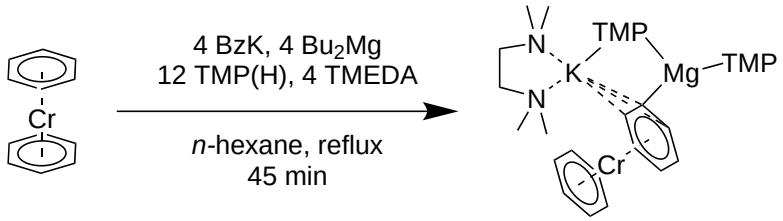

Scheme 2.4: Reaction of a potassium magnesiate with bis(benzene)chromium

In a similar vein to the $[Mg(HMDS)_3]^-$ anion in the previous publication,[86] Garcia-Alvarez and O'Hara et al. synthesised a series of potassium cations with chiral diamine ligands, with a corresponding $[Mg(HMDS)_3]^-$ anion.[87] This publication focused on the synthesis, solid-state and solution state structure of these compounds, without presenting any reactivity studies.

The first example of a structurally defined mixed alkyl-amido potassium magnesiate was isolated Conway and Mulvey *et al.*, and used in the *ortho*-magnesiation of the aromatic ether anisole.[88] When KCH_2SiMe_3, $MgBu_2$, TMP(H) and PMDETA were mixed in a 1:1:2:1 ratio, the mixed alkyl/amido magnesiate [(PMDETA)K(TMP)(CH_2SiMe_3)Mg(TMP)] was isolated. Interestingly, the authors were able to show through time-resolved NMR studies and crystallography that the kinetic product of the *ortho*-magnesiation of anisole was [(PMDETA)K(TMP)($o-C_6H_4OMe$)Mg(CH_2SiMe_3)] whereas the thermodynamic product was identified as [(PMDETA)K(TMP)($o-C_6H_4OMe$)Mg(TMP)] (see Scheme 2.5). In these two complexes, either amido or alkyl basicity were observed, respectively. Furthermore, all three complexes (the starting base, kinetic and thermodynamic product) were fully characterised by NMR and single-crystal X-ray diffraction studies.[88]

The most recent example of potassium magnesiates in the literature are the homoleptic complexes of the form [(C_6H_6)$KMgR_3$] formed from the addition of K(CH_2SiMe_3) and Mg(CH_2SiMe_3)$_2$ in a mixture of *n*-hexane and benzene. This initial mixture forms a

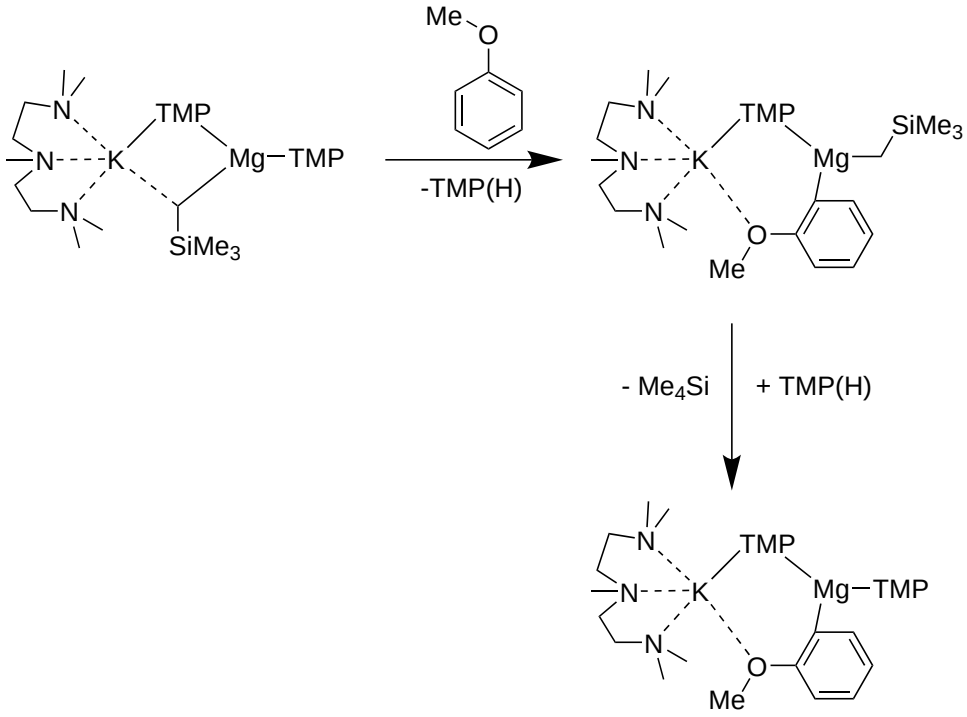

Scheme 2.5: Reaction of the potassium magnesiate [(PMDETA)K(TMP)(CH_2SiMe_3)Mg(TMP)] with anisole, highlighting both the kinetic amido basicity and the thermodynamic alkyl- basicity

lower-order magnesiate in the solid state, with an infinitely aggregated structure combining K-C and Mg-C bonds with medium-long K - Me eletrostatic interactions. When the Lewis donors TMEDA or PMDETA were added to this reaction mixture, a redistribution to higher-order magnesiates occurred, with the isolation of [$(PMDETA)_2K_2MgR_4$] and [$(TMEDA)_2K_2MgR_4$].[89]

2.0.1 DOSY NMR studies in organometallic chemistry

As previously outlined, while single crystal X-ray diffraction has been essential to the development of organometallic s-block chemistry, it does not necessarily translate into a full understanding of a molecules reactivity. In solution, organometallics are known to exist as complex equilibria of multiple co-existing aggregates. To fully understand the reactivity of these systems, it is therefore important to gain further insight into their solution state structure.

Pulsed gradient spin-echo (PGSE) diffusion NMR spectroscopy was designed in the mid

1960s as a tool to measure the hydrodynamic radius of molecules in solutions.[90–92] In 1992, the PGSE sequence was included in a psuedo two-dimensional NMR experiment allowing the comparison of chemical shift information with particle size, now commonly referred to as diffusion-ordered NMR spectroscopy (DOSY).[93] Since the early 2000s, it has been used extensively as a characterisation technique for reactive organometallic intermediates by a number of groups, allowing for the correlation of solution state aggregates and solvates with solid-state crystal structures and the determination of organolithium aggregates in dynamic equilibrium in solution.[94]

Highlighted in a recent study by Mulvey and Robertson, utilising ^{1}H-DOSY NMR the originally proposed lithium cadmate "LiCd(TMP)$_3$" as a cadmating (Cd-H exchange) agent, the reactivity observed is the result of a lithiation followed by a transmetallation with a cadmium reagent (see Figure 2.2).[32]

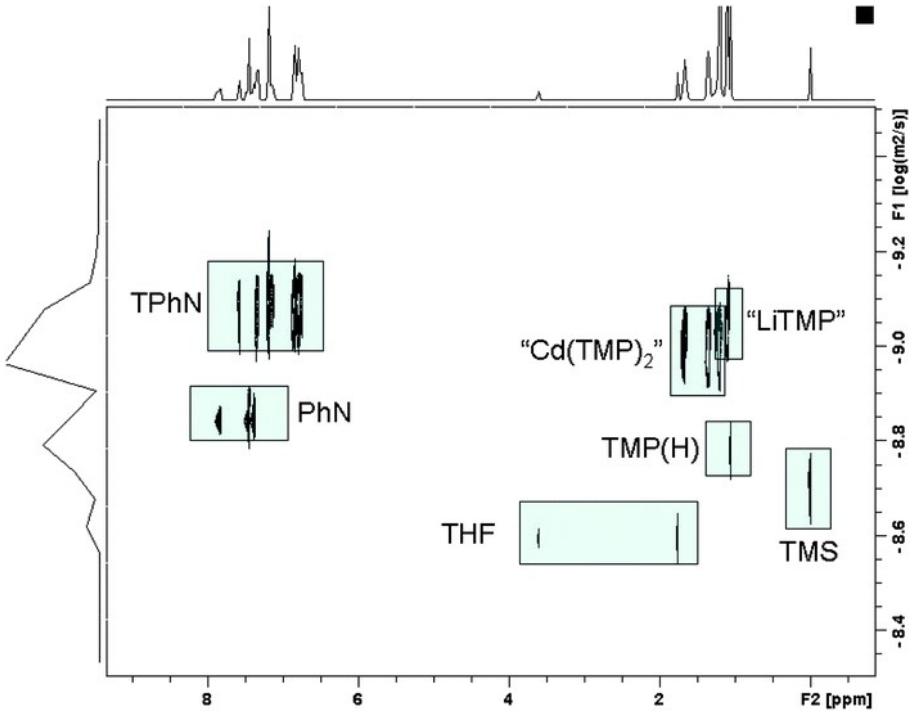

Figure 2.2: Pseudo 2D ^{1}H-DOSY spectrum of $CdCl_2$ + 3Li(TMP) in d_8−THF at 27 °C in the presence of the inert standards tetraphenylnapthalene (TPhN), phenylnapthalene (PhN) and tetramethylsilane(TMS). Reproduced with permission from the Royal Society of Chemistry

This has led to two distinct concepts within mixed metal metallations, that of co-complexation vs trans-metal trapping.[95] In co-complexation, base reactivity occurs syn-

ergistically, with the lower polarity metal performing a direct metallation of the desired substrate. Conversely, in trans-metal trapping, sequential reactivity is observed, with the more reactive alkali metal typically affording the metallation event, followed by transmetallation by the lower polarity metal. This enables the stabilisation of the kinetic products in many cases.[95] In both these reaction pathways, a combination of solid state and solution state characterisation was essential to elucidate the differential mechanism of reaction.

2.0.2 Aims and objectives

In this chapter, we aimed to synthesis a range of Group 1 heteroleptic metal magnesiates containing the alkyl- group CH_2SiMe_3 and amido group TMP, and fully characterise them in the solid state (by single crystal X-ray diffraction) and solution state (NMR studies as well as DOSY-NMR studies). Looking to the literature, only the sodium magnesiate [(TMEDA)Na(TMP)(CH_2SiMe_3)Mg(TMP)] **1** and the potassium magnesiate [(PMDETA)K(TMP)(CH_2SiMe_3)Mg(TMP)] have been previously reported. This study was initially inspired by some unexpected reactivity of the sodium magnesiate **1**, seen within this thesis as well as within other research projects within our group. Solution state studies presented in this chapter will be conducted in C_6D_{12}, as previous experience with these alkali metal magnesiates indicate they react with many other typical NMR solvents, such as C_6D_6, d_8-THF and d_8-toluene. Furthermore, deuterated cyclohexane (C_6D_{12}) will be the most representative of the solution state behaviour of these bases in *n*-hexane, the solvent they are typically utilised in, while being cost effective (deuterated *n*-hexane is cost prohibitive).

2.1 Synthesis of lithium magnesiate bases

2.1.1 Synthesis of [(TMEDA)Li(TMP)$_2$Mg(CH$_2$SiMe$_3$)]

To synthesise a lithium magnesiate base, LiCH$_2$SiMe$_3$ was reacted with an *in situ* mixture of MgTMP$_2$ (formed by refluxing 2 molar equivalents of TMP(H) with *n*MgBu$_2$ for 6 hours), followed by the addition of a molar equivalent of TMEDA to give a light yellow solution. After filtration and storage of the resulting solution at -30 °C, a crop of colourless crystals were deposited. X-ray crystallographic analysis of these crystals revealed them to be the anticipated lithium magnesiate complex [(TMEDA)Li(TMP)(CH$_2$SiMe$_3$)Mg(TMP)] **3**.

In an alternative method to synthesise **3**, *n*MgBu$_2$ can be replaced by Mg(CH$_2$SiMe$_3$)$_2$ to form Mg(TMP)$_2$, resulting in the same isolated lithium magnesiate.

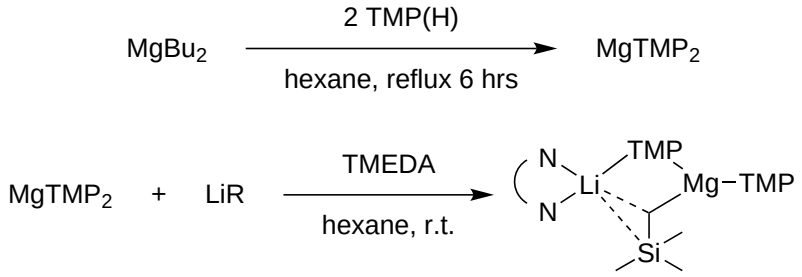

Scheme 2.6: Synthetic protocol for the synthesis of **3**, [(TMEDA)Li(TMP)$_2$Mg(CH$_2$SiMe$_3$)]

2.1.2 X-ray crystallography of complex 3

Complex **3** crystalises in the $Pna2_1$ space group. It exhibits a contact ion pair co-complex arrangement with a 4-atom Li-N-Mg-C ring motif core. The coordination environment of the magnesium atom is a N$_2$C trigonal planar arrangement, with one terminal TMP ligand (Mg - N distance 1.997(4) Å), and a bridging TMP (Mg - N distance 2.094(4) Å) and CH$_2$SiMe$_3$ unit (Mg - C distance 2.184(5) Å). The lithium atom has a distorted tetrahedral arrangement, with a bridging TMP (Li - N distance 2.143(10) Å), bridging CH$_2$SiMe$_3$

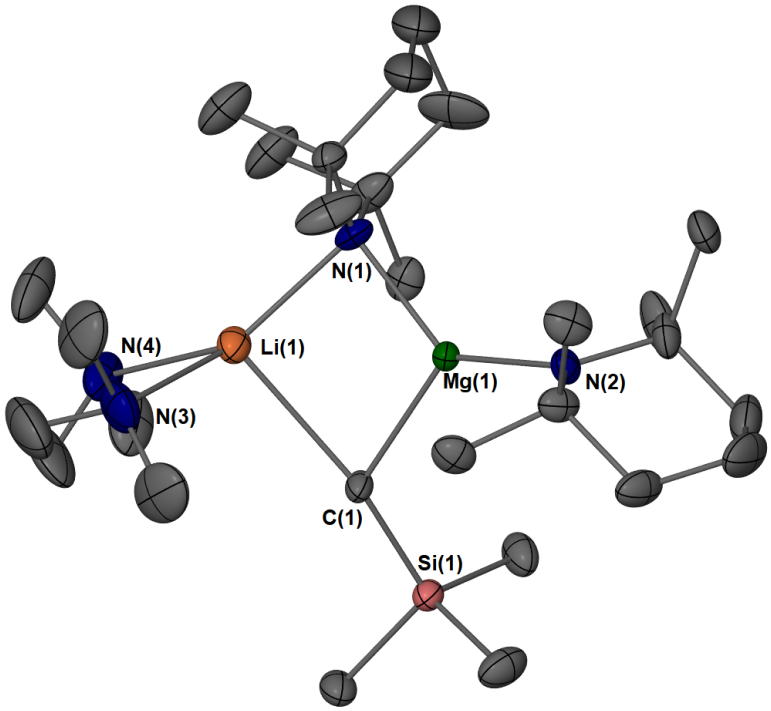

Figure 2.3: Molecular structure of [(TMEDA)Li(TMP)(CH_2SiMe_3)Mg(TMP)], **3**. Thermal ellipsoids shown at 40 % probability. Hydrogen atoms omitted for clarity. Selected bond lengths (Å) and angle (°): Li(1) – N(1), 2.143(10); N(1) – Mg(1), 2.094(4); Mg(1) – N(2), 1.997(4); Mg(1) – C(1), 2.184(5); Li(1) – C(1), 2.489(11); Li(1) – N(1) – Mg(1), 84.5(3) ; N(1) – Mg(1) – N(2), 132.9(2); N(2) – Mg(1) – C(1), 124.4(2).

(Li - C distance 2.489(11) Å) and a chelating bidentate TMEDA ligand completing the coordination environment.

To examine whether the crystal structure Figure 2.3 is representative of the bulk crystalline phase, a powder X-ray diffraction experiment was performed on bulk **3**. This analysis confirmed that the bulk crystalline solid phase matched the single-crystal X-ray diffraction structure of **3** (see Figure 2.4).

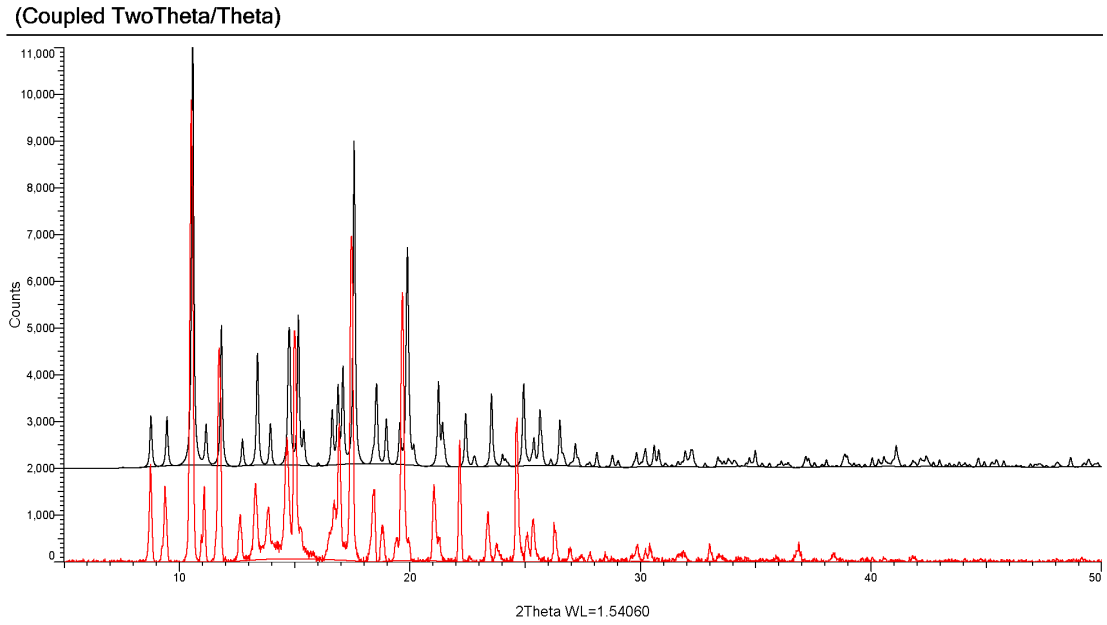

Figure 2.4: PXRD of a crystalline sample of **3** (bottom, red line) compared to a calculated pattern based on the crystal structure (top, black line)

2.1.3 Solution state studies of complex 3

^{1}H and ^{7}Li NMR spectroscopic analysis was performed on crystalline **3** in $d_{12}-$cyclohexane. The ^{1}H NMR spectrum elucidated that one dominant species was present, with signals assigned in Figure 2.5. However, some small impurities are noticeable. The dominant species shows signals related to coordinated TMEDA, deprotonated TMP as well as signals for the alkyl group CH_2SiMe_3. Impurities were particularly evident in the TMP region as well as the CH_2SiMe_3 region of the ^{1}H NMR spectrum. The ^{7}Li NMR spectrum is shown in Figure 2.6, which shows one dominant species at 1.08 ppm, with a minor ^{7}Li containing impurity present at 1.23 ppm.

To determine whether this major species was consistent with the solid state crystal structure, ^{1}H-DOSY NMR studies were performed, with the resulting DOSY plot shown in Figure 2.7. This spectrum indicated that the solid state structure of **3** is retained in solution, as indicated by a similar diffusion constant for all signals within the dominant species.

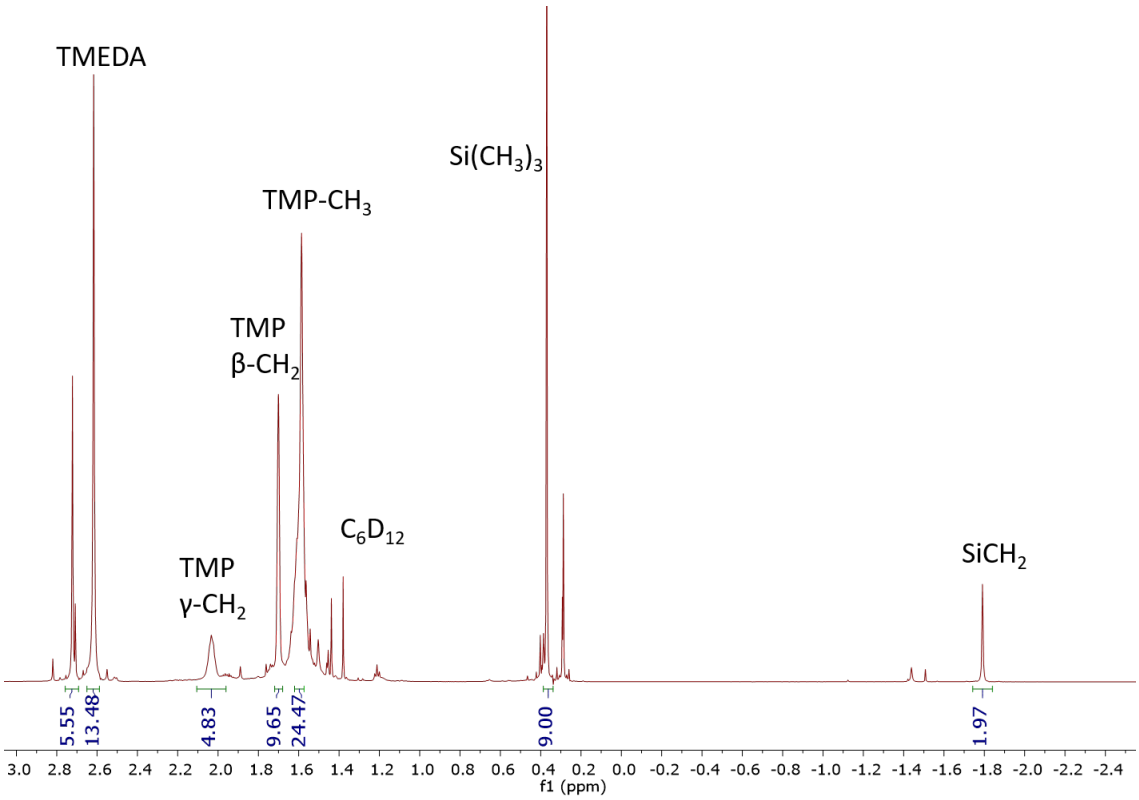

Figure 2.5: ^{1}H NMR spectrum of **3** in C_6D_{12} at 298 K

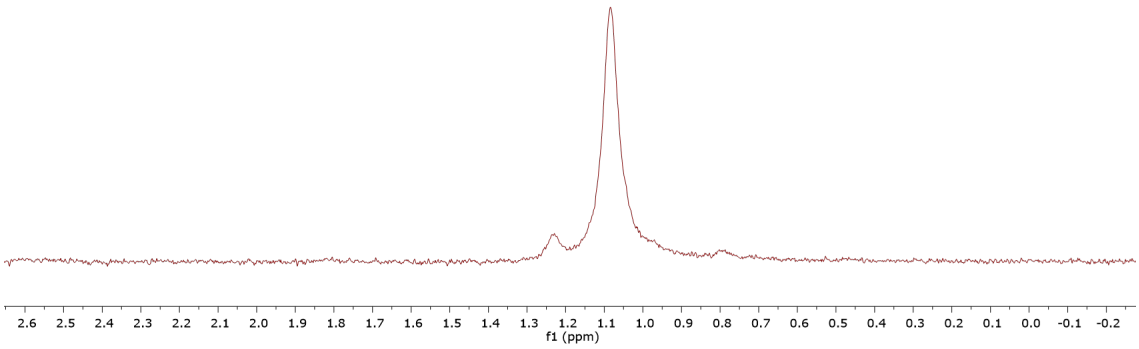

Figure 2.6: ^{7}Li NMR spectrum of **3** in C_6D_{12} at 298 K

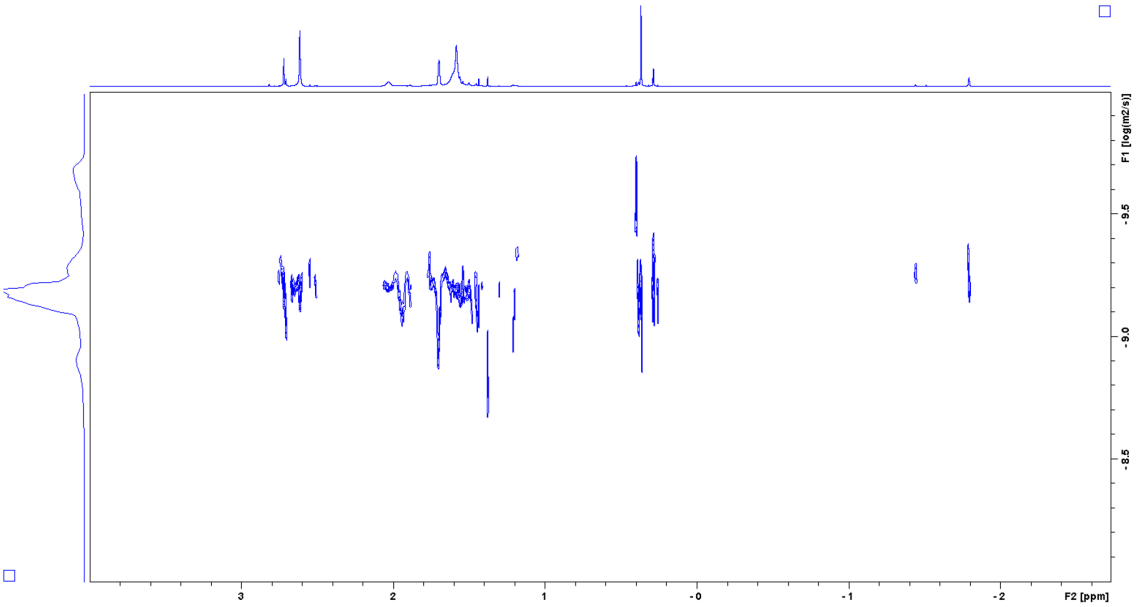

Figure 2.7: ^{1}H DOSY NMR spectrum of **3** in C_6D_{12} at 298 K

Interestingly, it became clear when monitoring the ^{1}H NMR spectrum over time that **3** was rearranging or decomposing in solution, with the appearance of new signals (see Figure 2.5). After six hours stored at room temperature, the dominant species is no longer **3**, and many other species (characterised by signals in the $SiCH_2$, $SiCH_3$ and TMP/TMEDA region of the spectra). These other species have not been identified. Multiple species are also present in the ^{7}Li NMR spectrum (see Figure 2.9). It is not clear at this stage whether this is a decomposition process, or a fluctional rearrangement occurring in solution.

It was also noticed that crystalline sample of **3** stored at room temperature in an argon glovebox decomposed over a period of a few weeks. It is not clear why this base is unstable in both solution (in C_6D_{12}) and solid state.

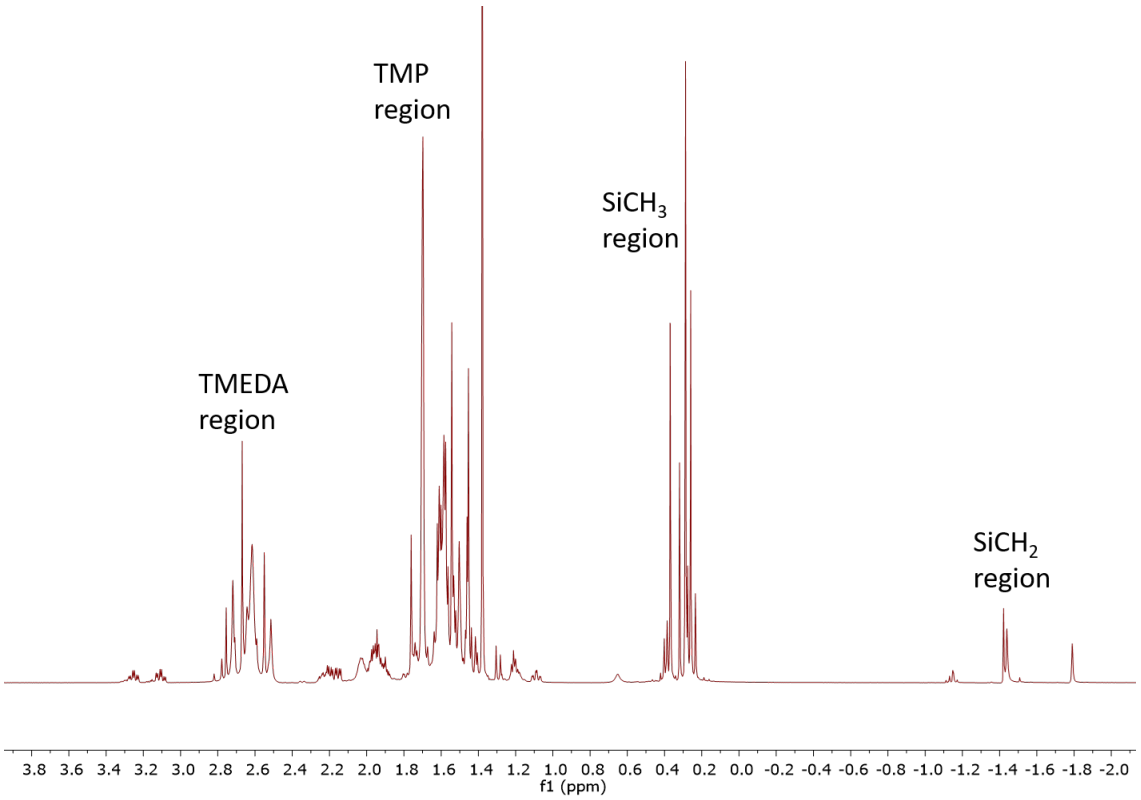

Figure 2.8: ^{1}H NMR spectrum of **3** in C_6D_{12} after 6 hours at 298 K

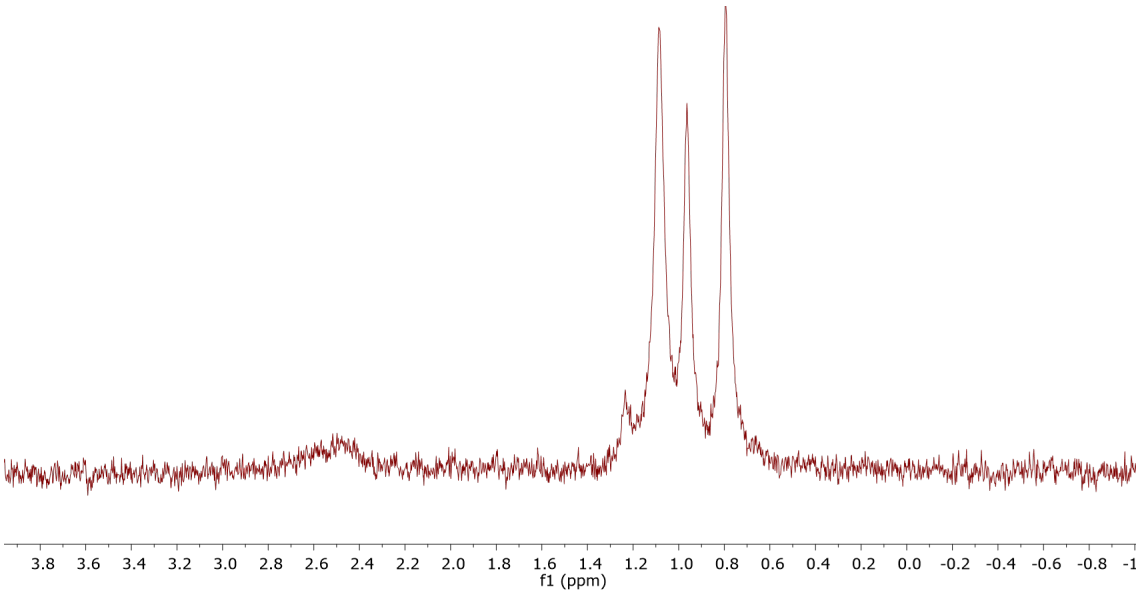

Figure 2.9: ^{7}Li NMR spectrum of **3** in C_6D_{12} after 6 hours at 298 K

2.2 Synthesis of [(PMDETA)Li(CH_2SiMe_3)Mg(TMP_2)]

Similarly to **3**, when $LiCH_2SiMe_3$ was reacted with an *in situ* mixture of $MgTMP_2$ (formed by refluxing 2 molar equivalents of TMP(H) with *n*$MgBu_2$ for 6 hours), followed by the molar addition of PMDETA, a light yellow solution developed. Upon storage of this solution at -30 °C, a large crop of colourless crystals were deposited. X-ray crystallographic analysis of these crystals revealed them to the be the unanticipated lithium magnesiate complex [(PMDETA)Li(CH_2SiMe_3)Mg(TMP_2)] **4**. An alternative synthesis of complex **4** is possible substituting *n*$MgBu_2$ for $Mg(CH_2SiMe_3)_2$ for the formation of $Mg(TMP)_2$.

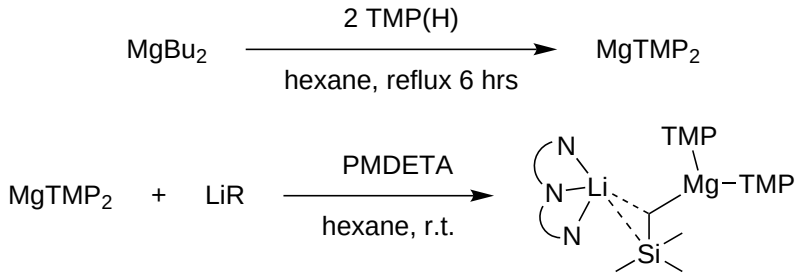

Scheme 2.7: Synthetic protocol for the synthesis of **4**, [(PMDETA)Li(CH_2SiMe_3)Mg(TMP_2)]

2.2.1 X-ray crystallography of complex 4

In the molecular structure of compound **4** [(PMDETA)Li(CH_2SiMe_3)Mg($TMP)_2$], the lithium cation exists in a different environment to the related TMEDA adduct **3**. The lithium cation is pulled further away from the anionic magnesium centre, interacting with the CH_2 and the silicon of the alkyl basic arm (Li-C bond length of 2.373(3) and Li-Si bond length of 3.160(3) Å) leaving a three-coordinate magnesium centre with two terminal TMP fragments (Mg-N distances of 2.0302(13) and 2.0101(12) Å). This species can be envisioned as an intermediate between a contact-ion pair co-complex, and a solvent separated ion pair. A similar structural motif is seen in the homoleptic lithium magnesiate complex [(PMDETA)$LiMg(CH_2SiMe_3)_3$].[83]

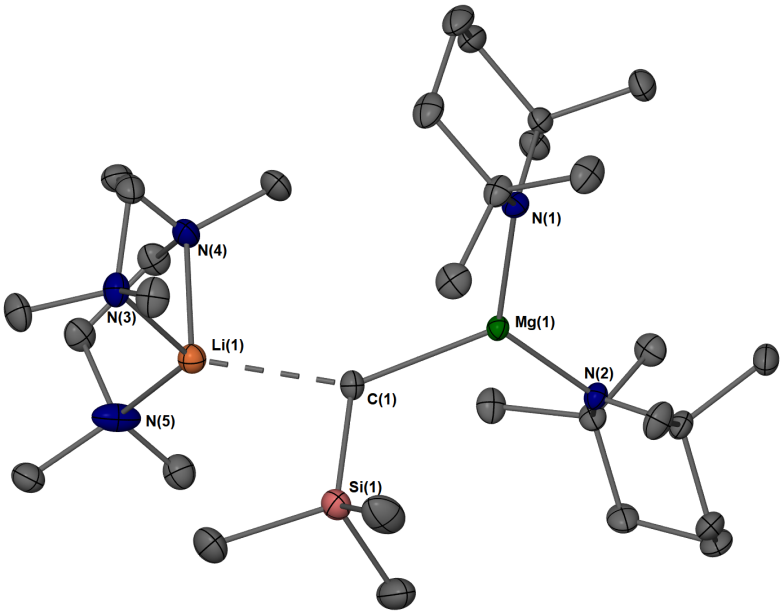

Figure 2.10: Molecular structure of [(PMDETA)Li(CH_2SiMe_3)Mg$(TMP)_2$], **4**. Thermal ellipsoids shown at 40 % probability. Hydrogen atoms omitted for clarity. Selected bond lengths (Å) and angle (°): Li(1) – C(1), 2.373(3); Li(1) – Si(1), 3.160(3); Mg(1) – C(1), 2.2328(15); Mg(1) – N(1), 2.0302(13); Mg(1) – N(2), 2.0101(12); N(1) – Mg(1) – N(2), 126.11(5); N(1) – Mg(1) – C(1), 115.62(6); N(2) – Mg(1) – C(1), 118.10(6).

To determine whether the bulk crystalline product matches the single-crystal structure, Powder X-ray Diffraction (PXRD) on a crystalline sample was undertaken (see Figure 2.11). This indicated that the bulk crystalline phase of **4** was consistent with the single-crystal X-ray diffraction structure. Crystalline sample will be used in the solution state studies to rule out co-crystallising species.

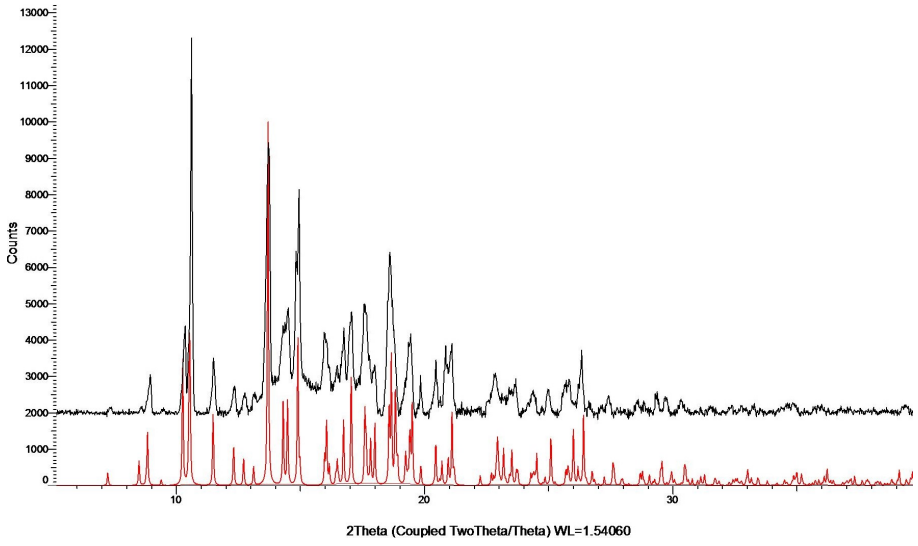

Figure 2.11: Powder XRD of crystalline complex **4** (top) vs calculated pattern (bottom)

2.2.2 Solution state studies of complex 4

Crystalline complex **4** was dissolved in C_6D_{12} and analysed by ^1H and ^7Li NMR spectroscopy. Similarly to **3**, this species was found to rapidly rearrange or decompose in C_6D_{12}, inhibiting any meaningful NMR analysis. It is unclear why these lithium magnesiates **3** and **4** decompose or rearrange in the solution phase - further work would be required to identify the exact composition of these species. To identify these species, reactivity studies could be particularly useful, if they selectively react with one species present in solution.

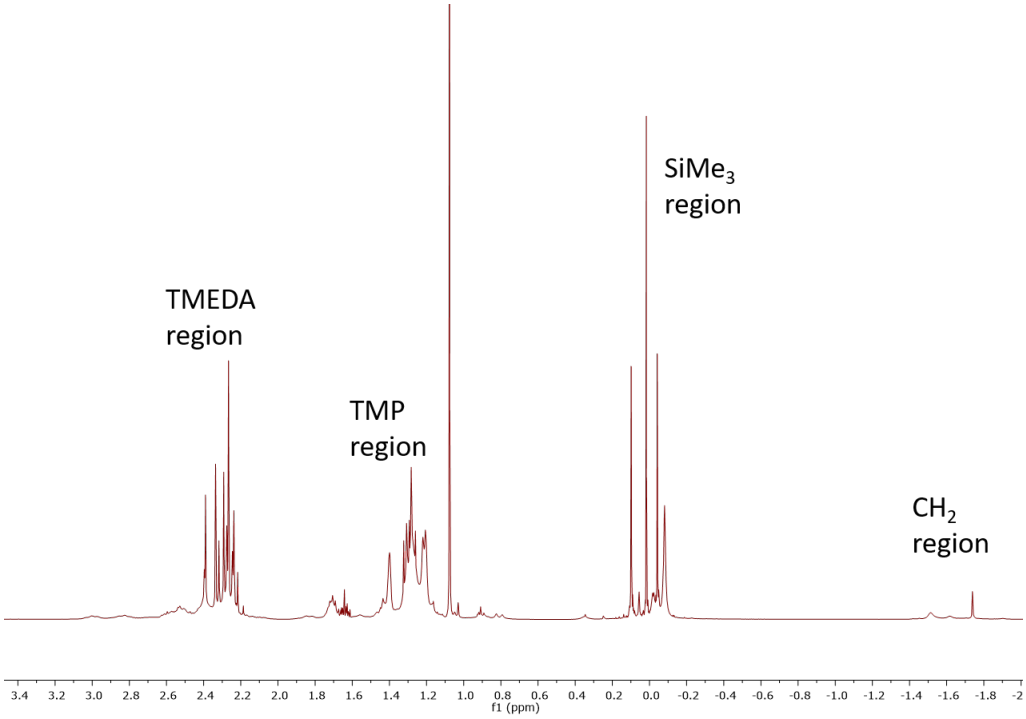

Figure 2.12: ^1H NMR spectrum of crystalline complex **4** in C_6D_{12} at 298 K, showing the presence of numerous species

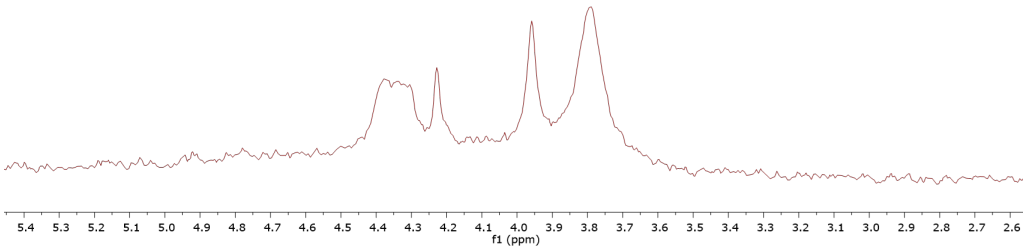

Figure 2.13: ^7Li NMR spectrum of crystalline complex **4** in C_6D_{12} at 298 K, showing the presence of numerous species

2.3 Synthesis of sodium magnesiate bases

2.3.1 Synthesis of [(TMEDA)Na(TMP)(CH_2SiMe_3)Mg(TMP)] 1

The sodium magnesiate base **1** was synthesised according to literature procedures.[67] The sodium magnesiate base **1** was synthesised by the reaction of molar equivalents of NaTMP, TMP(H), $Mg(CH_2SiMe_3)$ and TMEDA to give a light yellow solution. Storage of the resulting solution at -30 °C resulted in the deposition of a large crop of colourless crystals.

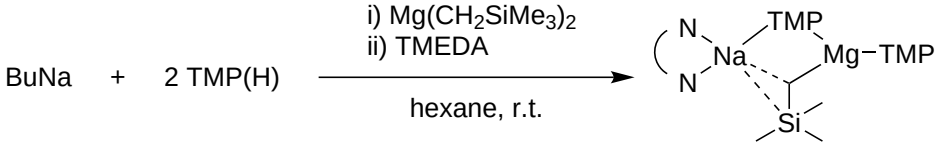

Scheme 2.8: Synthetic protocol for the synthesis of **1**, [(TMEDA)Na(TMP)(CH_2SiMe_3)Mg(TMP)]

2.3.2 X-ray crystallography of 1

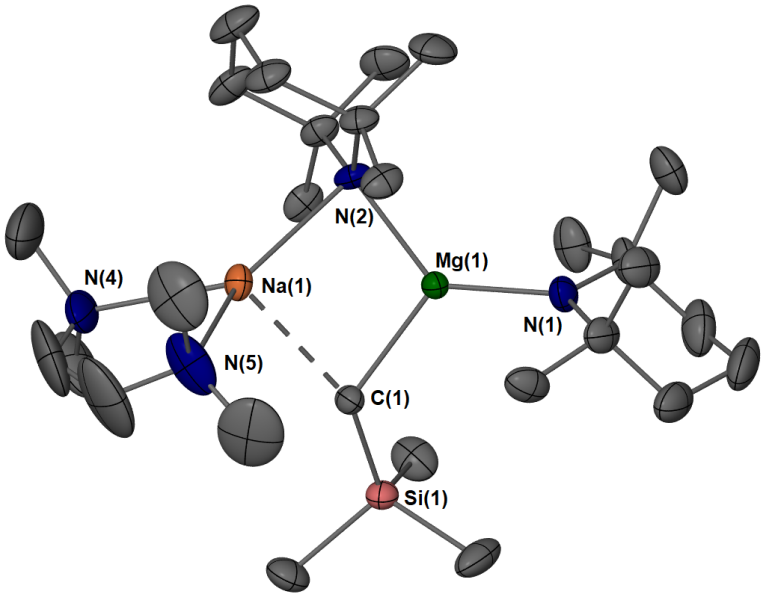

Figure 2.14: Molecular structure of [(TMEDA)Na(TMP)(CH_2SiMe_3)Mg(TMP)], **1**. Thermal ellipsoids shown at 40 % probability. Hydrogen atoms omitted for clarity. Selected bond lengths (Å) and angle (°): Mg(1) - C(1), 2.179(2); Mg(1) - N(1), 1.9895(18); Mg(1) - N(2), 2.068(3); Na(1) - C(1), 2.6783(2); Na(1) - N(2), 2.454(4); Na(1) - N(4), 2.433(2); Na(1) - N(5), 2.488(3); C(1) - Mg(1) - N(1), 123.36(10), C(1) - Mg(1) - N(2), 106.67(13); N(1) - Mg(1) - N(2), 128.70(14).

Similarly to complex **3**, the molecular structure of complex **1** features a trigonal planar magnesium centre, bonding to a terminal TMP (Mg - N bond length 1.9895(18) Å), a bridging TMP (Mg - N bond length 2.068(3) Å) and a bridging alkyl CH_2SiMe_3 group (Mg - C bond length 2.179(2) Å). The sodium atom is four coordinate, with a bridging TMP (Na - N bond length 2.454(4) Å), interacting with the CH_2 of the alkyl group (Na - C bond length 2.6783(2) Å), and a bidentate, chelating TMEDA (Na - N bond lengths of 2.433(2) and 2.488(3) Å).

To confirm the bulk crystalline phase was consistent with the crystal structure of **1**, PXRD of the bulk crystals was performed (see Figure 2.15). This confirmed that the bulk crystalline phase (to be used in solution state studies) is consistent with the crystal structure of **1**, and no co-crystalline impurities are present.

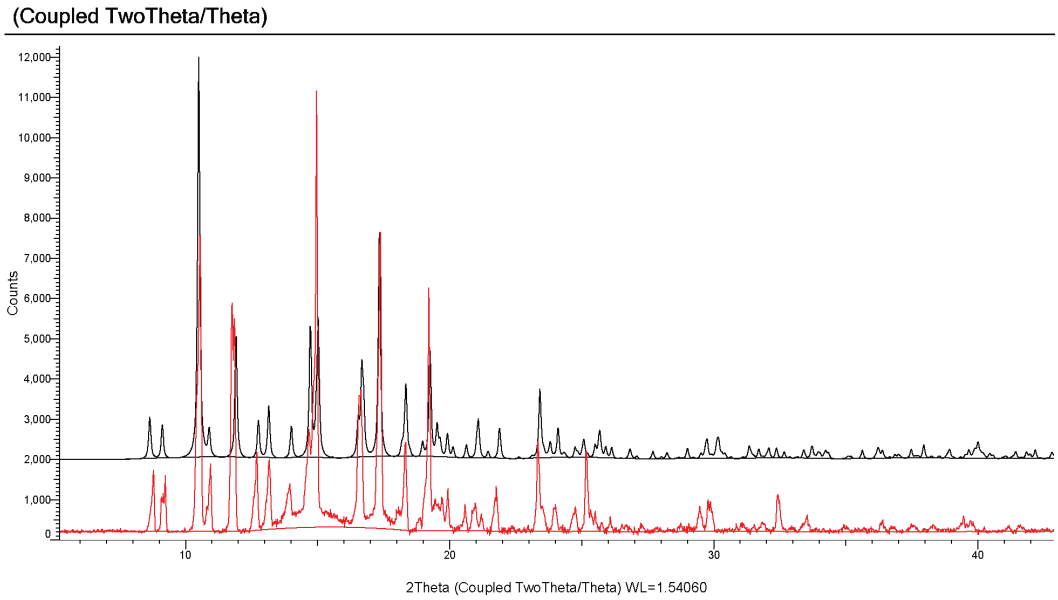

Figure 2.15: PXRD of a crystalline sample of **1** (bottom, red line) compared to a calculated pattern based on the crystal structure (top, black line)

2.3.3 Solution state studies of complex 1

Crystalline complex **1** was dissolved in C_6D_{12} and analysed by ^{1}H and ^{13}C NMR spectroscopy (see Figure 2.16). In agreement with the solid state structure, the ^{1}H spectrum matches well with the retention of the solid state structure in solution. Single signals

are present for coordinated TMEDA, TMP, and the alkyl CH_2SiMe_3 group. In order to investigate this further, ^{1}H-DOSY NMR studies were conducted. As can be seen in Figure 2.17, there is only one dominant species present in solution at room temperature. Complementary to this, a ^{1}H-^{1}H-NOESY study of **1** shows no interchange peaks present, indicating that no signals are interchanging on the NMR time-scale (see Figure 2.18).

In comparison to **3** and **4**, a sample of **1** in C_6D_{12} is stable for at least one week at room temperature.

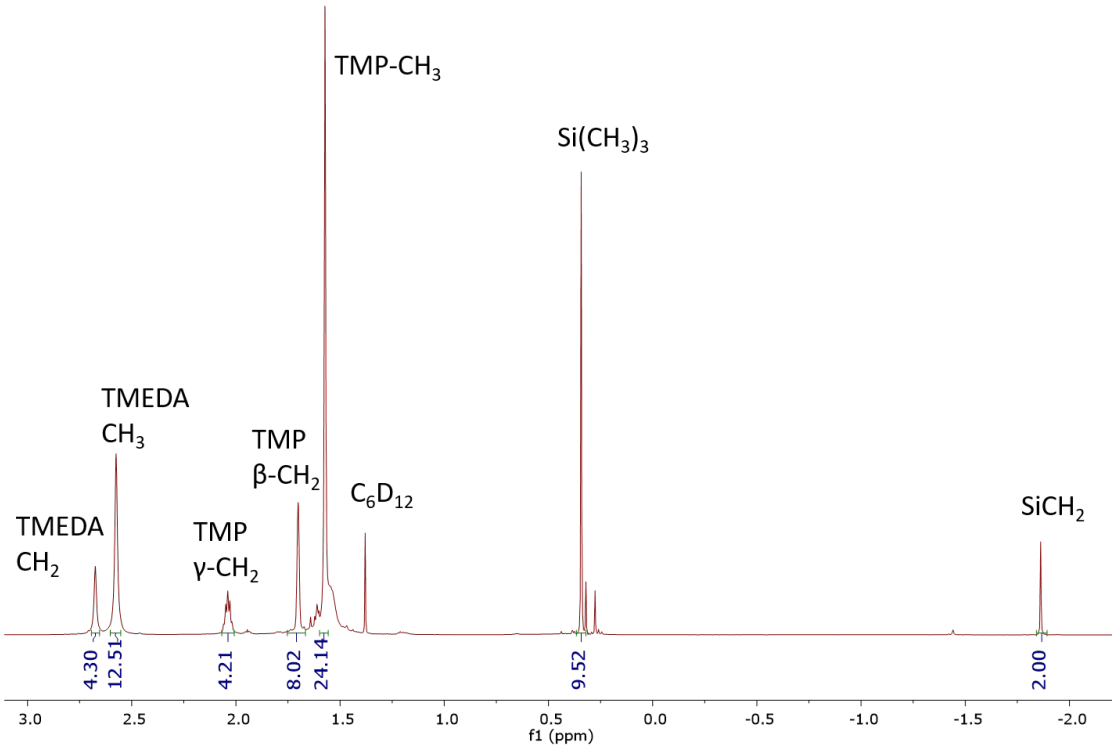

Figure 2.16: ^{1}H-NMR of complex **1** in C_6D_{12} at 298 K

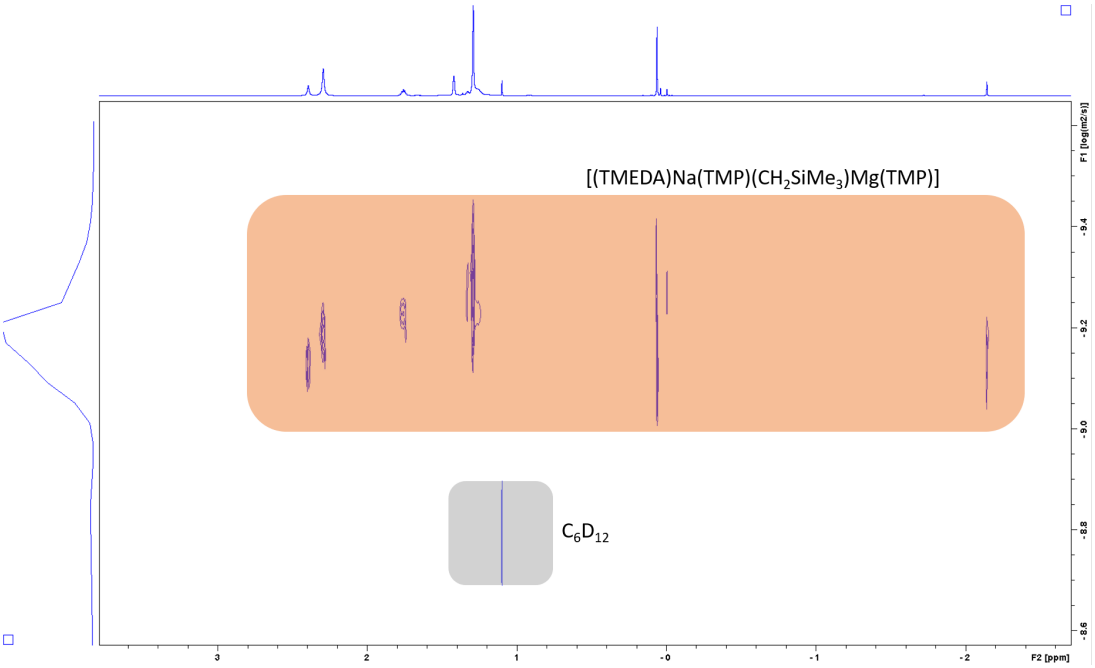

Figure 2.17: ^{1}H DOSY NMR sprectrum of complex **1** in C_6D_{12} at 298 K

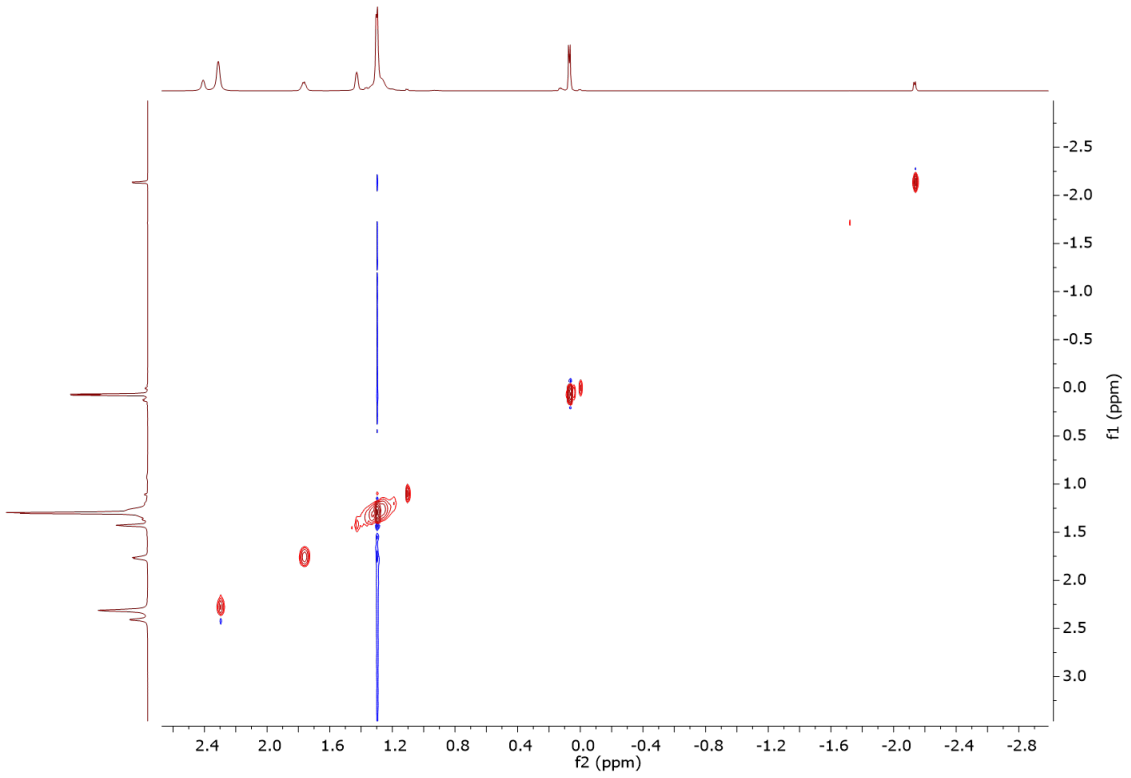

Figure 2.18: NOESY NMR spectrum of complex **1** in C_6D_{12} at 298 K

2.4 Synthesis of potassium magnesiate bases

2.4.1 Synthesis of $[(TMEDA)_3K]^+[Mg(TMP)_3]^-$

When attempting to isolate a potassium analogue of the aforementioned **1**, we unexpectedly isolated the solvent separated potassium magnesiate $[K(TMEDA)_3]^+[Mg(TMP)_3]^-$ **5**. The rational synthesis of this complex was also achieved, by refluxing $MgBu_2$ with three equivalents of TMP(H), followed by the addition of KCH_2SiMe_3 and three equivalents of the Lewis donor TMEDA. Storage of the resulting solution at - 30 °C resulted in the deposition of large colourless crystals.

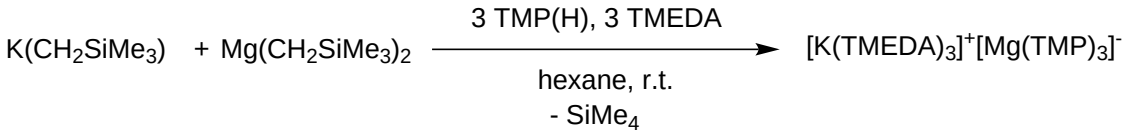

Scheme 2.9: Synthetic protocol for the synthesis of **5**, $[K(TMEDA)_3]^+[Mg(TMP)_3]^-$

2.4.2 X-ray crystallography of complex 5

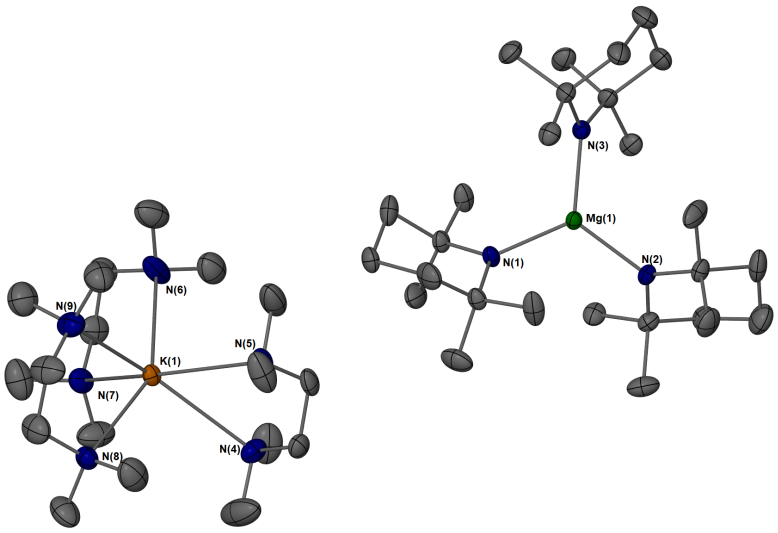

Figure 2.19: Molecular structure of $[(TMEDA)_3K]^+[Mg(TMP)_3]^-$, **5**. Thermal ellipsoids shown at 40 % probability. Hydrogen atoms omitted for clarity. Selected bond lengths (Å) and angle (°): Mg(1) – N(1), 2.0389(16); Mg(1) – N(2), 2.0493(16); Mg(1) – N(3), 2.0365(17); N(1) – Mg(1) – N(2), 120.23(7); N(2) – Mg(1) – N(3), 121.35(7); N(3) – Mg(1) – N(1), 118.40(7).

Complex **5** exists as the solvent separated ion pair $[(TMEDA)_3K]^+[Mg(TMP)_3]^-$. This complex features a three-coordinate trigonal planar anionic magnesium centre bonded to three basic TMP units (average Mg-N distance 2.0416 Å), and a charge separated potassium cation encapsulated by three TMEDA molecules to form a distorted octahedral environment. Complex **5** resembles the previously reported sodium magnesiate $[Na(PMDETA)_2]^+[Mg(TMP)_3]^-$[96] while having structural similarities to a variety of solvent separated alkali metal stabilised $[Mg(HMDS)_3]^-$ anionic complexes.[86,87,97]

2.4.3 Solution state analysis of complex 5

Crystalline complex **5** was dissolved in C_6D_{12} and analysed by ^1H NMR spectroscopy (see Figure 2.20). Signals corresponding to coordinated TMEDA, and deprotonated TMP(H) are evident. A small amount of free TMP(H) is also present, likely from residual TMP(H) from the synthesis.

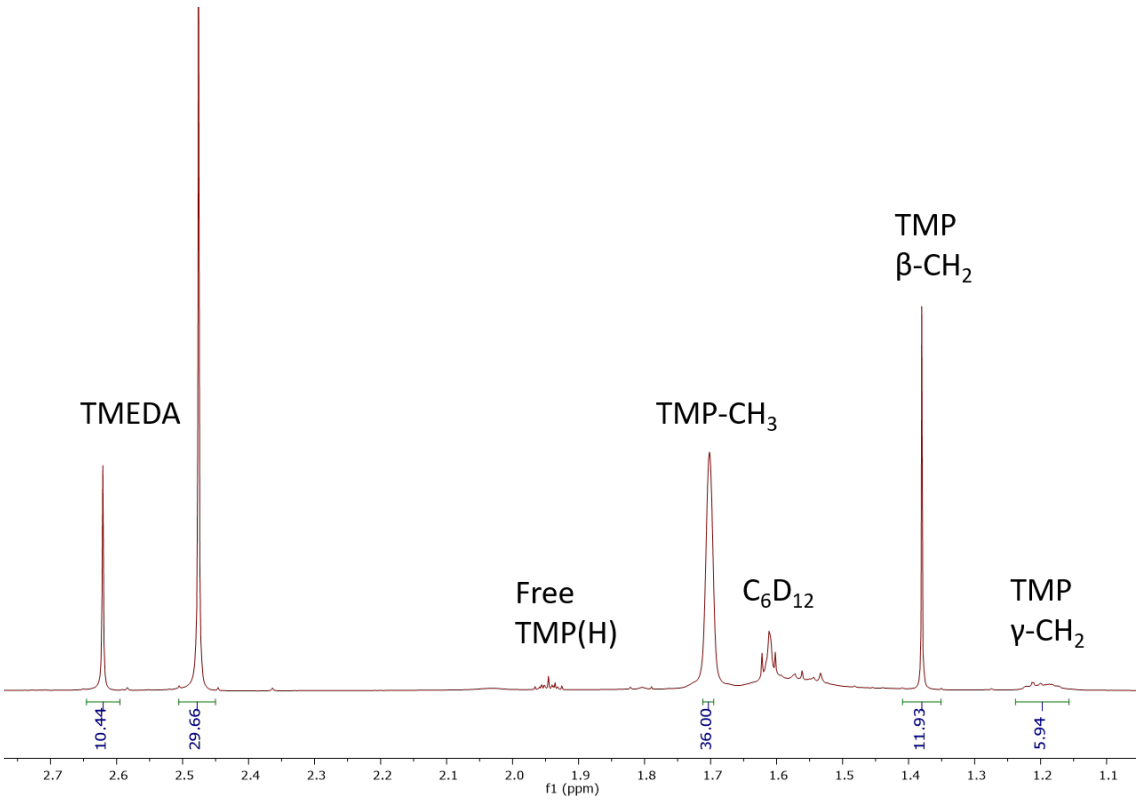

Figure 2.20: ^1H NMR spectra of **5** in C_6D_{12} at 298 K

Complex **5** was also analysed by ^{1}H-DOSY NMR, shown in Figure 2.21. In the DOSY spectra, signals are evident for K(TMEDA)$_3^-$ and Mg(TMP)$_3^+$, confirming their existence as a solvent separated ion pair. Some free TMP(H) is also present, likely from the initial synthesis. Due to the highly soluble nature of **5** in *n*-hexane, difficulties were experienced washing the obtained crystals without them redissolving.

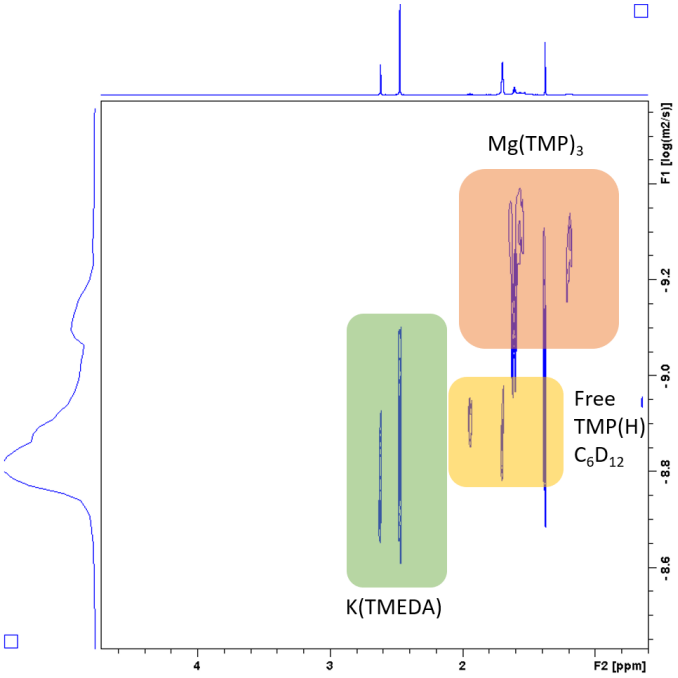

Figure 2.21: ^{1}H-DOSY NMR spectrum of complex **5** in C_6D_{12} at 298 K, showing K(TMEDA)$_3^+$, Mg(TMP)$_3^-$, and free TMP(H)

2.4.4 Reaction of 5 with aromatic solvents

Interestingly, when **5** was dissolved in C_6D_6 for NMR analysis, a crop of crystals were deposited in the NMR tube over the course of a few days. These crystals were suitable for single crystal X-ray diffraction and were analysed to be the previously reported 24-membered $(KNMgN)_6$ macrocyclic complex $[(TMP)_6K_6Mg_6(C_6H_5)_6]$ **6**,[85] which was synthesised originally by an *in situ* mixture of K(TMP)/Mg(TMP$_2$) with benzene.

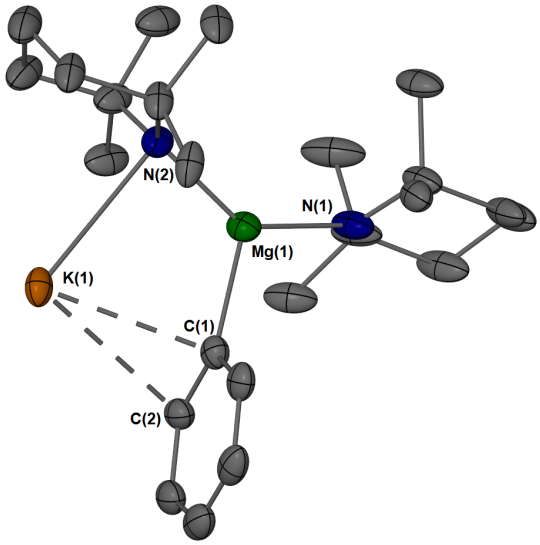

Figure 2.22: Asymmetric unit of complex **6**. Thermal ellipsoids shown at 40 % probability. Hydrogen atoms omitted for clarity. Selected bond lengths (Å) and angles (°): Mg(1) - C(1), 2.1797(7); Mg(1) - N(1), 2.0318(3); Mg(1) - N(2), 2.0258(3); K(1) - N(2), 3.0893(7); K(1) - C(1), 3.0692(5); K(1) - C(2), 3.3491(6); N(2) - Mg(1) - N(1), 136.2(1); N(2) - Mg(1) - C(1), 113.2(1); C(1) - Mg(1) - N(1), 110.6(2).

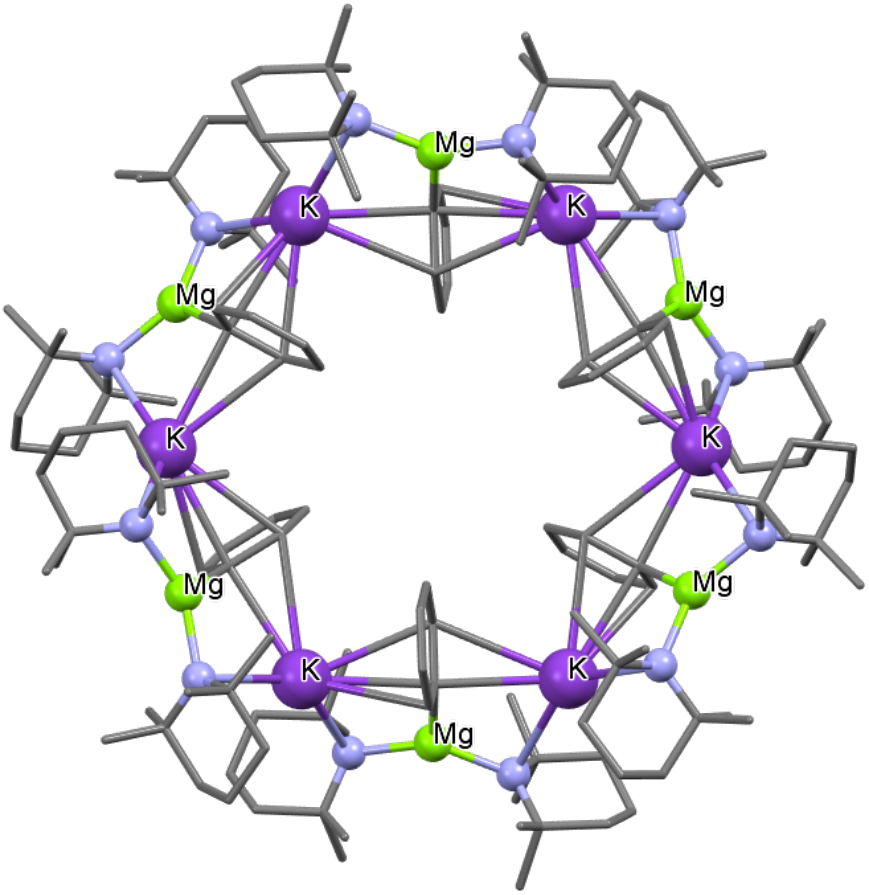

Figure 2.23: Full molecular structure of **6**

2.4.5 Synthesis of [(PMDETA)K(TMP)(CH_2SiMe_3)Mg(TMP)]

The potassium magnesiate base **7** was synthesised according to a literature procedure.[88] The addition of a *n*-hexane suspension of $Mg(TMP)_2$ to KCH_2SiMe_3 followed by the addition of PMDETA resulted in the formation of a clear, colourless solution. Upon storage at - 30 °C, a crop of colourless crystals were isolated. These were found to be the expected complex [(PMDETA)K(TMP)(CH_2SiMe_3)Mg(TMP)] **7**.

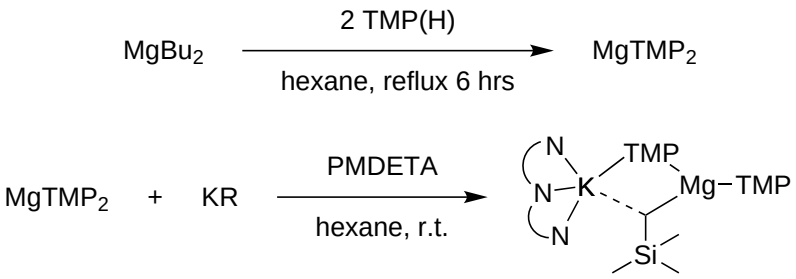

Scheme 2.10: Synthetic protocol for the synthesis of **7**, [(PMDETA)K(CH_2SiMe_3)Mg$(TMP)_2$]

2.4.6 X-ray crystallography of complex 7

Complex **7** features a trigonal planar Mg centre, bonding to a terminal TMP [Mg - N bond length 1.996(5) Å], a bridging TMP [Mg - N bond length 2.055(5) Å] and a bridging alkyl CH_2SiMe_3 group [Mg - C bond length 2.219(7) Å]. The potassium cation is five-coordinate, bonding to a bridging TMP [K - N bond length 2.925(4) Å], a bridging alkyl CH_2SiMe_3 [K - C bond length 3.033(8) Å], and a chelating, tridentate PMDETA ligand. Complex **7** adopts a similar structural motif to [(TMEDA)Li(TMP)(CH_2SiMe_3)Mg(TMP)] **3** and [(TMEDA)Na(TMP)(CH_2SiMe_3)Mg(TMP)] **1**.

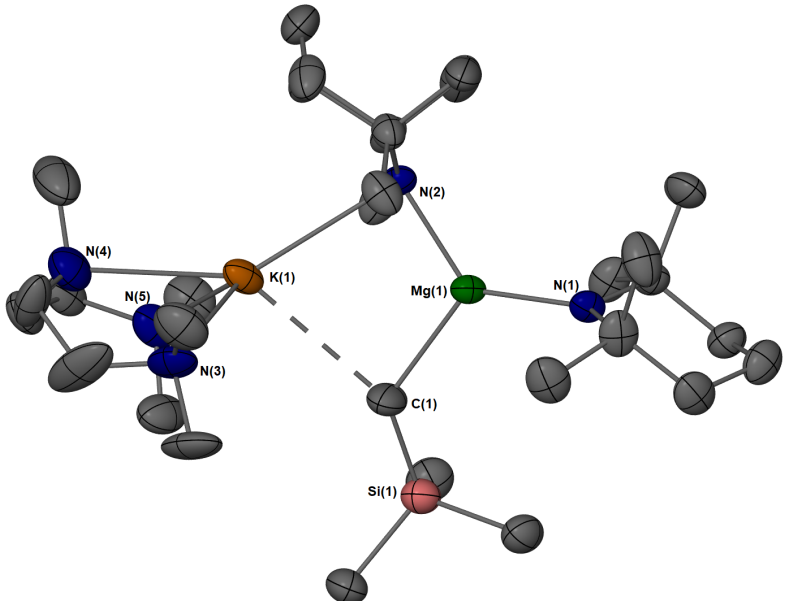

Figure 2.24: Molecular structure of [(PMDETA)K(CH_2SiMe_3)Mg($TMP)_2$], **7**. Thermal ellipsoids shown at 40 % probability. Hydrogen atoms omitted for clarity. Selected bond lengths (Å) and angle (°): Mg(1) - C(1), 2.219(7); Mg(1) - N(1), 1.996(5); Mg(1) - N(2), 2.055(5); K(1) - N(2), 2.925(4); K(1) - C(1), 3.033(8); N(2) - Mg(1) - N(1), 129.34(19); N(2) - Mg(1) - C(1), 110.6(2); C(1) - Mg(1) - N(1), 119.5(3); K(1) - N(2) - Mg(1), 90.94; K(1) - C(1) - Mg(1), 85.1(2).

2.4.7 Solution state analysis of complex 7

Complex **7** was dissolved in C_6D_{12} and analysed by ^{1}H NMR spectroscopy (see Figure 2.25). It would appear that only one species is present in solution, with minor impurities also present (TMP(H) predominately, as well as impurities related to the alkyl group). Signals are evident for coordinated PMDETA, deprotonated TMP(H) as well as signals corresponding to the alkyl group CH_2SiMe_3.

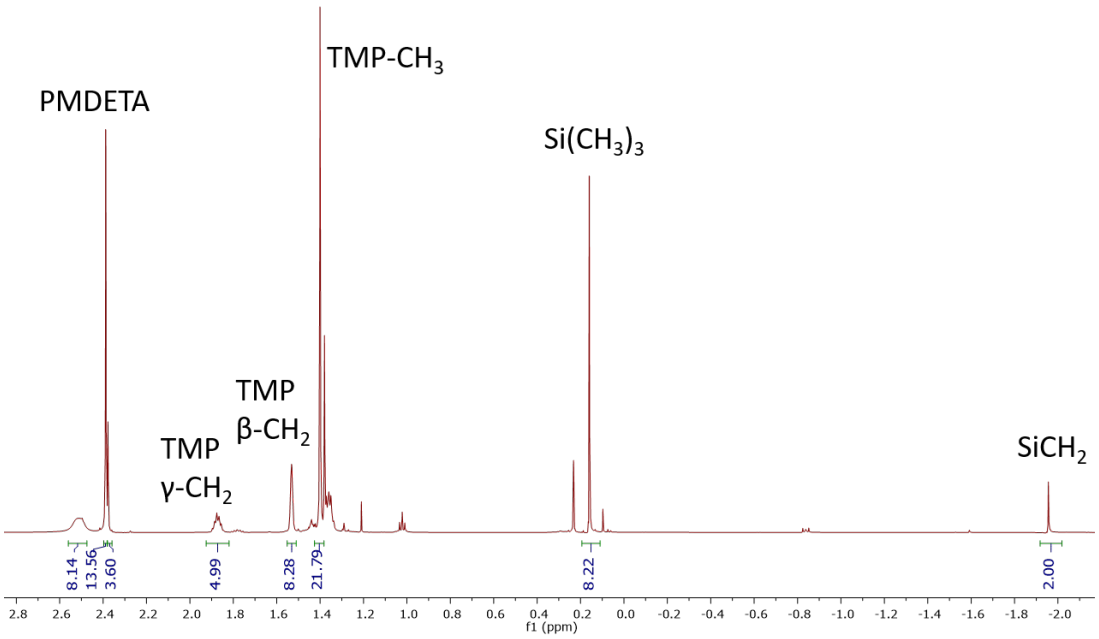

Figure 2.25: ^{1}H NMR spectrum of **7** in C_6D_{12} at 298 K

The ^{1}H-DOSY NMR spectrum of complex **7** was conducted, to confirm whether the solid state structure is retained in solution (see Figure 2.26). While one dominant species appears to be present in solution, the impurities present lead to a broadening in the diffusion coefficients of the overlapping signals. While attempts were made to further purify this complex, difficulties arose from the highly *n*-hexane soluble nature of complex **7**.

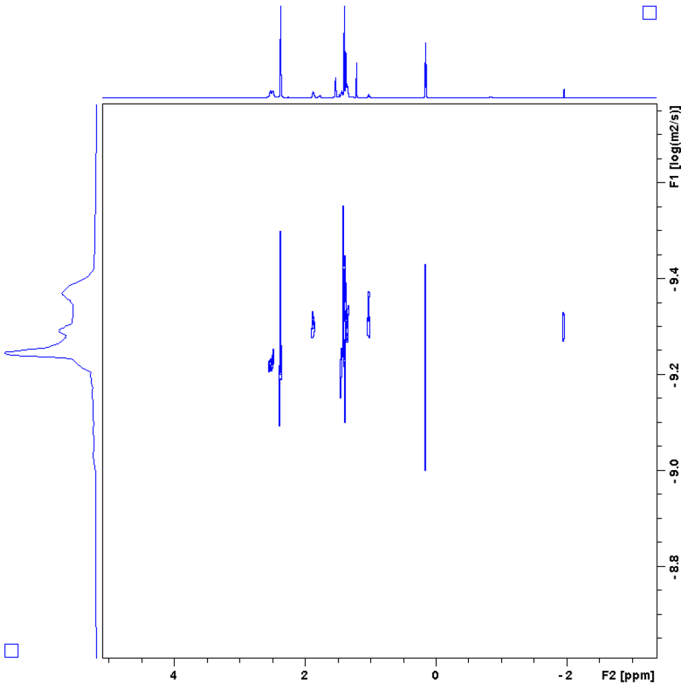

Figure 2.26: ^{1}H-DOSY NMR spectrum of complex **7** in C_6D_{12} at 298 K

2.5 Synthesis of $[(PMDETA)_2Rb]^+[MgTMP_3]^-$

Moving to the heavier alkali metal rubidium, the addition of $MgTMP_2$ to a hexane solution of $RbCH_2SiMe_3$ followed by the addition of two equivalents of PMDETA resulted in the formation of viscous yellow oils. Storage of these oils at - 30 °C afforded a crop of colourless crystals, which were suitable for single crystal X-ray diffraction. These were found to be the complex $[Rb(PMDETA)_2]^-[Mg(TMP)_3]^+$ **8**.

$$Rb(CH_2SiMe_3) + Mg(CH_2SiMe_3)_2 \xrightarrow[\text{hexane, r.t.}\\ \text{- } SiMe_4]{\text{3 TMP(H), 2 PMDETA}} [Rb(PMDETA)_2]^+[Mg(TMP)_3]^-$$

Scheme 2.11: Synthetic protocol for the synthesis of **8**, $[Rb(PMDETA)_2]^+[Mg(TMP)_3]^-$

2.5.1 X-ray crystallography of complex 8

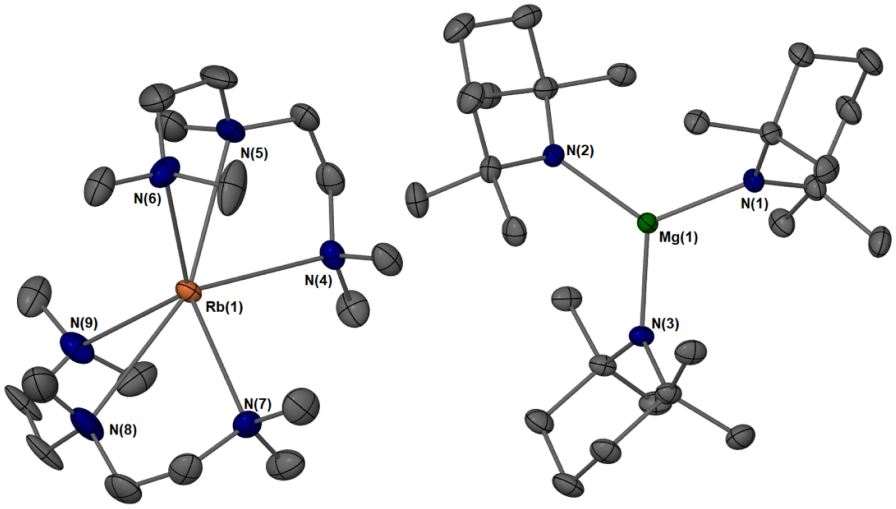

Figure 2.27: Molecular structure of $[(PMDETA)_2Rb]^+[MgTMP_3]^-$, **8**. Thermal ellipsoids shown at 40 % probability. Hydrogen atoms omitted for clarity. Selected bond lengths (Å) and angle (°): Mg(1) – N(1), 2.053(2); Mg(1) – N(2), 2.0471(19); Mg(1) – N(3), 2.0396(19); N(1) – Mg(1) – N(2), 122.16(8); N(2) – Mg(1) – N(3), 121.60(8); N(1) – Mg(1) – N(3), 116.21(8).

Similarly to its potassium analogue **5**, complex **8** features a trigonal planar magnesium centre bonded to three basic TMP units (average Mg-N bond 2.0416 Å) while the rubidium atom is encapsulated by two PMDETA molecules in a six-coordinate irregular coordination polyhedron. This geometry has previously being observed with $[(PMDETA)_2K]^+$ cation.[98,99] Looking to the literature, to the best of our knowledge complex **8** represents a rare structurally characterised example of a rubidium magnesiate, with only one previously reported complex $[Rb(toluene)_3]^+[Mg(HMDS)_3]^-$[100] to date (CCDC search 02/2021).

2.5.2 Solution state analysis of 8

Crystalline complex **8** was dissolved in C_6D_6 and analysed by ^{1}H NMR spectroscopy (see Figure 2.28, this complex was found too insoluble in C_6D_{12} for analysis). Signals are evident for coordinated PMDETA, as well as TMP. Unfortunately, a clean ^{1}H NMR spectrum of **8** was not possible, as the sample decomposed over a short period of time in C_6D_6.

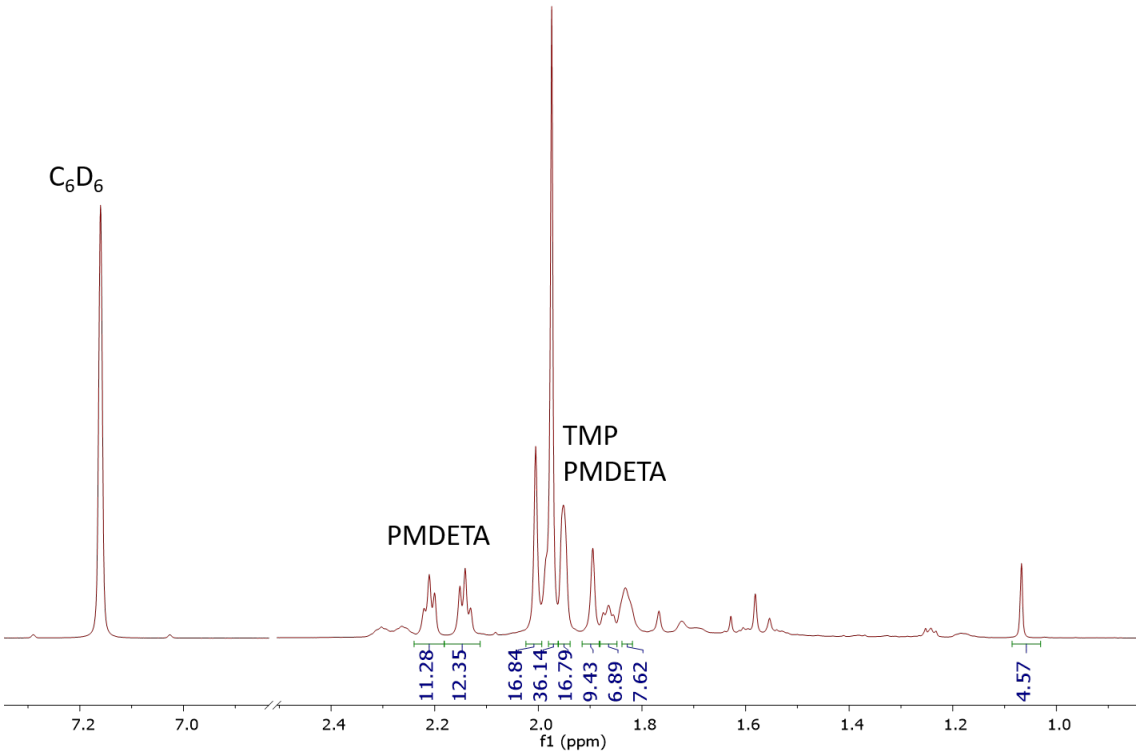

Figure 2.28: ^{1}H NMR spectrum of **8** in C_6D_6 at 298 K. Impurities are evident as the complex was unstable in solution, decomposing over a short period of time.

2.6 Comparison of structural chemistry

Complexes **1**, **3**, **4** and **7** exist as contact-ion pairs, while complexes **5** and **8** exist as solvent-separated ion pairs in the solid state. Complex **4** is the most distinct, featuring only one bridging alkyl group between the anionic magnesium centre and the cationic lithium. In comparison, **1**, **3** and **7** feature the more typical bridging amido and alkyl group seen in similar alkali metal magnesiate complexes. Similarly to the previously reported homoleptic complex [(PMDETA)Li(CH_2SiMe_3)Mg(CH_2SiMe_3)$_2$],[83] complex **4** can be seen as an intermediate between a solvent-separated ion pair and a contact ion pair species. As the alkali metal size increases between **3** (Li), **1** (Na) and **7** (K), a lengthening in the alkali metal bridging alkyl lengths (from 2.489(11) to 3.034(7) Å) and the alkali metal bridging amido lengths (from 2.142(10) to 2.929(4) Å) are observed. The coordination environment around the magnesium centre remains essentially unchanged. The anionic environments of complex **5** and **8** are essentially isostructural, with the cationic

Table 2.1: Comparison of the key bond lengths (Å) and angles (°) of complexes **3**,**4**,**1**,**5**,**7**,**8**

	Contact Ion Pairs Complexes				Solvent Separated Complexes	
	Complex **3** M = Li TMEDA	Complex **4** M = Li PMDETA	Complex **1** M = Na TMEDA	Complex **7** M = K PMDETA	Complex **5** M = K TMEDA	Complex **8** M = Rb PMDETA
Mg-C(alkyl)	2.184(5)	2.2328(15)	2.179(2)	2.218(6)		
Mg-TMP (bridging)	2.094(4)		2.068(3)	2.064(4)		
					2.0389(16)	2.053(2)
Mg-TMP (terminal)	1.997(4)	2.0302(13)	1.9895(18)	1.999(4)	2.0493(16)	2.0471(19)
		2.0101(12)			2.0365(17)	2.0396(19)
M-N(TMP)	2.142(10)		2.454(4)	2.929(4)		
					2.9399(19)	3.072(2)
		2.128(3)		2.828(5)	2.955(2)	2.991(2)
M-N(donor)	2.368(11)	2.096(3)	2.433(2)	2.777(7)	2.9164(18)	3.006(2)
	2.197(10)	2.187(3)	2.488(3)	2.928(5)	2.8955(18)	3.025(2)
					2.970(2)	3.008(2)
					2.981(2)	3.011(2)
M – C(alkyl)	2.489(11)	2.373(3)	2.678(2)	3.034(7)		
M – N – Mg	84.5(3)		85.42(11)	90.70(14)		
					120.23(7)	122.16(8)
N – Mg – N	132.9(2)	126.11(5)	128.70(14)	129.28(18)	121.35(7)	121.60(8)
					118.40(7)	116.21(8)
		115.62(6)	106.67(12)	110.7(2)		
N – Mg – C(alkyl)	124.4(2)	118.10(6)	123.36(10)	119.5(2)		

environments varying in their geometry based on the denticity of the Lewis donor (TMEDA in **5** vs PMDETA in **8**). A comparison of the bond lengths of the complexes **3**,**4**,**1**,**5**,**7**,**8** can be found in Table 2.1.

During the synthetic aspects of this chapter, it was noticed that the crystal structure for $Mg(CH_2SiMe_3)_2$.TMEDA was not known. As it was considered possible that this species may be an impurity present in a number of the magnesiates present, it was synthesised to allow comparison of the NMR chemical shifts.

2.7 Synthesis and characterisation of $Mg(CH_2SiMe_3)_2$.TMEDA

To a stirred suspension of $Mg(CH_2SiMe_3)_2$ in hexane, one molar equivalent of TMEDA was added dropwise at room temperature. This resulted in the complete dissolution of the suspension as the TMEDA coordinates to the magnesium centre. The resulting solution was stored overnight in a - 30 °C freezer, resulting in a large crop of colourless crystals which were suitable for single-crystal X-ray diffraction. These were identified to be the mononuclear $[(TMEDA)Mg(CH_2SiMe_3)_2]$ **9**.

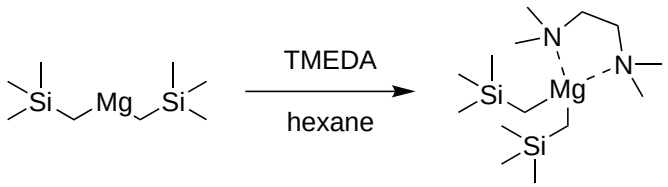

Scheme 2.12: Synthetic protocol for the synthesis of **9**, $[(TMEDA)Mg(CH_2SiMe_3)_2]$

2.7.1 X-ray crystallography of complex 9

In the molecular structure of complex **9**, the magnesium is in a distorted tetrahedral environment. The magnesium forms short bonds to the anionic C atoms (Mg-C bond lengths of 2.141(2) Å).

The polymeric structure of $Mg(CH_2SiMe_3)_2$ has been broken down into a monomeric unit by the bidentate nitrogen donor TMEDA (Mg - N bond lengths of 2.234(2) and 2.239(2) Å).

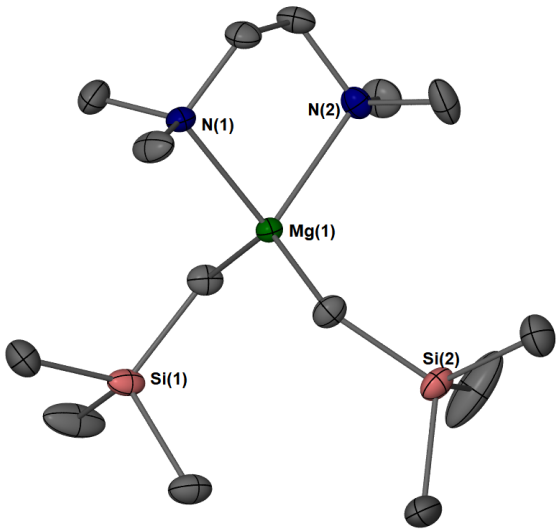

Figure 2.29: Molecular structure of MgR_2.TMEDA. Thermal ellipsoids shown at 40 % probability. Hydrogen atoms omitted for clarity. Selected bond lengths (Å) and angle (°): Mg(1) - C(4), 2.141(2); Mg(1) - C(5), 2.141(2); Mg(1) - N(1), 2.234(2); Mg(1) - N(2), 2.239(2); N(1) - Mg(1) - N(2), 81.99(7); N(1) - Mg(1) - C(4), 112.27(9); N(1) - Mg(1) - C(5), 104.68(8); N(2) - Mg(1) - C(4), 106.64(8); N(2) - Mg(1) - C(5), 113.33(9); C(4) - Mg(1) - C(5), 128.32(10).

2.7.2 Solution state analysis of complex 9

Crystalline complex **9** was dissolved in C_6D_6 and analysed by ^{1}H NMR spectroscopy. Signals were evident for TMEDA, as well as the CH_3 and CH_2 of the alkyl groups. The ^{1}H NMR spectrum was consistent with the retention of the solid state structure of **9** in solution.

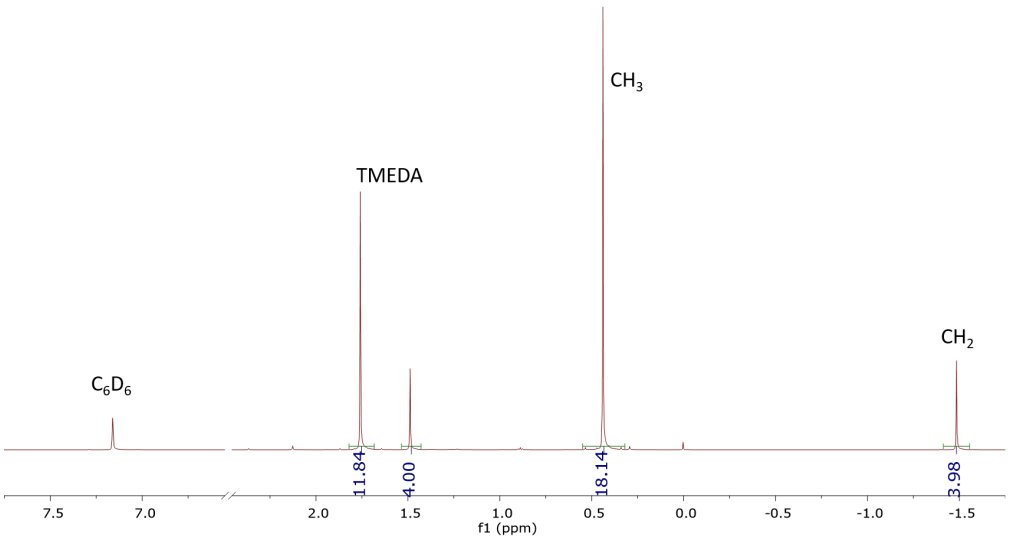

Figure 2.30: ^{1}H NMR spectrum of **9** in C_6D_6 at 298 K

2.8 Conclusions and further work

In this chapter, a series of alkali metal homo- and hetero-leptic magnesiates were synthesised, resulting in the isolation and characterisation of the novel lithium magnesiates [(TMEDA)Li(TMP)(CH_2SiMe_3)Mg(TMP)] and [(PMDETA)Li$(TMP)_2$Mg(CH_2SiMe_3)], potassium magnesiate [$(TMEDA)_3$K][$Mg(TMP)_3$] and the rubidium magnesiate [$(PMDETA)_3$Rb][$Mg(TMP)_3$]. The solution state chemistry of the lithium magnesiates was found to be complex - dynamic fluctional processes occurring in C_6D_{12}, not allowing the positive identification of the solution state species in each case. Further reactivity studies of the lithium magnesiates should be conducted, in order to gain insight into their solution state structure, as well as any potential synthetic utility.

3 Bimetallic metallations of *N,N*- and *P,P*-dialkyl substituted anilines and phenylphosphines

Anilines are a class of substituted aromatics that are weak *ortho* metallation directors in established organolithium chemistry.[64] This is a result of the delocalisation of the nitrogen lone pair into the aryl ring, not allowing the coordination of an incoming organolithium reagent. This results in the need for either harsh reactions conditions or activation of the organolithium reagent. For instance, the reaction of *N,N*-dimethyl or *N,N*-diethyl aniline with *n*-BuLi results in negligible *ortho*-lithiated product after one week, however when *n*-BuLi is activated by TMEDA the lithiation occurs in high yields within three hours.[101] The sodiation of *N,N*-dimethylaniline can be readily achieved at 0 °C with *n*-BuNa activated by TMEDA.[102]

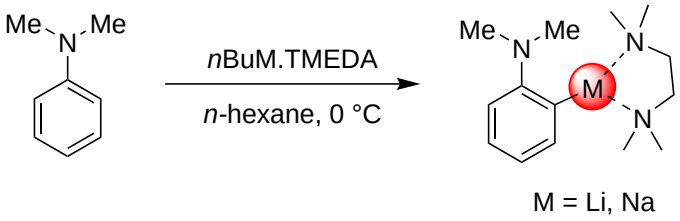

Scheme 3.1: Reaction of *n*BuLi·TMEDA and *n*BuNa·TMEDA with *N,N*-dimethylaniline to give the *ortho*-metallated complex

The metallation of *N,N*-dimethylaniline has been previously achieved with a bimetallic system, using the mixed sodium zincate [(TMEDA)Na(*t*Bu)(TMP)Zn(*t*Bu)], in which a novel *meta*-zincation was observed (Scheme 3.2).[103] Subsequent *in situ* electrophilic quenching studies with iodine revealed a mixture of *ortho*-, *meta*- and *para*- iodoanilines.[102]

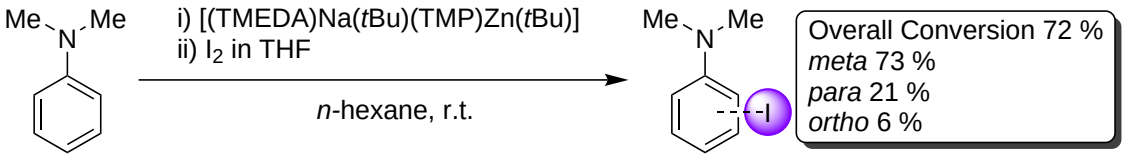

Scheme 3.2: Reaction of the zincate base [(TMEDA)Na(tBu)(TMP)Zn(tBu)] with *N,N*-dimethylaniline

3.1 Target anilines and phenylphosphines

Looking to extend the metallation chemistry of the sodium magnesiate **1**, [(TMEDA)Na(TMP)(CH_2SiMe_3)Mg(TMP)], a series of *N,N*-dialkylanilines and *P,P*-dialkylphenylphosphines were targeted (see Figure 3.1). The anilines targeted are commercially available, whereas the phosphines were synthesised from commercially available *P,P*-dichlorophenylphosphine and a corresponding Grignard reagent (this synthesis will be detailed later).

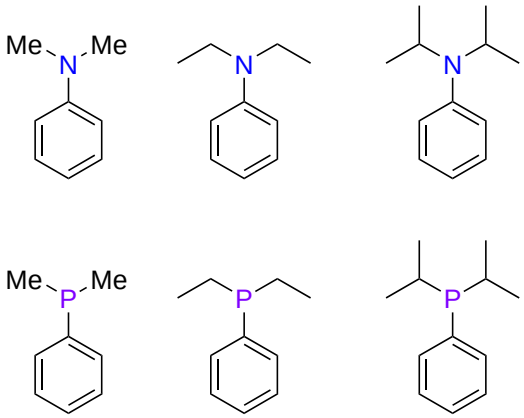

Figure 3.1: The target anilines and phenylphosphines in this study

3.2 Reaction of magnesiate base 1 with *N,N*-dimethylaniline

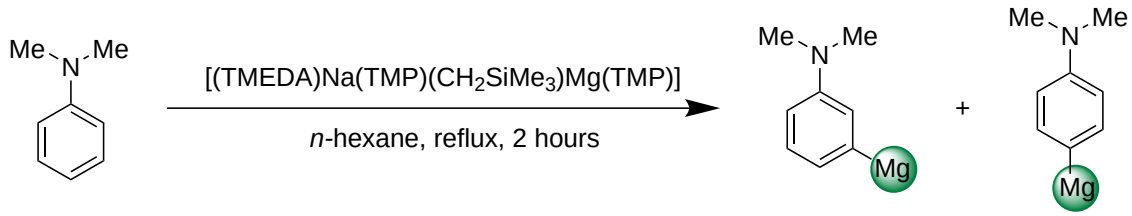

Scheme 3.3: Reaction of the magnesiate base **1** with *N,N*-dimethylaniline

Starting with the simplest benchmark methyl substituted aniline, reaction of **1** with *N,N*-dimethylaniline in *n*-hexane at room temperature resulted in a viscous oil identified (via ^{1}H NMR spectroscopy) as predominately starting material (<10 % metallated species). When the reaction mixture was heated to reflux (two hours), a mixture of *meta*- and *para*-magnesiated *N,N*-dimethylaniline products were observed (overall conversion 29%; *meta*-78 %, *para*-22 %, see Figure 3.2). Heating beyond two hours leads to decomposition of the base and an oil which was consistent with starting amine confirmed via NMR spectroscopy.

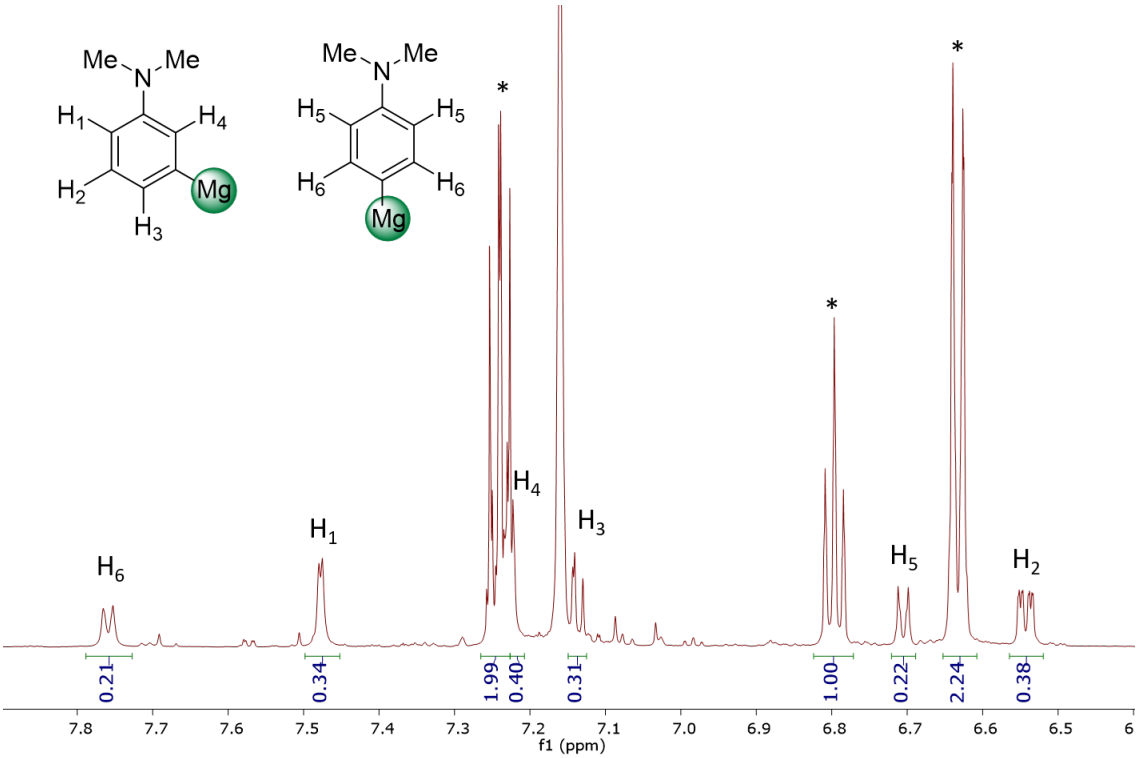

Figure 3.2: Aromatic section of the ^{1}H NMR spectrum (at 298 K) for the reaction of **1** with Me_2NPh for two hours at reflux. The black asterisks indicate the aromatic signals of unreacted *N,N*-dimethylaniline

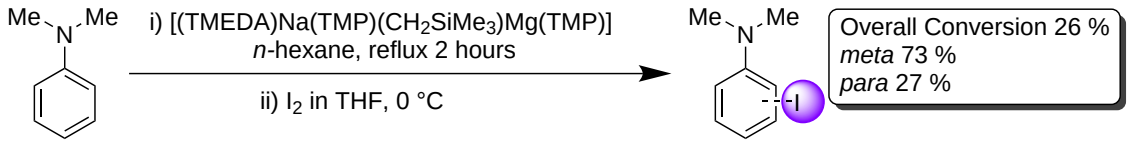

Scheme 3.4: Reaction of the magnesiate base **1** with *N,N*-dimethylaniline, followed by quenching with iodine

As no clean product could be obtained from this reaction, we turned to electrophilic quenching studies with I_2 to isolate the organic products (see Scheme 3.4). Taking our optimised metallation conditions (two hours reflux), we then proceeded to quench the reaction mixture with an excess of I_2 in THF (1 M). The ^{1}H NMR spectrum of the crude quenched product resulted in a 26 % overall conversion, with a *meta*:*para*- ratio of 73:27, in agreement with the reaction mixture pre-quench (see Figure 3.3).

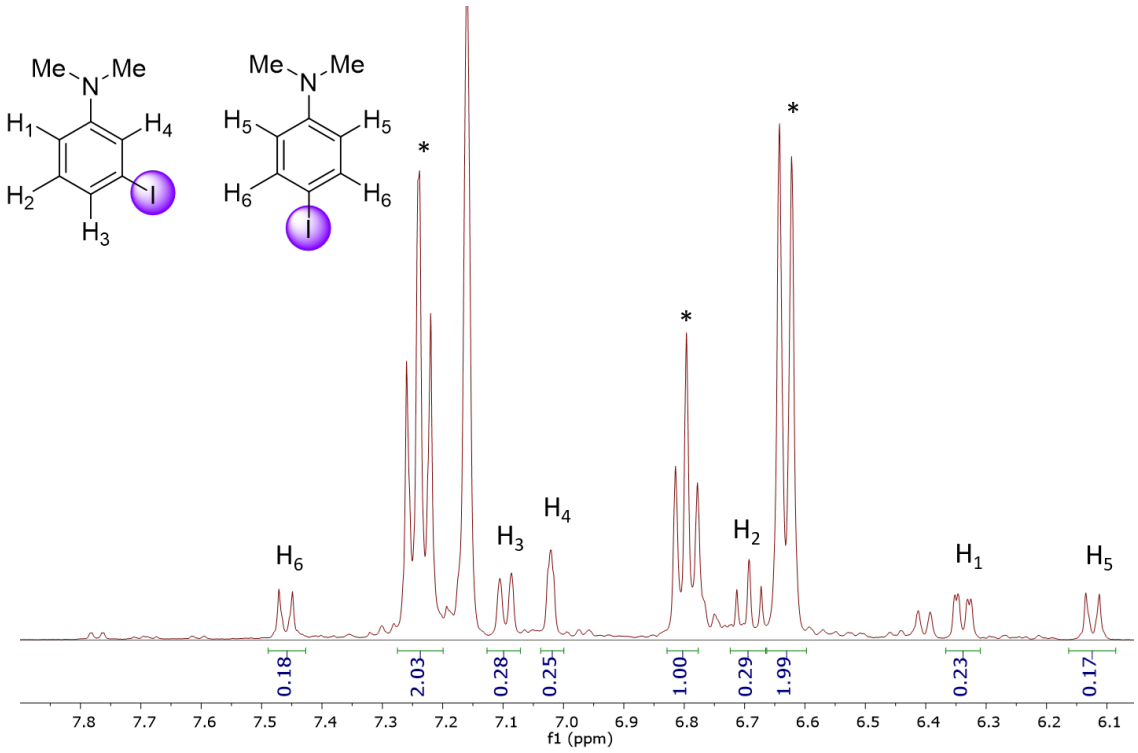

Figure 3.3: Aromatic section of the reaction of **1** with Me_2NPh for two hours at reflux, followed by quenching with iodine in C_6D_6. The black asterisks indicate the aromatic signals of unreacted *N,N*-dimethylaniline

3.3 Reaction of magnesiate base 1 with *N,N*-diethylaniline

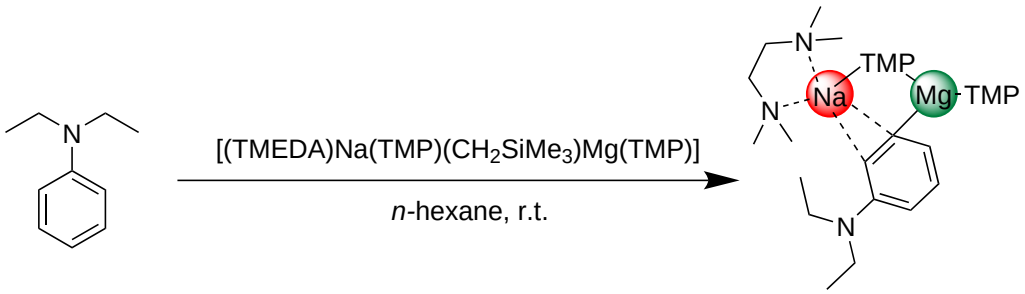

Scheme 3.5: Reaction of the magnesiate base **1** with *N,N*-diethylaniline, resulting in the selective *meta*-magnesiation

Moving to the bulkier *N,N*-diethylaniline, the addition of a molar equivalent of *N,N*-diethylaniline to a stirred hexane solution of **1** resulted in the deposition of a large quantity of white precipitate after stirring overnight (Scheme 3.5). This solid was isolated via filtration, washed with hexane and transferred to a glove box for storage. X-ray quality single crystals were obtained on one synthesis upon recrystallisation from *n*-hexane and slow cooling in an oil bath. This compound was identified as the *meta*- magnesiated [(TMEDA)Na(TMP)($m-C_6H_4NEt_2$)Mg(TMP)], isolated in a 65 % crystalline yield.

3.3.1 X-ray crystallographic analysis of 10

The molecular structure of **10** (Figure 3.4) retains a trigonal planar magnesium atom, bonding to a terminal TMP (Mg-N bond length 1.9989(17) Å), bridging TMP (Mg-N bond length 2.0794(16) Å) and a bridging *meta*-deprotonated *N,N*-diethylaniline based unit (Mg-C bond length 3.036(2) Å). As the terminal TMP unit has been retained, the product of this reaction can be seen as the result of alkyl basicity, with the elimination of a $SiMe_4$. Furthermore, the magnesium atom is coplanar to the aromatic ring, in comparison to the sodium which lies almost perpendicular to the ring, forming electrostatic interactions with both the *meta*- and *para*- positions (Na-C bond lengths of 3.036(2) and 2.648(2) Å respectively). The sodium is formally in a three coordinate environment, bonding to the bidentate Lewis donor TMEDA and a bridging TMP unit (Na(1) - N(3) bond

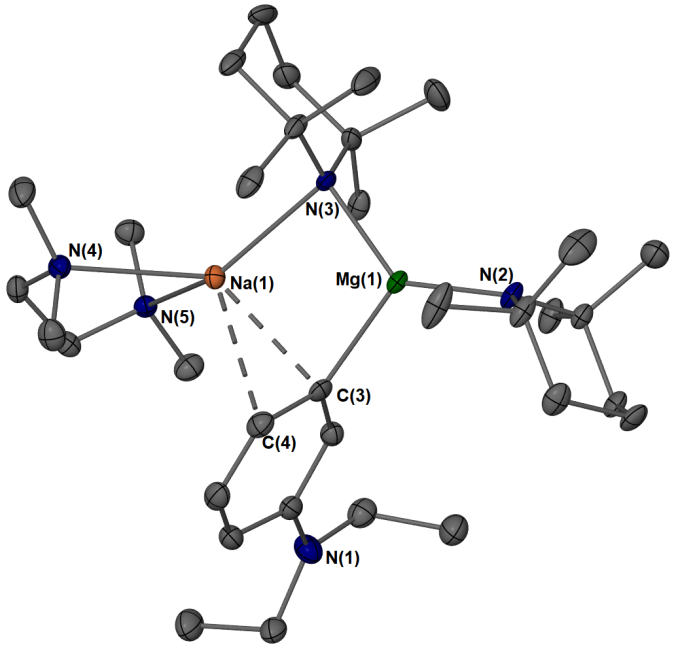

Figure 3.4: Molecular structure of [(TMEDA)Na(TMP)(*m*−$C_6H_4NEt_2$)Mg(TMP)] **10**. Hydrogen atoms omitted for clarity. Thermal ellipsoids shown at 40 % probability. Selected bond lengths (Å) and angles (°): Mg(1) - C(3), 2.182(2); Mg(1) - N(3), 2.0794(16); Mg(1) - N(2), 1.9989(17); Na(1) - C(3), 3.036(2); Na(1) - C(4), 2.648(2); Na(1) - N(3), 2.4779(18); Na(1) - N(4), 2.5401(18); Na(1) - N(5), 2.5291(18); N(2)- Mg(1)- C(3), 120.48(8); N(2)- Mg(1)- N(3), 134.32(7); N(3)- Mg(1) - C(3), 105.16(7); Na(1) - N(3) - Mg(1), 89.35(6).

length 2.4779(18) Å), while the electrostatic interactions with the phenyl ring complete its coordination environment.

3.3.2 Solution state analysis of 10

Crystalline material of compound **10** was dissolved in C_6D_6 and analysed by ^1H and $^{13}C\{^1H\}$ NMR spectroscopy. The disappearance of the aromatic signals at 7.24, 6.76 and 6.62 ppm corresponding to the parent aniline and the appearance of four new aromatic signals, at 7.45 (doublet), 7.12 (singlet), 7.11 (doublet) and 6.48 ppm (doublet of doublet of triplets) are characteristic of a *meta*-deprotonated species (see Figure 3.5). Signals at 3.17 (quartet, 4 H) and 1.04 ppm (triplet, 6 H) correspond to the ethyl groups present on the *N*-aniline. Signals evident at 1.98 - 1.87 (m, 4 H), 1.66 (s, 24 H) and 1.44 - 1.31 ppm (m, 8 H) correspond to the TMP unit and signals at 1.63 (s, 12 H) and 1.55 ppm (s, 6 H)

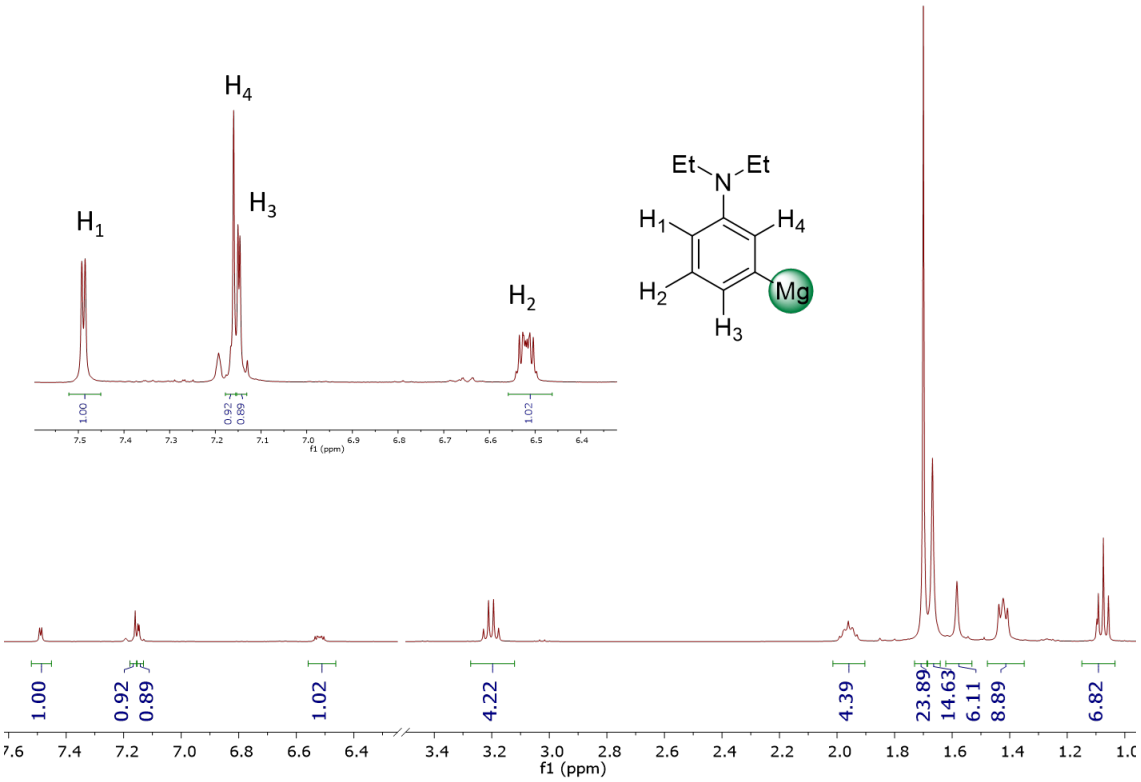

Figure 3.5: ^{1}H NMR spectra of **10**, [(TMEDA)Na(TMP)(*m*−$C_6H_4NEt_2$)Mg(TMP)] in C_6D_6 at 298 K

show the presence of coordinated TMEDA. Similarly, the appearance of a $^{13}C\{^{1}H\}$ NMR signal downfield at 173.41 ppm is characteristic of the newly formed Mg−C bond.

Iodolysis of the reaction mixture leads to the expected *N,N*-diethyl-3-iodoaniline in a reasonable unoptimised yield of 67 %. Interestingly, small quantities (<10 %) of *N,N*-diethyl-4-iodoaniline were also present, likely resulting from the electrophilic aromatic substitution of iodine with free *N,N*-diethylaniline.[104]

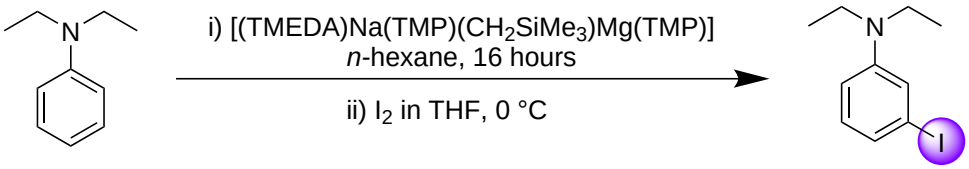

Scheme 3.6: Reaction of the magnesiate base **1** with *N,N*-diethylaniline followed by the *in situ* iodolysis to yield the expected *N,N*-diethyl-3-iodoaniline in a yield of 67 %

3.4 Reaction of NaTMP with *N,N*-diethylaniline

To investigate whether the reaction of magnesiate base **1** with *N,N*-diethylaniline was the result of synergistic character, the reaction of the individual homometallic components of **1**, namely NaTMP · TMEDA and $Mg(CH_2SiMe_3)_2$ were explored. The reaction of a molar equivalent of $Mg(CH_2SiMe_3)_2$ with *N,N*-diethylaniline resulted in quantitative return of starting material, even at reflux for 8 hours. Interestingly, the reaction of NaTMP · TMEDA with a molar equivalent of *N,N*-diethylaniline resulted in the isolation of the new sodium amide $[\{(TMEDA)Na(EtNC_6H_5)\}_2]$ **11** in a 46 % crystalline yield.

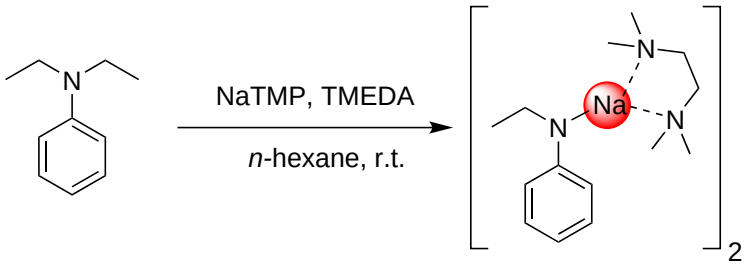

Scheme 3.7: Reaction of the monometallic NaTMP · TMEDA with *N,N*-diethylaniline

3.4.1 X-ray crystallographic analysis of complex 11

The centrosymmetric molecular structure of **11** shows that a β-hydrogen elimination process has occurred, eliminating one of the ethyl groups of *N,N*-diethylaniline (Figure 3.6). The molecular structure of **11** is a dimer with a planar Na_2N_2 core with the sodium atoms in a tetrahedral environment. The phenyl groups of the two *N*-ethylaniline units are orientated *trans* to each other. The sodium atoms make additional electrostatic interactions to both C(1) and C(2) of the phenyl ring (bond lengths of 2.8782(12) and 2.8805(13) Å respectively), as well as to the chelating bi-dentate ligand TMEDA. As NaTMP was generated *in situ*, this mono-metallic metallation is the product of an amido base. The active base in this reaction, $[(TMEDA)Na(TMP)]_2$ is known.[105]

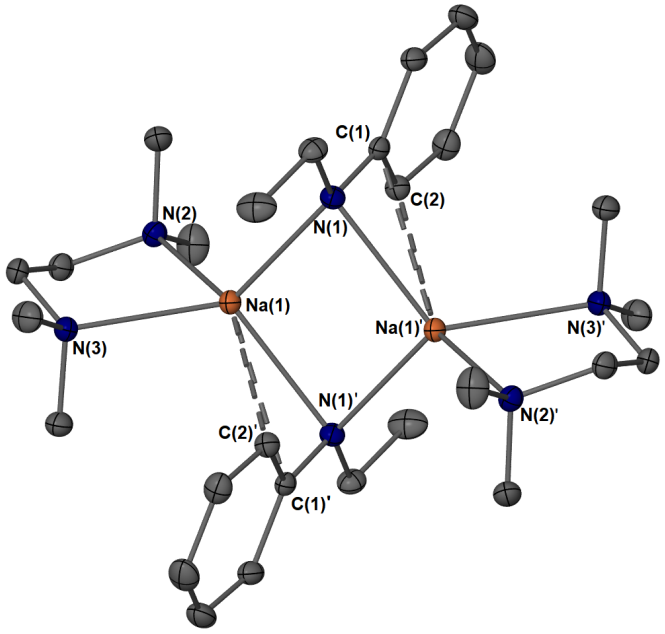

Figure 3.6: Molecular structure of [{(TMEDA)Na(EtNC$_6$H$_5$)}$_2$] **11**. Thermal ellipsoids shown at 40 % probability. Compound **11** is centrosymmetric, and thus the asymmetric unit contains half the molecule, symmetry operator ' = 1 - x, 1 -y, 1 -z. Hydrogen atoms omitted for clarity. Selected bond lengths (Å) and angles (°): Na(1)-N(4), 2.4116(10); Na(1)-C(1), 2.8782(12); Na(1)-C(2), 2.8805(13); Na(1)-N(2), 2.4744(11); Na(1)-N(3), 2.4825(10); Na(1)-N(4)-Na(1), 79.85(3); C(1)-N(4)-Na(1), 92.04(7)

3.4.2 Solution state analysis of complex 11

The ^{1}H NMR spectrum of complex **11** in C$_6$D$_6$ is consistent with the retention of the crystal structure in solution (Figure 3.7). A downfield shift of the remaining ethyl protons to 3.32 and 1.48 ppm (c.f. to 2.99 and 0.89 ppm in the parent compound *N,N*-diethylaniline) and integral analysis confirm the loss of one ethyl group. Resonance signals for the aromatic protons at 7.29 (broad signal), 6.61 (doublet) and 6.42 (triplet) ppm are observed, as well as signals for TMEDA at 1.77 and 1.66 ppm. The ^{13}C{^{1}H} NMR spectrum of complex **11** is consistent with the expected chemical shifts.

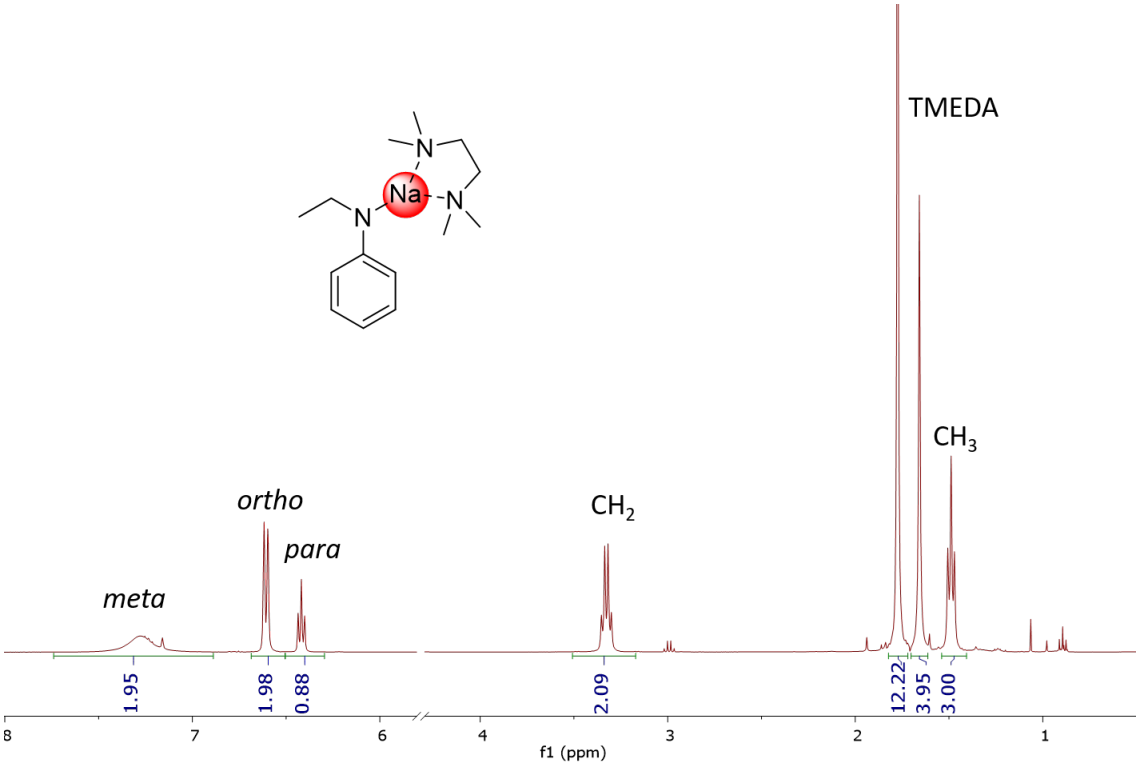

Figure 3.7: ^{1}H NMR spectrum of **11** in C_6D_6 at 298 K

3.5 Reaction of magnesiate base 1 with *N,N*-diisopropylaniline

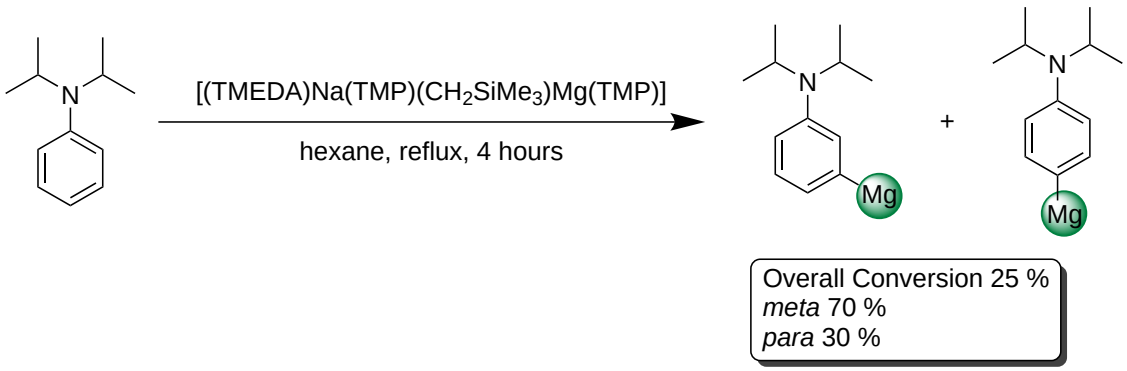

Scheme 3.8: Reaction of the magnesiate base **1** with *N,N*-diisopropylaniline, resulting in a mixture of the *meta*- and *para*- magnesiated *N,N*-diisopropylaniline as well as substantial starting material

Increasing the steric bulk on the directing group further, we next investigated the reaction of **1** with *N,N*-diisopropylaniline in *n*-hexane at room temperature which resulted in a viscous oil identified (via ^{1}H NMR spectroscopy) as predominately starting material (<10 % metallated species). When the reaction mixture was heated to reflux (four hours), a

mixture of *meta*- and *para*-magnesiated *N,N*-diisopropylaniline were observed (overall conversion 25 %; *meta*- 70 %, *para*- 30 %, see Figure 3.8). Heating beyond four hours lead to decomposition of the base and an oil which was consistent with starting amine confirmed via ^{1}H-NMR spectroscopy.

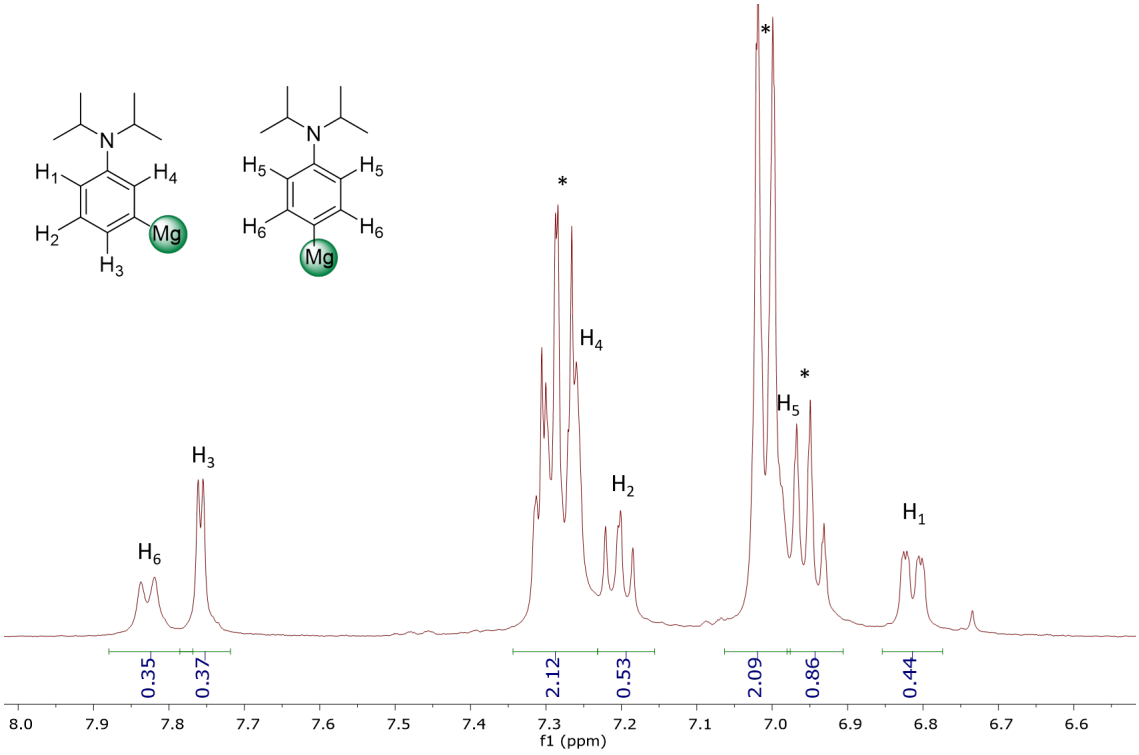

Figure 3.8: Aromatic section of the reaction of **1** with iPr_2NPh for 4 hours at reflux in C_6D_6, indicating *meta*- and *para*- magnesiation as well as substantial starting material, designated as black asterisks

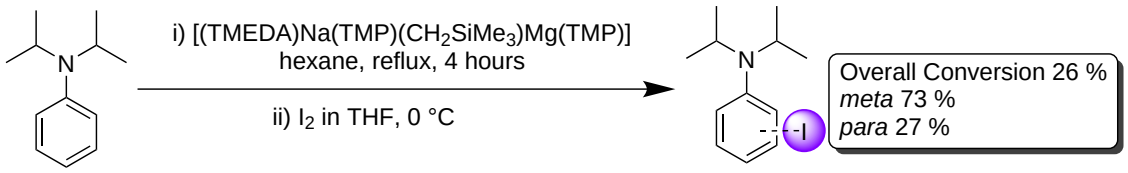

Scheme 3.9: Reaction of the magnesiate base **1** with *N,N*-diisopropylaniline, followed by quenching with iodine resulting in the formation of *N,N*-diisopropyl-3-iodoaniline and *N,N*-diisopropyl-4-iodoaniline

As no selective metallation product could be obtained from the reaction, we turned to electrophilic quenching studies with I_2 to isolate the organic products. Taking our optimised metallation conditions (four hours at reflux), we then proceeded to quench the reaction mixture with an excess of I_2 in THF at 0 ° C (see Scheme 3.9). This led to the

isolation of a mixture of *meta*- and *para*- iodinated species, as well as substantial starting material (see Figure 3.9). With an overall conversion of 25 %, the *meta*:*para*-iodo ratio was 7:3, identical to the ^{1}H NMR of the metallated species prior to the iodine quench (see Figure 3.9).

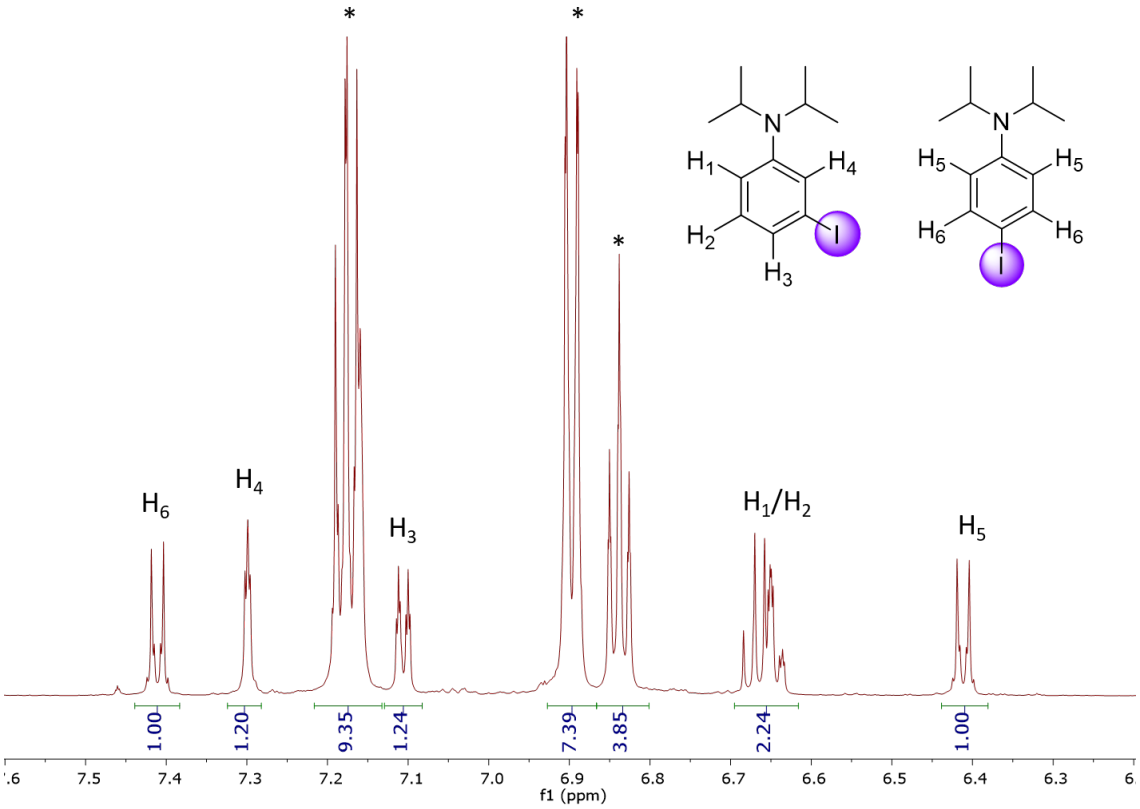

Figure 3.9: Aromatic section of the reaction of **1** with iPr_2NPh for 4 hours at reflux, followed by quenching with iodine. The asterisks indicate the aromatic signals of unreacted *N,N*-diisopropylaniline

3.6 Metallation of *P,P*-dialkylphenylphosphines

Phosphorus based ligands find extensive usage in catalyst design,[106] material chemistry and the stabilisation of main group and transition-metal complexes.[107] In comparison to the plethora of studies on the mono- and bi-metallic metallation chemistry of tertiary amines (such as anilines), studies on tertiary phosphines are scarce. While in medicinal chemistry, alkali metal amide complexes feature prominently,[108] phenylphosphines [P(III)] or phenylphosphine oxides [P(V)] have been generally overlooked. Recently, Brigatinib (AP26113), a promising drug for the treatment of lung cancer was approved by the FDA which contained an *ortho*-substituted dimethylphenylphosphine oxide unit, a unique structural feature.[103,109]

In comparison to their analogous anilines, *P,P*-dialkylphenylphosphines would have their lone pair localised on the phosphorus, which would result in acidic lateral protons. Confirming this, the selective lateral-lithiation of *P,P*-dimethylphenylphosphine can be achieved smoothly with nBuLi · TMEDA (see Scheme 3.10). When attempting to perform the lithiation with *t*BuLi, much longer reaction times are required and were poor yielding (43 % yield at 48 hours, as confirmed by carbonation). The authors note that the reactivity with *t*BuLi was complicated by the presence of unidentified dianionic species, which could be avoided using nBuLi · TMEDA.[110]

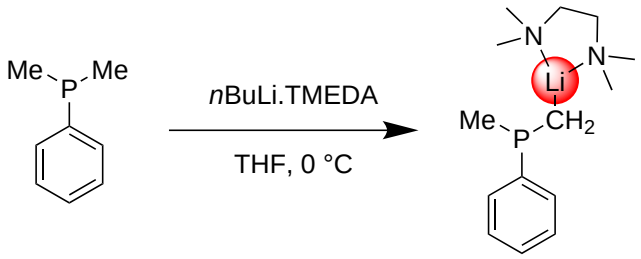

Scheme 3.10: Reaction of BuLi · TMEDA with *P,P*-dimethylphenylphosphine to yield lateral lithiation

3.7 Synthesis of *P,P*-dialkylphenylphosphines

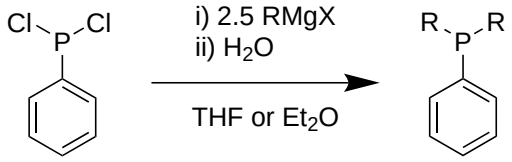

Scheme 3.11: Synthesis of compounds *P,P*-dialkylphenylphosphines from their corresponding Grignard reagent and *P,P*-dichlorophenylphosphine

The *P,P*-dialkylphenylphosphines (alkyl = methyl, ethyl or isopropyl) were synthesised by the addition of 2.5 equivalents of the corresponding Grignard reagent (RMgX, R = Me X = Br, R = Et X = Br,R = iPr X = Cl) to a solution of *P,P*-dichlorophenylphopshine in either diethyl ether (R = Me, Et) or THF (R = iPr) at 0 ° C. After stirring for two hours, the solution was quenched with deoxygenated water, the organic layer separated and solvent removed *in vacuo*. The resulting oils were vacuum distilled to yield the corresponding *P,P*-dialkylphenylphosphines as air-sensitive, viscous oils in reasonable to high yields (65 % - 81 %).

3.8 Reaction of magnesiate base 1 with *P,P*-dimethylphenylphosphine

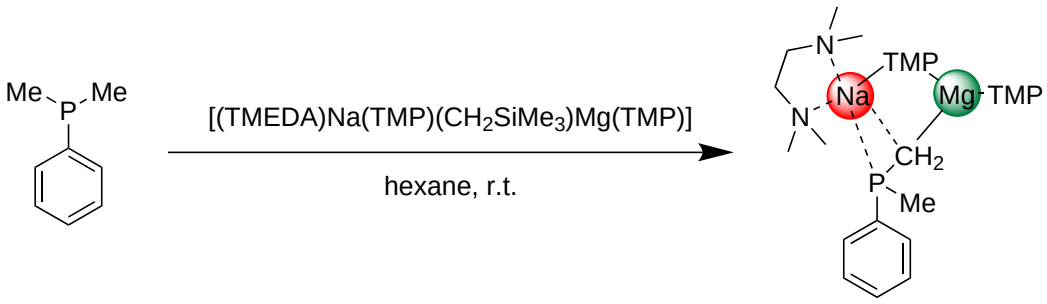

Scheme 3.12: Synthesis of complex [(TMEDA)Na(TMP)($C_6H_5PCH_3CH_2$)Mg(TMP)] **12**

Reacting a *n*-hexane solution of the synergic base **1** with a molar equivalent of *P,P*-dimethylphenylphosphine resulted in the deposition of a white precipitate overnight. Upon hot filtration and storage of the solution at 5 °C, a large crop of colourless crystals were deposited. These crystals were isolated in a 58 % crystalline yield, and

characterised by single crystal X-ray diffraction to be the lateral magnesiated complex [(TMEDA)Na(TMP)($C_6H_5PCH_3CH_2$)Mg(TMP)] **12** (see Scheme 3.12).

3.8.1 X-ray crystallographic analysis of complex 12

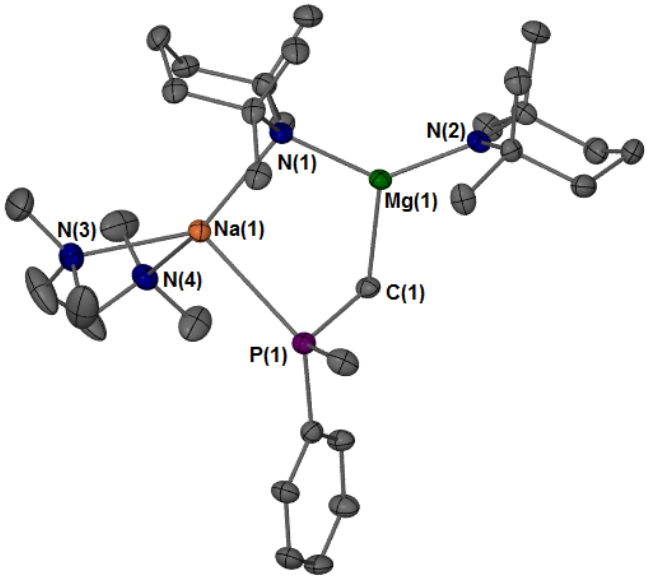

Figure 3.10: Molecular structure of [(TMEDA)Na(TMP)($C_6H_5PCH_3CH_2$)Mg(TMP)] **12**. Hydrogen atoms omitted for clarity. Thermal ellipsoids shown at 40 % probability. Selected bond lengths (Å) and angles (°): Mg(1)-N(1), 2.069(5); Mg(1)-N(2), 2.001(5); Mg(1)-C(1), 2.182(6); Na(1)-N(1), 2.463(5); Na(1)-N(3), 2.528(6); Na(1)-N(4), 2.495(5); Na(1)-P(1), 2.919(2); P(1)-C(1), 1.777(6); P(1)-C(2), 1.823(8); N(1)-Na(1)-P(1), 95.24(12); Na(1)-N(1)-Mg(1), 103.5(2); N(1)-Mg(1)-C(1), 108.8(2); Mg(1)-C(1)-P(1), 118.4(3); C(1)-P(1)-Na(1), 88.40(19).

The bimetallic monomer is composed of one sodium atom connected to magnesium via an amido TMP bridge (Mg-N bond length 2.069(5) Å) with the magnesium coordination completed by a further terminal TMP (Mg-N bond length 2.001(5) Å) and a CH_2 unit of a metallated phosphine (Mg-C bond length 2.182(6) Å). The sodium atom occupies a distorted tetrahedral environment (bond angles range 73.88°– 134.47°), comprising a TMP bridge (Na-N bond length 2.463(5) Å), a bridging anionic [[$C_6H_5PCH_3CH_2$]$^-$ (Na-P bond length 2.919(2) Å) and a bidentate chelating TMEDA ligand (Na-N bond lengths 2.528(6) and 2.495(5) Å). The sodium atom forms a strong bond with the phosphorus lone pair [Na(1) - P(1) 2.919(2) Å] to close a central 5-atom 5-element (NaNMgCP) ring. The coordination environment of the magnesium atom is essentially trigonal planar

($\sum$ bond angles = 359.96°) in common with this structural motif, with a terminal and bridging TMP molecule and a methyl magnesiated *P,P*-dimethylphenylphosphine anionic unit, with a typical covalent Mg - C bond length of 2.182(6) Å. Overall, **1** has executed alkyl basicity, with the loss of a $SiMe_4$ unit. Previous studies on the lateral metallation of *P,P*-dimethylphenylphosphine with *n*BuLi in the presence of the activating bidentate ligand TMEDA have been reported[110,111] revealing the dimer $[(TMEDA)Li(CH_2PCH_3Ph)]_2$.

3.8.2 Solution state analysis of 12

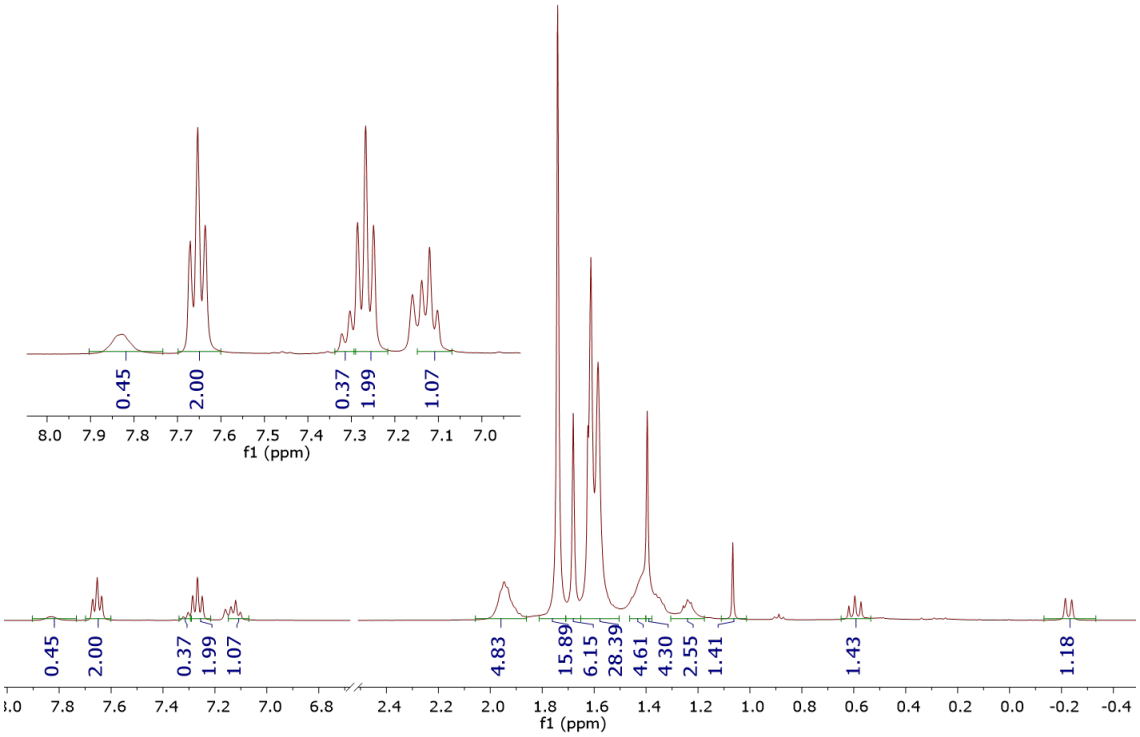

Figure 3.11: ^1H NMR spectra of **12** in C_6D_6 at 298 K

^1H and $^{31}P\{^1H\}$ NMR analysis of **12** was conducted in C_6D_6. Interestingly, this returned some unexpected results. While evident in the ^1H NMR spectrum (Figure 3.11), the appearance of a second set of signals is more evident in the ^{31}P NMR spectrum (Figure 3.12). In the proton NMR spectrums, the major species can be identified from a set of aromatic triplets at 7.65, 7.27 and 7.12 ppm (corresponding to the *ortho*-, *meta*- and *para*-protons respectively) and aliphatic signals at 1.40 ppm for the CH_3 and two non-equivalent signals for the $MgCH_2$ protons at 0.60 and -0.23 ppm (assigned by $^1H-^{13}C$ HSQC, see

Figure 3.11). In the $^{31}P\{^{1}H\}$ NMR spectrum, two signals are present, one dominate species at -29.67 ppm and a smaller signal present at -28.58 ppm (see Figure 3.12). The ^{1}H NMR spectrum also contains signals corresponding to resonances for TMEDA (1.68 ppm and 1.74 ppm) and TMP (1.95, 1.41 - 1.45 and 1.36 - 1.30 ppm).

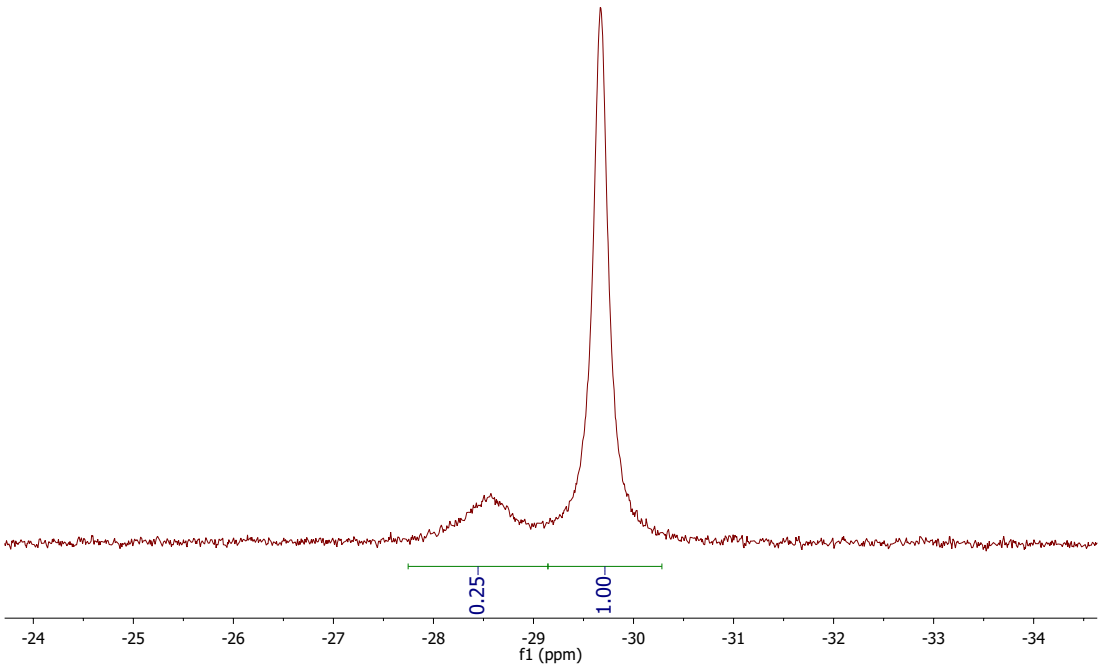

Figure 3.12: $^{31}P\{^{1}H\}$ NMR spectra of **12** in C_6D_6

In an attempt to identify the second species present, C:H:N analysis was carried out, which confirmed the expected ratio of C:H:N present for a mono-magnesiated *P,P*-dimethylphenylphosphine complex **12**. This indicated that either it is a solution state isomerisation, or multiple co-crystalline regioisomers. To further look into the observed reactivity, we next sought to complete electrophilic quenching studies, with both I_2 and D_2O. For ease of handling and purification, the quenched products were subject to aerial oxidation during workup to give the corresponding phosphorus(V) oxide organic compounds.

Iodine (and aerial oxidation) quenching studies revealed two dominant species, namely bis(iodomethylphenyl)phosphine oxide and iodomethylmethylphenylphosphine oxide, and

traces of (4-iodophenyl)dimethylphenylphosphine oxide. Unfortunately, this was not as conclusive at uncovering the solution state behaviour as one may have hoped. The presence of a di-iodinated species is curious, however as the base retains reactive arms during the initial metallation, it is possible that it is able to re-metallate another methyl-group following the initial quench.

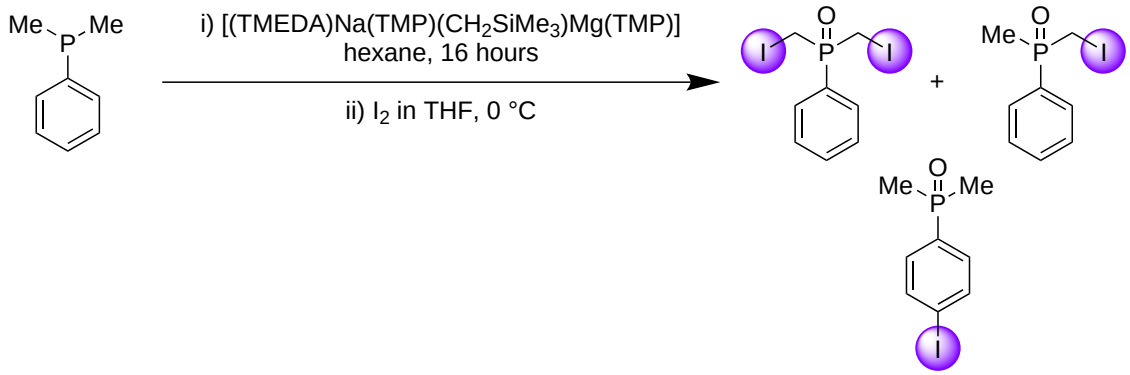

Scheme 3.13: Iodine quenching studies of **12**

3.9 Reaction of BuNa · TMEDA with *P,P*-dimethylphenylphosphine

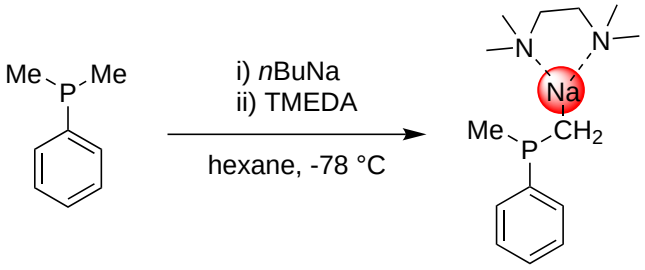

Scheme 3.14: Reaction of *n*BuNa · TMEDA with *P,P*-dimethylphenylphosphine

While the reaction of BuLi · TMEDA with *P,P*-dimethylphenylphosphine is known in the literature, the equivalent reaction with sodium organometallics have not been reported.[110] To investigate the monometallic reactivity of the components of the magnesiate **1** with *P,P*-dimethylphenylphosphine, a molar equivalent of the phosphine was added to a stirred suspension of BuNa at -78 ° C, followed by addition of a molar equivalent of TMEDA. After stirring overnight (18 hours), the resulting suspension was filtered, washed with *n*-hexane and dried *in vacuo*. The resulting solid was transferred to a glovebox for storage,

and found to be the lateral-sodiated complex [$PhPCH_3CH_2Na \cdot TMEDA$] **13**, supported by ^{1}H and $^{31}P\{^{1}H\}$ NMR spectroscopy.

3.9.1 Solution state analysis of complex 13

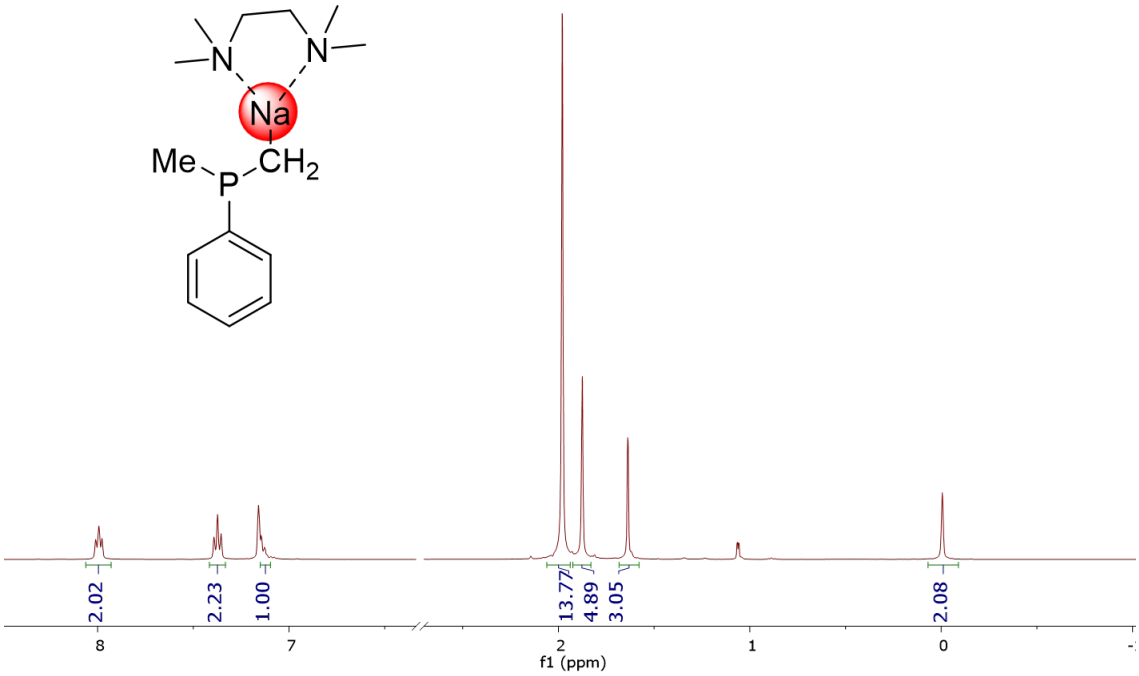

Figure 3.13: ^{1}H NMR spectrum of complex **13** in C_6D_6 at 298 K

The ^{1}H NMR spectrum of complex **13** in C_6D_6 revealed the *lateral*-sodiated complex is retained in solution (see Figure 3.14). The appearance of a new singlet at -0.01 ppm integrating as 2 H, with coupling (as evidenced by ^{1}H-^{1}H cosy NMR spectroscopy) to a singlet at 1.64 ppm is evident of a *lateral*-sodiated species. Aromatic signals at 7.99 (triplet), 7.37 (triplet) and 7.15 (multiplet) are evident, as well as TMEDA signals evident at 1.98 and 1.87 ppm, showing that complex **13** retains its composition in solution.

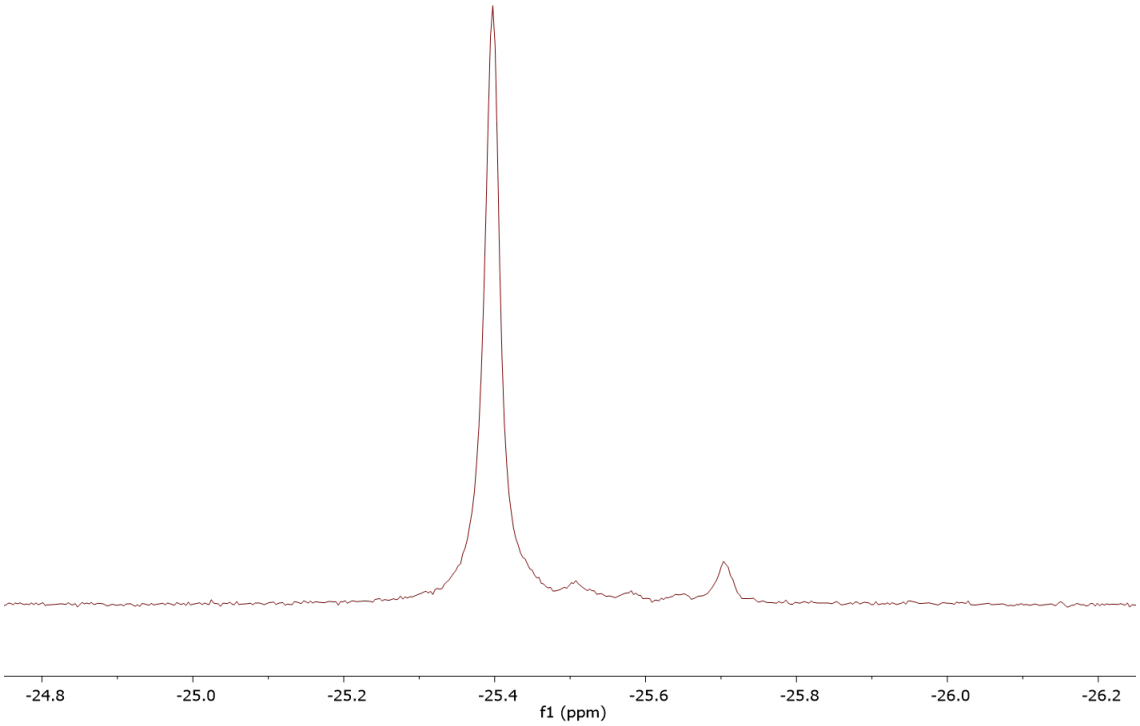

Figure 3.14: $^{31}P\{^{1}H\}$ NMR spectrum of complex **13** in C_6D_6

The $^{31}P\{^{1}H\}$ NMR spectrum of complex **13** in C_6D_6 revealed the presence of one main species at -25.40 ppm, and a minor species present at -25.70 ppm (c.f. $^{31}P\{^{1}H\}$ signal of -46.52 for free *P,P*-dimethylphenylphosphine). The identity of this apparent minor side species is unknown.

3.10 Reaction of magnesiate base 1 with *P,P*-diethylphenylphosphine

Moving to the ethyl substituted phosphine, the magnesiate **1** showed only negligible reactivity towards *P,P*-diethylphenylphosphine, even under reflux conditions. Solution studies of the oils produced from room temperature reactions indicated that no reaction had occurred, whereas heating to reflux led to minimal (<5 % metallation). As only trace quantities of reactive species were observed, further work to identify the species present was not conducted.

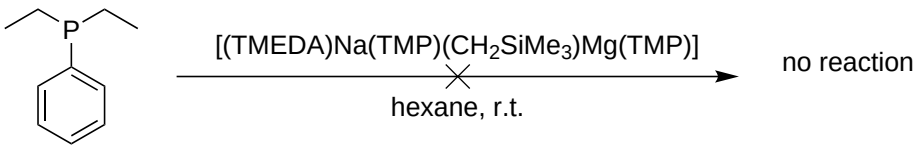

Scheme 3.15: Attempted reaction of **1** with *P,P*-diethylphenylphosphine

3.11 Reaction of NaTMP with *P,P*-diethylphenylphosphine

Looking to establish the monometallic reactivity of the components of complex **1** towards *P,P*-diethylphenylphosphine, we next investigated the potential for magnesiations using $Mg(CH_2SiMe_3)_2$. No reaction was observed between Et_2PPh and $Mg(CH_2SiMe_3)_2$, even at reflux for 16 hours in hexane.

Next, the reactivity towards NaTMP · TMEDA was investigated. Similarly to complex **11**, rather than ring metallation, β- elimination of an ethyl fragment was observed to generate the monometallic complex $[\{(TMEDA)Na(Et_2NC_6H_5)\}_2]$ **14** in a 70 % crystalline yield. Interestingly however, NaTMP · TMEDA reacts with half an equivalent of Et_2PPh to form a mixed sodium amido/sodium phosphido ladder complex, retaining basic NaTMP groups. The rational synthesis of this complex, using two molar equivalents of NaTMP · TMEDA with one equivalent of *P,P*-diethylphenylphosphine proceeds in high yield (70 %).

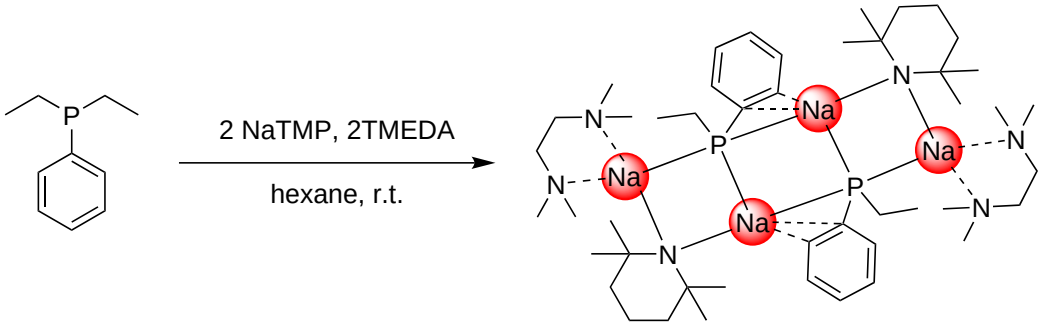

Scheme 3.16: Reaction of the monometallic NaTMP · TMEDA with *P,P*-diethylphenylphosphine

3.11.1 X-ray crystallographic analysis of complex 14

The mixed sodium-amide/sodium-phosphide ladder molecule is composed of a central (Na_2P_2) strictly planar core (Σ Na-P bond angles = 360°) and two outer planar (NaN-

NaP) rings lying out of the central plane by 26.87(4)°. Displaced from the central core ±1.230(1) Å, the outer Na atoms [Na(2) and Na(2)'] are capped by a chelating TMEDA molecule, while the inner two engage in two Na· · ·C electrostatic interactions, one short [Na(1)-C(1) 2.7474(19) Å] to the *ipso*-carbon and one long [Na(1) - C(2) 2.983(2) Å] to the *ortho*-carbon of the phenyl ring.[112] Comparable to the previously discussed complex **11**, the *P,P*-diethylphenylphosphine substrate has lost one of its ethyl limbs, most likely occurring from a β-elimination reaction and concurrent formation of ethene. Interestingly, unlike in complex **11**, where all the basic TMP arms have been consumed, two NaTMP units remain unreacted in **14**. Thus **14** can be regarded as an example of a hybrid co-complex between a sodium amide and a sodium phosphide, with the closest structurally characterised example being the monomeric amino-functionalised sodium phosphanide complex $[[(Me_3Si)_2CH(C_6H_4{-}2{-}NMe_2)P]Na(TMEDA)]$[113] and the pyridyl functionalised phosphanide $[(Me_3Si)_2CH(2\text{-}C_5H_4N)P]Na]_2.(Et_2O)]_2$[113] which adopts a

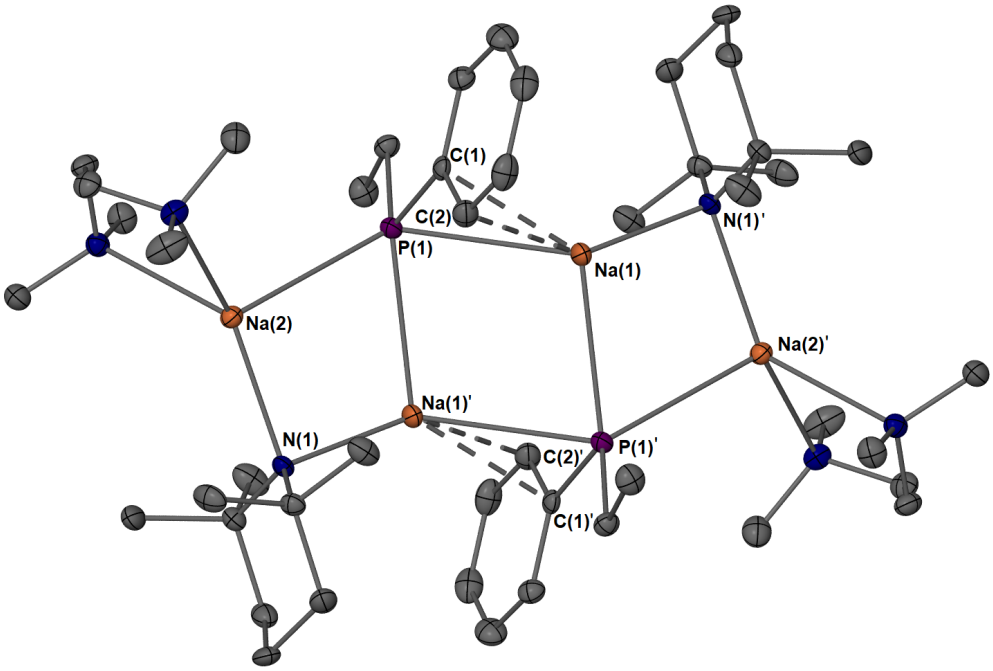

Figure 3.15: Molecular structure of $[(TMEDA)Na_2(TMP)(C_6H_5PEt)]_2$ **14**. Hydrogen atoms omitted for clarity. Thermal ellipsoids shown at 40 % probability. Symmetry operator ' = 1 - x, 1 - y, 1 - z, Selected bond lengths (Å) and angles (°): Na(1) - P(1), 2.9256(8); Na(1) - N(1)', 2.318 (4); Na(2) - P(1), 2.9891(9); Na(2) - N(1), 2.408(4); Na(1)' - P(1), 2.8848(8); Na(1) - C(1), 2.7474(19); Na(1) - C(2), 2.983(2); Na(2)-P(1)-Na(1), 68.41(2); P(1)-Na(1)-N(1)', 75.96(4); Na(1) - N(1)' - Na(2)', 88.64(5); P(1) - Na(1)' - N(1), 104.04(4); P(1) - Na(1)' - P(1)', 104.29(2); P(1)' - Na(2)' - N(1)', 98.80(4).

similar dimer of dimers motif to **14**. The composition of complex **14** fits the laddering principle established in lithium amide chemistry[114] with **14** representing a product of 'secondary laddering' assembly.

3.11.2 Solution state analysis of 14

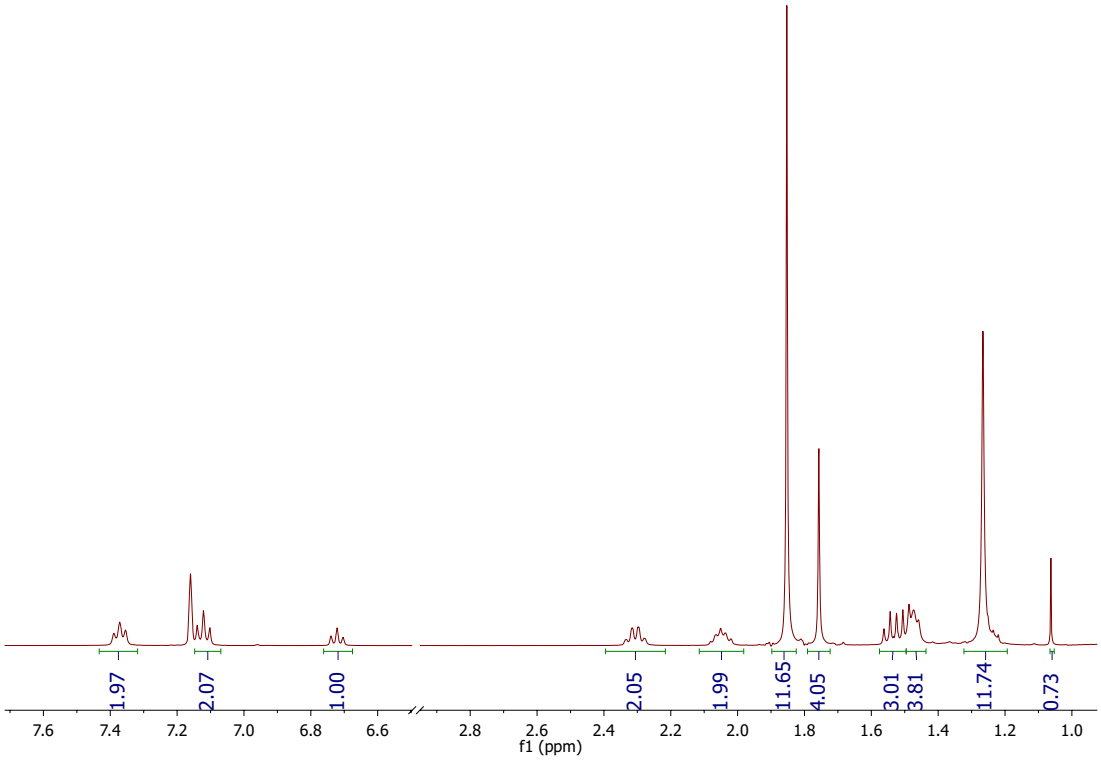

Figure 3.16: ^{1}H NMR analysis of **14** in C_6D_6 at 298 K

A crystalline sample of **14** was dissolved in C_6D_6 and analysed by ^{1}H, ^{31}P$\{^{1}$H$\}$ and ^{13}C$\{^{1}$H$\}$ NMR spectroscopy. A downfield shift of the remaining ethyl protons to 2.31 and 1.52 ppm (compared to 1.51 and 0.94 ppm in the parent compound *P,P*-diethylphenylphosphine) and integral analysis confirm the loss of an ethyl group. Resonance signals for the aromatic protons at 7.37 (triplet), 7.12 (triplet) and 6.72 (triplet) ppm are observed, as well as signals for TMEDA (1.85 and 1.76 ppm) and TMP (2.05, 1.49-1.43 and 1.27 ppm). The ^{31}P$\{^{1}$H$\}$ spectrum of **14** shows a substantial upfield shift from a sharp singlet at -16.59 ppm to a broad, less resolved signal at -55.85 ppm, which lies in the typical range for alkali-metal bis(*o*-anisyl)phosphides.[107,115]

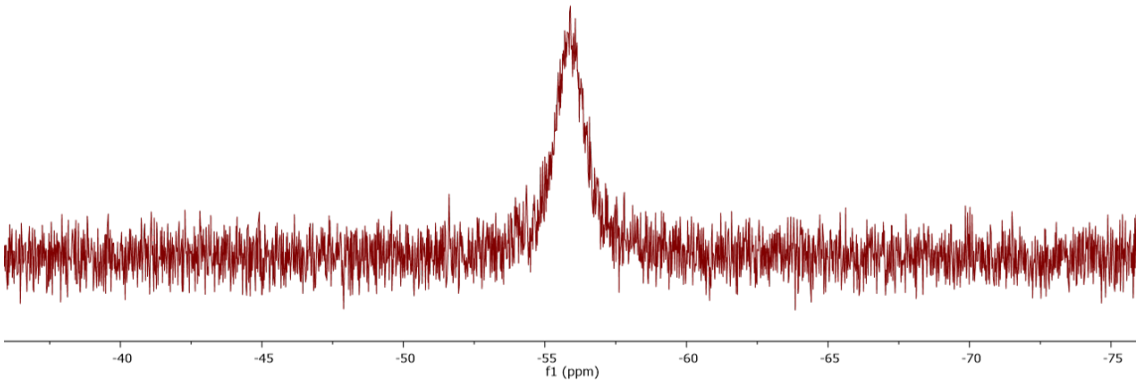

Figure 3.17: $^{31}P\{^{1}H\}$ NMR analysis of **14** in C_6D_6 at 298 K

3.12 Reaction of magnesiate base 1 with *P,P*-diisopropylphenylphosphine

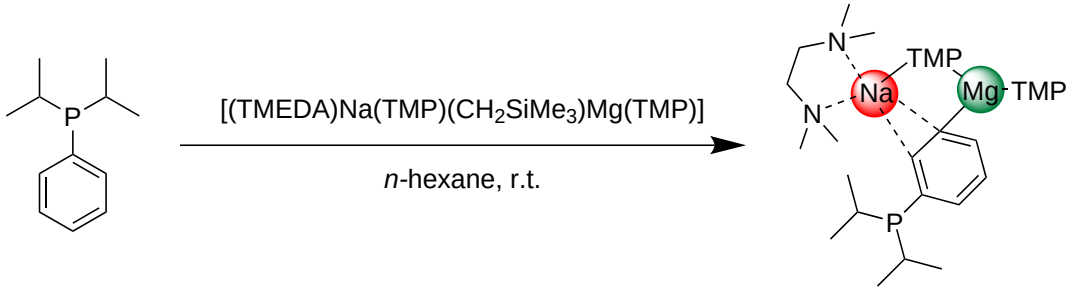

Scheme 3.17: Reaction of **1** with *P,P*-diisopropylphenylphosphine

Looking to increase the steric bulk further on the phenylphosphine substrate, *P,P*-diisopropylphenylphosphine was next investigated. Upon addition of a molar equivalent of *P,P*-diisopropylphenylphosphine to a stirred solution of the magnesiate base **1**, resulted in the immediate formation of a bright yellow solution (Scheme 3.17). Following stirring overnight, the solution was filtered and storage of the solution at -30 °C deposited a large crop of colourless crystals. These were suitable for X-ray analysis, and were found to be compound [(TMEDA)Na(TMP)(*m*−$C_6H_4PiPr_2$)Mg(TMP)] **15**, isolated in a 31 % crystalline yield.

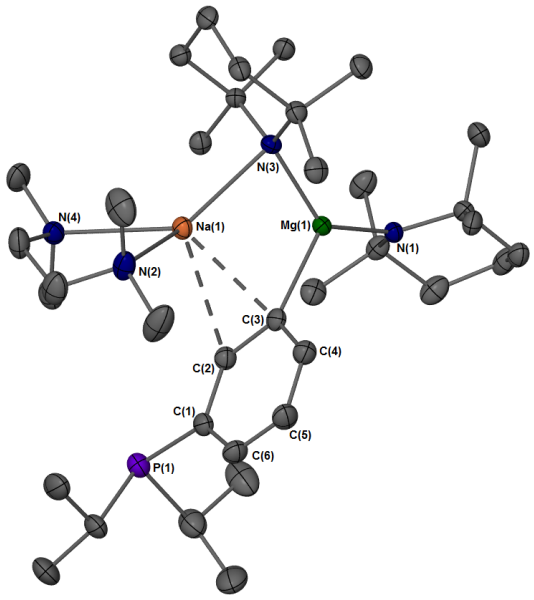

Figure 3.18: Molecular structure of [(TMEDA)Na(TMP)(*m*−$C_6H_4PiPr_2$)Mg(TMP)] **15**. Thermal ellipsoids shown at 40 % probability. Hydrogen atoms omitted for clarity. Selected bond lengths (Å) and angles (°): Mg(1)-C(3), 2.181(4); Mg(1)-N(1), 1.994(3); Mg(1)-N(3), 2.071(3); Na(1)-N(3), 2.485(3); Na(1)-N(2), 2.457(3); Na(1)-N(4), 2.569(3); Na(1)-C(2), 3.038(4); Na(1)-C(3), 2.684(4); N(1)-Mg(1)-N(3), 133.51(13); N(1)-Mg(1)-C(3), 119.21(14); C(3)-Mg(1)-N(3), 107.11(13); Na(1)-N(3)-Mg(1), 87.25(11).

3.12.1 X-ray crystallographic analysis of complex 15

The molecular structure of complex **15** (Figure 3.18) retains a trigonal planar magnesium atom, bonding to a terminal TMP [Mg(1) - N(1), 1.994(3) Å], a bridging TMP [Mg(1) - N(3), 2.0171(3) Å] and a bridging *P,P*-diisopropylphenylphosphine based unit [Mg(1) - C(3), 2.184(4) Å]. As the terminal TMP has been retained, the deprotonation can be seen as a product of alkyl basicity, eliminating $SiMe_4$. The magnesium atom is found to be bonding to the *meta*- position of the *P,P*-diisopropylphenylphosphine, as seen from the Mg(1) - C(3) bond length of 2.181(4) Å. Furthermore, the magnesium atom is coplanar to the aromatic ring, whereas the sodium atom lies almost perpendicular to the ring, forming electrostatic interactions with both the *ortho*- and *meta*- position [Na(1) - C(2), 3.038(4) and Na(1) - C(3), 2.686(4) Å respectively]. The sodium atom is formally in a three coordinate environment, while making close interactions with another two carbon atoms of the phenyl ring. The sodium atom is bound to a bridging TMP, a terminal TMEDA

chelating ligand as well as interacting with the metallated *P,P*-diisopropylphenylphosphine based unit.

3.13 Computational pKas of *N,N*-dialkylanilines and *P,P*-dialkylphenylphosphines

In an attempt to rationalise the different metallation regioselectivities observed by the homo- and hetero-bimetallic bases, DFT calculations[116] of the C−H acidities in THF (see Figure 3.19) of the different dialkyl-substituted phenylphosphine and aniline substrates were conducted in colloboration with Dr Ekaterina Izgorodina. All geometry optimisations were performed with the M06-2Z functional,[117] cc-pVTZ Dunnings basis set[118] and a universal solvation model based on density(SMD)[119] with THF as a solvent. Frequency calculations were carried out to ensure the location of the energy minima[117] which calculated the six substrates to have typical weak CH acidities covering a broad 35.5 - 53.6 pKa span in this polar solvent.

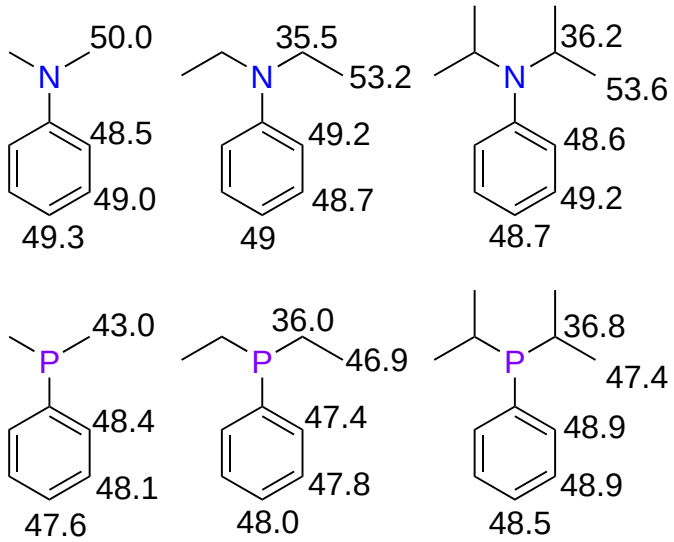

Figure 3.19: Calculated pKas of the various proton environments on *N,N*- dialkyl substituted anilines and *P,P*-dialkyl substituted phenylphosphines

Overall the acidity of the phenyl ring H atoms across all six substrates shows little to no variation comparing the *ortho*-, *meta*- and *para*-protons of the analogous P versus N substrates. These minor differences in pKa values rationalise the non-selective metallation seen for the reaction of **1** with dimethyl- and diisopropyl-aniline where a mixture of

regioisomers are observed (albeit predominately the *meta*-species). Interestingly, the experimentally observed regioselectivities of the isolated *meta*-isomers (**10** and **15**) of the *N,N*-diethylaniline and *P,P*-diisopropylphenylphosphine substrates conflict with the most acidic H atoms belonging to the methylene (pKa 35.5, **10**) and iPrC-H (pKa 36.8, **15**) groups (Figure 3.19). This would suggest metallation of these substrates is controlled by other contributing factors such as sterical orientation and electrostatic interactions.

The largest differences in calculated relative C-H acidity are seen upon changing the alkyl substituent on the P and N centres. In the dimethyl case, the $P-CH_3$ hydrogen atoms are significantly more acidic (pKa 43.0) than the analogous $N-CH_3$ atoms (pKa 50.0), consistent with the observed lateral metallation seen with phosphine complex **12**. In contrast, ring metallation is favoured for the nitrogen system, where pKa change is not so significant but still goes the other way and favours ring metallation (pKa ring average 48.9; methyl 50.0).

The experimental findings from the homometallic reaction of NaTMP with the *P,P*-diethylphenylphosphine and *N,N*-diethylaniline substrates fit the predicted acidity values well. Here the β-elimination of one of the ethyl groups via ethene evolution is supported by the most acidic methylene protons in both the N (pKa 35.5) and P (pKa 36.0) systems.

To further investigate the reactivity observed using computational methods, calculations were performed to determine the relative stability of the possible isomers in the systems where mixtures were observed. Geometry optimisations and subsequent frequency calculations were performed on the systems at the B3LYP/6+31(d) level of theory. The results found were in good agreement with the experimental results.

In the case of *N,N*-dimethylaniline (see Figure 3.20), the most stable regioisomer found was the *meta*-magnesiated complex (similar optimised geometry to the crystal structure of **10**). While overall metallation was low (26 % overall conversion), the *meta*-regioisomer was indeed the most favoured experimentally with a yield of 73 %. The remaining 27 % was *para*-magnesiated, which was only 2.7 kJ/mol higher in energy than the *meta*-system.

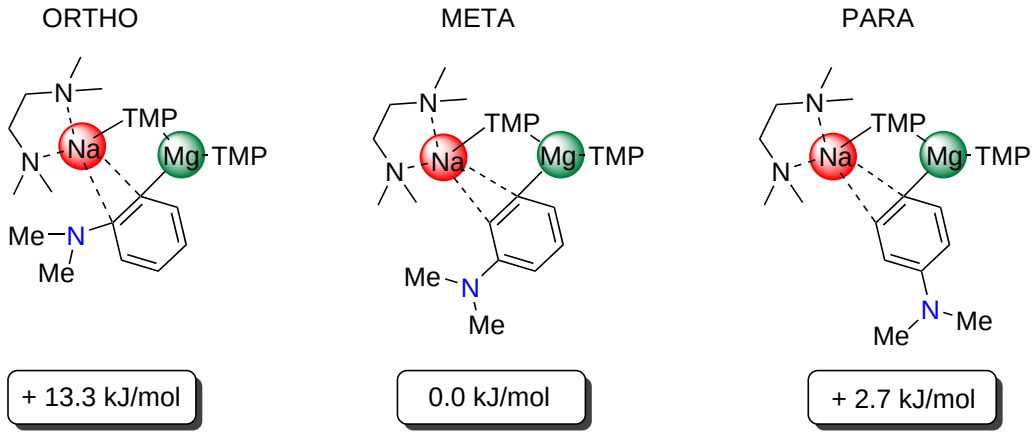

Figure 3.20: Computational studies of the relative energies of the regioisomers for the magnesiation of *N,N*-dimethylaniline with the sodium magnesiate **1**. The most stable regioisomer has been set as 0.0 kJ/mol. Modelled at the B3LYP/6+31(d) level of theory.

In comparison, the *ortho*-magnesiated species (not observed experimentally), was found to be +13.3 kJ/mol more unfavourable, significantly higher than the *meta*-species.

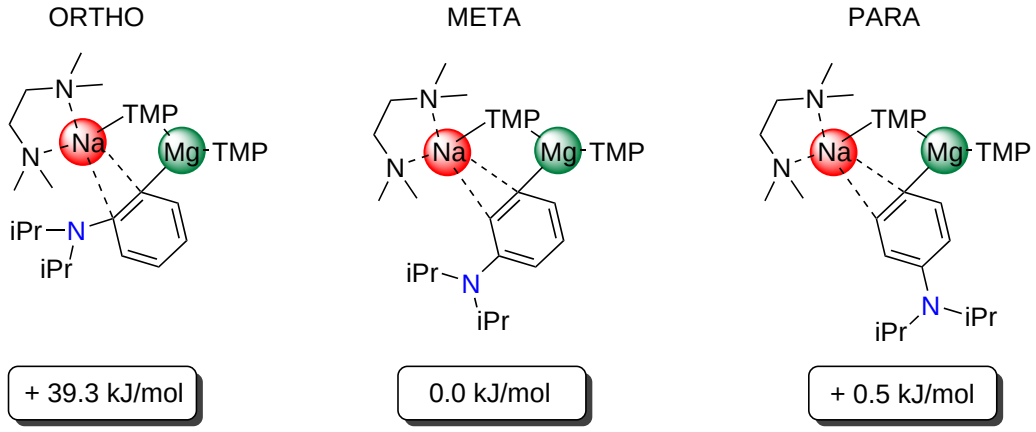

Figure 3.21: Computational studies of the relative energies of the regioisomers for the magnesiation of *N,N*-diisopropylphosphine with the sodium magnesiate **1**. The most stable regioisomer has been set as 0.0 kJ/mol. Modelled at the B3LYP/6+31(d) level of theory.

Similar results were found in the case of *N,N*-diisopropylaniline (see Figure 3.21). The most stable regioisomer observed once again was the *meta*-magnesiated species, however the *para*-magnesiated species was only 0.5 kJ/mol higher in energy - not significantly higher and within chemical accuracy (of 4 kJ/mol), indicating that these two species are very similar in energy. In comparison, the *ortho*-magnesiated species is dramatically higher in energy (39.3 kJ/mol), which would be expected based upon the increase in steric bulk around the nitrogen directing group.

Moving onto the simplest phosphorus substrate, *P,P*-dimethylphenylphosphine, where we found a mixture of *lateral*-magnesiated (by solid state) and a mixture of *lateral*- and *para*-magnesiation in solution state. Computationally, the most stable isomer was indeed observed to be the *lateral*-magnesiated product, which was observed experimentally in the solid state. The next most stable regioisomer computationally was the *para*-magnesiated product, which was 5.3 kJ/mol less stable. This aligns well with experimental results, where it was found that in solution a mixture of the *lateral*- and *para*-magnesiated species (in approximately a 75 % - 25 % ratio).

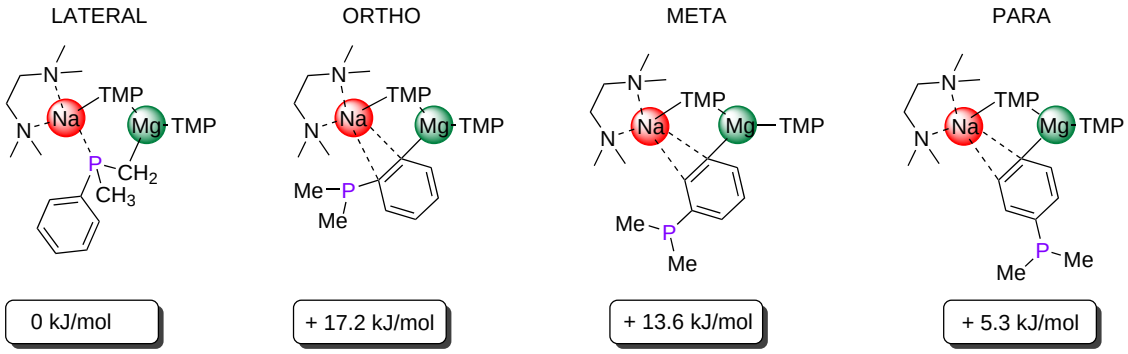

Figure 3.22: Computational studies of the relative energies of the regioisomers for the magnesiation of *P,P*-dimethylphenylphosphine with the sodium magnesiate **1**. The most stable regioisomer has been set as 0.0 kJ/mol. Modelled at the B3LYP/6+31(d) level of theory.

3.14 Conclusions for the reactivity of *N,N*- and *P,P*-dialkyl anilines and phenylphosphines

The reactivity profile of the sodium magnesiate **1** against a range of *N,N*-dialkylanilines and *P,P*-dialkylphenylphosphines has been established. Computational studies have been used to justify the reactivity observed.

In the case of *N,N*-diethylaniline, selective *meta*-magnesiation occurs resulting in the new magnesiate [(TMEDA)Na(TMP)(*m*−$C_6H_4NEt_2$)Mg(TMP)] - something not possible with more conventional monometallic reagents. The reactivity of the monometallic NaTMP and $Mg(CH_2SiMe_3)_2$ were also explored, giving rise to the new sodium amide $[\{(TMEDA)Na(EtNC_6H_5)\}_2]$ **11**.

In the case of both *N,N*-dimethyl and *N,N*-diisopropyl- aniline, non-selective magnesiation was found to occur at the *meta*- and *para*- positions, albeit in low yields. When iodolysed, the corresponding *meta*- and *para*- iodo-anilines could be isolated.

Moving onto the related phosphorus complexes, the *lateral*-magnesiation of *P,P*-dimethylphenylphosphine was achieved and characterised in both the solid-state and solution state. Interestingly, evident in the ^{1}H and $^{31}P\{^{1}H\}$ was the existence of a secondary minor species, which was identified to be the *para*- magnesiated species. Iodination of the magnesiated species unexpectedly led to the di-iodinated species bis(iodomethylphenyl)phosphine oxide being isolated, as well as iodomethyl-methylphenylphosphine oxide and traces of (4-iodophenyl)dimethylphenylphosphine oxide.

The sodium magnesiate **1** had minimal reactivity against *P,P*-diethylphenylphosphine, even under reflux conditions. On the other hand, the reactivity of NaTMP was established. This resulted in the β-elimination of an ethyl fragment to generate the monometallic complex $[(TMEDA)Na_2(TMP)(C_6H_5PEt)]_2$ **14**. This can be viewed as an example of a hybrid co-complex between a sodium amide and a sodium phosphide.

In the case of *P,P*-diisopropylphenylphosphine, selective *meta*-magnesiation was observed. In this case, the solution state behaviour was simpler, confirming the retention of the solid state structure in solution. The *meta*-iodinated species could be isolated.

Overall, this study has extended the reactivity profile of the sodium magnesiate **1** and offers new pathways to *meta*- and *para*- functionalised anilines, as well as lateral- and *meta*- functionalised phenylphosphines.

Extending the series to napthyl-based derivatives

To further extend this study, it was decided to vary the nature of the aromatic moiety present on the substrate. By moving to *N,N*-dimethyl-1-napthylamine, the reactivity can be compared to *N,N*-dimethylaniline, where a mixture of *meta*- and *para*- magnesiated products were observed. The corresponding *P,P*-dimethylnapthyl-1-phosphine was also able to be readily synthesised extending the corresponding phosphorus series (see Figure 3.23).

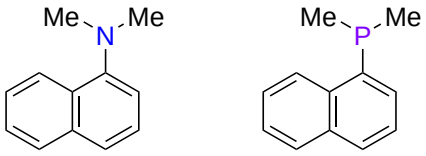

Figure 3.23: The napthyl-substituted amines and phenylphosphine targeted in this study

3.15 Reaction of magnesiate base 1 with *N,N*-dimethyl-1-napthylamine

To a stirred solution of the magnesiate base **1**, a molar equivalent of *N,N*-dimethyl-1-napthylamine was added dropwise. After stirring overnight, a large quantity of a white solid was deposited (see Scheme 3.18). This was isolated by filtration, washed with *n*-hexane and dried *in vacuo*. This solid was transferred to a glovebox for storage. On one repeat synthesis, crystals suitable for X-ray crystallographic analysis were obtained from a hot filtration of the suspension, and sitting at room temperature overnight. These crystals found to be the new 6-magnesiated product [(TMEDA)Na(TMP)(6 $-Me_2N-C_{10}H_6$)Mg(TMP)] **16**.

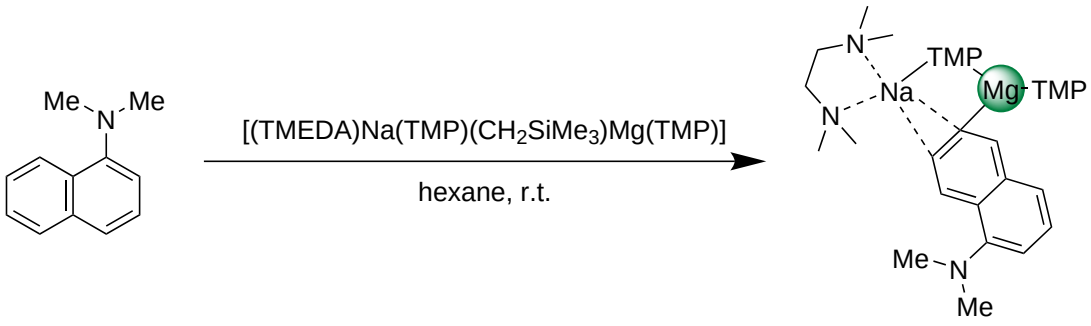

Scheme 3.18: Reaction of magnesiate base **1** with *N,N*-dimethylnapthyl-1-amine

3.15.1 X-ray crystallographic analysis of complex 16

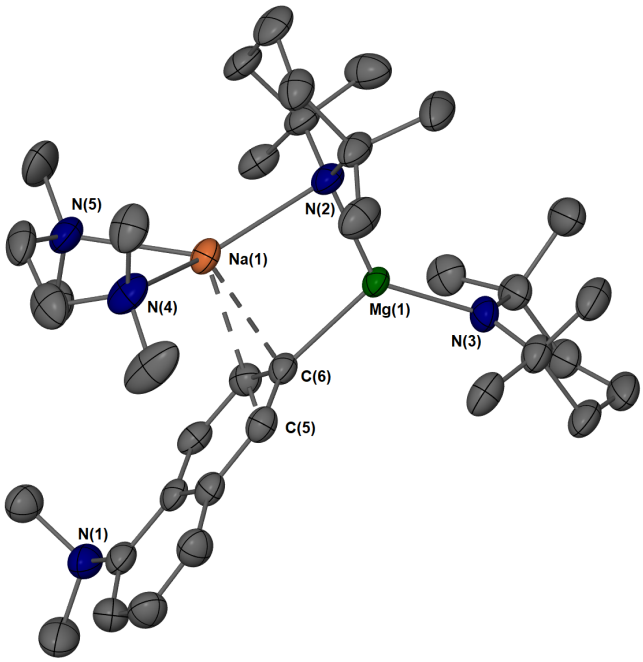

Figure 3.24: Molecular structure of [(TMEDA)Na(TMP)(6 −Me_2N−$C_{10}H_6$)Mg(TMP)] **16**. Thermal ellipsoids shown at 40 % probability. Hydrogen atoms omitted for clarity. Selected bond lengths (Å) and angles (°): Mg(1) - C(6), 2.182(6); Mg(1) - N(2), 2.073(5); Mg(1) - N(3), 1.990(5); Na(1) - C(5), 3.059(7); Na(1) - C(6), 2.706(6); Mg(1) - C(6) - Na(1), 79.71(18); Mg(1) - N(2) - Na(1), 86.7(2); N(2) - Mg(1) - C(6), 108.9(2); N(3) - Mg(1) - C(6), 117.7(2); N(3) - Mg(1) - N(2), 133.5(2); N(2) - Na(1) - C(5), 102.13(17); N(2) - Na(1) - C(6), 83.16(17).

The molecular structure of complex **16** (see Figure 3.24) features a distorted trigonal planar magnesium centre (bond angles range from 108.9(2)° to 133.5(2)°). The magnesium is bonded to the 6-position of the *N,N*-dimethylnapthyl-1-amine unit, indicated by the magnesium carbon bond length of 2.182(6) Å. The coordination environment of the magnesium is completed by a terminal TMP [Mg(1) - N(3) bond length 1.990(5) Å] and a bridging TMP unit [Mg(1) - N(2) bond length 2.073(5) Å]. The sodium atom makes close interactions with both the 5- and 6- positions of the napthyl-1-amine unit (Na - C bond lengths of 3.059(7) and 2.706(6) Å respectively). The sodium completes its coordination environment with a bridging TMP unit [Na(1) - N(2) bond length 2.073(5) Å] and the bidentate Lewis donor TMEDA. It can be seen from the crystal structure that the magnesiate base **1** loses a $SiMe_4$ group to afford this deprotonation, and therefore this is an example of alkyl-basicity.

3.15.2 Solution state analysis of complex 16

^{1}H and ^{13}C{^{1}H} NMR analysis of crystalline complex **16** was conducted in C_6D_6 (non-crystalline material was also studied, and found to be the same complex). The ^{1}H NMR spectrum was consistent with the retention of the solid-state structure in solution (see Figure 3.25). The appearance of a singlet at 8.33 ppm (corresponding to the lone proton at C5), and the downfield shift of two doublets to appear as an AB quartet at 8.24 and 8.17 ppm (corresponding to the protons on C7 and C8) are most indicative of a C6-magnesiated *N,N*-dimethylnapthyl-1-amine (see Figure 3.26). The methyl protons appear at 2.68 ppm. The presence of TMEDA (with signals at 1.43 and 1.25 ppm) and TMP (with signals at 1.91, 1.69 and 1.36 ppm) is also evident. In the ^{13}C{^{1}H} NMR spectrum of complex **16**, the most evident feature is a singlet at 170.31 ppm, corresponding to the newly formed Mg - C bond at C6.

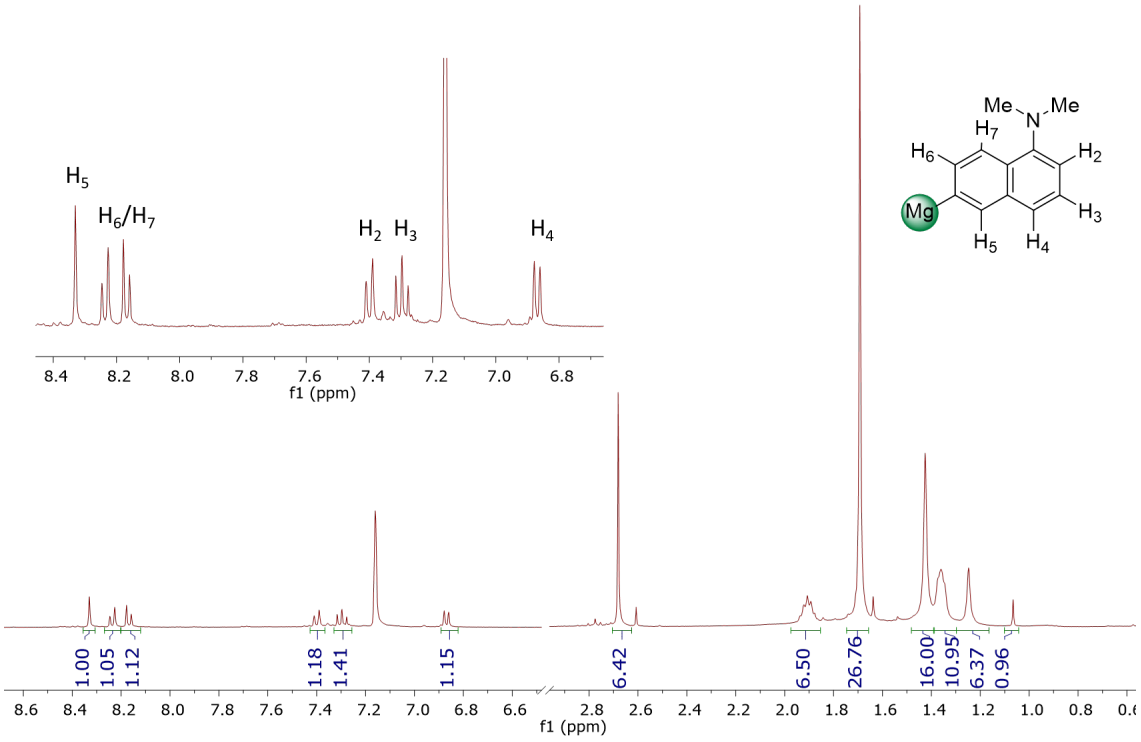

Figure 3.25: ^{1}H−NMR spectrum of **16** in C_6D_6 at 298 K

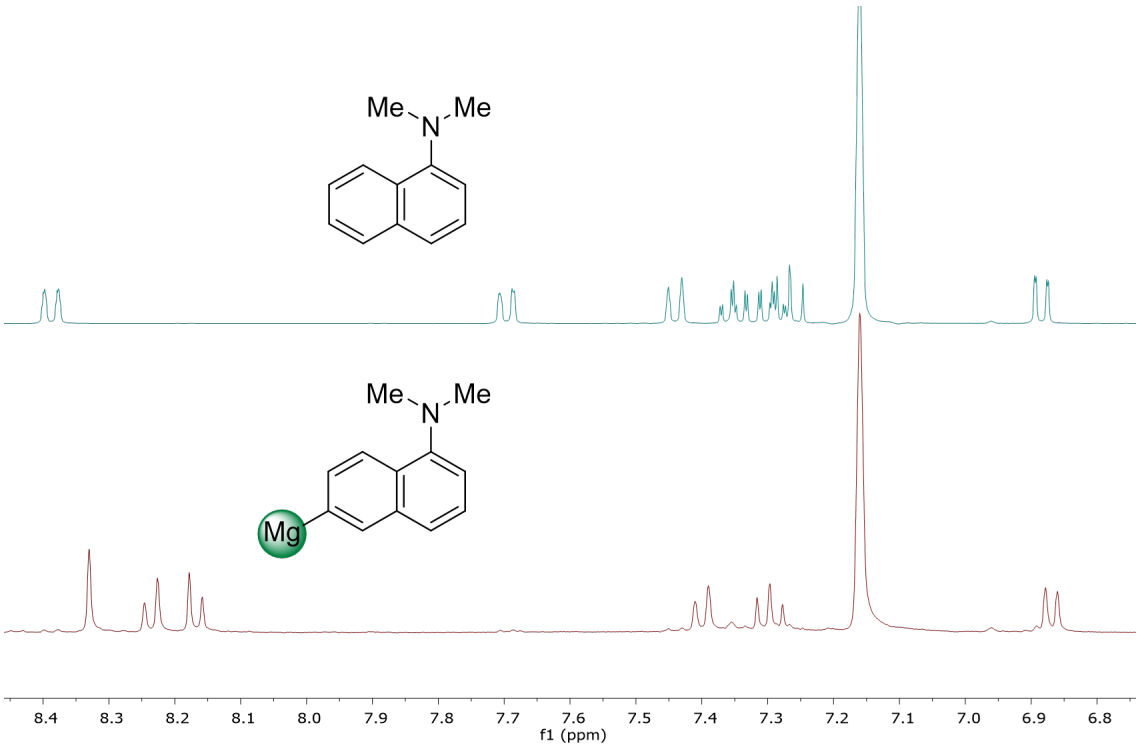

Figure 3.26: Comparison of the ^{1}H NMR spectrum of *N,N*-dimethylnapthyl-1-amine (top) and complex **16** (bottom) in C_6D_6

3.15.3 Electrophilic quenching studies of complex 16

A search of the Cambridge Structural Database (conducted on the 28/04/2020) reveals no hits for the 6-metallation of *N,N*-dimethylnapthyl-1-amine by any metal. This unprecedented reactivity opens new possiblities for the functionalisation of these napthylamine systems. To investigate the synthetic utility of this reaction, a number of electrophilic quenching studies were performed.

A 1 M solution of iodine in THF (5 equiv) was added dropwise at 0 ° C to a stirred solution of **16**, and allowed to warm to room temperature stirring overnight (16 hours). The reaction mixture was diluted with diethyl ether, before being quenched with saturated sodium thiosulphate solution to remove any residual iodine present. Following organic workup, the corresponding 6-iodo-*N,N*-dimethylnapthyl-1-amine was isolated in a high yield following purification by column chromatography (silica gel, 5 % EtOAc/petroleum benzene).

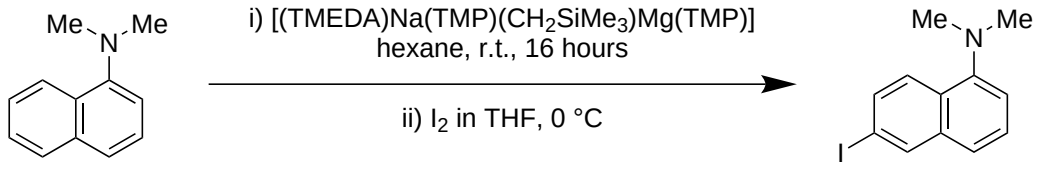

Scheme 3.19: Reaction of the magnesiate base **1** with *N,N*-dimethylnapthyl-1-amine followed by an electrophilic quench with iodine to afford the corresponding 6-iodo-*N,N*-dimethylnapthyl-1-amine species

Next, the possibility for direct reactions off the intermediate Mg-C bond were explored. Palladium-catalysed cross-couplings have been previously shown to be effective in these systems. First, the palladium catalysed cross-coupling of iodobenzene (2 equiv) with 6-magnesiated *N,N*-dimethylnapthyl-1-amine was explored using 4 mol % Pd(dppf)Cl_2. Upon addition of the Pd(dppf)Cl_2 and iodobenzene, the reaction mixture was heated to reflux overnight (16 hours). Upon cooling to room temperature, the reaction was diluted with diethyl ether and quenched with saturated NH_4Cl solution. Following standard organic workup, the corresponding 6-phenyl-*N,N*-dimethylnapthyl-1-amine was isolated in high yield following column chromatography (silica gel, 5 % EtOAc/petroleum benzine) (Scheme 3.20).

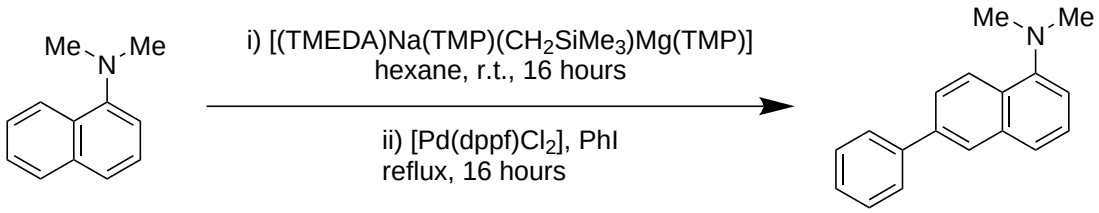

Scheme 3.20: Reaction of the magnesiate base **1** with *N,N*-dimethylnapthyl-1-amine followed by its use in a palladium catalysed cross-coupling with iodobenzene to afford the corresponding 6-phenyl-*N,N*-dimethylnapthyl-1-amine species

3.16 Synthesis of *P,P*-dimethyl(naphthalen-1-yl)phosphane

Following on from the unprecendented 6-magnesiation of *N,N*-dimethylnapthyl-1-amine, we next sought to extend to the corresponding phosphorus(III) equivalent *P,P*-dimethylnapthyl-1-phosphine (see Figure 3.27).

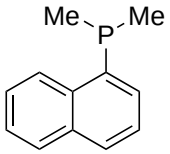

Figure 3.27: Synthetic target to extend the napthyl series

Initially, it was hoped that the target *P,P*-dichloronapthyl-1-phosphine could be synthesised by the addition of one equivalent of either 1-napthylmagnesium bromide or 1-lithio-napthalene to a solution of PCl_3 at low temperature. Unfortunately, this resulted in the formation of predominately trinapthyl-1-phosphine.

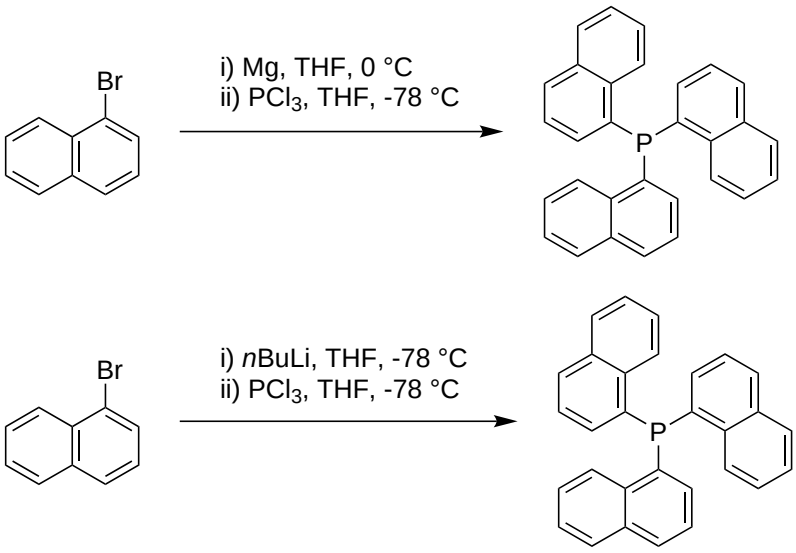

Scheme 3.21: Attempted synthesis of *P,P*-dichloronapthyl-1-phosphine via a Grignard or lithiated napthyl- species

By adapting a literature procedure for the preparation of aryl-phosphorus dichlorides from their corresponding Grignard reagent, *P,P*-dichloronapthyl-1-phosphine was successfully synthesised in a high yield.[120] Napthylmagnesium bromide was prepared as a dilute solution (< 0.5 M) in THF (to avoid slurry formation), to which an equimolar quantity

of $ZnCl_2$ in THF (1 M) was added dropwise at 0 ° C. Following this the new zinc based organometallic is added dropwise to PCl_3 in THF at -78 ° C. The solvent is removed *in vacuo* and replaced with diethyl ether to precipitate metal salts. The resulting solution is filtered, and the solvent removed *in vacuo*. The resulting *P,P*-dichloronapthylphosphine was isolated in high yield (> 80 % average yield, Scheme 3.22). This pale yellow solid is stable to glovebox storage for an extended period of time.

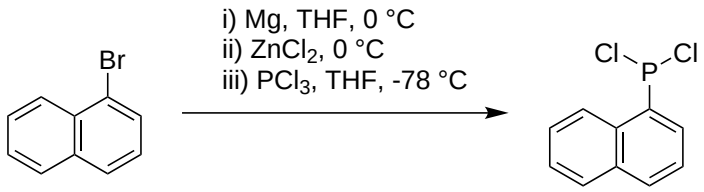

Scheme 3.22: Synthesis of *P,P*-dichloronapthyl-1-phosphine

To synthesise *P,P*-dimethylnapthylphosphine, 2.5 equivalents of MeMgBr was added to a stirred solution of *P,P*-dichloronapthylphosphine in THF (1 M) at 0 ° C (Scheme 3.23). The resulting solution is quenched with deoxygenated water, filtered and solvent removed *in vacuo* (under a nitrogen atmosphere to avoid oxidation). The resulting oil is vacuum distilled to afford *P,P*-dimethylnapthyl-1-phosphine in a high yield as a colourless oil. Interestingly, on a repeat synthesis of this compound it was discovered that it was reasonably stable to atmospheric oxygen, remaining predominately phosphorus (III) following aqueous work-up without exclusion of air and following purification by column chromatography (silica gel, 5% EtOAc/petroleum benzene).

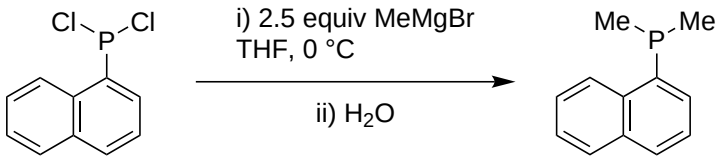

Scheme 3.23: Synthesis of *P,P*-dimethylnapthyl-1-phosphine

3.17 Reaction of magnesiate base 1 with *P,P*-dimethyl-1-napthylphosphine

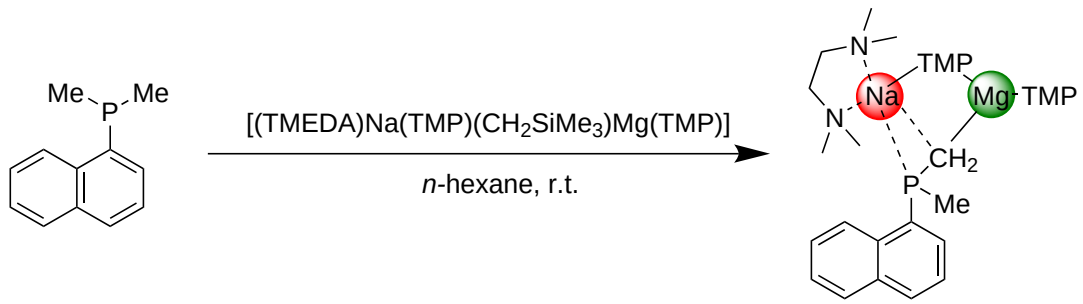

Scheme 3.24: Synthesis of complex **17**

To a stirred solution of [(TMEDA)Na(TMP)(CH_2SiMe_3)Mg(TMP)] in hexane, a molar equivalent of *P,P*-dimethylnapthylphosphine was added dropwise at room temperature. The resulting solution was stirred overnight, resulting in the deposition of a large quantity of a blue solid suspended in a blue solution. Upon filtration and storage at room temperature, crystals suitable for X-ray crystallographic analysis were deposited over the course of a week. These were found to be the lateral-magnesiated complex [(TMEDA)Na(TMP)($C_{10}H_7PCH_3CH_2$)Mg(TMP)], **17**.

3.17.1 X-ray crystallographic analysis of complex 17

Complex **17** shares similar structural features to complex **12**. Featuring a lateral magnesiation at one of the CH_3 groups, as a result of alkyl basicity through the loss of CH_3SiMe_3. The molecular structure features a trigonal planar magnesium centre, as is typical for other structures within this chapter. The magnesiums coordination environment features a terminal TMP (Mg - N bond length 2.0099(18) Å), bridging TMP (Mg - N bond length 2.0883(18) Å) and a bridging *P,P*-dimethylnapthyl-1-phosphine based unit (Mg - C bond length 2.197(2) Å). The sodium is in a four-coordinate molecule environment, bonded to a bridging TMP (Na - N bond length 2.4792(19) Å), a bidentate chelating TMEDA molecule (Mg - N bond lengths of 2.494(2) and 2.531(2) Å) and a strong interaction with the phosphorus lone pair, similarly to complex **12** (Na - P bond length 2.9123(10) Å). The

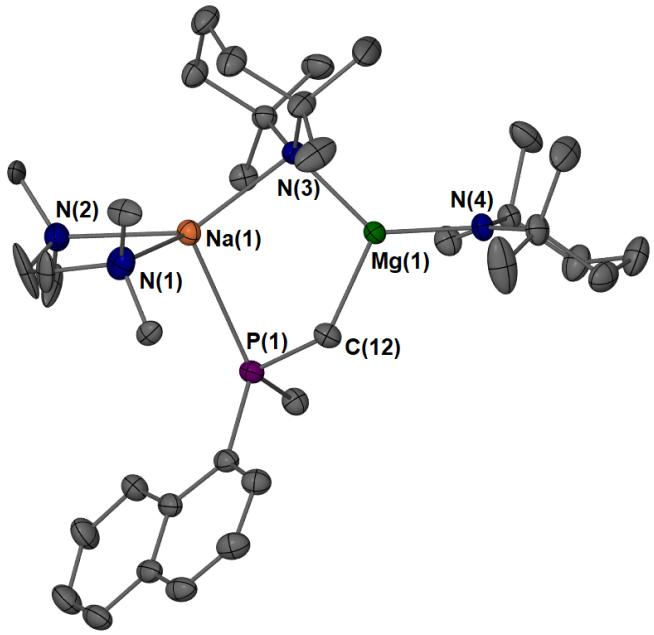

Figure 3.28: Molecular structure of **17**. Hydrogen atoms and a disordered TMEDA fragment omitted for clarity. Thermal ellipsoids shown at 40 % probability. Selected bond lengths (Å) and angles (°): Mg(1) - C(12), 2.197(2); Na(1) - P(1), 2.9123(10); Mg(1) - N(3), 2.0883(18); Mg(1) - N(4), 2.0099(18); Na(1) - N(3), 2.4792(19); Na(1) - N(1), 2.494(2); Na(1) - N(2), 2.531(2); N(3) - Mg(1) - N(4), 132.01(8); N(4) - Mg(1) - C(12), 119.07(9); C(12) - Mg(1) - N(3), 108.25(8); P(1) - C(12) - Mg(1), 117.91(12); Na(1) - P(1) - C(12), 81.17(8); P(1) - Na(1) - N(3), 99.00(5); Na(1) - N(3) - Mg(1), 98.24(7).

TMEDA molecule shows positional disorder, and is modelled as disordered across two sites (not shown in Figure 3.28 for simplicity).

3.17.2 Solution state analysis of 17

Crystalline solid **17** was dissolved in C_6D_6 and analysed by ^{1}H and $^{31}P\{^{1}H\}$ NMR spectroscopy. On inspection of the aromatic region of the ^{1}H NMR spectrum, it becomes evident that there is one dominant species present in solution, with potentially a number of other species present (see Figure 3.29). The dominant species present corresponds to the expected product based upon the crystal structure (see Figure 3.28). The presence of these minor products are also evident in the $^{31}P\{^{1}H\}$ NMR spectrum (see Figure 3.30). Unfortunately the identities of these side products have not been positively identified. While preliminary electrophile studies with iodine were conducted, this result was obtained in the

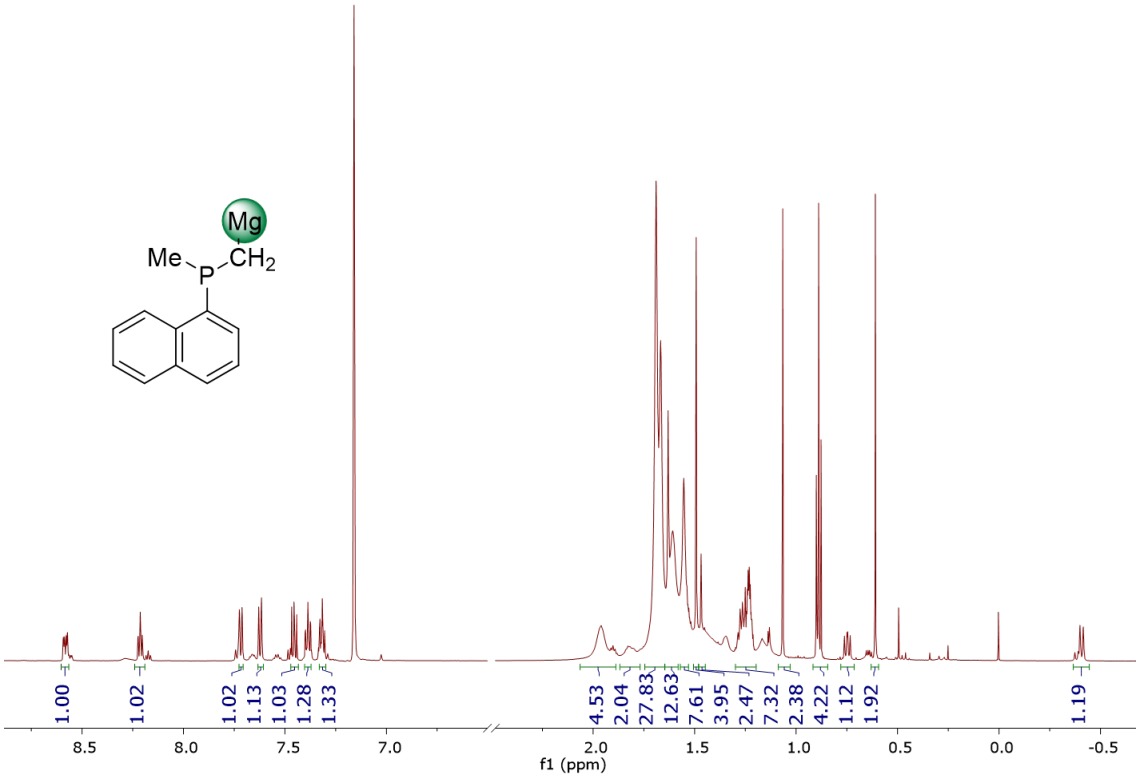

Figure 3.29: ^{1}H NMR spectrum of **17** in C_6D_6 at 298 K

final stages of this project, and time restraints did not allow full elucidation of the species present.

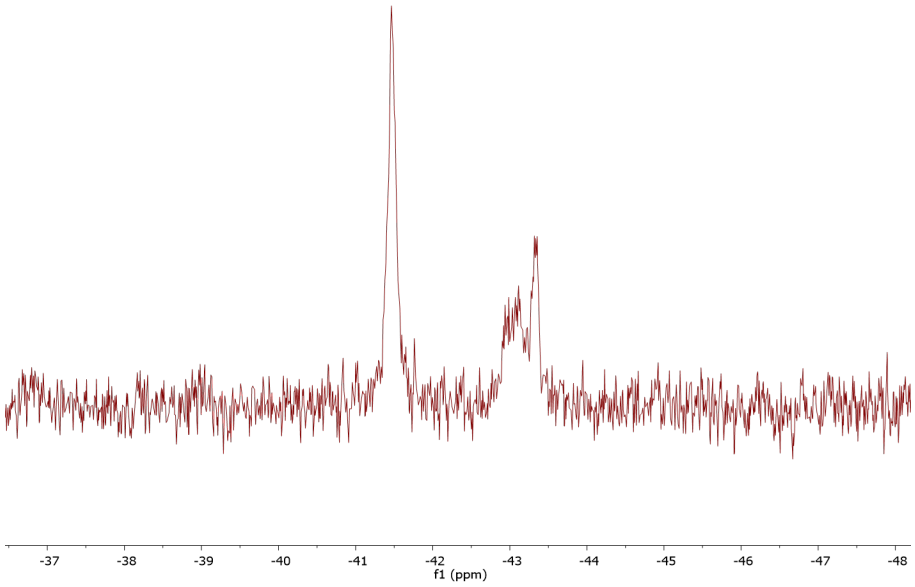

Figure 3.30: $^{31}P\{^{1}H\}$ NMR spectrum of **17** in C_6D_6 at 298 K, showing the existence of multiple ^{31}P containing species

3.18 Conclusions and Future Work

This chapter explored the reactivity of the sodium magnesiate **1** with a range of *N,N*- and *P,P*-dialkyl anilines and phenylphosphines, as well as an extension to related *N,N*-dimethylnapthyl-1-amine and *P,P*-dimethylnapthyl-1-phosphine. Selective *meta*-magnesiation was found in the case of *N,N*-diethylaniline and *P,P*-diisopropylphenylphosphine, which allowed access to the *meta*-iodinated species following electrophilic quenching with iodine. In the case of *P,P*-dimethylphenylphosphine and *P,P*-dimethylnapthyl-1-phosphine, a lateral magnesiated species was characterised by X-ray crystallographic studies. However, during solution state NMR studies as well as in electrophile studies, multiple species were detected. In the case of *P,P*-dimethylphosphine, both a di-lateral iodinated species [$(CH_2I)_2P(O)Ph$] and a *para*-iodinated species were identified. Unfortunately full elucidation of the multiple species has not been completed in the case of *P,P*-dimethylnapthyl-1-phosphine. Interestingly, the selective 6-magnesiation of *N,N*-dimethylnapthylamine was achieved with the sodium magnesiate **1**. There is no precedent in the literature for such regioselectivity. The corresponding 6-iodinated-*N,N*-dimethylnapthylamine was isolated in a high yield.

It would be worth exploring in the future of the reaction of the magnesiate base **1** with the corresponding phosphorus(V) oxides of the phosphines studied in this chapter. As will be seen in Chapter 5, these reactions may have the potential to produce radical species. Preliminary studies (not included in this thesis) indicate that this may indeed be the case. Further work is required to elucidate the nature and identity of these metallated species.

4 Bi-metallic metallations of *N*-heterocyclic molecules

Molecules containing *N*-heterocycles are critical to the natural environment and all known biological systems.[121] Likely the most common *N*-heterocycle, 1*H*-indole, is an aromatic bicyclic structure consisting of a six-membered benzene ring fused to a five-membered pyrrole ring. As an intercellular signalling molecule, indole containing molecules feature prominently in regulating many aspects of biological systems. For instance, the essential amino acid typtophan is an indole derivative, and is a precursor to the neurotransmitter serotonin. This prominent natural occurrence of indole containing molecules make them important scaffolds within medicinal chemistry, where they are considered a "privileged scaffold", and one of the most important structural subunits for drug discovery.[122] Indoles are found in a plethora of biologically significant natural compounds such as serotonin, reserpine, tryptophan and melatonin (see Figure 4.1). Indoles also feature prominently in a range of clinically important synthetic drugs (such as sumatriptan, tadalafil, rizatriptan and fluvastatin (see Figure 4.2).

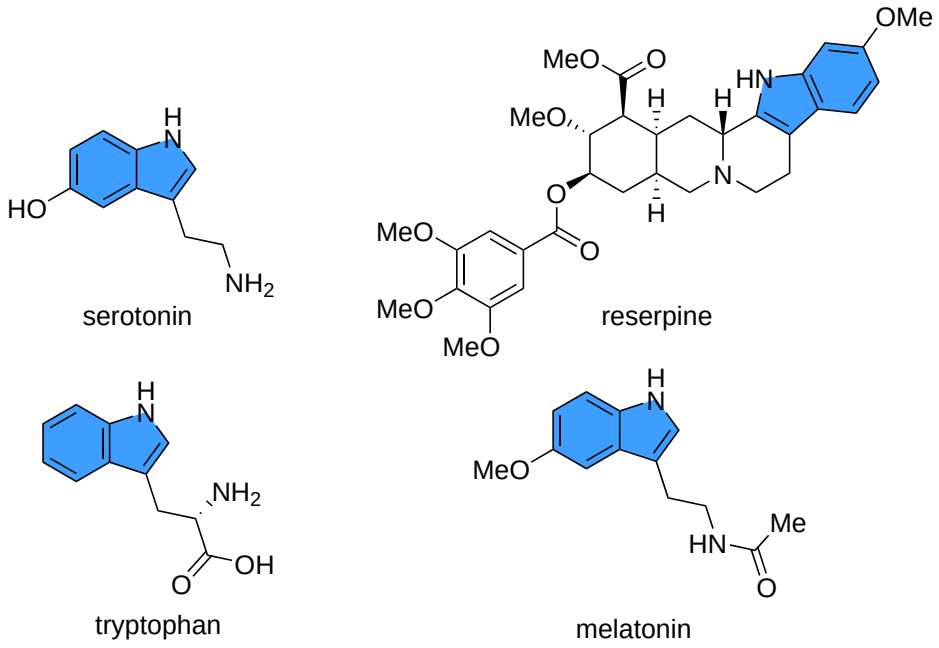

Figure 4.1: Four naturally occurring indoles

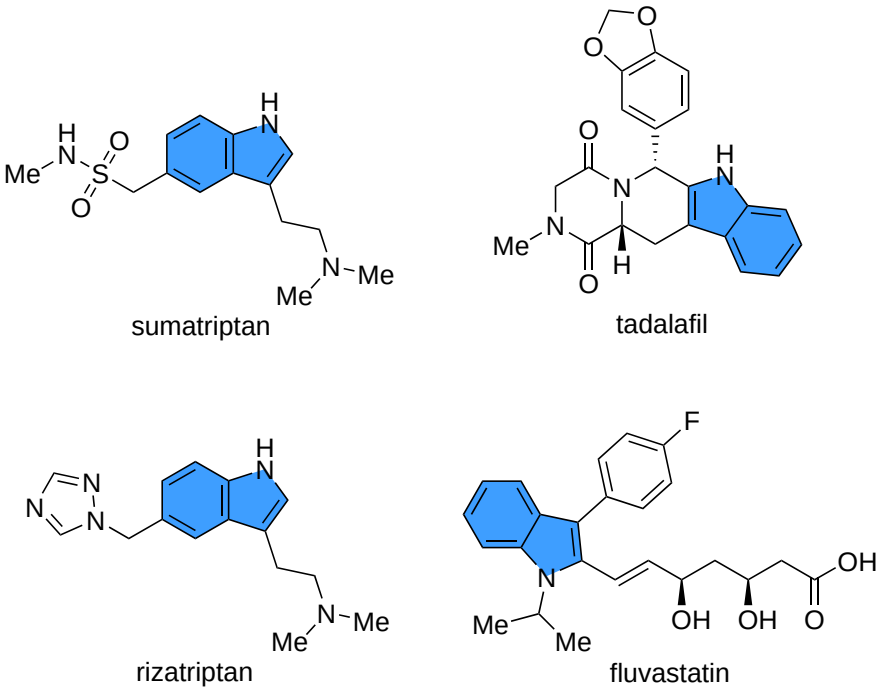

Figure 4.2: Four clinically relevant indole based drugs

Molecules containing *N*-heterocycles also find prominent uses throughout the entire chemical industry, such as in agrochemicals (e.g. auxins and Amisulbrom) and in pigments and dyes (indigoid and cyanine).[123]

The functionalisation of indoles is therefore of high importance in synthetic chemistry. There are two main synthetic routes used to functionalised indoles - direct functionalisation of preformed indole units, or most prominently the annulation of the five-membered pyrrole ring to an existing benzene ring bearing the appropriate functionality.[121] This chapter will focus on the first type - direct functionalisation of preformed indole rings.

4.0.1 Lithiation of substituted indoles

Lithiation of the C2 position of *N*-methylindole requires a 4-fold excess of *n*-butyllithium and prolonged heating (eight hours reflux in diethyl ether).[124] Electrophile quenches of the resulting 2-lithio-*N*-methylindole results in moderate to high yields of the corresponding 2-functionalised indole species, which is uncommon with non-metallation routes, which often result in 3-functionalised species (see Scheme 4.1).[124]

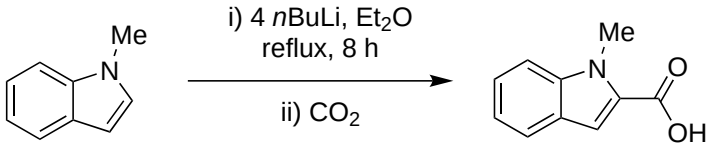

Scheme 4.1: C2 lithiation of *N*-methylindole by *n*BuLi, followed by carboxylation by CO_2

Boc-protected 1*H*-indole can be lithiated under milder conditions (albeit in low yield), likely due to the increased ability of the Boc group to coordinate and anchor the incoming organolithium reagent, directing lithiation *ortho* to the heteroatom. The lithiated species can be transmetallated with $n-Bu_3SnCl$, which can be employed in the subsequent Pd-catalysed cross-coupling reaction with aryl-bromides (Stille coupling, see Scheme 4.2). The Boc group can be easily removed to give the 2-arylated free 1*H*-indole in excellent yields.[125]

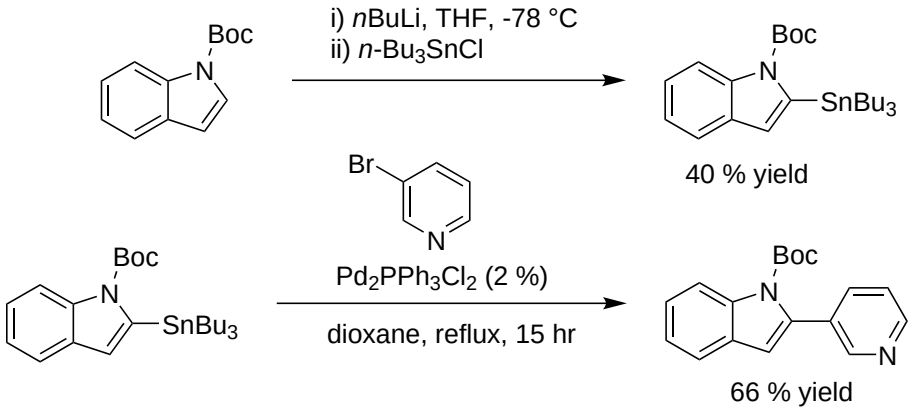

Scheme 4.2: Stille cross-coupling of *N*-protected indoles with 3-bromopyridine[125]

The selective 3-lithiation of an indole can be achieved using the bulky silyl-protecting group triisopropylsilyl (TIPS, see Scheme 4.3).[126] Optimal lithiation conditions were found to be the use of 1.5 equivalents of *t*BuLi with 1.8 equivalents of TMEDA in *n*-hexane at 0 ° C for 3 hours. The resulting 3-lithio-*N*-triisopropylsilyl-1*H*-indole can be trapped with various electrophiles, including MeI, TMSCl, DMF and CO_2. Interestingly, in all cases a small quantity of 2-triisopropylsilyl-1*H*-indole was isolated (2 - 3 %), formed from the C-2 lithiation of the indole followed by N to C migration of the triisopropylsilyl group. The silyl protecting group can be readily removed by treatment with TBAF, and therefore this method gives access to a range of 3-substituted indoles in moderate to high yields.[126]

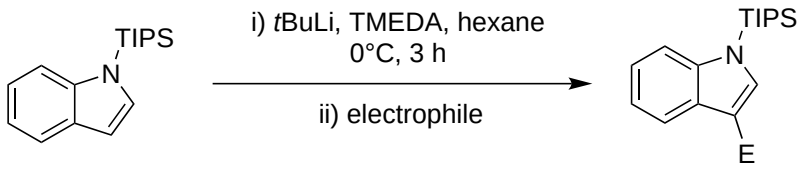

Scheme 4.3: Selective C-3 functionalisation of *N*-triisopropylsilyl-1*H*-indole, with various electrophiles including MeI (E = Me), TMSCl (E = TMS), DMF (E = CHO) and CO_2 (E = CO_2H)

The C3 lithiation can also be achieved with a less sterically demanding nitrogen based group, in the presence of a directing group at the C2 position. In this regard, 2-(*N*-methylindole)carboxamides were explored, with optimal lithiation conditions found using *N*-ethylcarboxamide with three equivalents of *t*BuLi/TMEDA (see Scheme 4.4).[127]

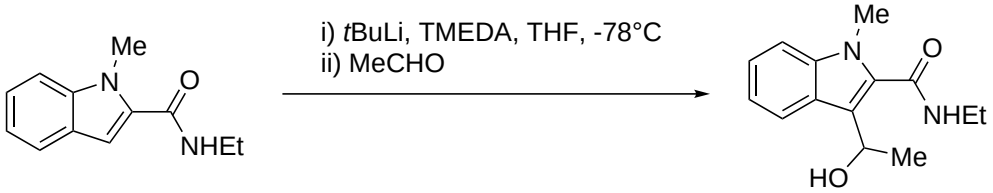

Scheme 4.4: Selective C3-lithiation of an indole derivative

Direct functionalisation of the benzenoid ring of the indole scaffold proves more challenging. Gramine is a naturally-occurring indole-based alkaloid with a dimethylaminomethylene group at the C3 position. This group can serve as a removable directing group, and can direct lithiation at the C4 position.[128] For instance, the *N*-triisopropylsilyl-gramine can be selectively lithiated at the C4 position (see Scheme 4.5).[129] In this case, optimal lithiation conditions were 1.2 equivalents of *t*BuLi at -78 ° C in diethyl ether. The resulting 4-lithio species can be trapped with various electrophiles, for example 3-methyl-2-butenal (see Scheme 4.5).

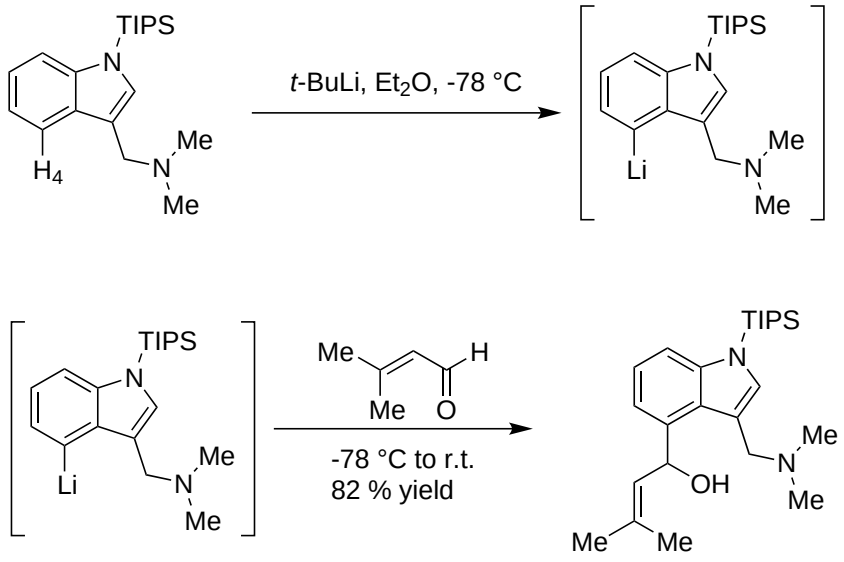

Scheme 4.5: Selective C4 lithiation of TIPS-protected gramine

The C5 and C6 positions of indoles are difficult to functionalise, as they lie remote from any nitrogen based directing group. The only known methods for C5 or C6 lithiation involve the use of lithium-halogen exchange with pre-installed halogens.

C7 lithiation can be achieved by the careful use of bulky directing groups present on the nitrogen functionality. The first report was from Iwao and co-workers, where they employed the bulky directing group 1-(2,2-diethylbutanoyl) to afford the C7 lithiation (see Scheme 4.6). This was achieved due to restricted rotation around the N−C=O bond, where predominately the Z-conformer (with the carbonyl oxygen directed towards the benzenoid ring) is retained during the deprotonation step, coordinating to the incoming organolithium and directing C7 lithiation. The *ethyl*- groups present in the directing group were crucial for inhibiting nucleophilic attack of the carbonyl followed by cleavage of the functional group. A small percentage of C2 lithiation was also observed with these conditions.[130]

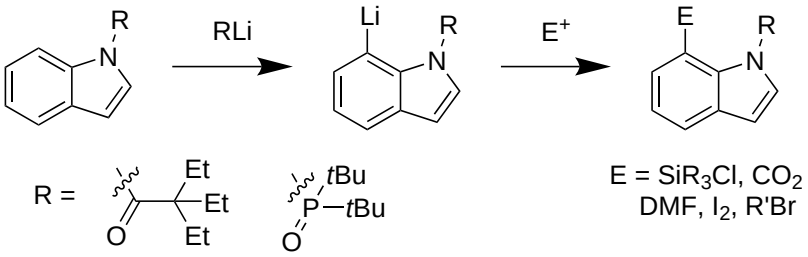

Scheme 4.6: Selective C7-lithiation of indole

Snieckus and co-workers improved on this method with the powerful P(O)($t-$Bu)$_2$ directing group, which afforded selective C2 or C7 lithiation depending on the lithium reagent used. When LDA is employed at 0 ° C, selective C2 lithiation was observed in 15 minutes (as confirmed by subsequent TMSCl quench). When *n*-BuLi was selected as the lithiation reagent, C7 functionalisation was exclusively observed, followed by a range of electrophilic quenches (see Scheme 4.6).[131]

4.0.2 Magnesiation of indoles

The magnesiation of indoles have been achieved utilising both Hauser bases (R_2NMgBr) or magnesium diamides ($(R_2N)_2Mg$).[132] The reaction of *N*-phenylsulfonylindole with both of these magnesium reagents resulted in the 2-magnesioindole being produced, which could subsequently be trapped with a range of electrophiles to produce C2-substituted indoles (see Scheme 4.7). Interestingly, *N*-methylindole did not react even at elevated temperatures, suggesting the phenylsulfonyl- group is critical for this reactivity.

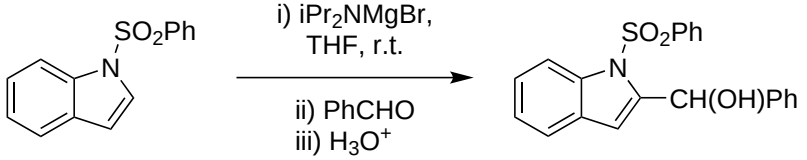

Scheme 4.7: Reaction of the Hauser base iPr_2NMgBr with *N*-phenylsulfonylindole

Mulvey and coworkers found the sodium tetraalkylmagnesiate [(TMEDA)$_2$Na$_2$Mg(nBu)$_4$] reacts with four equivalents of *N*-methylindole to produce the disodium tetraindol-2-ylmagnesiate [(Na $\cdot$ TMEDA)$_2$Mg($\alpha-$C$_9$H$_8$N)$_4$].[133] The magnesiated species could sub-

sequently be used in *in situ* Pd-catalysed cross-couplings with iodobenzene to yield *N*-methyl-2-phenylindole in a high yield of 84 %.

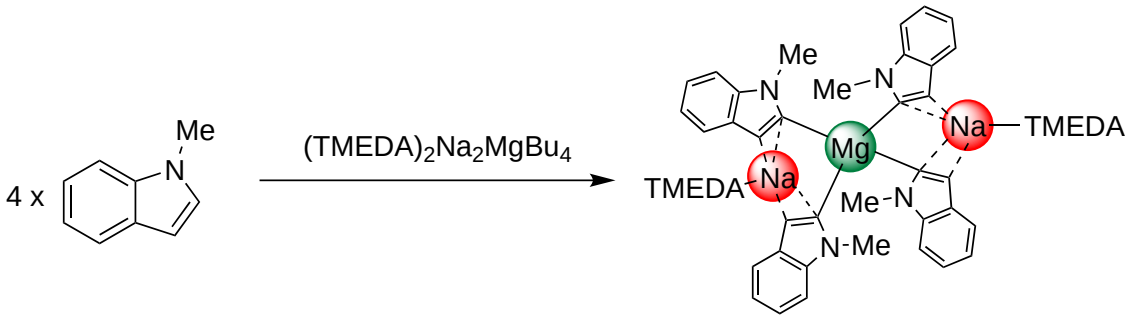

Scheme 4.8: Reaction of the disodium tetraalkylmagnesiate [$(TMEDA)_2Na_2Mg$*n*Bu_4] with *N*-methylindole

4.0.3 Alkali metal mediated metallation of indoles

More broadly, the alkali metal mediated metallaton of indoles has been achieved with numerous metal pairings.

Uchiyama and co-workers developed the direct *alpha*-cupration and -alumination of *N*-boc-indoles using the lithium cuprate [$MeCu(TMP)(CN)Li_2$][35] and lithium aluminate [$i Bu_3Al(TMP)Li$],[34] where selective C2- metallations were observed in both cases (see Scheme 4.9). However, both mixed metal reagents required sub-ambient temperatures (-40 °C or -78 °C) and/or an excess of metallating reagent.

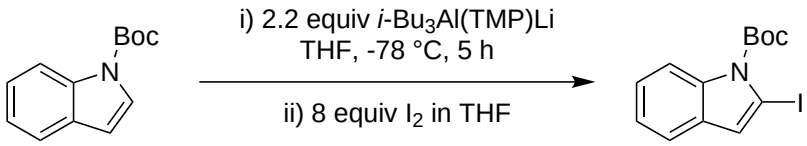

Scheme 4.9: Reaction of the lithium aluminate [$i Bu_3Al(TMP)Li$] with *N*-boc-indole

Mongin and co-workers have developed a lithium zincate, $ZnCl_2$.TMEDA / LiTMP, which is able to functionalise a diverse range of functionalised indoles and pyrrole species, giving rise to predominately 2-iodo derivatives in excellent yields.[24,134,135] A range of other metal pairings have been explored by Mongin and co-workers, including cadmium and indium.[25]

Following on from the literature precedents discussed so far, we decided to start simply with *N*-alkyl substituted 1*H*-indoles, and their reaction with the sodium magnesiate [(TMEDA)Na(TMP)(CH_2SiMe_3)Mg(TMP)] **1**.

4.1 Synthesis of *N*-substituted indoles

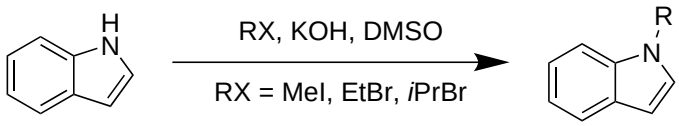

Scheme 4.10: Synthesis of *N*-substituted indoles

N-methylindole, *N*-ethylindole and *N*-isopropylindole were synthesised by the addition of RX (Me = MeI, Et = EtBr, iPr = iPrBr) to a stirred solution of 1*H*-indole and potassium hydroxide (Scheme 4.10) in DMSO. The reaction was monitored by TLC, and once full consumption of 1*H*-indole was observed the reaction was quenched with H_2O. Following organic work-up, the synthesised *N*-substituted indoles were purified by vacuum distillation and stored over 4 Å molecular sieves.

4.2 Reaction of magnesiate base 1 with *N*-methylindole

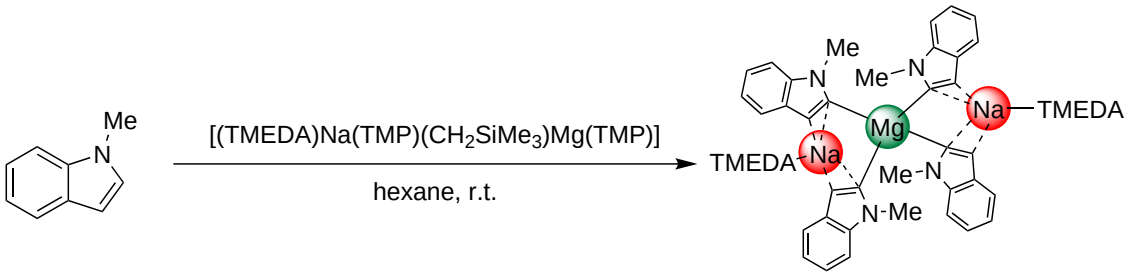

Scheme 4.11: Synthesis of complex **18**, $[(Na \cdot TMEDA)_2Mg(\alpha{-}C_9H_8N)_4]$

Reacting a hexane solution of the base **1** with one molar equivalent of *N*-methylindole resulted in the deposition of a large quantity of white precipitate after approximately five minutes (Scheme 4.11). When the reaction was repeated with stirring stopped upon

addition of *N*-methylindole, large colourless crystals were deposited over one hour. These crystals were suitable for single crystal X-ray analysis and were found to be the compound $[(Na \cdot TMEDA)_2Mg(o{-}C_9H_8N)_4]$ **18** (Figure 4.3).

It became evident when inspecting the crystal structure of **18** that the maximum possible yield of the reaction would only be 25 %. The rational synthesis of **18** was achieved by reacting NaTMP, $Mg(CH_2SiMe_3)_2$ and TMEDA in a 2:1:2 ratio with four equivalents of the *N*-methylindole (see Scheme 4.12). This led to the desired product being isolated in a high crystalline yield of 81 % (no residual starting material was detected by ^{1}H NMR, suggesting the reaction was quantitative).

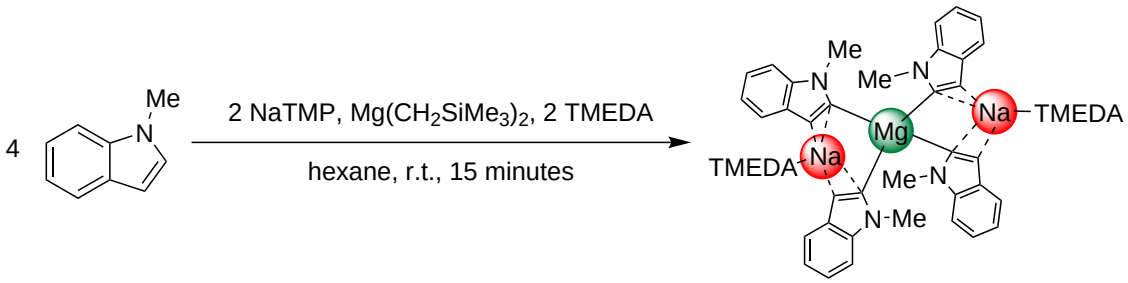

Scheme 4.12: Rational synthesis of complex **18**, $[(Na \cdot TMEDA)_2Mg(\alpha{-}C_9H_8N)_4]$

4.2.1 Solid state analysis of $[(Na \cdot TMEDA)_2Mg(\alpha{-}C_9H_8N)_4]$ 18

From the crystal structure of complex **18** (Figure 4.3), it can be seen that the magnesium atom is in a tetrahedral environment (mean bond angle 109.28°). The magnesium atom is bound to four different *N*-methylindole substituents at the *alpha* position (range of Mg(1)-C bond distances between 2.193(8) - 2.247(8) Å). Each sodium atom makes close electrostatic interactions with the α- and β- carbons from two different *N*-methylindole substitutents, while not making a formal bond [Na(1)-C(11) 2.657(9) and Na(1)-C(10) 2.882(9) Å]. The sodium interactions can be seen as a contact-ion pair arrangement, as they are needed to balance the charge on the magnesium centre. Each sodium atoms coordination environment is completed with a bidentate, chelating TMEDA.

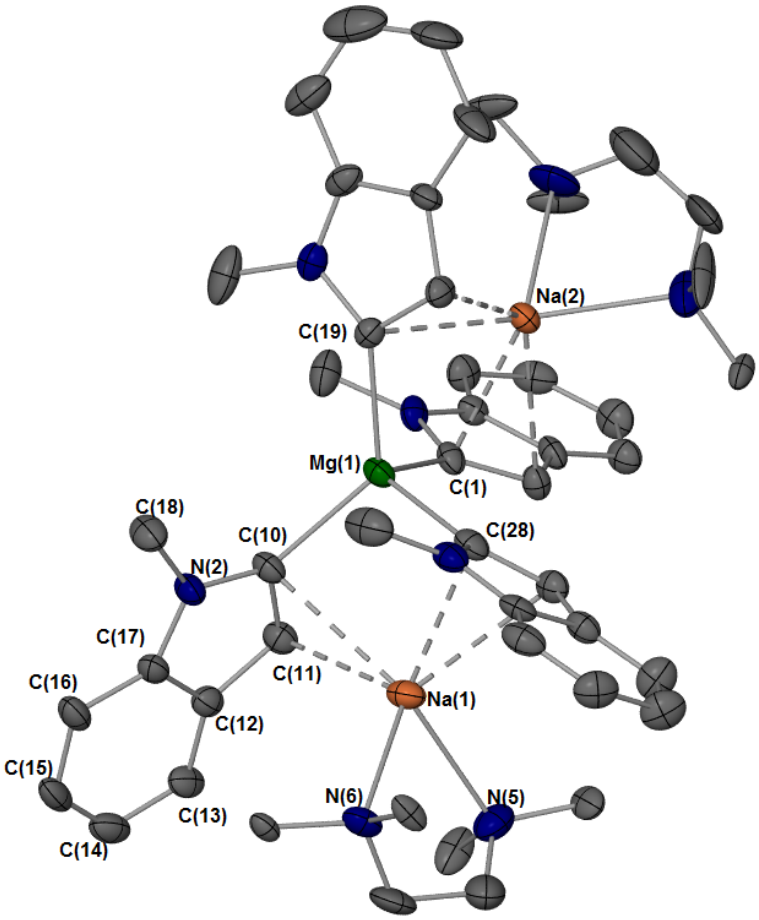

Figure 4.3: Molecular structure of **18**, $[(Na \cdot TMEDA)_2Mg(\alpha{-}C_9H_8N)_4]$. Thermal ellipsoids shown at 40 % probability. Hydrogen atoms omitted for clarity. Selected bond lengths (Å) and angles (°): Mg(1)-C(10), 2.193(8); Mg(1)-C(1), 2.234(7); Mg(1)-C(19), 2.201(7); Mg(1)-C(28), 2.247(8); Na(1)-C(10), 2.882(9); Na(1)-C(11), 2.657(9); N(2)-C(10), 1.393(10); C(10)-C(11), 1.389(11); C(11)-C(12), 1.440(11); C(1)-Mg(1)-C(28), 108.2(3); C(28)-Mg(1)-C(10), 104.8(3); C(10)-Mg(1)-C(19), 127.9(3); C(19)-Mg(1)-C(1), 103.6(3); C(1)-Mg(1)-C(10), 105.6(8); C(28)-Mg(1)-C(19), 105.2(3).

In the molecular structure of **18**, the bi-metallic base **1** has lost both its alkyl (CH_2SiMe_3) and two amido (TMP) 'basic arms'. While it was initially unexpected to see dual basicity of the base, similar reactivity has been previously observed when reacting **1** with thiophene.[66] The authors isolated the compound $[(TMEDA)Na(\mu{-}C_4H_3S)_3Mg(TMEDA)]$ **19** (Figure 4.4). In the study, the authors found that the active base was not **1**, as the logical synthesis involving $Mg(CH_2SiMe_3)_2$, *n*BuNa and two equivalents of TMEDA resulted in the same isolated structure, albeit in a higher yield. While similar, in that all the basic arms of the base have been lost, in the case of **18** the active base appears to differ from that in both **19** and **1**. Furthermore, four *alpha* deprotonations have occurred in the

case of **18**. In both cases, it appears that the isolated complex observed is the result of a disproportionation of **1**. Similar overall reactivity was observed with the homoleptic sodium tetraalkylmagnesiate $[(TMEDA)_2Na_2Mg(n\text{Bu})_4]$, where the same crystal structure was isolated.[133]

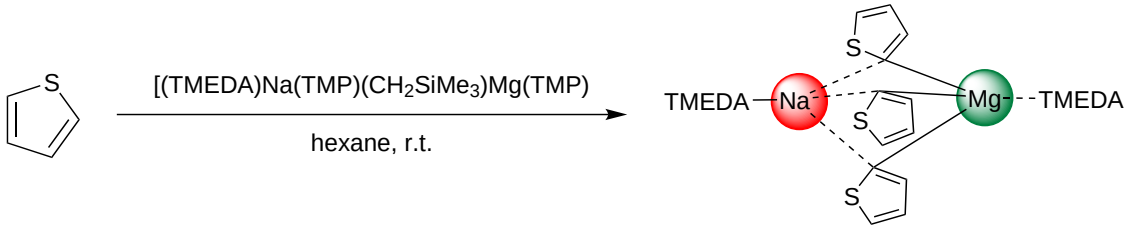

Figure 4.4: Reaction of the magnesiate base **1** with thiophene

Attempts were made to isolate the suspected active basic species in the reaction of **1** with *N*-methylindole. To achieve this, two equivalents of NaTMP, one equivalent of $Mg(CH_2SiMe_3)_2$ and two equivalents of TMEDA. Unfortunately, only the sodium magnesiate base **1** could be isolated from this reaction, likely indicating that some fluctional behaviour of this species exists in solution.

In order to examine whether the dialkyl magnesium species $Mg(CH_2SiMe_3)_2$ could effect deprotonation of the *N*-methylindole substrate, one molar equivalent of N-methylindole was added to a stirred suspension of $Mg(CH_2SiMe_3)_2$. No reaction was found to occur, whether at room temperature or at reflux for four hours. Therefore it can be concluded that $Mg(CH_2SiMe_3)_2$ is not reactive enough on its own, therefore the sodium is essential to the observed reactivity. This can therefore be considered an example of Alkali Metal Mediated *Magnesiation*.

While unique regio-selectivity was not obtained in **18**, the use of **1** has some advantages over more traditional metallating agents, especially from a green chemistry perspective. For instance, the bi-metallic base **1** used may be advantageous over the more commonly used *n*BuLi as the reaction can be completed at room temperature and takes minimal time for the reaction to occur. Also, only one base unit is required per four substrate units, thus requiring significantly lower quantities of these pyrophoric metallation reagents and making it a more atom economical reaction.

4.2.2 Solution studies of 18

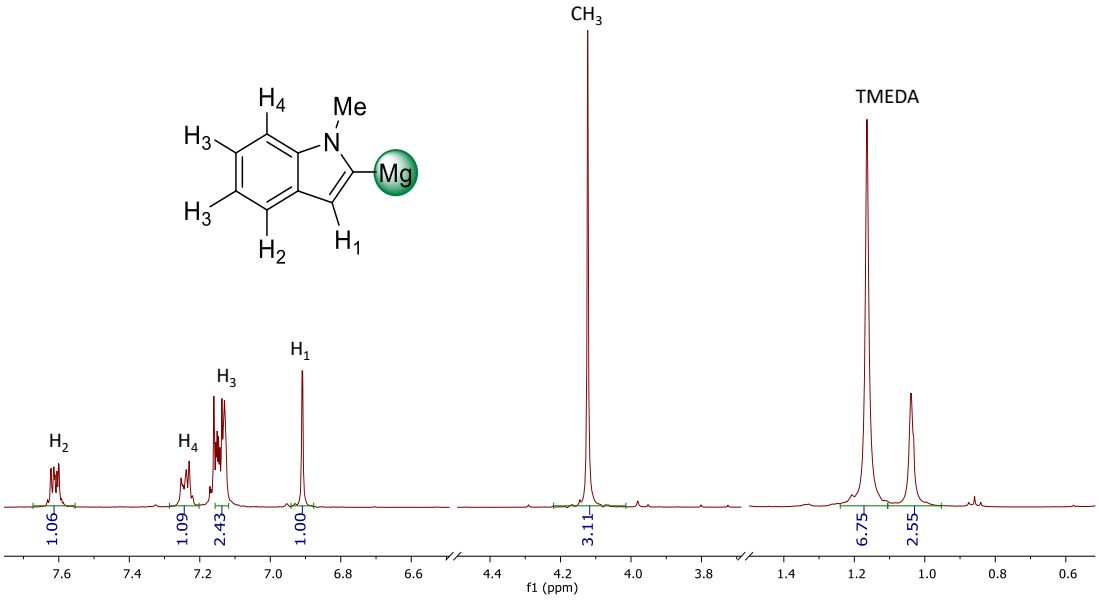

Figure 4.5: ^{1}H NMR spectrum of complex **18** in C_6D_6 at 298 K

Crystalline complex **18** was dissolved in C_6D_6 and analysed by ^{1}H and $^{13}C\{^{1}H\}$ NMR spectroscopy (see Figure 4.5). In support of the crystal structure, the NMR spectrum shows only α substituted N-methylindole in a 2:1 ratio with TMEDA. The disappearance of two doublet signals in the aromatic region of the proton spectrum corresponding to the parent indole, and the appearance of a singlet at 6.53 ppm are indicative of an α-substituted *N*-methylindole unit. A large down field chemical shift for the alpha carbon ^{13}C resonance to 180.39 ppm (from 129.05 ppm in the parent *N*-methylindole are indicative of a magnesiation occurring.

4.2.3 Electrophilic quenching studies of 18

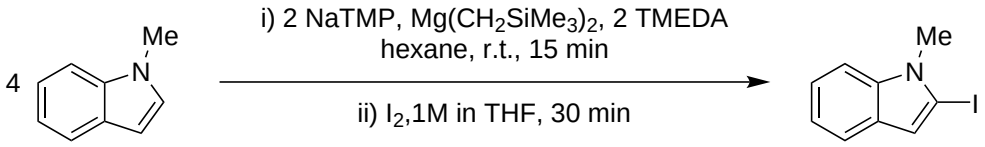

Scheme 4.13: Electrophilic quench of **18** with iodine, to give the α- iodinated species *N*-methyl-2-iodo-indole

To investigate the synthetic utility of the newly formed Mg-C bond in **18**, its use in *in situ* iodolysis and Pd-catalysed cross-coupling reactions were explored. In a one pot procedure, both the expected *N*-methyl-2-iodoindole and *N*-methyl-2-phenylindole were isolated in high unoptimised yields (79 % for iodolysis, 82 % for cross-coupling, see Scheme 4.13 and Scheme 4.14).

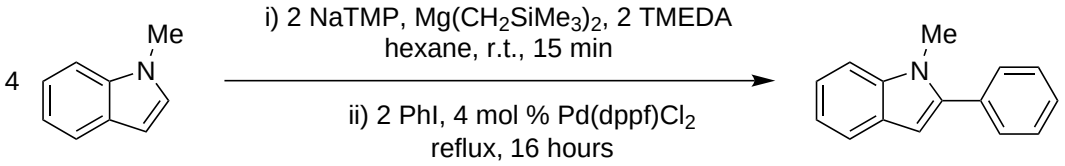

Scheme 4.14: Use of the magnesiated species $[(\mathrm{Na}\cdot\mathrm{TMEDA})_2\mathrm{Mg}(\alpha{-}\mathrm{C_9H_8N})_4]$, **18** in palladium catalysed cross coupling with iodobenzene to yield *N*-methyl-2-phenylindole

4.3 Reaction of magnesiate base 1 with *N*-ethylindole

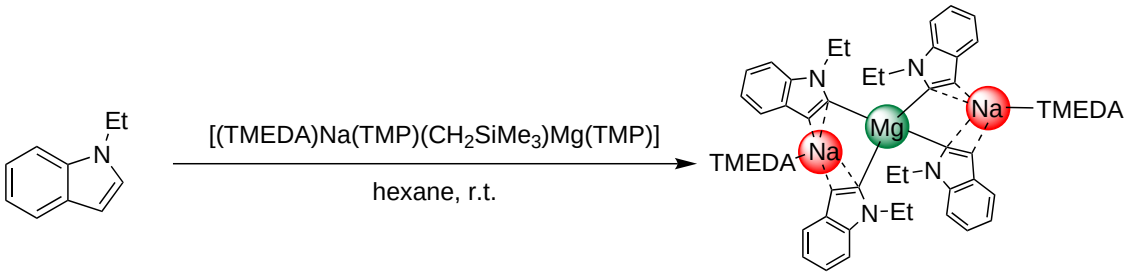

Scheme 4.15: Synthesis of complex **20**, $[(\mathrm{Na}\cdot\mathrm{TMEDA})_2\mathrm{Mg}(\alpha{-}\mathrm{C_{10}H_{10}N})_4]$

Reacting a hexane solution of the base **1** with one molar equivalent of *N*-ethylindole resulted in the deposition of a large quantity of white precipitate after approximately five minutes (Scheme 4.15). The solid was isolated by filtration, washed with *n*-hexane and transferred to a glovebox for storage. On one repeat synthesis, the solid was recrystallised from toluene to yield large, colourless crystals suitable for single crystal X-ray diffraction and were found to be the compound $[(\mathrm{Na}\cdot\mathrm{TMEDA})_2\mathrm{Mg}(\alpha{-}\mathrm{C_{10}H_{10}N})_4]$ **20**. Similarly to complex **18**, this reactivity appears to be the result of a different *in situ* active species. The rational synthesis of **20** was achieved similarly to **18**, where NaTMP, $\mathrm{Mg(CH_2SiMe_3)_2}$ and TMEDA were reacted in a 2:1:2 ratio with four equivalents of *N*-ethylindole (see Scheme 4.16).

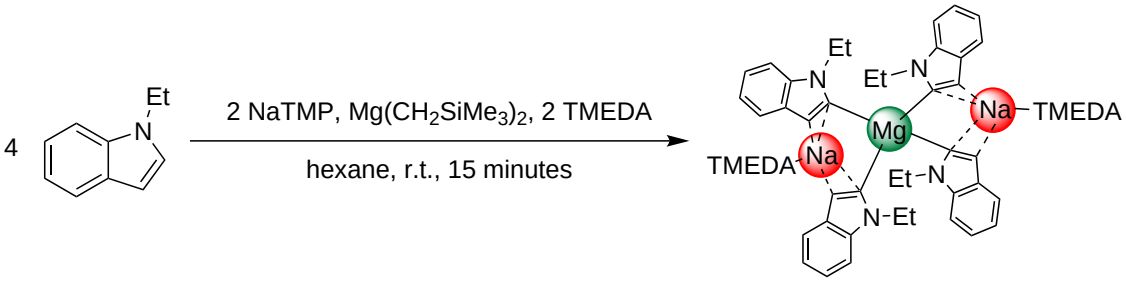

Scheme 4.16: Rational synthesis of complex $[(\mathrm{Na}\cdot\mathrm{TMEDA})_2\mathrm{Mg}(\alpha{-}\mathrm{C_{10}H_{10}N})_4]$, **20**

4.3.1 Solid state analysis of complex 20

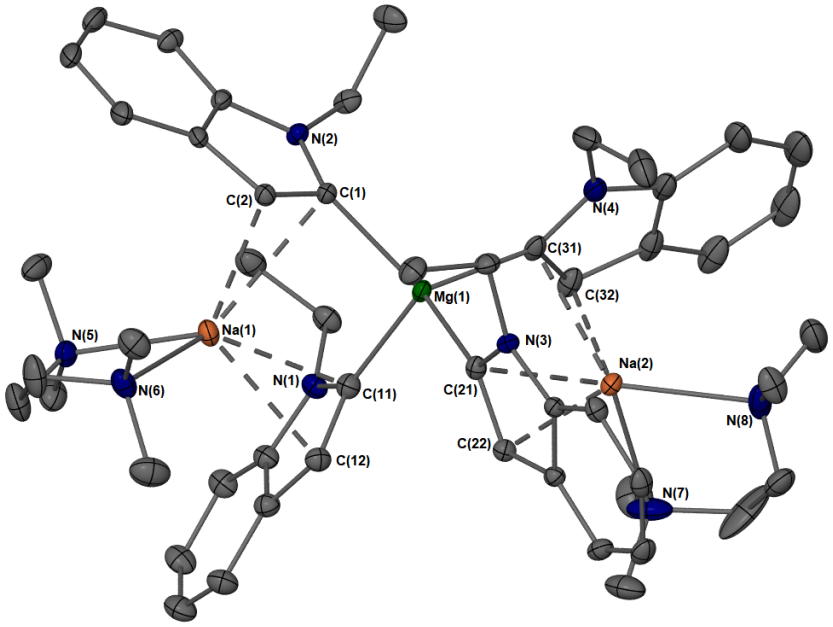

Figure 4.6: Molecular structure of **20**, $[(\mathrm{Na}\cdot\mathrm{TMEDA})_2\mathrm{Mg}(o{-}\mathrm{C_9H_8N})_4]$. Thermal ellipsoids shown at 40 % probability. Hydrogen atoms omitted for clarity. Selected bond lengths (Å) and angles (°): Mg(1)-C(1), 2.2086(16); Mg(1)-C(11), 2.2120(18); Mg(1)-C(21), 2.2331(16); Mg(1)-C(31), 2.2377(17); Na(1)-C(1), 2.9184(17); Na(1)-C(2), 2.6993(17), Na(1)-C(11), 2.6905(18); Na(1)-C(12), 2.7420(18); Na(2)-C(21), 2.8580(17); Na(2)-C(22), 2.6159(17); Na(2)-C(31), 2.6492(18); Na(2)-C(32), 2.7225(18); C(1)-Mg(1)-C(11), 102.76(6); C(1)-Mg(1)-C(21), 119.67(6); C(1)-Mg(1)-C(31), 116.16(6); C(11)-Mg(1)-C(21), 102.00(6); C(11)-Mg(1)-C(31), 112.06(7); C(21)-Mg(1)-C(31), 103.46(6).

Essentially isostructural to **18**, complex **20** contains a central distorted tetrahedral (mean bond angle 109.34 °) magnesium atom bonded to four separate α-magnesiated indole substitutents [C(1), C(11), C(21) and C(31)] with an average Mg-C bond length 2.222 Å. Each sodium atom in **20** makes electrostatic η^2-interactions with the 2-C and 3-C atoms of

each deprotonated indole unit [range of lengths Na-C: 2.6159(17)-2.9184(17) Å]. Each sodium atoms coordination sphere is completed by a complexed bidentate molecule of TMEDA making the sodium atoms overall six coordinate.

4.3.2 Solution studies of complex 20

Crystalline complex **20** was dissolved in C_6D_6 and analysed by ^{1}H and $^{13}C\{^{1}H\}$ NMR spectroscopy (Figure 4.7). In support of the crystal structure, the NMR spectrum shows only an *alpha*substituted *N*-ethylindole in a 2:1 ratio with TMEDA. The disappearance of two doublet signals in the aromatic region of the proton spectrum corresponding to the parent indole at 6.54 and 6.68 ppm, and the appearance of a singlet at 6.53 ppm are indicative of an α-substituted *N*-ethylindole unit. A large down field chemical shift for the *alpha* carbon ^{13}C resonance to 181.49 ppm (from 126.5 ppm in the parent *N*-ethylindole are indicative of a magnesiation occurring.

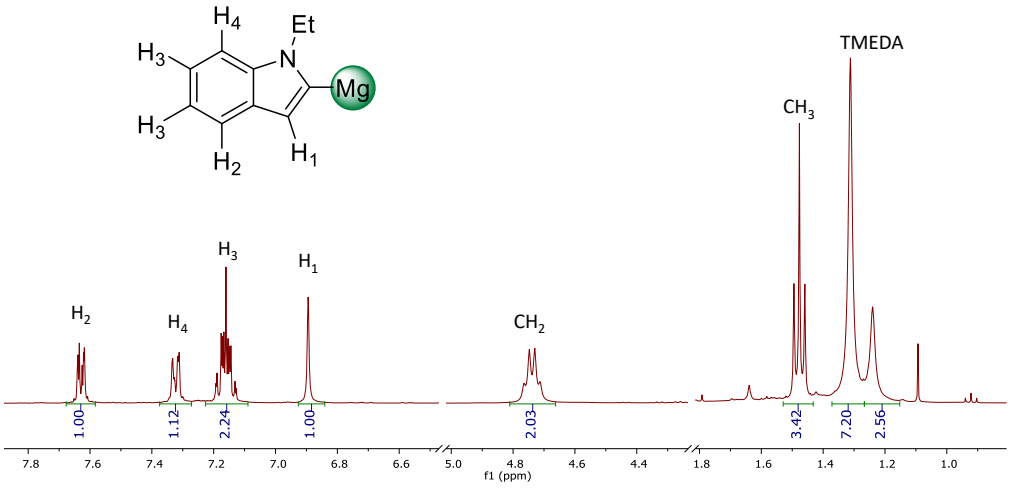

Figure 4.7: ^{1}H NMR spectrum of complex **20** in C_6D_6 at 298 K

4.3.3 Electrophilic quenching studies of complex 20

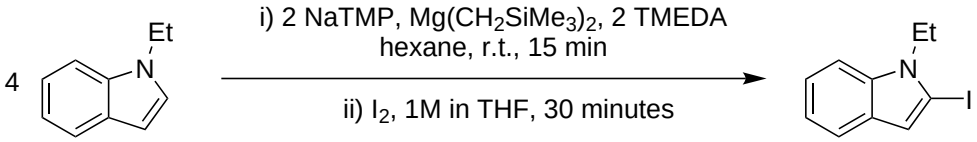

Scheme 4.17: Electrophilic quench of **20** with iodine, to give the α- iodinated species *N*-ethyl-2-iodo-indole

To investigate the synthetic utility of the newly formed Mg-C bond in **20**, its use in *in situ* iodolysis and Pd-catalysed cross-coupling reactions were explored. In a one pot procedure, both the expected *N*-ethyl-2-iodoindole and *N*-ethyl-2-phenylindole were isolated in high unoptimised yields (66 % for iodolysis, 68 % for cross-coupling, see Scheme 4.17 and Scheme 4.18 respectively).

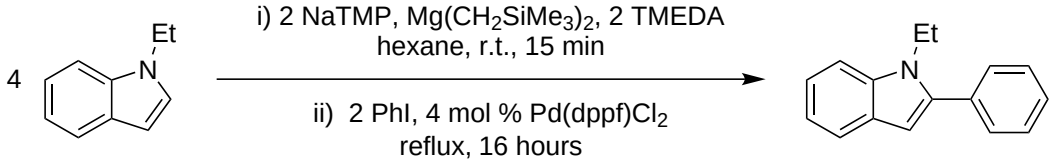

Scheme 4.18: Use of the magnesiated species $[(\mathrm{Na}\cdot\mathrm{TMEDA})_2\mathrm{Mg}(\alpha{-}\mathrm{C_{10}H_{10}N})_4]$, **20** in palladium catalysed cross coupling with iodobenzene to yield *N*-ethyl-2-phenylindole

4.4 Reaction of magnesiate base 1 with *N*-isopropylindole

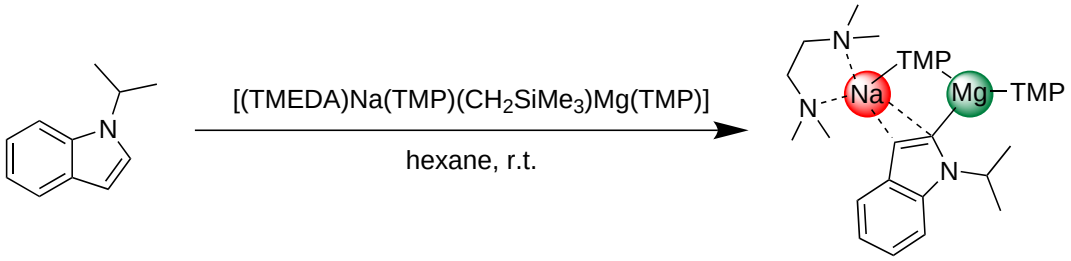

Scheme 4.19: Synthesis of complex **21**, $[(\mathrm{TMEDA})\mathrm{Na}(\mathrm{TMP})(\alpha{-}\mathrm{C_{11}H_{12}N})\mathrm{Mg}(\mathrm{TMP})]$

Increasing the steric bulk further on the indole substrate, *N*-isopropylindole was next investigated. To a stirred hexane solution of the magnesiate base **1**, freshly distilled *N*-isopropylindole was added dropwise at room temperature (Scheme 4.19). After stirring

overnight, a large amount of white precipitate had formed. This was isolated by filtration and transferred to a glovebox for storage. The mother-liquor deposited colourless, block crystals overnight when stored at -30°C. These were suitable for X-ray crystallographic analysis and found to be the compound [(TMEDA)Na(TMP)($\alpha-C_3H_7NC_8H_5$)Mg(TMP)] **21** (Scheme 4.19). Both the crystalline material and the solid precipitate were found to be the same complex by ^{1}H-NMR spectroscopy.

4.4.1 Solid state studies of complex 21

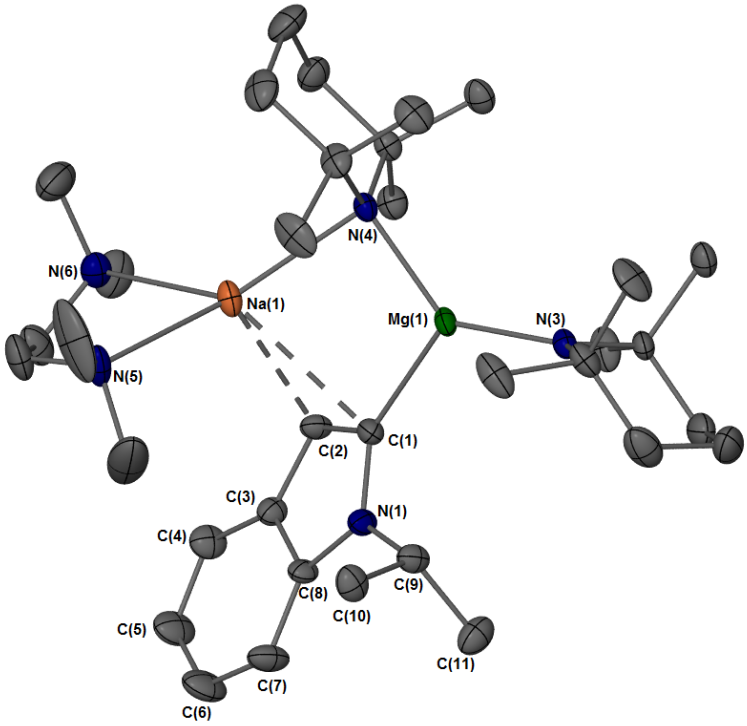

Figure 4.8: Molecular structure of [(TMEDA)Na(TMP)($\alpha-C_{11}H_{12}N$)Mg(TMP)], **21**. Thermal ellipsoids shown at 40 % probability. Hydrogen atoms omitted for clarity. Only one of two essentially the same molecules is shown. Selected bond lengths (Å) and angles (°): Mg(1)-C(1), 2.192(4); Mg(1)-N(4), 2.070(3); Mg(1)-N(3), 2.009(3); Na(1)-N(4), 2.464(3); Na(1)-N(5), 2.499(4); Na(1)-N(6), 2.457(4); Na(1)-C(1), 2.857(4); Na(1)-C(2), 2.646(4); C(1)-Mg(1)-N(3), 121.72(15); N(3)-Mg(1)-N(4), 133.32(14); N(4)-Mg(1)-C(1), 104.94(15).

Complex **21** has two crystallographically independent molecules in its unit cell. As these are nearly identical, only one is shown (Figure 4.8). The molecular structure of **21** includes a central trigonal planar magnesium atom, bonding to a bridging TMP, terminal TMP, as well as bonding to the *N*-isopropylindole in the α position (C(1)-Mg(1) bond distance

2.192(4) Å). The sodium atom is interacting electrostatically with both the C(1) and C(2) of the *N*-isopropylindole molecule, as indicated by the Na-C bond lengths of 2.857(4) and 2.646(4) Å respectively. The loss of the CH_2SiMe_3 substituent of the base **1** indicates that this is a product of alkyl basicity.

4.4.2 Solution state studies of complex 21

Crystalline compound **21** was dissolved in C_6D_6 and analysed by ^{1}H and ^{13}C NMR spectroscopy (Figure 4.9). The solution state structure is consistent with the solid state structure. Once again, the disappearance of two doublet signals at 6.57 and 6.88 ppm and the appearance of a singlet further upfield at 6.21 ppm is indicative of loss the α proton. It is evident that TMP and TMEDA are present in solution. In the ^{13}C-NMR spectrum, the large down field shifts for the alpha-carbon to 178.79 ppm (compared to 123.0 ppm in *N*-isopropylindole) is indicative of a newly formed magnesium-carbon bond.

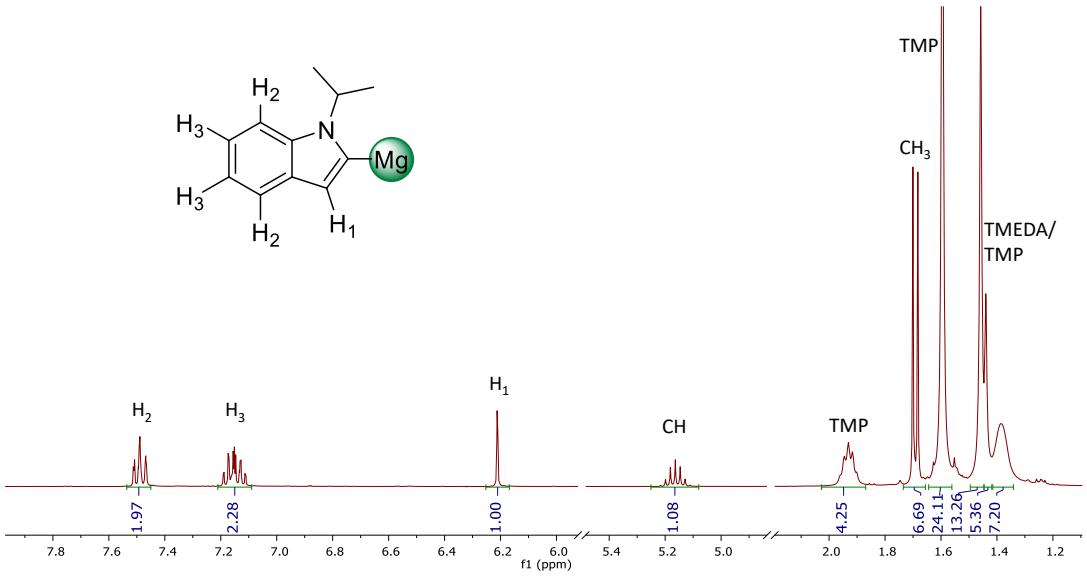

Figure 4.9: ^{1}H NMR spectrum of complex **21** in C_6D_6 at 298 K

4.4.3 Electophilic quenching studies of complex 21

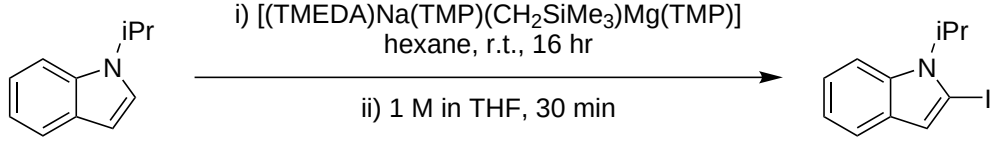

Scheme 4.20: Electrophilic quench of [(TMEDA)Na(TMP)($\alpha-C_{11}H_{12}N$)Mg(TMP)], complex **21** with iodine, to give the α- iodinated species *N*-isopropyl-2-iodo-indole

To investigate the synthetic utility of the newly formed Mg-C bond in **21**, its use in *in situ* iodolysis and Pd-catalysed cross-coupling reactions were explored. In a one pot procedure, both the expected *N*-isopropyl-2-iodoindole and *N*-isopropyl-2-phenylindole were isolated in high unoptimised yields (78 % for iodolysis, 71 % for cross-coupling, see Scheme 4.20 and Scheme 4.21 respectively).

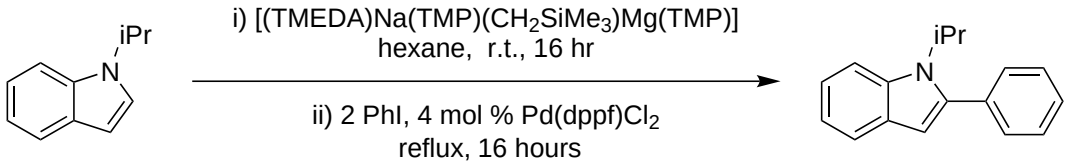

Scheme 4.21: Use of the magnesiated species **21** in palladium catalysed cross coupling with iodobenzene to yield *N*-isopropyl-2-phenylindole

4.5 Synthesis of *N*-alkyl-3-methyl-indoles

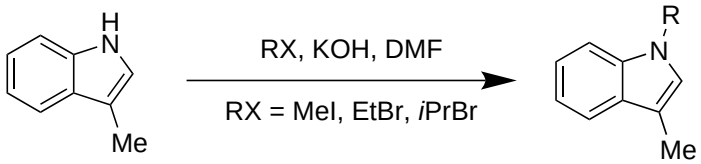

Scheme 4.22: Synthesis of *N*-alkyl-3-methyl-indoles

The 3-substituted indoles *N*,3-dimethylindole, *N*-ethyl-3-methyl-indole and *N*-isopropyl-3-methyl-indole were synthesised by the addition of RX (Me = MeI, Et = EtBr, iPr = iPrBr) to a stirred solution of 3-methyl-1*H*-indole and potassium hydroxide in DMF (see

Scheme 4.22). The reaction was monitored by TLC, and once full consumption of 3-methyl-1*H*-indole was observed the reaction was quenched with H_2O. Following organic work-up, the synthesised *N*-substituted indoles were purified by vacuum distillation and stored over 4 Å molecular sieves. In the case of *N*-isopropyl-3-methyl-indole, complete conversion was not achieved and the product was purified by flash column chromatography (silica gel, 10 % EtOAc/petroleum benzine).

4.6 Reaction of magnesiate base 1 with *N*-3-dimethylindole

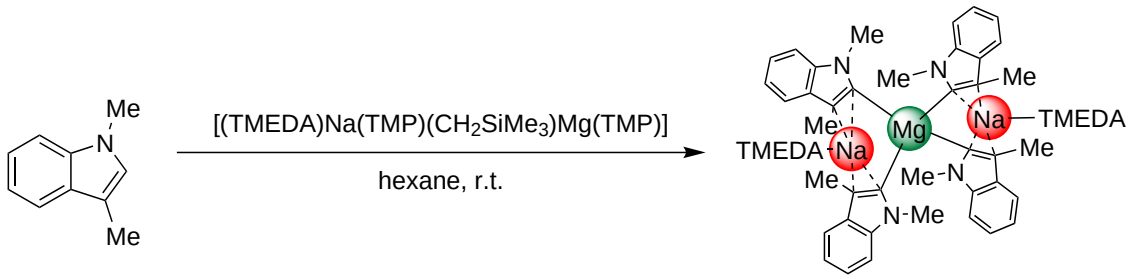

Scheme 4.23: Synthesis of $[(Na \cdot TMEDA)_2Mg(\alpha{-}C_{10}H_{11}N)_4]$, complex **22**

To a hexane solution of **1**, a molar equivalent of *N*,3-dimethylindole was added dropwise at room temperature. This resulted in a large quantity of white precipitate after approximately five minutes (Scheme 4.23). This solid was isolated, and dissolved in C_6D_6 for ^1H and $^{13}C\{^1H\}$ NMR analysis. Similarly to compound **18**, the product was identified to be the higher order magnesiate $[(Na \cdot TMEDA)_2Mg(\alpha{-}C_{10}H_{11}N)_4]$ **22**.

Indeed, the rational synthesis of **22** was achieved by reacting NaTMP, $Mg(CH_2SiMe_3)_2$ and TMEDA in a 2:1:2 ratio with four equivalents of *N*,3-dimethylindole (Scheme 4.24). Upon hot filtration, crystals were grown from the mother-liquor at room temperature overnight. These crystals were analysed by single crystal X-ray diffraction and found to be the expected compound $[(Na \cdot TMEDA)_2Mg(\alpha{-}C_{10}H_{11}N)_4]$.

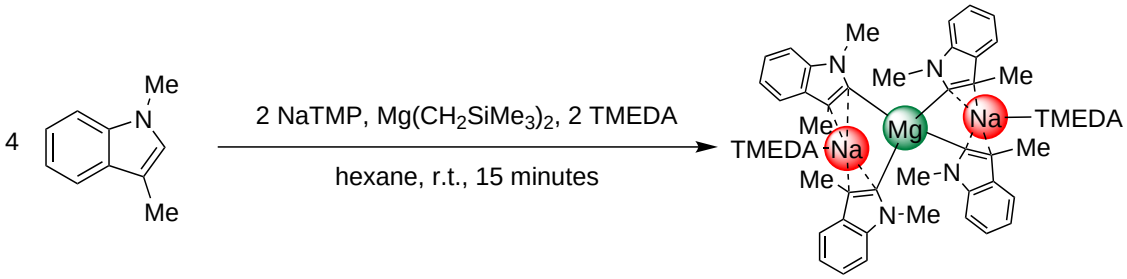

Scheme 4.24: Rational synthesis of complex **22**

4.6.1 X-ray crystallographic analysis of complex 22

Single crystals of **22** were grown from a saturated *n*-hexane solution stored at room temperature. These were suitable for single crystal X-ray diffraction studies, and were found to be the complex $[(Na \cdot TMEDA)_2Mg(\alpha{-}C_{10}H_{11}N)_4]$. A similar structural motif to **18** and **20** is found. The molecular structure of **22** features a tetrahedral magnesium centre, bonding to four α - deprotonated *N,3*-dimethylindole units (Mg - C bond lengths range from 2.219(5) - 2.245(5) Å). The sodium atoms make close electrostatic interactions with the nitrogen as well as the α- and β- carbons from two different *N,3*-dimethylindole based units. The coordination environment of each sodium is completed by a bidentate, chelating TMEDA ligand.

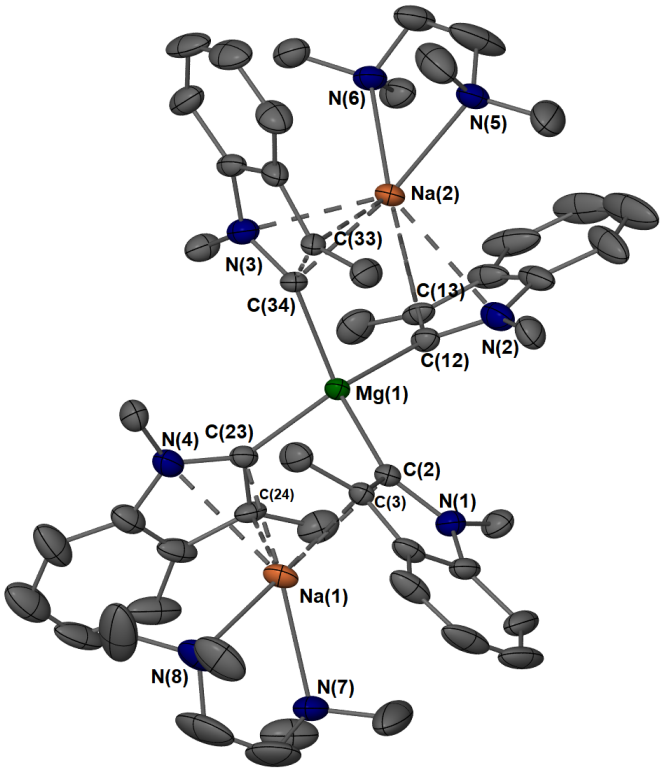

Figure 4.10: Molecular structure of **22**, $[(Na \cdot TMEDA)_2Mg(\alpha{-}C_9H_8N)_4]$. Thermal ellipsoids shown at 40 % probability. Hydrogen atoms and an ordered *n*-hexane solvent molecule omitted for clarity. Selected bond lengths (Å) and angles (°): Mg(1) - C(2), 2.245(5); Mg(1) - C(12), 2.233(5); Mg(1) - C(23), 2.223(5); Mg(1) - C(34), 2.219(5); Na(1) - C(2), 2.689(5); Na(1) - C(3), 2.866(6); Na(1) - C(24), 2.823(6); Na(1) - C(23), 2.688(5); Na(2) - N(2), 2.871(6); Na(2) - C(12), 2.734(5); Na(2) - C(13), 2.985(6); Na(2) - N(3), 2.783(5); Na(2) - C(34), 2.719(5); Na(2) - C(33), 3.110(6); C(2) - Mg(1) - C(12), 111.59(19); C(2) - Mg(1) - C(23), 100.55(18); C(2) - Mg(1) - C(34), 117.1(2); C(12) - Mg(1) - C(34), 98.92(19); C(12) - Mg(1) - C(23), 118.2(2); C(23) - Mg(1) - C(34), 111.36(19).

4.6.2 Solution state studies of complex 22

Compound **22** was dissolved in C_6D_6 and analysed by ^1H and ^{13}C NMR spectroscopy. On examination of the ^1H NMR spectrum (see Figure 4.11), it becomes clear that the $N{-}CH_3$ and the $C{-}CH_3$ groups are disordered throughout the crystal structure, giving rise to multiple CH_3 species resent in the 2.70 - 3.00 ppm (for $C{-}CH_3$) and 3.90 - 4.30 ppm (for $N{-}CH_3$) ranges. Otherwise, protons assignable to the deprotonated indole moiety are present in a 2:1 ratio with TMEDA, indicating that the crystal structure is indicative of the solution state species. The disappearance of a doublet at 6.33 ppm is indicative

of an α-deprotonation occurring. In the ^{13}C NMR spectrum, the appearance of a singlet downfield at 179.68 ppm is indicative of the newly formed Mg-C bond.

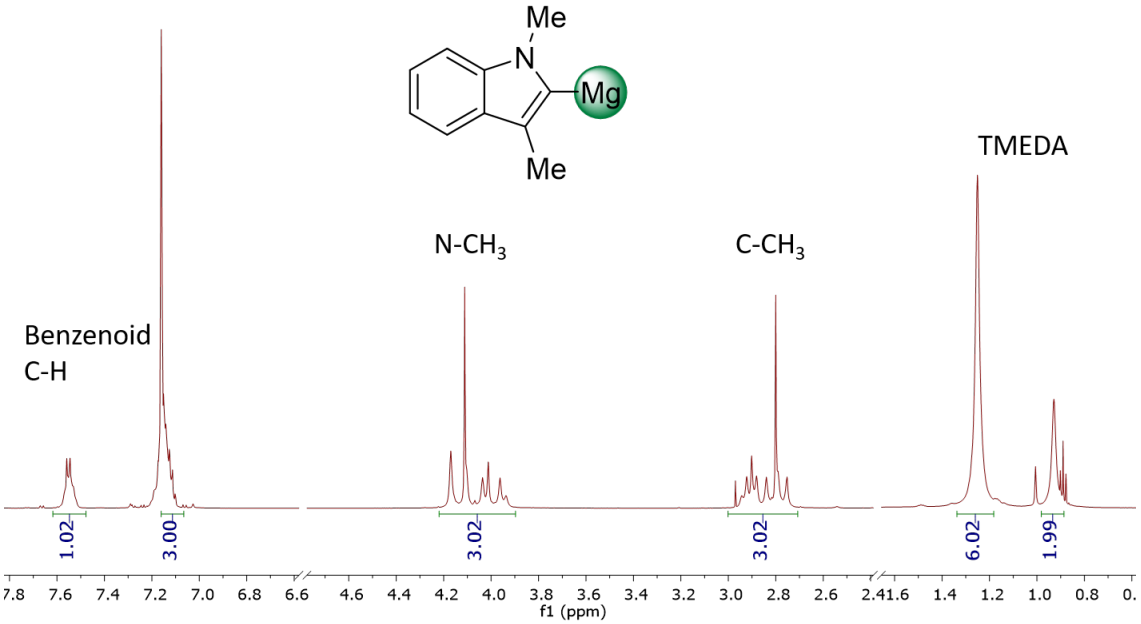

Figure 4.11: ^{1}H NMR spectrum of **22** in C_6D_6 at 298 K

To confirm the multiple signals related to the N$-$CH$_3$ and the C$-$CH$_3$ groups are infact a solution state, fluctional behaviour, a ^{1}H-^{1}H-NOESY spectrum was obtained (see Figure 4.12). The presence of off-diagonal negative NOE peaks in the NOESY spectrum indicated that these signals are interchanging.

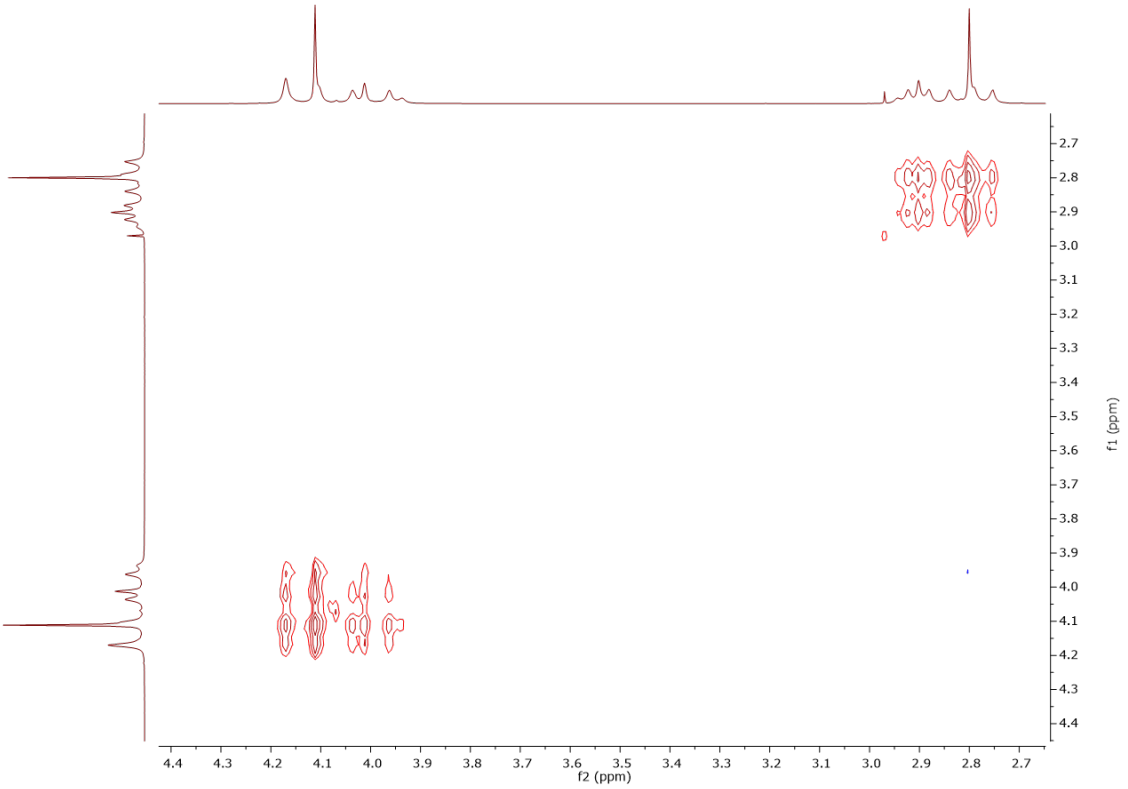

Figure 4.12: ^{1}H-^{1}H NOESY NMR spectrum of **22** in C_6D_6

Complex **22** can be quenched *in situ* with a THF solution of iodine to produce the expected *N*,3-dimethyl-2-iodo-1*H*-indole in a high yield of 89 % as a crystalline solid (see Scheme 4.25).

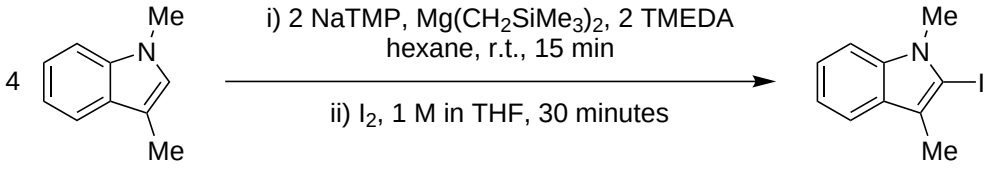

Scheme 4.25: Electrophilic quench of **22** with iodine

4.7 Reaction of magnesiate base 1 with *N*−ethyl−3−methyl−1*H*−indole

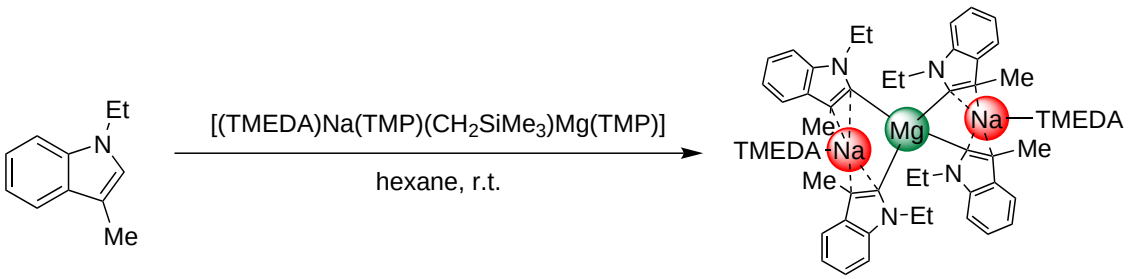

Scheme 4.26: Initial synthesis of $[(\mathrm{Na}\cdot\mathrm{TMEDA})_2\mathrm{Mg}(\alpha{-}\mathrm{C}_{11}\mathrm{H}_{13}\mathrm{N})_4]$, complex **23**

To a hexane solution of **1**, a molar equivalent of *N*,3-ethylindole was added dropwise at room temperature (see Scheme 4.26). This resulted in a large quantity of white precipitate after approximately five minutes. This solid was isolated, and dissolved in C_6D_6 for ^{1}H and ^{13}C$\{^1$H$\}$ NMR analysis. Similarly to compound **18**, the product was identified to be the higher order magnesiate $[(\mathrm{Na}\cdot\mathrm{TMEDA})_2\mathrm{Mg}(\alpha{-}\mathrm{C}_{11}\mathrm{H}_{13}\mathrm{N})_4]$ **23** by NMR spectroscopy. Unfortunately, growing single crystals proved difficult - however the complex could be positively identified by solution state analysis.

Scheme 4.27: Rational synthesis of $[(\mathrm{Na}\cdot\mathrm{TMEDA})_2\mathrm{Mg}(\alpha{-}\mathrm{C}_{11}\mathrm{H}_{13}\mathrm{N})_4]$, complex **23**

The rational synthesis of **23** was achieved by reacting NaTMP, $Mg(CH_2SiMe_3)_2$ and TMEDA in a 2:1:2 ratio with four equivalents of *N*-ethyl-3-methylindole (Scheme 4.27).

4.7.1 Solution state studies of complex 23

Complex **23** was dissolved in C_6D_6 and analysed by ^{1}H and ^{13}C NMR spectroscopy. The disappearance of a singlet at 6.46 ppm is indicative of the newly formed Mg-C bond. There

is an upfield shift of the N−CH_2 protons from 3.47 ppm to 4.74 ppm, the C−CH_3 protons from 2.31 ppm to 2.80 ppm, and the N−CH_3 protons from 0.92 ppm to 1.36 ppm. Signals are also evident for TMEDA, and overall the deprotonated indole species is in a 2:1 ratio with TMEDA, indicating that similar reactivity is observed as with **24**. In the ^{13}C-NMR spectrum, the appearance of a singlet downfield at 180.72 ppm is indicative of the newly formed Mg-C bond.

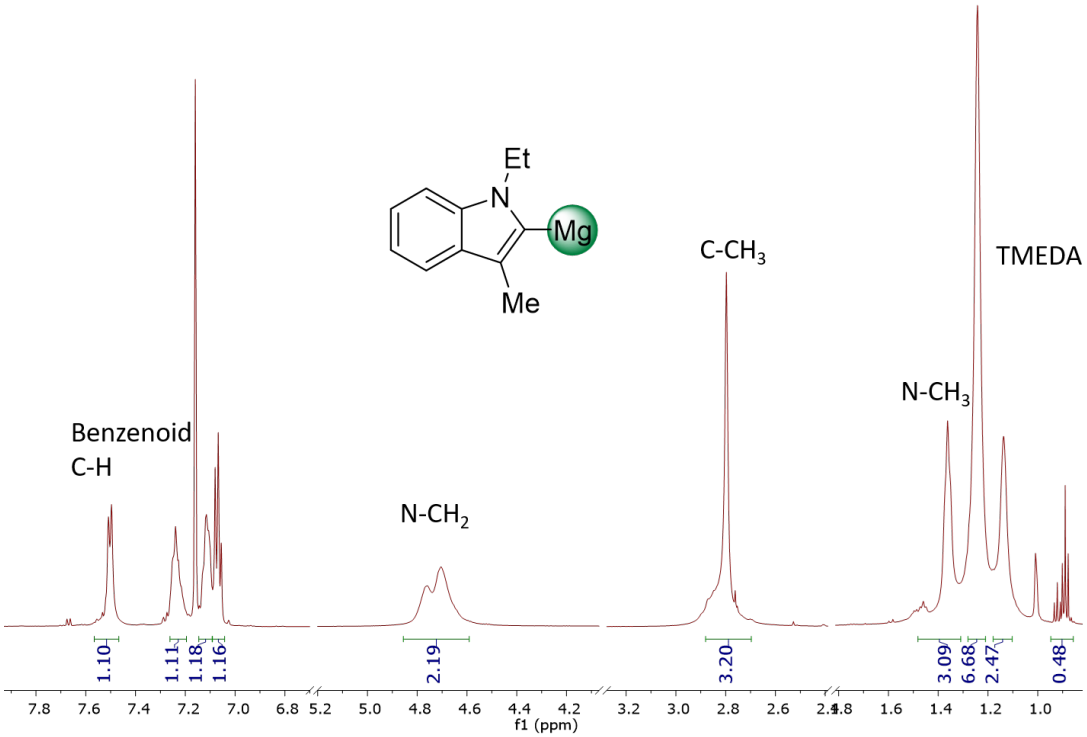

Figure 4.13: ^{1}H NMR spectrum of **23** in C_6D_6 at 298 K

Complex **23** can be quenched with a THF solution of iodine to produce the expected *N*-ethyl-2-iodo-3-methyl-1*H*-indole in a high yield of 84 % (see Scheme 4.28).

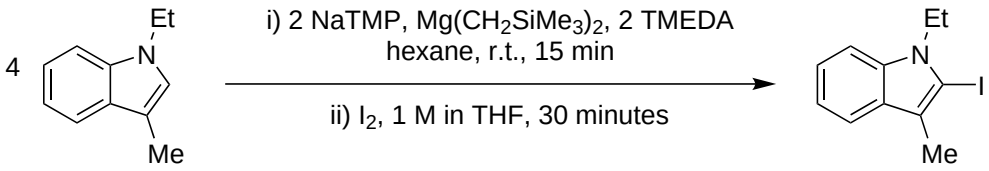

Scheme 4.28: Electrophilic quench of **23** with iodine

4.8 Reaction of magnesiate base 1 with N−isopropyl−3−methyl−1*H*−indole

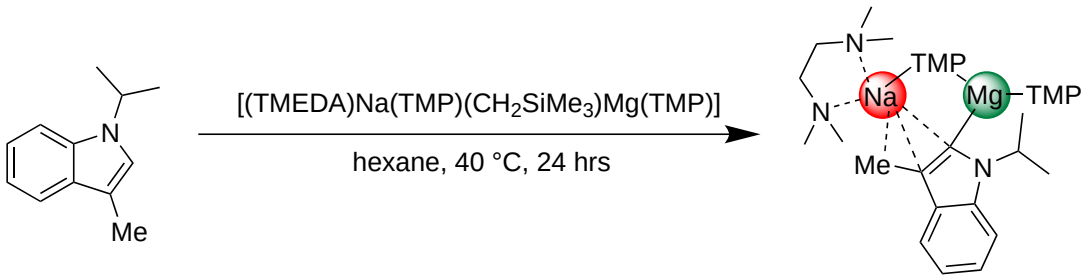

To a hexane solution of **1**, a molar equivalent of *N*-isopropyl-3-methyl-1*H*-indole was added dropwise at room temperature. The resulting solution was stirred overnight, before the solvent was removed *in vacuo* and the resulting oil transferred to a glovebox. The oil was dissolved in C_6D_6 and analysed by ^{1}H NMR spectroscopy. This indicated that while some α-magnesiation had occurred, a substantial quantity of the starting indole remained (approximately 20:80 product:starting material). In an attempt to push the reaction towards completion, the reaction was repeated and heated at 40 ° C overnight (24 hours), before the solvent was removed *in vacuo* and transferred to a glovebox. The resulting oil was dissolved in C_6D_6 and analysed by ^{1}H NMR spectroscopy. Heating this reaction led to a higher conversion (approximately 55:45 product:starting material, see Figure 4.14), however some starting material remained. Interestingly, crystals of the α-magnesiated species crystallised from C_6D_6 remaining in the Schlenk flask. These were analysed by single-crystal X-ray diffraction and found to be the expected α-magnesiated product [(TMEDA)Na(TMP)($\alpha-C_{12}H_{14}N$)Mg(TMP)] **24**.

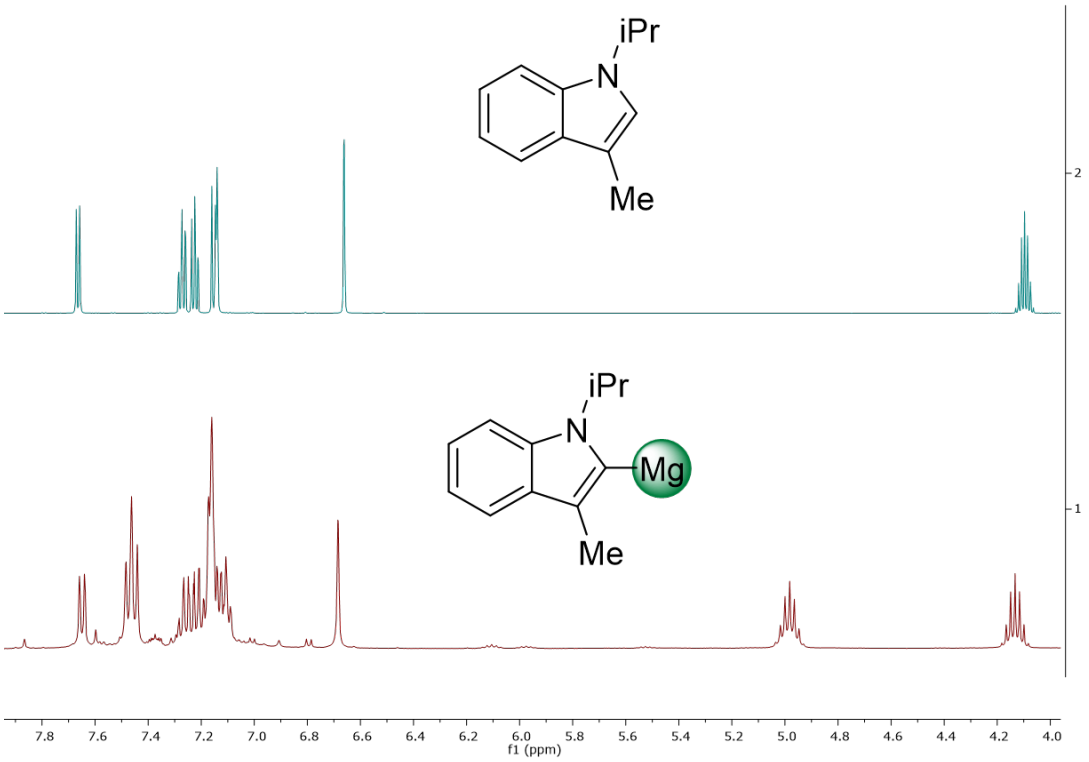

Figure 4.14: ^{1}H NMR spectrum of the oil obtained from heating at 40 ° C for 24 hours

4.8.1 Solid state studies of complex 24

The molecular structure of **24** features a trigonal planar magnesium atom, bonding to an α-deprotonated *N*-isopropyl-3-methyl-1*H*-indole unit (Mg - C bond length of 2.2158(17) Å), a terminal anionic TMP unit (Mg - N bond length of 2.0033(14) Å) and a bridging anionic TMP unit (Mg - N bond length of 2.0739(15) Å). This bridging unit connects to the other metal centre, a sodium atom (Na - N bond length of 2.5059(15) Å). The sodium atoms coordination environment is fulfilled with a bidentate, chelating TMEDA unit as well as making electrostatic interactions to the *alpha*- and *beta*- carbons of the *N*-isopropyl-3-methyl-1*H*-indole unit (Na - C bond lengths of 2.6930(17) and 2.9217(18) Å respectively), as well as the methyl group present on the C3 position (Na - C bond length of 2.979(2) Å). This can be seen as a magnesiation, as the magnesium atom lies essentially co-planar with the deprotonated *N*-isopropyl-3-methyl-1*H*-indole unit, in comparison to the sodium which is out of the plane, making interactions with the double bond system.

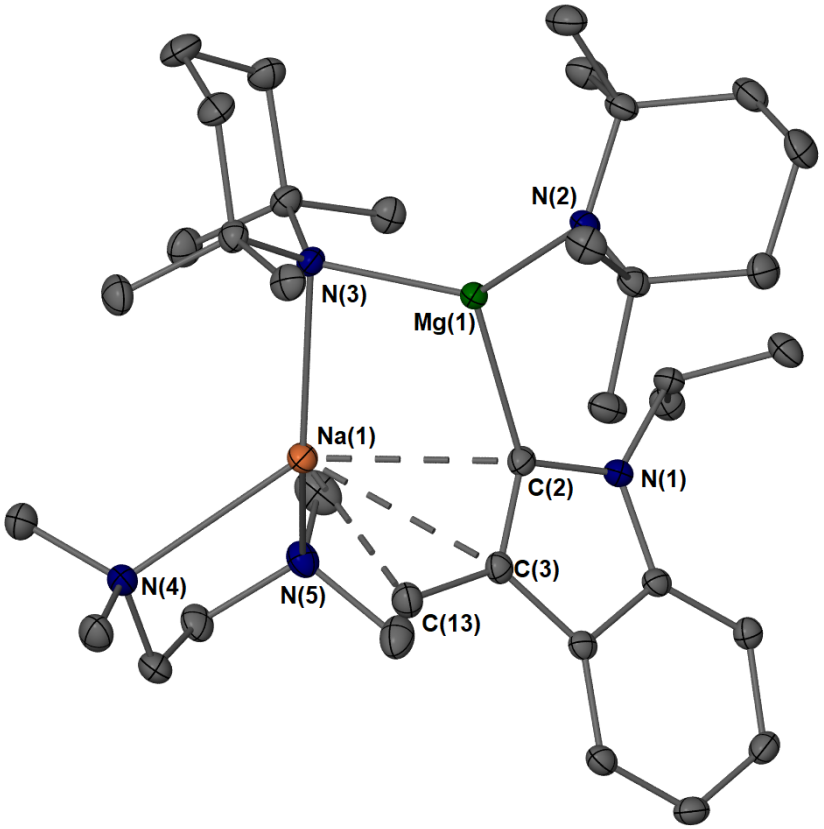

Figure 4.15: Molecular structure of [(TMEDA)Na(TMP)(α $-C_{12}H_{14}N$)Mg(TMP)], **24**. Thermal ellipsoids shown at 40 % probability. Hydrogen atoms omitted for clarity. Selected bond lengths (Å) and angles (°): Mg(1) - C(2), 2.2158(17); Mg(1) - N(2), 2.0033(14); Mg(1) - N(3), 2.0739(15); Na(1) - C(2), 2.6930(17); Na(1) - C(3), 2.9217(18); Na(1) - C(13), 2.979(2); Na(1) - N(3), 2.5059(15); C(2) - Mg(1) - N(2), 116.42(6); N(2) - Mg(1) - N(3), 135.68(6); N(3) - Mg(1) - C(2), 107.58(6); Na(1) - N(3) - Mg(1), 87.74(5).

4.8.2 Solution state studies of complex 24

A crystalline sample of **24** was dissolved in C_6D_6 and analysed by ^{1}H and $^{13}C\{^{1}H\}$ NMR spectroscopy. Unfortunately, trace amounts of the starting *N*-isopropyl-3-methyl-1*H*-indole were difficult to remove, however the peaks corresponding to the magnesiated species **24** can be clearly assigned. The isopropyl-CH signal is shifted downfield from 4.13 ppm to 4.98 ppm, the $C-CH_3$ from 2.32 ppm to 2.47 ppm and the *i*$Pr-CH_3$ from 1.02 ppm to 1.07 ppm. The lowering of the singlet at 6.66 ppm is indicative of an α-magnesiation occurring. In the ^{13}C NMR spectrum, a downfield shift of the $\alpha-CH_2$ to 174.80 ppm is indicative of a magnesiation occuring.

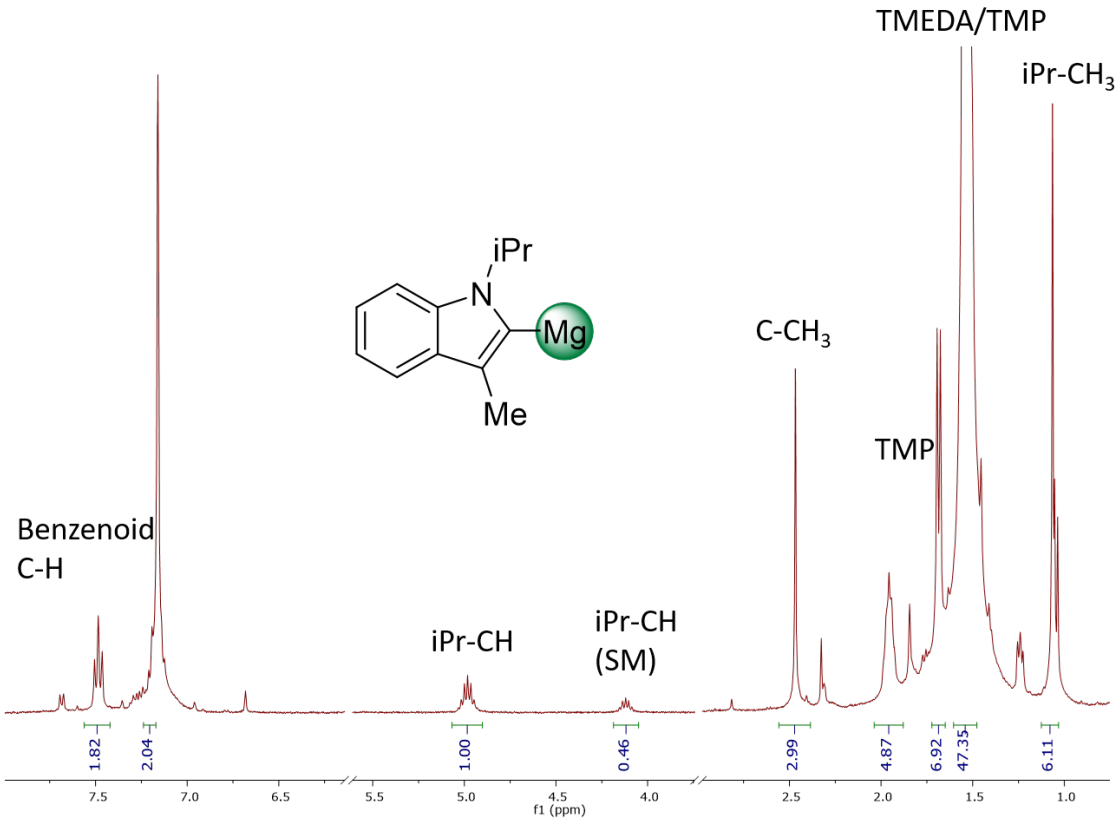

Figure 4.16: ^{1}H NMR spectrum of **24** in C_6D_6 at 298 K

The α-magnesiated species **24** can be utilised in *in situ* iodolysis by the addition of a THF solution of iodine, to produce the expected *N*-isopropyl-2-iodo-3-methyl-1*H*-indole in a moderate yield of 60 % (see Scheme 4.29).

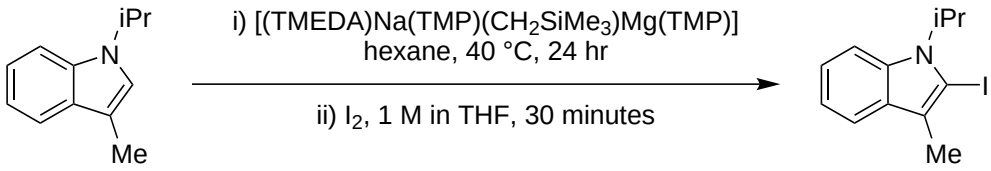

Scheme 4.29: Electrophilic quench of **24** with iodine

4.9 Synthesis of *N*-phenylindole

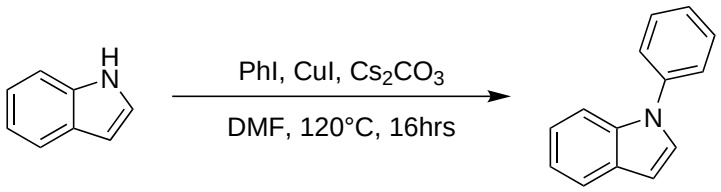

Scheme 4.30: Synthesis of *N*-phenylindole under Ullmann coupling conditions

The synthesis of *N*-phenylindole was achieved under Ullmann coupling conditions (see Scheme 4.30). One equivalent of 1*H*-indole was reacted with two equivalents of iodobenzene, in the presence of catalytic amounts of copper(I) iodide and caesium carbonate. The resulting suspension was heated to 120 ° C for 16 hours, before being diluted with diethylether and quenched with aqueous $NaHCO_3$. The organic layer was collected, dried and evaporated to leave a pale yellow oil. This oil was purified by flash column chromatography (silica gel, 5 % EtOAc/petroleum benzene) to yield *N*-phenyl-1*H*-indole in a high yield (80 %) as a pale yellow oil.

4.10 Reaction of magnesiate base 1 with N−phenylindole

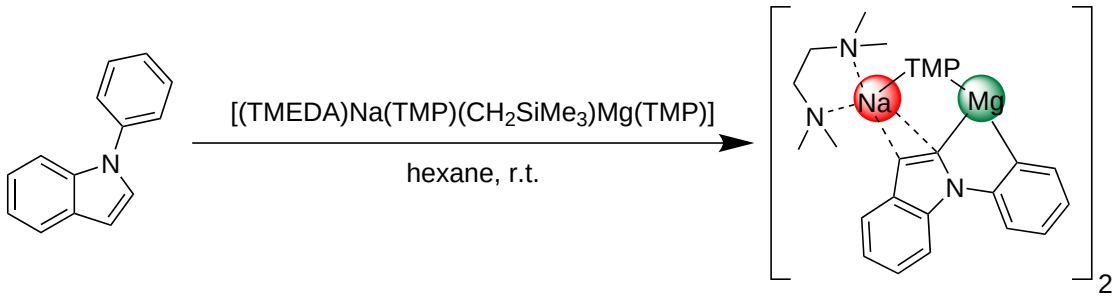

Scheme 4.31: Synthesis of [(TMEDA)Na(TMP)($\alpha-C_8H_5N-o-C_6H_4$)Mg]$_2$

To a stirred solution of the magnesiate base **1** in *n*-hexane was added a molar equivalent of *N*-phenyl-1*H*-indole at room temperature. The resulting solution was stirred overnight, leading to the deposition of a large quantity of a white precipitate. This solid was isolated by filtration, washed with *n*-hexane and dried *in vacuo*, before being transferred to a

glovebox for storage and analysis. On one repeat synthesis, the suspension was hot filtered, and the filtrate allowed to cool in a hot oil bath. This led to the deposition of a large crop of crystals, which were analysed by single-crystal X-ray diffraction to be the di-magnesiated complex [(TMEDA)Na(TMP)($\alpha-C_8H_5N-o-C_6H_4$)Mg]$_2$ **25**.

4.10.1 Solid state analysis of complex 25

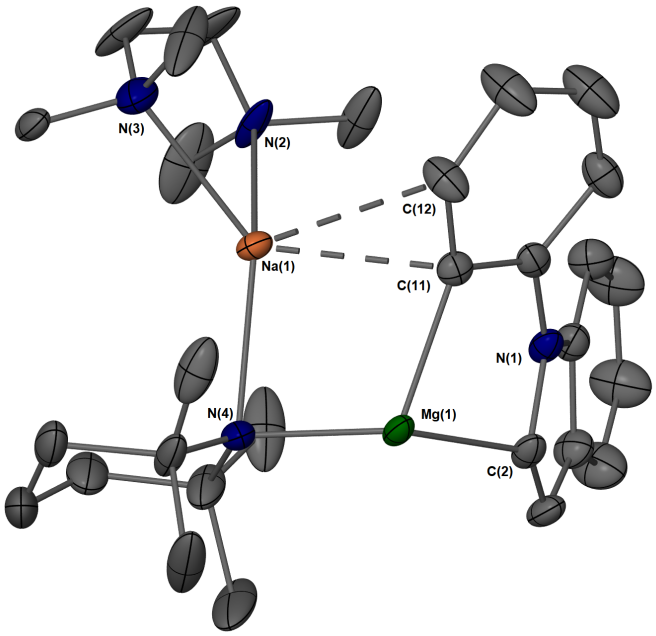

Figure 4.17: Molecular structure of complex **25**. Thermal ellipsoids shown at 40 % probability. Hydrogen atoms omitted for clarity. Selected bond lengths (Å) and angles (°): Mg(1) - C(2), 2.320(3); Mg(1) - C(11), 2.185(3); Mg(1) - N(2), 2.072(3); Na(1) - C(11), 2.658(3); Na(1) - C(12), 2.979(4); C(2) - Mg(1) - C(11), 80.42(12).

Complex **25** crystallises as a dimer, with the asymmetric unit shown in Figure 4.17 and the full molecular structure shown in Figure 4.18. It can be seen that the magnesium atom is bonding to both the α-position of the indole ring [Mg(1) - C(2) bond length 2.320(3) Å] and the *ortho*-position of the phenyl group [Mg(1) - C(11) bond length 2.185(3) Å]. In the full molecular structure, it can be seen that each magnesium atom is in a distorted tetrahedral environment, bridging between two deprotonated *N*-phenyl-1*H*-indole units. The magnesium lies within the plane of the phenyl ring, yet deviates from the plane of the indole ring. Each sodium atom makes electrostatic interactions with the deprotonated

ortho- and *meta*- position of the phenyl group [Na(1) - C bond lengths of 2.658(3) and 2.979(4) Å respectively], completing its coordination environment with a bridging TMP and a bidendate, chelating TMEDA.

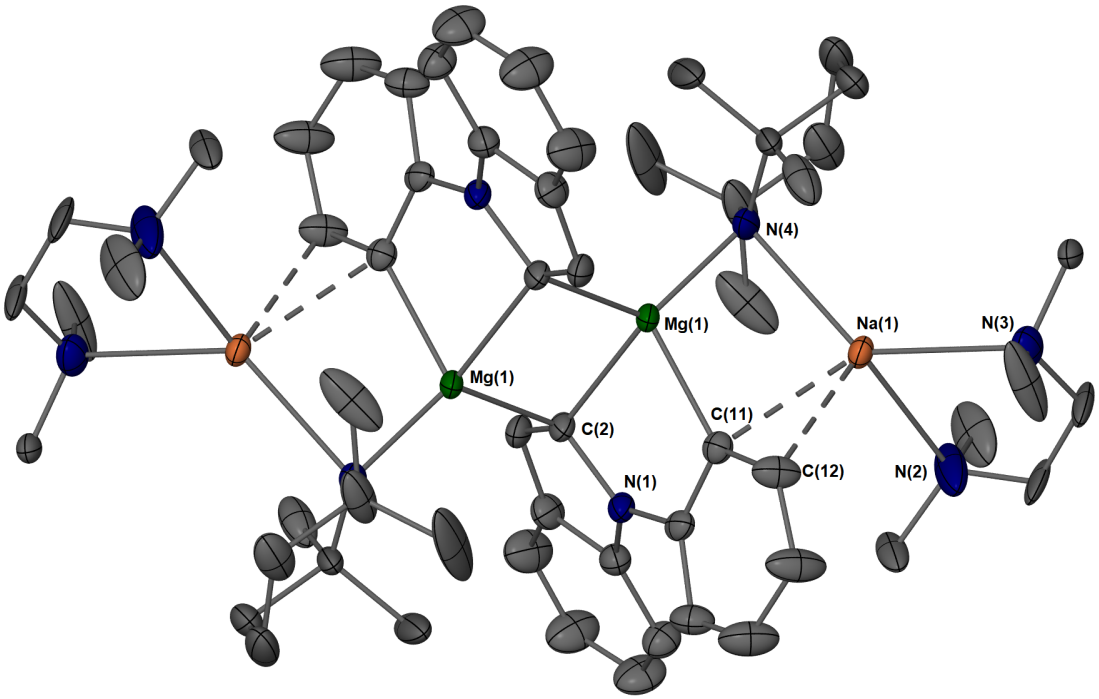

Figure 4.18: The full molecular structure of complex **25**. Thermal ellipsoids shown at 40 % probability. Hydrogen atoms omitted for clarity. Symmetry operator 1 - x, 1 - y, 1 - z.

4.10.2 Solution state analysis of 25

Crystalline complex **25** was dissolved in C_6D_6 and analysed by ^{1}H and ^{13}C NMR spectroscopy. Interestingly, this revealed that the dimeric species found in the solid state was non-equivalent in solution, leading to a doubling of all signals related to the dianionic *N*-phenyl-1*H*-indole based unit (see Figure 4.19 and Figure 4.20). This is presumably a solution state phenomenon, where each half of the dimeric species is slightly different, due to solvation effects. Signals relating to the TMP and TMEDA are also doubled. This doubling is also seen in the ^{13}C NMR spectrum (see Figure 4.21).

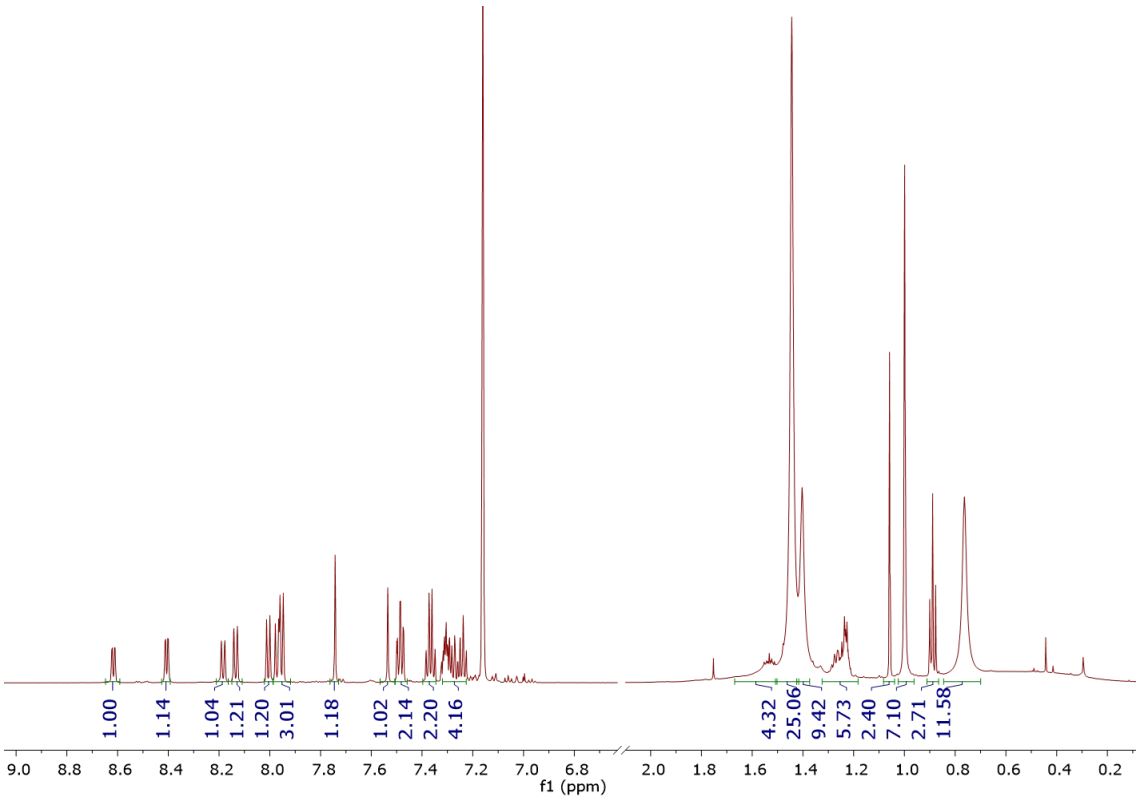

Figure 4.19: ^{1}H NMR spectrum of **25** in C_6D_6 at 298 K

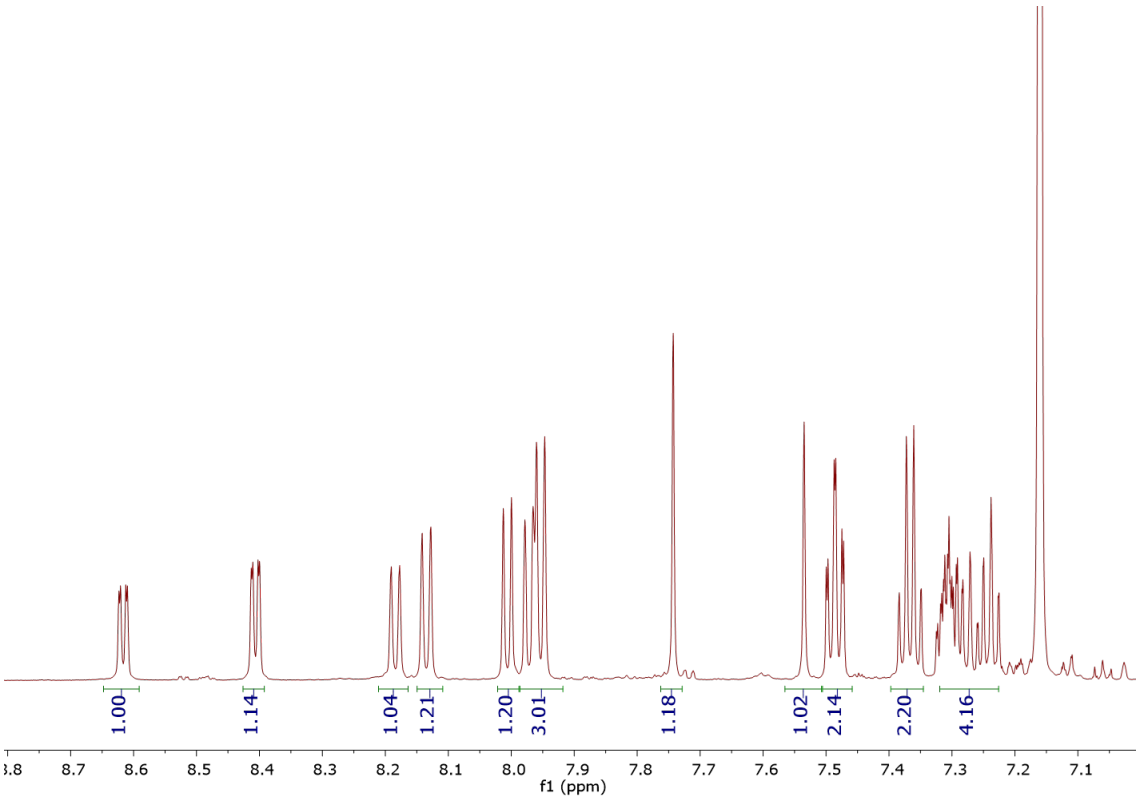

Figure 4.20: Aromatic region of the ^{1}H NMR spectrum of **25** in C_6D_6 at 298 K

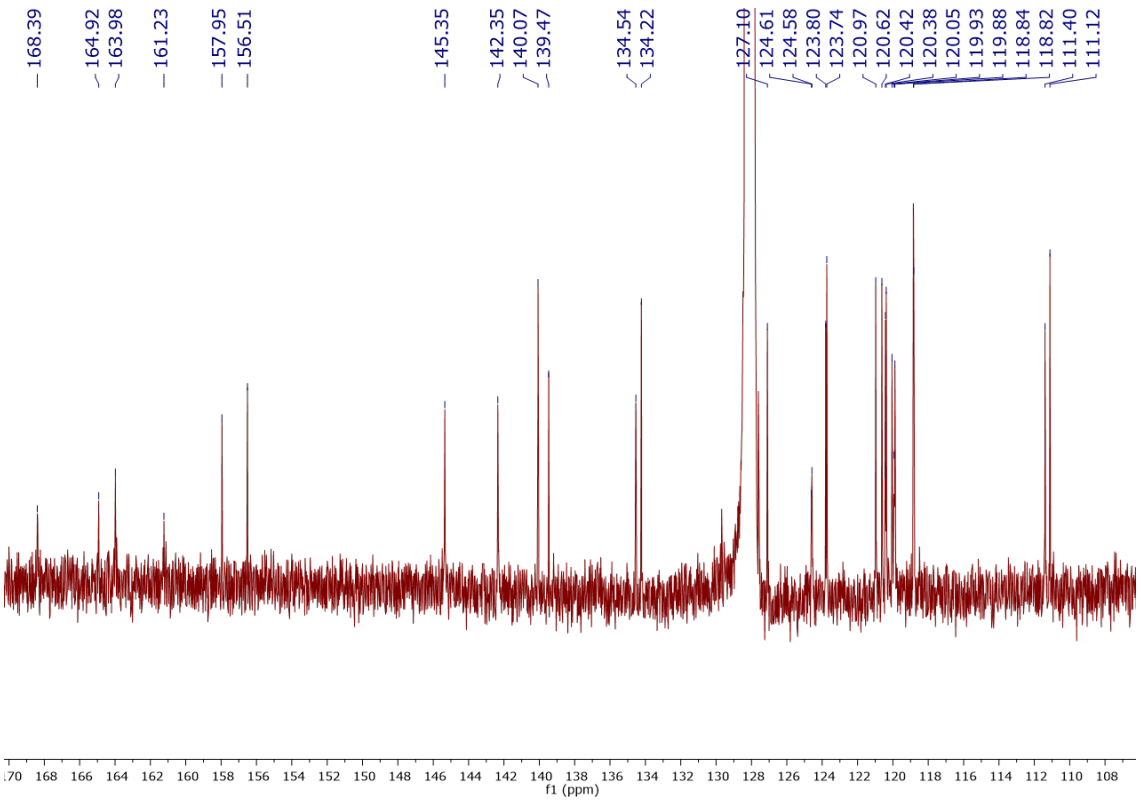

Figure 4.21: Aromatic region of the ^{13}C NMR spectrum of **25** in C_6D_6 at 298 K

When dissolved in d_8-THF, this collapses down to one set of signals (see Figure 4.22). The d_8-THF competitively binds to the sodium atoms, as evidenced by sharp signals observed for the TMEDA (see Figure 4.23). An appearance of a singlet at 6.42 ppm is indicative of the remaining C3-H. A complex multiplet from 6.70-6.79 ppm integrating to three protons and a multiplet at 6.91 - 6.97 ppm integrating to one proton are the residual protons left on the deprotonated phenyl group.

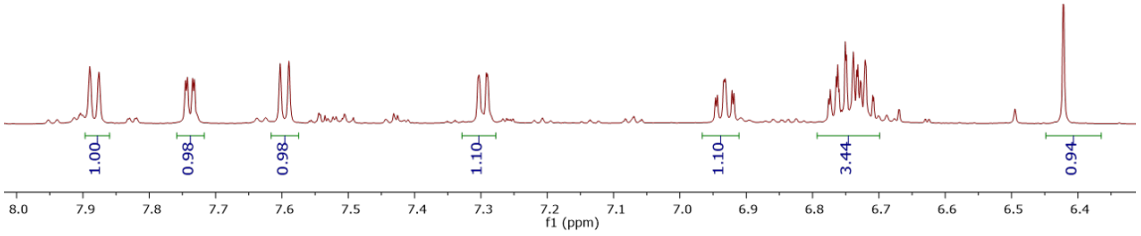

Figure 4.22: Aromatic region of the ^{1}H NMR spectrum of **25** in d_8-THF at 298 K

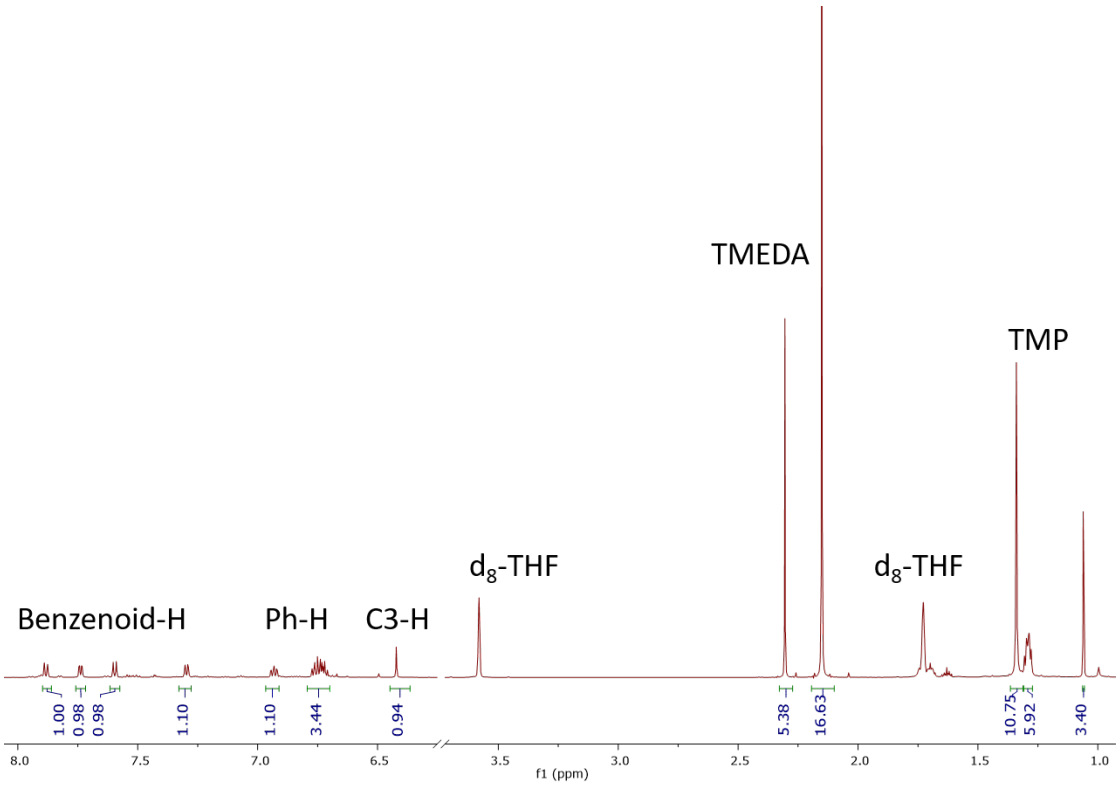

Figure 4.23: ^{1}H NMR of **25** in d_8-THF

The dianionic complex **25** can be utilised in *in situ* iodolysis reactions by the addition of a THF solution of iodine, to yield the diiodinated species 2-iodo-1-(2-iodophenyl)-1*H*-indole in a high yield (76 %) following purification by flash column chromatography (petroleum benzine/EtOAc 10/90).

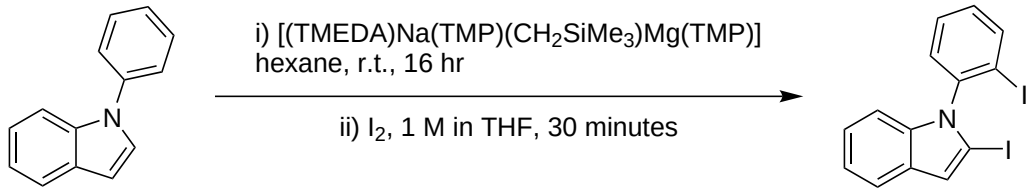

Scheme 4.32: Electrophilic quench of complex **25** with iodine

4.11 Synthesis of *N*-benzyl-1*H*-indole

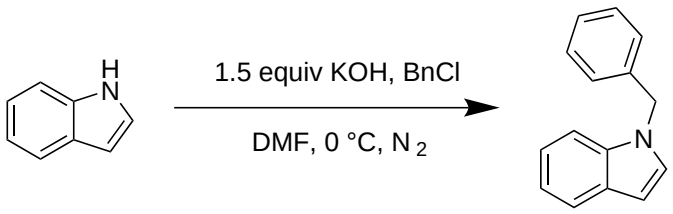

Scheme 4.33: Synthesis of *N*-benzyl-1*H*-indole

N-benzyl-1*H*-indole was synthesised by the addition of benzylchloride (BnCl) to a stirred solution of 1*H*-indole and potassium hydroxide in DMF under N_2 at 0 ° C. *N*-benzyl-1*H*-indole was isolated as a colourless solid following purification by flash column chromatography (silica gel, petroleum benzine/EtOAc 15/1).

4.12 Reaction of magnesiate base 1 with *N*-benzylindole

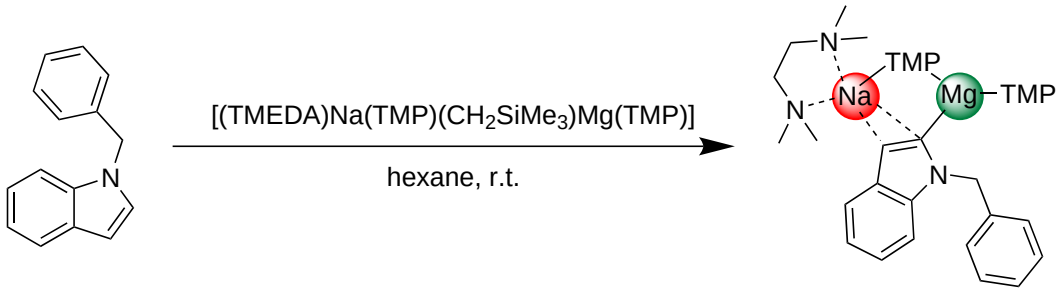

N-benzyl-1*H*-indole was added as a solid in one portion to a stirred solution of the magnesiate base **1**, and sonicated to break up the suspended solid. After stirring overnight, a large quantity of a white precipitate is observed, which was isolated by filtration, washed with *n*-hexane and dried *in vacuo*. This solid was transferred to a glovebox for storage. On a repeat synthesis, the solid was hot filtered allowed to cool undisturbed, leading to the deposition of a large crop of colourless crystals. These were identified by single-crystal X-ray diffraction to be the α-magnesiated species [(TMEDA)Na(TMP)($\alpha-C_8H_5N-$Bn)Mg(TMP)] **26**.

4.12.1 X-ray crystallographic analysis of complex 26

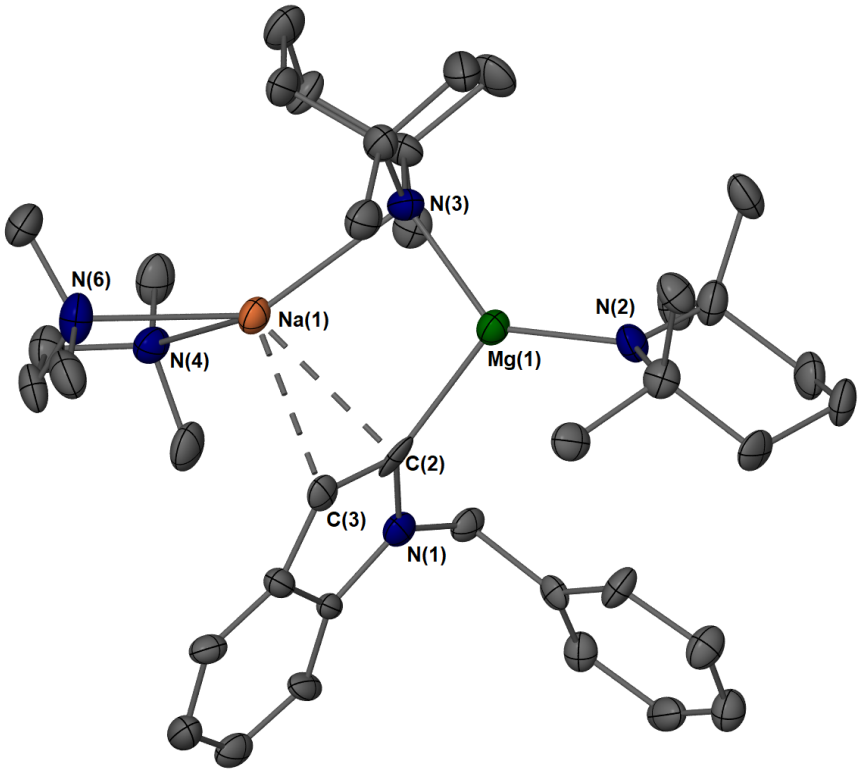

Figure 4.24: Molecular structure of [(TMEDA)Na(TMP)($\alpha-C_8H_5N-$Bz)Mg(TMP)] , **26**. Thermal ellipsoids shown at 40 % probability. Hydrogen atoms omitted for clarity. Selected bond lengths (Å) and angles (°): Mg(1) - C(2), 2.169(17); Mg(1) - N(2), 1.974(12); Mg(1) - N(3), 2.038(10); Na(1) - N(3), 2.523(12); Na(1) - C(2), 2.702(12); Na(1) - C(3), 2.813(11); C(2) - Mg(1) - N(2), 120.9(4); C(2) - Mg(1) - N(3), 106.0(5); N(3) - Mg(1) - N(2), 132.7(5); Mg(1) - N(3) - Na(1), 90.6(4).

The molecular structure of **26** (see Figure 4.24) features a trigonal planar magnesium centre, bonding to the α-position of a *N*-benzyl-1*H*-indole unit [Mg(1) - C(2) bond length 2.169(17) Å], a terminal TMP [Mg(1) - N(2) bond length 1.974(12) Å] and a bridging TMP [Mg(1) - N(3) bond length 2.038(10) Å]. The sodium atom makes electrostatic interactions with the α and β position of the indole ring [Na - C bond lengths of 2.702(12) and 2.813(11) Å respectively] and a bridging TMP unit [Na(1) - N(3) bond length 2.523(12) Å]. The sodium atoms coordination environment is completed by a bidentate, chelating TMEDA unit.

4.13 Synthesis of 1-(triisopropylsilyl)-1*H*-indole

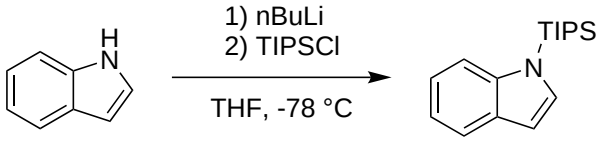

Triisopropylsilyl-1*H*-indole was synthesised by the lithiation of 1*H*-indole by *n*-butyllithium at -78 ° C in anhydrous THF (see section 4.13). After stirring for 30 minutes at this temperature, a molar equivalent of triisopropylsilylchloride was added dropwise at -78 ° C. The resulting solution was allowed to warm to room temperature stirring. The reaction was diluted with diethyl ether and quenched with saturated aqueous NH_4Cl solution. The ethereal layer was collected, washed with brine and dried over anhydrous $MgSO_4$. Triisopropylsilyl-1*H*-indole was isolated as an orange oil, in quantitative yield. The triisopropylsilyl- protecting group will be referred to as TIPS. This silyl- protecting group can be removed via addition of a F^- source, commonly TBAF.

4.14 Reaction of magnesiate base 1 with *N*-triisopropylsilyl-1*H*-indole

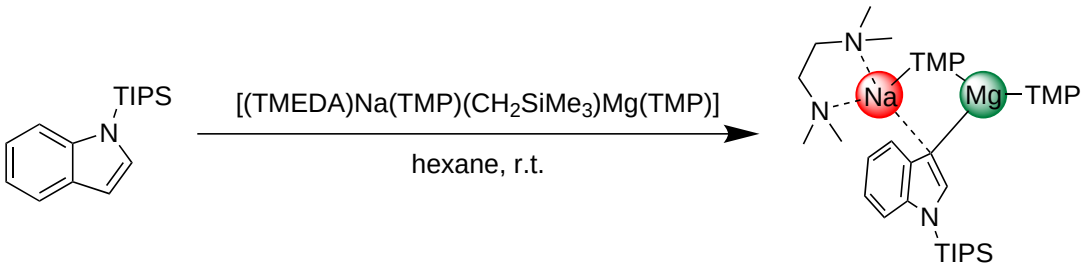

Scheme 4.34: Synthesis of complex **27**, [(TMEDA)Na(TMP)(β $-C_{17}H_{26}NSi$)Mg(TMP)]

To a stirred *n*-hexane solution of the sodium magnesiate **1**, a molar equivalent of *N*-triisopropylsilyl-1*H*-indole was added dropwise at room temperature. The resulting solution was stirred overnight for 16 hours, resulting in the deposition of a large quantity of an off-white solid. Upon gentle heating, the solid redissolved in solution. Filtration of this solution and storage at -30 ° C over three days resulted in a large crop of colourless

crystals, which were identified by NMR analysis and single-crystal X-ray diffraction studies to be the *beta*-magnesiated species [(TMEDA)Na(TMP)(β $-C_{17}H_{26}NSi$)Mg(TMP)] (see Scheme 4.34). On repeat synthesis, the solid can be isolated and was identified to be the same species as the crystallised product by ^{1}H NMR spectroscopy.

4.14.1 Solid state studies of complex 27

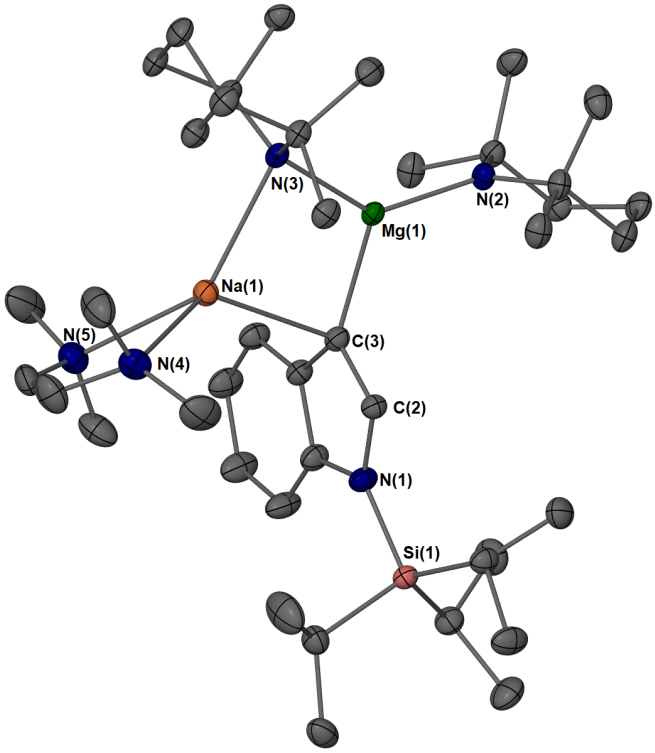

Figure 4.25: Molecular structure of [(TMEDA)Na(TMP)(β $-C_{17}H_{26}NSi$)Mg(TMP)], **27**. Thermal ellipsoids shown at 40 % probability. Hydrogen atoms and a minor disorder component in the TMEDA ligand is not shown for clarity. Selected bond lengths (Å) and angles (°): Mg(1) - C(3), 2.1734(16); Mg(1) - N(2), 1.9976(13); Mg(1) - N(3), 2.0925(12); Na(1) - C(3), 2.5305(14); Na(1) - N(3), 2.5305(14); Na(1) - N(4), 2.5912(16); Na(1) - N(5), 2.5582(16); C(3) - Mg(1) - N(2), 118.17(6); N(2) - Mg(1) - N(3), 133.09(6); N(3) - Mg(1) - C(3), 108.75(6); Na(1) - N(3) - Mg(1), 85.75(4); N(3) - N(1) - C(3), 84.06(5).

The crystal structure of complex **27** reveals a β -magnesiated *N*-triisopropylsilyl-1*H*-indole species [Mg(1) - C(3) 2.1734(16) Å]. The coordination sphere of the magnesium atom is completed by a terminal TMP unit [Mg(1) - N(2) 1.9976(13) Å] and a bridging TMP [Mg(1) - N(3) 2.5305(14) Å]. The sodium atom interacts solely with the magnesiated carbon [Na(1) - C(3) 2.6477Å]. The sodium atoms coordination sphere is completed by a

bridging TMP unit [Na(1) - N(3) 2.5305(14) Å], and a bidentate chelating TMEDA [Na(1) - N(4) 2.5912(16) Å, Na(1) - N(5) 2.5582(16) Å]. This can be seen as a magnesiation, as the magnesium atom co-planar to the indole ring, whereas the sodium sits almost perpendicular.

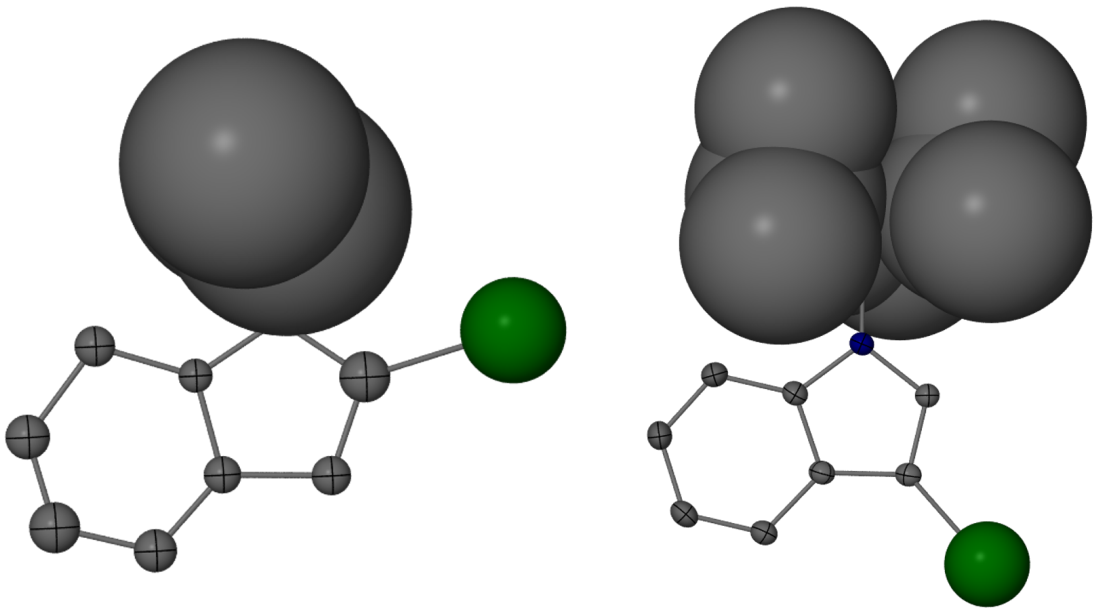

Figure 4.26: Space filling diagram of the isopropyl (left) vs TIPS group (right), with only the magnesium atom (shown in green) of the base shown for clarity

It can be seen that the steric demands of the triisopropylsilyl- group on the nitrogen of the indole likely restricts the base **1** from accessing the α- position, resulting in the observed β- position metallation (see Figure 4.26 right). For comparison, the steric demands of a single isopropyl group on the nitrogen, as in the case of [(TMEDA)Na(TMP)($\alpha-C_{11}H_{12}N$)Mg(TMP)] **21** is shown in the left of Figure 4.26.

4.14.2 Solution state analysis of complex 27

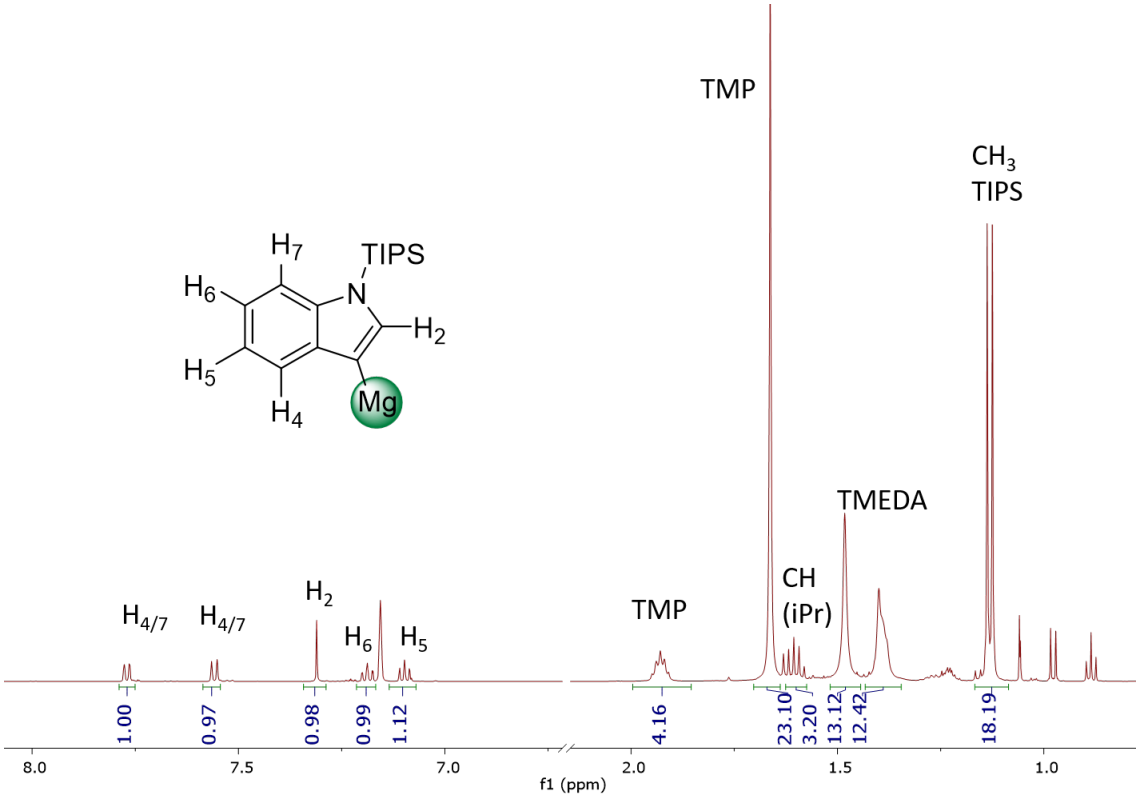

Figure 4.27: ^{1}H NMR spectrum of complex **27** in C_6D_6 at 298 K

Crystalline complex **27** was dissolved in C_6D_6 and analysed by ^{1}H and $^{13}C\{^{1}H\}$ NMR spectroscopy (see Figure 4.27). Non-crystalline material isolated from the same reaction was also analysed, and shown to be identical to the crystalline product. The disappearance of a doublet at 6.70 ppm, corresponding to the C3 proton indicates that a deprotonation has occurred. A sharp singlet is present at 7.31 ppm, corresponding to the lone proton at the C2 position, a shift downfield from the corresponding doublet at 7.08 ppm in the free *N*-triisopropylsilyl-1*H*-indole (see Figure 4.28 for a comparison of the free and magnesiated indole). Signals are evident for the triisopropylsilyl- group, as well as signals present for the TMP group and coordinated TMEDA. In the $^{13}C\{^{1}H\}$ NMR spectrum, the upfield shift of the C3 carbon to 143.7 ppm (compared to 105.3 in the parent indole) is indicative of a magnesiation occurring.

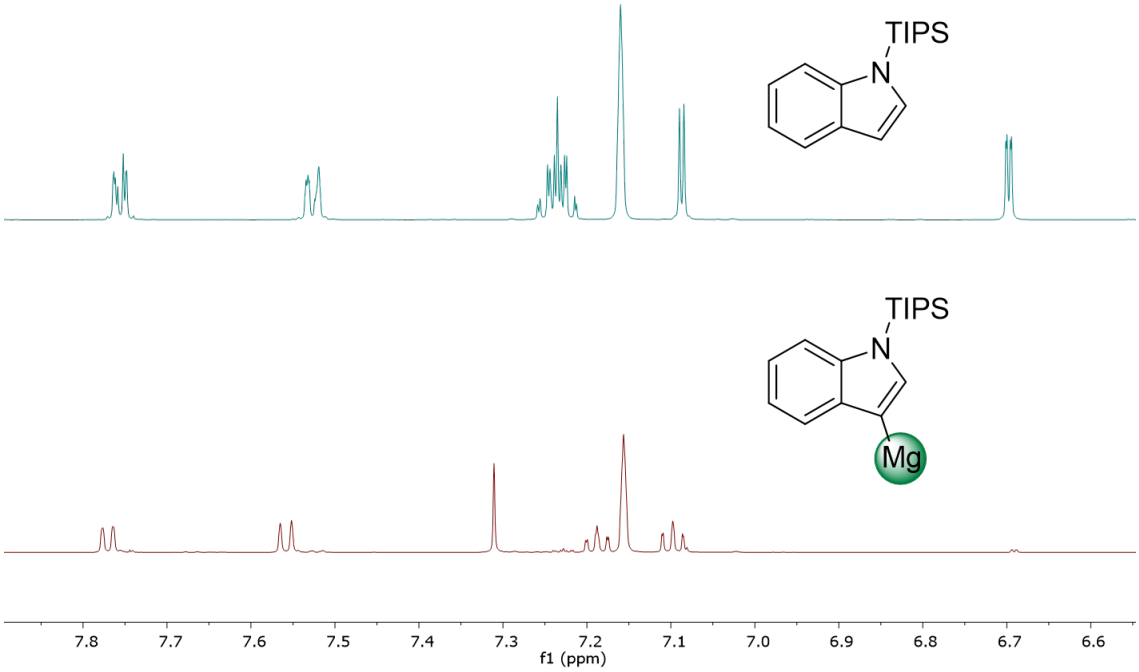

Figure 4.28: Comparison of the aromatic region of ^{1}H-NMR spectrum of *N*-triisopropyl-1*H*-indole (top) and complex **27** in C_6D_6

In a one-pot procedure, the expected *N*-triisopropylsilyl-3-iodo-1*H*-indole could be isolated in a high yield following the addition of a 1 M iodine in THF solution (see Scheme 4.35).

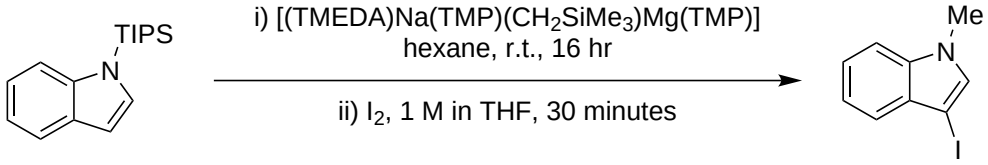

Scheme 4.35: Reaction of the magnesiate base **1** with *N*-triisopropylsilyl-1*H*-indole, followed by iodine quenching to yield the corresponding *N*-triisopropylsilyl-3-iodo-1*H*-indole

4.15 Synthetic utility of 7-azaindoles

The 7-azaindole scaffold has received considerable interest in the field of drug discovery. 7-Azaindole is a bicyclic heteroaromatic system containing a π-electron deficient pyridine ring fused with an π-electron excessive pyrrole ring.[136] Whilst rare in natural products, the 7-azaindole ring is considered a bioiostere for indole.

4.16 Synthesis of *N*- substituted 7-azaindoles

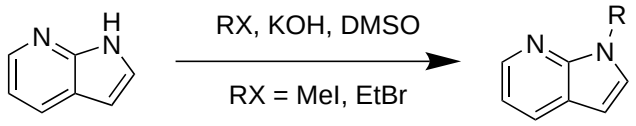

Scheme 4.36: Synthesis of *N*-substituted 7-azaindoles

N-methyl-7-azaindole and *N*-ethyl-7-azaindole were synthesised by the addition of RX (Me = MeI, Et = EtBr) to a stirred solution of 7-azaindole and potassium hydroxide in DMF (see Scheme 4.36). The reaction was monitored by TLC, and once full consumption of 7-azaindole was observed the reaction was diluted with Et_2O and quenched by addition of H_2O. To remove traces of DMF, the combined organic layers were washed repeatedly with H_2O. The synthesised *N*-substituted 7-azaindoles could be used as is, or further purified by vacuum distillation and stored over 4 Å molecular sieves prior to use.

4.17 Reaction of magnesiate base 1 with *N*-methyl-7-azaindole

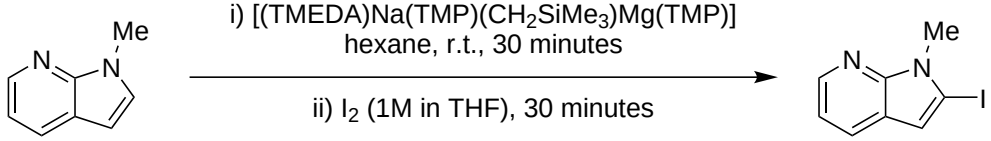

Scheme 4.37: Reaction of the magnesiate base **1** with *N*-methyl-7-azaindole, followed by iodine quenching

Starting simply, a molar equivalent of *N*-methyl-7-azaindole was added dropwise to a stirred solution of the magnesiate base **1**. This led to the immediate deposition of a white precipitate. On continued stirring, this precipitate redissolved into an oily biphasic solution in *n*-hexane. Attempts to analyse the resulting oil by ^{1}H NMR spectroscopy proved difficult, where both solubility and poorly resolved signals were major factors. Instead, we turned to electrophile studies to gain further insight into the regioselectivity of the reaction. When a molar equivalent of *N*-methyl-7-azaindole was added dropwise to a stirred solution of the magnesiate base **1**, and stirred for approximately 30 minutes resulting in the oily

biphasic mixture. Following this, a 1 M iodine solution in THF was added dropwise (five equivalents), and stirred for a further 30 minutes. The resulting solution was diluted with diethyl ether, and quenched with aqueous sodium thiosulphate until bleaching occurred. Following workup, *N*-methyl-2-iodo-7-azaindole was isolated as a crystalline solid (see Scheme 4.37).

While the metallated intermediate was not determined from this reaction, it can be concluded that the dominant species present is likely an alpha-metallated *N*-methyl-7-azaindole based complex.

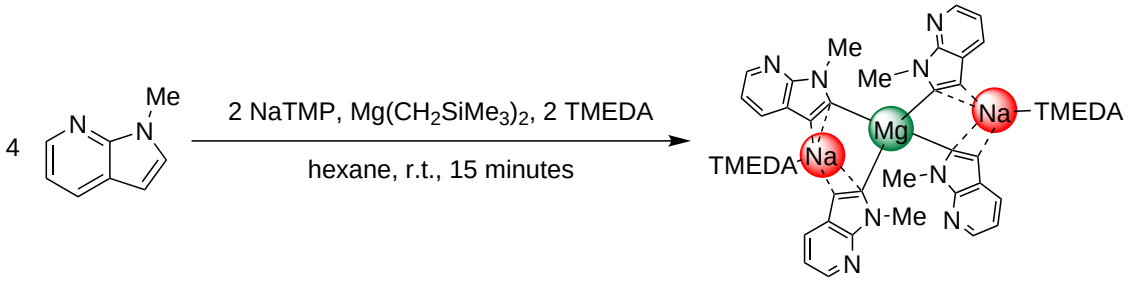

Scheme 4.38: Alternative base mixture and its reaction with *N*-methyl-7-azaindole to give **28**

Following this, we next decided to investigate the effects of stoichiometry on the reaction. The obvious first choice was to use the alternate base mixture, which was found in the case of *N*-methylindole and *N,3*-dimethylindole to be the active base mixture. Four equivalents of *N*-methyl-7-azaindole was added to an *in situ* mixture of NaTMP, $Mg(CH_2SiMe_3)_2$ and TMEDA in a 2:1:2 ratio. This resulted in the deposition of a large quantity of a white solid, which could be isolated by filtration and analysed by ^{1}H NMR spectroscopy. Indeed, the species was identified by solution state analysis to be the higher order magnesiate, $[Na \cdot TMEDA)_2Mg(\alpha{-}C_8H_7N_2)_4]$ **28**. Unfortunately, it proved difficult to obtain single-crystals of this species, however it can be clearly identified by ^{1}H NMR spectroscopy (see Figure 4.29).

Complex **28** was dissolved in $d_8{-}$THF and analysed by ^{1}H NMR spectroscopy (see Figure 4.29). In support of our hypothesised metallated structure, it is evident that there is an α- deprotonated *N*-methyl-7-azaindole species. A lack of signals related to TMP is evident, as well as a decoordinated TMEDA species present. The azaindole species is

in a 2:1 ratio with TMEDA. Unfortunately, splitting patterns are not observable on the *N*-methyl-7-azaindole related signals, where they are broad and poorly defined.

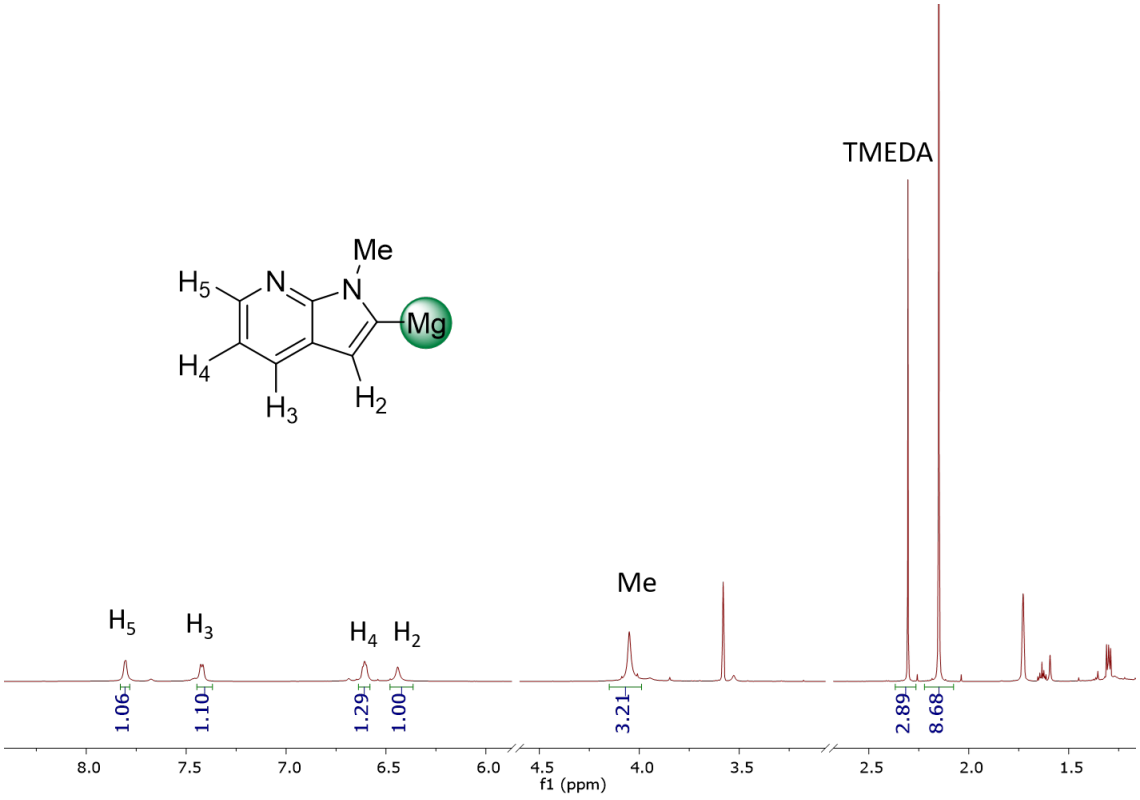

Figure 4.29: ^{1}H NMR spectrum of complex **28** in d_8-THF at 298 K

In order to fully confirm the regioselectivity of the metallated species present, an *in situ* iodolysis was performed (see Scheme 4.39). A 1 M iodine in THF solution was added dropwise to a suspension of **28**, and allowed to stir for 30 minutes. The resulting solution was diluted with diethyl ether, and quenched with aqueous sodium thiosulphate until bleaching occurred. The organic layer was separated and its solvent removed. The resulting *N*-methyl-2-iodo-7-azaindole was isolated as a crystalline solid in a yield of 84 %.

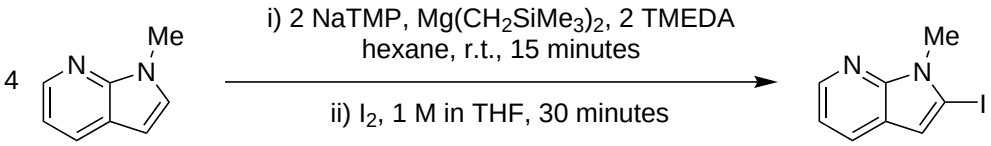

Scheme 4.39: Electrophile quench of **28** with iodine, to give the α- iodinated species *N*-methyl-2-iodo-7-azaindole

Interestingly, when 1.5 equivalents of *N*-methyl-7-azaindole was added to a *n*-hexane solution of the magnesiate **1**, within seconds a large quantity of a white precipitate forms, impeding stirring. The solid can be isolated by filtration, washed with *n*-hexane and dried *in vacuo*, and transferred to a glovebox for storage. Interestingly, two distinct 7-azaindole species are present - one can be clearly identified as the α- magnesiated species, however the other species does not correspond to the starting *N*-methyl-7-azaindole (see Figure 4.30). Based on analysis of the integrals, it appears possible that the species is a laterally metallated species - however, a large shift in the chemical shift of the new $N-CH_2-Mg$ signals would likely be expected. Attempts to crystallise this compound were not successful. Similarly to the previous base ratios, the reaction was quenched with a 1 M solution of iodine in THF, which resulted in the isolation of *N*-methyl-2-iodo-7-azaindole in a high yield as a crystalline solid. GC/MS analysis of the crude reaction mixture did not detect the presence of any other iodinated species.

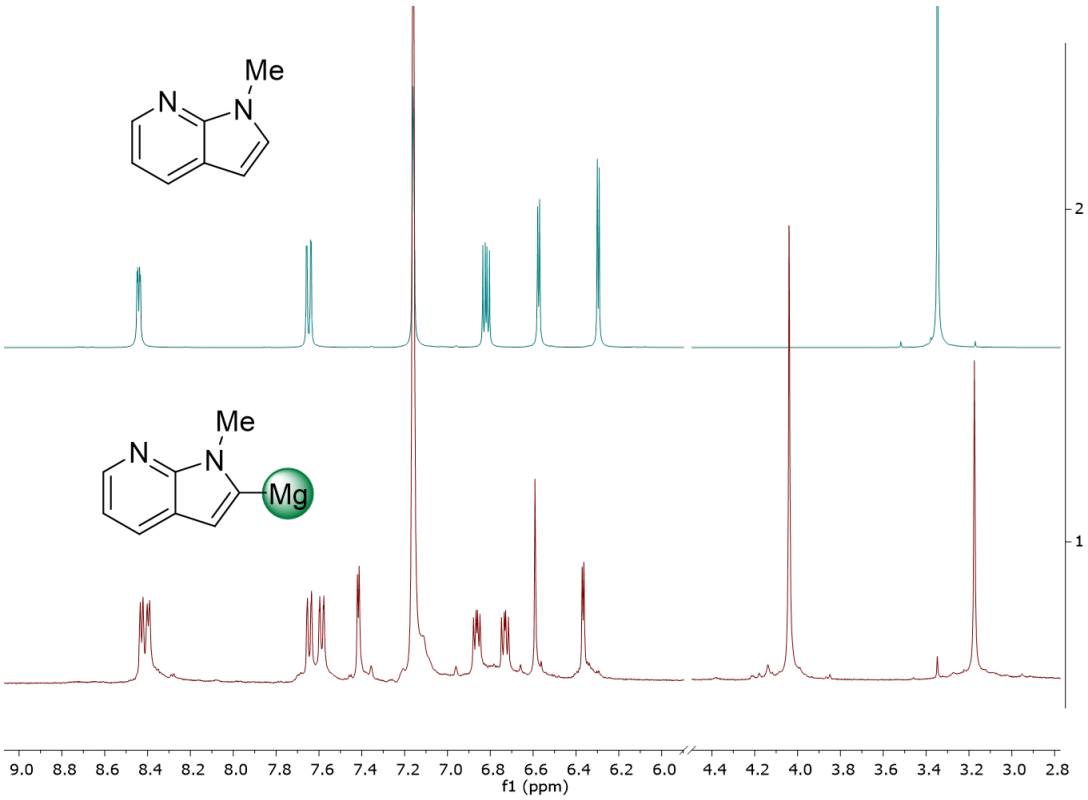

Figure 4.30: ^{1}H NMR spectrum of the reaction between 1.5 equivalents of *N*-methyl-7-azaindole and the magnesiate **1** in C_6D_6 on the bottom, with a standard of *N*-methyl-7-azaindole on top

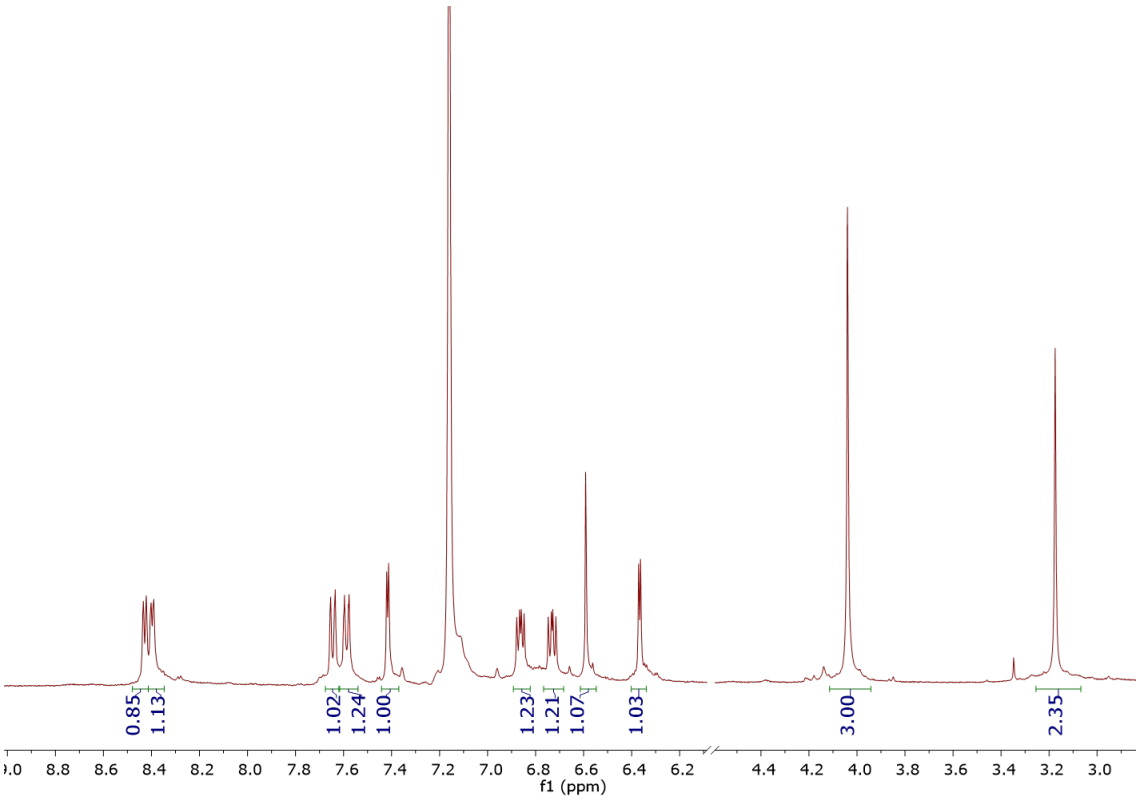

Figure 4.31: ^{1}H NMR spectrum of the reaction between 1.5 equivalents of *N*-methyl-7-azaindole and the magnesiate **1** in C_6D_6 at 298 K

While further work is required to chase up the exact solution state composition of these metallated *N*-methyl-7-azaindole, it does appear that selective α-magnesiation is occurring.

4.18 Reaction of magnesiate base 1 with *N*-ethyl-7-azaindole

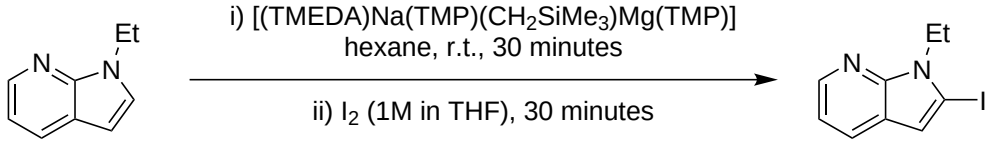

Scheme 4.40: Reaction of the magnesiate base **1** with *N*-ethyl-7-azaindole, followed by iodine quenching

To a stirred hexane solution of the magnesiate base **1**, was added a molar equivalent of *N*-ethyl-7-azaindole at room temperature. This resulted in the formation of a large quantity of a white precipitate, which did not form an oily bi-phasic mixture like *N*-methyl-7-

azaindole. This solid was isolated by filtration, washed with *n*-hexane and dried *in vacuo*. It was transferred to a glovebox for analysis.

The solid was dissolved in C_6D_6 and analysed by ^{1}H NMR spectroscopy. While substantial starting material was present, two distinct metallated species were present, as indicated by the two singlets (at 6.83 and 6.21 ppm) and the two Et$-CH_2$ signals. This is hypothesised to be a mixture of the α- and β- magnesiated species. Turning to an electrophile quench, a 1 M iodine solution in THF was added dropwise to a stirred solution of the magnesiate base **1** and *N*-ethyl-7-azaindole. This resulted in the isolation of the selective α- iodinated species *N*-ethyl-2-iodo-7-azaindole in a high yield (76 %, see Scheme 4.40).

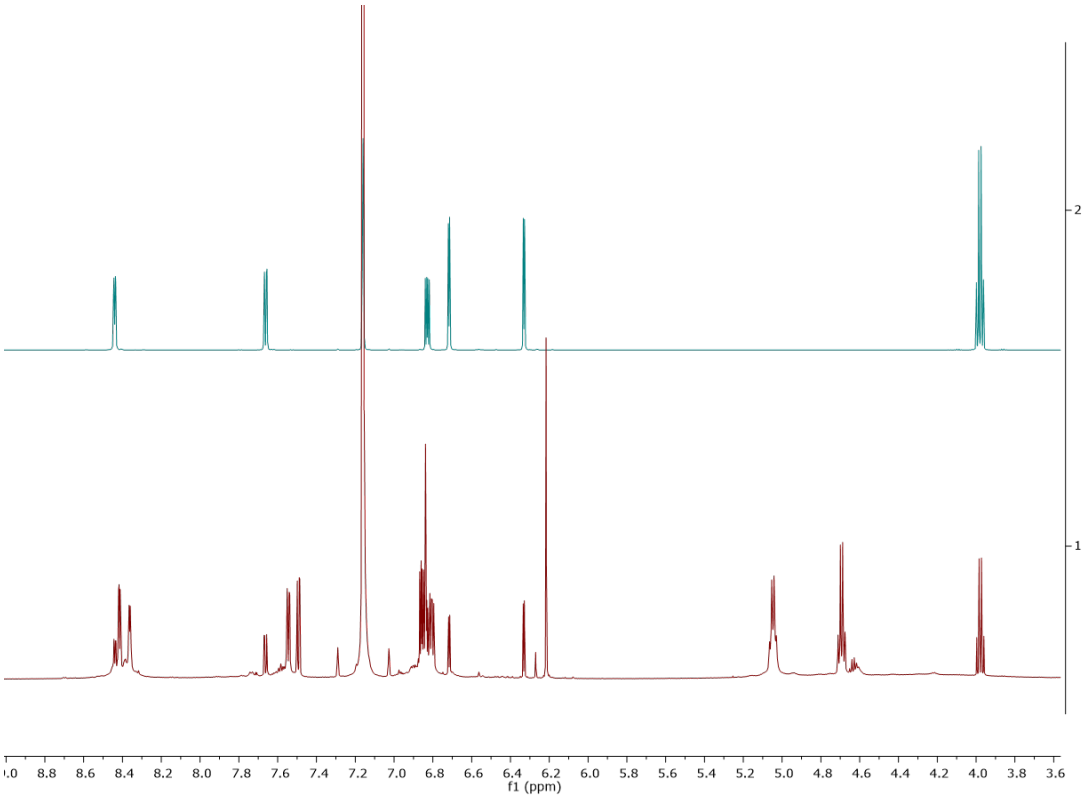

Figure 4.32: ^{1}H NMR spectrum of the reaction between 1 equivalent of *N*-ethyl-7-azaindole and the magnesiate **1** in C_6D_6 on the bottom, with a standard of *N*-ethyl-7-azaindole on top

As with *N*-methyl-7-azaindole, we next decided to try the alternative base mixture that was used in *N*-methyl and *N*-ethyl indole. Four equivalents of *N*-ethyl-7-azaindole was added to a stirred solution of *n*BuNa, $Mg(CH_2SiMe_3)_2$ and TMEDA in a 2:1:2 ratio. This resulted in the deposition of a large quantity of a white solid **29**. This solid was isolated

and dissolved in C_6D_6 for ^{1}H NMR analysis (see Figure 4.33). Interestingly, this appears to result in selectively one magnesiation product being observed (as compared to the reaction of **1** with *N*-ethyl-7-azaindole). Indeed, when comparing the two NMR spectra (see Figure 4.34), we do see that this appears to be the other species present in the reaction of **1** with *N*-ethyl-7-azaindole. Despite numerous attempts to crystallise this mixture, unfortunately no structural information has been gathered about these species.

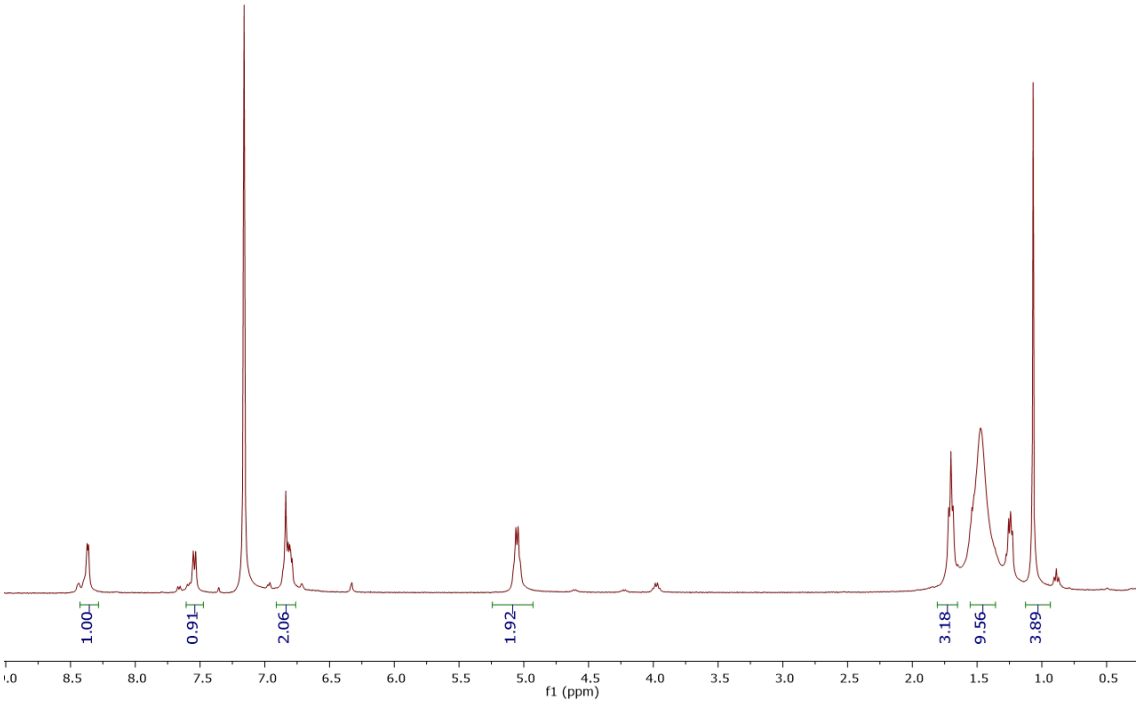

Figure 4.33: ^{1}H NMR spectrum of the reaction between the 'alternative' base mixture and four equivalents of *N*-ethyl-7-azaindole at 298 K

Looking to confirm the regioselectivity of this 'alternative base mixture', a 1 M iodine solution was added dropwise to **29**. Following organic workup, this resulted in the isolation of *N*-ethyl-2-iodo-7-azaindole (see Scheme 4.41). This leads us to the conclusion that the reaction of *N*-ethyl-7-azaindole with the magnesiate base **1** likely leads to a mixture of alpha- magnesiated [(TMEDA)Na(TMP)($\alpha-C_6H_4N_2-$Et)Mg(TMP)] and [$(Na \cdot TMEDA)_2Mg(\alpha-C_6H_4N_2-Et)_4$].

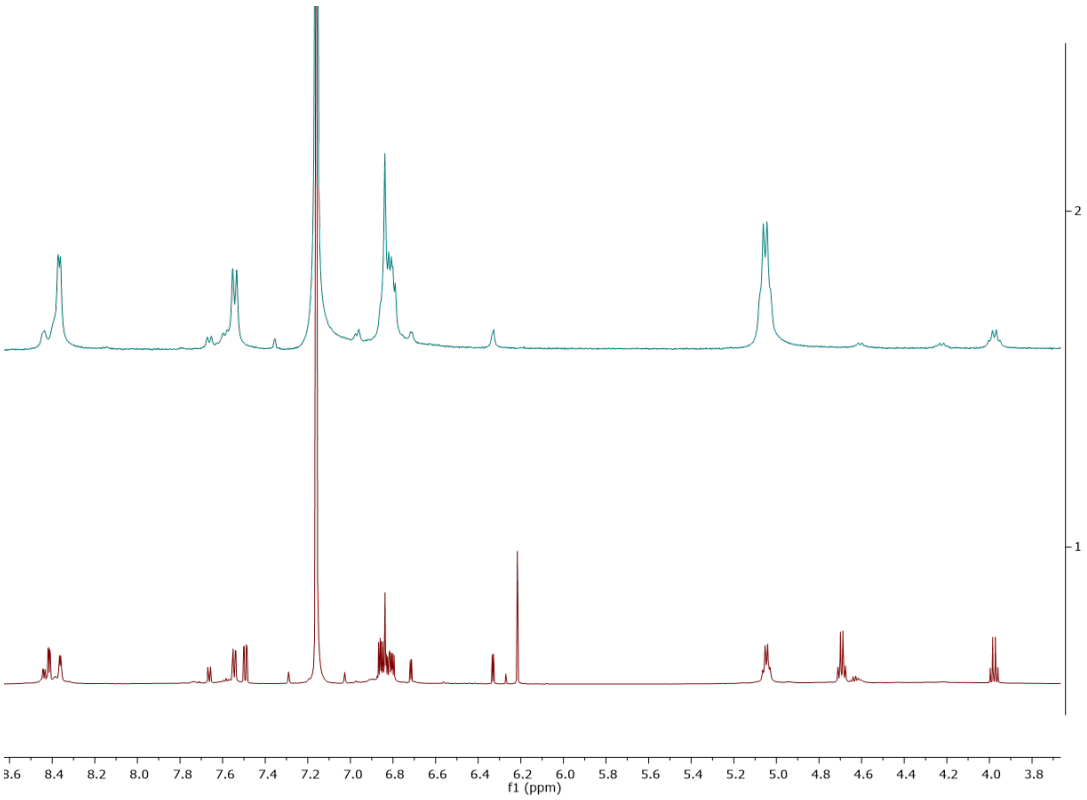

Figure 4.34: Comparison of the reaction of **1** with *N*-ethyl-7-azaindole (top) and the 'alternative base mixture' (bottom)

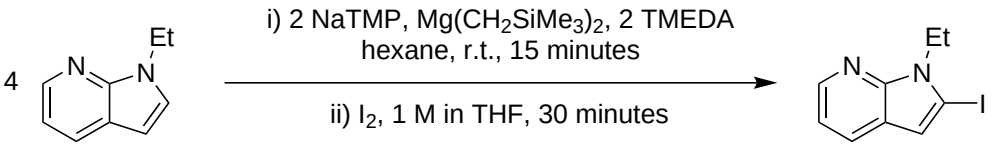

Scheme 4.41: Electrophilic quench of **29** with iodine, to give the α- iodinated species *N*-ethyl-2-iodo-7-azaindole

4.19 Conclusions and Future Work

This chapter focused on the reaction of the magnesiate base **1** with a variety of *N*-heterocyclic indoles and 7-azaindoles. It found almost exclusively α magnesiation to occur, except for when the bulky TIPS protecting group was used in the case of *N*-triisopropylsilyl-1*H*-indole.

When *N*-methyl and *N*-ethyl indoles were employed, a disproportionation reaction was found to occur, to give the disodium tetraindol-2-ylmagnesiates [Na $\cdot$ TMEDA)$_2$Mg($\alpha-$C$_9$H$_8$N)$_4$] and [(Na $\cdot$ TMEDA)$_2$Mg($\alpha-$C$_{10}$H$_{11}$N)$_4$]. These complexes

could be rationalised synthesised by mixing *n*BuNa, $Mg(CH_2SiMe_3)_2$ and TMEDA in a 2:1:2 ratio, and the addition of four equivalents of the corresponding indole. These magnesiated complexes were subsequently used in *in situ* iodolysis and Pd-catalysed cross-coupling reactions with PhI. Similar reactivity was observed when exploring the *N,3*-dimethyl- and *N*-methyl-3-ethyl-1*H*-indole species. With both *N*-isopropyl-1*H*-indole and *N*-isopropyl-3-methyl-1*H*-indole, the sodium magnesiate stays 'intact', giving rise to the α magnesiation selectively.

A di-magnesiation was found to occur in the case of *N*-phenyl-1*H*-indole, with both the α-position of the indole ring and the *ortho-* position of the phenyl group magnesiated. The corresponding di-iodo species was isolated following an iodine quench of the metallated intermediate. Preliminary work has been conducted on the use of this species in Pd-catalysed cross-coupling, however this is not included in this thesis.

The bulky triisopropylsilyl- protecting group leads to the selective β-magnesiation of TIPS-indole, allowing access to *N*-triisopropylsilyl-3-iodo-1*H*-indole. This TIPS protecting group can be removed with a source of the F^- ion, such as TBAF, to give the 3-substituted free indole.

Further work is required to fully elucidate the reactivity observed when magnesiating 7-azaindoles. While it does appear that electrophile quenches result in the selective α-iodination, it is not currently clear what the metallated species are. Further crystallographic evidence would allow the precise nature of these complex species to be elucidated.

5 Bi-metallic metallations of *P*-heterocyclic compounds

After previous success in the magnesiation of a variety of *N*-substituted indoles, it was decided to explore the analogous phosphorus compound - phosphindole.

Benzo[*b*]phosphole derivatives have attracted significant interested for their semiconducting, fluorescent and coordinating properties, holding promise in various areas including organic electronics, bioimaging, coordination chemistry and catalysis.[137–141]

The metallation chemistry of substituted phosphindoles has only briefly been explored in the literature. For example, the lithiation of 5-phenyl-dibenzophosphole oxide with LDA, followed by electrophilic quench results in predominately α-functionalised 5-phenyl-dibenzophosphole, as well as small quantities of the di-substituted product (see Scheme 5.1).[142]

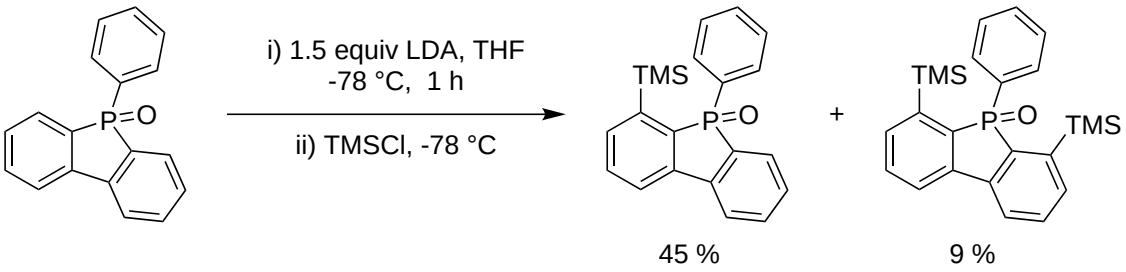

Scheme 5.1: Reaction of LDA with 5-phenyl-dibenzophosphole oxide

Similarly, the synthesis of 7-substituted 1,2,3-triphenylphosphindole oxide was explored using LiTMP, which could then be trapped with 1,2-diiodoethane (see Scheme 5.2).[143] With the corresponding 7-iodo species, the authors explored a variety of palladium cross coupling reactions, giving access to a large variety of 7-functionalised 1,2,3-triphenylphosphindole oxide molecules.[143] Interestingly, high molar equivalents of LiTMP (3.6 equivalents) were required to optimise the yield of the lithiated intermediate, while still being overall low yielding (47 % yield).

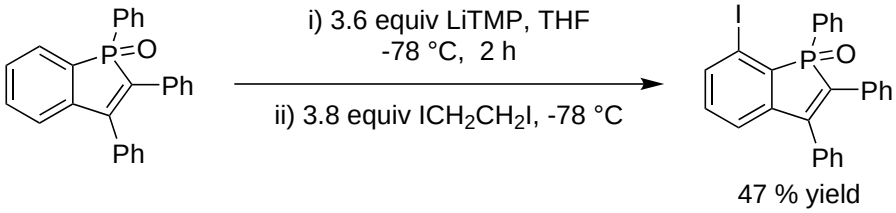

Scheme 5.2: Reaction of LiTMP with 1,2,3-triphenylphosphindole oxide

Encouraged by these lithium-metallation studies, our initial targets for this study were the analogous phosphorus equivalents of *N*-phenylindole - namely; *P*-phenylphosphindole and *P*-phenylphosphindole oxide (see Figure 5.1). In the nitrogen system, we observed a di-magnesiation, selectively at the α- position of the indole ring and the *ortho*- position of the phenyl ring (see Figure 5.1).

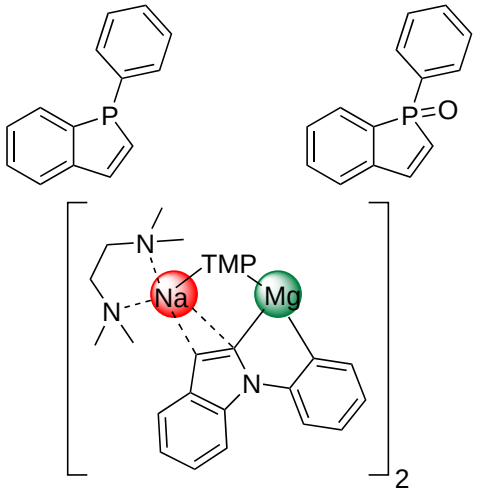

Figure 5.1: Target phosphindole molecules (top) and outcome of the magnesiation of the analagous *N*-phenylindole (bottom)

5.1 Synthesis of *P*-phenylphosphindole

Since the phenylphosphindoles are not commercially available, we used a range of literature procedures to aid in their synthesis. While a number of literature procedures were found for *P*-phenylphosphindole (III) and its oxide, they were found to be generally unreliable, poor yielding or difficult to purify. The route proposed by Tsuchiya et al.[144], and further optimised by Decken et al.[145] was chosen as a starting point. Unfortunately, trichlorosilane (used to reduce the phospindole oxide to the phosphindole) is not commercially available in

Australia, and cannot be imported. Nevertheless, this method seemed the most promising, and careful exclusion of oxygen could avoid the oxidation to phosphorus(V) present in this method.

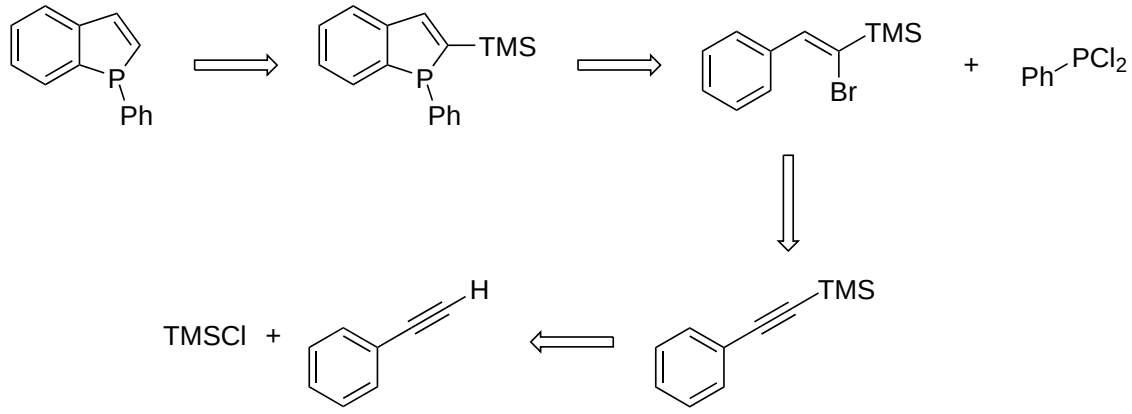

Scheme 5.3: Retrosynthesis of the target *P*-phenylphoshindole, starting from commercially available phenylacetylene

To a stirred solution of phenylacetylene in THF, *n*-BuLi was added dropwise at -78 ° C. This resulted in the formation of a bright blue suspension, likely due to trace amounts of the dianion. After stirring at -78 ° C for 30 minutes, the solution was quenched with trimethylsilylchloride to afford the desired product, 1-trimethylsilyl-phenylacetylene as a pale yellow oil in a quantitative yield and high purity (see Scheme 5.4).

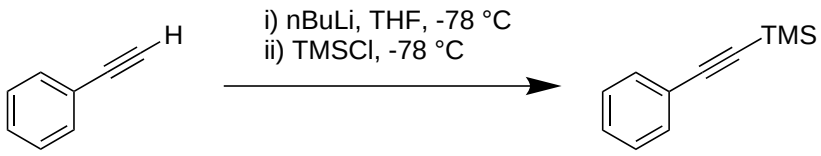

Scheme 5.4: Synthesis of 1-trimethylsilylphenylacetylene from phenylacetylene

The next step in the synthetic sequence involves the hydralumination of 1-trimethylsilylphenylacetylene with diisobutylaluminium hydride (DIBAL-Hdr and subsequent treatment with *N*-bromosuccinimide (NBS). The resulting (Z)-β-bromo-β-trimethylsilylstyrene was isolated regio- and stero-selectively in a high yield (ca. 80 % yield, see Scheme 5.5).

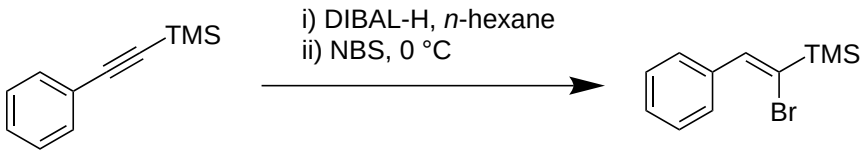

Scheme 5.5: Synthesis of (Z)-β-bromo-β-trimethylsilylstyrene from 1-trimethylsilylphenylacetylene

To form the phosphindole, the (Z)-β-bromo-β-trimethylsilylstyrene can be di-lithiated with two equivalents of *n*-BuLi, followed by addition of phenylphosphine dichloride to afford ring closure and the desired phosphorus heterocycle (see Scheme 5.6). While the literature reports of this step were vague, it was found through extensive optimisation that this reaction was highly sensitive to the quality of *n*-BuLi used, the precise stoichiometry and the rate of addition of both the *n*-BuLi and the phenylphosphorus dichloride. Optimal synthesis used freshly titrated *n*-BuLi added slowly dropwise (over 30 minutes), as well as the addition of a dilute solution ($<$ 0.2 M in diethyl ether) of phenylphosphine dichloride.

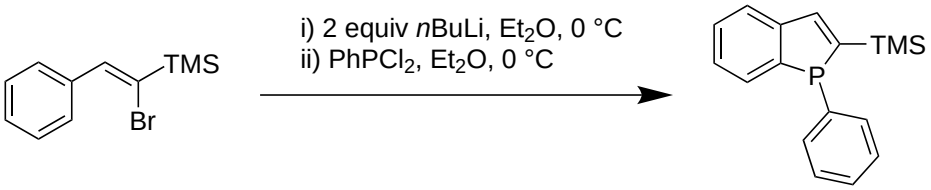

Scheme 5.6: Synthesis of 2-trimethylsilyl-*P*-phenylphosphindole

The final step in the synthetic sequence to *P*-phenylphosphindole involves the deprotection of the trimethylsilyl protecting group. This could be achieved using tetrabutylammonium fluoride (TBAF) as a F^- source (see Scheme 5.7). Attempts to use CsF as a F^- source were unsuccessful, resulting in quantitative return of starting material (in contrast to what is reported by Tsuchiya et al.[146]). This reaction was not found to be sensitive to oxygen or moisture, and so inert conditions were not required. In a modification from reported methods, this deprotection step can be conveniently performed in a pressurised microwave reactor, where a more reliable reaction outcome was achieved (in a shorter time period). Following organic workup, pure *P*-phenylphosphindole was isolated as a yellow, crystalline solid which can be used without further purification.

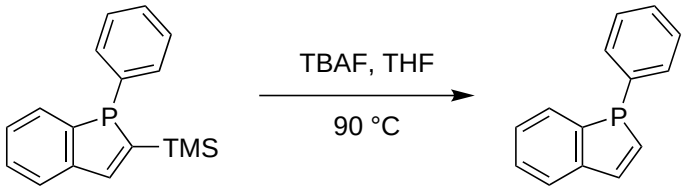

Scheme 5.7: Deprotection of the the trimethylsilyl group from *P*-phenyl-2-trimethylsilyl-phosphindole

The corresponding phosphorus(V) oxide can be obtained at either step (Scheme 5.6 or Scheme 5.7), simply by the addition of H_2O_2 to a THF solution of the phosphorus heterocycle with vigorous stirring (see Scheme 5.8). This step leads to quantitative conversion to the corresponding phosphorus(V) *P*-phenyl-2-trimethylsilyl-phosphindole oxide or *P*-phenyl-phosphindole oxide.

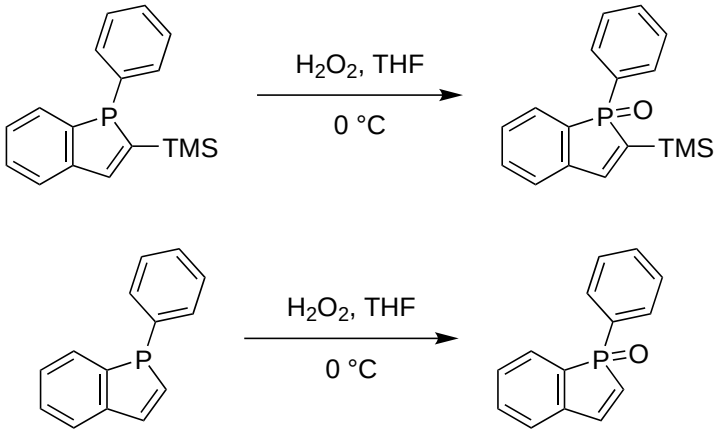

Scheme 5.8: Oxidation of *P*-phenylphosphindole and *P*-phenyl-2-trimethylsilyl-phosphindole

5.2 Isolation of the di-lithio intermediate in the synthesis of P-phenylphosphindole

Interested in the structure of the di-lithiated intermediate (see Scheme 5.6) present in the synthetic strategy, we attempted to crystallise this intermediate species. In one repeat synthesis, addition of one equivalent of the bidentate Lewis base TMEDA and storage of the solution at -30 °C yielded a crop of red crystals, which were identified by single-crystal X-ray diffraction to be the di-lithiated complex $[(TMEDA)Li(PhC_2H_1SiMe_3)Li]_2$ **30**.

5.2.1 Solid state analysis of complex 30

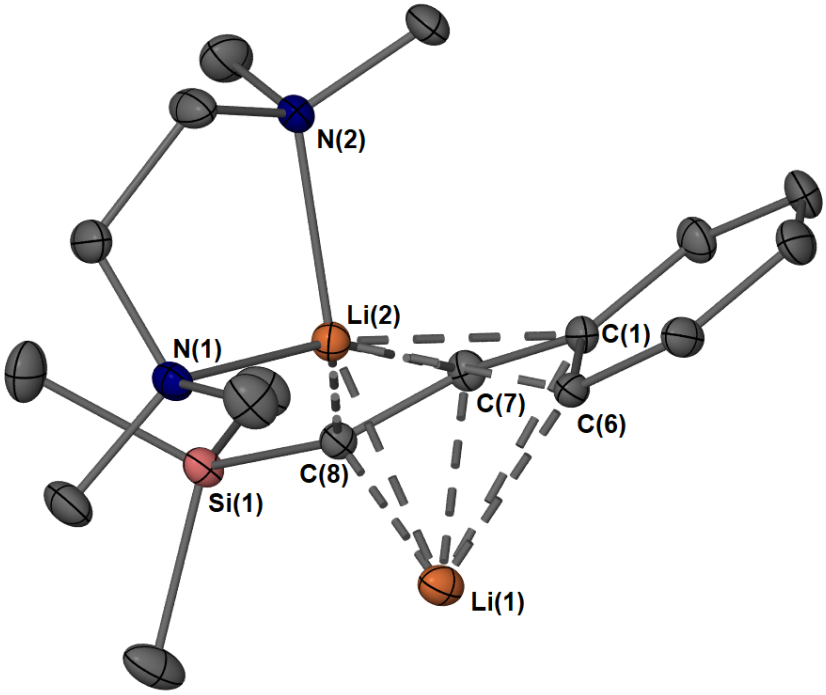

Figure 5.2: The asymmetric unit of **30**. Thermal ellipsoids shown at 40 % probability. Hydrogen atoms omitted for clarity. Selected bond lengths (Å) and angles (°): Li(1) - C(8), 2.090(2); Li(1) - C(7), 2.531(2); Li(1) - C(1), 2.668(2); Li(1) - C(6), 2.254(2); Li(2) - C(8), 2.160(2); Li(2) - C(7), 2.558(2); Li(2) - C(1), 2.574(2); Li(2) - C(6), 2.223(2), N(1) - Li(2), 2.096(2); N(2) - Li(2), 2.103(2).

Complex **30** crystallises as a dimeric species, consisting of two di-lithiated units (the asymmetric unit is shown in Figure 5.2). The full molecular structure is seen in Figure 5.3. In the molecular structure of **30**, the dimeric species has two lithium atoms on the periphery, interacting with the π- electron system of the double bond (Li(2) - C bond lengths range from 2.160(2) - 2.558(2) Å) and capped by a bidentate, chelating TMEDA (Li - N bond lengths of 2.096(2) and 2.103(2) Å). Two lithium atoms are internal to the dimeric species, interacting with the π- electron density of the double bond (Li(1) - C bond lengths range from 2.090(2) - 2.668(2) Å), as well as bridging to two carbons within the aromatic ring of the second unit (Li(1) - C bond lengths of 2.156(2) and 2.472(2) Å). The structure of **30** results from two distinct lithiation events: a Li−Br exchange as well as a C−H deprotonation at the *ortho*-position of the aromatic ring.

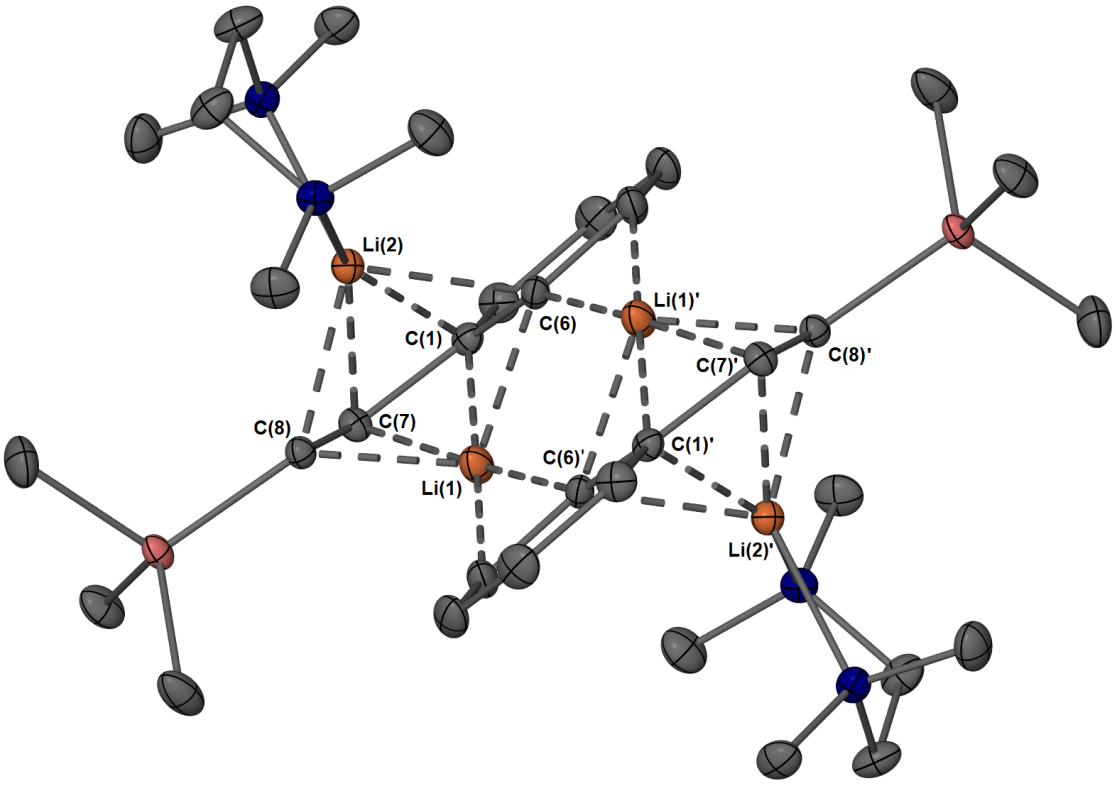

Figure 5.3: Full molecular structure of **30**. Symmetry operator ' = 1 - x, 1 - y, 1 - z. Li(1) - C(5)', 2.472(2); Li(1) - C(6)', 2.156(2).

5.3 Solution state analysis of complex 30

Complex **30** was dissolved in C_6D_6 and analysed by ^{1}H and ^{7}Li NMR spectroscopy. Signals associated with the phenyl group are present between 7.25 - 8.5 ppm, and the Ph−CH proton is evident at 9.24 ppm. A broad, undefined signal is evident from 1 ppm - 2.25 ppm, which corresponds to the coordinated TMEDA ligand (see Figure 5.4). Interestingly, only one broad ^{7}Li signal is observed at 2.13 ppm (see Figure 5.5).

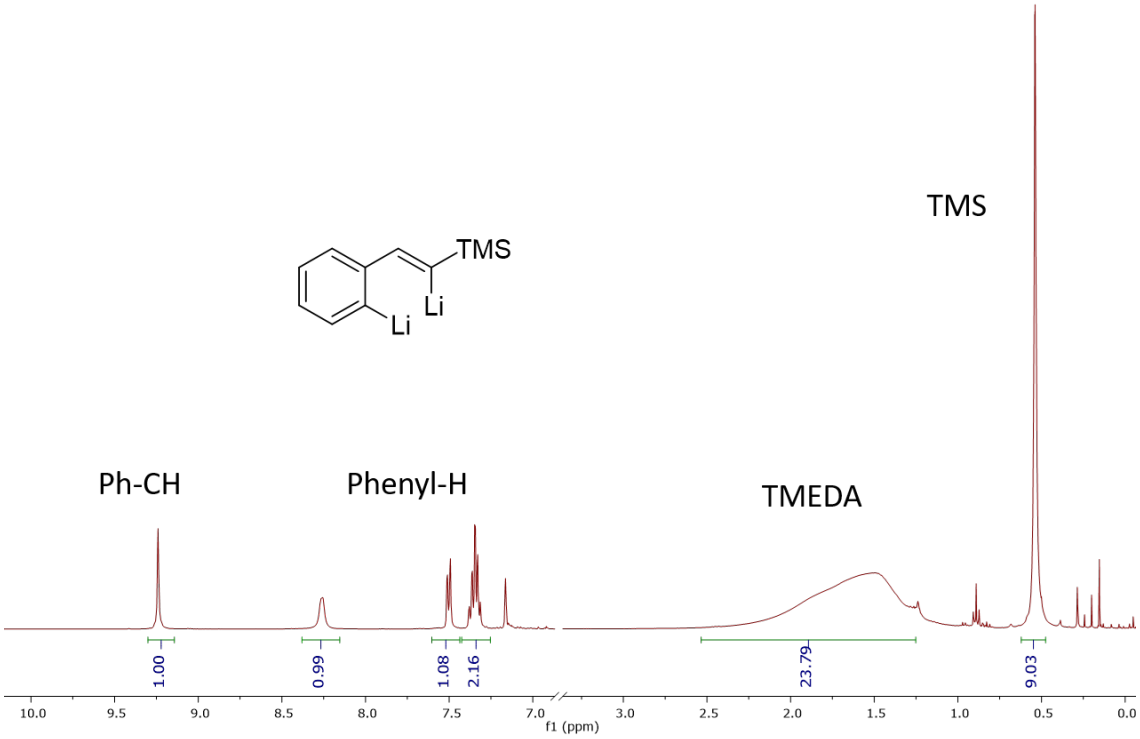

Figure 5.4: ^{1}H NMR spectrum of **30** in C_6D_6 at 298 K

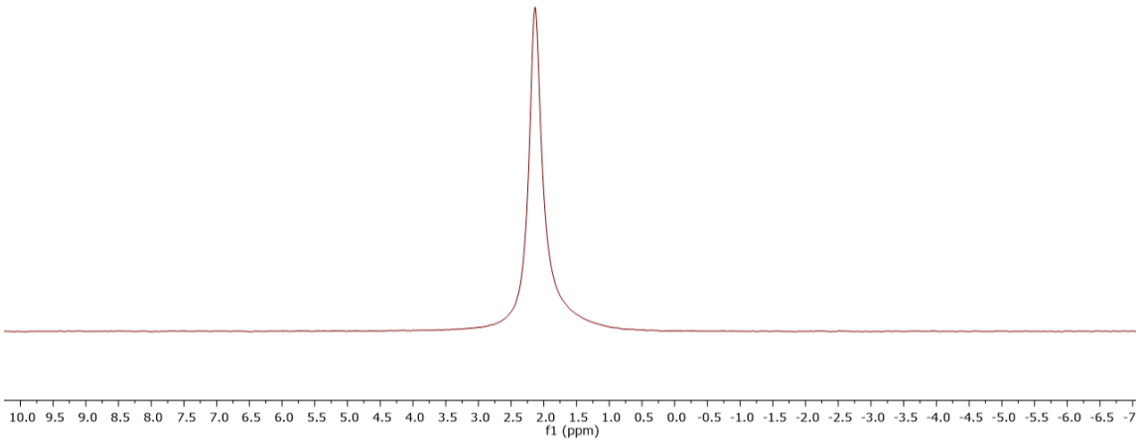

Figure 5.5: ^{7}Li NMR spectrum of **30** in C_6D_6 at 298 K

5.4 Reaction of the magnesiate base 1 with *P*-phenylphosphindole

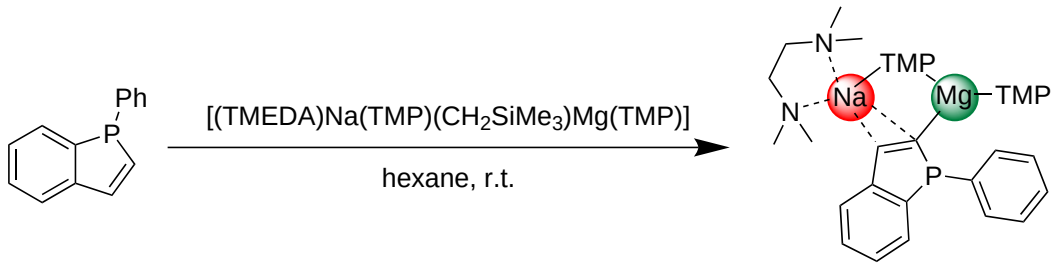

Scheme 5.9: Reaction of the magnesiate base **1** with *P*-phenylphosphindole

After the successful synthesis of the phosphindole, we next began our reactivity studies with the bimetallic base **1**. A molar equivalent of *P*-phenylphosphindole was added via a solid addition tube to a solution of the magnesiate base **1**. Stirring the reaction overnight (16 hours) resulted in the deposition of a large quantity of a brown solid. This solid was isolated by filtration, washed with *n*-hexane and dried *in vacuo*. On one repeat synthesis, crystals were grown following hot filtration and slow cooling of the solution in a hot oil bath. Analysis by single-crystal X-ray diffraction revealed the α magnesiated complex [(TMEDA)Na(TMP)($\alpha-C_8H_5P-$Ph)Mg(TMP)] **31**.

5.4.1 Solid state structure of 31

The molecular structure of **31** features an α-magnesiated *P*-phenylphosphindole unit (Mg-C(2) bond length 2.194(9) Å). The magnesium atom is in a trigonal planar geometry, completing its coordination environment with a terminal TMP (Mg - N(1) bond length 1.993(6) Å) and a bridging TMP (Mg - N(2) bond length 2.068(7) Å). The sodium atom has electrostatic interactions with both the alpha- and beta- position of the *P*-phenylphosphindole (Na - C bond lengths of 2.798(8) and 2.945(8) Å respectively). The sodium atoms coordination environment is completed by a bridging TMP (Na - N(2) bond length 2.508(7) Å) and a chelating, bidentate TMEDA.

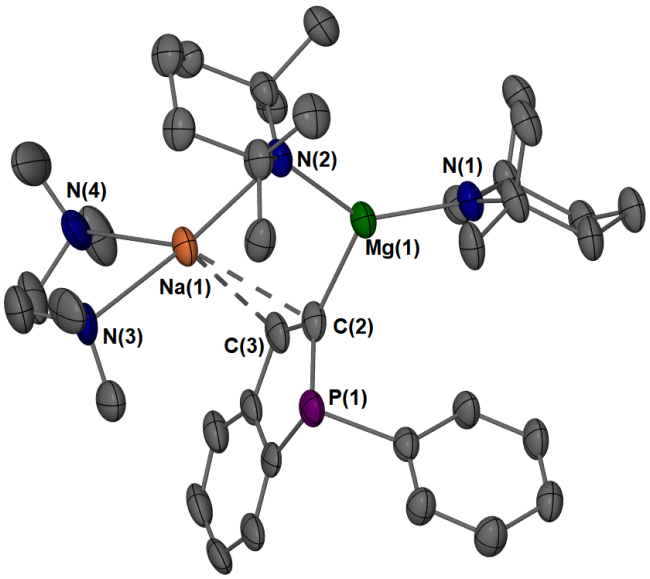

Figure 5.6: Molecular structure of **31**. Thermal ellipsoids shown at 40 % probability. Hydrogen atoms and a hexane solvent molecule omitted for clarity. Selected bond lengths (Å) and angles (°): Mg(1) - C(2), 2.194(9); Mg(1) - N(1), 1.993(6); Mg(1) - N(2), 2.068(7); Na(1) - C(2), 2.798(8) ; Na(1) - C(3), 2.945(8); N(2) - Mg(1) - C(2), 107.1(3); N(1) - Mg(1) - N(2), 133.3(3); C(1) - Mg(1) - N(1), 119.4(3); Na(1) - N(3) - Mg(1), 90.8(3).

5.4.2 Solution state analysis of 31

Complex **31** was dissolved in C_6D_6 and analysed by ^{1}H and $^{31}P\{^{1}H\}$ NMR spectroscopy (see Figure 5.7). While the coupling within the phosphindole leads to a complicated aromatic region, the phenyl-group protons and the C3-H can be identified by integration and coupling to ^{31}P nuclei respectively. Signals are evident for coordinated TMEDA, as well as TMP. The $^{31}P\{^{1}H\}$ NMR spectrum (see Figure 5.8) shows one sharp signal at 29.74 ppm (compared to 0.43 ppm in free *P*-phenylphosphindole).

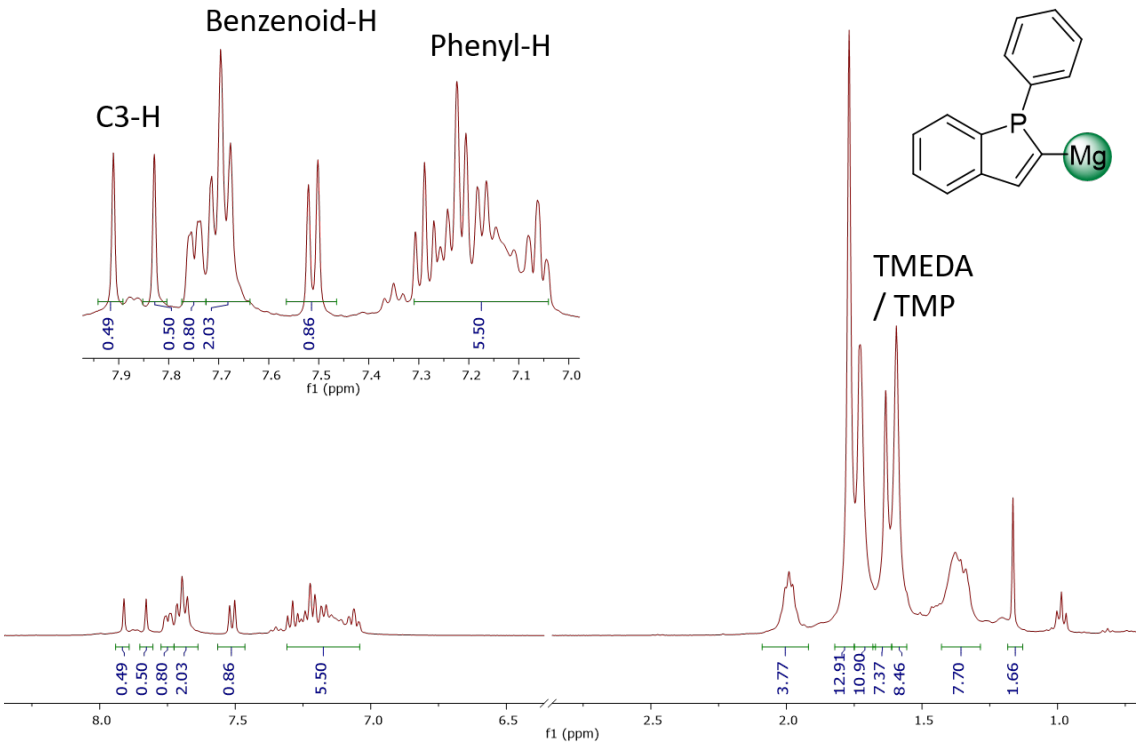

Figure 5.7: ^{1}H NMR spectrum of **31** in C_6D_6 at 298 K

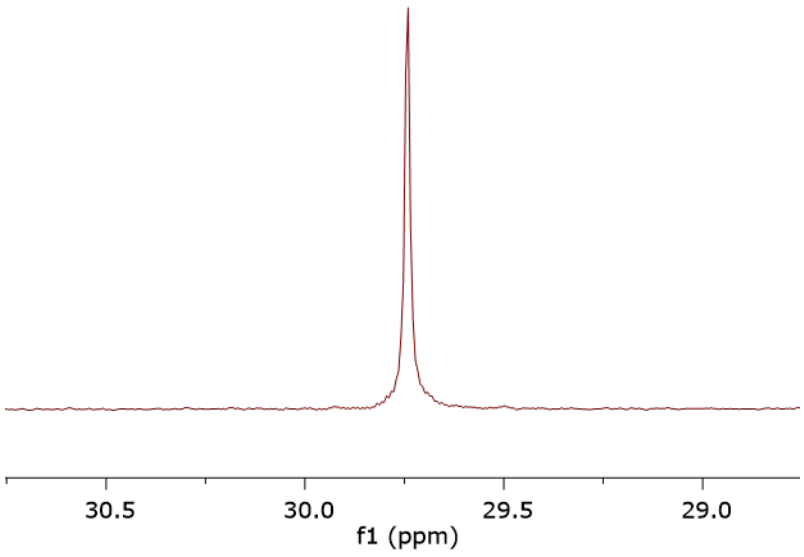

Figure 5.8: $^{31}P\{^{1}H\}$ NMR spectrum of **31** in C_6D_6 at 298 K

To an *in situ* reaction mixture of **32**, an iodine solution (1 M in THF) was added dropwise

at room temperature. The resulting suspension was stirred for 30 minutes, before the addition of sodium thiosulphate until bleaching occurred. The organic layer was washed with 5 % HCl (3 x 10 mL), to remove any amines present. *P*-phenyl-2-iodo-phosphindole oxide was isolated as a crystalline solid in a high yield of 73 % (see Scheme 5.10).

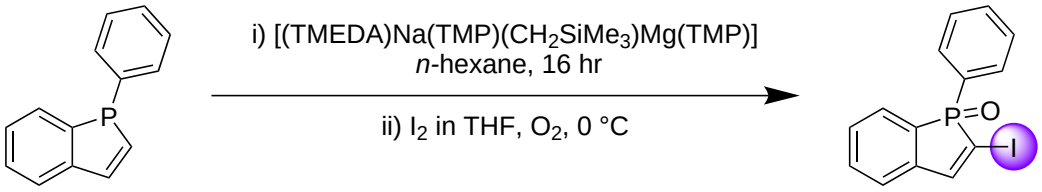

Scheme 5.10: Iodine quench of complex **31**

5.5 Reaction of the magnesiate base 1 with *P*-phenylphosphindole oxide

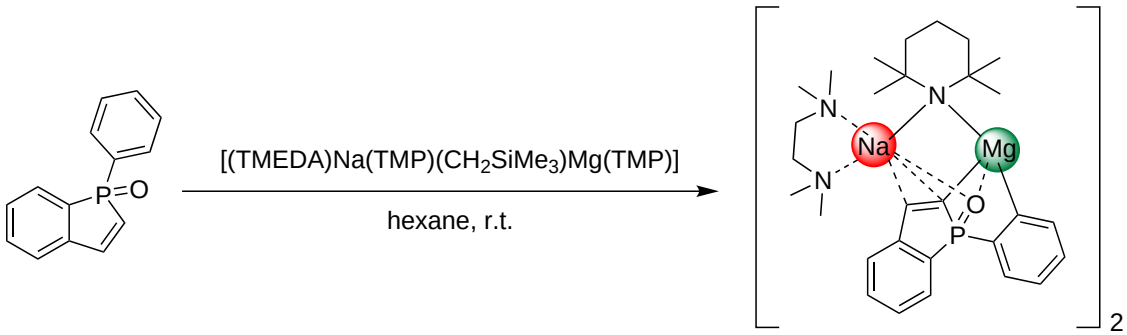

Scheme 5.11: Reaction of the magnesiate base **1** with *P*-phenylphosphindole oxide

The magnesiate base **1** was prepared as a hexane solution, before being transferred via cannula to a Schlenk containing a molar equivalent of *P*-phenylphosphindole oxide. Overnight, a large quantity of a brown precipitate formed. Following hot filtration, single crystals grew which were found to be the di-magnesiated structure [(TMEDA)Na(TMP)($\alpha-C_8H_5PO-$*ortho*$-C_6H_4$)Mg]$_2$ **33**.

5.6 Solid state analysis of 33

The molecular structure of **33** shows a di-deprotonated *P*-phenylphosphindole oxide, in both the α position of the phosphindole ring and the *ortho*-position of the phenyl ring (Mg

- C bond lengths of 2.217(3) and 2.205(3) Å respectively). Interestingly, this manifests as an intermolecular di-magnesiation, as the magnesium bridges between two separate phosphindole units (see Figure 5.10 for full molecular structure). Both the magnesium atom and the sodium atom are interacting with the oxygen of the phosphine oxide (M - O bond lengths of 2.0443(18) and 2.320(2) Å respectively). The magnesium bonds to a bridging TMP (Mg - N bond length 2.101(2) Å). The sodium atoms are four coordinate, bonding to a bridging TMP (Na - N bond length 2.484(2) Å), the previously mentioned oxygen, and a chelating, bidentate TMEDA (Na - N bond lengths of 2.570(2) and 2.455(2) Å).

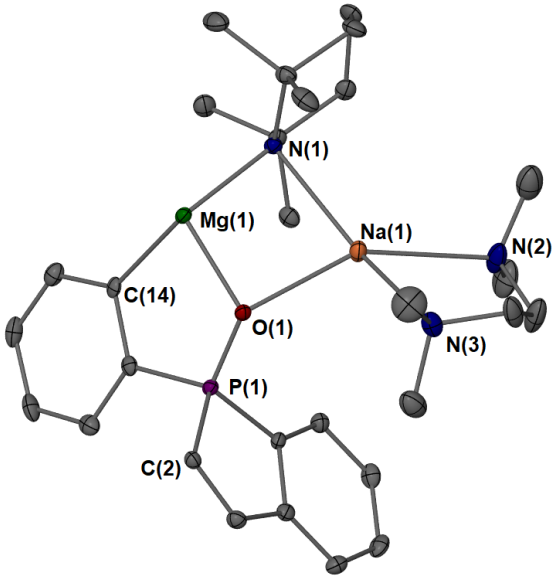

Figure 5.9: Molecular structure of **33**. Thermal ellipsoids shown at 40 % probability. Hydrogen atoms omitted for clarity. Selected bond lengths (Å) and angles (°): P(1) - O(1), 1.5254(17); Mg(1) - C(14), 2.205(3); Mg(1) - O(1), 2.0443(18); Na(1) - O(1), 2.320(2); Na(1) - N(1), 2.484(2); Mg(1) - N(1), 2.101(2); Na(1) - N(2), 2.570(2); Na(1) - N(3), 2.455(2); C(14) - Mg(1) - O(1), 86.08(8); N(1) - Mg(1) - O(1), 99.65(8); Mg(1) - N(1) - Na(1), 91.48(7); Na(1) - O(1) - P(1), 132.27(10).

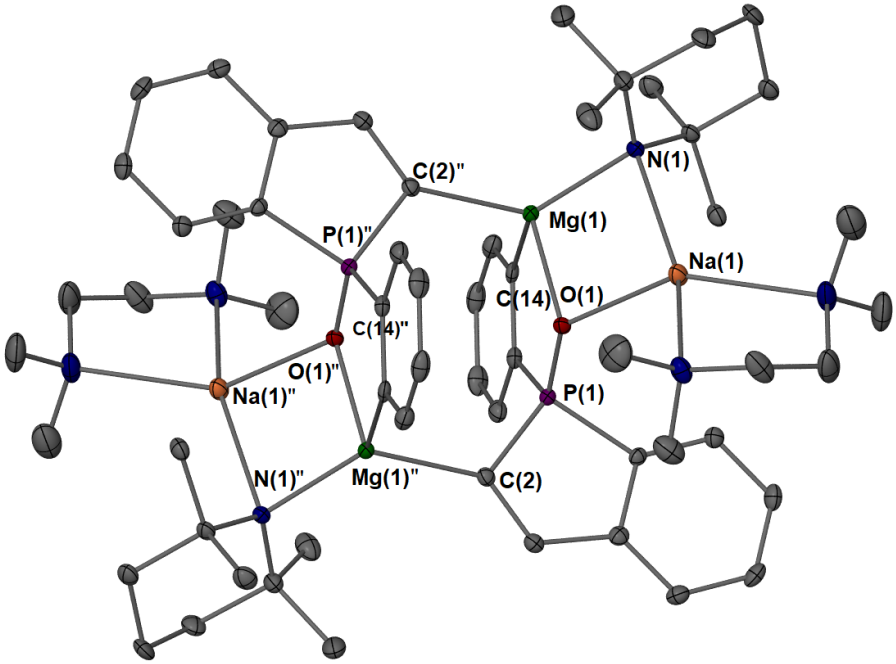

Figure 5.10: Molecular structure of **33**. Thermal ellipsoids shown at 40 % probability. Hydrogen atoms omitted for clarity. Selected bond lengths (Å) and angles (°): P(1) - O(1), 1.5254(17); Mg(1) - C(14), 2.205(3); Na(1) - O(1), 2.320(2); Na(1) - N(1), 2.484(2); Mg(1) - N(1), 2.101(2); Na(1) - N(2), 2.570(2); Na(1) - N(3), 2.455(2); C(14) - Mg(1) - O(1), 86.08(8); N(1) - Mg(1) - O(1), 99.65(8); Mg(1) - N(1) - Na(1), 91.48(7); Na(1) - O(1) - P(1), 132.27(10); Mg(1) - C(2)", 2.217(3)

5.6.1 Solution state analysis of complex 33

Compound **33** was dissolved in C_6D_6 and analysed by ^{1}H and ^{31}P NMR spectroscopy. Interestingly, no signals are evident for the deprotonated *P*-phenylphosphindole oxide unit (see Figure 5.11) - instead, only signals relating to the TMP and TMEDA are visible. The $^{31}P\{^{1}H\}$ NMR spectrum shows no signal at all (see Figure 5.12).

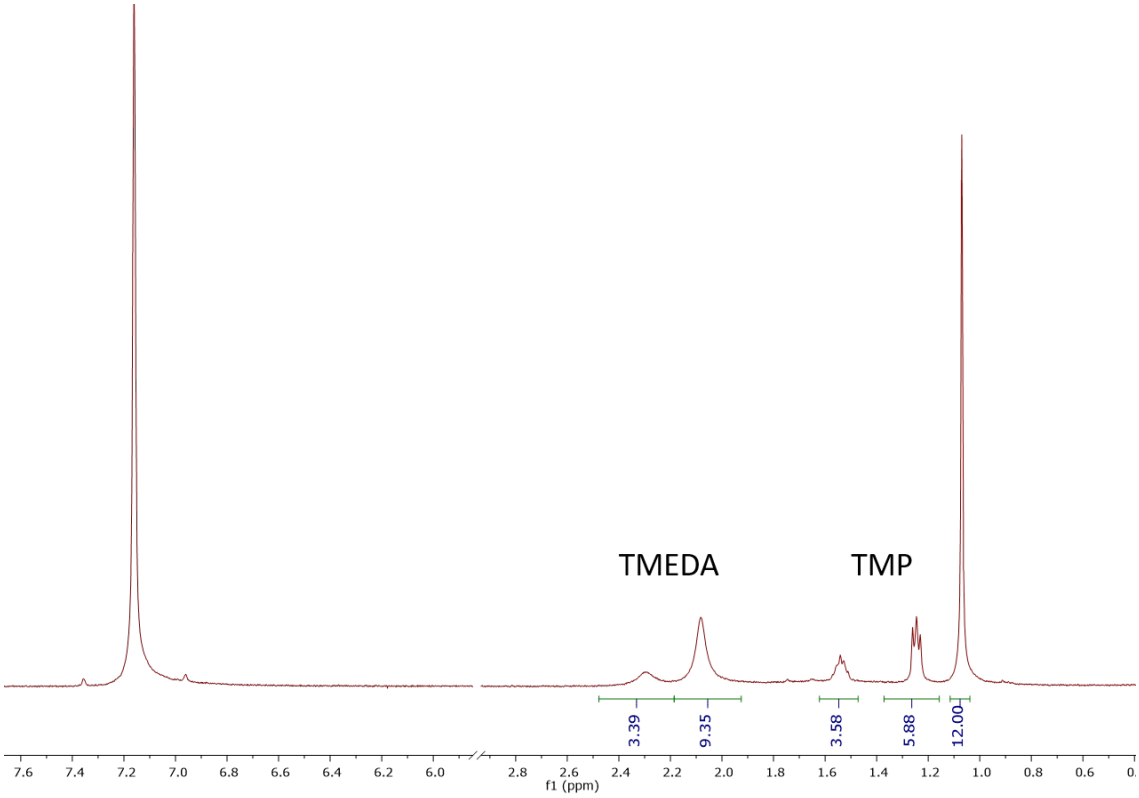

Figure 5.11: ^{1}H NMR spectrum of **33** in C_6D_6 at 298 K

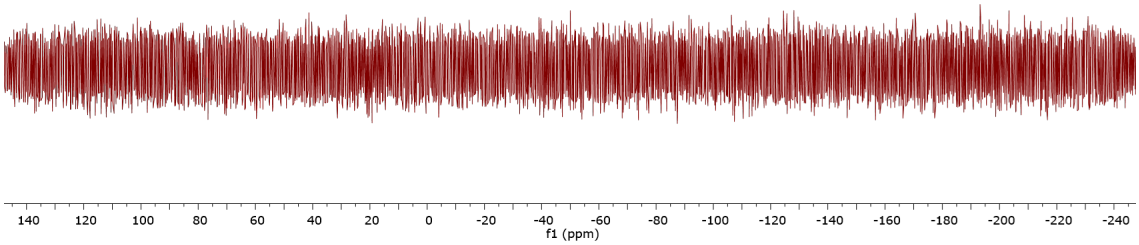

Figure 5.12: $^{31}P\{^{1}H\}$ NMR spectrum of **33** in C_6D_6 at 298 K

In order to determine if their was any phosphindole in the NMR sample, MeOD was added (0.1 mL), to quench any reactive metal species and return deuterated starting material. Interestingly, this led to signals being present for the phosphindole species, including in the $^{31}P\{^{1}H\}$ NMR spectrum (see Figure 5.13 and Figure 5.14). The presence of the *P*-phenylphosphindole oxide was also supported by GC/MS analysis to be present.

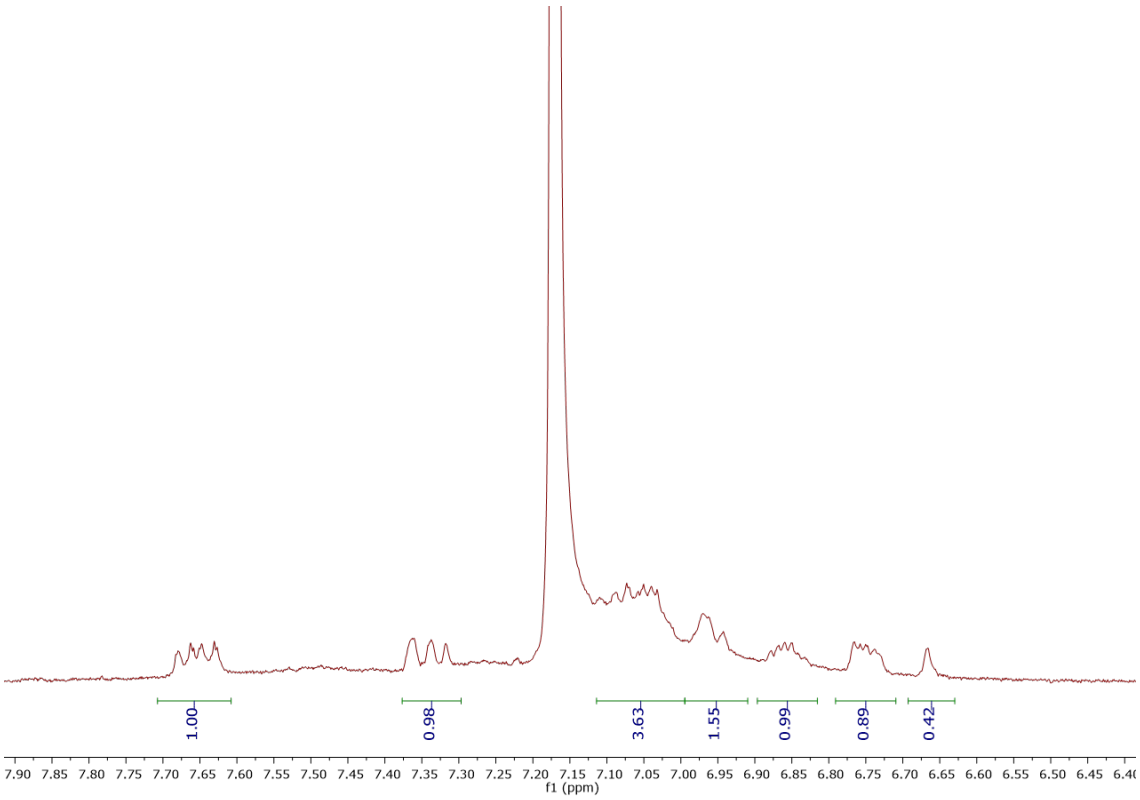

Figure 5.13: ^{1}H NMR spectrum of **33** in C_6D_6 after the addition of 0.1 mL MeOD at 298 K

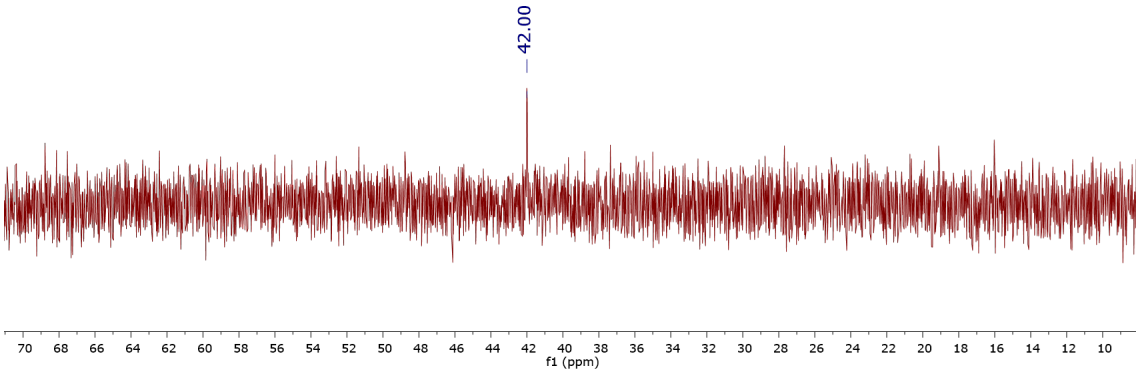

Figure 5.14: ^{31}H NMR spectrum of **33** in C_6D_6 after the addition of 0.1 mL MeOD at 298 K

5.6.2 EPR characterisation of complex 33

As it seemed likely we were dealing with a NMR silent radical species, we sought new collaborations to conduct EPR (electron paramagnetic resonance) measurements of **33**. These measurements and the subsequent data analysis were conducted at the Australian National University in collaboration with Assoc. Prof. Nick Cox and Martyna Judd.

CW X-band *EPR* (Solution Phase and Solid Phase, low temperature)

The solution-phase EPR spectrum of the sample is shown in Figure 5.15. The dominant structure is a three-line 44 MHz (1.57 mT) splitting indicative of a strongly localized (43 % spin density) ^{14}N-centred radical (I = 1). Each of the three derivative shaped lines is further split by a fine structure consisting of two main features: (i) a $<$ 1 MHz multiline splitting on each main nitrogen derivative feature, and (ii) a broader 5 MHz splitting manifesting as shoulder structures about each nitrogen line. The former multiline pattern (i) was attributed to a 0.56 MHz splitting from two pairs of six equivalent methyl-group protons closest to the nitrogen radical, in addition to a 0.92 MHz and 0.78 MHz hyperfine contribution from the ^{23}Na (I = 3/2) and ^{31}P (I = 1/2) nuclei respectively. The broader shoulder feature (ii) could be fit by including a 5.0 MHz contribution from the 10 % abundant ^{25}Mg (I = 5/2) nucleus. These hyperfine contributions were determined in tandem with the double resonance pulse measurements detailed in the sections that follow. Details of the simulation best-fit parameters are summarized in table 5.1.

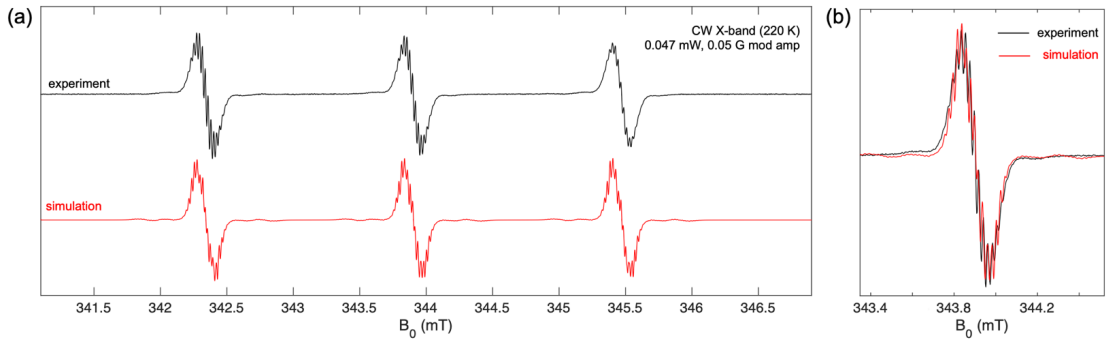

Figure 5.15: CW X-band spectrum of the radical sample in toluene at 220 K comparing the experimental (black trace) and simulated (red trace) spectra, where the simulation was modelled using the parameters in table 5.1. The insert in (b) shows the central feature in (a) enlarged with the experimental and simulated traces superimposed.

Table 5.1: Fitting parameters for simulations of the CW EPR radical spectrum in Figure 5.15. Spectral features were modelled using the EasySpin package garlic.

Parameter	Modelled Value
g-value	2.00748
Linewidth (Lorentzian)	0.012 mT
Hyperfine couplings \MHz (% spin density)	
A(N)	43.9 (43 %)
A(Mg)	5.00 (5.7 %)
A(Na)	0.92 (<1 %)
A(P)	0.78 (<1 %)
A(H) x 6	0.56 (6.6 % for all 6 H)

The solid-phase spectrum (see Figure 5.16) was obtained by cooling the sample to 120 K, i.e. below the freezing point of toluene where the spectrum is dominated by the anisotropic component of the nitrogen hyperfine interaction. The sample was measured using a power of 0.0047 mW (45 dB attenuation) to meet non-saturating conditions, using a field modulation amplitude of 1 G. Simulations used the EasySpin solid-state CW program pepper. The simulation fitting parameters used are shown in table 5.2. The spectrum can be modelled by assuming a rhombic g-tensor with the large component of the hyperfine splitting along the A_{zz} axis of the hyperfine tensor A. To model the linewidths, H-strain, which specifies a Gaussian broadening in each axis direction, was included to account for unresolved hyperfine splittings along the A_{xx} and A_{yy} axes. The modelled A-tensor agrees with the isotropic component fit to the solution spectrum: A = A_{iso} + A_{dip}, where A_{dip} is the anisotropic dipolar traceless tensor [$^{d}A_{xx}$ $^{d}A_{yy}$ $^{d}A_{zz}$], and A/3 = A_{iso}, i.e. [2 35 93]/3= 43.7 MHz.

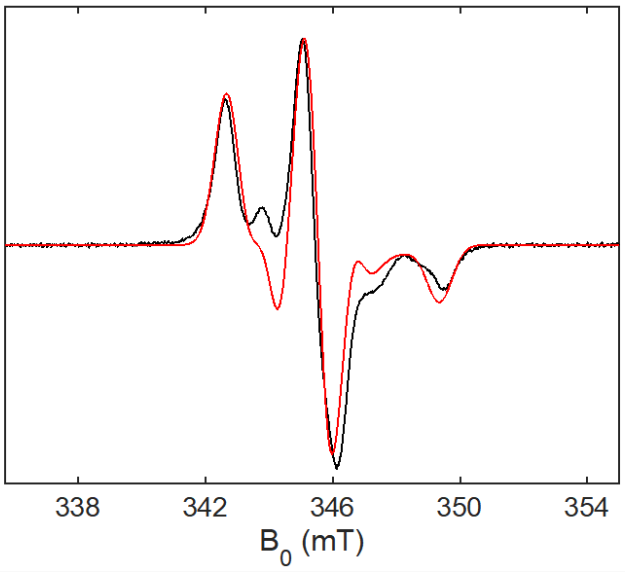

Figure 5.16: CW X-band solid state spectrum of the radical sample in toluene at 120 K comparing the experimental (black trace) and simulated (red trace) spectra, where the simulation was modelled using the parameters in table 5.1.

Table 5.2: Fitting parameters for simulations of the CW EPR low-temperature spectrum in Figure 5.16. Simulation was run using the EasySpin package pepper

Parameter	Modelled Value
g-tensor	[2.0110 2.0068 2.0038]
Linewidth (Gaussian)	0.63 mT
^{14}N hyperfine [$A_{xx}A_{yy}A_{zz}$] (MHz)	[2 35 93]
H-Strain [$A_{xx}A_{yy}A_{zz}$] (MHz)	[20 10 15]

Mims ENDOR on ^{31}P, ^{23}Na and ^{1}H

The measured Mims ENDOR spectra are depicted in Figure 5.17, scaled and normalized to the maximum intensity of each spectrum. Both ^{1}H spectra show a clear proton matrix line as well as suggestions of broader 5-11 MHz couplings. The ^{23}Na spectrum appears to similarly average to a matrix-line peak, with a possible broader 4.8 MHz structure as well. The ^{31}P spectrum gives the most structured spectrum of the three nuclei, with clear shoulder features arising as 2.7 MHz and 5.2 MHz couplings. These results are more or less consistent with the X-band HYSCORE detailed in the section below.

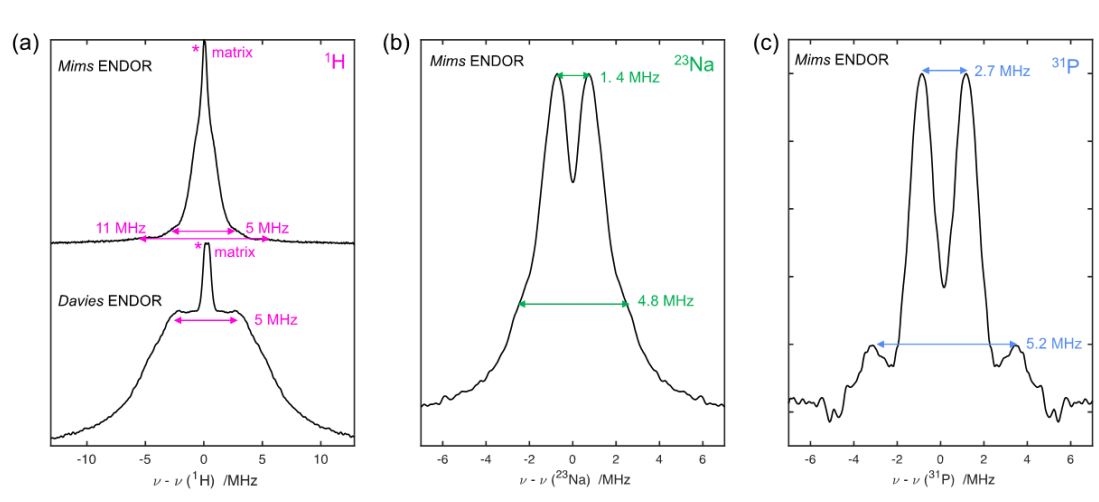

Figure 5.17: *MIMS ENDOR spectra (a-c)* for ^{1}H, ^{23}Na and ^{31}P couplings respectively, and ^{1}H *Davies* ENDOR in (a) for comparison. *Davies* could only be performed at the proton frequency owing to blind spotting at the centre of the ^{23}Na and ^{31}P positions

ESEEM and HYSCORE for ^{25}Mg Hyperfine

ESEEM and HYSCORE are coherence-transfer experiments that lend themselves to detecting low-frequency nuclear couplings, and at W-band can be useful to extracting the Magnesium couplings in this system ($\nu(^{25}\text{Mg})$ = 8.7 MHz at W-band). Three-pulse ESEEM experiments were performed using the sequence $\pi/2 - \tau - \pi/2 - \text{T}+d\text{t} - \pi/2 - \tau -$ echo, recorded as a function of T+dt, using $\pi/2$ = 20 ns, T = 80 ns, dt = 4 ns at different fixed values of τ. Figure 5.18 shows the experimental and simulated spectra for τ = 200, 450, 700 and 950 ns in both the time (Figure 5.18a) and Fourier-transformed (Figure 5.18b) frequency domain. The spectra were simulated using the EasySpin program saffron for pulse experiments, and were fit by including ^{25}Mg and ^{14}N couplings. The ^{25}Mg coupling accounts for the larger peaks around 9 MHz in the fft spectrum (Figure 5.18b) and was modelled as A(^{25}Mg) = 5.044 + [-1.68, -2.52, 4.2] MHz, where the first term is the isotropic hyperfine value A_{iso} obtained in the CW solution spectrum (Figure 5.15), and the second tensor term is the anisotropic traceless dipolar interaction [A_{xx} A_{yy} A_{zz}]. A quadrupole interaction of [2.0. 0.0] MHz was also included in the simulation. The ^{14}N accounts for the feature around 30 MHz (for a nucleus in the strong coupling regime, the signal will appear at half the hyperfine, split by twice the Larmor frequency). The coupling was originally fit

to the same anisotropic **A** tensor that was modelled for the X-band solid-state spectrum in Figure 5.16, but a better fit was obtained using the values **A** = 44.0 + [-11.7 -14.3 26.0] MHz (= [32.3 29.7 70.0 MHz]) This is substantially different from the tensor fit to the CW 120 K spectrum. However, the W-band is subject to bandwidth limitations – only a component of the nitrogen interaction will ever be excited meaning a direct comparison cannot be made to the X-band data, and it is therefore also difficult to simulate accurately.

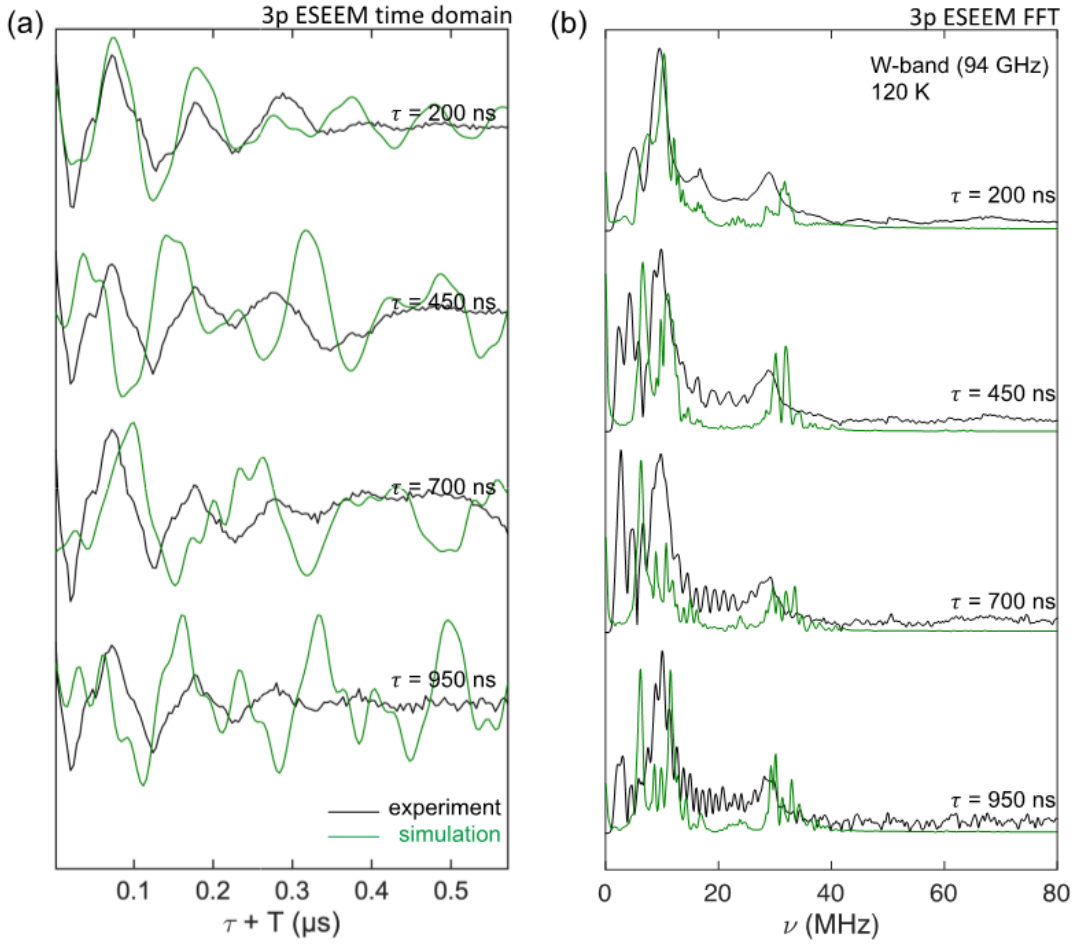

Figure 5.18: 3-p ESEEM in the time domain (a) and frequency domain (b) comparing the experimental (black trace) and simulated (green trance) spectra at different values of τ, as annotated on each spectrum

The HYSCORE experiment is a 2D version of the 3-pulse ESEEM experiment and discriminates between interactions in the strong and weak coupling regimes. Weakly coupled nuclei appear at the nuclear Larmor frequency in the (+, +) quadrant (upper right), split by the hyperfine frequency about the antidiagonal. Strongly coupled nuclei appear

in the (+, -) quadrant (upper left) at half the hyperfine frequency (A/2), split by twice the Larmor frequency 2νN about the diagonal. Like in 3-pulse ESEEM, the spectrum is collected over several fixed τ values and averaged in the time domain before Fourier transforming.

The W-band HYSCORE spectrum for this system is shown in Figure 5.19. The vertical lines in the two quadrants indicate the expected weak vs strong couplings given the ^{25}Mg interactions predicted so far. The HYSCORE shows signals that could be roughly ascribed to an Mg interaction in both quadrants, although the apparent ^{25}Mg hyperfine visualized in the HYSCORE in the (+, -) quadrant is larger than what was modelled in the CW EPR spectrum and the ESEEM. However, both the HYSCORE and 3-pulse ESEEM were subject to artefacts (appearing as dips or oscillations at T + t = τ), meaning the low-frequency regions could be distorted. Regardless, the presence of distinct real features in both the (+,-) and (+, +) quadrants suggests that the ^{25}Mg interaction is likely intermediate between the strong and weak coupling regimes.

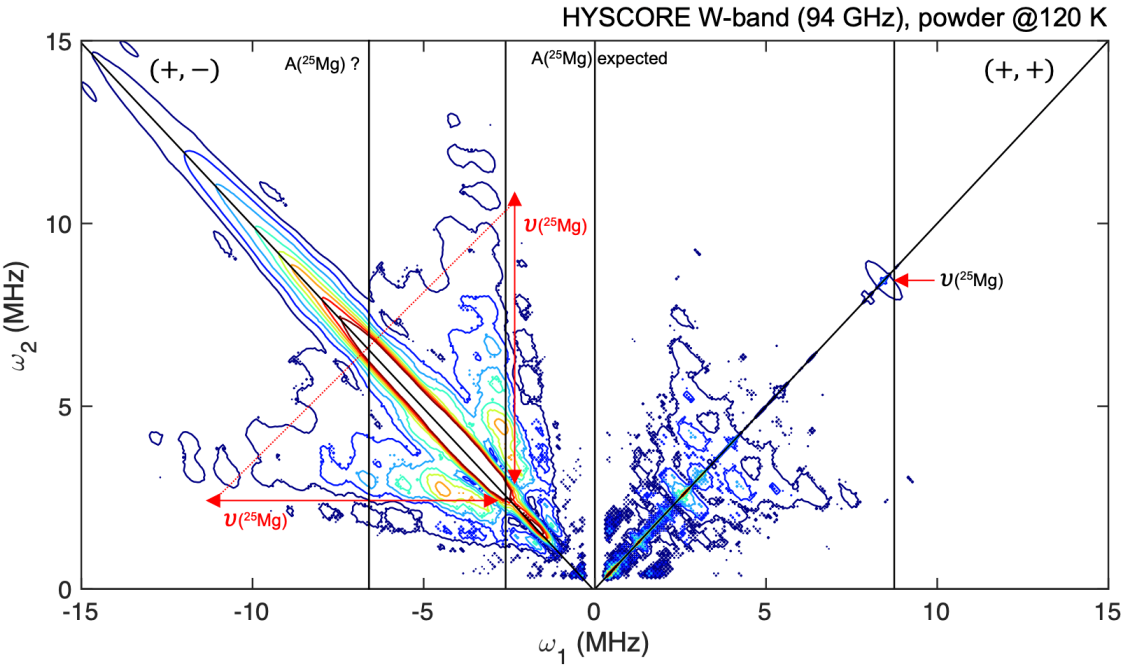

Figure 5.19: W-band HYSCORE annotated with the strong (+,-) vs weak (+,+) coupling regimes and possible ^{25}Mg signals.

HYSCORE was also performed at X-band on a frozen solution (toluene solvent) sample

at 50 K (using liquid Helium). This spectrum is shown in Figure 5.20 and supports both the CW and ENDOR measurements detailed above. The ^{1}H, ^{23}Na and ^{31}P nuclei are clearly in the weak coupling regime, which supports the proposition that the spin density of the system is delocalized from the nitrogen towards the direction of the Mg nucleus, rather than towards the Na nucleus. The couplings observed in the X-band HYSCORE are broadly consistent with those observed in the W-band ENDOR experiments, with the exception of the large ^{31}P (12 MHz) coupling, which could not be resolved from the noise in ENDOR.

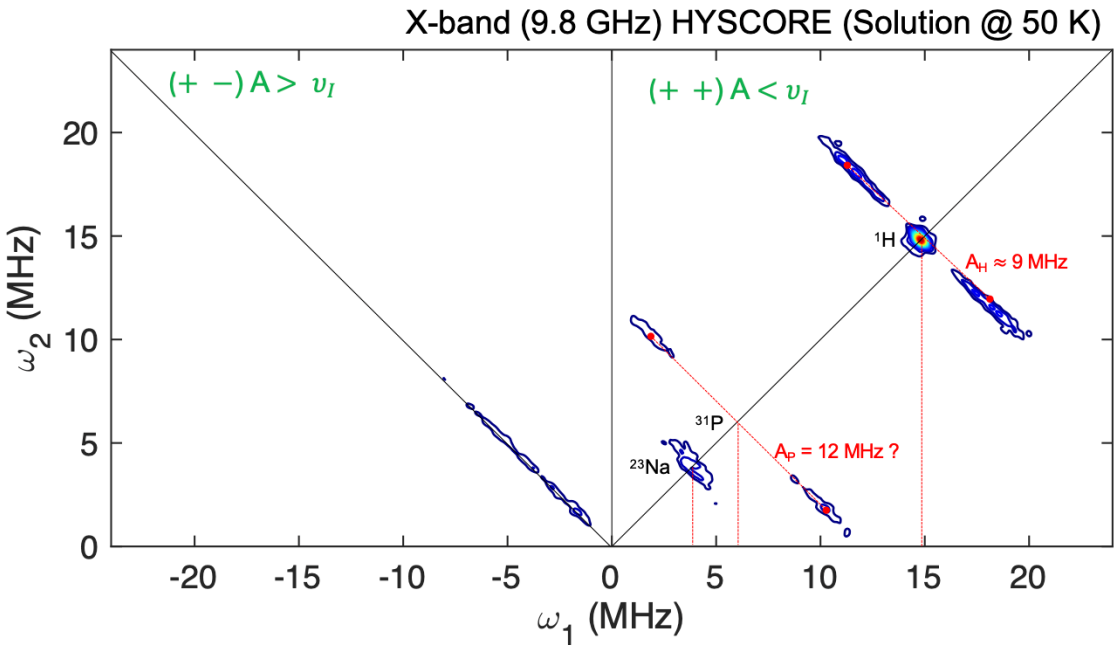

Figure 5.20: X-band HYSCORE annotated with the strong (+,-) vs weak (+,+) coupling regimes and showing the weakly-coupled nuclear signals.

Conclusions of EPR studies of 33

At this stage, one interpretation of the information presented points towards a nitrogen centred radical species. The hypothesised structure is pictured in Figure 5.21. Further work is ongoing to determine the precise nature of this radical species, as well as computational work to model the structure and position of the radical.

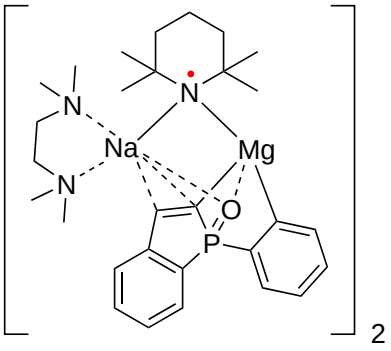

Figure 5.21: Proposed structure of the radical species of **33**

5.7 Synthesis of 5-phenyl-5H-benzo[b]phosphindole oxide

Looking to extend the phosphindole oxide series, we next sought to explore the reactivity of 5-phenyl-5H-benzo[b]phosphindole oxide (see Figure 5.22).

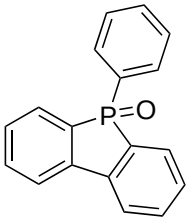

Figure 5.22: Target benzo[b]phosphindole

To synthesise these target molecules, we first targeted the synthesis of 2,2'-dibromobiphenyl, which could then be di-lithiated and quenched with *P,P*-dichlorophenylphosphine to form the corresponding 5-phenyl-5H-benzo[b]phosphindole. 2,2'-Dibromobiphenyl could be readily synthesised by the addition of a half molar equivalent of *n*-BuLi to 1,2-dibromobenzene in THF at -78 ° C, and allowing the mixture to warm to room temperature. Following the addition of water, the corresponding 2,2'-dibromobiphenyl could be isolated in a high yield, and recrystallised from *n*-hexane (see Scheme 5.12).

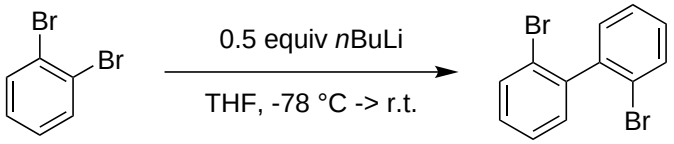

Scheme 5.12: Synthesis of 2,2'-dibromobiphenyl

To a solution of 2,2'-dibromobiphenyl in diethyl ether was added two equivalents of *n*-BuLi at 0 ° C. After two hours stirring, a solution of *P,P*-dichlorophenylphosphine in diethyl ether was added dropwise, resulting in the formation of the desired 5-phenyl-5H-benzo[b]phosphindole (see Scheme 5.13).

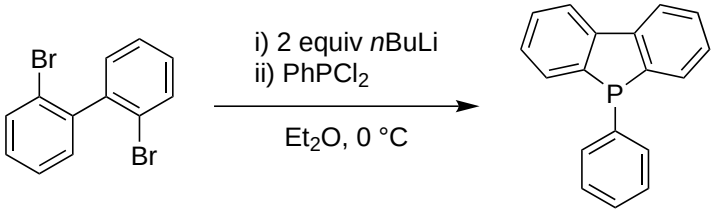

Scheme 5.13: Synthesis of 5-phenyl-5H-benzo[b]phosphindole

While this method was convenient, shortage of the 1,2-dibromobenzene led us to explore another synthesis method. Two molar equivalents of phenyllithium were added to a solution of triphenylphosphine oxide in THF, resulting in a dark red solution. This solution was heated to reflux overnight (16 hrs), before being cooled to room temperature and quenched with aqueous $NaHCO_3$. The crude residue was purified by column chromatography (silica gel, EtOAc, compound was dry loaded on celite), to give the desired product in a high crystalline yield (typical yields > 80 %). The desired phosphine oxide could be readily obtained by the addition of H_2O_2 to a stirred THF solution of the phosphindole.

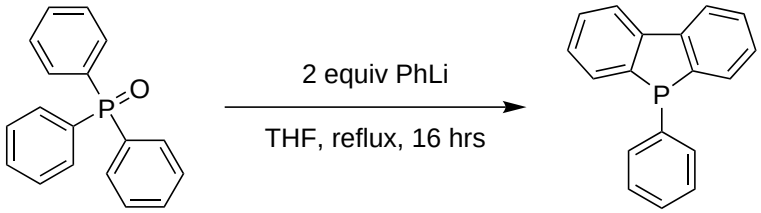

Scheme 5.14: Alternative synthesis of 5-phenyl-5H-benzo[b]phosphindole from triphenylphosphine oxide and phenyllithium

5.7.1 Reaction of the magnesiate base 1 with 5-phenyl-5H-benzo[b]phosphindole oxide

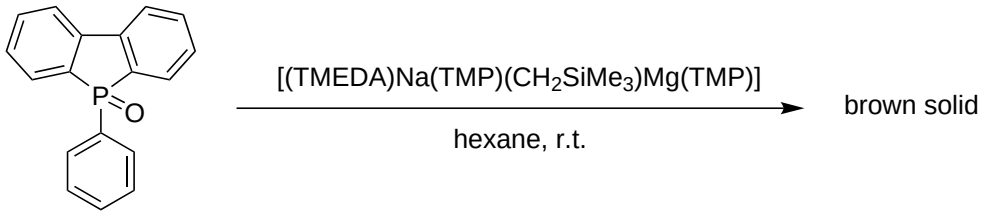

Scheme 5.15: Reaction of the magnesiate base **1** with 5-phenyl-5H-benzo[b]phosphindole oxide

A molar equivalent of 5-phenyl-5H-benzo[b]phosphindole oxide was added as a solid portion to a stirred solution of the magnesiate base **1**. This resulted in the deposition of a large quantity of a brown solid (see Scheme 5.15). This was isolated by filtration, washed with *n*-hexane and dried *in vacuo*. It was transferred to a glovebox for storage. This complex will be referred to as complex **34**.

The brown solid was dissolved in C_6D_6 and analysed by ^{1}H and $^{31}P\{^{1}H\}$ NMR spectroscopy (see Figure 5.23 and Figure 5.24 respectively). Unfortunately, similarly to **33**, the isolated species here is NMR silent, and no signals corresponding to the benzo[b]phosphindole could be observed in either the ^{1}H or $^{31}P\{^{1}H\}$ NMR spectrum.

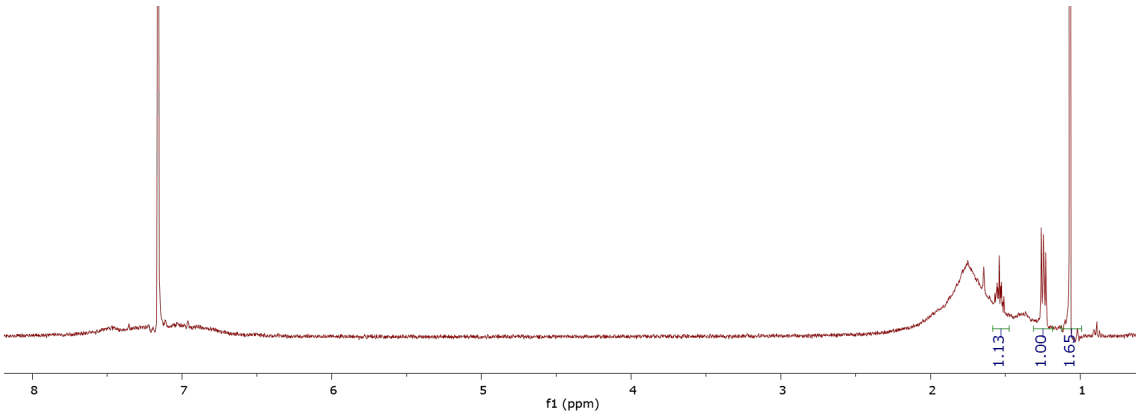

Figure 5.23: ^{1}H NMR spectrum in C_6D_6 of the brown solid from the reaction of the magnesiate base **1** with 5-phenyl-5H-benzo[b]phosphindole oxide at 298 K

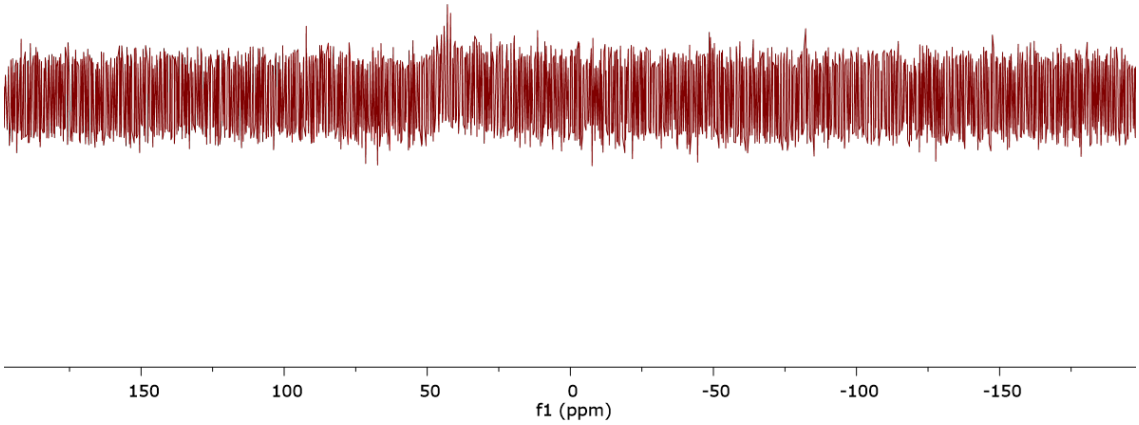

Figure 5.24: $^{31}P\{^{1}H\}$ NMR spectrum in C_6D_6 of the brown solid from the reaction of the magnesiate base **1** with 5-phenyl-5H-benzo[b]phosphindole oxide at 298 K

Similarly to **33**, the addition of 0.1 mL of MeOD to quench any metallated species resulted in the reappearance of signals corresponding to the benzo[b]phosphindole (see Figure 5.25 and Figure 5.26).

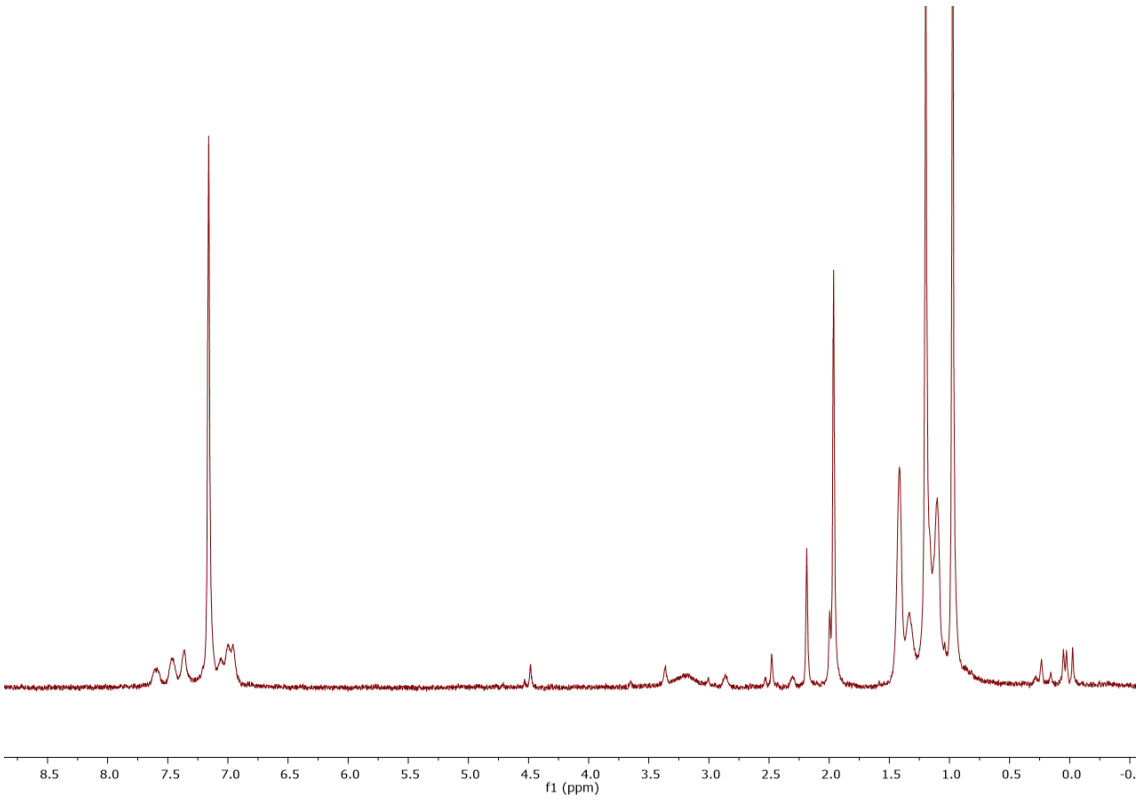

Figure 5.25: ^{1}H NMR spectrum in C_6D_6 of the brown solid from the reaction of the magnesiate base **1** with 5-phenyl-5H-benzo[b]phosphindole oxide after the addition of 0.1 mL MeOD at 298 K

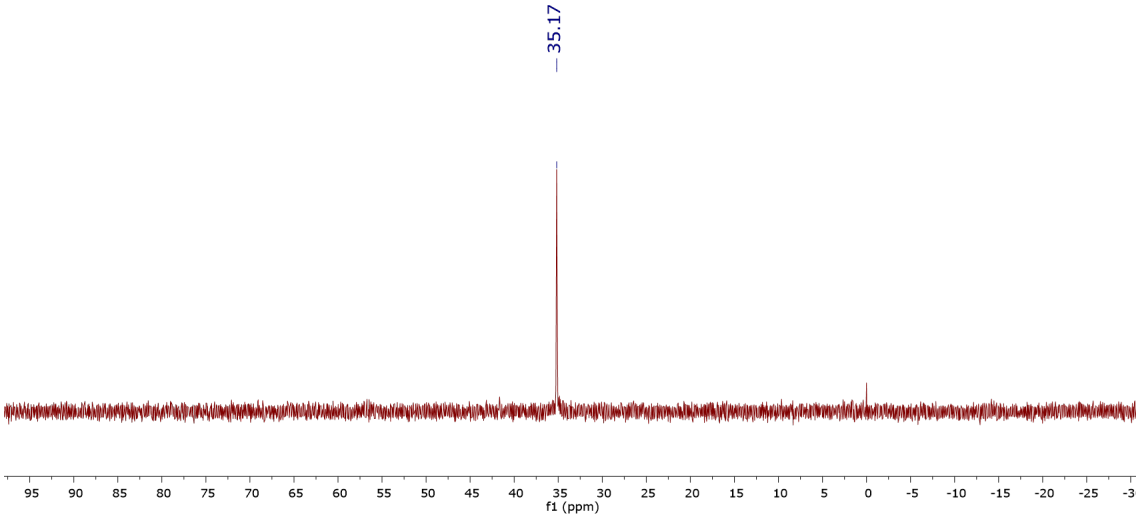

Figure 5.26: $^{31}P\{^{1}H\}$ NMR spectrum in C_6D_6 of the brown solid from the reaction of the magnesiate base **1** with 5-phenyl-5H-benzo[b]phosphindole oxide after the addition of 0.1 mL MeOD at 298 K

As it appeared we were dealing with another radical species, samples were sent for EPR analysis at the Australian National University. Unfortunately, only a very weak signal was

obtained during this analysis, suggesting the possibility that the radical species in this case was a minor impurity, rather than the dominant species present.

To try and confirm what metallation position (if any) was present in this sample, we next sought to do an iodine quench of the *in situ* mixture. The resulting residue was analysed by ^{1}H and $^{31}P\{^{1}H\}$ NMR spectroscopy, as well as GC/MS. Interestingly, a mixture of all six possible regioisomers is observed, as well as substantial starting material (see Figure 5.27 for the GC/MS chromatogram and MS spectrum). After this result, further work was not pursued as it became clear that no selective metallation would be achieved.

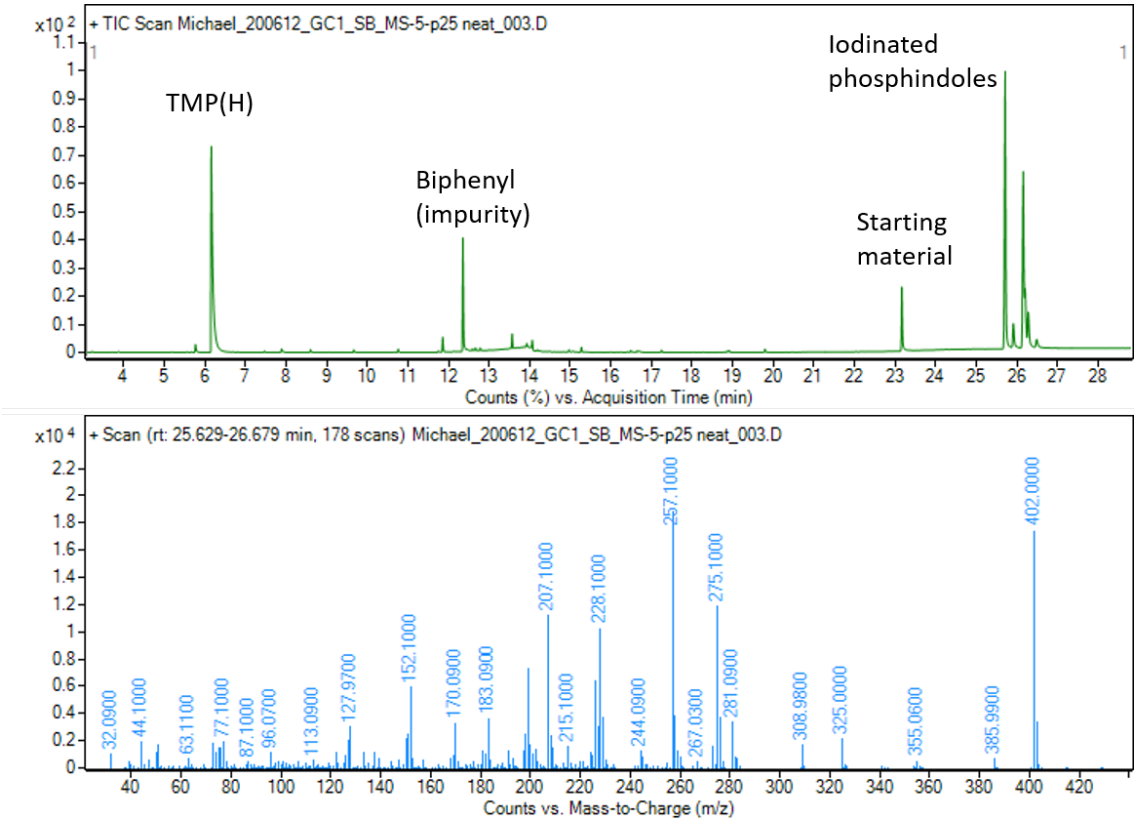

Figure 5.27: GC/MS analysis of the crude reaction product of the iodine quench of complex **34**

5.8 Conclusions and future work

This work has reported the first magnesiations of *P*-heterocyclic molecules. In the case of *P*-phenylphosphindoles, it was found that differing reactivity was observed dependent on the oxidation state of the phosphorus atom, where phosphorus(III) complexes led

to single deprotonations, whereas phosphorus(V) oxides favoured di-deprotonations, as well as the generation of NMR silent paramagnetic species. When moving to *P*-phenyl-benzo[b]phosphindole oxide, it appears another paramagnetic species is been generated, however this needs further exploration.

Further work is necessary to tie down the exact nature of the radical species generated in the reaction of the magnesiate base **1** with phosphorus(V) heterocyclic molecules. Preliminary experiments involving radical traps (such as TEMPO) have been conducted, however more extensive studies are required. The synthesis of a variety of phosphindoles and their corresponding phosphine oxides could also be explored. These can be readily synthesised by varying the phosphine dichloride species used when quenching the dilithio-species in the synthesis of *P*-phenylphosphindole.

Unfortunately this aspect of the overall research project was heavily affected by the global COVID-19 pandemic, and the associated university shutdowns and border closures within Australia. This was further exacerbated by the breakdown of key analytical facilities within Monash University in 2020.

6 Overall Project Conclusions and Future Work

This research project has extended the reactivity profile of the sodium magnesiate [(TMEDA)Na(TMP)(CH_2SiMe_3)Mg(TMP)] **1**, exploring its metallation chemistry with a variety of *N*- and *P*- containing molecules. This includes the first reported magnesiations of *P,P*-dialkylphenylphosphines as well as *P*-heterocyclic phosphindoles. This has led to the surprising outcome of the generation of stable radical species, which require a more detailed, comprehensive study to fully understand. This study would include the synthesis of a range of *P*-substituted phosphindoles and phosphindole oxides. Additionally, a study on their corresponding reactivity with the sodium magnesiate **1** would allow the full elucidation and synthetic potential of these new radical species to be examined. It should also be extended to a range of mono- and bi-metallic bases, to see what the necessary components are for the generation of these radical species. The exploration of a variety of phosphine oxides, as well as other phosphorus (V) species (for example, phosphorus (V) sulfides, boranes), could also be explored. Detailed computational studies should also be conducted, to gain further insight into the nature of the radical species generated.

The reactivity of the sodium magnesiate **1** could also be explored against a larger range of functionalised aromatics, as well as other traditionally sensitive functional groups (halides, aldehydes, ketones, esters, etc).

Investigating a range of *N*-heterocyclic molecules with **1** as predominately returned α-magnesiations, with atom efficient metallations occurring when *N*-methyl and *N*-ethyl directing groups are present. Further work should focus on changing the steric and electronic nature of the directing groups present, to attempt to access the magnesiation of the benzenoid ring. For instance, *N*-triisopropylsilyl-3-dimethylaminomethyl-indole allows access to the C4 position in established lithium chemistry, and should be explored with the sodium magnesiate **1**. Furthermore, the extension to other cross-coupling reactions,

such as iron catalysed cross-coupling should be explored to fully understand the synthetic potential of these species.

This research project has also developed two new lithium magnesiate bases, [(TMEDA)Li(TMP)(CH_2SiMe_3)Mg(TMP)] and [(TMEDA)Li(TMP)$_2$(CHSiMe_3)Mg]. While initial solution state studies of these bases indicated a large degree of fluctional behaviour, an in-depth study into the reactivity of these bases against a variety functionalised aromatic substrates should be conducted to further understand the structure and reactivity of these new bases. If similar reactivity is observed with these lithium magnesiates (when compared to the sodium magnesiate **1**), they could offer a more practical alternative for the average synthetic chemist, who may not have access to inert-atmosphere gloveboxes or the extensive air-free techniques required for the synthesis of **1**. These lithium magnesiates can be synthesised from entirely commercially available chemicals, using basic Schlenk line techniques.

7 Experimental Section

7.1 Instrumentation

7.1.1 ^{1}H-NMR spectra

Proton NMR spectra were recorded on a Bruker AVANCE 400 (400 MHz) or 600 (600 MHz) spectrometer. Chemical shifts were recorded on the δ scale in parts per million (ppm). Spectra were measured in *d*-chloroform ($CDCl_3$) using the residual 7.26 ppm signal, d_6-benzene (C_6D_6) using the residual 7.16 ppm signal, d_8-toluene using the residual 2.09 and 6.98 ppm signals, d_{12}-cyclohexane using the residual 1.38 ppm signal and d_8-tetrahydrofuran (d_8-THF) using the residual 1.73 and 3.58 ppm signals. The residual signal of each solvent was used as an internal reference. The resonance was reported according to the following convention: chemical shift (δ ppm) [multiplicity, number of hydrogens, coupling constant, and assignment]. Multiplicities are designated as (s) = singlet, (br) = broad signal, (d) = doublet, (dd) = doublet of doublets, (t) = triple, (m) = multiplet. Coupling constants were recorded on Hz scale.

7.1.2 ^{13}C-NMR spectra

Carbon NMR spectra were recorded at 100 MHz on a Bruker AVANCE DRX 400 spectrometer. Chemical shifts were recorded on the δ scale in parts per million (ppm). Spectra were measuring in *d*-chloroform using the triplet carbon signal (77.16 ppm) signal, C_6D_6 using the triplet carbon (128.06 ppm) signal and d_8-tetrahydrofuran using the pentent carbon (25.37 and 67.57 ppm) signals.

7.1.3 ^{31}P-NMR spectra

^{31}P- NMR spectra were collected using a Bruker Avance400 spectrometer operating at 162 MHz. Spectra were assigned chemical shifts in parts per million (ppm), and reported relative to external H_3PO_4 at 0 ppm. Coupled spectra are denoted as ^{31}P-NMR and decoupled spectra are denoted as $^{31}P\{^1H\}$-NMR.

7.1.4 GC/MS analysis

Analysis was carried out at the Monash Analytical Platform, Australia (School of Chemistry, Monash University). GC/MS analysis was conducted on a Agilent 6890 GC coupled to a 5973 MS system (Santa Clara, CA, USA) with an EI source. A 1 µL injection volume of test compound was used in conjunction with a 100:1 split ratio and a He carrier gas with a constant flow of 1 mL/min. Analytes were separated on an Aglent DB-5MS 30m column with a film thickness of 0.25 uM and a diameter of 0.25 mm on a temperature gradient starting at 50 °C for 3 minutes and ramping to 300 °C at a rate of 12 °C. A final hold time of 5 minutes was employed. The MS was operated in scan mode with a mass range of m/z 30-550 units.

7.1.5 Fourier Transform Infrared (FTIR) analysis

Fourier Transform Infrared (FTIR) spectra were obtained on an Agilent Cary 630 diamond attenuated total deflection (ATR) spectrometer with MicroLab software. Absorptions are reported in wavenumbers (cm^{-1}), with relative intensities described by the abbreviations: strong (s), medium (m), weak (w) and prefixed broad (b) where appropriate.

7.1.6 Reactions under anhydrous conditions - Schlenk protocol

All reactions requiring anhydrous conditions were conducted with oven dried glassware under an atmosphere of dry nitrogen using a vacuum / nitrogen line and Schlenk techniques. All glassware was dried at 105 °C for at least 18 hours prior to use and allowed to cool under

vacuum to minimise water content. The Schlenk assembly was purged of air and moisture under high vacuum and backfilled with nitrogen three times. Liquids and solutions of dissolved solids were transferred through rubber seals using oven dried, nitrogen purged syringes or cannulas. Filtering of solutions was carried out through rubber seals using oven dried / nitrogen purged cannula equipped with glass fibre micro filters (GF/A, circles Ø 42.5 cm, Whatman ®) which were fixed with Teflon rubber. Air-sensitive compounds were stored in a high purity argon recirculating dry box, with oxygen and moisture levels typically lower than 0.5 ppm. All analytical samples of air-sensitive compounds were prepared using a high purity argon recirculating dry box.

7.1.7 Microanalysis

Microanalyses were carried out by the Science Centre, London Metropolitan University. Air and moisture sensitive samples were prepared in air tight sealed glass ampules.

7.1.8 DOSY NMR

All spectra were acquired in 5 mm NMR tubes. Sample spinning was deactivated during the measurements. All DOSY experiments were performed using a double stimulated echo sequence with bipolar gradient pulses and three spoil gradients with convection compensation (dstebpgp3s). The diffusion time was Δ = 0.1 s. The duration of the magnetic field pulse gradients $\delta/2$ was adjusted for each temperature in a range of 400–3500 µs. The delay for gradient recovery was 0.2 ms and the eddy current delay 5 ms. For each DOSY-NMR experiment, a series of 16 spectra on 32 K data points were collected. The pulse gradients (g) were incremented from 2 to 98% of the maximum gradient strength in a linear ramp with a total experiment time of 45 min. The temperature was set and controlled at 298 K with an air flow of 400 l h^{-1} in order to avoid any temperature fluctuations due to sample heating during the magnetic field pulse gradients. After Fourier transformation and baseline correction, the diffusion dimension was processed with the Topspin 3.1 software.

Diffusion coefficients, processed with a line broadening of 2 Hz, were calculated by Gaussian fits with the T1/T2 software of Topspin.

7.1.9 X-ray crystallographic analysis

Crystallographic data was collected on either a Bruker X8 APEXII CCD diffractometer equipped with an OXFORD Cryosystems 700 (at 123(1) K), a Rigaku Xtalab Synergy Dualflex diffractometer with monochromatic (graphite) Mo (λ = 0.71073 Å) or Cu (λ = 1.54180 Å) Kα radiation (at 123(1) K) or at the MX1 or MX2 beamlines at the Australian Synchrotron, Melbourne, Victoria, Australia (λ = 0.71070 Å, at 100 K). At the MX1 and MX2 beamlines, the software used for data collection and reduction of the data were BluIce[147] and XDS.[148]. Lorentz, polarisation and absorption corrections (multi-scan - SADABS)[149] were applied to all datasets.

All crystal structures were solved and refined with SHELX-2014[150] and X-seed interface[151] or Olex2.[152] All non-hydrogen atoms were refined with anisotropic thermal parameters unless otherwise indicated and hydrogen atoms were placed in calculated positions using a riding model with C-H = 0.95-0.98 Å and U_{iso}(H) = xU_{iso}(C), x = 1.2 or 1.5.

7.1.10 Powder X-ray diffraction analysis

Powder X-ray diffraction (PXRD) data was collected at room temperature using a Bruker D8 Advance Eco diffractometer equipped with a Cu Kα (λ = 1.5418 Å) radiation. The sample was mounted on a zero background silicon single crystal stage and sealed under high purity argon in a glovebox. Data was collected in the angle interval 2θ = 5 - 55 ° with a step size of 0.02 °. The data was collected at 298 K and compared to predicted patterns based on the single crystal data (collected at 123 K).

7.1.11 Flash Column Chromatography

Flash column chromatography was performed on silica gel (Davisil LC60A, 40-63 μm silica) using compressed air. Thin layer chromatography (TLC) was performed using aluminium-backed plates coated with 0.2 mm silica (Merck, DC Kieselgel 60 F_{254} plates). Eluted plates were visualised using a 254 nm UV lamp and treated with a suitable stain.

7.1.12 EPR characterisation of 33

CW X-band measurements in the solution phase were performed on a 9.4 GHz X-band EPR spectrometer equipped with an EN 4118X-MD4 pulse resonator. The solution-phase experiments were run at 220 K which was found to be the optimum temperature for resolving the fine structure of the spectrum whilst remaining above the melting point of the toluene solvent (178 K). Spectra were recorded with a field modulation amplitude of 0.05 G and a microwave power of 0.047 mW. Simulations were performed using the fast-motion CW EPR program garlic in the EasySpin package[153] in MATLAB, and were optimized using a Nelder-Mead minimization algorithm.

Pulse W-band EPR, Powder Sample

All pulse W-band experiments were measured on a 94 GHz W-band EPR spectrometer (Bruker ELEXSYS E580) equipped with a cylindrical resonator. Experiments were performed at 120 K (Liquid N_2) to afford slower T_2 relaxation times. At W-band the sample was measured as a solid powder owing to the sensitivity of the sample to air, which proved problematic when using W-band capillaries (10 μL quartz tubes) requiring a small sample size (3 μL). The maximum field position was determined by an Electron-Spin-Echo (ESE) Field Sweep, using the pulse sequence $\pi/2$ - τ - π - τ - echo, with $\pi/2$ = 20 ns, and τ = 200 ns. In this case, the ESE of the powder sample does not allow resolution of the g-anisotropy, and so was useful primarily for determining the field position for maximum echo response.

Mims ENDOR on ^{31}P, ^{23}Na and ^{1}H

The ENDOR experiment resolves couplings to nuclei via a double resonance pulse sequence, using an RF pulse that is matched to the Larmor frequency of the nucleus, and a MW detection sequence at the frequency of the system's electronic spin transition. Mims ENDOR spectra were measured using the pulse sequence: τ_p - τ - τ_p – τ_{RF} - T - τ_p - τ - echo, with varied τ (100-900 ns), τ_p = 20 ns, T = 5000 ns. The optimal RF pulse length (t_{RF}) was measured by RF nutation, giving t_{RF} = 28 µs for ^{31}P ENDOR and t_{RF} = 50 µs for ^{23}Na ENDOR and t_{RF} = 16 ns for ^{1}H ENDOR. The RF attenuator and sum attenuator were both set to 0 dB, and spectra were measured at the maximum field position (3352.5 mT). Davies ENDOR was also measured at the ^{1}H frequency for comparison, using the pulse sequence π - T - t_RF - T – π/2 - τ - π - echo using selective, soft pulses of π = 80 ns. Mims ENDOR spectra were τ-averaged and scaled to the echo intensity to remove blind spotting artefacts. The ^{25}Mg nucleus cannot be measured by ENDOR owing to resonator and excitation bandwidth limitations.

7.2 Precursor Synthesis

7.2.1 Synthesis of $[Mg(CH_2SiMe_3)_2]_\infty$

To a 500 mL round bottom flask equipped with a condenser and a pressure-equalising dropping funnel, magnesium turnings (4.5 g, 145 mmol) were added and the system flushed three times. The magnesium turnings were suspended in 100 mL of dried Et_2O. A solution of Me_3SiCH_2Cl (15 mL, 139 mmol) in 75 mL of dry Et_2O was added dropwise via the dropping funnel. Following the addition, the reaction was refluxed for one hour, following which dried 1,4-dioxane (8 mL, 93 mmol) in 75 mL of dried Et_2O was added dropwise to afford a thick grey suspension. The reaction was allowed to stir at room temperature for 2 days, then filtered through Celite and glass wool and washed with 2 x 40 mL of ether to give a clear solution. The solvent was removed *in vacuo* leaving a white

solid, which was purified via sublimation (0.15 torr, 174 °C) to yield a crystalline white solid. This was stored in the glove box prior to use. Typical yield = 8 - 9 g, 28 - 32 %.

^{1}H NMR (400 MHz, C_6D_6, 300K): δ 0.25 (s, 18 H, CH_3), -1.49 (s, 4 H, CH_2).

^{13}C NMR (100 MHz, C_6D_6, 300K): δ 4.8 ($SiCH_3$, s), -7.5 ($MgCH_2$).

7.2.2 Synthesis of *n*-BuNa

*n*BuNa was prepared according to the literature procedure.[154] *n*BuLi (18.75 mL, [1.6 M solution in hexane], 30 mmol) was added dropwise to a stirred suspension of sodium *tert*-butoxide (2.88 g, 30 mmol) in 50 mL of hexane at 0 °C. The solution was allowed to warm to room temperature and left stirring overnight. The resulting white precipitate was collected by filtration and washed thoroughly with hexane (2 $\times$ 50 mL) and then dried under vacuum. The highly pyrophoric solid was stored under argon in a recirculating dry box. Typical yield 1.7 g, 70 %.

7.2.3 Synthesis of *n*-BuK

*n*BuK was prepared according to the literature procedure.[154] *n*-BuLi (18.75 mL, [1.6 M solutionn in hexane], 30 mmol) was added dropwise to a stirred suspension of potassium *tert*-butoxide (3.36 g, 30 mmol) in 50 mL of hexane at 0 ° C. The soluton was allowed to warm to toom temperature and left stirring overnight. The resulting brown precipitate was collected by filtration and washed thoroughly with hexane (2 $\times$ 50 mL) and then dried under vacuum. The highly pyrophoric solid was stored under argon at -30 ° C in a recirculating dry box.

7.2.4 Synthesis of Na(CH_2SiMe_3)

$LiCH_2SiMe_3$ (25 mL, [1 M solution in pentane], 25 mmol) was added dropwise to a stirred suspension of sodium *tert*-butoxide (2.3 g, 24 mmol) in *n*-hexane at 0 ° C. The resulting suspension was allowed to warm to room temperature stirring overnight. The precipitate of

$NaCH_2SiMe_3$ was isolated by filtration, and thoroughly washed with *n*-hexane and dried under vacuum. The highly pyrophoric solid was stored under argon in a recirculating dry box. Typical yield 2.25 g, 85 %.

7.2.5 Synthesis of $K(CH_2SiMe_3)$

$LiCH_2SiMe_3$ (25 mL, [1 M solution in pentane], 25 mmol) was added dropwise to a stirred suspension of potassium *tert*-butoxide (2.7 g, 24 mmol) in *n*-hexane at 0 ° C. The resulting suspension was allowed to warm to room temperature stirring overnight. The precipitate of KCH_2SiMe_3 was isolated by filtration, and thoroughly washed with *n*-hexane and dried under vacuum. The highly pyrophoric solid was stored under argon in a recirculating dry box. Typical yield 1.97 g, 65 %.

7.2.6 Synthesis of $Rb(CH_2SiMe_3)$

$LiCH_2SiMe_3$ (25 mL, [1 M solution in pentane], 25 mmol) was added dropwise to a stirred suspension of rubidium fluoride (2.5 g, 24 mmol) in *n*-hexane. The resulting suspension was heated to reflux for 16 hours. The precipitate of $RbCH_2SiMe_3$ was isolated by filtration, and thoroughly washed with *n*-hexane and dried under vacuum. The highly pyrophoric solid was stored under argon in a recirculating dry box. Some residual rubidium fluoride was always present, however this did not seem to impact the compounds reactivity. Due to the rapid decomposition of this compound in typical NMR solvents, no characterisation by NMR spectroscopy was possible.

7.2.7 Synthesis of $Cs(CH_2SiMe_3)$

$LiCH_2SiMe_3$ (25 mL, [1 M solution in pentane], 25 mmol) was added dropwise to a stirred suspension of caesium fluoride (3.65 g, 24 mmol) in *n*-hexane. The resulting suspension was heated to reflux for 16 hours. The precipitate of $CsCH_2SiMe_3$ was isolated by filtration, and thoroughly washed with *n*-hexane and dried under vacuum. The highly pyrophoric

solid was stored under argon in a recirculating dry box. Some residual caesium fluoride was always present, however this did not seem to impact the compounds reactivity. Due to the rapid decomposition of this compound in typical NMR solvents, no characterisation by NMR spectroscopy was possible.

7.2.8 General Reaction Procedure 1 (GP1)

Synthesis of [(TMEDA)Na(TMP)(CH_2SiMe_3)Mg(TMP)] 1

*n*BuNa (0.08 g, 1 mmol) was suspended in 5 mL of dry *n*-hexane. To this suspension TMP(H) (0.34 mL, 2 mmol) was added dropwise and the resulting suspension was stirred for at least 30 minutes at room temperature. This resulted in a pale yellow suspension. Next $Mg(CH_2SiMe_3)_2$ (0.2 g, 1 mmol) was added via solid addition tube with subsequent addition of TMEDA (0.15 mL, 1 mmol) affording a pale-yellow, transparent solution that was used without further purification. If clumps of solid remained in solution following addition of TMEDA, the solution was sonicated until complete dissolution occurred.

7.2.9 General Reaction Procedure 2 (GP2)

*n*BuNa (0.16 g, 2 mmol) was suspended in 10 mL of dry *n*-hexane. To this suspension TMP(H) (0.34 mL, 2 mmol) was added dropwise and the resulting suspension was stirred for at least 30 minutes at room temperature. This resulted in a pale yellow suspension. Next $Mg(CH_2SiMe_3)_2$ (0.2 g, 1 mmol) was added via solid addition tube with subsequent addition of TMEDA (0.3 mL, 2 mmol) affording a pale-yellow, cloudy solution that was used *in situ* without further purification.

7.3 Investigation into the solution state structure and stability of mixed metal magnesiate bases

7.3.1 Synthesis of [(TMEDA)Li(TMP)(CH_2SiMe_3)Mg(TMP)]

n-Hexane (5 mL) was added to an oven-dried Schlenk followed by nBu_2Mg (1 mL, [1 M in hexanes], 1 mmol) and TMP(H) (0.34 mL, 2 mmol). The reaction mixture was heated to reflux for 5 h, following which LiCH_2SiMe_3 (1 mL,[1 M in pentane], 1 mmol) was added dropwise. Next TMEDA (0.15 mL, 1 mmol) was added to produce a clear yellow solution. Storage of the Schlenk at - 28 ° C yielded colourless crystals (0.21 g, 41 %). ^{1}H NMR spectrums were obtained in C_6D_{12}, however they displayed a high degree of fluctionality, and will not be included here.

Crystal data for $C_{28}H_{63}LiMgN_4Si$: M = 515.16, colourless prism, 0.2 x 0.15 x 0.12 mm^3, monoclinic, space group $P2a2_1$, a = 14.9595(3), b = 18.6845(3), c = 11.9703(2), α = 90°, β = 90°, γ = 90°, V = 3345.83(10) Å^3, Z = 4, D_c = 1.023 g/cm^3, F_{000} = 1152, T = 123(2) K, 22839 reflections collected, 6299 unique (R_{int} = 0.0745), Final GooF = 1.041, *R1* = 0.0733, *wR2* = 0.1976, 319 parameters, 1 restraint. Lp and absorption corrections applied, μ = 0.937 mm^{-1}. Absolute structure parameter = 0.02(3).[155]

7.3.2 Synthesis of [(PMDETA)Li(CH_2SiMe_3)Mg($TMP)_2$]

n-Hexane (5 mL) was added to an oven-dried Schlenk followed by nBu_2Mg (1 mL, [1 M in hexanes], 1 mmol) and TMP(H) (0.34 mL, 2 mmol). The reaction mixture was heated to reflux for 5 h, following which LiCH_2SiMe_3 (1 mL,[1 M in pentane], 1 mmol) was added dropwise. Next PMDETA (0.21 mL, 1 mmol) was added to produce a clear yellow solution. Storage of the Schlenk at - 28 ° C yielded pale yellow crystals (0.34 g, 59 %). ^{1}H NMR spectrums were obtained in C_6D_{12}, however they displayed a high degree of fluctionality, and will not be included here.

Crystal data for $C_{31}H_{70}LiMgN_5Si$: M = 572.26, pale yellow prism, 0.3 x 0.25 x 0.15 mm^3,

monoclinic, space group *P21/n*, *a* = 11.893(1), *b* = 15.3957(10), *c* = 19.9922(10), α = 90°, β = 92.242(10)°, γ = 90°, *V* = 3657.79(4) Å^3, *Z* = 4, D_c = 1.039 g/cm^3, F_{000} = 1280, T = 123(2) K, 29048 reflections collected, 7503 unique (R_{int} = 0.0267), Final GooF = 1.045, *R1* = 0.0483, *wR2* = 0.1371, 423 parameters, 0 restraint. Lp and absorption corrections applied, μ = 0.906 mm^{-1}.

7.3.3 Synthesis of [(TMEDA)Na(TMP)(CH_2SiMe_3)Mg(TMP)]

*n*BuNa (0.08 g, 1 mmol) was suspended in 5 mL of *n*-hexane. To this suspension, TMP(H) (0.34 mL, 2 mmol) is added dropwise, and the resulting yellow suspension allowed to stir for at least 30 minutes. Following this, $Mg(CH_2SiMe_3)_2$ (0.2 g, 1 mmol) is added as a single portion via a solid addition tube. Next, TMEDA (0.15 mL, 1 mmol) is added, resulting in the formation of a clear, yellow solution. If solid clumps remain, the solution is sonicated to ensure full dissolution occurs. Storage of the resulting yellow solution at -30 ° C resulted in the deposition of a large quantity of colourless crystals.

^{1}H NMR (600 MHz, Cyclohexane$-d_{12}$, 298.2 K): δ 2.67 (4 H, s, CH_2-TMEDA), 2.57 (12 H, s, CH_3-TMEDA), 2.04 (4 H, p, *J* 6.1, CH_2-TMP), 1.70 (8 H, s, CH_2-TMP), 1.57 (24 H, s, CH_3-TMP), 0.34 (9 H, s, $SiMe_3$), -1.86 (2 H, CH_2-SiMe_3).

^{13}C NMR (150.95 MHz, Cyclohexane$-d_{12}$, 298.2 K): δ 57.17, 51.86, 45.81, 41.60, 34.87, 19.71, 3.94, 0.16.

7.3.4 Synthesis of [(PMDETA)K(TMP)(CH_2SiMe_3)Mg(TMP)]

n-Hexane (5 mL) was added to an oven-dried Schlenk followed by nBu_2Mg (1 mL, [1 M in hexanes], 1 mmol) and TMP(H) (0.34 mL, 2 mmol). The reaction mixture was heated to reflux for 5 h, following which KCH_2SiMe_3 (0.126 g, 1 mmol) was added via solid addition tube. Next PMDETA (0.21 mL, 1 mmol) was added to produce a clear yellow solution. Storage of the Schlenk at - 28 ° C yielded yellow crystals (0.31 g, 52 %).

^{1}H NMR (600 MHz, C_6D_6, 298.2 K): δ 2.50 (8 H, bs), 2.39 (12 H, s), 2.38 (3 H, s), 1.95 – 1.83 (4 H, m), 1.53 (8 H, s), 1.40 (24 H, s), 0.16 (9 H, s), -1.96 (2 H, s).

^{13}C NMR (150.95 MHz, C_6D_6, 298.2 K): δ 58.11, 56.36, 52.99, 46.02, 42.06, 35.90, 35.73, 20.88, 5.10.

7.3.5 Synthesis of $[(TMEDA)_3K]^+[Mg(TMP)_3]^-$

n-Hexane (5 mL) was added to an oven-dried Schlenk followed by nBu_2Mg (1 mL, [1 M in hexanes], 1 mmol) and TMP(H) (0.51 mL, 3 mmol). The reaction mixture was heated to reflux for 5 h, following which KCH_2SiMe_3 (0.126 g, 1 mmol) was added via solid addition tube. Next TMEDA (0.45 mL, 3 mmol) was added to produce a clear yellow solution. Storage of the Schlenk at - 28 ° C yielded colourless crystals (0.55 g, 66 %).

^{1}H NMR (600 MHz, C_6D_6, 298.2 K): δ 2.40 (12 H, s, TMEDA-CH_2), 2.26 (36 H, s, TMEDA-CH_3), 1.48 (32 H, s, TMP-CH_3), 1.38 - 1.40 (12 H, m, TMP), 0.91 - 1.03 (6 H, m, TMP).

^{13}C NMR (150.95 MHz, C_6D_6, 298.2 K): δ 58.85, 50.02, 46.19, 39.26, 32.39, 26.97.

7.3.6 Synthesis of $[(PMDETA)_2Rb]^+[Mg(TMP)_3]^-$

n-Hexane (5 mL) was added to an oven-dried Schlenk followed by nBu_2Mg (1 mL, [1 M in hexanes], 1 mmol) and TMP(H) (0.51 mL, 3 mmol). The reaction mixture was heated to reflux for 5 h, following which $RbCH_2SiMe_3$ (0.171 g, 1 mmol) was added via solid addition tube. Next PMDETA (0.42 mL, 2 mmol) was added to produce a clear yellow solution. Storage of the Schlenk at - 28 ° C yielded yellow crystals, which were extremely sensitive to moisture and oxygen.

^{1}H NMR (600 MHz, C_6D_6, 298.2 K): δ (12 H, s, TMEDA-CH_2, (36 H, s, TMEDA-CH_3), (32 H, s, TMP-CH_3), (12 H, m, TMP), (6 H, m, TMP).

Crystal data for $C_{45}H_{100}MgN_9Rb$: M = 877.11, clear yellow blocks, 0.15 x 0.12 x 0.09 mm^3, monoclinic, space group *P-1*, *a* = 10.3798(14), *b* = 15.9233(2), *c* = 16.8318(2), α

= 95.5549(11)°, β = 92.4073(10)°, γ = 106.1455(12)°, *V* = 2652.77(6) Å^3, *Z* = 2, D_c = 1.098 g/cm^3, F_{000} = 964, T = 123(2) K, 34408 reflections collected, 10777 unique (R_{int} = 0.0686), Final GooF = 1.061, *R1* = 0.0487, *wR2* = 0.1232, 521 parameters, 12 restraints. Lp and absorption corrections applied, μ = 1.665 mm^{-1}.

7.3.7 Synthesis of MgR_2TMEDA

$Mg(CH_2SiMe_3)_2$ (0.1 g, 0.5 mmol) was suspended in 5 mL of *n*-hexane. To this suspension, TMEDA (0.08 mL, 0.5 mmol) was added, resulting in a clear yellow solution. This solution was placed in a - 30 °C freezer overnight, resulting in the deposition of a large crop of colourless, rod-like crystals.

^{1}H NMR (600 MHz, C_6D_6, 298.2 K): δ 1.75 (s, 12 H), 1.48 (s, 4 H), 0.43 (s, 18 H), -1.49 (s, 4 H).

^{13}C NMR (150.95 MHz, C_6D_6, 298.2 K): δ 55.97, 46.53, 5.27, -6.87.

Crystal data for $C_{14}H_{38}MgN_2Si_2$: M = 314.95, clear colourless block, 0.25 x 0.2 x 0.15 mm^3, triclinic, space group *P-1*, *a* = 9.8642(3), *b* = 10.0031(4), *c* = 13.0953(4), α = 106.685(3)°, β = 90.869(3)°, γ = 117.883(4)°, *V* = 1076.87(8) Å^3, *Z* = 2, D_c = 0.971 g/cm^3, F_{000} = 352, T = 123(2) K, 13467 reflections collected, 5279 unique (R_{int} = 0.0345), Final GooF = 1.097, *R1* = 0.0525, *wR2* = 0.1415, 182 parameters, 0 restraints. Lp and absorption corrections applied, μ = 0.187 mm^{-1}.

7.4 Bimetallic metallations of *N,N*- and *P,P*-dialkyl substituted anilines and phenylphosphines

7.4.1 Synthesis of *P,P*-dimethylphenylphosphine

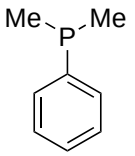

MeMgBr (25 mL, [3 M solution in Et_2O], 75 mmol) was added dropwise to a stirred solution containing *P,P*-dichlorophenylphosphine ($PPhCl_2$, 5 mL, 37 mmol) in 60 mL of Et_2O at 0 °C over 60 minutes. This was stirred overnight. After filtration, the reaction was quenched with 10 mL of de-oxygenated water. The ethereal layer was cannula filtered to another round bottom flask, where the solvent was removed under vacuum. The phosphine was purified by vacuum distillation at 0.15 torr, 30 °C, resulting in a colourless liquid. Typical yield: 4.5 g, 88 %. This compound has been previously reported.[156]

^{1}H NMR (400 MHz, C_6D_6, 300K): δ 7.48 (tt, 2 H, J = 6.83, 1.63 Hz, *ortho*-H) 7.15 - 7.28 (m, 3H, *meta/para*-H), 1.17 (d, J = 3.32 Hz, CH_3).

^{13}C NMR (100 MHz, C_6D_6, 300K): δ 143.0 (d, quaternary-C), 130.6 (d, *ortho*-C), 128.2 (d, *meta*-C), 127.8 (s, *para*-C), 14.3 (d, CH_3).

^{31}P NMR (162 MHz, C_6D_6, 300K): δ -46.52 (s).

7.4.2 Synthesis of *P,P*-diethylphenylphosphine

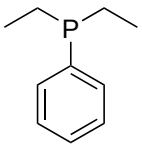

EtMgBr (25 mL, [3 M solution in Et_2O], 75 mmol) was added dropwise to a stirred solution of $PPhCl_2$ (5 mL, 37 mmol) in 60 mL of ether at 0 °C over 60 minutes. After

filtration, the reaction was quenched with 15 mL of de-oxygenated water. The ethereal layer was cannula filtered to another round bottom flask, where the solvent was removed under vacuum. The phosphine was purified by vacuum distillation at 0.15 torr, 30 °C resulting in a colourless liquid. Typical yield: 4.3 mL, 65 %. This compound has been previously reported.[157]

^{1}H NMR (400 MHz, C_6D_6, 300K): δ 7.56 (m, 2 H, *ortho*-H), 7.1 - 7.3 (m, 3 H, *meta/para* -H), 1.61 (m, 4 H, CH_2), 1.05 (dt, 6 H, J = 7.6, 7.2 Hz, CH_3).

^{13}C NMR (100 MHz, C_6D_6, 300K): δ 139.1 (d, quaternary-C), 132.4 (d, *ortho*-C), 128.4 (s, *para*-C), 128.2 (d, *meta*-C), 20.3 (d, CH_2), 9.7 (d, CH_3).

^{31}P NMR (162 MHz, C_6D_6, 300K): δ -16.59 (s).

7.4.3 Synthesis of *P,P*-diisopropylphenylphosphine

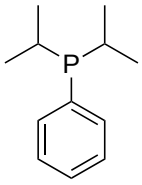

*i*PrMgBr (25 mL, [1 M solution in THF], 25 mmol) was added dropwise to a stirred solution of $PPhCl_2$ (1.65 mL, 12.34 mmol) in 50 mL of THF at 0 °C over 60 minutes. After filtration, the reaction was quenched with 10 mL of de-oxygenated water. The ethereal layer was cannula filtered to another round bottom flask, where the solvent was removed under vacuum. The phosphine was purified by vacuum distillation at 0.15 torr, 46 °C resulting in a colourless liquid. Typical yield: 2 g, 81 %. This compound has been previously reported.[158]

^{1}H NMR (400 MHz, C_6D_6, 300K): δ 7.53 - 7.62 (m, *ortho*-H), 7.21 - 7.30 (m, 3 H, *meta/para*-H), 2.06 (ds, 2 H, J = 7.2, 1.6 Hz, CH), 1.16 (dd, 6 H, J = 14.8, 7.2 Hz, CH_3), 1.00 (dd, 6 H, J = 10.8, 7.2 Hz, CH_3).

^{13}C NMR (100 MHz, C_6D_6, 300K): δ 135.3 (d, quaternary-C), 134.6 (d, *ortho*-C), 128.6 (s, *para*-C), 127.8 (d, *meta*-C), 22.8 (d, CH), 19.7 (d, CH_3), 18.6 (d, CH_3).

^{31}P NMR (162 MHz, C_6D_6, 300K): δ 10.35 (s).

7.4.4 Synthesis of *P,P*-dichloro(napthalen-1-yl)phosphine

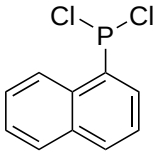

In a 500 mL round bottom flask equipped with a condenser, magnesium turnings (1.22 g, 50 mmol) was added and the system evacuated three times. The magnesium turnings were suspended in 200 mL of dry THF. 1,2-Dibromoethane (0.1 mL, 1.2 mmol) was added and the solution heated to reflux to initiate the Grignard reaction. Next, 1-bromonapthalene (7 mL, 50 mmol) was added dropwise such that a gentle reflux was maintained. Upon complete addition, the solution was refluxed for a further 30 minutes, before allowing to cool to room temperature. This can result either in a homogeneous solution or a slurry. To this mixture, $ZnCl_2$ (50 mL, [1 M in THF], 50 mmol) was added dropwise, resulting in the formation of a white slurry. This was stirred for a further 1 hour. Next, this solution was cooled to -78 °C, following which a solution of PCl_3 in THF (4.35 mL in 30 mL THF) was added dropwise. The resulting suspension was allowed to warm to room temperature stirring overnight. The solvent was removed *in vacuo*, following which the solids were extracted with diethyl ether. After filtration via filter cannula, the solvent was removed to yield the title compound as a yellow solid. This compound has been previously characterised.[159]

^{1}H NMR (600 MHz, C_6D_6, 298.2 K): δ 8.45 – 8.14 (1 H, m), 7.72 (1 H, dd, J 11.3, 7.2), 7.24 (2 H, m), 6.98 (1 H, ddd, J 8.5, 6.9, 1.6), 6.93 – 6.89 (1 H, m), 6.76 (1 H, ddd, J 8.3, 7.1, 1.1).

^{31}P NMR (162.0 MHz, C_6D_6, 298.3 K) δ 164.15 (s).

7.4.5 Synthesis of *P,P*-dimethylnapthyl-1-phosphine

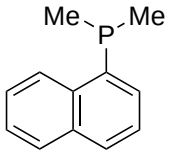

P,P-dichloro(napthalen-1-yl)phosphine (4.58 g, 20 mmol) was dissolved in anhydrous diethyl ether (100 mL). MeMgBr (20 mL, [3 M in diethyl ether], 60 mmol) was added dropwise at 0 ° C, resulting in the formation of a precipitate. The resulting suspension was stirred overnight, warming to room temperature. The following day, degassed H_2O (20 mL) is added carefully at 0 ° C (a large excess of MeMgBr is used, resulting in an exothermic quench). The reaction is filtered under a protective nitrogen atmosphere and the solvent removed *in vacuo*. The resulting oil is vacuum distilled to afford *P,P*-dimethylnapthyl-1-phosphine in a high yield as a colourless oil. This compound can be purified by column chromatography (silica gel, 5 % EtOAc/pteroleum benzene) with minimal oxidation.

^{1}H NMR (600 MHz, $CDCl_3$, 298.2 K): δ 7.88 – 7.61 (4 H, m), 7.40 – 7.34 (3 H, m), 1.30 (6 H, d, J 3.2).

^{13}C NMR (150.95 MHz, $CDCl_3$, 298.2 K): δ 134.97 (d, J 21.0), 133.45 (d, J 4.4), 128.91 (d, J 6.3), 128.66, 128.06, 127.80, 126.62, 126.41, 125.97, 125.48, 14.15 (d, J 12.3).

^{31}P NMR (162.0 MHz, $CDCl_3$, 298.3 K) δ -56.92 (s).

7.4.6 Reaction of 1 with *N,N*-dimethylaniline

Attempts were made to metallate *N,N*-dimethylaniline with the sodium magnesiate **1** [(TMEDA)Na(TMP)(CH_2SiMe_3)Mg(TMP)]. Reactions were conducted at room temperature, and at reflux for 2, 4, 6 and 18 hours. Reactions at room temperature return predominately starting material (trace metallated species present by ^{1}H NMR analysis of reaction aliquots). Optimal yield of metallated species was found at 2 hour reflux, beyond this predominately starting material was returned (presumably through a decomposition

process). For iodolysis, an iodine solution (7 mL, 1 M in THF, 7 mmol) was added dropwise at ambient temperature and allowed to stir overnight. The resulting solution was quenched with aqueous sodium thiosulphate (20 mL). The solution was diluted with DCM and the organic layer separated from the aqueous, dried over anhydrous $MgSO_4$ and the solvent removed *in vacuo*. Integral ratios of either a solution aliquot or of the crude material post iodolysis were used to determine relative yields.

7.4.6.1 Characterisation of iodinated species

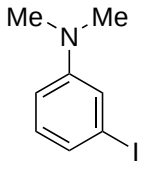

N,N-dimethyl-3-iodoaniline[102] ^{1}H NMR (400 MHz, C_6D_6, 298.2 K): δ 7.10 (1 H, d, J 7.3), 7.02 (1 H, m), 6.69 (1 H, t, J 8.1), 6.34 (1 H, dd, J = 8.4, 2.6), 2.27 (1 H, s).

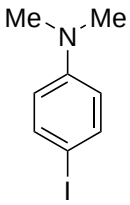

N,N-dimethyl-4-iodoaniline[102] ^{1}H NMR (400 MHz, C_6D_6, 298.2 K): δ 7.45 (2 H, d, J = 9.0), 6.13 (2 H, d, J = 9.0), 2.32 (6 H, s).

7.4.7 Reaction of 1 with *N,N*-diethylaniline

*n*BuNa (0.16 g, 2 mmol) was suspended in 10 mL of dry *n*-hexane. To this suspension TMP(H) (0.68 mL, 4 mmol) was added dropwise and the resulting suspension was stirred for at least 30 minutes at room temperature. This resulted in a pale yellow suspension. Next $Mg(CH_2SiMe_3)_2$ (0.4 g, 2 mmol) was added via solid addition tube with subsequent addition of TMEDA (0.3 mL, 2mmol) affording a pale-yellow, transparent solution that was used without further purification. If clumps of solid remained in solution following

addition of TMEDA, the solution was sonicated until complete dissolution occurred. To this solution, *N,N*-diethylaniline (0.32 mL, 2 mmol) was added dropwise at room temperature. The resulting solution was stirred overnight, resulting in the formation of a large amount of white precipitate. This was isolated by filtration and transferred to an argon glovebox for storage. X-ray quality single crystals were obtained upon recrystallisation from *n*-hexane and slow cooling in a hot oil bath. Yield = 0.77 g, 65 %.

^{1}H NMR (600 MHz, C_6D_6, 298.2 K): δ 7.45 (d, 1 H, *J* = 2.9 Hz), 7.12 (s, 1 H), 7.11 (d, 1 H, *J* = 1.8 Hz), 6.48 (m, 1 H, *meta*-H), 3.17 (q, 4 H, *J* = 7 Hz, Ethyl-CH_2), 1.98 – 1.87 (m, 4 H, γ CH_2TMP), 1.66 (s (br), 24 H, CH_3 TMP), 1.63 (s (br), 12 H, CH_3-TMEDA), 1.55 (s, 6 H, CH_2TMEDA), 1.44 – 1.31 (m, 8 H, $\beta-CH_2-$TMP), 1.04 (t, 6 H, J = 7 Hz, Ethyl-CH_3).

^{13}C NMR (150.95 MHz, C_6D_6, 298.2 K): 173.41 (s, Mg-C), 147.22, 127.51, 126.03, 110.33 (meta'-C), 57.30 (CH_2TMEDA), 46.34 (CH_3TMEDA), 45.06 (CH_3), 42.76 (β-CH_2-TMP), 36.26 (CH_3 TMP), 20.76 (γ-CH_2 TMP), 13.48 (CH_3).

Crystal data for $C_{34}H_{66}MgN_5Na$: M = 592.21, clear yellow block, 0.25 x 0.2 x 0.15 mm^3, monoclinic, space group *P21/n*, a = 8.4765(7), b = 18.7027(17), c = 24.956(2), α = 90 °, β = 90.886 °, γ = 90 °, V = 3955.9(6) Å, Z = 4, Dc = 1.067 g/cm3, F_{000} = 1400, T = 123(2) K, 45712 reflections collected, 7903 unique (R_{int} = 0.1175), Final GooF = 1.035, R_1 = 0.0717, wR_2 = 0.1829, 404 parameters, 0 restraints. Lp and absorption corrections applied, μ = 0.124 mm^{-1}.

7.4.7.1 Characterisation of iodinated species

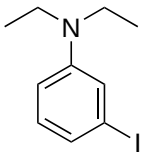

N,N-diethyl-3-iodoaniline was isolated as a colourless liquid (yield 0.37 g, 67 %). ^{1}H NMR (400 MHz, $CDCl_3$, 298.2 K): δ 7.05 – 6.80 (3 H, m), 6.61 (1 H, d, J = 8.1), 3.31 (4 H, q, J = 7.0), 1.15 (6 H, t, J = 7.0). ^{1}H NMR (600 MHz, C_6D_6, 298.2 K): δ 7.81 (1 H, d, J

= 8.9), 7.54 (1 H, s), 7.45 (1 H, d, J = 3.0), 6.65 (1 H, dd, J = 8.9, 3.0), 3.56 (4 H, q, J = 7.1), 1.43 (6 H, t, J = 7.1).

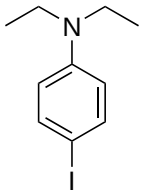

Small quantities of *N,N*-diethyl-4-iodoaniline were detected, presumably from the electrophilic aromatic substitution of residual *N,N*-diethylaniline. *N,N*-diethyl-4-iodoaniline ^{1}H NMR (600 MHz, C_6D_6, 298.2 K): δ 7.71 (2 H, d, J = 8.5), 6.73 (2 H, d, J = 8.5), 3.56 (4 H, q, J = 7.1), 1.43 (6 H, t, J = 7.1).

7.4.8 Reaction of 1 with *N,N*-diisopropylaniline

Attempts were made to metallate *N,N*-diisopropylaniline with the sodium magnesiate **1** [(TMEDA)Na(TMP)(CH_2SiMe_3)Mg(TMP)]. Reactions were conducted at room temperature, and at reflux for 2, 4, 6 and 18 hours. Reactions at room temperature return predominately starting material (trace metallated species present by ^{1}H NMR analysis of reaction aliquots). Optimal yield of metallated species was found at 4 hour reflux, beyond this predominately starting material was returned (presumably through a decomposition process). For iodolysis, an iodine solution (7 mL, 1 M in THF, 7 mmol) was added dropwise at ambient temperature and allowed to stir overnight. The resulting solution was quenched with aqueous sodium thiosulphate (20 mL). The solution was diluted with DCM and the organic layer separated from the aqueous, dried over anhydrous $MgSO_4$ and the solvent removed *in vacuo*. Integral ratios of either a solution aliquot or of the crude material post iodolysis were used to determine relative yields.

7.4.8.1 Characterisation of iodinated species

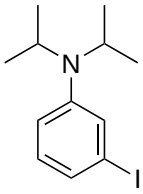

N,N-diisopropyl-3-iodoaniline ^{1}H NMR (400 MHz, C_6D_6, 298.2 K): δ 7.30 (1 H, t, J 2.0), 7.11 (1 H, d, J 7.2), 6.75 - 6.59 (2 H, m)

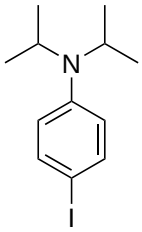

N,N-diisopropyl-3-iodoaniline ^{1}H NMR (400 MHz, C_6D_6, 298.2 K): δ 7.41 (2 H, d, J 9.0), 6.41 (2 H, d, J 9.0)

7.4.9 Reaction of 1 with *P,P*-dimethylphenylphosphine

*n*BuNa (0.16 g, 2 mmol) was suspended in 10 mL of dry *n*-hexane. To this suspension TMP(H) (0.68 mL, 4 mmol) was added dropwise and the resulting suspension was stirred for at least 30 minutes at room temperature. This resulted in a pale yellow suspension. Next $Mg(CH_2SiMe_3)_2$ (0.4 g, 2 mmol) was added via solid addition tube with subsequent addition of TMEDA (0.3 mL, 2mmol) affording a pale-yellow, transparent solution that was used without further purification. If clumps of solid remained in solution following addition of TMEDA, the solution was sonicated until complete dissolution occurred. To this solution, *P,P*-dimethylphenylphosphine (0.28 mL, 2 mmol) was added dropwise at room temperature. The resulting solution was stirred overnight, resulting in the formation of a large amount of white precipitate. This was isolated by filtration and transferred to an argon glovebox for storage. X-ray quality single crystals were obtained upon

recrystallisation from *n*-hexane and slow cooling in a hot oil bath. Crystalline yield = 0.67 g, 58 %.

^{1}H NMR (400 MHz, C_6D_6, 298.2 K): δ 7.65 (t, 2 H, J = 6.84 Hz ortho-H), 7.27 (t, 2 H, J = 7.36 Hz, meta-H), 7.12 (t, 1 H, J = 7.24 Hz, para-H), 1.95 (m (br), 4 H, γ-CH_2, TMP), 1.74 (s (br), 12 H, CH_3 TMEDA), 1.68 (s (br), 4 H, CH_2 TMEDA), 1.55 - 1.65 (m (br), 24 H, CH_3 TMP), 1.45 – 1.41 (m (br), 4 H, β-CH_2 TMP) 1.40 (s, 3 H, CH_3), 1.36 - 1.30 (m (br), 4 H, β-CH_2 TMP), 0.60 (t, 1 H, J = 9.6 Hz, CH_2Mg), -0.23 (d, 1 H, J = 10 Hz, CH_2Mg).

^{13}C NMR (100 MHz, C_6D_6, 298.2 K): δ 150.25 (d, ipso-C), 130.4 (ortho-C), 127.1 (para-C), 57.4 (CH_2-TMEDA), 46.4 (CH_3-TMEDA), 42.8 (β-C TMP), 36.21 (CH_3 TMP), 20.66 (γ-C TMP), 18.78 (CH_3), 8.0 (CH_2-Mg) Note: meta-C signal appears under the C_6D_6 residual peak (as determined by HSQC experiment).

^{31}P NMR (162.0 MHz, C_6D_6, 298.3 K) δ -28.58 (s (br)), -29.68 (s (br)).

Microanalysis: Calculated for $C_{32}H_{62}N_4MgNaP$: C, 66.14; H, 10.75; N, 9.64. Found: C, 65.88; H, 10.53; N, 9.45.

Crystal data for $C_{32}H_{62}N_4MgNaP$ **12**: M = 581.12, colourless plates, 0.19 x 0.17 x 0.11 mm^3, monoclinic, space group *P21*, *a* = 10.1805(9), *b* = 11.1263(13), *c* = 15.4179(17), α = 90°, β = 97.364(6)°, γ = 90°, *V* = 1732.0(3) $Å^3$, *Z* = 2, D_c = 1.114 g/cm^3, F_{000} = 640, T = 123(2) K, 56126 reflections collected, 8476 unique (R_{int} = 0.1395), Final GooF = 1.035, *R1* = 0.0660, *wR2* = 0.1489, 366 parameters, 1 restraints. Lp and absorption corrections applied, μ = 0.136 mm^{-1}.

7.4.9.1 Characterisation of iodinated species

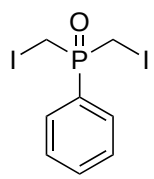

Bis(iodomethyl)(phenyl)phosphine oxide was isolated as a colourless crystalline solid (0.42 g, 52 % yield) following flash chromatography (silica gel, ethyl acetate).

^{1}H NMR (400 MHz, $CDCl_3$, 298.2 K): δ 7.94 – 7.79 (2 H, m), 7.67 – 7.59 (1 H, m), 7.59 – 7.45 (2 H, m), 3.66 – 3.42 (4 H, m).

^{13}C NMR (100 MHz, $CDCl_3$, 298.2 K): δ 133.20 (d, J 2.8), 131.74 (d, J 8.9), 129.03 (d, J 12.2), -8.02 (d, J 69.7).

^{31}P NMR (162 MHz, $CDCl_3$, 298.2 K): δ 29.85 (s).

HRMS (ESI) ($[M + H]^+$) calcd. for $C_8H_9I_2OP$: 406.8559, found 406.8551. Single crystals were obtained from ethyl acetate.

Crystal data for $C_8H_9PI_2O$: M = 405.92, colourless blocks, 0.2 x 0.18 x 0.15 mm^3, monoclinic, space group *P21/n*, a = 9.8572(5), b = 5.2264(2), c = 21.9562(10), α = 90 °, β = 100.336(2) °, γ = 90 °, V = 1112.78 Å, Z = 4, Dc = 2.423 g/cm3, F_{000} = 744, T = 123(2) K, 15166 reflections collected, 2655 unique (R_{int} = 0.0313), Final GooF = 1.316, R_1 = 0.0322, wR_2 = 0.0678, 109 parameters, 0 restraints. Lp and absorption corrections applied, μ = 5.751 mm^{-1}.

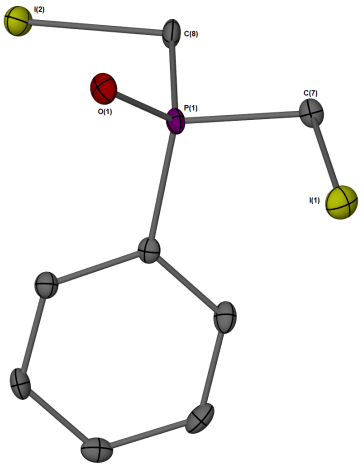

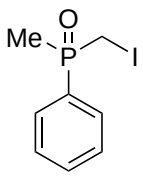

Iodomethyl(methyl)(phenyl)phosphine oxide was isolated as a colourless oil (0.19 g, 35 % yield).

^{1}H NMR (400 MHz, $CDCl_3$, 298.2 K): δ 7.84 – 7.71 (2 H, m), 7.63 – 7.55 (1 H, m), 7.55 – 7.45 (2 H, m), 3.32 – 3.22, (2 H, m), 1.97 (3 H, dt, J 13.1, 1.7).

^{13}C NMR (151 MHz, $CDCl_3$, 298.2 K): δ 132.61 (d, J = 2.9, para-C), 131.13 (d, J = 102.1, ipso-C), 130.68 (d, J = 9.3, meta-C), 128.95 (d, J = 12.1, ortho-C), 14.64 (d, J = 75.5, CH_3), -3.71 (d, J = 64.5, CH_2I).

^{31}P NMR (162 MHz, $CDCl_3$, 298.2 K): δ 33.57 (s).

HRMS (ESI) ($[M + H]^+$) calcd. for $C_8H_{11}IOP$: 280.9592, found: 280.9583.

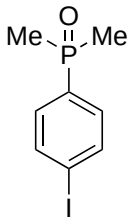

Para-iodo-*P,P*-dimethylphenylphosphine oxide was detected in mixed column fractions. It was not able to be isolated as a pure compound.

^{1}H NMR (400 MHz, $CDCl_3$, 298.2 K): δ 8.12 (2 H, (br)), 7.28 – 7.25 (2 H, m), 1.89 – 1.80 (6 H, broad).

7.4.10 Reaction of 1 with *P,P*-diisopropylphenylphosphine

To a stirred solution of the magnesiate base **1** (see **GP1**), *P,P*-diisopropylphenylphosphine (0.2 g, 1 mmol) was added dropwise at room temperature. Upon addition, an immediate formation of a bright yellow solution was observed. After stirring overnight, the solution was filtered and its volume reduced *in vacuo*, where storage at - 30 ° C resulted in the deposition of a large crop of yellow, block crystals. Crystalline yield = 0.2 g, 31 %.

^{1}H NMR (600 MHz, C_6D_6, 300K): δ 8.15 (dd, 1 H, *J* = 8.4, 1.2 Hz, H^6), 7.83 (d, 1 H, *J* = 4.4 Hz, H^4), 7.23 (m, 1 H, H^5), 7.17 (t, 1 H, *J* = 6.6 Hz, H^2), 2.10 (septet, 2 H, *J* = 6.6

Hz, CH), 1.90 (t (br), 4 H, *J* = 6 Hz, γ-CH_2 TMP), 1.61 (s (br), 36 H, CH_3 TMP/TMEDA), 1.36 (s (br), 6 H, CH_2 TMEDA), 1.19 (dd, 6 H, *J* = 14.7, 6.9 Hz, *i*Pr, 1.07 (d, *J* = 1.2 Hz, TMP), 1.02 (dd, 6 H, *J* = 10.5, 6.9 Hz, *i*Pr).

^{31}P NMR (162 MHz, C_6D_6, 300K): δ 9.42 (s).

Unfortunately ^{13}C NMR studies have been inconclusive due to the poor solubility and instability of compound **35** in solution.

Crystal data for $C_{36}H_{68}MgN_4NaP$ **35**: M = 635.21, yellow blocks, 0.26 x 0.20 x 0.18 mm^3, monoclinic, space group *P21/n*, *a* = 8.4765(7), *b* = 18.7027(17), *c* = 24.956(2), α = 90°, β = 90.886(4)°, γ = 90°, *V* = 3955.9(6) Å^3, *Z* = 4, D_c = 1.067 g/cm^3, F_{000} = 1400, T = 123(2) K, 45712 reflections collected, 7903 unique (R_{int} = 0.1175), Final GooF = 1.035, *R1* = 0.0717, *wR2* = 0.1829, 404 parameters, 0 restraints. Lp and absorption corrections applied, μ = 0.124 mm^{-1}.

7.4.11 Reaction of 1 with *N,N*-dimethylnapthyl-1-amine

To a stirred solution of the magnesiate base **1** (see **GP1**), distilled *N,N*-dimethylnapthyl-1-amine (0.16 g, 1 mmol) was added dropwise at room temperature. Note: Samples of *N,N*-dimethylnapthyl-1-amine from SigmaAldrich were found to have an unidentified impurity, which interfered with the reaction. Distillation from CaH_2 resolved this issue. The resulting solution was stirred overnight (16 hours), resulting in a large quantity of a white precipitate. This was isolated by filtration, washed with *n*-hexane and dried *in vacuo*. Yield = 0.50 g, 78 %.

^{1}H NMR (400 MHz, C_6D_6, 298.2 K): δ 8.33 (1 H, s), 8.24 (1 H, d, J 7.9), 8.17 (1 H, d, J 7.9), 7.40 (1 H, d, J 8.1), 7.30 (1 H, t, J 7.7), 6.87 (1 H, d, J 7.3), 2.68 (6 H, s), 1.91 (5 H, p, J 6.2), 1.69 (25 H, s), 1.43 (14 H, s), 1.36 (11 H, s), 1.25 (6 H, s).

^{13}C NMR (151 MHz, C_6D_6, 298.2 K): δ 169.91, 150.89, 139.34, 137.99, 134.94, 124.34, 122.22, 121.35, 111.86, 56.27, 51.92, 45.41, 44.82, 44.79, 44.77, 41.99, 38.25, 35.59, 31.67, 19.97.

Crystal data for MS207 $C_{36}H_{64}MgN_5Na$: M = 635.21, yellow blocks, 0.24 x 0.18 x 0.16 mm^3, orthorhombic, space group *Pna21*, *a* = 22.8425(13), *b* = 9.5028(4), *c* = 17.6401(5), $\alpha = 90°$, $\beta = 90°$, $\gamma = 90°$, *V* = 3829.1(3) $Å^3$, *Z* = 4, D_c = 1.065 g/cm^3, F_{000} = 1352, T = 123(2) K, 29724 reflections collected, 7367 unique (R_{int} = 0.1146), Final GooF = 1.091, *R1* = 0.0967, *wR2* = 0.2228, 403 parameters, 1 restraints. Lp and absorption corrections applied, μ = 0.720 mm^{-1}. Absolute structure parameter = 0.18(12).[155]

7.4.12 Reaction of 1 with *P,P*-dimethylnapthyl-1-phosphine

To a stirred solution of the magnesiate base **1** (see **GP1**), distilled *P,P*-dimethylnapthyl-1-phosphine (0.19 g, 1 mmol) was added dropwise at room temperature. The resulting blue solution was stirred overnight (16 hours), resulting in a large quantity of a blue precipitate. This was isolated by filtration, washed with *n*-hexane and dried *in vacuo*. Yield = 0.45 g, 72 %.

Crystal data for MS213 $C_{36}H_{64}MgN_4NaP$: M = 631.20, clear yellow block, 0.2 x 0.15 x 0.09 mm^3, triclinic, space group *P -1*, *a* = 9.85701(11), *b* = 13.72889(16), *c* = 14.7301(2), $\alpha = 82.4430(11)°$, $\beta = 85.0865(10)°$, $\gamma = 73.9304(10)°$, *V* = 1897.29(4) $Å^3$, *Z* = 2, D_c = 1.105 g/cm^3, F_{000} = 692, T = 123(2) K, 7071 reflections collected, 4365 unique (R_{int} = 0.0206), Final GooF = 1.091, *R1* = 0.0459, *wR2* = 0.1180, 457 parameters, 0 restraints. Lp and absorption corrections applied, μ = 1.118mm^{-1}.

7.5 Bimetallic metallations of *N*-heterocyclic molecules

7.5.1 Synthesis of *N*-ethylindole

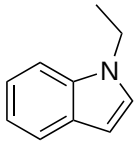

To a stirred solution of indole (1 g, 8.54 mmol) and KOH (1.44 g, 25.61 mmol) in DMF (10 mL), ethyl bromide (1.27 mL, 17.07 mmol) was added at room temperature. The mixture was stirred for three hours before being extracted with diethyl ether. The combined organic layers were washed with H_2O and brine, dried over anhydrous magnesium sulphate and concentrated by rotary evaporation. The crude product was vacuum distilled at 0.15 torr, 60 °C to afford N-ethylindole as a colourless liquid. Yield: 0.92 g, 80 %. This compound has been previously reported.[160]

^{1}H NMR (400 MHz, C_6D_6, 300K): δ 7.74 (d, 1 H, J = 7.88 Hz, H^4), 7.23 (m, 2 H, H^5 H^6), 7.11 (d, 1 H, J = 8 Hz, H^7), 6.68 (d, 1 H, J = 3 Hz, H^1), 6.53 (d, 1 H, J = 3 Hz, H^2), 3.44 (q, 2 H, J = 7.2 Hz, CH_2), 0.87 (t, 3 H, J = 7.2 Hz, CH_3).

^{13}C NMR (100 MHz, C_6D_6, 300K): δ 135.9 (quaternary-C), 129.2 (quaternary-C), 126.5 (C^1), 121.4 (C^4), 121.2 (C^6), 119.4 (C^5), 109.2 (C^7), 101.2 (C^2), 40.3 (CH_2), 14.9 (CH_3).

7.5.2 Synthesis of *N*-isopropylindole

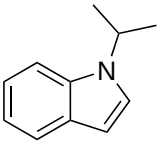

To a stirred solution of indole (1 g, 8.54 mmol) and KOH (1.44 g, 25.61 mmol) in DMF (10 mL), 2-bromopropane (1.6 mL, 17.07 mmol) was added at room temperature. The mixture was stirred for 3 hours before being extracted with ethyl acetate. The combined

organic layers were washed with H_2O and brine, dried over anhydrous magnesium sulphate and concentrated by rotary evaporation. The crude product was vacuum distilled at 0.15 torr, 60 °C to afford N-isopropylindole (0.8 g, 59 % yield) as a colourless liquid. This compound has been previously reported.[161]

^{1}H NMR (400 MHz, C_6D_6, 300K): δ 7.75 (d, 1 H, J = 8 Hz, H^4), 7.16 - 7.28 (m, 3 H, $H^5H^6H^7$, 6.87 (d, 1 H, J = 3.2 Hz, H^1), 6.56 ppm (d, 1 H, J = 3.2 Hz, H^2), 4.09 (septet, 1 H, J = 6.8 Hz, CH), 1.01 (d, 9 H, J = 6.8 Hz, CH_3).

^{13}C NMR (100 MHz, C_6D_6 300K): δ 135.8 (quaternary-C), 129.2 (quaternary-C), 123.0 (C^1), 121.2 (C^6), 120.8 (C^4), 119.5 (C^5), 109.4 (C^7), 101.5 (C^2), 46.5 (CH), 22.1 (CH_3).

7.5.3 Synthesis of *N*-phenyl-1*H*-indole

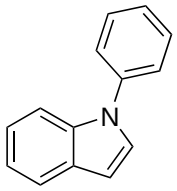

This compound was prepared according to the literature.[162] Indole (1.64 g, 14 mmol), iodobenzene (2.04 g, 10 mmol), CuI (382 mg, 2 mmol) and Cs_2CO_3 (6.52 g, 20 mmol) was added to a Schlenk. The Schlenk was evacuated, and refilled with nitrogen x 3. DMF (20 mL) was added. The resulting mixture was stirred at 120 °C under a nitrogen atmosphere for 16 hours. After cooling to ambient temperature, the reaction mixture was diluted with diethyl ether (40 mL), and washed with H_2O (2 x 30 mL). The aqueous phase was extracted with diethyl ether (2 x 30 mL), and the combined organic phases were dried over $MgSO_4$. After filtration, the solvent was removed, and the crude product purified by column chromatography on silica gel (10 % EtOAc/petroleum benzine) to give *N*-phenylindole as a light yellow oil. Typical yield = 1.55 g, 80 %.

^{1}H NMR (400 MHz, C_6D_6, 300K): δ 7.72 (1 H, dt, J 7.9, 1.0), 7.48 (1 H, dq, J 7.9, 1.0), 7.26 – 7.15 (2 H, m), 7.15 – 7.09 (2 H, m), 7.09 – 7.02 (2 H, m), 7.05 – 6.93 (2 H, m), 6.62 (1 H, dd, J 3.2, 0.9).

^{13}C NMR (100 MHz, C_6D_6, 300K): 139.86, 136.13, 129.74, 129.31, 127.55, 125.98, 124.22, 122.46, 121.25, 120.54, 110.52, 103.78.

7.5.4 Synthesis of *N*-benzyl-1*H*-indole

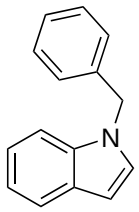

Indole (1 g, 8.54 mmol) was dissolved in 10 mL of DMF. Powdered KOH (0.96 g, 17 mmol) was added, and stirred for at least 30 minutes. Benzylchloride (1.96 mL, 17 mmol) was added dropwise. The resulting suspension was stirred overnight (16 hours). The reaction mixture was then diluted with diethyl ether, and 20 mL of H_2O added. The layers were separated and the aqueous layer extracted with 2 x 20 mL diethyl ether. The solvent was removed to leave an oily solid, which was purified by flash chromatography (silica gel) to yield *N*-benyzlindole as a crystalline colourless solid. Typical yield = 1.33 g, 75 %. This compound has been previously reported.[163]

^{1}H NMR (600 MHz, C_6D_6, 300K): δ 7.79 – 7.66 (1 H, m), 7.20 – 7.16 (2 H, m), 7.11 – 7.05 (1 H, m), 7.02 – 6.85 (3 H, m), 6.79 – 6.72 (2 H, m), 6.70 (1 H, d, J 3.2), 6.55 (1 H, dd, J 3.2, 0.9), 4.66 (2 H, s).

7.5.5 Synthesis of *N*-methyl-7-azaindole

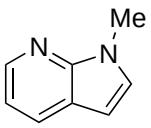

7-azaindole (2.36 g, 20 mmol) was dissolved in 15 mL of DMF. To this solution, powdered KOH (2.24 g, 40 mmol) was added and the mixture stirred for 30 minutes. MeI (2.49 mL, 40 mmol) was added dropwise and the solution was stirred for 30 minutes. The reaction

was monitored by TLC (ethyl acetate/petroleum benzine 50/50). After 30 minutes, the reaction was diluted with diethyl ether, and quenched with 20 mL of H_2O. The layers were separated and the aqueous layer extracted with 2 x 20 mL diethyl ether. The combined organic layers were washed with 10 x 20 mL of distilled water (to remove trace DMF) and washed with brine. The organic layer was dried with $MgSO_4$, filtered and solvent removed to yield a fluorescent yellow oil. Typical yield = 2 g, 76 %. This compound has been previously reported.[164]

^{1}H NMR (400 MHz, $CDCl_3$, 300K): δ 8.34 (1 H, dd, J 4.7, 1.6), 7.90 (1 H, dd, J 7.8, 1.6), 7.18 (1 H, d, J 3.4), 7.05 (1 H, dd, J 7.8, 4.7), 6.45 (1 H, d, J 3.4), 3.90 (3 H, s).

^{13}C NMR (100 MHz, $CDCl_3$, 300K): δ 147.95, 142.97, 129.12, 128.84, 120.65, 115.62, 99.41, 31.38.

^{1}H NMR (600 MHz, C_6D_6, 300K): δ 8.45 (1 H, dd, J 4.6, 1.6), 7.65 (1 H, dd, J 7.8, 1.6), 6.82 (1 H, dd, J 7.8, 4.6), 6.58 (1 H, d, J 3.5), 6.30 (1 H, d, J 3.4), 3.35 (3 H, s).

^{13}C NMR (151 MHz, C_6D_6, 300K): δ 148.62, 143.34, 128.81, 128.36, 120.69, 115.83, 99.42, 30.62.

7.5.6 Synthesis of *N*-ethyl-7-azaindole

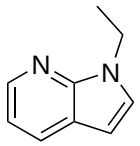

7-azaindole (2.36 g, 20 mmol) was dissolved in 15 mL of DMF. To this solution, powdered KOH (2.24 g, 40 mmol) was added and the mixture stirred for 20 minutes. MeI (2.49 mL, 40 mmol) was added dropwise and the solution was stirred for 20 minutes. The reaction was monitored by TLC (ethyl acetate/petroleum benzine 50/50). After 20 minutes, the reaction was diluted with diethylether, and quenched with 20 mL of H_2O. The layers were separated and the aqueous layer extracted with 2 x 20 mL diethylether. The combined organic layers were washed with 10 x 20 mL of distilled water (to remove trace DMF) and

washed with brine. The organic layer was dried with $MgSO_4$, filtered and solvent removed to yield a yellow oil. Typical yield = 2.43 g, 83 %. This compound has been previously reported.[165]

^{1}H NMR (400 MHz, $CDCl_3$, 300K): δ 8.33 (1 H, dd, J 4.7, 1.6), 7.90 (1 H, dd, J 7.8, 1.6), 7.24 (1 H, d, J 3.5), 7.05 (1 H, dd, J 7.8, 4.7), 6.45 (1 H, d, J 3.5), 4.36 (2 H, q, J 7.3), 1.49 (3 H, t, J 7.3).

^{13}C NMR (100 MHz, $CDCl_3$, 300K): δ 147.35, 142.79, 128.82, 127.41, 120.78, 115.65, 99.48, 39.43, 15.84.

^{1}H NMR (600 MHz, C_6D_6, 300K): δ 8.43 (1 H, d, J 4.6), 7.66 (1 H, dd, J 7.8, 1.1), 6.82 (1 H, ddd, J 7.8, 4.6, 0.7), 6.71 (1 H, d, J 3.5), 6.32 (1 H, dd, J 3.5, 0.8), 3.97 (2 H, q, J 7.3), 1.06 (3 H, t, J 7.3).

^{13}C NMR (151 MHz, C_6D_6, 300K): δ 148.07, 143.20, 128.43, 127.27, 120.90, 115.93, 99.55, 39.27, 15.61.

7.5.7 Synthesis of *N*-isopropyl-7-azaindole

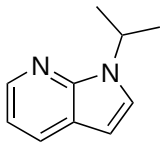

7-azaindole (2.36 g, 20 mmol) was dissolved in 15 mL of DMF. To this solution, powdered KOH (2.24 g, 40 mmol) was added and the mixture stirred for 20 minutes. MeI (2.49 mL, 40 mmol) was added dropwise and the solution was stirred for 20 minutes. The reaction was monitored by TLC (ethyl acetate/petroleum benzine 50/50). After 20 minutes, the reaction was diluted with diethylether, and quenched with 20 mL of H_2O. The layers were separated and the aqueous layer extracted with 2 x 20 mL diethylether. The combined organic layers were washed with 10 x 20 mL of distilled water (to remove trace DMF) and washed with brine. The organic layer was dried with $MgSO_4$, filtered and solvent removed

to yield a pale yellow oil. Typical yield = 2.5 g, 78 %. This compound has been previously reported.[166]

^{1}H NMR (400 MHz, $CDCl_3$, 300K): δ 8.34 (1 H, dd, J 4.6, 1.6), 7.92 (1 H, dd, J 7.8, 1.6), 7.35 (1 H, d, J 3.6), 7.07 (1 H, dd, J 7.8, 4.7), 6.49 (1 H, d, J 3.6), 5.24 (1 H, dt, J 13.5, 6.8), 1.55 (6 H, d, J 6.8).

^{13}C NMR (100 MHz, $CDCl_3$, 300K): δ 147.12, 142.59, 128.76, 124.21, 120.84, 115.73, 99.58, 45.35, 23.06.

7.5.8 Synthesis of *N*-phenyl-7-azaindole

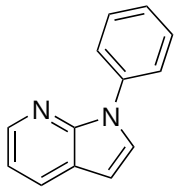

7-Azaindole (1.65 g, 14 mmol), iodobenzene (2.04 g, 10 mmol), CuI (382 mg, 2 mmol) and Cs_2CO_3 (6.52 g, 20 mmol) was added to a Schlenk. The Schlenk was evacuated, and refilled with nitrogen x 3. DMF (20 mL) was added. The resulting mixture was stirred at 120 °C under a nitrogen atmosphere for 16 hours. After cooling to ambient temperature, the reaction mixture was diluted with EtOAc (40 mL), and washed with H_2O (2 x 30 mL). The aqueous phase was extracted with EtOAC (2 x 30 mL), and the combined organic phases were dried over $MgSO_4$. After filtration, the solvent was removed, and the crude product purified by column chromatography on silica gel (10 % EtOAc/petroleum spirits) to give *N*-phenyl-7-azaindole as a light yellow oil (2.1 g, 81 %). This compound has been previously reported.[164]

7.5.9 Synthesis of *N*,3-dimethyl-1*H*-indole

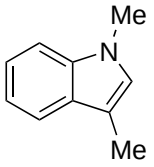

3-Methyl-1*H*-indole (1.5 g, 11.4 mmol) was dissolved in 15 mL of DMF. To this solution, powdered KOH (1.28 g, 22.9 mmol) was added and the mixture stirred for 30 minutes. MeI (3.25 g, 22.9 mmol) was added dropwise and the solution was stirred for 30 minutes. The reaction was monitored by TLC (ethyl acetate/petroleum benzine 50/50). After 30 minutes, the reaction was diluted with diethyl ether, and quenched with 20 mL of H_2O. The layers were separated and the aqueous layer extracted with 2 x 20 mL diethyl ether. The combined organic layers were washed with 10 x 20 mL of distilled water (to remove trace DMF) and washed with brine. The organic layer was dried with $MgSO_4$, filtered and solvent removed to yield a pale yellow oil. Typical yield = 2 g, 76 %. This compound has been previously reported.[167]

^{1}H NMR (400 MHz, $CDCl_3$, 300K): δ 7.59 (1 H, dt, J 7.9, 1.0), 7.30 (1 H, dt, J 8.2, 1.0), 7.26 – 7.21 (1 H, m), 7.13 (1 H, ddd, J 8.0, 6.8, 1.2), 6.84 (1 H, d, J 1.1), 3.75 (3 H, s), 2.35 (3 H, d, J 1.1).

^{13}C NMR (100 MHz, $CDCl_3$, 300K): δ 137.11, 128.76, 126.62, 121.52, 119.05, 118.60, 110.22, 109.11, 32.61, 9.67.

^{1}H NMR (400 MHz, C_6D_6, 300K): δ 7.70 – 7.63 (1 H, m), 7.33 – 7.19 (2 H, m), 7.06 (1 H, dt, J 8.2, 1.0), 6.33 (1 H, d, J 1.2), 2.96 (3 H, s), 2.30 (3 H, d, J 1.1).

7.5.10 Synthesis of *N*-ethyl-3-methyl-1*H*-indole

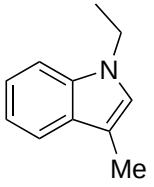

3-Methyl-1*H*-indole (1.5 g, 11.4 mmol) was dissolved in 15 mL of DMF. To this solution, powdered KOH (1.28 g, 22.9 mmol) was added and the mixture stirred for 30 minutes. EtBr (2.5 g, 22.9 mmol) was added dropwise and the solution was stirred for 30 minutes. The reaction was monitored by TLC (ethyl acetate/petroleum benzine 50/50). After 30 minutes, the reaction was diluted with diethyl ether, and quenched with 20 mL of H_2O. The layers were separated and the aqueous layer extracted with 2 x 20 mL diethyl ether. The combined organic layers were washed with 10 x 20 mL of distilled water (to remove trace DMF) and washed with brine. The organic layer was dried with $MgSO_4$, filtered and solvent removed to yield a pale yellow oil. Typical yield = 1.6 g, 88 %. This compound has been previously reported.[168]

^{1}H NMR (400 MHz, $CDCl_3$, 300K): δ 7.63 – 7.56 (1 H, m), 7.37 – 7.29 (1 H, m), 7.27 – 7.18 (1 H, m), 7.17 – 7.08 (1 H, m), 6.91 (1 H, d, J 1.1), 4.13 (2 H, q, J 7.2), 2.36 (3 H, d, J 1.1), 1.45 (3 H, t, J 7.3).

^{13}C NMR (100 MHz, $CDCl_3$, 300K): δ 136.10, 128.88, 124.81, 121.38, 119.15, 118.56, 110.30, 109.17, 40.75, 15.68, 9.73.

^{1}H NMR (400 MHz, C_6D_6, 300K): δ 7.71 – 7.64 (1 H, m), 7.33 – 7.19 (2 H, m), 7.14 – 7.07 (1 H, m), 6.46 (1 H, s), 3.47 (2 H, q, J 7.2), 2.31 (3 H, d, J 1.1), 0.92 (3 H, t, J 7.3).

^{13}C NMR (100 MHz, C_6D_6, 300K): δ 136.68, 129.64, 124.73, 121.71, 119.55, 119.02, 110.28, 109.37, 40.40, 15.40, 9.86.

7.5.11 Synthesis of *N*-isopropyl-3-methyl-1*H*-indole

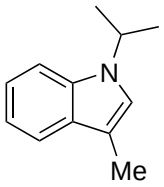

3-Methyl-1*H*-indole (1.5 g, 11.4 mmol) was dissolved in 15 mL of DMF. To this solution, powdered KOH (1.28 g, 22.9 mmol) was added and the mixture stirred for 30 minutes.

iPrBr (2.5 g, 22.9 mmol) was added dropwise and the solution was stirred for 30 minutes. The reaction was monitored by TLC (ethyl acetate/petroleum benzine 50/50). After stirring overnight, the reaction was diluted with diethyl ether, and quenched with 20 mL of H_2O. The layers were separated and the aqueous layer extracted with 2 x 20 mL diethyl ether. The combined organic layers were washed with 10 x 20 mL of distilled water (to remove trace DMF) and washed with brine. The organic layer was dried with $MgSO_4$, filtered and solvent removed. This was further purified by flash column chromatography (silica gel, 10 % EtOAc/petroleum benzine) to yield *N*-isopropyl-3-methyl-1*H*-indole as a pale yellow oil. Typical yield = 1.07 g, 54 %. This compound has been previously reported.[169]

7.5.12 Synthesis of *N*-triisopropylsilyl-1*H*-indole

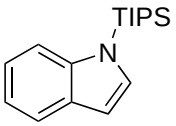

1*H*-indole (1.17 g, 10 mmol) was dissolved in 20 mL of anhydrous THF. The resulting solution was cooled to -78 ° C, and *n*-butyllithium (7.5 mL, [1.6 M in hexanes], 12 mmol) was added dropwise. The resulting solution was allowed to stir at -78 ° C for 30 minutes. Following this, triisopropylsilylchloride (2.57 mL, 12 mmol) was added dropwise at -78 ° C. The resulting solution was allowed to warm to room temperature, following which it was diluted with diethylether (50 mL) and quenched with aqueous NH_4Cl. The organic layer was collected, washed with H_2O and brine, and dried over anhydrous $MgSO_4$. The product was dried *in vacuo*, resulting in a pale yellow oil (2.6 g, 95 % yield). This compound has been previously reported.[170]

^{1}H NMR (400 MHz, $CDCl_3$, 300K): δ 7.64 (1 H, dd, J 7.2, 1.8), 7.52 (1 H, d, J 7.9), 7.27 (1 H, s), 7.22 – 7.07 (2 H, m), 6.63 (1 H, d, J 3.2), 1.72 (3 H, hept, J 7.5), 1.16 (18 H, d, J 7.5).

^{13}C NMR (100 MHz, $CDCl_3$, 300K): δ 140.95, 131.56, 131.28, 121.45, 120.67, 119.88, 114.01, 104.83, 18.29, 13.00.

^{1}H NMR (600 MHz, C_6D_6, 300K): δ 7.92 – 7.63 (1 H, m), 7.57 – 7.37 (1 H, m), 7.30 – 7.17 (2 H, m), 7.09 (1 H, d, J 3.2), 6.70 (1 H, dd, J 3.2, 0.9), 1.43 (4 H, h, J 7.5), 0.98 (18 H, d, J 7.6).

^{13}C NMR (100 MHz, C_6D_6, 300K): δ 144.11, 143.87, 141.08, 133.64, 124.21, 120.54, 118.91, 113.69, 56.88, 52.64, 45.72, 42.30, 36.06, 20.50, 18.65, 13.37.

7.5.13 Reaction of 1 with *N*-methyl-1*H*-indole

*n*BuNa (0.16 g, 2 mmol) was suspended in 10 mL of dry *n*-hexane. To this suspension TMP(H) (0.68 mL, 4 mmol) was added dropwise and the resulting suspension was stirred for at least 30 minutes at room temperature. This resulted in a pale yellow suspension. Next $Mg(CH_2SiMe_3)_2$ (0.4 g, 2 mmol) was added via solid addition tube with subsequent addition of TMEDA (0.3 mL, 2mmol) affording a pale-yellow, transparent solution that was used without further purification. If clumps of solid remained in solution following addition of TMEDA, the solution was sonicated until complete dissolution occurred. To this solution, *N*-methyl-1*H*-indole (0.26 mL, 2 mmol) was added dropwise at room temperature. After approximately 5 minutes stirring at room temperature, a white precipitate formed. This was isolated by filtration and transferred to an argon glovebox for storage. On a repeat synthesis, stirring was stopped following addition of *N*-methyl-1*H*-indole, which resulted in the formation of single crystals.

Rational synthesis of **18**: *n*BuNa (0.16 g, 2 mmol) was suspended in 5 mL of dry *n*-hexane. To this suspension TMP(H) (0.34 mL, 2 mmol) was added dropwise, and the resulting suspension was stirred for at least 30 minutes at room temperature. Next, $Mg(CH_2SiMe_3)_2$ (0.2 g, 1 mmol) was added via a solid addition tube with subsequent addition of TMEDA (0.3 mL, 2 mmol). This afforded a pale yellow, cloudly solution that was used without further purification. To this suspension was added *N*-methylindole (0.5 mL, 4 mmol) was added dropwise, resulting in the immediate formation of a clear solution. After approximately 5 - 10 minutes, a large quantity of a white precipitate was observed, which

was identified by NMR as the title species. Isolated crystalline yield: 0.67 g, 81 % (quantitative by NMR).

^{1}H NMR (400 MHz, C_6D_6, 300K): δ 7.68 – 7.60 (m, 1H, H3), 7.27 (m, 1H, H6), 7.21 – 7.16 (m, 2H, H4/H5), 6.94 (d, *J* = 0.9 Hz, 1H, H2), 4.15 (s, 3H, CH_3), 1.19 (s, 6H, CH_3-TMEDA), 1.06 (s, 2H, CH_2-TMEDA).

^{13}C NMR (101 MHz, C_6D_6, 300K): δ 180.39 (Mg-C2), 141.17, 131.79, 118.52, 117.97, 117.65, 109.71, 108.62, 55.84 (CH_2-TMEDA), 44.46 (CH_3-TMEDA), 36.57 (CH_3) ppm.

Crystal data for complex **18** $C_{48}H_{64}MgN_8Na_2$ **18**: M = 823.38, colourless plates, 0.21 x 0.20 x 0.14 mm^3, monoclinic, space group *P21/c*, *a* = 17.6570(16), *b* = 16.8891(15), *c* = 15.9701(14), α = 90°, β = 90.628(4)°, γ = 90°, *V* = 4762.2(7) Å^3, *Z* = 4, D_c = 1.148 g/cm^3, F_{000} = 1768, T = 123(2) K, 82061 reflections collected, 10691 unique (R_{int} = 0.1037), Final GooF = 1.022, *R1* = 0.0794, *wR2* = 0.2648, 545 parameters, 0 restraints. Lp and absorption corrections applied, μ = 0.096 mm^{-1}. Refined as a two-component twin (Twin law -1 0 0 0 -1 0 0 0 1), BASF = [0.1492(19)].

7.5.14 Reaction of 1 with *N*-ethyl-1*H*-indole

N-ethylindole (0.15 g, 1 mmol) was added dropwise to a stirred solution of the magnesiate base **1**. After approximately five minutes, formation of a white precipitate was observed. The precipitate was isolated via filtration, washed with hexane and dried in vacuo, before storage in an argon glove box. X-ray quality crystals were obtained upon recrystallisation in toluene. Both the crystalline material and the powder were found to be the same product by NMR analysis. Yield = 0.2 g, 24 % (maximum yield 25 % based on consumption of N-ethylindole).

Rational synthesis of **20**. To a stirred suspension of GP2, N-ethylindole (0.58 g, 4 mmol) was added dropwise, resulting in the immediate formation of a clear solution. After approximately 10-20 minutes, a large quantity of a white precipitate was observed, which

was identified by NMR as the title species. Isolated crystalline yield: 0.586 g, 70 % (quantitative by NMR).

Crystal data for $C_{52}H_{72}MgN_8Na_2$: M = 1198.37, colourless plates, 0.04 x 0.03 x 0.02 mm^3, triclinic, space group Pbca, a = 16.682(3), b = 16.236(3), c = 38.216(8), α = 90 °, β = 90 °, γ = 90 °, V = 10351(4) Å, Z = 8, Dc = 1.129 g/cm3, F_{000} = 3792.0, T = 100(2) K, 85955 reflections collected, 12826 unique (R_{int} = 0.706), Final GooF = 1.056, R_1 = 0.0706, wR_2 = 0.1528, 612 parameters, 0 restraints. Lp and absorption corrections applied, μ = 0.090 mm^{-1}.

^{1}H NMR (600 MHz, C_6D_6, 300K): δ 7.63 – 7.56 (m, 1H, H4), 7.29 (m, 1H, H7), 7.17 – 7.08 (m, 2H, H5/H6), 6.86 (s, 1H, H3), 4.70 (q, 2H, *J* = 7.0 Hz, CH_2), 1.44 (t, 3H, 3JHH = 7.1 Hz, CH_3), 1.28 (s, 6H, TMEDA-CH_3), 1.21 (s, 3H, TMEDA-CH_2).

^{13}C NMR (100 MHz, C_6D_6, 300K): δ 181.49 (Mg-C2), 140.45, 132.73, 119.01, 118.58, 118.23, 109.88, 109.64, 56.79 (CH_2-TMEDA), 45.25 (CH_3-TMEDA), 45.14 (CH_2), 17.31 (CH_3) ppm.

7.5.15 Reaction of 1 with *N*-isopropyl-1*H*-indole

To a stirred solution of **GP1**, *N*-isopropyl-1*H*-indole (0.16 g, 1 mmol) was added dropwise at room temperature. The resulting solution was stirred overnight, resulting in the deposition of a large quantity of a white precipitate. This was isolated by filtraton, washed with *n*-hexane and dried *in vacuo*. The solid was transferred to a glovebox for storage. On one repeat synthesis, X-ray quality crystals were obtained upon recrystallisation from *n*-hexane. Both the crystalline product and the solid powder were found to be the same product by ^{1}H NMR spectroscopy. Yield = 0.35 g, 58 %.

^{1}H NMR (600 MHz, C_6D_6, 300K): δ 7.49 (m, 2 H, H^5 / H^6), 7.1 - 7.2 (m, 2 H, H^4 & H^7), 6.21 (d, 1 H, *J* = 0.8 Hz, H^2), 5.16 (septet, 1 H, *J* = 6.8 Hz, CH), 1.69 (d, 6 H, *J* = 6.8 Hz, CH_3), 1.88 (m, 4 H, γ-CH_2 TMP), 1.59 (s (br), 24 H, CH_3 TMP), 1.46 (s (br), 12 H, CH_3, TMEDA), 1.44 (s (br), 4 H, CH_2, TMEDA), 1.39 (s (br), 6 H, β-CH_2 TMP).

^{13}C NMR (100 MHz, C_6D_6, 300K): δ 138.0 (quaternary-C^8), 133.4 (quaternary-C^3), 118.4 (C^4), 117.8 (C^7), 117.7 (C^5), 111.1 (C^6), 106.4 (C^2), 56.4 (CH_2 TMEDA), 54.1 (CH -isopropyl), 52.2 (C^1), 45.2 (CH_3 TMEDA), 41.8 (β-CH_2 TMP), 35.7 (CH_3 TMP), 22.3 (CH_3 isopropyl), 20.0 (γ-CH_2 TMP).

Crystal data for MS-001 $C_{70}H_{122}Mg_2N_{10}Na_2$ **21**: M = 1198.37, colourless plates, 0.18 x 0.16 x 0.10 mm^3, triclinic, space group *P -1*, *a* = 11.5469(4), *b* = 16.3939(6), *c* = 20.4362(8), α = 81.102(2)°, β = 85.116(2)°, γ = 72.647(2)°, *V* = 3644.9(2) Å^3, *Z* = 2, D_c = 1.092 g/cm^3, F_{000} = 1316, T = 123(2) K, 49988 reflections collected, 14416 unique (R_{int} = 0.1065), Final GooF = 1.038, *R1* = 0.0794, *wR2* = 0.2291, 783 parameters, 0 restraints. Lp and absorption corrections applied, μ = 0.090 mm^{-1}.

7.5.16 Iodolysis procedure for complexes 18, 20 and 21

To a stirred solution of either **18**, **20** or **21** a 1 M iodine in THF solution (10 mL for **18** and **20**, 5 mL for **21**) was added dropwise at room temperature. The resulting solution was stirred overnight and quenched with saturated sodium thiosulphate (20 mL). The solution was diluted with CH_2Cl_2, dried over $MgSO_4$ and the solvent removed in vacuo. *N*-methyl-2-iodoindole was isolated as a crystalline solid.[171] *N*-ethyl-2-iodoindole and *N*-isopropyl-2-iodoindole were isolated as pale yellow oils following purification by flash chromatography (silica gel, n-hexane).

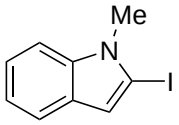

^{1}H NMR (400 MHz, C_6D_6, 300K): δ 7.57 (1 H, d, J = 7.9), 7.34 (1 H, d, J = 8.3), 7.19 (1 H, d, J = 7.4), 7.11 (1 H, t, J = 7.4), 6.84 (1 H, s), 3.79 (3 H, s).

^{13}C NMR (101 MHz, C_6D_6, 300K): δ 138.19, 129.74, 121.96, 119.93, 119.62, 111.94, 109.82, 84.10, 34.19.

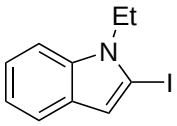

^{1}H NMR (400 MHz, C_6D_6, 300K): δ 7.53 (1 H, dt, J = 7.9, J = 1.0 Hz), 7.33 (1 H, dd, J = 8.3, 0.9 Hz), 7.15 (1 H, ddd, J = 8.3, 7.1, 1.2 Hz), 7.06 (1 H, ddd, J = 7.9, 7.1, 1.0 Hz), 6.78 (1 H, d, J = 0.8 Hz), 4.23 (2 H, q, J = 7.2 Hz), 1.35 (3 H, t, J = 7.2 Hz).

^{13}C NMR (101 MHz, C_6D_6, 300K): δ 137.01, 130.08, 121.87, 119.89, 119.76, 112.11, 109.74, 82.58, 42.25 (CH2), 15.35 (CH3).

ESI-MS: *m/z* $[M+H]^+$ calcd for $C_{10}H_{10}IN$: 271.9936; found: 271.9925.

FT-IR (neat) *V*max (cm^{-1}): 3052 (w), 2939 (w), 1602 (w), 1512 (m), 1463 (s), 1420 (m), 1385 (m), 1316 (s), 1241 (s), 1205 (m) 1130 (m), 1075 (s), 1008 (s), 919 (m), 837 (m), 733 (s), 698 (s).

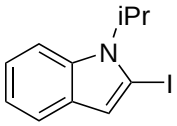

^{1}H NMR (400 MHz, C_6D_6, 300K): δ 7.50 – 7.45 (2 H, m), 7.05 – 7.00 (2 H, m), 6.67 (d, 1 H, J = 0.9), 4.78 (1 H, septet, J = 7.1), 1.56 (9 H, d, J = 7.1).

^{13}C NMR (101 MHz, C_6D_6, 300K): δ 123.00, 120.91, 120.85, 119.68, 111.19, 57.96, 21.12.

ESI-MS: *m/z* $[M+H]^+$ calcd for $C_{11}H_{12}IN$: 286.0082 found: 286.0082.

FT-IR (neat) *V*max (cm^{-1}): 2967 (m), 2931 (m), 2440 (w), 1701 (w), 1457 (s), 1438 (s), 1400 (s), 1383 (m), 1336 (m), 1303 (s), 1260 (m), 1220 (s), 1087 (s), 1011 (s), 906 (m), 800 (m), 738 (s).

7.5.17 Cross-coupling procedure for complexes 18, 20 and 21

To a stirred solution of either **18**, **20** or **21**, iodobenzene (5 equiv. for **18** and **20**, 2 equiv. for **21** was added followed by the addition of 4 mol % of Pd(dppf)Cl_2. The reaction was refluxed for 16 hours. After cooling to room temperature, the solution was quenched with saturated NH_4Cl, extracted with DCM, dried over anhydrous $MgSO_4$ and the solvent was removed *in vacuo*. *N*-methyl-2-phenylindole[164] (0.68 g, 82 %) and *N*-ethyl-2-phenylindole[172] (0.60 g, 68 %) were isolated as crystalline solids, and *N*-isopropyl-2-phenylindole[173] (0.17 g, 71 %) was isolated as a pale yellow oil following flash chromatography (silica gel, n-hexane).

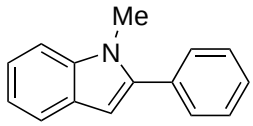

^{1}H NMR (400 MHz, C_6D_6, 300K): δ 7.57 (1 H, d, J = 7.9), 7.34 (1 H, d, J = 8.3), 7.19 (1 H, d, J = 7.4), 7.11 (1 H, t, J = 7.4), 6.84 (1 H, s), 3.79 (3 H, s).

^{1}H NMR (600 MHz, C_6D_6, 300K): = 7.65 (d, 1H, J = 7.7 Hz), 7.52 (dd, 2H, J = 8.3, 1.3 Hz), 7.48 (t, 2H, J = 7.6 Hz), 7.41 (t, 1H, J = 7.3 Hz), 7.38 (d, 1H, J = 8.2 Hz), 7.28 – 7.23 (m, 2H), 7.18 – 7.13 (m, 1H), 6.57 (s, 1H), 3.76 (s, 3H) ppm.

^{13}C NMR (151 MHz, C_6D_6, 300K): δ = 141.79, 138.55, 133.07, 129.60, 128.70, 128.17, 128.07, 121.87, 120.68, 120.07, 109.81, 101.86, 31.40 ppm.

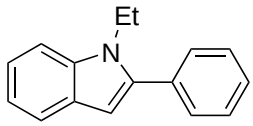

^{1}H NMR (400 MHz, C_6D_6, 300K): δ 7.63 (dt, 1H, J =7.8, 1.0 Hz), 7.53 – 7.36 (m, 6H), 7.26 – 7.19 (m, 1H), 7.13 (ddd, 1H, J = 8.0, 7.0, 1.0 Hz), 6.52 (d, 1H, J = 0.9 Hz), 4.18 (t, 2H, J = 7.2 Hz), 1.32 (d, 3H, J = 7.2 Hz) ppm.

^{13}C NMR (101 MHz, C_6D_6, 300K): δ 141.30, 137.31, 133.44, 129.59, 128.69, 128.53, 128.14, 121.74, 120.80, 119.98 (C5), 110.08 (C7), 102.31 (C3), 38.96 (CH2), 15.59 (CH3).

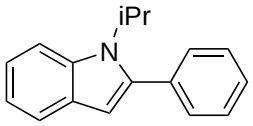

^{1}H NMR (400 MHz, C_6D_6, 300K): δ 7.64 – 7.59 (m, 2 H), 7.5 - 7.4 (m, 5 H), 7.20 – 7.15 (m, 2 H), 6.45 (d, 1 H, J = 0.8), 4.68 (septet, 1 H, J = 7.0), 1.6 (d, 1H, J = 7.0).

^{13}C NMR (101 MHz, C_6D_6, 300K): δ 141.41, 135.44, 133.81, 131.98, 129.64, 128.42, 127.93, 121.01, 120.85, 119.44, 112.40, 102.21, 47.90, 21.57.

7.5.18 Reaction of 1 with *N*,3-dimethyl-1*H*-indole

*n*BuNa (0.16 g, 2 mmol) was suspended in 10 mL of dry *n*-hexane. To this suspension TMP(H) (0.68 mL, 4 mmol) was added dropwise and the resulting suspension was stirred for at least 30 minutes at room temperature. This resulted in a pale yellow suspension. Next $Mg(CH_2SiMe_3)_2$ (0.4 g, 2 mmol) was added via solid addition tube with subsequent addition of TMEDA (0.3 mL, 2mmol) affording a pale-yellow, transparent solution that was used without further purification. If clumps of solid remained in solution following addition of TMEDA, the solution was sonicated until complete dissolution occurred. To this solution, *N*-methyl-1*H*-indole (0.26 mL, 2 mmol) was added dropwise at room temperature. After approximately 5 minutes stirring at room temperature, a white precipitate formed. This was isolated by filtration and transferred to an argon glovebox for storage. On a repeat synthesis, stirring was stopped following addition of *N*-methyl-1*H*-indole, which resulted in the formation of single crystals.

Rational synthesis of **22**: *n*BuNa (0.16 g, 2 mmol) was suspended in 5 mL of dry *n*-hexane. To this suspension TMP(H) (0.34 mL, 2 mmol) was added dropwise, and the resulting suspension was stirred for at least 30 minutes at room temperature. Next, $Mg(CH_2SiMe_3)_2$ (0.2 g, 1 mmol) was added via a solid addition tube with subsequent addition of TMEDA (0.3 mL, 2 mmol). This afforded a pale yellow, cloudly solution that was used without further purification. To this suspension was added *N*-methylindole (0.5 mL, 4 mmol) was added dropwise, resulting in the immediate formation of a clear solution. After

approximately 5 - 10 minutes, a large quantity of a white precipitate was observed, which was identified by NMR as the title species. Isolated crystalline yield: 0.67 g, 81 % (quantitative by NMR).

^{1}H NMR (400 MHz, C_6D_6, 300K): δ 7.62 – 7.48 (1 H, m), 7.21 – 7.08 (3 H, m), 4.22 – 3.90 (3 H, m), 3.00 – 2.71 (3 H, m), 1.25 (6 H, s), 0.93 (2 H, s).

^{13}C NMR (101 MHz, C_6D_6, 300K): δ 179.68, 141.82, 131.44, 118.39, 117.35, 116.76, 116.48, 109.12, 56.55, 45.96, 35.74, 31.98.

Crystal data for $C_{48}H_{64}MgN_8Na_2$ **18**: M = 823.38, colourless plates, 0.21 x 0.20 x 0.14 mm^3, monoclinic, space group *P21/c*, *a* = 17.6570(16), *b* = 16.8891(15), *c* = 15.9701(14), α = 90°, β = 90.628(4)°, γ = 90°, *V* = 4762.2(7) Å^3, *Z* = 4, D_c = 1.148 g/cm^3, F_{000} = 1768, T = 123(2) K, 82061 reflections collected, 10691 unique (R_{int} = 0.1037), Final GooF = 1.022, *R1* = 0.0794, *wR2* = 0.2648, 545 parameters, 0 restraints. Lp and absorption corrections applied, μ = 0.096 mm^{-1}. Refined as a two-component twin (Twin law -1 0 0 0 -1 0 0 0 1), BASF = [0.1492(19)].

7.5.19 Reaction of 1 with *N*-ethyl-3-methyl-1*H*-indole

N-ethyl-3-methyl-1*H*-indole (0.159 g, 1 mmol) was added dropwise to a stirred solution of the magnesiate base **1**. After approximately five minutes, formation of a white precipitate was observed. The precipitate was isolated via filtration, washed with hexane and dried in vacuo, before storage in an argon glove box. Yield = 0.2 g, 24 % (maximum yield 25 % based on consumption of *N*-ethyl-3-methyl-1*H*-indole).

Rational synthesis of **23**. To a stirred suspension of GP2, *N*-ethyl-3-methyl-1*H*-indole (0.64 g, 4 mmol) was added dropwise, resulting in the immediate formation of a clear solution. After approximately 10-20 minutes, a large quantity of a white precipitate was observed, which was identified by NMR as the title species. Isolated yield: g, % (quantitative by NMR).

^{1}H NMR (600 MHz, C_6D_6, 300K): δ 7.63 – 7.56 (m, 1H, H4), 7.29 (m, 1H, H7), 7.17 –

7.08 (m, 2H, H5/H6), 6.86 (s, 1H, H3), 4.70 (q, 2H, *J* = 7.0 Hz, CH_2), 1.44 (t, 3H, 3JHH = 7.1 Hz, CH_3), 1.28 (s, 6H, TMEDA-CH_3), 1.21 (s, 3H, TMEDA-CH_2).

^{13}C NMR (100 MHz, C_6D_6, 300K): δ 181.49 (Mg-C2), 140.45, 132.73, 119.01, 118.58, 118.23, 109.88, 109.64, 56.79 (CH_2-TMEDA), 45.25 (CH_3-TMEDA), 45.14 (CH_2), 17.31 (CH_3) ppm.

7.5.20 Reaction of 1 with *N*-isopropyl-3-methyl-1*H*-indole

N-isopropyl-3-methyl-1*H*-indole (0.17 g, 1 mmol) was added dropwise to a stirred solution of the magnesiate base **1**. The resulting solution was heated at 40 ° C for 24 hours, before the solvent was removed *in vacuo* and the resulting oil transferred to a glovebox. ^{1}H NMR analysis indicated a conversion of approximately 55 %. Single crystals of the α magnesiated product grew from a C_6D_6 solution.

^{1}H NMR (600 MHz, C_6D_6, 300K): δ 7.48 (1 H, t, J 8.4), 7.34 – 7.1 (3 H, m), 4.99 (1 H, sept, J 6.8), 2.47 (3 H, s), 1.96 (4 H, t, J 6.2), 1.69 (2 H, d, J 7.0), 1.55 (36 H, s, TMP/TMEDA), 1.06 (3 H, s).

^{13}C NMR (100 MHz, C_6D_6, 300K): δ 174.40 (Mg - C signal).

Crystal data for MS-221 $C_{36}H_{66}MgN_5Na$: M = 616.24, colourless blocks, 0.21 x 0.16 x 0.10 mm^3, monoclinic, space group *P21/n*, *a* = 8.49940(12), *b* = 29.2404(5), *c* = 14.88946(19), α = 90°, β = 92.6831(13)°, γ = 90°, *V* = 3686.36(9) Å^3, *Z* = 4, D_c = 1.107 g/cm^3, F_{000} = 1360, T = 123(2) K, 30097 reflections collected, 7676 unique (R_{int} = 0.0544), Final GooF = 1.110, *R1* = 0.0481, *wR2* = 0.1233, 404 parameters, 0 restraints. Lp and absorption corrections applied, μ = 0.746 mm^{-1}.

7.5.21 Iodolysis procedure for complexes 22 and 23

To a stirred solution of either **22** or **23**, a 1 M iodine in THF solution (10 mL, 10 mmol) was added dropwise at room temperature. The resulting solution was stirred overnight

and quenched with saturated sodium thiosulphate (20 mL). The solution was diluted with CH_2Cl_2, dried over $MgSO_4$ and the solvent removed in vacuo.

7.5.22 Characterisation of *N*-3-dimethyl-2-iodo-indole

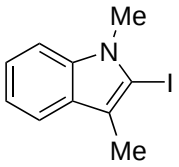

N-3-dimethyl-2-iodo-indole was isolated as a yellow solid in an 85 % yield.

^{1}H NMR (600 MHz, $CDCl_3$, 300K): δ 7.52 (1 H, dq, J 7.8, 1.2), 7.32 – 7.27 (1 H, m), 7.17 (1 H, ddt, J 8.3, 7.1, 1.2), 7.08 (1 H, ddq, J 8.6, 7.2, 1.6), 3.75 (3 H, s), 2.33 (3 H, s).

^{13}C NMR (151 MHz, $CDCl_3$, 300K): δ 138.51, 128.37, 121.86, 119.16, 118.39, 117.03, 109.57, 87.44, 34.25, 12.56.

ESI-MS: *m/z* $[M+H]^+$ calcd for $C_{10}H_{10}NI$: 271.9936; found: 271.9930.

7.5.23 Characterisation of *N*-ethyl-3-methyl-2-iodo-indole

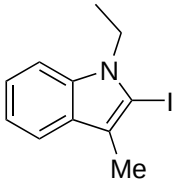

N-ethyl-3-methyl-2-iodo-indole was isolated as a yellow solid in an 85 % yield.

^{1}H NMR (600 MHz, $CDCl_3$, 300K): δ 7.55 – 7.50 (1 H, m), 7.34 – 7.30 (1 H, m), 7.15 (1 H, ddd, J 8.2, 7.0, 1.2), 7.07 (1 H, ddd, J 8.2, 7.0, 0.9), 4.23 (2 H, q, J 7.2), 2.32 (3 H, s), 1.32 (3 H, t, J 7.2).

^{13}C NMR (151 MHz, $CDCl_3$, 300K): δ 137.35, 128.70, 124.81, 121.77, 119.13, 118.52, 117.07, 109.49, 85.96, 42.19, 15.31.

ESI-MS: *m/z* $[M+H]^+$ calcd for $C_{10}H_{10}NI$: 285.0014; found: 285.0011.

7.5.24 Reaction of the magnesiate base with *N*-triisopropylsilyl-1*H*-indole

To a stirred solution of the magnesiate base **1** (see **GP1**), *N*-triisopropylsilyl-1*H*-indole (0.27 g, 1 mmol) was added dropwise at room temperature. Upon addition, an immediate formation of a bright yellow solution was observed. The solution was stirred overnight, resulting in the deposition of a large quantity of a white precipitate. This was gently heated back into solution, and the solution was filtered into a new schlenk. Storage of this solution at -30 ° C over three days resulted in a large crop of colourless crystals, which were isolated and dried under vacuum, before being transferred to a glovebox for storage. Yield = 0.6 g, 84 %.

^{1}H NMR (600 MHz, C_6D_6, 300K): δ 7.77 (1 H, dd, J 7.6, 1.3), 7.55 (1 H, d, J 0.8), 7.31 (1 H, s), 7.19 (1 H, ddd, J 8.2, 7.0, 1.3), 7.10 (1 H, ddd, J 7.8, 7.0, 1.0), 1.93 (4 H, p, J 6.1), 1.66 (26 H, s), 1.61 (3 H, dt, J 15.0, 7.5), 1.48 (14 H, s), 1.13 (18 H, d, J 7.6).

^{13}C NMR (100 MHz, C_6D_6, 300K): δ 143.72, 143.48, 140.68, 133.25, 123.82, 120.15, 118.52, 113.30, 56.49, 52.25, 45.33, 41.91, 35.67, 20.10, 18.26, 12.98.

Crystal data for MS223 $C_{41}H_{78}MgN_5NaSi$: M = 716.47, colourless blocks, 0.25 x 0.2 x 0.2 mm^3, space group $P2_1/c$, a = 18.8373(2), b = 11.0648(1), c = 22.4078(3), α = 90°, β = 107.78(1) °, γ = 90 °, V = 4447.34(8) Å^3, Z = 4, D_c = 1.070 g/cm^3, F_{000} = 1584, T = 123(2) K, 35155 reflections collected, 9212 unique (R_{int} = 0.0493), Final GooF = 1.058, *R1* = 0.0465, *wR2* = 0.1234, 519 parameters, 0 restraints. Lp and absorption corrections applied, μ = 0.928 mm^{-1}.

7.5.25 Reaction of magnesiate base 1 with *N*-phenylindole

To a stirred solution of the magnesiate base **1** (see **GP1**), *N*-phenyl-1*H*-indole (0.193 g, 1 mmol) was added dropwise at room temperature. The solution was stirred overnight, resulting in the deposition of a large quantity of a white precipitate. Recrystallisation

from *n*-hexane resulted in single crystals being deposited which were found to be the di-magnesiated complex [(TMEDA)Na(TMP)($\alpha-C_8H_5N-o-C_6H_4$)Mg]$_2$ **25**. Isolated yield = 0.35 g, 70 %.

^{1}H NMR (600 MHz, C_6D_6, 300K): δ 8.62 (1 H, dd, J 6.6, 1.7), 8.41 (1 H, dd, J 6.4, 1.7), 8.18 (1 H, d, J 8.1), 8.13 (1 H, d, J 8.2), 8.01 (1 H, d, J 7.7), 7.96 (3 H, dd, J 11.1, 7.8), 7.74 (1 H, s), 7.53 (1 H, s), 7.49 (2 H, td, J 7.5, 1.7), 7.37 (2 H, q, J 6.9), 7.34 – 7.17 (4 H, m), 1.60 – 1.50 (4 H, m), 1.44 (24 H, s), 1.40 (8 H, s), 1.00 (8 H, s), 0.89 (2 H, t, J 7.1), 0.76 (12 H, s).

^{13}C NMR (100 MHz, C_6D_6, 300K): δ 175.40, 166.18, 153.58, 138.69, 136.20, 133.19, 121.45, 118.87, 115.70, 115.21, 114.61, 112.70, 109.91, 108.82, 56.08, 49.67, 43.36, 39.95, 36.39, 36.37, 33.58, 29.69, 29.42, 29.36, 20.68, 18.32, 16.50, 11.59.

Crystal data for MS081 $(C_{29}H_{43}MgN_4Na)_2$: M = 989.95, colourless blocks, 0.25 x 0.2 x 0.2 mm^3, space group *P -1*, *a* = 10.9550(7), *b* = 11.1736(7), *c* = 13.3095(9), α = 67.403(2) °, β = 82.765(2) °, γ = 72.739(2) °, *V* = 1436.23(16) Å^3, *Z* = 1, D_c = 1.145 g/cm^3, F_{000} = 536, T = 123(2) K, 22292 reflections collected, 5677 unique (R_{int} = 0.0595), Final GooF = 1.020, *R1* = 0.0663, *wR2* = 0.1678, 383 parameters, 6 restraints. Lp and absorption corrections applied, μ = 0.100 mm^{-1}.

7.5.26 Iodolysis procedure for complex 25

To a stirred suspension of **25**, a 1 M iodine in THF solution (10 mL, 10 mmol) was added dropwise at room temperature. The resulting solution was stirred for 30 minutes and quenched with saturated sodium thiosulphate (20 mL). The solution was diluted with diethyl ether, dried over $MgSO_4$ and the solvent removed *in vacuo*. The crude residue was purified by flash column chromatography (silcia gel, 90 % EtOAc/petroleum benzine) to yield 2-iodo-1-(2-iodophenyl)-1*H*-indole in a high, crystalline yield (82 %).

7.5.27 2-iodo-1-(2-iodophenyl)-1*H*-indole

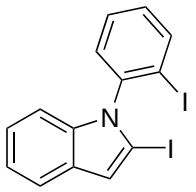

^{1}H NMR (400 MHz, $CDCl_3$, 300K): δ 8.05 (1 H, dd, J 8.0, 1.4), 7.63 – 7.59 (1 H, m), 7.54 (1 H, td, J 7.6, 1.4), 7.34 (1 H, dd, J 7.8, 1.6), 7.27 (1 H, ddd, J 7.9, 7.5, 1.6), 7.12 (2 H, pd, J 7.1, 1.4), 6.99 (1 H, d, J 0.8).

^{13}C NMR (100 MHz, $CDCl_3$, 300K): δ 141.77, 140.06, 138.96, 131.36, 130.97, 129.77, 129.44, 122.63, 120.69, 119.57, 113.59, 111.04, 100.84, 83.53, 77.36.

ESI-MS: *m/z* $[M+H]^+$ calcd for $C_{14}H_9I_2N$: 445.8903; found: 445.8904, $[M-I]^+$ calcd for $C_{14}H_9IN^+$: 318.9858; found: 318.9867.

FT-IR (neat) *V*max (cm^{-1}): 3058 (bw), 2922 (bw), 2852 (bw), 1577 (w), 1475 (s), 1434 (s), 1295 (s), 1211 (m), 1146 (w), 1047 (w), 1023 (m), 963 (w), 781 (m), 755 (m), 743 (s), 714 (m).

7.6 Bimetallic metallations of *P*-heterocyclic compounds

7.6.1 Synthesis of trimethyl(phenylethynyl)silane

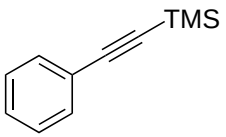

Phenylacetylene (10.96 mL, 100 mmol) was dissolved in 100 mL of THF. This solution was cooled to -78 °C in a dry-ice/acetone bath, following which *n*-BuLi (65 mL, [1.6 M in hexanes], 1.05 equiv) was added dropwise. After complete addition, the mixture transitions to a deep blue colour (presumably due to trace quantities of the di-anion). This solution is stirred at - 78 °C for 1 hour, following which TMSCl (13.3 mL, 105 mmol) was added dropwise at -78 °C. The resulting suspension was allowed to warm to room temperature, following which it was diluted with diethylether and quenched with H_2O. The organic layer was separated, dried and the solvent removed. Typical yield = 17 g, 97 % yield.

^{1}H NMR (600 MHz, C_6D_6, 298.2 K): δ 7.49 – 7.43 (2 H, m), 7.33 – 7.27 (3 H, m), 0.25 (9 H, s).

7.6.2 Synthesis of (Z)-β-bromo-β-trimethylsilylstyrene

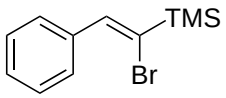

Trimethyl(phenylethynyl)silane (17.43 g, 100 mmol) was dissolved in 100 mL of *n*-hexane. To this solution, DIBAL-H (105 mL, [1 M in hexanes], 105 mmol) was added dropwise. The resulting solution was allowed to stir overnight. Following this, the solution was cooled to 0 °C, where *n*-bromosuccinimide (18.69 g, 105 mmol) was added in portions. Following complete addition, the resulting heterogenous solution was stirred at 0 °C for 30 minutes, after which it was diluted with diethylether. To this solution, 4 mL of H_2O

was added slowly dropwise. Following complete addition, 4 mL of 15 % NaOH in H_2O was added slowly dropwise. After complete addition, 10 mL of H_2O was added slowly dropwise. Anhydrous magnesium sulfate was added, and the resulting mixture allowed to warm to room temperature stirring. The mixture was filtered, organic layer separated and washed with H_2O (3 x 100 mL), brine (1 x 100 mL) and dried over $MgSO_4$. The solvent was removed, yielding a light yellow oil. Typical yield = 24.25 g, 95 % yield. This compound has been previously reported.[144]

7.6.3 Synthesis of P-phenyl-2-trimethylsilyl-phosphindole

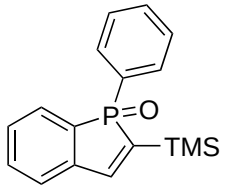

To a stirred, dilute solution of (Z)-β-bromo-β-trimethylsilylstyrene (4.2 g, 20 mmol) in diethyl ether (200 mL) at 0 °C was added 2.1 equivalents of *n*-BuLi (26.25 mL, 42 mmol) dropwise. The resulting orange solution is stirred for two hours at 0 °C, following which a dilute diethyl ether solution of phenylphosphine dichloride (3.94 g, 22 mmol) is added slowly at 0 °C. It is crucial that this step is completed slowly and a dilute solution ($<$ 0.2 M) is used for the purity of the phosphindole. The resulting solution is stirred for at least 4 hours warming to room temperature, before being quenched with degassed saturated $NaHCO_3$. The solution is then vigorously stirred until full dissolution occurs. The organic layer is collected, dried and solvent removed to leave a yellow oil. This can either be purified by flash column chromatography (silica gel, *n*-hexane), or allowed to crystallise over a number of days at room temperature. This compound has been previously reported.[144]

^{1}H NMR (400 MHz, $CDCl_3$, 298.2 K): δ 7.62 – 7.58 (2 H, m), 7.51 (1 H, dd, J 15.4, 0.7), 7.36 (1 H, td, J 7.5, 1.2), 7.32 – 7.26 (2 H, m), 7.25 – 7.20 (4 H, m), 0.08 (9 H, s).

^{31}P NMR (162.0 MHz, $CDCl_3$, 298.2 K δ 13.71.

P-phenyl-2-trimethylsilyl-phosphindole can be readily converted to its oxide by the addition of H_2O_2.

^{1}H NMR (400 MHz, $CDCl_3$, 298.2 K): δ 7.26 - 7.70 (m, 10 H), 0.1 (s, 9 H).

^{31}P NMR (162.0 MHz, $CDCl_3$, 298.2 K δ 48.67.

7.6.4 Synthesis of P-phenylphosphindole

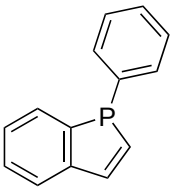

P-phenyl-2-trimethylsilyl-phosphindole (0.85 g, 3 mmol) was dissolved in approximately 3 mL of THF in a 10 mL microwave tube. To this solution, TBAF (4 mL, [1 M in THF], 4 mmol) was added. The resulting dark red solution was heated in a pressurised microwave reactor for 30 minutes at 90 ° C. After cooling to room temperature, the solution was diluted with diethyl ether (50 mL) and quenched with saturated NH_4Cl solution (20 mL). The organic layer was washed with NH_4Cl x 3, dilute HCl (5 %), and with brine. The solvent is removed to leave *P*-phenylphosphindole as a crystalline solid. This compound has been previously reported.[144]

^{1}H NMR (400 MHz, $CDCl_3$, 298.2 K): δ 7.58 – 7.45 (1 H, m), 7.42 (1 H, d, J 7.6), 7.26 – 7.10 (8 H, m), 6.75 (1 H, dd, J 39.3, 7.5).

^{31}P NMR (162.0 MHz, $CDCl_3$, 298.2 K δ 0.24 (s).

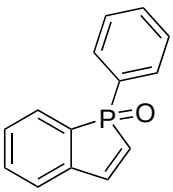

P-phenylphosphindole can be readily converted to its oxide by the addition of H_2O_2. This compound has been previously reported.[144]

^{1}H NMR (400 MHz, $CDCl_3$, 298.2 K): δ 7.70 – 7.55 (2 H, m), 7.52 (1 H, ddd, J 9.3, 7.2, 1.0), 7.47 – 7.19 (7 H, m), 6.36 (1 H, dd, J 25.7, 8.5).

^{31}P NMR (162.0 MHz, $CDCl_3$, 298.2 K δ 41.03 (s).

7.6.5 Synthesis of 2,2'-dibromobiphenyl

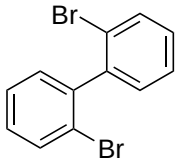

1,2-Bromobenzene (15 g, 63.6 mmol) was dissolved in approximately 100 mL anhydrous THF. *n*-Butyllithium (21 mL, 33.4 mmol) was added dropwise over 1 hour at - 78 °C. The mixture was stirred at room temperature overnight and the reaction quenched with water. The crude product was extracted into diethyl ether, dried over magnesium sulfate and solvent removed *in vacuo*. The crude solid was purified by recrystallisation from *n*-hexane.

7.6.6 Synthesis of 5-phenyl-5H-benzo[b]phosphindole

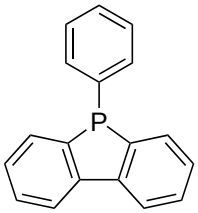

2,2'-dibromobiphenyl (3.12 g, 10 mmol) was dissolved in 50 mL of anhydrous THF and cooled to -78 ° C. To this solution, *n*BuLi (13.2 mL, [1.6 M in hexanes], 21 mmol) was added dropwise. The resulting solution was stirred for two hours. At -78 ° C, dichlorophenylphosphine (1.97 g, 11 mmol) was added dropwise slowly via syringe pump. The resulting suspension was stirred warming to room temperature. The reaction was diluted with diethyl ether and quenched with aqueous NH_4Cl. Following standard organic workup, the crude product was purified by column chromatography (silica gel, ethyl

acetate) to give *P*-phenyl-5H-benzo[b]phosphindole as a yellow crystalline solid. Yield 1.66 grams, 60 %. The corresponding oxide could be obtained by treating *P*-phenyl-5H-benzo[b]phosphindole with H_2O_2.

In an alternative synthesis, triphenylphosphine oxide (2.8 g, 10 mmol) was dissolved in 80 mL of anhydrous THF. Phenyllithium (11.2 mL, [20 % solution in dibutyl ether], 21 mmol) was added dropwise, resulting in a dark red solution. This solution was heated to reflux for 16 hours. After hydrolysis, the solvent was removed, and 100 mL of water was added. The solution was neutralised with dilute HCl and extracted with DCM. The combined organic layers were dried over $MgSO_4$, solvent removed and purified by column chromatography (silica gel, dry-loaded, ethyl acetate). The oxide could be obtained by oxidation with H_2O_2. Yield = 2.76 g, 76 %. This compound has been previously reported.[174]

References

[1] R. E. Mulvey and S. D. Robertson, *Angew. Chem. Int. Ed.*, **2013**, 52, 11470–11487.

[2] P. Gros and Y. Fort, *Eur. J. Org. Chem.*, **2002**, 3375–3383.

[3] P. C. Gros and Y. Fort, *Eur. J. Org. Chem.*, **2009**, 4199–4209.

[4] G. R. Bedford and D. N. Richardson, *Nature*, **1966**, 212, 733–734.

[5] World Health Organization (WHO), *Model list of essential medicines - 21st List*, 2019.

[6] R. M. Peltzer, O. Eisenstein, A. Nova and M. Cascella, *J. Phys. Chem. B*, **2017**, 121, 4226–4237.

[7] G. E. Parris and E. C. Ashby, *J. Am. Chem. Soc.*, **1971**, 93, 1206–1213.

[8] H. J. Reich, *Chem. Rev.*, **2013**, 113, 7130–7178.

[9] T. Kottke and D. Stalke, *Angew. Chemie Int. Ed. English*, **1993**, 32, 580–582.

[10] U. Schümann, J. Kopf and E. Weiss, *Angew. Chemie Int. Ed. English*, **1985**, 24, 215–216.

[11] A. S. Galiano-Roth and D. B. Collum, *J. Am. Chem. Soc.*, **1989**, 111, 6772–6778.

[12] P. G. Williard and J. M. Salvino, *J. Org. Chem.*, **1993**, 58, 1–3.

[13] F. E. Romesberg and D. B. Collum, *J. Am. Chem. Soc.*, **1994**, 116, 9198–9202.

[14] N. D. Barnett, R. E. Mulvey, W. Clegg and P. A. O'Neil, *J. Am. Chem. Soc.*, **1991**, 113, 8187–8188.

[15] M. F. Lappert, M. J. Slade, A. Singh, J. L. Atwood, R. D. Rogers and R. Shakir, *J. Am. Chem. Soc.*, **1983**, 105, 302–304.

[16] B. L. Lucht and D. B. Collum, *J. Am. Chem. Soc.*, **1994**, 116, 7949–7950.

[17] E. Hevia, A. R. Kennedy, R. E. Mulvey, D. L. Ramsay and S. D. Robertson, *Chem. - A Eur. J.*, **2013**, 19, 14069–14075.

[18] P. G. Williard and Q. Y. Liu, *J. Am. Chem. Soc.*, **1993**, 115, 3380–3381.

[19] D. R. Armstrong, P. García-ÃÁlvarez, A. R. Kennedy, R. E. Mulvey and S. D. Robertson, *Chem. - A Eur. J.*, **2011**, 17, 6725–6730.

[20] L. S. Bennie, W. J. Kerr, M. Middleditch and A. J. Watson, *Chem. Commun.*, **2011**, 47, 2264–2266.

[21] J. S. Nicholson and S. S. Adams, *GB971700*, 1964.

[22] P. Gros, S. Choppin and Y. Fort, *J. Org. Chem.*, **2003**, 68, 2243–2247.

[23] H. K. Khartabil, P. C. Gros, Y. Fort and M. F. Ruiz-López, *J. Am. Chem. Soc.*, **2010**, 132, 2410–2416.

[24] A. Seggio, M. I. Lannou, F. Chevallier, D. Nobuto, M. Uchiyama, S. Golhen, T. Roisnel and F. Mongin, *Chem. - A Eur. J.*, **2007**, 13, 9982–9989.

[25] K. Snégaroff, J. M. L'Helgoual'ch, G. Bentabed-Ababsa, T. T. Nguyen, F. Chevallier, M. Yonehara, M. Uchiyama, A. Derdour and F. Mongin, *Chem. - A Eur. J.*, **2009**, 15, 10280–10290.

[26] K. Snégaroff, S. Komagawa, F. Chevallier, P. C. Gros, S. Golhen, T. Roisnel, M. Uchiyama and F. Mongin, *Chem. - A Eur. J.*, **2010**, 16, 8191–8201.

[27] T. T. Nguyen, F. Chevallier, V. Jouikov and F. Mongin, *Tetrahedron Lett.*, **2009**, 50, 6787–6790.

[28] G. Dayaker, F. Chevallier, P. C. Gros and F. Mongin, *Tetrahedron*, **2010**, 66, 8904–8910.

[29] E. Nagaradja, F. Chevallier, T. Roisnel, V. Jouikov and F. Mongin, *Tetrahedron*, **2012**, 68, 3063–3073.

[30] O. Bayh, H. Awad, F. Mongin, C. Hoarau, F. Trécourt, G. Quéguiner, F. Marsais, F. Blanco, B. Abarca and R. Ballesteros, *Tetrahedron*, **2005**, 61, 4779–4784.

[31] F. Mongin, A. Bucher, J. P. Bazureau, O. Bayh, H. Awad and F. Trécourt, *Tetrahedron Lett.*, **2005**, 46, 7989–7992.

[32] D. R. Armstrong, A. R. Kennedy, R. E. Mulvey, J. A. Parkinson and S. D. Robertson, *Chem. Sci.*, **2012**, 3, 2700–2707.

[33] M. Uchiyama, H. Naka, Y. Matsumoto and T. Ohwada, *J. Am. Chem. Soc.*, **2004**, 126, 10526–10527.

[34] H. Naka, M. Uchiyama, Y. Matsumoto, A. E. Wheatley, M. McPartlin, J. V. Morey and Y. Kondo, *J. Am. Chem. Soc.*, **2007**, 129, 1921–1930.

[35] S. Usui, Y. Hashimoto, J. V. Morey, A. E. Wheatley and M. Uchiyama, *J. Am. Chem. Soc.*, **2007**, 129, 15102–15103.

[36] A. J. Peel, N. Tezuka, J. M. D'Rozario, M. Uchiyama and A. E. Wheatley, *Chem. Sci.*, **2019**, 10, 3385–3400.

[37] R. E. Mulvey, F. Mongin, M. Uchiyama and Y. Kondo, *Angew. Chem. Int. Ed.*, **2007**, 46, 3802–3824.

[38] A. Krasovskiy and P. Knochel, *Angew. Chem. Int. Ed.*, **2004**, 43, 3333–3336.

[39] R. Li-Yuan Bao, R. Zhao and L. Shi, *Chem. Commun.*, **2015**, 51, 6884–6900.

[40] C. R. Hauser and H. G. Walker, *J. Am. Chem. Soc.*, **1947**, 69, 295–297.

[41] A. Krasovskiy, V. Krasovskaya and P. Knochel, *Angew. Chem. Int. Ed.*, **2006**, 45, 2958–2961.

[42] P. García-Álvarez, D. V. Graham, E. Hevia, A. R. Kennedy, J. Klett, R. E. Mulvey, C. T. O'Hara and S. Weatherstone, *Angew. Chem. Int. Ed.*, **2008**, 47, 8079–8081.

[43] T. P. Petersen, M. R. Becker and P. Knochel, *Angew. Chem. Int. Ed.*, **2014**, 53, 7933–7937.

[44] M. R. Becker, M. A. Ganiek and P. Knochel, *Chem. Sci.*, **2015**, 6, 6649–6653.

[45] M. R. Becker and P. Knochel, *Angew. Chem. Int. Ed.*, **2015**, 54, 12501–12505.

[46] M. A. Ganiek, M. R. Becker, M. Ketels and P. Knochel, *Org. Lett.*, **2016**, 18, 828–831.

[47] M. Ketels, D. B. Konrad, K. Karaghiosoff, D. Trauner and P. Knochel, *Org. Lett.*, **2017**, 19, 1666–1669.

[48] N. Weidmann, M. Ketels and P. Knochel, *Angew. Chem. Int. Ed.*, **2018**, 57, 10748–10751.

[49] B. Heinz, D. Djukanovic, M. A. Ganiek, B. Martin, B. Schenkel and P. Knochel, *Org. Lett.*, **2020**, 22, 493–496.

[50] A. J. Martínez-Martínez, M. Á. Fuentes, A. Hernán-Gõmez, E. Hevia, A. R. Kennedy, R. E. Mulvey and C. T. O'Hara, *Angew. Chem. Int. Ed.*, **2015**, 54, 14075–14079.

[51] D. R. Armstrong, W. Clegg, S. H. Dale, D. V. Graham, E. Hevia, L. M. Hogg, G. W. Honeyman, A. R. Kennedy and R. E. Mulvey, *Chem. Commun.*, **2007**, 598–600.

[52] M. Uchiyama, Y. Matsumoto, D. Nobuto, T. Furuyama, K. Yamaguchi and K. Morokuma, *J. Am. Chem. Soc.*, **2006**, 128, 8748–8750.

[53] H. Naka, M. Uchiyama, Y. Matsumoto, A. E. Wheatley, M. McPartlin, J. V. Morey and Y. Kondo, *J. Am. Chem. Soc.*, **2007**, 129, 1921–1930.

[54] V. L. Blair, W. Clegg, R. E. Mulvey and L. Russo, *Inorg. Chem.*, **2009**, 48, 8863–8870.

[55] R. E. Mulvey, *Acc. Chem. Res.*, **2009**, 42, 743–755.

[56] R. E. Mulvey, *Dalt. Trans.*, **2013**, 42, 6676–6693.

[57] S. D. Robertson, M. Uzelac and R. E. Mulvey, *Chem. Rev.*, **2019**, 119, 8332–8405.

[58] V. L. Blair, L. M. Carrella, W. Clegg, B. Conway, R. W. Harrington, L. M. Hogg, J. Klett, R. E. Mulvey, E. Rentschler and L. Russo, *Angew. Chem. Int. Ed.*, **2008**, 47, 6208–6211.

[59] E. Hevia, D. J. Gallagher, A. R. Kennedy, R. E. Mulvey, C. T. O'Hara and C. Talmard, *Chem. Commun.*, **2004**, 10, 2422–2423.

[60] S. Harder, J. Boersma, L. Brandsma and J. A. Kanters, *J. Organomet. Chem.*, **1988**, 339, 7–15.

[61] W. Bauer and P. von Ragué Schleyer, *J. Am. Chem. Soc.*, **1989**, 111, 7191–7198.

[62] J. M. Saa, P. M. Deya, G. A. Suner and A. Frontera, *J. Am. Chem. Soc.*, **1992**, 114, 9093–9100.

[63] S. T. Chadwick, R. A. Rennels, J. L. Rutherford and D. B. Collum, *J. Am. Chem. Soc.*, **2000**, 122, 8640–8647.

[64] A. J. Martínez-Martínez, A. R. Kennedy, R. E. Mulvey and C. T. O'Hara, *Science*, **2014**, 346, 834–837.

[65] A. J. Martínez-Martínez, S. Justice, B. J. Fleming, A. R. Kennedy, I. D. Oswald and C. T. O'Hara, *Sci. Adv.*, **2017**, 3, 1–8.

[66] V. L. Blair, A. R. Kennedy, R. E. Mulvey and C. T. O'Hara, *Chem. Eur. J.*, **2010**, 16, 8600–8604.

[67] V. L. Blair, A. R. Kennedy, J. Klett and R. E. Mulvey, *Chem. Commun.*, **2008**, 129, 5426–5428.

[68] R. E. Mulvey, V. L. Blair, W. Clegg, A. R. Kennedy, J. Klett and L. Russo, *Nat. Chem.*, **2010**, 2, 588–591.

[69] A. J. Martínez-Martínez and C. T. O'Hara, *Adv. Organomet. Chem.*, Academic Press, 2016, vol. 65, 1–46.

[70] A. Maercker, *Angew. Chemie Int. Ed. English*, **1987**, 26, 972–989.

[71] M. Schlosser, *Organometallics Synth. Third Man.*, John Wiley & Sons, Inc., 2013, ch. Chap. 1.

[72] H. Gilman and B. J. Gaj, *J. Org. Chem.*, **1957**, 22, 1165–1168.

[73] S. C. Honeycutt, *J. Organomet. Chem.*, **1971**, 29, 1–5.

[74] J. Clayden and S. A. Yasin, *New J. Chem.*, **2002**, 26, 191–192.

[75] R. B. Bates, L. M. Kroposki and D. E. Potter, *J. Org. Chem.*, **1972**, 37, 560–562.

[76] A. R. Kennedy, J. Klett, R. E. Mulvey and D. S. Wright, *Science*, **2009**, 326, 706–708.

[77] A. J. Martínez-Martínez, A. R. Kennedy, R. E. Mulvey and C. T. O'Hara, *Science*, **2014**, 346, 834–837.

[78] M. Uzelac, A. R. Kennedy and E. Hevia, *Inorg. Chem.*, **2017**, 56, 8615–8626.

[79] V. G. Wittig, F. J. Meyer and G. Lange, *Ann.*, **1951**, 571, 167.

[80] G. Wittig, *Q. Rev. Chem. Soc.*, **1966**, 20, 191–210.

[81] F. Bickelhaupt, *Chem. Soc. Rev.*, **1999**, 28, 17–23.

[82] S. Y. Lau, G. Hughes, P. D. O'Shea and I. W. Davies, *Org. Lett.*, **2007**, 9, 2239–2242.

[83] S. E. Baillie, W. Clegg, P. García-Álvarez, E. Hevia, A. R. Kennedy, J. Klett and L. Russo, *Organometallics*, **2012**, 31, 5131–5142.

[84] S. Zaragoza-Calero, J. Francos, A. R. Kennedy and C. T. O'Hara, *Dalt. Trans.*, **2015**, 44, 7258–7267.

[85] P. C. Andrews, A. R. Kennedy, R. E. Mulvey, C. L. Raston, B. A. Roberts and R. B. Rowlings, *Angew. Chem. Int. Ed.*, **2000**, 39, 1960–1962.

[86] E. Hevia, G. W. Honeyman, A. R. Kennedy, R. E. Mulvey and D. C. Sherrington, *Angew. Chem. Int. Ed.*, **2004**, 44, 68–72.

[87] P. García-Álvarez, A. R. Kennedy, C. T. O'Hara, K. Reilly and G. M. Robertson, *Dalt. Trans.*, **2011**, 40, 5332–5341.

[88] W. Clegg, B. Conway, P. García-Álvarez, A. R. Kennedy, R. E. Mulvey, L. Russo, J. Sassmannshausen and T. Tuttle, *Chem. - A Eur. J.*, **2009**, 15, 10702–10706.

[89] S. E. Baillie, T. D. Bluemke, W. Clegg, A. R. Kennedy, J. Klett, L. Russo, M. De Tullio and E. Hevia, *Chem. Commun.*, **2014**, 50, 12859–12862.

[90] E. O. Stejskal, *J. Chem. Phys.*, **1965**, 43, 3597–3603.

[91] E. O. Stejskal and J. E. Tanner, *J. Chem. Phys.*, **1965**, 42, 288–292.

[92] J. E. Tanner, *Rev. Sci. Instrum.*, **1965**, 36, 1086–1087.

[93] K. F. Morris and C. S. Johnson, *J. Am. Chem. Soc.*, **1992**, 114, 3139–3141.

[94] D. Li, I. Keresztes, R. Hopson and P. G. Williard, *Acc. Chem. Res.*, **2009**, 42, 270–280.

[95] M. Uzelac and R. E. Mulvey, *Chem. - A Eur. J.*, **2018**, 24, 7786–7793.

[96] D. V. Graham, E. Hevia, A. R. Kennedy, R. E. Mulvey, C. T. O'Hara and C. Talmard, *Chem. Commun.*, **2006**, 417–419.

[97] G. C. Forbes, A. R. Kennedy, R. E. Mulvey, P. J. A. Rodger and R. B. Rowlings, *J. Chem. Soc., Dalt. Trans.*, **2001**, 1477–1484.

[98] I. Fanjul, F. García, R. A. Kowenicki, M. E. Mosquera, M. McPartlin and D. S. Wright, *Inorganica Chim. Acta*, **2007**, 360, 1266–1273.

[99] F. J. Craig, A. R. Kennedy, R. E. Mulvey and M. D. Spicer, *Chem. Commun.*, **1996**, 1951–1952.

[100] G. C. Forbes, A. R. Kennedy, R. E. Mulvey, B. A. Roberts and R. B. Rowlings, *Organometallics*, **2002**, 21, 5115–5121.

[101] H. T. Al-Masri, J. Sieler, P. Lönnecke, S. Blaurock, K. Domasevitch and E. Hey-Hawkins, *Tetrahedron*, **2004**, 60, 333–339.

[102] D. R. Armstrong, L. Balloch, E. Hevia, A. R. Kennedy, R. E. Mulvey, C. T. O'Hara and S. D. Robertson, *Beilstein J. Org. Chem.*, **2011**, 7, 1234–1248.

[103] D. R. Armstrong, W. Clegg, S. H. Dale, E. Hevia, L. M. Hogg, G. W. Honeyman and R. E. Mulvey, *Angew. Chem. Int. Ed.*, **2006**, 45, 3775–3778.

[104] C. Monnereau, E. Blart and F. Odobel, *Tetrahedron Lett.*, **2005**, 46, 5421–5423.

[105] D. R. Armstrong, A. R. Kennedy, R. E. Mulvey and S. D. Robertson, *Chem. Eur. J.*, **2011**, 17, 8820–8831.

[106] J. M. Bayne and D. W. Stephan, *Chem. Soc. Rev.*, **2016**, 45, 765–774.

[107] K. Izod, *Adv. Inorg. Chem.*, **2000**, 50, 33–107.

[108] M. Lappert, A. Protchenko, P. Power and A. Seeber, *Metal Amide Chemistry*, John Wiley & Sons, Ltd, Chichester, UK, 2008, 1–355.

[109] W. S. Huang, S. Liu, D. Zou, M. Thomas, Y. Wang, T. Zhou, J. Romero, A. Kohlmann, F. Li, J. Qi, L. Cai, T. A. Dwight, Y. Xu, R. Xu, R. Dodd, A. Toms, L. Parillon, X. Lu, R. Anjum, S. Zhang, F. Wang, J. Keats, S. D. Wardwell, Y. Ning, Q. Xu, L. E. Moran, Q. K. Mohemmad, H. G. Jang, T. Clackson, N. I. Narasimhan, V. M. Rivera, X. Zhu, D. Dalgarno and W. C. Shakespeare, *J. Med. Chem.*, **2016**, 59, 4948–4964.

[110] D. J. Peterson, *J. Organomet. Chem.*, **1967**, 8, 199–208.

[111] L. T. Byrne, L. M. Engelhardt, G. E. Jacobsen, W. P. Leung, R. I. Papasergio, C. L. Raston, B. W. Skelton, P. Twiss and A. H. White, *J. Chem. Soc. Dalt. Trans.*, **1989**, 105–113.

[112] S. A. Orr, A. R. Kennedy, J. J. Liggat, R. McLellan, R. E. Mulvey and S. D. Robertson, *Dalt. Trans.*, **2016**, 45, 6234–6240.

[113] K. Izod, J. C. Stewart, W. Clegg and R. W. Harrington, *Dalt. Trans.*, **2007**, 257–264.

[114] A. Downard and T. Chivers, *Eur. J. Inorg. Chem.*, **2001**, 2001, 2193–2201.

[115] H. C. Aspinall and M. R. Tillotson, *Inorg. Chem.*, **1996**, 35, 5–8.

[116] E. I. Izgorodina, C. Yeh Lin and M. L. Coote, *Phys. Chem. Chem. Phys.*, **2007**, 9, 2507–2516.

[117] Y. Zhao and D. G. Truhlar, *Theor. Chem. Acc.*, **2008**, 120, 215–241.

[118] T. H. Dunning, *J. Chem. Phys.*, **1989**, 90, 1007–1023.

[119] A. V. Marenich, C. J. Cramer and D. G. Truhlar, *J. Phys. Chem. B*, **2009**, 113, 6378–6396.

[120] C. Hettstedt, M. Unglert, R. J. Mayer, A. Frank and K. Karaghiosoff, *Eur. J. Inorg. Chem.*, **2016**, 2016, 1405–1414.

[121] M. Inman and C. J. Moody, *Chem. Sci.*, **2013**, 4, 29–41.

[122] F. R. de Sá Alves, E. J. Barreiro and C. A. M. Fraga, *Mini Rev. Med. Chem.*, **2009**, 9, 782–793.

[123] T. C. Barden, *Top. Heterocycl. Chem.*, **2011**, 26, 31–46.

[124] D. A. Shirley and P. A. Roussel, *J. Am. Chem. Soc.*, **1953**, 75, 375–378.

[125] S. S. Labadie and E. Teng, *J. Org. Chem.*, **1994**, 59, 4250–4254.

[126] M. Matsuzono, T. Fukuda and M. Iwao, *Tetrahedron Lett.*, **2001**, 42, 7621–7623.

[127] T. Grimaldi, M. Romero and M. D. Pujol, *Synlett*, **2000**, 2000, 1788–1792.

[128] J. Kalepu, P. Gandeepan, L. Ackermann and L. T. Pilarski, *Chem. Sci.*, **2018**, 9, 4203–4216.

[129] M. Iwao and F. Ishibashi, *Tetrahedron*, **1997**, 53, 51–58.

[130] T. Fukuda, R. Maeda and M. Iwao, *Tetrahedron*, **1999**, 55, 9151–9162.

[131] C. G. Hartung, A. Fecher, B. Chapell and V. Snieckus, *Org. Lett.*, **2003**, 5, 1899–1902.

[132] Y. Kondo, A. Yoshida and T. Sakamoto, *J. Chem. Soc. - Perkin Trans. 1*, **1996**, 34, 2331–2332.

[133] B. Conway, E. Hevia, A. R. Kennedy and R. E. Mulvey, *Chem. Commun.*, **2007**, 25, 2864.

[134] J. M. L'Helgoual'ch, A. Seggio, F. Chevallier, M. Yonehara, E. Jeanneau, M. Uchiyama and F. Mongin, *J. Org. Chem.*, **2008**, 73, 177–183.

[135] M. Y. A. Messaoud, G. Bentabed-Ababsa, M. Hedidi, A. Derdour, F. Chevallier, Y. S. Halauko, O. A. Ivashkevich, V. E. Matulis, L. Picot, V. Thiéry, T. Roisnel, V. Dorcet and F. Mongin, *Beilstein J. Org. Chem.*, **2015**, 11, 1475–1485.

[136] P. Kannaboina, K. Mondal, J. K. Laha and P. Das, *Chem. Commun.*, **2020**, 56, 11749–11762.

[137] F. Mathey, *Angew. Chem. Int. Ed.*, **2003**, 42, 1578–1604.

[138] M. Hissler, P. W. Dyer and R. Réau, *Coord. Chem. Rev.*, **2003**, 244, 1–44.

[139] T. Baumgartner and R. Réau, *Chem. Rev.*, **2006**, 106, 4681–4727.

[140] Y. Matano and H. Imahori, *Org. Biomol. Chem.*, **2009**, 7, 1258–1271.

[141] B. Wu, R. Chopra and N. Yoshikai, *Org. Lett.*, **2015**, 17, 5666–5669.

[142] M. Widhalm, L. Brecker and K. Mereiter, *Tetrahedron Asymmetry*, **2006**, 17, 1355–1369.

[143] A. Wakatsuki, M. Yukimoto, M. Minoura, K. Fujii, Y. Kimura and Y. Matano, *Dalt. Trans.*, **2018**, 47, 7123–7127.

[144] J. Kurita, M. Ishii, S. Yasuike and T. Tsuchiya, *Chem. Pharm. Bull.*, **1994**, 42, 1437–1441.

[145] A. Decken, F. Bottomley, B. E. Wilkins and E. D. Gill, *Organometallics*, **2004**, 23, 3683–3693.

[146] T. Kurita, Jyoji, Ishii Makoto, Yasuike, Shuji, Tsuchiya, *Chem. Commun.*, **1993**, 1993, 1309–1310.

[147] T. M. McPhillips, S. E. McPhillips, H.-J. Chiu, A. E. Cohen, A. M. Deacon, P. J. Ellis, E. Garman, A. Gonzalez, N. K. Sauter, R. P. Phizackerley, S. M. Soltis and P. Kuhn, *J. Synchrotron Radiat.*, **2002**, 9, 401–406.

[148] W. Kabsch, *J. Appl. Crystallogr.*, **1993**, 26, 795–800.

[149] G. M. Sheldrick, *SADABS v2.30, Unversity of Gottingen*, **2002**.

[150] G. M. Sheldrick, *Acta Crystallogr C*, **2015**, 71, 3–8.

[151] L. J. Barbour, *J. Supramol. Chem.*, **2001**, 1, 189–191.

[152] O. V. Dolomanov, L. J. Bourhis, R. J. Gildea, J. A. K. Howard and H. Puschmann, *J. Appl. Crystallogr.*, **2009**, 42, 339–341.

[153] S. Stoll and A. Schweiger, *J. Magn. Reson.*, **2006**, 178, 42–55.

[154] L. Lochmann, J. Pospíšil and D. Lím, *Tetrahedron Lett.*, **1966**, 7, 257–262.

[155] H. D. Flack, *Acta Crystallogr. Sect. A*, **1983**, 39, 876–881.

[156] C. Frajerman, B. Meunier and M. E. Strem, in *Preparation of Dimethylphenylphosphine*, John Wiley & Sons, Inc., 2006, vol. 22, 133–135.

[157] M. Kuroboshi, T. Kita, A. Aono, T. Katagiri, S. Kikuchi, S. Yamane, H. Kawakubo and H. Tanaka, *Tetrahedron Lett.*, **2015**, 56, 918–920.

[158] J. M. Tukacs, D. Király, A. Strádi, G. Novodarszki, Z. Eke, G. Dibó, T. Kégl and L. T. Mika, *Green Chem.*, **2012**, 14, 2057–2065.

[159] D. Dailler, R. Rocaboy and O. Baudoin, *Angew. Chem. Int. Ed.*, **2017**, 56, 7218–7222.

[160] Y. Wu, X. Peng, B. Luo, F. Wu, B. Liu, F. Song, P. Huang and S. Wen, *Org. Biomol. Chem.*, **2014**, 12, 9777–9780.

[161] P. Y. Choy, C. P. Lau and F. Y. Kwong, *J. Org. Chem.*, **2011**, 76, 80–84.

[162] P. Xu, E. U. Würthwein, C. G. Daniliuc and A. Studer, *Angew. Chem. Int. Ed.*, **2017**, 56, 13872–13875.

[163] X. Li, X. Gu, Y. Li and P. Li, *ACS Catal.*, **2014**, 4, 1897–1900.

[164] X. Hong, Q. Tan, B. Liu and B. Xu, *Angew. Chem. Int. Ed.*, **2017**, 56, 3961–3965.

[165] I. Kazi, S. Guha and G. Sekar, *J. Org. Chem.*, **2019**, 84, 6642–6654.

[166] C. Pan, G. Huang, Y. Shan, Y. Li and J. T. Yu, *Org. Biomol. Chem.*, **2020**, 18, 3038–3042.

[167] I. Medina-Mercado, E. O. Asomoza-Solís, E. Martínez-González, V. M. Ugalde-Saldívar, L. G. Ledesma-Olvera, J. E. Barquera-Lozada, V. Gómez-Vidales, J. Barroso-Flores, B. A. Frontana-Uribe and S. Porcel, *Chem. - A Eur. J.*, **2020**, 26, 634–642.

[168] C. Shao, G. Shi, Y. Zhang, S. Pan and X. Guan, *Org. Lett.*, **2015**, 17, 2652–2655.

[169] T. R. Pradhan, H. W. Kim and J. K. Park, *Org. Lett.*, **2018**, 20, 5286–5290.

[170] A. Das, K. Watanabe, H. Morimoto and T. Ohshima, *Org. Lett.*, **2017**, 19, 5794–5797.

[171] H. Miyamoto, T. Hirano, Y. Okawa, A. Nakazaki and S. Kobayashi, *Tetrahedron*, **2013**, 69, 9481–9493.

[172] L. Zhang, P. Li, C. Liu, J. Yang, M. Wang and L. Wang, *Catal. Sci. Technol.*, **2014**, 4, 1979–1988.

[173] A. K. Bachon and T. Opatz, *J. Org. Chem.*, **2016**, 81, 1858–1869.

[174] S. Ogawa, Y. Tajiri and N. Furukawa, *Bull. Chem. Soc. Jpn.*, **1991**, 64, 3182–3184.

ChemPubSoc Europe

DOI: 10.1002/ejic.201701317

EurJIC European Journal of Inorganic Chemistry

Full Paper

Magnesiation of Indoles | *Very Important Paper* |

Atom Efficient Magnesiation of *N*-Substituted Alkyl Indoles with a Mixed Sodium-Magnesium Base

Michael A. Stevens[a] and Victoria L. Blair*[a]

Abstract: This study presents the alkali metal mediated magnesiation (AMM*Mg*) of three *N*-alkylated indoles with the mixed Na/Mg base [(TMEDA)Na(TMP)$_2$Mg(CH$_2$SiMe$_3$)] **1** (TMEDA = *N*,*N*,*N*′,*N*′-tetramethylethylenediamine, TMP = 2,2,6,6-tetramethylpiperidine). All three magnesiated indoles have been successfully characterised by single-crystal X-ray diffraction and solution state NMR studies, whereas iodolysis and Pd-catalysed cross coupling have been investigated. The steric nature of the *N*-alkyl group changes the reactivity and efficiency of **1** to give either atom efficient disodium tetraindol-2-ylmagnesiates [(Na-TMEDA)$_2$Mg(α-C$_9$H$_8$N)$_4$] **2** and [(Na-TMEDA)$_2$Mg(α-C$_{10}$H$_{11}$N)$_4$] **3**, or [(TMEDA)Na(TMP)(α-C$_{11}$H$_{12}$N)Mg(TMP)] **4**, whereby only one indole molecule is selectively deprotonated.

Introduction

Indoles and their derivatives play a prominent role in a large number of biologically active compounds, as well as in many diverse products across the entire chemical industry.[1] It is considered a "privileged structural scaffold"[2] present in many important natural products (such as serotonin, tryptamine, tryptophan),[1] pharmaceuticals (such as Sumatriptan and Rizatriptan),[3] agrochemicals (such as auxins and Amisulbrom)[4] and pigments and dyes (indigoid and cyanine).[4] With the majority (88 %)[5] of active pharmaceutical drugs on the market containing aromatic heterocyclic components dominated by N-heterocyclic compounds, the synthesis and functionalisation of indoles and their derivatives is of significant interest to both synthetic and medicinal chemists.[6]

Metalation reactions have proven indispensable in the conversion of simple indole containing synthons into complex functionalised indole-based products.[7] This has predominately been achieved through the use of alkyllithium reagents through direct metalation or metathesis and/or lithium secondary-amides. However, these methods commonly require low temperatures, long reaction times and reagent excess to be employed to ensure selectivity.

In the last fifteen years, numerous research groups have developed mixed metal reagents as new tools to deprotometallate sensitive aromatic compounds.[8] In the context of indoles, Uchiyama et al. have studied both the direct *ortho*-cupration and -alumination of *N*-boc-indoles using the lithium cuprate [MeCu(TMP)(CN)Li$_2$][9] and lithium aluminate [*i*Bu$_3$Al(TMP)Li] reagents achieving C2-selective outcomes.[10] However, both mixed metal reagents required sub-ambient temperatures (–40 °C or –78 °C) and/or an excess of metalating reagent.

Recent studies by Mongin et al. focused on the room temperature metalation of a diverse range of functionalised indole and pyrrole species using a mixture of ZnCl$_2$·TMEDA/LiTMP in various ratios,[11,12] which report, after subsequent iodolysis, predominately 2-iodo derivatives in excellent yields.

Mulvey and Hevia et al. also reported the direct magnesiation and zincation of *N*-methylindole using the sodium magnesiate and zincate reagents [(TMEDA)$_2$Na$_2$MgBu$_4$] and [(TMEDA)Na(*t*Bu)(TMP)Zn(*t*Bu)] at room temperature[13] revealing the first structurally characterised C-magnesiated [(Na-TMEDA)$_2$Mg(α-C$_9$H$_8$N)$_4$] and C-zincated [(TMEDA)Zn(α-C$_9$H$_8$N)$_2$] examples of N-heterocyclic compounds.

In this study, we report the room temperature magnesiation of a range of *N*-alkyl functionalised indoles (*N*-alkyl = Me, Et and *i*Pr) with the sodium magnesium base [(TMEDA)Na(TMP)(CH$_2$SiMe$_3$)Mg(TMP)][14] **1**. Rapid reaction times (under 20 min) and atom-efficient metalation are defined by the steric bulk of the *N*-alkyl substituent with X-ray crystallography and solution NMR studies revealing different complex architectures.

Results and Discussion

Reaction of **1** with either *N*-methyl or *N*-ethyl-indole resulted in the deposition of a yellow precipitate, which when re-crystallised from *n*-hexane or toluene respectively afforded X-ray quality single crystals, identified as the disodium tetraindol-2-ylmagnesiates [(Na-TMEDA)$_2$Mg(α-C$_9$H$_8$N)$_4$][13] **2** and [(Na-TMEDA)$_2$Mg(α-C$_{10}$H$_{11}$N)$_4$] **3** (Figure 1).

Using a different metalation route, complex **2** has been previously reported in the literature[13] and will not be discussed in detail (see Supporting Information). Essentially isostructural to **2**, complex **3** contains a central distorted tetrahedral (mean 109.34°) magnesium atom [Mg(1)] bonded to four separate α-

[a] *School of Chemistry, Monash University, Clayton, Melbourne, VIC 3800 Australia*
E-mail: Victoria.Blair@monash.edu

Supporting information for this article is available on the WWW under https://doi.org/10.1002/ejic.201701317.

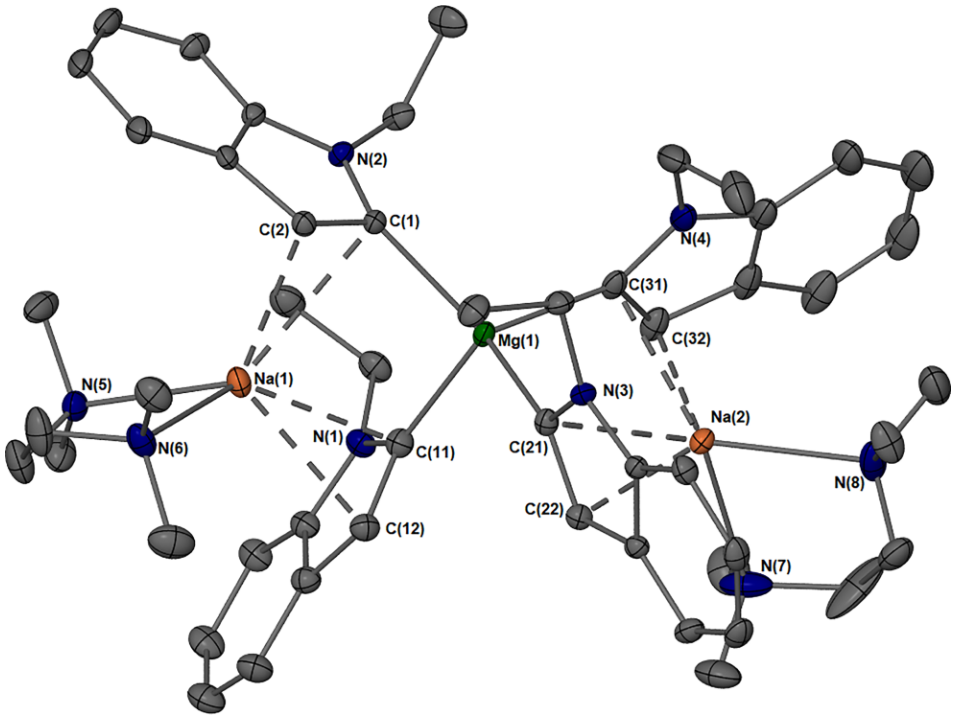

Figure 1. Molecular structure of $[(Na\text{-}TMEDA)_2Mg(\alpha\text{-}C_{10}H_{10}N)_4]$ (**3**) with thermal ellipsoids at 40 % probability. Hydrogen atoms and one disordered TMEDA molecule have been omitted for clarity. Selected bond lengths [Å]: Mg(1)–C(1), 2.2086(16); Mg(1)–C(11), 2.2120(18); Mg(1)–C(21), 2.2331(16); Mg(1)–C(31), 2.2377(17); Na(1)–C(1), 2.9184(17); Na(1)–C(2), 2.6993(17), Na(1)–C(11), 2.6905(18); Na(1)–C(12), 2.7420(18); Na(2)–C(21), 2.8580(17); Na(2)–C(22), 2.6159(17); Na(2)–C(31), 2.6492(18); Na(2)–C(32), 2.7225(18); C(1)–Mg(1)–C(11), 102.76(6); C(1)–Mg(1)–C(21), 119.67(6); C(1)–Mg(1)–C(31), 116.16(6); C(11)–Mg(1)–C(21), 102.00(6); C(11)–Mg(1)–C(31), 112.06(7); C(21)–Mg(1)–C(31), 103.46(6).

metalated indole substituents [C(1), C(11), C(21) and C(31)] with an average Mg–C bond length of 2.222 Å (mean 2.216 Å in **2**[13]). Each sodium atom in **3** makes electrostatic η^2-interactions with the 2-C and 3-C atoms of each deprotonated indole unit [range of lengths Na–C: 2.6159(17)–2.9184(17) Å]. Its coordination sphere is completed by a complexed bidentate molecule of TMEDA making the Na atoms overall six coordinate.

The rational synthesis of both **2** and **3** was achieved by reacting NaTMP, $Mg(CH_2SiMe_3)_2$, and TMEDA in a 2:1:2 ratio with four equivalents of the respective indole (Scheme 1). In both cases the desired product was isolated in a high crystalline yield (unoptimised 81 % and 72 % respectively). The original synthesis is likely to occur by a disproportionation reaction similar to that which has been previously reported for **1** with thiophene[15] and the mixed zincate bases $[(TMEDA)Na(tBu)_2Zn(TMP)]$ and $[Li(nBu)_2Zn(TMP)(TMEDA)]$ and their reactivity towards indoles and ferrocene respectively.[13,16]

Reaction of **1** with the more sterically encumbered *N*-isopropylindole substrate at room temperature resulted in the deposition of a yellow precipitate, which when recrystallised from *n*-hexane afforded X-ray quality single crystals. These were identified as $[(TMEDA)Na(TMP)(\alpha\text{-}C_{11}H_{12}N)Mg(TMP)]$ **4** (Scheme 1 and Figure 2). Complex **4** adopts a familiar structural motif,[17–20] whereby **1** has exhibited overall alkyl basicity, losing the CH_2SiMe_3 group and replacing it with an α-deprotonated *N*-isopropylindole unit. The molecular structure of **4** contains a central trigonal planar magnesium atom, bonding to a bridging and terminal TMP molecule and an α-deprotonated *N*-isopropylindole [C(1)–Mg(1), 2.192(4) Å]. Similar to **3**, the sodium atom is interacting electrostatically with both the C(1) and C(2) atoms of the *N*-isopropylindole in a η^2-manner, as indicated by the Na–C bond lengths of 2.857(4) and 2.646(4) Å respectively.

When comparing complexes **2** and **3** to **4**, although the overall regioselectivity of **1** does not change, different complex architectures are uncovered. The α-magnesiation of both *N*-methyl and *N*-ethyl indole results in **1** or "$[(TMEDA)_2Na(TMP)_2Mg(CH_2SiMe_3)_2]$" replacing all the available (potentially) basic arms with α-magnesiated indole units, whereas in **4**, only one basic (CH_2SiMe_3) arm is lost. This makes **2** and **3** the products of a more atom efficient process. Complexes **2** and **3** are obtained swiftly under ambient conditions (quantitative at room temperature, 15 min), with no cooling or reflux conditions (cf. lithiation of *N*-methylindole[21]) required to retain selectivity, whereas **4** needs longer reaction times to achieve quantitation (16 h). Attempts to force **4** to be more atom-efficient and react faster unfortunately failed, even when an excess of *N*-isopropylindole was employed under both room temperature and reflux conditions. It would therefore appear that the added steric bulk of the *N*-isopropyl group in **4** inhibits the formation of a structural motif similar to **2** or **3**. Examining the space filling diagram of **3** (Figure 3) demonstrates the steric congestion already present around the metal centres when an ethyl group is present, most likely hindering the isolation of an isopropyl analogue. To the best of our knowledge, structurally characterised

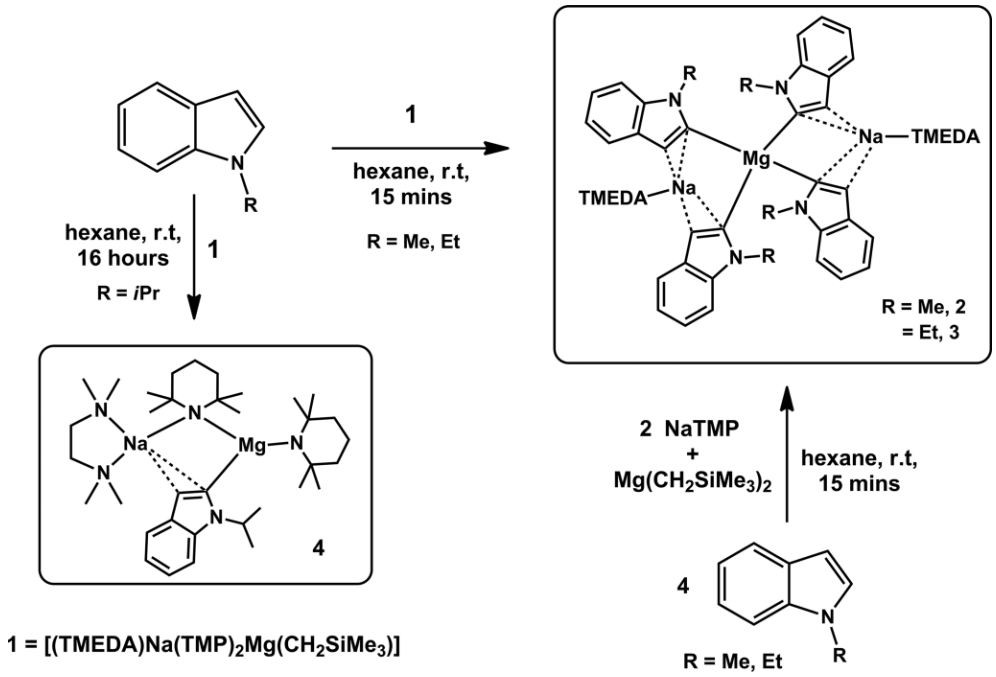

Scheme 1. Reaction of **1** with methyl, ethyl and isopropyl *N*-alkyl indoles.

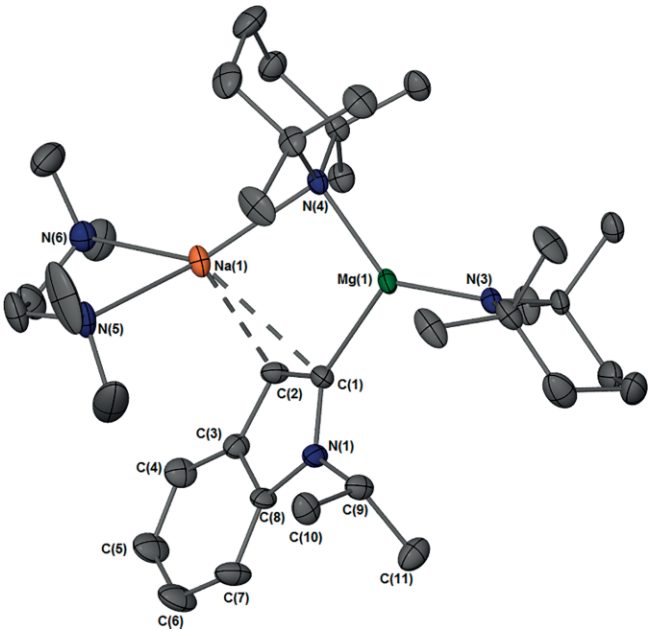

Figure 2. Molecular structure of [(TMEDA)Na(TMP)(α-$C_{11}H_{12}N$)Mg(TMP)] (**4**) with thermal ellipsoids at 40 % probability. Hydrogen atoms are omitted for clarity. Selected bond lengths [Å] and angles [°]: Mg(1)–C(1), 2.192(4); Mg(1)–N(4), 2.070(3); Mg(1)–N(3), 2.009(3); Na(1)–N(4), 2.464(3); Na(1)–N(5), 2.499(4); Na(1)–N(6), 2.457(4); Na(1)–C(1), 2.857(4); Na(1)–C(2), 2.646(4); C(1)–Mg(1)–N(3), 121.72(15); N(3)–Mg(1)–N(4), 133.32(14); N(4)–Mg(1)C(1), 104.94(15).

Mg–C or Mg–N bonded indole complexes are rare with only one previously reported Mg–C indole complex [(Na-TMEDA)$_2$Mg(α-C_9H_8N)$_4$][13] and two Mg–N bonded bis-indolyl complexes [($C_{14}H_{12}SN$)$_2$Mg(THF)$_2$] and [($C_{14}H_{12}ON$)$_2$Mg(THF)$_2$] reported in the literature.[22]

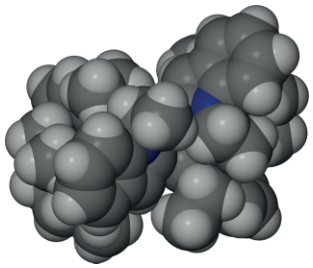

Figure 3. Space-filling diagram of compound **3**.

Crystalline **2**–**4** were dissolved in C_6D_6 and analysed by ^{1}H and ^{13}C NMR spectroscopy. The spectra indicate an α-substituted *N*-alkyl indole in a 2:1 ratio with TMEDA for **2** and **3** and a 1:1 ratio for **4**, with all three complexes preserving their solid state composition in solution. The disappearance of the two doublet signals (6.51 and 6.55 ppm for **2**; 6.54 and 6.68 ppm for **3**; 6.57 and 6.88 ppm for **4**) in the aromatic region corresponding to the parent indole, and the appearance of a singlet at δ = 6.53, 6.86 and 6.21 ppm respectively are indicative of an α-magnesiated species. Large down field chemical shifts for the 2-C ^{13}C resonance to 180.39, 181.49 and 178.79 ppm (parent indole: 129.05, 126.5 and 123.0 ppm) in **2**–**4** respectively are indicative of a magnesiation.

Utilising the Mg–C bond in complexes **2**–**4**, we examined their potential use in both in situ iodolysis and Pd-catalysed cross-coupling reactions[23] with iodobenzene. In a "one pot" procedure, all three complexes successfully gave their expected 2-iodo-1-alkylindole or 2-phenyl-1-alkylindole products in unoptimised high to moderate yields (I_2 79–66 %; cross-coupling 82–68 %, Scheme 2).

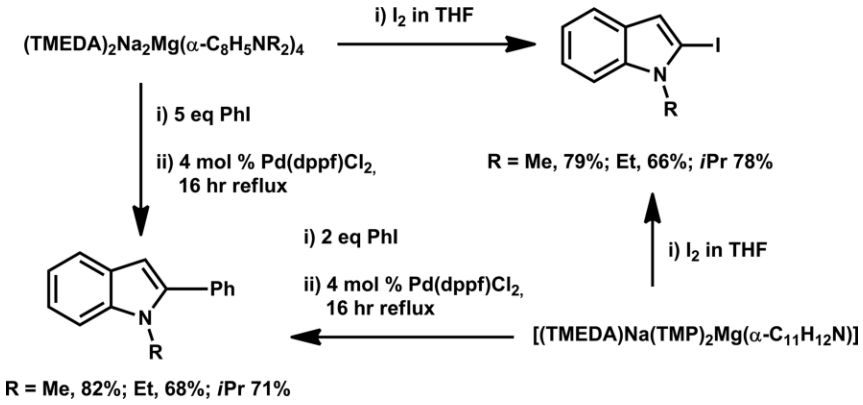

Scheme 2. In situ iodolysis and cross coupling reactions of **2**–**4**.

Conclusion

We have demonstrated that AMM*Mg* with **1** can successfully α-magnesiate three N-alkylated indoles selectively and under mild reaction conditions. We have revealed, through X-ray crystallographic and solution characterisation, that the efficiency of **1** is influenced by the steric nature of the *N*-alkyl group, leading to a less atom efficient magnesiation as steric bulk is increased. Utilising these selective indol-2-magnsiates in both in situ iodolysis and Pd-catalysed cross-coupling reactions leads to the isolation of the corresponding 2-iodo-1-alkylindole or 2-phenyl-1-alkylindole products in high to moderate yields.

Experimental Section

General Experimental Details: All reactions (unless otherwise stated) were completed under an atmosphere of dinitrogen and anhydrous conditions using standard Schlenk-line techniques. Water and oxygen were removed from *n*-hexane and diethyl ether using a MBRAUN SPS-800 solvent purification system and were stored over 4 Å molecular sieves under a dinitrogen atmosphere. TMEDA was dried by reflux over CaH_2 and stored over 4 Å molecular sieves. TMP(H) was purchased from Oakwood Chemicals and stored over 4 Å molecular sieves. ^{1}H and ^{13}C NMR spectra were recorded on Bruker DRX 400 MHz or 600 MHz Cryo spectrometers with chemical shifts internally referenced to C_6D_6 or $CDCl_3$. Microanalysis were carried out at the Science Centre, London Metropolitan University, with samples prepared in air-tight sealed glass ampules. *N*-methylindole was purchased from Aldrich and stored over 4 Å molecular sieves. *N*-ethylindole,[24] *N*-isopropylindole,[25] *n*BuNa,[26] and $Mg(CH_2SiMe_3)_2$[14] were prepared according to literature procedures.

GP1: *n*BuNa (0.08 g, 1 mmol) was suspended in 10 mL of dry *n*-hexane. To this suspension was added TMP(H) (0.34 mL, 2 mmol) dropwise, and the reaction was stirred at room temperature for at least 30 min. Next, $Mg(CH_2SiMe_3)_2$ (0.2 g, 1 mmol) was added with subsequent addition of TMEDA (0.15 mL, 1 mmol), affording a pale yellow, clear solution, which was used in situ. **GP2:** *n*BuNa (0.16 g, 2 mmol) was suspended in 10 mL of dry *n*-hexane. To this suspension was added TMP(H) (0.34 mL, 2 mmol) dropwise, and the reaction was stirred at room temperature for at least 30 min. Next $Mg(CH_2SiMe_3)_2$ (0.2 g, 1 mmol) was added with subsequent addition of TMEDA (0.3 mL, 2 mmol). The resulting pale yellow, cloudy solution was used in situ.

X-ray Data Collection, Reduction, Solution and Refinement

X-ray crystallographic data for **2** and **4** were obtained on a Bruker X8 Nonius Kappa CCD diffractometer with graphite-monochromated Mo-K_α (λ_0 = 0.71073 Å) radiation at 123 K. All single crystals were mounted on a glass fibre under oil. Data was collected and processed using the Bruker Apex2 v.2012.2.0 software; Lorentz, polarisation and absorption corrections (multi-scan – SADABS)[27] were applied. Crystallographic data of compound **3** was collected at the MX1 beamline at the Australian Synchrotron, Melbourne, Victoria, Australia (γ = 0.71070 A). All data was collected at 100 K, maintained using an open flow of nitrogen. The software used for data collection and reduction of the data were Blulce[28] and XDS.[29] Multi-scan absorption corrections (SADABS[27]) were applied. Compounds **2**, **3** and **4** were solved and refined with SHELX-2016[30] and X-seed interface[31] or Olex2.[32] Compound **2** was modelled as a two component twin (twin law −1 0 0 0 −1 0 0 0 1), BASF = 0.1492(19). Compound **3** had a disordered TMEDA molecule which was modelled as disordered across two sites.

CCDC 1578143 (for **2**), 1578142 (for **3**), and 1578141 (for **4**) contain the supplementary crystallographic data for this paper. These data can be obtained free of charge from The Cambridge Crystallographic Data Centre.

[(Na-TMEDA)$_2$Mg(α-C$_9$H$_8$N)$_4$] (2): *N*-Methylindole (0.13 mL, 1 mmol) was added to a stirred solution of **GP1**. A large quantity of white precipitate was observed after roughly 10–15 min, which was isolated by filtration and transferred to an argon glovebox for storage. X-ray quality crystals were obtained upon recrystallisation from *n*-hexane. Yield = 0.2 g, 24 % (max yield 25 % based on consumption of *N*-methylindole). Rational synthesis of **2** was achieved using **GP2**. *N*-methylindole (0.52 mL, 4 mmol) was added to a stirred solution of **GP2**. This resulted in the immediate formation of a clear solution. After approximately 10–20 min, a large quantity of a white precipitate was observed, which was identified by NMR as **2**. Isolated crystalline yield = 0.67 g, 81 % (quantitative by NMR). ^{1}H NMR (400 MHz, C_6D_6, 300 K): δ = 7.68–7.60 (m, 1 H, H3), 7.27 (m, 1 H, H6), 7.21–7.16 (m, 2 H, H4/H5), 6.94 (d, $^4J_{HH}$ = 0.9 Hz, 1 H, H2), 4.15 (s, 3 H, CH_3), 1.19 (s, 6 H, CH_3-TMEDA), 1.06 (s, 2 H, CH_2-TMEDA) ppm. ^{13}C NMR (101 MHz, C_6D_6, 300 K): δ = 180.39 (Mg-C2), 141.17, 131.79, 118.52 (C5/6), 117.97 (C4), 117.65 (C5/6), 109.71 (C3), 108.62 (C7), 55.84 (CH_2-TMEDA), 44.46 (CH_3-TMEDA), 36.57 (CH_3) ppm. $C_{48}H_{64}MgN_8Na_2$ (823.37): calcd. C 70.19, H 7.61, N 13.64; found C 69.73, H 7.65, N 13.41. Crystal data for compound **2** $C_{48}H_{64}MgN_8Na_2$: M = 823.38, colourless plates, 0.21 × 0.20 × 0.14 mm^3, monoclinic, space group $P2_1/c$, a = 17.6570(16), b = 16.8891(15), c = 15.9701(14),

α = 90°, β = 90.628(4)°, γ = 90°, V = 4762.2(7) Å ^{3}, Z = 4, D_c = 1.148 g/cm^3, F(000) = 1768, T = 123(2) K, 82061 reflections collected, 10691 unique (R_{int} = 0.1037), Final GooF = 1.022, $R1$ = 0.0794, $wR2$ = 0.2648, 545 parameters, 0 restraints. Lp and absorption corrections applied, μ = 0.096 mm^{-1}. Refined as a two-component twin (Twin law –1 0 0 0 –1 0 0 0 1), BASF = [0.1492(19)].

[(Na-TMEDA)$_2$Mg(α-C$_{10}$H$_{11}$N)$_4$] (3): *N*-Ethylindole (0.15 g, 1 mmol) was added dropwise to a stirred solution of **GP1**. After approximately five minutes, formation of a white precipitate was observed. The precipitate was isolated by filtration, washed with *n*-hexane and dried in vacuo, before storage in an argon glove box. X-ray quality crystals were obtained upon recrystallisation in toluene. Both the crystalline material and the powder were found to be the same product by NMR analysis. Yield = 0.2 g, 24 % (maximum yield 25 % based on consumption of *N*-ethylindole). Rational synthesis of **3**: To a stirred suspension of **GP2** was added *N*-ethylindole (0.58 g, 4 mmol) dropwise, resulting in the immediate formation of a clear solution. After approximately 10–20 min, a large quantity of a white precipitate was observed, which was identified by NMR as the title species. Isolated crystalline yield: 0.586 g, 70 % (quantitative by NMR). ^{1}H NMR (400 MHz, C_6D_6, 300 K): δ = 7.63–7.56 (m, 1 H, H4), 7.29 (m, 1 H, H7), 7.17–7.08 (m, 2 H, H5/H6), 6.86 (s, 1 H, H3), 4.70 (q, $^3J_{HH}$ = 7.0 Hz, 2 H, CH_2), 1.44 (t, $^3J_{HH}$ = 7.1 Hz, 3 H, CH_3), 1.28 (s, 6 H, TMEDA-CH_3), 1.21 (s, 3 H, TMEDA-CH_2) ppm. ^{13}C NMR (101 MHz, C_6D_6, 300 K): δ = 181.49 (Mg-C2), 140.45, 132.73, 119.01 (C5/6), 118.58 (C5/6), 118.23 (C4), 109.88 (C7), 109.64 (C3), 56.79 (CH_2-TMEDA), 45.25 (CH_3-TMEDA), 45.14 (CH_2), 17.31 (CH_3) ppm. Crystal data for Compound **3** $C_{52}H_{72}MgN_8Na_2$: M = 1198.37, colourless plates, 0.04 × 0.03 × 0.02 mm^3, triclinic, space group *Pbca*, a = 16.682(3), b = 16.236(3), c = 38.216(8), α = 90°, β = 90°, γ = 90°, V = 10351(4) Å^3, Z = 8, D_c = 1.129 g/cm^3, F(000) = 3792.0, T = 100(2) K, 85955 reflections collected, 12826 unique (*R*int = 0.706), Final GooF = 1.056, $R1$ = 0.0706, $wR2$ = 0.1528, 612 parameters, 0 restraints. Lp and absorption corrections applied, μ = 0.090 mm^{-1}.

[(TMEDA)Na(TMP)(α-C$_{11}$H$_{12}$N)Mg(TMP)] (4): *N*-Isopropylindole (0.16 g, 1 mmol) was added dropwise to a stirred solution of **GP1**. After stirring overnight, a white precipitate was observed and collected via filtration, washed with *n*-hexane and dried in vacuo, before storage in a glovebox. X-ray quality single crystals were obtained upon recrystallisation from *n*-hexane. Both the crystalline material and the powder were found to be the same product by NMR analysis. Yield: 0.35 g, 58 %. ^{1}H NMR (400 MHz, C_6D_6, 300 K): δ = 7.49 (m, 2 H, H3/6), 7.1–7.2 (m, 2 H, H4/5), 6.21 (d, $^4J_{HH}$ = 0.8 Hz, 1 H, H_2), 5.16 (septet, $^3J_{HH}$ = 6.8 Hz, 1 H, CH), 1.69 (d, $^3J_{HH}$ = 6.8 Hz, 6 H, CH_3), 1.88 (m, 4 H, γ-CH_2 TMP), 1.59 [s (br), 24 H, CH_3 TMP], 1.46 [s (br), 12 H, CH_3, TMEDA], 1.44 [s (br), 4 H, CH_2, TMEDA], 1.39 [s (br), 6 H, β-CH_2 TMP] ppm. ^{13}C NMR (100 MHz, C_6D_6, 300 K): δ = 178.79 (Mg-C2), 138.0, 133.4, 118.4 (C4), 117.8 (C7), 117.7 (C5), 111.1 (C6), 106.4 (C3), 56.4 (CH_2 TMEDA), 54.1 (CH-isopropyl), 52.2 (TMP-quaternary), 45.2 (CH_3 TMEDA), 41.8 (β-CH_2 TMP), 35.7 (CH_3 TMP), 22.3 (CH_3 isopropyl), 20.0 (γ-CH_2 TMP) ppm. $C_{70}H_{122}Mg_2N_{10}Na$ (1175.40): calcd. C 69.80, H 10.71, N 11.63; found C 69.88, H 9.96, N 11.45. Crystal data for compound **4** $C_{70}H_{122}Mg_2N_{10}Na_2$: M = 1198.37, colourless plates, 0.18 × 0.16 × 0.10 mm^3, triclinic, space group $P\bar{1}$, a = 11.5469(4), b = 16.3939(6), c = 20.4362(8), α = 81.102(2)°, β = 85.116(2)°, γ = 72.647(2)°, V = 3644.9(2) Å^3, Z = 2, D_c = 1.092 g/cm^3, F(000) = 1316, T = 123(2) K, 49988 reflections collected, 14416 unique (*R*int = 0.1065), Final GooF = 1.038, $R1$ = 0.0794, $wR2$ = 0.2291, 783 parameters, 0 restraints. Lp and absorption corrections applied, μ = 0.090 mm^{-1}.

Iodolysis Protocol: To a stirred solution of **2**, **3** or **4**, was added a 1 M solution of iodine in THF (10 mL for **2** and **3**, 5 mL for **4**) dropwise at room temperature. The resulting solution was stirred overnight and quenched with saturated $Na_2S_2O_3$ sodium thiosulfate (20 mL). The solution was diluted with CH_2Cl_2, dried with $MgSO_4$ and the solvent removed in vacuo. *N*-methyl-2-iodoindole was isolated as a crystalline solid. *N*-ethyl-2-iodoindole and *N*-isopropyl-2-iodoindole were isolated as pale yellow oils following purification by flash chromatography (silica gel, *n*-hexane). ***N*-methyl-2-iodoindole**: 0.81 g, 79 %: ^{1}H NMR (400 MHz, $CDCl_3$, 300 K): δ = 7.57 (d, $^3J_{HH}$ = 7.9 Hz, 1 H, H3), 7.34 (d, $^3J_{HH}$ = 8.3 Hz, 1 H, H6), 7.19 (d, $^3J_{HH}$ = 7.4 Hz, 1 H, H5), 7.11 (t, $^3J_{HH}$ = 7.4 Hz, 1 H, H4), 6.84 (s, 1 H, H2), 3.79 (s, 3 H) ppm. ^{13}C NMR (101 MHz, $CDCl_3$, 300 K): δ = 138.19, 129.74, 121.96 (C4), 119.93 (C5), 119.62 (C6), 111.94 (C2), 109.82 (C7), 84.10 (C1), 34.19 (CH_3) ppm. ***N*-ethyl-2-iodoindole**: 0.72 g, 66 %: ^{1}H NMR (600 MHz, $CDCl_3$, 300 K): δ = 7.53 (dt, $^3J_{HH}$ = 7.9, $^4J_{HH}$ = 1.0 Hz, 1 H, H3), 7.33 (dd, $^3J_{HH}$ = 8.3, $^4J_{HH}$ = 0.9 Hz, 1 H, H6), 7.15 (ddd, $^3J_{HH}$ = 8.3, 7.1, $^4J_{HH}$ = 1.2 Hz, 1 H, H5), 7.06 (ddd, $^3J_{HH}$ = 7.9, 7.1, $^4J_{HH}$ = 1.0 Hz, 1 H, H4), 6.78 (d, $^4J_{HH}$ = 0.8 Hz, 1 H, H2), 4.23 (q, $^3J_{HH}$ = 7.2 Hz, 2 H, CH_2), 1.35 (t, $^3J_{HH}$ = 7.2 Hz, 3 H, CH_3) ppm. ^{13}C NMR (151 MHz, $CDCl_3$, 300 K): δ = 137.01, 130.08, 121.87 (C5), 119.89 (C4), 119.76 (C3), 112.11 (C2), 109.74 (C6), 82.58 (C1), 42.25 (CH_2), 15.35 (CH_3) ppm. HRMS (ESI) ([M + H]$^+$) calcd. for $C_{10}H_{10}IN$: 271.9936, found 271.9925. IR: $\tilde{\nu}$ = (ax =) 3052 (w), 2939 (w), 1602 (w), 1512 (m), 1463 (s), 1420 (m), 1385 (m), 1316 (s), 1241 (s), 1205 (m) 1130 (m), 1075 (s), 1008 (s), 919 (m), 837 (m), 733 (s), 698 (s) cm^{-1}. ***N*-isopropyl-2-iodoindole**: 0.22 g, 78 %: ^{1}H NMR (400 MHz, $CDCl_3$, 300 K): δ = 7.50–7.45 (m, 2 H, H4/7), 7.05–7.00 (m, 2 H, H5/6), 6.67 (d, $^3J_{HH}$ = 0.9 Hz, 1 H, H2),4.78 (septet, $^3J_{HH}$ = 7.1 Hz, 1 H, CH), 1.56 (d, $^3J_{HH}$ = 7.1 Hz, 9 H, CH_3) ppm. ^{13}C NMR (101 MHz, $CDCl_3$, 300 K): δ = 123.00 (C4/7), 120.91 (C5/6), 120.85 (C5/6), 119.68 (C4/7), 111.19 (C3), 57.96 (CH), 21.12 (CH_3) ppm. HRMS (ESI) ([M + H]$^+$) calcd. for $C_{11}H_{12}IN$: 286.0093, found 286.0082. IR: $\tilde{\nu}$ = (ax =) 2967 (m), 2931 (m), 2440 (w), 1701 (w), 1457 (s), 1438 (s), 1400 (s), 1383 (m), 1336 (m), 1303 (s), 1260 (m), 1220 (s), 1087 (s), 1011 (s), 906 (m), 800 (m), 738 (s) cm^{-1}.

Cross-Coupling Protocol: To a stirred solution of either **2**, **3** or **4**, was added iodobenzene (5 equiv. for **2** and **3**, 2 equiv. for **4**), followed by the addition of 4 mol-% of Pd(dbbf)Cl_2. The reaction was refluxed for 16 hours. After cooling to room temperature, the solution was quenched with saturated NH_4Cl, extracted with dichloromethane, dried with anhydrous $MgSO_4$ and the solvent was removed in vacuo. *N*-methyl-2-phenylindole and *N*-ethyl-2-phenylindole were isolated as crystalline solids, and *N*-isopropyl-2-phenylindole was isolated as a pale yellow oil following flash chromatography (silica gel, *n*-hexane). Compounds prepared were consistent with literature values. ***N*-methyl-2-phenylindole**:[13] 0.68 g, 82 %: ^{1}H NMR (600 MHz, $CDCl_3$, 300 K): δ = 7.65 (d, $^3J_{HH}$ = 7.7 Hz, 1 H, H4), 7.52 (dd, $^3J_{HH}$ = 8.3, $^4J_{HH}$ = 1.3 Hz, 2 H, *ortho*-H), 7.48 (t, $^3J_{HH}$ = 7.6 Hz, 2 H, *meta*-H), 7.41 (t, $^3J_{HH}$ = 7.3 Hz, 1 H, *para*-H), 7.38 (d, $^3J_{HH}$ = 8.2 Hz, 1 H, H7), 7.28–7.23 (m, 2 H, H6), 7.18–7.13 (m, 1 H, H5), 6.57 (s, 1 H, H3), 3.76 (s, 3 H, CH_3) ppm. ^{13}C NMR (151 MHz, $CDCl_3$, 300 K): δ = 141.79, 138.55, 133.07, 129.60 (*meta*-C), 128.70 (*ortho*-C), 128.17, 128.07 (*para*-C), 121.87 (C6), 120.68 (C5), 120.07 (C4), 109.81 (C7), 101.86 (C3), 31.40 (CH_3) ppm. ***N*-ethyl-2-phenylindole**:[33] 0.60 g, 68 %: ^{1}H NMR (400 MHz, $CDCl_3$, 300 K): δ = 7.63 (dt, $^3J_{HH}$ = 7.8, $^4J_{HH}$ = 1.0 Hz, 1 H, H4), 7.53–7.36 (m, 6 H, Ph + H7), 7.26–7.19 (m, 1 H, H6), 7.13 (ddd, $^3J_{HH}$ = 8.0, 7.0, $^4J_{HH}$ = 1.0 Hz, 1 H, H5), 6.52 (d, $^4J_{HH}$ = 0.9 Hz, 1 H, H3), 4.18 (t, $^3J_{HH}$ = 7.2 Hz, 2 H, CH_2), 1.32 (d, $^3J_{HH}$ = 7.2 Hz, 3 H, CH_3) ppm. ^{13}C NMR (101 MHz, $CDCl_3$, 300 K): δ = 141.30, 137.31, 133.44, 129.59 (*meta*-C), 128.69 (*ortho*-C), 128.53, 128.14 (*para*-C), 121.74 (C6), 120.80 (C4), 119.98 (C5), 110.08 (C7), 102.31 (C3), 38.96 (CH_2), 15.59 (CH_3) ppm. ***N*-isopropyl-2-phenylindole**:[34] 0.17 g, 71 %: 7.64–7.59 (m, 2 H, H4/7), 7.5–7.4 (m, 5 H, phenyl-H), 7.20–7.15 (m, 1 H, H5/6), 6.45 (d, 1 H, J = 0.8,

H3), 4.68 (septet, 1 H, J = 7.0, CH), 1.6 (d, 1 H, J = 7.0, CH_3). ^{13}C NMR (101 MHz, $CDCl_3$, 300 K): δ = 141.41, 135.44, 133.81, 131.98, 129.64 (*meta*-C), 128.42 (*ortho*-C), 127.93 (*para*-C), 121.01 (C5/6), 120.85 (C5/6), 119.44 (C4/7), 112.40 (C4/7), 102.21 (C3), 47.90 (CH), 21.57 (CH_3) ppm.

Acknowledgments

We thank the Australian Research Council (DE140101137) and Monash University for financial support. This research was supported by an Australian Government Research Training Program (RTP) Scholarship. The authors acknowledge that part of this research was undertaken on the MX1 beamline at the Australian Synchrotron, Victoria, Australia.

Keywords: Functionalised indoles · Metallation · Magnesiation · Cross-coupling · Iodolysis

[1] N. Kaushik, N. Kaushik, P. Attri, N. Kumar, C. Kim, A. Verma, E. Choi, *Molecules* **2013**, *18*, 6620–6662.
[2] F. R. de Sá Alves, E. J. Barreiro, C. A. M. Fraga, *Mini-Rev. Med. Chem.* **2009**, *9*, 782–793.
[3] M. Inman, C. J. Moody, *Chem. Sci.* **2013**, *4*, 29–41.
[4] T. C. Barden, *Top. Heterocycl. Chem.* **2011**, *26*, 31–46.
[5] R. P. Jumde, F. Lanza, M. J. Veenstra, S. R. Harutyunyan, *Science* **2016**, *352*, 433–437.
[6] G. R. Humphrey, J. T. Kuethe, *Chem. Rev.* **2006**, *106*, 2875–2911.
[7] E. T. Pelkey in *Heterocyclic Scaffolds II Reactions and Applications of Indoles* (Ed.: W. G. Gribble), Springer, Berlin, Heidelberg, **2010**, pp. 141–191.
[8] F. Mongin, A. Harrison-Marchand, *Chem. Rev.* **2013**, *113*, 7563–7727.
[9] S. Usui, Y. Hashimoto, J. V. Morey, A. E. H. Wheatley, M. Uchiyama, *J. Am. Chem. Soc.* **2007**, *129*, 15102–15103.
[10] H. Naka, M. Uchiyama, Y. Matsumoto, A. E. H. Wheatley, M. McPartlin, J. V. Morey, Y. Kondo, *J. Am. Chem. Soc.* **2007**, *129*, 1921–1930.
[11] A. Seggio, M. I. Lannou, F. Chevallier, D. Nobuto, M. Uchiyama, S. Golhen, T. Roisnel, F. Mongin, *Chem. Eur. J.* **2007**, *13*, 9982–9989.
[12] M. Y. A. Messaoud, G. Bentabed-Ababsa, M. Hedidi, A. Derdour, F. Chevallier, Y. S. Halauko, O. A. Ivashkevich, V. E. Matulis, L. Picot, V. Thiéry, T. Roisnel, V. Dorcet, F. Mongin, *Beilstein J. Org. Chem.* **2015**, *11*, 1475–1485.
[13] B. Conway, E. Hevia, A. R. Kennedy, R. E. Mulvey, *Chem. Commun.* **2007**, 2864.
[14] V. L. Blair, A. R. Kennedy, J. Klett, R. E. Mulvey, *Chem. Commun.* **2008**, 5426–5428.
[15] V. L. Blair, A. R. Kennedy, R. E. Mulvey, C. T. O'Hara, *Chem. Eur. J.* **2010**, *16*, 8600–8604.
[16] H. R. L. Barley, W. Clegg, S. H. Dale, E. Hevia, G. W. Honeyman, A. R. Kennedy, R. E. Mulvey, *Angew. Chem. Int. Ed.* **2005**, *44*, 6018–6021; *Angew. Chem.* **2005**, *117*, 6172.
[17] R. E. Mulvey, V. L. Blair, W. Clegg, A. R. Kennedy, J. Klett, L. Russo, *Nat. Chem.* **2010**, *2*, 588–591.
[18] V. L. Blair, W. Clegg, B. Conway, E. Hevia, A. Kennedy, J. Klett, R. E. Mulvey, L. Russo, *Chem. Eur. J.* **2008**, *14*, 65–72.
[19] D. R. Armstrong, W. Clegg, S. H. Dale, E. Hevia, L. M. Hogg, G. W. Honeyman, R. E. Mulvey, *Angew. Chem. Int. Ed.* **2006**, *45*, 3775–3778; *Angew. Chem.* **2006**, *118*, 3859.
[20] A. R. Kennedy, R. E. Mulvey, D. L. Ramsay, S. D. Robertson, *Dalton Trans.* **2015**, *44*, 5875–5887.
[21] D. A. Shirley, P. A. Roussel, *J. Am. Chem. Soc.* **1953**, *75*, 375–378.
[22] K.-F. Peng, Y. Chen, C.-T. Chen, *Dalton Trans.* **2015**, *44*, 9610–9619.
[23] S. Dumouchel, F. Mongin, F. Trécourt, G. Quéguiner, *Tetrahedron Lett.* **2003**, *44*, 3877–3880.
[24] Y. Wu, X. Peng, B. Luo, F. Wu, B. Liu, F. Song, P. Huang, S. Wen, *Org. Biomol. Chem.* **2014**, *12*, 9777–9780.
[25] X. Hong, Q. Tan, B. Liu, B. Xu, *Angew. Chem. Int. Ed.* **2017**, *56*, 3961–3965; *Angew. Chem.* **2017**, *129*, 4019.
[26] L. Lochmann, J. Pospíšil, D. Lím, *Tetrahedron Lett.* **1966**, *7*, 257–262.
[27] G. M. Sheldrick, *SADABS v2.30, University of Gottingen* **2002**.
[28] T. M. McPhillips, S. E. McPhillips, H.-J. Chiu, A. E. Cohen, A. M. Deacon, P. J. Ellis, E. Garman, A. Gonzalez, N. K. Sauter, R. P. Phizackerley, M. S. Soltis, P. Kuhn, *J. Synchrotron Radiat.* **2002**, *9*, 401–406.
[29] W. Kabsch, *J. Appl. Crystallogr.* **1993**, *26*, 795–800.
[30] G. M. Sheldrick, *Acta Crystallogr., Sect. C Struct. Chem.* **2015**, *71*, 3–8.
[31] L. J. Barbour, *J. Supramol. Chem.* **2001**, *1*, 189–191.
[32] O. V. Dolomanov, L. J. Bourhis, R. J. Gildea, J. A. K. Howard, H. Puschmann, *J. Appl. Crystallogr.* **2009**, *42*, 339–341.
[33] L. Zhang, P. H. Li, C. Liu, J. Yang, M. Wang, L. Wang, *Catal. Sci. Technol.* **2014**, *4*, 1979–1988.
[34] A. K. Bachon, T. Opatz, *J. Org. Chem.* **2016**, *81*, 1858–1869.

Received: November 9, 2017

ChemPubSoc Europe

DOI: 10.1002/chem.201803477

CHEMISTRY A European Journal Full Paper

Synthetic Methods

Contrasting Synergistic Heterobimetallic (Na–Mg) and Homometallic (Na or Mg) Bases in Metallation Reactions of Dialkylphenylphosphines and Dialkylanilines: Lateral versus Ring Selectivities

Michael A. Stevens,[a] Fairuz H. Hashim,[a] Eunice S. H. Gwee,[a] Ekaterina I. Izgorodina,[a] Robert E. Mulvey,[b] and Victoria L. Blair*[a]

Abstract: A series of dialkylphenylphosphines and their analogous aniline substrates have been metallated with the synergistic mixed-metal base [(TMEDA)Na(TMP)(CH_2SiMe_3)-Mg(TMP)] **1**. Different metallation regioselectivities for the substrates were observed, with predominately lateral or *meta*-magnesiated products isolated from solution. Three novel heterobimetallic complexes [(TMEDA)Na(TMP)-(CH_2PCH_3Ph)Mg(TMP)] **2**, [(TMEDA)Na(TMP)(*m*-$C_6H_4PiPr_2$)-Mg(TMP)] **3** and [(TMEDA)Na(TMP)(*m*-$C_6H_4NEt_2$)Mg(TMP)] **4** and two homometallic complexes [{(TMEDA)Na($EtNC_6H_5$)}$_2$] **5** and [(TMEDA)Na_2(TMP)(C_6H_5PEt)]$_2$ **6** derived from homometallic metallation have been crystallographically characterised. Complex **6** is an unprecedented sodium-amide, sodium-phosphide hybrid with a rare $(NaNNaP)_2$ ladder motif. These products reveal contrasting heterobimetallic deprotonation with homometallic induced ethene elimination reactivity. Solution studies of metallation mixtures and electrophilic iodine quenching reactions confirmed the metallation sites. In an attempt to rationalise the regioselectivity of the magnesiation reactions the C–H acidities of the six substrates were determined in THF solution using DFT calculations employing the M06-2X functional and cc-pVTZ Dunning's basis set.

Introduction

A fundamental challenge within synthetic chemistry is to control the chemo- and regioselectivity when functionalising organic molecules. Organometallic alkyl- and aryl-lithium compounds and the lithium secondary amides (the "utility amides"[1]) have a long-established role in the synthetic chemists repertoire.[1–3] Synthetic approaches including directed *ortho*-metallation (DoM) is without doubt the classical concept in organo-alkali chemistry, allowing the selective functionalisation of aromatic molecules. DoM is of particular importance in the synthesis of pharmaceutical products.[4] However, exceptions to *ortho*-metallation are relatively scarce.[2] The demand to develop new methods to selectively functionalise neighbouring *meta* and *para* positions led to several new classes of bimetallic reagents emerging in the past two decades. Most prominent are 'turbo-Grignard' reagents pioneered by Knochel. Typified by the mixed lithium halide-magnesium amide complex (TMPMgCl.LiCl),[5,6] these salt-modulated organometallic reagents can regiospecifically functionalize an impressive variety of aromatic and heteroaromatic compounds and offer good compatibility with sensitive functional groups. Recently, a new halogen–magnesium exchange reagent *s*BuMgOR·*x*LiOR ($x = 1$ or 2; R = 2-ethylhexyl) has been developed allowing fast Br/Mg or Cl/Mg exchange reactions producing heteroaryl magnesium alkoxides in non-polar solvents.[7] Mongin and co-workers have developed a range of bimetallic ate complexes for the metallation of many functionalised aromatics, combining lithium with a variety of secondary metals including zinc,[8–12] copper[13] or magnesium.[14,15] These metallating agents usually consist of a mixed alkyl or amido lithium species with either a divalent metal salt or a dialkyl/amido metallic species. Of particular relevance to this work are the bimetallic bases formed by the co-complexation of an alkali metal amide (most commonly NaTMP) and a dialkyl subordinate metal partner, typically zinc,[12,16–18] magnesium[14,15,19,20] aluminium[21,22] or manganese.[23–25] Early examples of the effectiveness of these bases include the magnesiation (C–H to C–Mg) of benzene[26] and the selective *meta*-magnesiation of toluene,[27] both achieved utilising the sodium magnesiate base [(TMEDA)Na(*n*Bu)-(TMP)Mg(TMP)].[26,27] There are precedents in the literature for these bimetallic systems metallating aniline based substrates. A notable example is with the sodium zincate, [(TMEDA)-

[a] M. A. Stevens, F. H. Hashim, E. S. H. Gwee, Dr. E. I. Izgorodina, Dr. V. L. Blair
School of Chemistry, Monash University
Melbourne, VIC, 3800 (Australia)
E-mail: Victoria.Blair@monash.edu

[b] Prof. Dr. R. E. Mulvey
WestCHEM
Department of Pure and Applied Chemistry
University of Strathclyde
295 Cathedral Street, Glasgow, G1 1XL (UK)

Supporting information and the ORCID identification number(s) for the author(s) of this article can be found under: https://doi.org/10.1002/chem.201803477.

Na(*t*Bu)(TMP)Zn(*t*Bu)], in which a novel *meta*-zincation of *N*,*N*-dimethylaniline[28] (Scheme 1) was achieved. However, subsequent in situ electrophilic quenching studies with iodine revealed a mixture of *ortho*-, *meta*- and *para*- iodoanilines.[29]

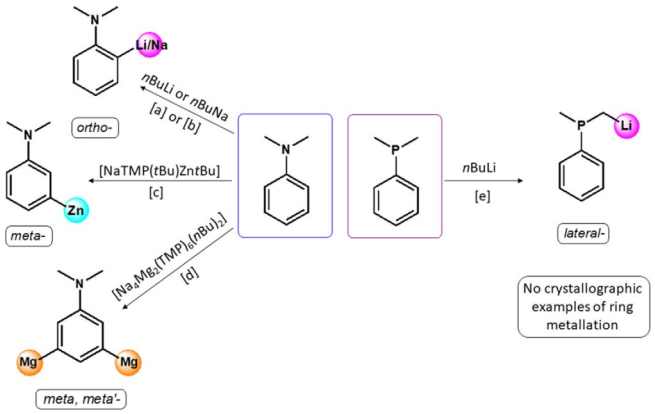

Scheme 1. Structurally characterised examples of the products of metallation of *N*,*N*-dimethylaniline and dimethylphenylphosphine. Note only metals shown for clarity. Reagents and conditions: [a] *n*BuLi, hexane, reflux, 16 h;[33] [b] *n*BuNa, hexane, 0 °C;[29] [c] [NaTMP(*t*Bu)Zn(*t*Bu)], hexane, reflux, 2 h,[28] [d] $[Na_4Mg_2(TMP)_6(nBu)_2]$, methylcyclohexane, reflux, 4 h,[31] [e] *n*BuLi.TMEDA, hexane.[34]

More recently a sophisticated template approach[30] has been reported employing the sodium magnesiate base $[Na_4Mg_2(TMP)_6(nBu)_2]$. This powerful method relies on the azametallo ring scaffold, which can override acidity criteria and direct remarkable selective and regiospecific polymetallations. For example *ortho–meta"* or *meta–meta"* di-metallations of substituted arenes and anilines (Scheme 1)[31] have been accomplished, whereas reactions with the polyaryl substrate *para*-terphenyl result in di- or even tetra-metallated substrates.[32]

Surprisingly, compared to the established mono- and bimetallic metallation chemistry of tertiary amines, analogous studies based on tertiary phosphines are relatively scarce. Given the synthetic utility of phosphorus-based ligands in catalyst design,[35] material chemistry and the stabilisation of main group and transition-metal complexes[36] investigation of their functionalisation and reactivity is of special importance. In context to synthetic medicinal chemistry, alkali metal amide complexes feature prominently,[37] while related phosphorus containing compounds have been generally overlooked. Recently, a phosphine-oxide-containing compound Brigatinib (AP26113), developed by Huang and co-workers, was approved by the FDA for the treatment of lung cancer,[38] making the metallation of phosphorus containing compounds of high interest, providing new prospects in medicinal chemistry.

This study reports, the selective magnesiation of a range of dialkyl substituted phenylphosphines and their aniline counterparts employing the sodium magnesiate base [(TMEDA)Na(TMP)(CH_2SiMe_3)Mg(TMP)] **1** (TMEDA = *N*,*N*,*N*′,*N*′-tetramethylethylenediamine, TMP = 2,2,6,6-tetramethylpiperdide). To the best of our knowledge, no phosphorus containing substrates have been investigated to date, whereas, **1** has previously been used in metallation of furan,[20] thiophene[39] and most recently N-substituted indoles.[40] This work discloses the subtle electronic and steric influences of N versus P substitution, showcasing in some instances unexpected metallation sites. To provide a rational for the different selectivities observed, pK_a calculations have been performed.

Results and Discussion

Synthesis

Starting with the simplest benchmark methyl substituted analogues, reaction of **1** with *N*,*N*-dimethylaniline in hexane at room temperature resulted in a viscous oil identified (via ^{1}H NMR spectroscopy) as predominately starting material (< 10% metallated species). When the reaction mixture was heated to reflux (2 hours), a mixture of *meta*- and *para*-magnesiated *N*,*N*-dimethylaniline was observed (overall conversion 29%; *meta*- 78%, *para*- 22%). Heating beyond 2 hours leads to decomposition of the base and an oil which was consistent with starting amine confirmed via NMR spectroscopy (see Supporting Information). In contrast, reaction of a hexane solution of **1** with *P*,*P*-dimethylphenylphosphine at room temperature resulted in the isolation of a white crystalline solid identified by X-ray crystallography as the laterally magnesiated phosphinomethanide complex [(TMEDA)Na(TMP)(CH_2PCH_3Ph)-Mg(TMP)] **2**, in a 58% crystalline yield. Moving on to the ethyl-analogues, *N*,*N*-diethylaniline could be successfully *meta*-magnesiated upon reaction with **1** in hexane solution to afford the crystalline compound [(TMEDA)Na(TMP)(*m*-$C_6H_4NEt_2$)-Mg(TMP)] **3** in a 65% crystalline yield. Contrastingly, when **1** was treated with a molar equivalent of *P*,*P*-diethylphenylphosphine, no reaction was observed, even under reflux conditions, resulting in quantitative recovery of the phosphine substrate. Lastly, reaction of **1** at room temperature with the more sterically encumbered *N*,*N*-diisopropylaniline at room temperature results in an oil identified as starting material. When the reaction mixture is heated to reflux, a mixture of *meta*- and *para*-magnesiated anilinophenyl species are obtained (overall conversion 25%; *meta*- 70%, *para*- 30%), as well as significant unreacted starting amine (see Supporting Information), whereas reaction of **1** with *P*,*P*-diisopropylphenylphosphine affords the crystalline *meta*-magnesiated phosphinophenyl complex [(TMEDA)Na(TMP)(*m*-$C_6H_4PiPr_2$)Mg(TMP)] **4** selectively in a 31% crystalline yield.

Solid-state structures

To the best of our knowledge complexes **2** and **4** represent the first structurally characterised magnesiated dialkylphenylphosphines,[41] while complex **3** is a rare structural example of a ring-magnesiated aniline[31] with the only other reported literature examples being of in situ magnesiations followed by electrophilic quenching studies.[5,6,42,43]

X-ray crystallographic analysis of compound **2** (Figure 1) reveals the first example of lateral magnesiation of *P*,*P*-dimethyl-

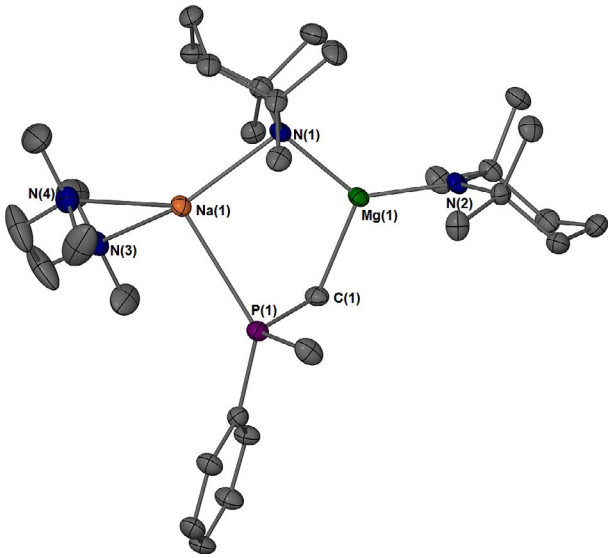

Figure 1. Molecular structure of [(TMEDA)Na(TMP)(CH_2PCH_3Ph)Mg(TMP)] **2** with thermal ellipsoids at 40% probability. Hydrogen atoms have been omitted for clarity. Selected bond lengths (Å) and angles (°): Mg(1)–N(1), 2.069(5); Mg(1)–N(2), 2.001(5); Mg(1)–C(1), 2.182(6); Na(1)–N(1), 2.463(5); Na(1)–N(3), 2.528(6); Na(1)–N(4), 2.495(5); Na(1)–P(1), 2.919(2); P(1)–C(1), 1.777(6); P(1)–C(2), 1.823(8); N(1)-Na(1)-P(1), 95.24(12); Na(1)-N(1)-Mg(1), 103.5(2); N(1)-Mg(1)-C(1), 108.8(2); Mg(1)-C(1)-P(1), 118.4(3); C(1)-P(1)-Na(1), 88.40(19).

phenylphosphine. The bimetallic monomer is composed of one sodium atom connected to magnesium via an amido TMP bridge, with the magnesium coordination completed by a further TMP (terminal) and a CH_2 unit of a metallated phosphine. The sodium atom occupies a distorted tetrahedral environment (bond angles range 73.88°–134.47°), comprising a TMP bridge, a bridging $[C_6H_5PCH_3CH_2]^-$ and a bidentate chelating TMEDA ligand. The sodium atom forms a strong bond with the phosphorus lone pair [Na(1)–P(1) 2.919(2) Å] to close a central 5-atom 5-element (NaNMgCP) ring. The coordination environment of the magnesium atom is essentially trigonal planar (Σ bond angles = 359.96°) in common with this structural motif, with a terminal and bridging TMP molecule and a methyl magnesiated *P,P*-dimethylphenylphosphine anionic unit, with a typical covalent Mg–C bond length of 2.182(6) Å. Overall, **1** has executed alkyl basicity, with the loss of $SiMe_4$. Previous studies on the lateral metallation of *P,P*-dimethylphenylphosphine with *n*BuLi in the presence of the activating bidentate ligand TMEDA have been reported[34,44] revealing the dimer [(TMEDA)-Li(CH_2PCH_3Ph)]$_2$. Contrasting the reactivity of the analogous dimethyl P/N substrates with **1**, a distinction in metallation site is observed, namely, lateral versus ring (Scheme 1). These differences can be rationalised at least in part by considering the electronic nature of the different directing groups. The poor directing ability of the dimethyl amino group,[45] attributed to lone pair delocalisation into the aromatic ring, makes the aryl H atoms weakly acidic, resulting in *ortho*-metallation. In contrast, the lone pairs on the dimethyl phosphorus system are not delocalised, resulting in increased acidity of the methyl substituents and hence directing metallation to the methyl group.

The molecular structures of **3** (Figure 2) and **4** (Figure 3) display a similar structural backbone {(TMEDA)Na(TMP)Mg(TMP)} to that of **2**, completed by a selectively *meta*-magnesiated dialkyl N or P substrate. In both **3** and **4** the magnesium atom lies coplanar to the aromatic ring, indicative of a strong Mg–C σ-

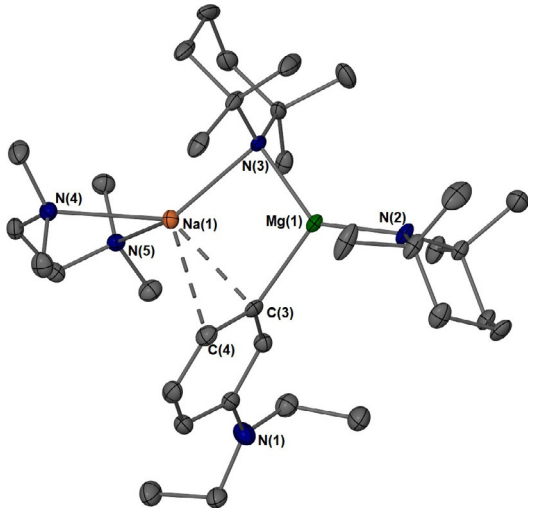

Figure 2. Molecular structure of [(TMEDA)Na(TMP)(*m*-$C_6H_4NEt_2$)Mg(TMP)] **3** with thermal ellipsoids at 40% probability. Hydrogen atoms have been omitted for clarity. Selected bond lengths (Å) and angles (°): Mg(1)–C(3), 2.182(2); Mg(1)–N(3), 2.0794(16); Mg(1)–N(2), 1.9989(17); Na(1)–C(3), 3.036(2); Na(1)–C(4), 2.648(2); Na(1)–N(3), 2.4779(18); Na(1)–N(4), 2.5401(18); Na(1)–N(5), 2.5291(18); N(2)-Mg(1)-C(3), 120.48(8); N(2)-Mg(1)-N(3), 134.32(7); N(3)-Mg(1)-C(3), 105.16(7); Na(1)-N(3)-Mg(1), 89.35(6).

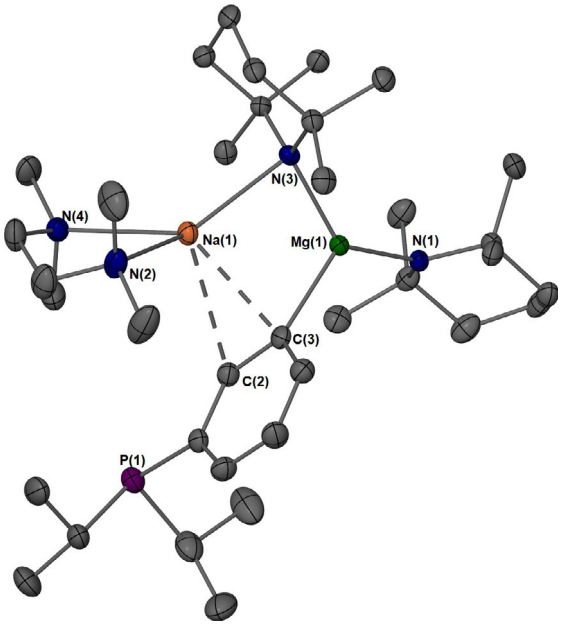

Figure 3. Molecular structure of [(TMEDA)Na(TMP)(*m*-$C_6H_4PiPr_2$)Mg(TMP)] **4** with thermal ellipsoids at 40% probability. Hydrogen atoms have been omitted for clarity. Selected bond lengths (Å) and angles (°): Mg(1)–C(3), 2.181(4); Mg(1)–N(1), 1.994(3); Mg(1)–N(3), 2.071(3); Na(1)–N(3), 2.485(3); Na(1)–N(2), 2.457(3); Na(1)–N(4), 2.569(3); Na(1)–C(2), 3.038(4); Na(1)–C(3), 2.684(4); N(1)-Mg(1)-N(3), 133.51(13); N(1)-Mg(1)-C(3), 119.21(14); C(3)-Mg(1)-N(3), 107.11(13); Na(1)-N(3)Mg(1), 87.25(11).

bond to the *meta*-carbon of the aromatic ring [2.182(2) and 2.181(4) Å in **3** and **4** respectively]. In contrast, the sodium atom lies almost perpendicular to the magnesiated ring, forming modest Na–π interactions with the π-system of the aromatic ring, primarily with the deprotonated *meta*-carbon [Na(1)–C(3) 2.648(2) and Na(1)–C(2) 3.036(2) Å in **3**; Na(1)–C(3) 2.684 and Na(1)–C(2) 3.038(4) Å in **4**].[46] A distinction here is that the Ph ring engages with the sodium through a η^2 C_{meta}–$C(H)_{para}$ interaction in **3**, but through a η^2C_{meta}–$C(H)_{ortho}$ interaction in **4**. Interestingly, in comparison to laterally metallated **2**, where the sodium atom binds to the phosphorus, here in **3** and **4** the heteroatom is orientated away from the metal centres, with the sodium atom opting to predominately π-engaging with the arene-ring opposed to typical dative bonding through the N/P atoms. As far as we can ascertain, the only reported, structurally characterised example of a ring metallated *N,N*-diethylaniline complex is the *para*-metallated dirhenium complex $[Re_2(CO)_8(\mu\text{-H})(p\text{-}C_6H_4NEt_2)]$,[47] while hitherto no structurally characterised examples of ring-metallated dialkylphenylphosphine complexes exist.

Solution studies and quenching

To build up a solution picture of complexes **2**–**4** NMR spectroscopic studies were performed in C_6D_6 followed by a series of I_2 and D_2O quenching studies. Interestingly this revealed some unexpected solution behaviour.

^{1}H and ^{31}P NMR spectra of complex **2** each revealed two sets of signals, suggesting a second species, other than the solid-state structure, coexists in solution. In the $^{31}P\{^1H\}$ spectrum two resonances are present, a broad singlet at −29.7 ppm (belonging to **2**) and a smaller signal at −28.6 ppm attributed to **2a** (Scheme 2). Similarly, the ^{1}H and $^{13}C\{^1H\}$ NMR spectra indicate the presence of two species, the major species being assigned as **2** by three triplets 7.85, 7.27 and 7.12 ppm (corresponding to the *ortho*-, *meta*- and *para*-protons) and aliphatic signals at 1.40 ppm for the CH_3 and two non-equivalent signals for the $MgCH_2$ protons at 0.60 and −0.23 ppm (assigned by ^{1}H-^{13}C HSQC). While in the same spectra a second minor species can be identified as **2a** by a set of resonances at 7.83, 7.30 and 1.40 ppm. Note that this solution also contains resonances for TMEDA and TMP (see Supporting Information). In an attempt to confirm the presence of the regioisomer **2a** and not another product within the sample C:H:N analysis was also carried out. Microanalysis and NMR spectroscopic studies are consistent with the minor species being the *para*-magnesiated *P,P*-dimethylphenylphosphine regioisomer complex **2a**. For further confirmation, attempts to isolate the observed *para*-isomer **2a** were made via electrophilic iodine and D_2O quenches. For ease of handling and purification, the quenched products were subject to aerial oxidation during workup to give the corresponding phosphorus(V) oxide compounds. Iodination of a crystalline sample of **2** lead to a mixture of multi-iodinated products (see Supporting Information). However, quenching studies with D_2O afforded the expected corresponding single deuterated product, $CH_3(CH_2D)P{=}OPh$ with no other deutero-regioisomer isolated, suggesting **2a** to be a solution artefact.

^{1}H and ^{13}C NMR spectroscopic studies of complexes **3** and **4** returned no such complications and are consistent with the retention of their structures in solution. For **3**, the disappearance of the aromatic signals related to the parent aniline (7.24, 6.76 and 6.62 ppm) and appearance of four new aromatic signals, at 7.45 (doublet), 7.12 (singlet), 7.11 (doublet) and 6.48 ppm (doublet of doublet of triplets) are characteristic of a *meta*-deprotonated species. Similarly, the presence of four new aromatic resonances in the ^{1}H NMR spectrum of compound **4** at 8.15

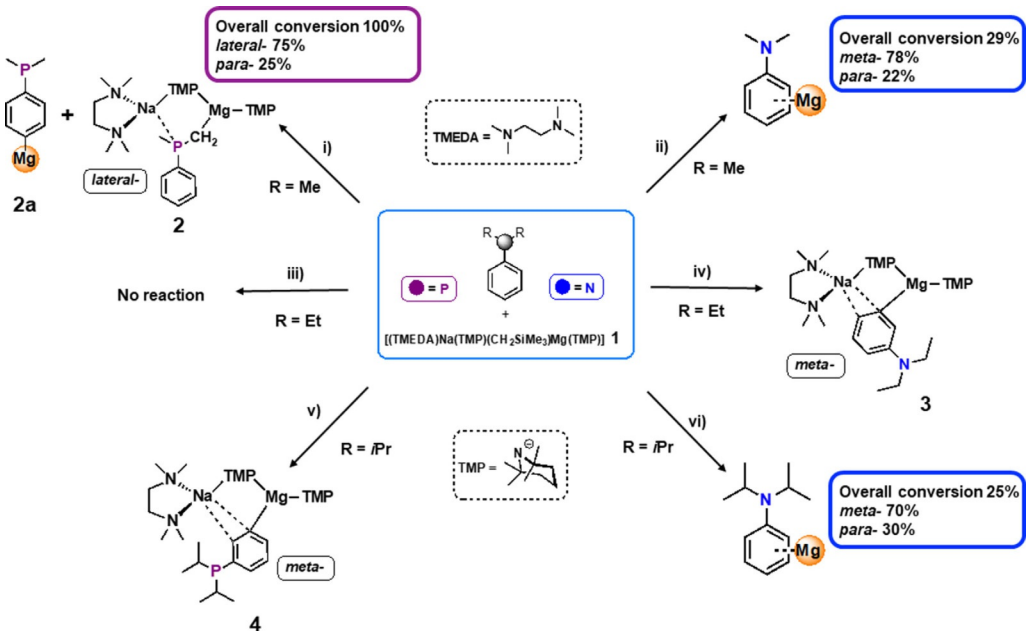

Scheme 2. Reagents and conditions: i) hexane, r.t., overnight ii) hexane, reflux, 2 hours iii) hexane, no reaction observed at r.t. for 1–7 days or reflux for 1, 2, 6 or 18 h, iv) hexane, r.t., overnight, v) hexane, r.t., overnight, vi) hexane, reflux, 3 hours.

(doublet of doublets), 7.83 (doublet), 7.23 (multiplet) and 7.17 ppm (triplet) indicate the formation of a *meta*-deprotonated species. The $^{31}P\{^{1}H\}$ NMR spectrum shows an upfield shift of the phosphorus signal from 10.42 ppm (parent phosphine) to 9.42 ppm in the metallated species **4**.

Iodolysis of **3** and **4** resulted in the expected *N*,*N*-diethyl-3-iodoaniline and (3-iodophenyl)diisopropylphosphine, respectively. Interestingly, small quantities (< 10%) of *N*,*N*-diethyl-4-iodoaniline were also present from **3**, likely resulting from the electrophilic aromatic substitution of iodine with free *N*,*N*-diethylaniline.[48]

Due to the lack of isolable magnesiated intermediates for *N*,*N*-dimethyl- and *N*,*N*-diisopropyl-aniline substrates, iodolysis of the reaction mixtures were conducted to gain insight into the metallation site selectivity observed in solution. A ^{1}H NMR study of the crude material obtained following iodolysis of the reaction mixture of **1** with *N*,*N*-dimethylaniline at room temperature was found to have an overall conversion of 26%, with an iodo-*meta*:*para* ratio of 73:27, which is in agreement with the in situ monitoring (compared to 29% for metallated species and *meta*:*para* ratio 78:22, Scheme 2, see the Supporting Information). Switching the reaction conditions to 4 hours reflux and then quenching with iodine, resulted in predominantly the *para*-product *N*,*N*-dimethyl-4-iodoaniline being isolated, as well as small amounts of residual starting material. In a similar fashion, iodolysis of the reaction of **1** with *N*,*N*-diisopropylaniline resulted in an overall conversion of 25% with an iodo-*meta*:*para* ratio of 7:3 (identical to the ^{1}H NMR identified metallated species prior to iodine quench, Scheme 2, see Supporting Information). In both magnesiation reactions no *ortho*-iodonated products were isolated. In keeping with our findings that the *meta*-isomer monopolized the selectivity the reported metallation of *N*,*N*-dimethylaniline with the mixed metal zincate reagent [(TMEDA)Na(TMP)(*t*Bu)Zn(*t*Bu)] also results in the isolation of a mixture of the regioisomers[29] upon iodolysis quenching studies, with the *meta*-isomer the major product.

Homo-metallic studies

Wanting to determine if the reactions of base **1** displayed any synergistic character we next sought to probe the reactivity of the homo-metallic components of **1**, NaTMP·TMEDA and $Mg(CH_2SiMe_3)_2$. Literature examples for the mono-metallation of the dimethyl N/P substrates (Scheme 1) have been reported,[29,33,34] prompting us to investigate the reactivity of the diethyl analogues *N*,*N*-diethylaniline and *P*,*P*-diethylphenylphosphine. Reaction of a molar equivalent of *N*,*N*-diethylaniline or *P*,*P*-diethylphenylphosphine with (NaTMP·TMEDA) at room temperature resulted in the isolation of the crystalline compounds $[\{(TMEDA)Na(EtNC_6H_5)\}_2]$ **5** and $[(TMEDA)Na_2(TMP)(C_6H_5PEt)]_2$ **6** in a 46 and 35% (max yield 50%) yield, respectively. On the other hand, reaction with $Mg(CH_2SiMe_3)_2$, even under forcing reflux conditions, resulted in quantitative recovery of the starting materials (Scheme 3).

The centrosymmetric molecular structure of **5** indicates that instead of a deprotonative ring metallation as seen in **3**, the β-elimination of one ethyl group on the *N*,*N*-diethylaniline substrate has occurred (Figure 4). The complex is dimeric with a planar (NaNNaN) ring core (ΣNa–N bond angles = 360°) with each sodium atom in a tetrahedral N_4 environment. The

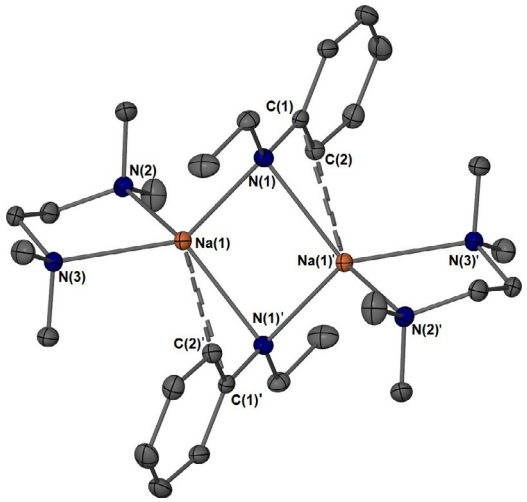

Figure 4. Molecular structure of $[\{(TMEDA)Na(EtNC_6H_5)\}_2]$ **5** with thermal ellipsoids at 40% probability. Hydrogen atoms have been omitted for clarity. Symmetry operator ′ = 1−*x*, 1−*y*, 1−*z*. Hydrogen atoms omitted for clarity. Selected bond lengths (Å) and angles (°): Na(1)–N(1), 2.4116(10); Na(1)–C(1)′, 2.8782(12); Na(1)–C(2)′, 2.8805(13); Na(1)–N(2), 2.4744(11); Na(1)–N(3), 2.4825(10); Na(1)-N(1)-Na(1)′, 79.85(3); C(1)-N(1)-Na(1)′, 92.04(7), N(1)-Na(1)′-N(1)′, 100.15(3).

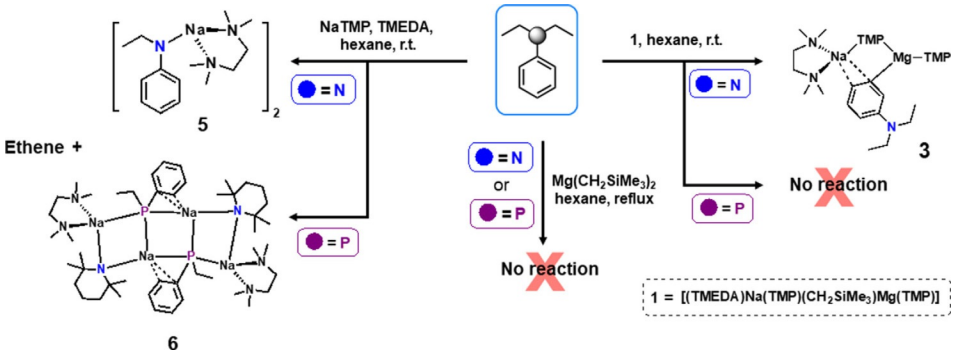

Scheme 3. Contrasting homometallic metallations of *N*,*N*-diethylaniline and *P*,*P*-diethylphenylphosphine with sodium TMP and bis(trimethylsilylmethyl)magnesium.

phenyl groups of the *N*-ethylaniline units are disposed *trans* to each other maximising Na···C electrostatic interactions to both *ipso*- and *ortho*-Ph sites (Na–C bond lengths of 2.8782(12) and 2.8805(13) Å respectively). TMEDA completes the Na coordination sphere in its common bidentate fashion.

Akin to complex **5**, **6** adopts a dimeric composition in the crystal, but with an overall ladder-type arrangement (Figure 5).

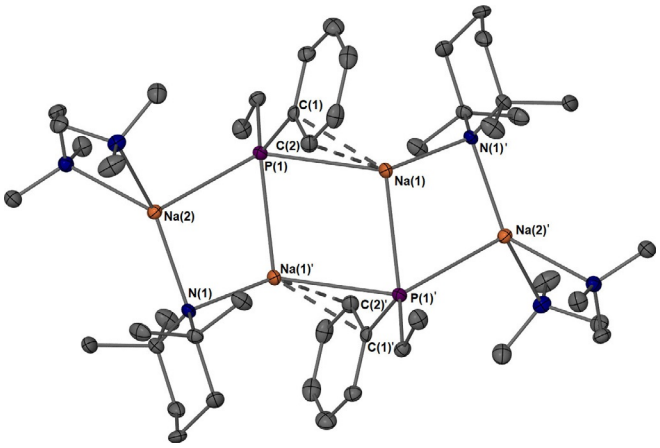

Figure 5. Molecular structure of $[(TMEDA)Na_2(TMP)(C_6H_5PEt)]_2$ **6** with thermal ellipsoids shown at 40% probability. Hydrogen atoms are omitted for clarity. Symmetry operator ′ = 1−*x*, 1−*y*, 1−*z*. Selected bond lengths (Å) and angles (°): Na(1)–P(1), 2.9256(8); Na(1)–N(1)′, 2.318 (4); Na(2)–P(1), 2.9891(9); Na(2)–N(1), 2.408 (4) Na(1)′–P(1), 2.8848(8); Na(1)–C(1), 2.7474(19); Na(1)–C(2), 2.983(2); Na(2)-P(1)-Na(1), 68.41(2); P(1)-Na(1)-N(1)′, 75.96(4); Na(1)-N(1)′-Na(2)′, 88.64(5), P(1)-Na(1)′-N(1), 104.04(4); P(1)-Na(1)′-P(1)′, 104.29(2); P(1)′-Na(2)′-N(1)′, 98.80(4).

The mixed sodium amide/sodium phosphide ladder molecule is composed of a central (Na_2P_2) strictly planar core (ΣNa–P bond angles = 360°) and two outer planar (NaNNaP) rings lying out of the central plane by 26.87(4)°. Displaced from the central core ±1.230(1) Å, the outer Na atoms [Na(2) and Na(2)′] are capped by a chelating TMEDA molecule, while the inner two engage in two Na···C electrostatic interactions, one short [Na(1)–C(1) 2.7474(19) Å] to the *ipso*-carbon and one long [Na(1)–C(2) 2.983(2) Å] to the *ortho*-carbon of the phenyl ring.[49] Comparable to **5**, the *P,P*-diethylphenylphosphine substrate has lost one of its ethyl limbs, most likely occurring from a β-elimination reaction and concurrent formation of ethene. Interestingly, unlike in **5**, where all the basic TMP arms have been consumed, two NaTMP units remain unreacted in **6**. Thus **6** can be regarded as an example of a hybrid co-complex between a sodium amide and a sodium phosphide, with the closest structurally characterised example being the monomeric amino-functionalised sodium phosphanide complex $[[\{(Me_3Si)_2CH\}(C_6H_4\text{-}2\text{-}NMe_2)P]Na(TMEDA)]$[50] and the pyridyl-functionalised phosphanide $[\{(Me_3Si)_2CH\}(2\text{-}C_5H_4N)P]Na\}_2\cdot(Et_2O)]_2$[50] which adopts a similar dimer of dimers motif to **6**. The composition of complex **6** fits the laddering principle established in lithium amide chemistry[51] with **6** representing a product of "secondary laddering" assembly.

^1H and ^{13}C NMR spectroscopy of compounds **5** and **6** confirmed the retention of their crystal structure in solution. A downfield shift of the remaining ethyl protons to 3.32 and 1.48 ppm and 2.31 and 1.52 ppm for **5** and **6** respectively (parent *N,N*-diethylaniline 2.99 and 0.89 ppm and *P,P*-diethylphenylphosphine 1.51 and 0.94 ppm, respectively) and integration analysis confirm the loss of an ethyl group. The $^{31}P\{^1H\}$ spectrum of **6** shows a substantial upfield shift from a sharp singlet at −16.59 ppm to a broad, less resolved signal at −55.85 ppm, which lies in the same range as previously reported alkali-metal bis(*o*-anisyl)phosphides.[36,52]

Highlighting the power of the bimetallic alliance of **1** in the effective deprotonation of these substrates, no ring metallation is observed in **5** or **6**, with an alternative ethene elimination pathway predominating. This elimination reaction, resulting from a P–C and N–C cleavage fits nicely with the theme of 'cleave and capture chemistry'—a new concept recently introduced in the literature.[24,53,54]

Computational aspects

In an attempt to rationalize the different metallation regioselectivities afforded by the homo- and heterobimetallic bases, DFT calculations[55] of the C–H acidities in THF (Figure 6) of the different dialkyl-substituted phenylphosphine and aniline substrates where conducted (see Supporting Information for full information). All geometry optimizations were performed with

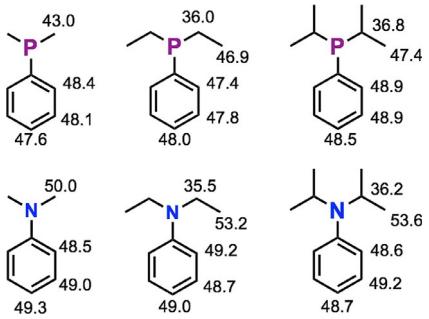

Figure 6. Calculated values of pK_a(THF) of the dialkyl substituted phenylphosphine and aniline substrates.

the M06-2Z functional,[56] cc-pVTZ Dunnings basis set[57] and a universal solvation model based on density(SMD)[58] with THF as a solvent. Frequency calculations were carried out to ensure the location of the energy minima[56] which calculated the six substrates to have typical weak CH acidities covering a broad 35.5–53.6 pK_a span in this polar solvent.

Overall the acidity of the phenyl ring H atoms across all six substrates shows little to no variation comparing the *ortho*-, *meta*- and *para*-protons of the analogous P versus N substrates. These minor differences in pK_a values rationalise the non-selective metallation seen for the reaction of **1** with dimethyl- and diisopropylaniline where a mixture of regioisomers are observed (albeit predominately the *meta*-species). Interestingly, the experimentally observed regioselectivities of the isolated *meta*-isomers (**3** and **4**) of the diethylaniline and diisopro-

pylphenylphosphine substrates conflict with the most acidic H atoms belonging to the methylene (pK_a 35.5, **3**) and ^{iPr}C–H (pK_a 36.8, **4**) groups (Figure 6). This would suggest metallation of these substrates is controlled by other contributing factors such as sterical orientation and electrostatic interactions.

The largest differences in calculated relative C–H acidity are seen upon changing the alkyl substituent on the P and N centres. In the dimethyl case, the PCH_3 hydrogen atoms are significantly more acidic (pK_a 43.0) than the analogous NCH_3 atoms (pK_a 50.0), consistent with the observed lateral metallation seen with phosphine complex **2**. In contrast, ring metallation is favoured for the nitrogen system, where pK_a change is not so significant but still goes the other way and favours ring metallation (pK_a ring average 48.9; methyl 50.0).

The experimental findings from the homometallic reaction of NaTMP with the diethyl phenylphosphine and aniline substrates fit the predicted acidity values well. Here the elimination of one of the ethyl groups via initial alpha-deprotonation and ethene evolution, is supported by the most acidic methylene protons in both the N (pK_a 35.5) and P (pK_a 36.0) systems and reactivity similar to the alkali metal decomposition and cleavage pathways of ethers and similar substrates.[59]

Conclusions

In this systematic metallation study, we have shown for the first time the successful alkali-metal-mediated magnesiation of a series of dialkylphenylphosphines and their aniline counterparts. Contradicting lateral versus *meta*-magnesiation products were seen for the dimethyl substituted phenylphosphine and aniline substrates, respectively, while predominately *meta*-magnesiation was observed for the other diethyl and diisopropyl substrates. These findings were in agreement with the theoretically calculated pK_a values indicating little to no variation in the relative acidity of the *ortho*- *meta*- and *para*-ring protons across all substrates. Highlighting the cooperative effect of bimetallic base **1**, mono-metallic studies (NaTMP) on the diethylphenylphosphine and aniline substrates lead to no ring metallation and a competitive ethene elimination pathway. In summary, this reactivity study has shown exchanging the nitrogen for a softer phosphorus centre results in more selective metallation outcomes, eliminating competitive regioisomer mixtures seen predominately for their nitrogen analogues.

Experimental Section

All reactions (unless otherwise stated) were completed under an atmosphere of dinitrogen and anhydrous conditions using standard Schlenk-line techniques. Water and oxygen were removed from *n*-hexane and diethyl ether using a MBRAUN SPS-800 solvent purification system and were stored over 4 Å molecular sieves under a dinitrogen atmosphere. TMEDA and TMP(H) were dried by reflux over CaH_2 and stored over 4 Å molecular sieves. ^{1}H and ^{13}C NMR spectra were recorded on Bruker DRX 400 MHz or 600 MHz Cryo spectrometers with chemical shifts internally referenced to C_6D_6 or $CDCl_3$. Microanalysis were carried out at the Science Centre, London Metropolitan University, with samples prepared in air-tight sealed glass ampules. *n*BuNa,[60] $Mg(CH_2SiMe_3)_2$[20] and *N*,*N*-diisopropylaniline[61] were prepared according to literature procedures. See Supporting Information for full details of X-ray crystallographic information and electrophilic quenching studies. CCDC 1831594 (2), 1831592 (3), 1831590 (4), 1831593 (5), 1850750 (6), and 1831591 (7) contain the supplementary crystallographic data for this paper. These data can be obtained free of charge from The Cambridge Crystallographic Data Centre.

Synthesis of *P,P*-diethylphenylphosphine: Ethylmagnesium bromide (25 mL, [3 M in diethyl ether], 75 mmol) was added dropwise to a stirred solution of phenylphosphorus dichloride (5 mL, 37 mmol) in 60 mL of diethyl ether at 0 °C over 60 minutes. After filtration, the reaction was quenched with 5 mL of deoxygenated water. The aqueous layer was removed via a gas-tight syringe, and the ethereal layer dried with anhydrous magnesium sulphate. The solution was filtered, the solvent removed under vacuum and the phosphine purified by vacuum distillation (0.15 torr, 30 °C) to afford the product as a colourless air-sensitive liquid. Typical yield 4.3 mL, 65%. ^{1}H NMR (400 MHz, C_6D_6, 300 K): δ = 7.56 (m, 2H, *ortho*-H), 7.1–7.3 (m, 3H, *meta*/*para*-H), 1.61 (m, 4H, CH_2), 1.05 ppm (dt, 6H, J = 7.6, 7.2 Hz, CH_3). ^{13}C NMR (100 MHz, C_6D_6, 300 K): δ = 139.1 (d, quaternary-C), 132.4 (d, *ortho*-*C*), 128.4 (s, *para*-C), 128.2 (d, *meta*-C), 20.3 (d, CH_2), 9.7 ppm (d, CH_3). ^{31}P{^{1}H} NMR (162 MHz, C_6D_6, 300 K): δ = −16.59 ppm (s).

Synthesis of *P,P*-diisopropylphenylphosphine: Isopropylmagnesium chloride (25 mL, [1 M in tetrahydrofuran], 25 mmol) was added dropwise to a stirred solution of phenylphosphorus dichloride (1.65 mL, 12.34 mmol) in 50 mL of anhydrous tetrahydrofuran at 0 °C over 60 minutes. After stirring overnight, the reaction was quenched with 5 mL of deoxygenated water. The aqueous layer was removed via a gas-tight syringe, and the tetrahydrofuran was removed under vacuum and replaced with diethyl ether. This solution was filtered, solvent removed and the phosphine purified by vacuum distillation (0.15 torr, 46 °C) to afford the product as a colourless air-sensitive liquid. Typical yield: 2 g, 81%. ^{1}H NMR (400 MHz, C_6D_6, 300 K): δ = 7.53–7.62 (m, 2H, *ortho*-H), 7.21–7.3 (m, 3H, *meta*/*para*-H), 2.06 (ds, 2H, J = 7.2, 1.6 Hz, CH), 1.16 (dd, 6H, J = 14.8, 7.2 Hz, CH_3), 1.00 ppm (dd, 6H, J = 14.8, 7.2 Hz, CH_3). ^{13}C NMR (100 MHz, C_6D_6, 300 K): δ = 135.3 (d, quaternary-C), 134.6 (d, *ortho*-*C*), 128.6 (s, *para*-C), 127.8 (d, *meta*-C), 22.8 (d, CH), 19.7 (d, CH_3), 18.6 ppm (d, CH_3). ^{31}P{^{1}H} NMR (162 MHz, C_6D_6, 300 K): δ = 10.35 ppm (s).

General procedure (GP): *n*BuNa (0.16 g, 2 mmol) was suspended in 10 mL of dry hexane. To this suspension TMP(H) (0.68 mL, 4 mmol) was added dropwise and the reaction allowed to stir at room temperature for at least 30 minutes. Next $Mg(CH_2SiMe_3)_2$ (0.4 g, 2 mmol) was introduced with subsequent addition of TMEDA (0.3 mL, 2 mmol) affording a pale-yellow, transparent solution that was used without further purification. If clumps of solid remained in solution following addition of TMEDA, the solution was sonicated until complete dissolution occurred.

Synthesis of [(TMEDA)Na(TMP)(CH_2PCH_3Ph)Mg(TMP)] (2): To a stirred solution of **GP**, 0.28 mL of *P,P*-dimethylphenylphosphine was added dropwise at room temperature. The resulting solution was stirred overnight, resulting in the formation of a large amount of white precipitate. This was isolated by filtration and transferred to an argon glovebox for storage. X-ray quality crystals were obtained upon recrystallisation from *n*-hexane. Crystalline yield = 0.67 g, 58%. ^{1}H NMR (400 MHz, C_6D_6, 300 K): δ = 7.65 (t, 2H, J = 6.84 Hz *ortho*-H), 7.27 (t, 2H, J = 7.36 Hz, *meta*-H), 7.12 (t, 1H, J = 7.24 Hz, *para*-H), 1.95 (m (br), 4H, γ-CH_2, TMP), 1.74 (s (br), 12H, CH_3 TMEDA), 1.68 (s (br), 4H, CH_2 TMEDA), 1.55–1.65 (m (br), 24H, CH_3 TMP), 1.45–1.41 (m (br), 4H, β-CH_2 TMP) 1.40 (s, 3H, CH_3), 1.36–1.30 (m (br), 4H, β-CH_2 TMP), 0.60 (t, 1H, J = 9.6 Hz, CH_2Mg), −0.23 ppm

(d, 1H, $J=10$ Hz, CH_2Mg). ^{13}C NMR (100 MHz, C_6D_6, 300 K): $\delta=$ 150.25 (d, *ipso*-C), 130.4 (*ortho*-C), 127.1 (*para*-C), 57.4 (CH_2-TMEDA), 46.4 (CH_3-TMEDA), 42.8 (β-C TMP), 36.21 (CH_3 TMP), 20.66 (γ-C TMP), 18.78 (CH_3), 8.0 ppm (CH_2-Mg) Note: *meta*-C signal appears under the C_6D_6 residual peak (as determined by HSQC experiment). ^{31}P{^{1}H} NMR (162 MHz, C_6D_6, 300 K): $\delta=-28.58$ (s (br)), -29.68 ppm (s (br)). Microanalysis: Calculated for $C_{32}H_{62}N_4MgNaP$: C 66.14, H 10.75, N 9.64; found: C 65.88, H 10.53, N 9.45. **[(TMEDA)Na(TMP)(*p*-PMe$_2$Ph)Mg(TMP)] 2a**: ^{1}H NMR (400 MHz, C_6D_6, 300 K): $\delta=8.83$ (s (br), 0.5H), 7.30 (m, 0.3H), 1.40 ppm (s, 1.3H, CH_3).

Synthesis of [(TMEDA)Na(TMP)(*m*-C$_6$H$_4$NEt$_2$)Mg(TMP)] (3): To a stirred solution of **GP**, *N*,*N*-diethylaniline (0.32 mL, 2 mmol) was added dropwise at room temperature. The resulting solution was stirred overnight, resulting in the formation of a large amount of white precipitate. This was isolated by filtration and transferred to an argon glovebox for storage. X-ray quality crystals were obtained upon recrystallisation from *n*-hexane and slow cooling in a hot oil bath. Yield = 0.77 g, 65%. ^{1}H NMR (600 MHz, C_6D_6, 300 K): $\delta=7.45$ (d, 1H, $J=2.9$ Hz), 7.12 (s, 1H, C2), 7.11 (d, 1H, $J=1.8$ Hz), 6.48 (m, 1H, *meta*′-H), 3.17 (q, 4H, $J=7$ Hz, ethyl-CH_2), 1.98–1.87 (m, 4H, γ-CH_2 TMP), 1.66 (s (br), 24H, CH_3 TMP), 1.63 (s (br), 12H, CH_3-TMEDA), 1.55 (s, 6H, CH_2 TMEDA), 1.44–1.31 (m, 8H, β-CH_2-TMP), 1.04 ppm (t, 6H, $J=7$ Hz, Ethyl-CH_3). ^{13}C NMR (151 MHz, C_6D_6, 300 K): $\delta=173.41$ (s, Mg-C), 147.22, 127.51, 126.03, 110.33 (*meta*′-C), 57.30 (CH_2 TMEDA), 46.34 (CH_3 TMEDA), 45.06 (CH_3), 42.76 (β-CH_2-TMP), 36.26 (CH_3 TMP), 20.76 (γ-CH_2 TMP), 13.48 ppm (CH_3). Despite multiple attempts, satisfactory elemental analysis was not possible.

Synthesis of [(TMEDA)Na(TMP)(*m*-C$_6$H$_4$P*i*Pr$_2$)Mg(TMP)] 4: To a stirred solution of **GP**, *P*,*P*-diisopropylphenylphosphine (0.4 g, 2 mmol) was added dropwise at room temperature. Upon addition, an immediate formation of a bright yellow solution was observed. After stirring overnight, the solution was filtered and its volume reduced in vacuo, where storage at $-30\,^\circ$C resulted in the deposition of a large crop of yellow, block crystals Crystalline yield = 0.4 g, 31%. ^{1}H NMR (600 MHz, C_6D_6, 300 K): $\delta=8.15$ (dd, 1H, $J=8.4$, 1.2 Hz, H), 7.83 (d, 1H, $J=4.4$ Hz, H^4), 7.23 (m, 1H, H^5), 7.17 (t, 1H, $J=6.6$ Hz, H^2), 2.10 (septet, 2H, $J=6.6$ Hz, CH), 1.90 (t (br), 4H, $J=$ 6 Hz, γ-CH_2 TMP), 1.61 (s (br), 36H, CH_3 TMP/TMEDA), 1.36 (s (br), 6H, CH_2 TMEDA), 1.19 (dd, 6H, $J=14.7$, 6.9 Hz, *i*Pr) 1.07 (d, $J=$ 1.2 Hz, TMP), 1.02 ppm (dd, 6H, $J=10.5$, 6.9 Hz, *i*Pr). ^{31}P{^{1}H} NMR (162 MHz, C_6D_6, 300 K): $\delta=9.42$ (s). Satisfactory ^{13}C NMR has not been possible due to solubility issues. Despite multiple attempts, satisfactory elemental analysis was not possible.

Synthesis of [{(TMEDA)Na(EtNC$_6$H$_5$)}$_2$] (5): *N*,*N*-diethylaniline (0.32 mL, 2 mmol) was added dropwise at room temperature to a stirred suspension of *n*BuNa (0.16 g, 2 mmol), TMP(H) (0.36 mL, 2 mmol) and TMEDA (0.3 mL, 2 mmol). The resulting solution was stirred overnight at room temperature, and then filtered and its volume reduced in vacuo. Storage at room temperature deposited crystals of the title compound over one week. Crystalline yield: 0.12 g, 46%. ^{1}H NMR (400 MHz, C_6D_6, 300 K): $\delta=7.26$ (br, 2H, *meta*-H), 6.61 (d, 2H, $J=7.6$ Hz, *ortho*-H), 6.42 (t, 1H, $J=7.2$ Hz, *para*-H), 3.33 (q, 2H, $J=7.2$ Hz, CH_2), 1.77 (s (br), 12H, CH_3-TMEDA), 1.66 (s (br), 4H, CH_2-TMEDA), 1.49 ppm (t, 3H, $J=7.2$ Hz). ^{13}C NMR (100 MHz, C_6D_6, 300 K): $\delta=129.4$ (*meta*-C, determined by HMBC), 107.6 (*ortho*-C, determined by HMBC), 101.27 (s, *para*-C), 57.27 (s, CH_3-TMEDA), 45.41 (CH_2-TMEDA), 45.06 (s, CH_2), 19.32 ppm (s, CH_3); elemental analysis calcd (%) for $C_{14}H_{26}N_3Na$: C 64.83, H 10.10, N 16.20; found: C 64.68, H 9.88, N 15.91.

Synthesis of [(TMEDA)Na$_2$(TMP)(C$_6$H$_5$PEt)]$_2$ (6): *P*,*P*-diethylphenylphosphine (0.18 mL, 1 mmol) was added dropwise at room temperature to a stirred suspension of *n*BuNa (0.08 g, 1 mmol), TMP(H) (0.18 mL, 1 mmol) and TMEDA (0.15 mL, 1 mmol). The resulting solution was stirred overnight at room temperature, and then filtered and its volume reduced in vacuo. Storage at room temperature deposited crystals of the title compound over one week. Crystalline yield: 0.15 g, 35% (Maximum yield = 50% based on consumption of TMP(H)). ^{1}H NMR (400 MHz, C_6D_6, 300 K) $\delta=7.37$ (2H, t, J 7.0, *ortho*-H), 7.12 (2H, t, J 7.5, *meta*-H), 6.72 (1H, tt, J 7.2, 1.2, *para*-H), 2.31 (2H, qd, J 7.5, 1.8, CH_2), 2.10–2.00 (2H, m, γ-CH_2 TMP), 1.85 (12H, s, CH_3-TMEDA), 1.76 (4H, s, CH_2-TMEDA), 1.52 (3H, dt, $J=$ 14.9, 7.4, CH_3), 1.49–1.43 (4H, m, β-CH_2 TMP), 1.27 ppm (12H, s, CH_3-TMP). ^{31}P{^{1}H} NMR (162 MHz, C_6D_6, 300 K): $\delta=-55.87$ ppm (bs). ^{13}C NMR (100 MHz, C_6D_6, 300 K): $\delta=128.27$ (d, *ortho*-C), 125.67 (d, *meta*-C), 117.98 (d, *para*-C), 56.89 (CH_2-TMEDA), 52.31, 45.58 (CH_3-TMEDA), 42.08 (s, β-CH_2 TMP), 37.22 (s, CH_3-TMP), 21.03 (s, γ-CH_2 TMP), 16.07 (d, CH_2), 13.98 ppm (d, CH_3). Despite multiple attempts, satisfactory elemental analysis has not proved possible.

Acknowledgements

We thank the Australian Research Council (DE140101137) and Monash University for financial support. This research was supported by an Australian Government Research Training Program (RTP) Scholarship. REM is grateful to the Alexander von Humboldt foundation for a Humboldt research award (host: Universität Regensburg, Germany). We thank Dr. Samantha Orr for help with figures and proof reading and Dr. Craig Forsyth for assistance with X-ray crystallography.

Conflict of interest

The authors declare no conflict of interest.

Keywords: anilines · dialkylphenyphosphines · metallation · regioselectivity · synergistic effect

[1] R. E. Mulvey, S. D. Robertson, *Angew. Chem. Int. Ed.* **2013**, *52*, 11470 – 11487; *Angew. Chem.* **2013**, *125*, 11682 – 11700.
[2] M. Schlosser in *Organometallics Synth. Third Man.* (Ed.: M. Schlosser), Wiley, **2013**.
[3] V. Snieckus, *Chem. Rev.* **1990**, *90*, 879 – 933.
[4] See references therein: a) C. G. Hartung, V. Snieckus in *Modern Arene Chemistry*, Wiley, **2004**, pp. 330 – 367; b) S. Florio, A. Salomone, *Synthesis* **2016**, *48*, 1993 – 2008.
[5] G. Monzón, I. Tirotta, Y. Nishii, P. Knochel, *Angew. Chem. Int. Ed.* **2012**, *51*, 10624 – 10627; *Angew. Chem.* **2012**, *124*, 10776 – 10779.
[6] A. H. Stoll, P. Knochel, *Org. Lett.* **2008**, *10*, 113 – 116.
[7] D. S. Ziegler, K. Karaghiosoff, P. Knochel, *Angew. Chem. Int. Ed.* **2018**, *57*, 6701 – 6704; *Angew. Chem.* **2018**, *130*, 6811 – 6815.
[8] R. E. Mulvey, *Acc. Chem. Res.* **2009**, *42*, 743 – 755.
[9] G. Dayaker, A. Sreeshailam, F. Chevallier, T. Roisnel, P. Radha Krishna, F. Mongin, *Chem. Commun.* **2010**, *46*, 2862 – 2864.
[10] G. Dayaker, D. Tilly, F. Chevallier, G. Hilmersson, P. C. Gros, F. Mongin, *Eur. J. Org. Chem.* **2012**, 6051 – 6057.
[11] K. Snégaroff, J. M. L'Helgoual'ch, G. Bentabed-Ababsa, T. T. Nguyen, F. Chevallier, M. Yonehara, M. Uchiyama, A. Derdour, F. Mongin, *Chem. Eur. J.* **2009**, *15*, 10280 – 10290.
[12] K. Snégaroff, S. Komagawa, F. Chevallier, P. C. Gros, S. Golhen, T. Roisnel, M. Uchiyama, F. Mongin, *Chem. Eur. J.* **2010**, *16*, 8191 – 8201.
[13] T. T. Nguyen, F. Chevallier, V. Jouikov, F. Mongin, *Tetrahedron Lett.* **2009**, *50*, 6787 – 6790.

[14] O. Bayh, H. Awad, F. Mongin, C. Hoarau, F. Trécourt, G. Quéguiner, F. Marsais, F. Blanco, B. Abarca, R. Ballesteros, *Tetrahedron* **2005**, *61*, 4779 – 4784.
[15] F. Mongin, A. Bucher, J. P. Bazureau, O. Bayh, H. Awad, F. Trécourt, *Tetrahedron Lett.* **2005**, *46*, 7989 – 7992.
[16] H. R. L. Barley, W. Clegg, S. H. Dale, E. Hevia, G. W. Honeyman, A. R. Kennedy, R. E. Mulvey, *Angew. Chem. Int. Ed.* **2005**, *44*, 6018 – 6021; *Angew. Chem.* **2005**, *117*, 6172 – 6175.
[17] J. M. L'Helgoual'ch, A. Seggio, F. Chevallier, M. Yonehara, E. Jeanneau, M. Uchiyama, F. Mongin, *J. Org. Chem.* **2008**, *73*, 177 – 183.
[18] M. Y. A. Messaoud, G. Bentabed-Ababsa, M. Hedidi, A. Derdour, F. Chevallier, Y. S. Halauko, O. A. Ivashkevich, V. E. Matulis, L. Picot, V. Thiéry, V. Dorcet, F. Mongin, *Beilstein J. Org. Chem.* **2015**, *11*, 1475 – 1485.
[19] V. L. Blair, L. M. Carrella, W. Clegg, B. Conway, R. W. Harrington, L. M. Hogg, J. Klett, R. E. Mulvey, E. Rentschler, L. Russo, *Angew. Chem. Int. Ed.* **2008**, *47*, 6208 – 6211; *Angew. Chem.* **2008**, *120*, 6304 – 6307.
[20] V. L. Blair, A. R. Kennedy, J. Klett, R. E. Mulvey, *Chem. Commun.* **2008**, 5426 – 5428.
[21] M. Uchiyama, H. Naka, Y. Matsumoto, T. Ohwada, *J. Am. Chem. Soc.* **2004**, *126*, 10526 – 10527.
[22] H. Naka, M. Uchiyama, Y. Matsumoto, A. E. H. Wheatley, M. McPartlin, J. V. Morey, Y. Kondo, *J. Am. Chem. Soc.* **2007**, *129*, 1921 – 1930.
[23] J. Garcia-Álvarez, A. R. Kennedy, J. Klett, R. E. Mulvey, *Angew. Chem. Int. Ed.* **2007**, *46*, 1105 – 1108; *Angew. Chem.* **2007**, *119*, 1123 – 1126.
[24] R. E. Mulvey, V. L. Blair, W. Clegg, A. R. Kennedy, J. Klett, L. Russo, *Nat. Chem.* **2010**, *2*, 588 – 591.
[25] V. L. Blair, W. Clegg, B. Conway, E. Hevia, A. Kennedy, J. Klett, R. E. Mulvey, L. Russo, *Chem. Eur. J.* **2008**, *14*, 65 – 72.
[26] E. Hevia, D. J. Gallagher, A. R. Kennedy, R. E. Mulvey, C. T. O'Hara, C. Talmard, *Chem. Commun.* **2004**, 2422 – 2423.
[27] P. C. Andrikopoulos, D. R. Armstrong, D. V. Graham, E. Hevia, A. R. Kennedy, R. E. Mulvey, C. T. O'Hara, C. Talmard, *Angew. Chem. Int. Ed.* **2005**, *44*, 3459 – 3462; *Angew. Chem.* **2005**, *117*, 3525 – 3528.
[28] D. R. Armstrong, W. Clegg, S. H. Dale, E. Hevia, L. M. Hogg, G. W. Honeyman, R. E. Mulvey, *Angew. Chem. Int. Ed.* **2006**, *45*, 3775 – 3778; *Angew. Chem.* **2006**, *118*, 3859 – 3862.
[29] D. R. Armstrong, L. Balloch, E. Hevia, A. R. Kennedy, R. E. Mulvey, C. T. O'Hara, S. D. Robertson, *Beilstein J. Org. Chem.* **2011**, *7*, 1234 – 1248.
[30] M. Uzelac, R. E. Mulvey, *Chem. Eur. J.* **2018**, *24*, 7786 – 7793.
[31] A. J. Martinez-Martinez, A. R. Kennedy, R. E. Mulvey, C. T. O'Hara, *Science* **2014**, *346*, 834 – 837.
[32] A. J. Martínez-Martínez, S. Justice, B. J. Fleming, A. R. Kennedy, I. D. H. Oswald, C. T. O'Hara, *Sci. Adv.* **2017**, *3*, e1700832.
[33] A. R. Lepley, W. A. Khan, A. B. Giumanini, A. G. Giumanini, *J. Org. Chem.* **1966**, *31*, 2047 – 2051.
[34] D. J. Peterson, *J. Organomet. Chem.* **1967**, *8*, 199 – 208.
[35] J. M. Bayne, D. W. Stephan, *Chem. Soc. Rev.* **2016**, *45*, 765 – 774.
[36] K. Izod, *Adv. Inorg. Chem.* **2000**, *50*, 33 – 107.
[37] M. Lappert, A. Protchenko, P. Power, A. Seeber in *Metal Amide Chemistry*, Wiley, Chichester, UK, **2008**.
[38] W. S. Huang, S. Liu, D. Zou, M. Thomas, Y. Wang, T. Zhou, J. Romero, A. Kohlmann, F. Li, J. Qi, L. Cai, T. A. Dwight, Y. Xu, R. Xu, R. Dodd, A. Toms, L. Parillon, X. Lu, R. Anjum, S. Zhang, F. Wang, J. Keats, S. D. Wardwell, Y. Ning, Q. Xu, L. E. Moran, Q. K. Mohemmad, H. G. Jang, T. Clackson, N. I. Narasimhan, V. M. Rivera, X. Zhu, D. Dalgarno, W. C. Shakespeare, *J. Med. Chem.* **2016**, *59*, 4948 – 4964.
[39] V. L. Blair, A. R. Kennedy, R. E. Mulvey, C. T. O'Hara, *Chem. Eur. J.* **2010**, *16*, 8600 – 8604.
[40] M. A. Stevens, V. L. Blair, *Eur. J. Inorg. Chem.* **2018**, 74 – 79.
[41] CCDB Search Date 21-06-2018.
[42] G. Varchi, A. E. Jensen, W. Dohle, A. Ricci, G. Cahiez, P. Knochel, *Synlett* **2001**, 0477 – 0480.
[43] W. Dohle, A. D. M. Lindsay, P. Knochel, *Org. Lett.* **2001**, *3*, 2871 – 2873.
[44] L. T. Byrne, L. M. Engelhardt, G. E. Jacobsen, W.-P. Leung, R. I. Papasergio, C. L. Raston, B. W. Skelton, P. Twiss, A. H. White, *J. Chem. Soc. Dalton Trans.* **1989**, 105 – 113.
[45] J. Clayden, *Organolithiums: Selectivity for Synthesis* Pergamon, Oxford, **2002**.
[46] D. O. Khristolyubov, D. M. Lyubov, A. V. Cherkasov, G. K. Fukin, A. S. Shavyrin, A. A. Trifonov, *Organometallics* **2018**, *37*, 1627 – 1634.
[47] R. D. Adams, V. Rassolov, Y. O. Wong, *Angew. Chem. Int. Ed.* **2016**, *55*, 1324 – 1327; *Angew. Chem.* **2016**, *128*, 1346 – 1349.
[48] C. Monnereau, E. Blart, F. Odobel, *Tetrahedron Lett.* **2005**, *46*, 5421 – 5423.
[49] S. A. Orr, A. R. Kennedy, J. J. Liggat, R. McLellan, R. E. Mulvey, S. D. Robertson, *Dalton Trans.* **2016**, *45*, 6234 – 6240.
[50] K. Izod, J. C. Stewart, W. Clegg, R. W. Harrington, *Dalton Trans.* **2007**, 257 – 264.
[51] A. Downard, T. Chivers, *Eur. J. Inorg. Chem.* **2001**, 2193 – 2201.
[52] H. C. Aspinall, M. R. Tillotson, *Inorg. Chem.* **1996**, *35*, 5 – 8.
[53] P. C. Andrews, V. L. Blair, E. C. Border, A. C. Peatt, J. G. Maclellan, C. D. Thompson, *Organometallics* **2013**, *32*, 7509 – 7519.
[54] R. E. Mulvey, *Dalton Trans.* **2013**, *42*, 6676 – 6693.
[55] E. I. Izgorodina, C. Yeh Lin, M. L. Coote, *Phys. Chem. Chem. Phys.* **2007**, *9*, 2507.
[56] Y. Zhao, D. G. Truhlar, *Theor. Chem. Acc.* **2008**, *120*, 215 – 241.
[57] T. H. Dunning, *J. Chem. Phys.* **1989**, *90*, 1007 – 1023.
[58] A. V. Marenich, C. J. Cramer, D. G. Truhlar, *J. Phys. Chem. B* **2009**, *113*, 6378 – 6396.
[59] A. Maercker, *Angew. Chem. Int. Ed. Engl.* **1987**, *26*, 972 – 989; *Angew. Chem.* **1987**, *99*, 1002 – 1019.
[60] L. Lochmann, J. Pospíšil, D. Lím, *Tetrahedron Lett.* **1966**, *7*, 257 – 262.
[61] D. Wang, M. R. Talipov, M. V. Ivanov, R. Rathore, *J. Am. Chem. Soc.* **2016**, *138*, 16337 – 16344.

Manuscript received: July 9, 2018
Accepted manuscript online: August 12, 2018
Version of record online: September 20, 2018

ORGANOMETALLICS

pubs.acs.org/Organometallics Article

Synthesis, Structure, and Solution Studies of Lithiated Allylic Phosphines and Phosphine Oxides

Nimrod M. Eren, Samantha A. Orr, Christopher D. Thompson, Emily C. Border, Michael A. Stevens, and Victoria L. Blair*

Cite This: *Organometallics* 2020, 39, 2080–2090 Read Online

ACCESS | Metrics & More | Article Recommendations | Supporting Information

ABSTRACT: This study reports a new series of 12 α-lithiated allylic phosphines and phosphine oxides. By incorporating Lewis base donors including diethyl ether (Et_2O), tetrahydrofuran (THF), *N,N,N′,N′*-tetramethylethylenediamine (TMEDA), and *N,N,N′,N′,N″*-pentamethyldiethylenetriamine (PMDETA), nine complexes were structurally characterized by single-crystal X-ray crystallography. This includes novel dilithiated allylic phosphine **4** [$PhP\{CHCHCH_2Li(TMEDA)\}_2$] and a rare hemisolvated lithiated phosphine oxide **6** [$\{Ph_2P(O)CHC(Me)CH_2Li\}_2(TMEDA)$]. Interestingly, in the solid state, P(III) complexes take advantage of Li–π interactions to the newly formed delocalized system, in comparison to P(V) complexes where the oxophillic nature of the lithium atom dominates. All 12 complexes were fully characterized in the solution state by multinuclear NMR spectroscopy. DFT calculations on isomers of monomeric lithiated complex **3** [$Ph_2PCHC(Me)CH_2Li(PMDETA)$] described the low energy barrier between transition steps of the subtle delocalization of the allylic chain.

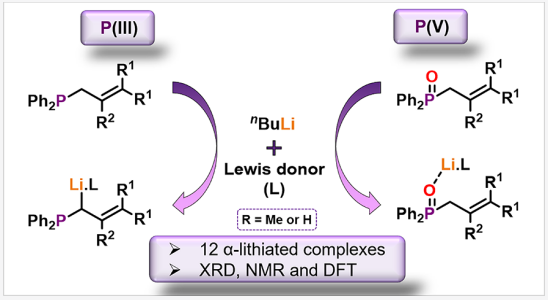

INTRODUCTION

Organophosphines are undergoing a long-awaited renaissance compared with their well-developed group 15 nitrogen analogues. To date, research efforts have focused on understanding the synthesis, reactivity, and structural chemistry, in both solid and solution states, of alkali metal amides,[1] yet the phosphine derivatives have not received as much attention.

It is well-established in the literature that phosphines are a crucial ligand class in the field of metal catalysis,[2] such as Buchwald-type dialkylbiaryl phosphine ligands[3] (Figure 1) or

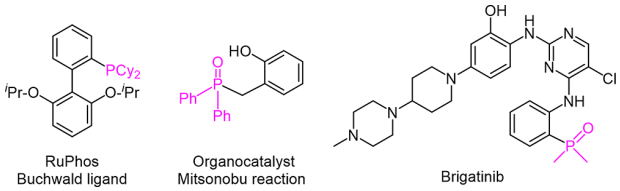

Figure 1. Examples of some prominent phosphorus containing molecules in synthetic and medicinal chemistry.

2,2′-bis(diphenylphosphino)-1,1′-binnaphthyl (BINAP) ligand employed in asymmetric synthesis,[4] while tertiary phosphines can also be employed independently as organocatalysts for various organic transformations.[5] Alongside synthetic applications, the past decade has seen the development of cyclic phosphorus compounds evolve for the use in organic electronics such as organic light-emitting diodes (OLEDs).[6] Interestingly, phosphorus-containing compounds can exhibit beneficial biological activity in medicinal chemistry.[7] In particular interest to this work is the recent FDA approval of the lung cancer drug Brigatinib[8] (Figure 1). The incorporation of a phosphine oxide functionality enhanced its desirable medicinal properties and has revived interest in understanding the importance of this functional group in medicinal chemistry. As a result of these developments, the formation of C–P bonds as a route to access novel organophosphines has been expanded,[2,9,10] while continuing to understand their structure and reactivity patterns is crucial.

In recent years, we have studied alkali metal allylic amide systems[11−13] owing to the simple building block having a significant role in accessing many valuable N-containing compounds such as β-amino acids and β-lactams,[14,15] chiral β-branched esters,[16] chiral 1,2 diamines,[17] and peptide isosteres.[18] Our ongoing interest in allylic amide systems and their applications has led us to delve into the phosphorus derivatives exploiting both oxidation states, where P(V) is air-

Received: February 28, 2020
Published: May 26, 2020

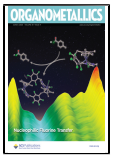

https://dx.doi.org/10.1021/acs.organomet.0c00144
Organometallics 2020, 39, 2080–2090

stable over the P(III) analogues. Allyl phosphines have not featured extensively in the literature, although they have been incorporated into bifunctional phosphine borane FLP systems[19] and appear as donor ligands in transition metal complexes.[20,21] However, phosphine oxides feature in the literature mainly in the renowned Wittig−Horner reaction,[22−24] alongside cycloadditions,[25,26] diene synthesis,[27,28] and most recently as a superior redox-free organocatalyst for Mitsunobu reactions (Figure 1).[29]

Our group recently reported the contrasting lithiation reactivity of a N- and P-diphenylallyl system with *n*-BuLi.[30] Interestingly, notable differences were observed upon increasing the Lewis donor denticity resulting in P−C bond cleavage compared with traditional deprotonation pathways in nitrogen systems (Scheme 1). In order to extend this chemistry, the

Scheme 1. Previous Work Illustrating Lithiation of N- and P-Allyl Systems

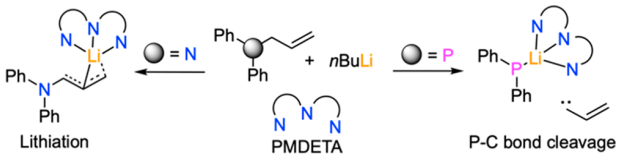

work herein focuses on understanding the lithiations of closely related substituted allyl groups including 2-methylallyl, 3,3-dimethylallyl, and diallyl phenyl phosphine compounds exploring steric and electronic influences. The analogous phosphine oxides will also be discussed and compared illustrating the impact of oxidation states on metalation patterns.

RESULTS AND DISCUSSION

Ligand Synthesis. The synthesis of P(III) allylic substrates **P1**−**P3** was achieved through an established metathesis route,[30] reacting lithium diphenyl phosphide and the corresponding allyl halide. Diallyl substrate **P4** was prepared via the Grignard reaction of phenyl phosphine dichloride with two equivalents of allyl magnesium halide (Scheme 2). All four phosphine substrates (**P1**−**P4**) were isolated as viscous colorless oils in yields ranging from 50 to 80% and fully characterized by NMR spectroscopy. The oxide derivatives

Scheme 2. Synthesis of Allylic Phenyl Phosphines and Oxides

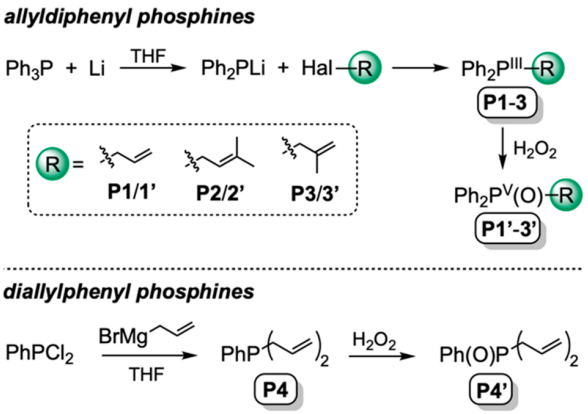

were obtained via an additional oxidation step with hydrogen peroxide to yield corresponding allylic phosphine oxides **P1′**−**P3′** as microcrystalline solids in near-quantitative yields. All four oxides where fully characterized by NMR spectroscopy and X-ray crystallography (see the Supporting Information).

Lithiation synthesis. Lithium complexes of **P2**−**P4** and **P1′**−**P3′** were synthesized by reacting the parent P-allyl substrate with *n*-BuLi at −78 °C in hexane for P(III) or diethyl ether for P(V) followed by the addition of the appropriate Lewis donor: Et_2O, THF, TMEDA, or PMDETA (Scheme 3).

Scheme 3. Summary of Lithiation of Allyl Phosphines and Oxides

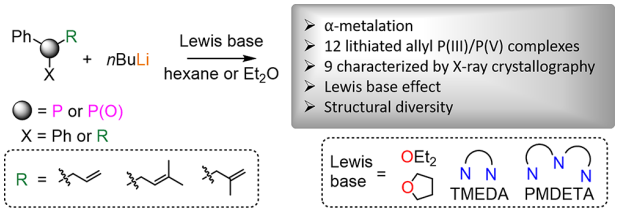

Isolation of 12 new α-lithiated complexes was achieved with nine complexes amenable to single-crystal X-ray diffraction (XRD). All complexes **1**−**12** were fully characterized by multinuclear NMR spectroscopy and microanalysis (where possible).

Structural Studies of P(III) Complexes. Single crystals suitable for XRD analysis could be obtained for four of the lithiated allyl diphenyl phosphine complexes, namely, **1** [$\{Ph_2PCHCHCMe_2Li(Et_2O)\}_2$], **2** [$\{Ph_2PCHCHCMe_2Li(TMEDA)\}_2$], **3** [$Ph_2PCHC(Me)CH_2Li(PMDETA)$], and **4** [$PhP\{CHCHCH_2Li(TMEDA)\}_2$] (Scheme 4). A summary of comparative bond lengths can be seen in Table 1.

Scheme 4. General Synthesis and Structural Diversity of Lithiated Allylic Phosphines

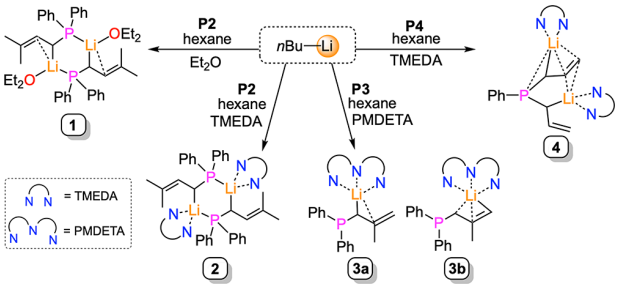

Colorless block crystals of lithiated **P2** were obtained from a hexane solution stored at −40 °C, affording α-lithiated dimer **1** [$\{Ph_2PCHCHCMe_2Li(Et_2O)\}_2$] (Figure 2). The central $(LiPC)_2$ ring core in **1** displays a distinct twist boat conformation (Figure 4) with each lithium atom formally three coordinate adopting a distorted trigonal planar olefinic carbon atom (Li1−C2, 2.250(6) Å; Li2−C7, 2.173(6) Å) increasing its coordination number to four. Notably, subtle delocalization is seen following deprotonation of the α-carbon, highlighted by contraction of the P1−C1 and C1−C2 bonds [1.752(3) and 1.434(4) Å, respectively] and elongation of the C=C bond length [1.357(4) Å]. Moving to the bidentate donor TMEDA, crystallization of lithiated **P2** from hexane and

https://dx.doi.org/10.1021/acs.organomet.0c00144
Organometallics 2020, 39, 2080−2090

Table 1. Summary of Bond Lengths for Crystallographically Characterized Complexes 1−9

	P(III) complexes					P(V) complexes				
	1	**2**	**3a**	**3b**	**4**	**5**	**6**	**7**	**8**	**9**
bond	dimer	dimer	monomer	monomer	monomer	dimer	dimer	monomer	monomer	monomer
P1−C1−C4	1.752(3)	1.753(2)	1.7636(12)	1.7620(13)	1.797(6) 1.707(9)	1.7083(12)	1.7056(14)	1.7003(17)	1.696(2)	1.7073(16)
P1−O1						1.5240(10)	1.5190(9)	1.5123(11)	1.5197(15)	1.5226(11)
Li1−O1						1.884(2)	1.860(2)	1.804(3)	1.801(4)	1.837(3)
Li1−O1′						1.990(2)				
Li2−O1							2.043(3)			
Li1−C1	2.224(6)	2.216(4)	2.282(2)	2.494(3)	2.296(10)		2.435(2)			
−C2	2.250(6)		2.760(3)	2.412(3)	2.194(10)	2.691(3)	2.512(2)			
−C3				2.303(3)	2.335(9)	2.403(3)				
Li2−C2					2.531(10)					
−C3					2.520(11)					
−C4					2.289(11)					
−C6	2.192(6)									
−C7	2.173(6)									
C1−C2	1.434(4)	1.419(3)	1.4447(17)	1.4168(18)	1.414(8)	1.4259(16)	1.437(2)	1.433(2)	1.436(2)	1.421(2)
C4−C5					1.444(9)					
C2−C3	1.357(4)	1.354(4)	1.367(2)	1.3732(19)	1.356(8)	1.3689(16)	1.346(2)	1.361(3)	1.348(3)	1.356(2)
C5−C6					1.375(10)					

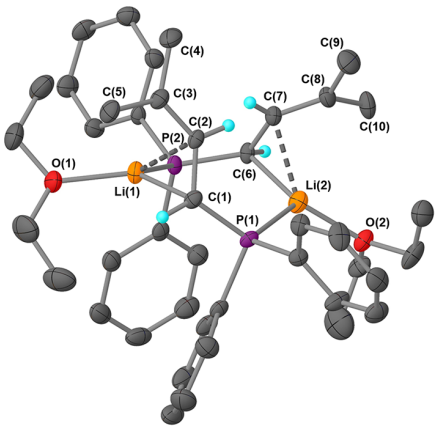

Figure 2. Molecular structure of $[\{Ph_2PCHCHCMe_2Li(Et_2O)\}_2]$ **1**. Hydrogen atoms (except allylic) are omitted for clarity. Thermal ellipsoids are shown at a 40% probability.

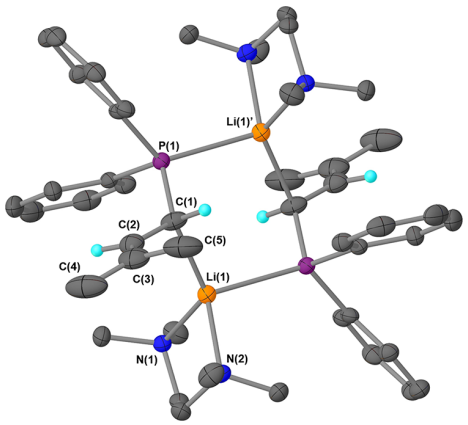

Figure 3. Molecular structure of $[\{Ph_2PCHCHCMe_2Li(TMEDA)\}_2]$ **2**. Hydrogen atoms (except allylic) are omitted for clarity. Thermal ellipsoids are shown at a 40% probability. Symmetry operator (′) = 1 − *x*, 1 − *y*, 1 − *z*.

addition of TMEDA afforded complex **2** $[\{Ph_2PCHCHCMe_2Li(TMEDA)\}_2]$ (Figure 3) in a 79% yield.

Complex **2** adopts a traditional centrosymmetric dimeric assembly with a central six-membered $(PCLi)_2$ ring assuming a chair conformation (Figure 4). Each lithium atom adopts a distorted tetrahedral geometry ($\sum$ 653.87°) with its coordination environment comprising a phosphorus atom, an α-deprotonated carbon atom [Li1−C1, 2.216(4) Å], and a bidentate chelating TMEDA molecule. Consistent with **1**, the mild delocalization of the allyl component is observed with elongated P−C and C−C bonds [1.753(2) and 1.419(3) Å, respectively], while a slight shortening of the olefinic C2−C3 bond [1.354(4) Å] is observed. Addition of bidentate TMEDA inhibits any additional Li−π electrostatic interactions, as seen in ether solvated **1**. Overall, the bonding parameters of **2** are in agreement with the reported TMEDA solvated lithiophosphine $[\{Ph_2PCH_2Li(TMEDA)\}_2]$.[31]

Moving on to phosphine **P3**, lithiation in hexane and addition of 1 equiv of PMDETA afforded a crop of single crystals identified as **3** $[Ph_2PCHC(Me)CH_2Li(PMDETA)]$.

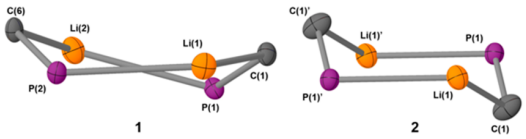

Figure 4. Comparison of $(PCLi)_2$ cores within complexes **1** and **2**.

Surprisingly, upon further inspection of the crystalline material, two distinct morphologies and crystal colors were present, namely, orange blocks **3a** and yellow blocks **3b**, both of which were suitable for XRD analysis (Figure 5). Monomeric **3a** and **3b** differ only by the interactions the lithium cation makes with the allyl component of metalated phosphine **P3**. Polymorphs **3a** and **3b** are both α-deprotonated at C1. Compound **3a** makes its shortest Li−C bond to C1 [Li1−C1 2.282(2) Å], while in isomer **3b** the lithium atom is positioned to maximize interactions with C1, C2, and C3 (average Li−C bond length 2.403 Å) with Li1−C3 displaying the shortest bond length at

https://dx.doi.org/10.1021/acs.organomet.0c00144
Organometallics 2020, 39, 2080−2090

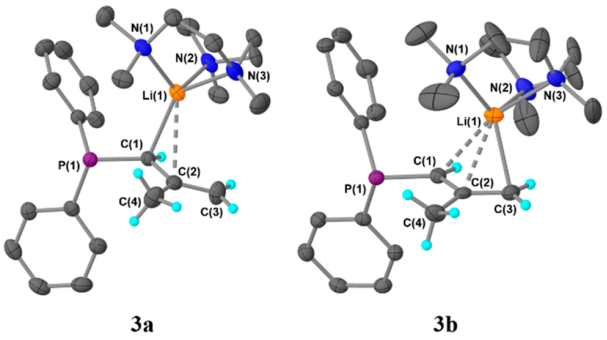

Figure 5. Molecular structures of [$Ph_2PCHC(Me)CH_2Li$-(PMDETA)] **3a** and **3b**. Hydrogen atoms (except allylic) are omitted for clarity. Thermal ellipsoids are shown at a 40% probability.

2.303(3) Å. Interestingly, despite the differing Li atom interactions on the allylic chain the C−C bond lengths in **3a** and **3b** are relatively comparable [C1−C2 1.4447(17), 1.4168(18) Å and C2−C3 1.367(2), 1.3732(19) Å, respectively]. Similar to complexes **1** and **2**, contraction of the C1−C2 bond supports moving toward a delocalized allyl chain system which is more pronounced in Li-electrostatic-rich **3b**. In contrast to our previously reported P-allylic system where PMDETA induces P−C bond cleavage,[30] here it maximizes Li-allylic electrostatic interactions to afford a stable complex.

As established in previous reported studies, nitrogen systems are well-known to form desirable aza-allyl species.[32−34] Since two isomeric forms of complex **3** were isolated in the solid state, we sought to determine the transition between **3a** and **3b**. Density functional theory (DFT) calculations were employed using the Gaussian 16[35] suite of software to help understand the cocrystallization of two isomeric forms of [$Ph_2PCHC(Me)CH_2Li$(PMDETA)] (**3a** and **3b**) observed when using PMDETA as a ligand (Figure 6). Geometry optimization and frequency calculations were performed using the B3LYP/6-311+G(d) level and basis set which were in good agreement with the XRD structures.

Complex **3b** was found to be more stable than **3a** by ΔG = −5.6 kJ mol^{-1}, a sufficiently small difference to suggest these two structures are of comparable stability. The energy barrier between **3a** and **3b** was calculated to be marginal, ΔG = +1.5 kJ mol^{-1}. This relatively small energy difference helps explain why a mixture of products is isolated experimentally over one isomeric form. It would be reasonable to assume that the lowest energy complex, **3b**, is preferential due to the steric bulk of PMDETA, resulting in the lithium atom located further along the deprotonated allylic chain.

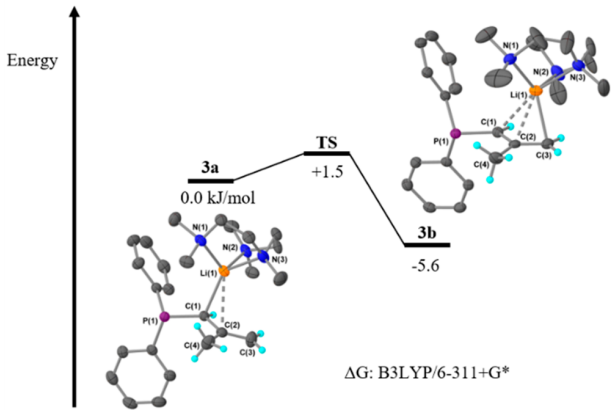

Figure 6. DFT calculations illustrating the ΔG values for the transformation between solid state isomers **3a** and **3b**.

As the phenyl ligands appear to be innocent in the structural makeup of the complex, the diallyl analogue **P4** was next investigated. **P4** was reacted with two equivalents of *n*-BuLi in hexane, which upon addition of 2 equiv of TMEDA yielded novel dilithiated diallylphenylphosphine complex **4** [PhP-{$CHCHCH_2Li$(TMEDA)}$_2$] (Figure 7).

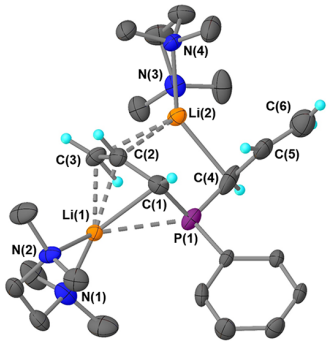

Figure 7. Molecular structure of **4** [PhP{$CHCHCH_2Li$(TMEDA)}$_2$]. Hydrogen atoms (except allylic) are omitted for clarity. Thermal ellipsoids are shown at a 40% probability.

In monomeric **4**, both allylic chains have been selectively α-deprotonated with each lithium cation solvated by one TMEDA molecule. Both lithium atoms are distinct in their coordination environments with Li1 adopting an η^4-binding mode to the P1, C1, C2, and C3 atoms on one allyl chain with the shortest Li−C bond to C2 [2.194(10) Å]. In contrast, Li2 is sandwiched between both deprotonated allylic chains making its shortest bond to α-deprotonated C4 (Li2−C4, 2.289(11) Å) and an η^2-interaction to only one of the deprotonated allylic chains via carbon atoms C2 and C3. Interestingly, despite the different electronic environments about both the deprotonated allylic chains in **4**, the C1−3 and C4−6 chain fragments are essentially equivalent in their bond lengths, with an overall contraction of the deprotonated single C1−C2 and C4−C5 bonds suggesting a dual sp^3/sp^2 nature. The cis/trans geometries of the allyl chains resonate with the bonding mode observed to the lithium cations. One notable difference in complex **4** is the asymmetric P−$C_{allylic}$ bonds [P1−C1, 1.797(6) Å; P1−C4 1.707(9) Å] in comparison to those of complexes **1**−**3** which consistently show a shortening of the P−C bond upon lithiation (avg 1.758 Å).

Structural Studies of P(V) Complexes. Upon moving to the P(V) oxidation state, a series of six new lithiated allyl phosphine oxides were isolated, of which five were characterized by XRD analysis as summarized in Scheme 5 and Table 1. Phosphine oxide **P3′** was the most successful in yielding single crystals suitable for X-ray crystallography. Lithiation of **P3′** with *n*-BuLi in diethyl ether solution and addition of THF to aid crystallization yielded a crop of orange needle crystals identified as **5** [{$Ph_2P(O)CHC(Me)CH_2Li$-(THF)}$_2$] (Figure 8). The discrete centrosymmetric dimer exhibits a central four-atom $(LiO)_2$ core, reminiscent of a typical lithium alkoxide motif.[36,37] The bridging oxygen atom

https://dx.doi.org/10.1021/acs.organomet.0c00144
Organometallics 2020, 39, 2080−2090

Scheme 5. General Synthesis and Structural Diversity of Lithiated Allylic Phosphine Oxides

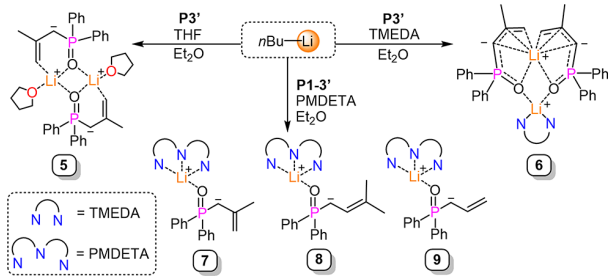

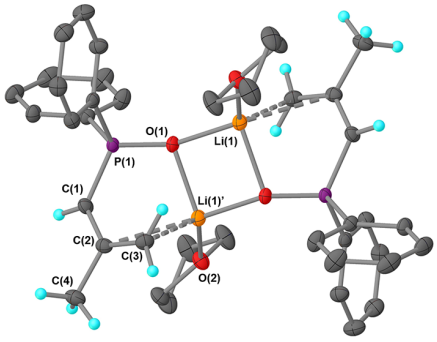

Figure 8. Molecular structure of $[\{Ph_2P(O)CHC(Me)CH_2Li(THF)\}_2]$ **5**. Hydrogen atoms (except allylic) are omitted for clarity. Thermal ellipsoids are shown at a 40% probability. Symmetry operator (′) = $-x$, $1 - y$, $1 - z$.

belonging to the phosphine oxide binds the two monomeric units together [Li1–O1 and Li1′–O1 are 1.884(2) and 1.990(2) Å, respectively], while the Li cation makes an η^2-electrostatic contact to carbon atoms C2, 2.691(3) Å, and C3, 2.403(3) Å which lie in the region of typical Li–C_{allyl} contacts.[11] The Li atoms coordination sphere is completed by a coordinating THF molecule. Overall, in the final dimeric complex the α-deprotonated allyl groups are positioned trans to each other possibly to ease steric strain.

Changing the Lewis donor to TMEDA resulted in the isolation and crystallization of rare dinuclear hemisolvated complex **6** $[\{Ph_2P(O)CHC(Me)CH_2Li\}_2(TMEDA)]$ (Figure 9). The core of **6** is composed of a $(LiO)_2$ ring in a rhombic arrangement with each lithium atom having a distinct coordination environment. The outermost lithium atom Li1 is bonded to two oxygen atoms of two α-deprotonated phosphine oxide ligands and chelated by one molecule of TMEDA in an essentially tetrahedral geometry. This appears to influence the deprotonated allyl arms into a cis arrangement encapsulating the secondary lithium cation Li2 in an η^8-fashion. The electrostatic contacts from the lithium atom Li2 to the oxygen [2.043(3) Å], phosphorus [2.6570(8) Å], and carbon [avg 2.539 Å] atoms form a stable, protective η^8-environment for the Li metal center which is persistent even upon addition of excess TMEDA. Interestingly, the bonding characteristics of the allylic chain are consistent, with shortening of the single C1–C2 bond [1.437(2) Å] and lengthening of the double C2–C3 bond [1.346(2) Å] indicating a degree of delocalization within the allylic system. Such a structural motif is unique with only limited examples observed in alkali metal chemistry. Most similar is the organophosphorous enamine complex $[\{Ph_2P(O)CH{=}C\text{-}(Bu^t)N(H)Li\}_2(TMEDA)]$,[38] which exhibits a dimeric tetranuclear species in sharp contrast to the cage like motif observed in **6** emphasizing the influence of the allyl moiety in the final complex architecture.

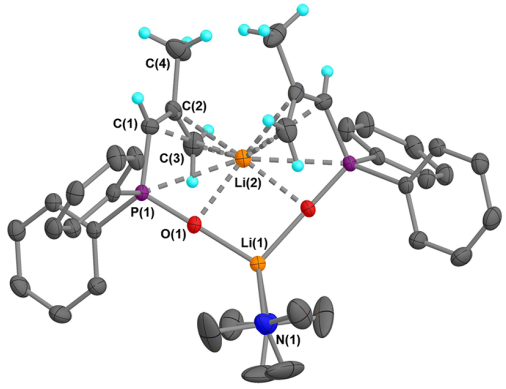

Figure 9. Molecular structure of $[\{Ph_2P(O)CHC(Me)\text{-}CH_2Li\}_2(TMEDA)]$ **6**. Hydrogen atoms (except allylic) are omitted for clarity. Thermal ellipsoids are shown at a 40% probability. Symmetry operator (′) = 1 − x, + y, 3/2 −z.

Complexes **7** $[Ph_2P(O)CHC(Me)CH_2Li(PMDETA)]$, **8** $[Ph_2P(O)CHCHC(Me)_2Li(PMDETA)]$, and **9** $[Ph_2P(O)\text{-}CHCHCH_2Li(PMDETA)]$ were synthesized by treating **P3′**, **P2′**, or **P1′** with 1 equiv of *n*-BuLi followed by the addition of the Lewis donor PMDETA, respectively (Scheme 5). Crystals suitable for XRD analysis of compounds **7**–**9** revealed a series of isostructural PMDETA solvated lithiated diphenyl allyl phosphine oxides. Due to their isostructural nature, only **7** has been discussed in detail (see the Supporting Information). Monomeric **7** (Figure 10) has undergone α-deprotonation

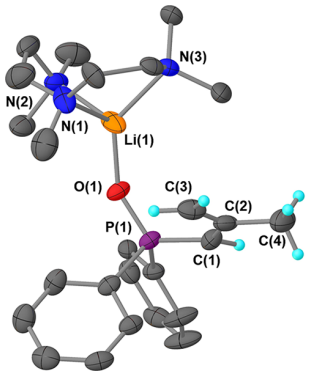

Figure 10. Molecular structure of $[Ph_2P(O)CHC(Me)CH_2Li\text{-}(PMDETA)]$ **7**. Hydrogen atoms (except allylic) are omitted for clarity. Thermal ellipsoids are shown at a 40% probability.

with the lithium atom bonded to the oxygen atom of the phosphine oxide ligand [Li1–O1, 1.804(3) Å] and capped by a tridentate molecule of PMDETA. Neither the phosphorus atom nor the allyl chain display any interaction to the metal center illustrating the strong oxophillic nature of the Li cation.

Notably, there is a high degree of delocalization through the P1–C1 and P1–O1 bonds, showing considerable bond contraction (average of complexes **7**–**9** are 1.7012 and 1.5182 Å, respectively; see Table 1). This demonstrates that functionalization of the allyl chain with methyl groups at C2 or C3 does not influence the electronics of the α-deprotonated

https://dx.doi.org/10.1021/acs.organomet.0c00144
Organometallics 2020, 39, 2080–2090

allyl group. However, a point of difference among the three complexes is the angle around the oxygen atom. The P1−O1−Li1 angles across **7**, **8**, and **9** are 147.03(14), 137.33(16), and 133.79(10)° where the least branched allyl chain shows the largest bond angle.

In summary, α-lithiation of the P-allylic systems result in complexes **1**−**9** exhibiting a degree of delocalization across the allyl chain fragment. This can be described as an intermediary species where the delocalization is subtle compared to nitrogen analogues where the aza-allyl nature is prominent. Interestingly, P(V) complexes **7**−**9** display additional delocalization through the P−O bond. The molecular architectures are influenced by the denticity of the Lewis base employed.

Solution-State Characterization. All 12 complexes, including three not amenable to XRD analysis, were characterized by multinuclear NMR spectroscopy (^{1}H, ^{7}Li, ^{31}P{^{1}H}, ^{13}C, COSY, and HSQC) in C_6D_6 or THF-d_8. The three additional complexes from the reaction of *n*-BuLi with parent ligands **P2**, **P3**, and **P1′** were identified as **10** [$Ph_2PCHCHCMe_2Li$(PMDETA)], **11** [Ph_2PCHC(Me)-CH_2Li(TMEDA)], and **12** [Ph_2P(O)$CHCHCH_2Li\cdot Et_2O$], respectively (Scheme 6).

Scheme 6. Synthesis of Complexes 10−12

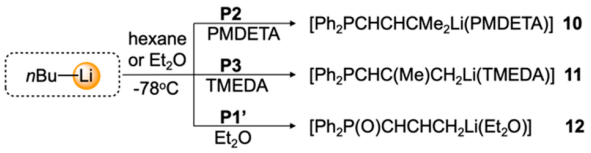

The ^{1}H NMR spectra confirm all compounds **1**−**12** have undergone selective α-lithiation, indicated by the general downfield shift of the remaining α-proton and significant downfield shift of the β-protons relative to those of the free parent phosphine or phosphine oxide (see the Supporting Information). In each complex, the corresponding donor ligand is present in the relevant ratio. The ^{7}Li NMR spectra of each complex **1**−**12** are comparable, appearing as a sharp singlet in the range of −3.73 to −5.14 ppm. Notably, the ^{31}P{^{1}H} NMR chemical shifts vary considerably across complexes **1**−**12** dependent on the coordination environment and oxidation state of the complex. This will be discussed in more detail herein.

Solution Studies P(III). In dimeric P(III) complexes **1** and **2**, which contain a direct P−Li bond, a considerable downfield shift in the ^{31}P{^{1}H} NMR signal is observed to −6.8 and −1.6 ppm, respectively (cf. parent phosphine **P2** at −15.8 ppm).

Due to the cocrystallization of monomeric isomers **3a** and **3b**, individual isolation and purification was not feasible. ^{1}H and ^{13}C NMR spectroscopic studies revealed both **3a** and **3b** exist as one species in solution, where subtle differences in their electrostatic interactions in the solid state are not observed. The ^{31}P{^{1}H} NMR resonance is less shielded appearing at −13.6 ppm compared to that of parent phosphine **P3** (cf. −17.9 ppm).

Solution studies of dilithiated complex **4** revealed that the two distinct Li cation environments in the solid state are not retained in solution with a sharp singlet at −5.14 ppm observed in the ^{7}Li NMR spectrum. In comparison, the ^{1}H NMR spectrum appears notably broad (Figure 11) which can be attributed to the fluxional nature of the allyl groups.

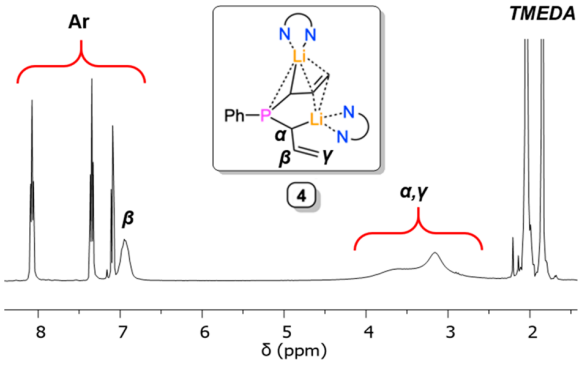

Figure 11. ^{1}H NMR spectrum of complex **4** in C_6D_6 at 25 °C.

Compound **4** is the anomaly across the P(III) complexes revealing a large upfield shift in the ^{31}P{^{1}H} NMR spectrum to −35.2 ppm (cf. parent **P4**, −26.6 ppm).

Complex **10**, which was not amenable to XRD analysis, has a ^{31}P{^{1}H} NMR spectrum chemical shift (−2.5 ppm) and a NMR profile similar to those of complexes **1** and **2**, suggesting a dimeric assembly (see the Supporting Information). In comparison, the ^{31}P{^{1}H} NMR spectrum of complex **11** in C_6D_6 is more complex, displaying three resonances at −19.7, −27.6, and −32.7 ppm. Analysis of **11** in THF-d_8 revealed a single peak at −17.4 ppm in the ^{31}P{^{1}H} NMR spectrum, suggesting the complexity and broadness of **11** in C_6D_6 could be attributed to the fluxional behavior of the allyl moiety.

Solution Studies P(V). P(V) complexes **5**−**7** possessing the same deprotonated 2-methylallyl moiety (**P3**) illustrate the influence of Lewis base donor on aggregation state. ^{1}H and ^{7}Li NMR analyses are comparable across complexes **5**−**7** with no significant differences in shift or splitting patterns observed. However, it must be noted that at room temperature in C_6D_6 compound **5** displays an extremely broad ^{1}H NMR spectrum, while the ^{31}P{^{1}H} NMR spectrum displays two broad resonances at 36.2 and 38.2 ppm, akin to the spectrum of complex **11** (see the Supporting Information). Upon performing the analysis of complex **5** in THF-d_8, the ^{1}H NMR spectrum becomes more resolved, while the ^{31}P{^{1}H} NMR spectrum displays one major resonance at 26.5 ppm in the presence of some other minor resonances (see the Supporting Information for full analysis). To confirm **5** is a single species undergoing fluxional behavior, we conducted variable-temperature studies in toluene-d_8 from 25 to 100 °C in 20 °C increments (Figure 12). As the temperature reaches 60 °C, the α- and γ-signals become resolved, while the concomitant ^{31}P{^{1}H} NMR resonances coalesce to one sharp signal at 36.8 ppm. This supports the notion that the allyl groups are displaying fluxional behavior, inducing broad spectra similar to those of complexes **4** and **11**. Post-heating analysis of the sample produced an identical spectrum to that initially collected at room temperature, ruling out a possible decomposition pathway or product.

Contrasting the ^{31}P{^{1}H} NMR profiles of **5**−**7**, they vary notably observing signals at 36.2 and 38.2 ppm (**5**), 33.3 ppm (**6**), and 26.1 ppm (**7**) upon moving from a dimer to a hemisolvated species to a monomer, where monomeric complex **7** is closest to parent phosphine **P3′** (25.9 ppm). Analogous monomeric compounds **8** and **9** have chemical shifts in a range similar to that of **7**. Comparing **7**−**9** facilitates investigating the influence of the allyl substituent, where having

https://dx.doi.org/10.1021/acs.organomet.0c00144
Organometallics 2020, 39, 2080−2090

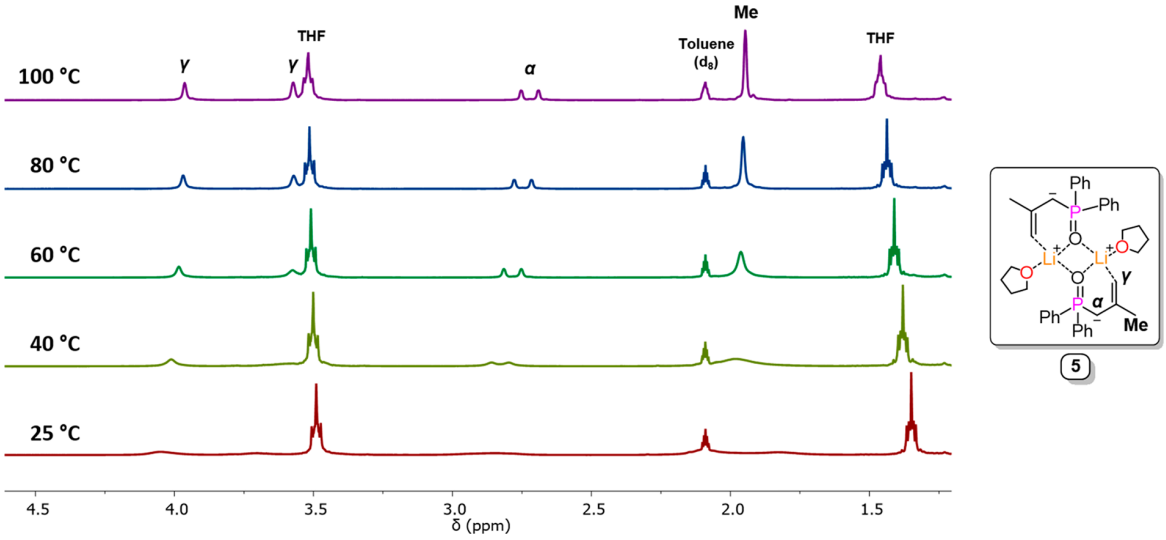

Figure 12. ^{1}H NMR spectra overlay of variable-temperature study of complex **5** in toluene-d_8.

an unbranched allyl chain (**9**) results in the most downfield shift observed in the ^{31}P{^{1}H} NMR data.

NMR analysis of **12** confirmed α-metalation with β-resonances shifting downfield relative to the resonance of the free parent phosphine oxide. The ^{31}P{^{1}H} NMR (38.8 ppm) is in line with that observed for dimeric **5** (36.2 and 38.2 ppm).

CONCLUSION

A series of α-lithiated allylic substrates have been isolated and characterized in the solid and solution states, including a novel dilithiated allylic phosphine. X-ray crystallography revealed the molecular assembly was dependent on the donor denticity, whereby the aggregation state was dimeric in the case of mono- or bidentate donors Et_2O, THF, and TMEDA but monomeric in the case of the tridentate donor PMDETA. The allylic portion of the solid-state structures, supported by DFT calculations of complexes **3a** and **3b**, displays subtle delocalization of the chain following metalation, akin to the nitrogen analogues forming aza-allylic species. Solution studies are in agreement with the solid-state structures, with delocalization of the allylic chain retained. Ongoing studies are investigating their reactivity in comparative nitrogen based cyclization pathways.

EXPERIMENTAL SECTION

All manipulations were carried under an atmosphere of argon or nitrogen using Schlenk techniques and a glovebox. Et_2O, *n*-hexane, and THF were dried and degassed using MBRAUN SPS-800 solvent purification system (SPS). Other chemicals were purchased commercially and used as received with the exception of TMEDA and PMDETA which were distilled distilled and dried over 4 Å molar sieves prior to use.

NMR Analysis. NMR spectra were recorded on a Bruker AVANCE 400 spectrometer (^{1}H, 400.13 MHz; ^{7}Li, 155.5 MHz; ^{13}C, 100.62 MHz; ^{31}P, 162.0 MHz). All ^{13}C and ^{31}P spectra were proton-decoupled. ^{1}H and ^{13}C spectra were referenced against the appropriate solvent signal. ^{7}Li and ^{31}P spectra were referenced against 9.7 M LiCl and 85% H_3PO_4 in D_2O, respectively. The proton and carbon signals were assigned by analysis of ^{1}H, ^{13}C{H}, ^{1}H−^{1}H COSY, ^{1}H−^{13}C HSQC, and ^{1}H−^{13}C HMBC.

X-ray Data. Single-crystal X-ray diffraction data were collected with a Bruker X8 APEXII CCD diffractometer with monochromatic (graphite) Mo Kα radiation processed using the Bruker Apex2 v2012.2.0 software;[39] Lorentz, polarization and absorption corrections (multiscan − SADABS)[40] were applied or a Rigaku Xtalab Synergy Dualflex diffractometer with monochromatic (graphite) Mo or Cu Kα radiation; or the MX1 synchrotron beamline at the Australian synchrotron.[41] Compounds **1**−**9** and **P1′**−**P4′** were solved and refined with SHELXT 2014/5[42] and SHELXL.[43]

Synthesis of 1 [{Ph$_2$PCHCHCMe$_2$Li(Et$_2$O)}$_2$]. 3,3-Dimethylallyldiphenylphosphine (**P2**) (0.2543 g, 1.00 mmol) was dissolved in dry *n*-hexane (10 mL). *n*-Butyllithium (0.69 mL, 1.6 M in hexane, 1.1 mmol) was then added dropwise at −78 °C, forming a yellow solution. After warming to room temperature and stirring for a further 2 h, Et_2O (0.12 mL (1.1 mmol) was added dropwise with stirring, turning the solution a brighter yellow. The solution was concentrated under reduced pressure forming a yellow-orange oil. Crystals suitable for X-ray diffraction were grown from a filtered, highly concentrated solution of hexane at −40 °C as blocks (0.087 g, 26%). ^{1}H NMR (C_6D_6, 400.20 MHz): δ 0.82 (t, $^{3}J_{H-H}$ = 7.1 Hz, 6H, Et_2O−Me), 1.90 (s, 3H, −CH═CMeMe(trans)), 2.08 (s, 3H, −CH═CMeMe(cis)), 2.61 (dd, $^{3}J_{H-H}$ = 12.7 Hz, $^{2}J_{H-P}$ = 5.1 Hz, 1H, P−CH−), 3.04 (q, $^{3}J_{H-H}$ = 7.1 Hz, 4H, Et_2O−CH_2) 6.45 (t, $^{3}J_{H-P}$ = 14.3 Hz, $^{3}J_{H-H}$ = 12.7 Hz, 1H, −CH═), 7.06 (m, 2H, *p*-H), 7.14 (m, 4H, *m*-H), 7.65 (m, 4H, *o*-H). ^{7}Li NMR (C6D6, 155.53 MHz): δ −3.73. ^{13}C NMR (C_6D_6, 100.6 MHz): δ 14.46 (s, Et_2O−CH_3), 18.93 (d, $^{4}J_{C-P}$ = 2.1 Hz, ═CMeMe(trans)), 26.57 (s, −CH═CMeMe(cis)), 34.64 (m, P−CH−), 66.29 (s, Et_2O−CH_2), 102.93 (m, ═CMe_2), 127.05 (s, *p*-C), 128.1 (m, *m*-C), 132.36 (d, $^{2}J_{C-P}$ = 14.0 Hz, *o*-C), 132.53 (m, −CH═), 146.34 (m, *i*-C). ^{31}P{H} NMR (C_6D_6, 162.0 MHz): δ −6.8. Due to the highly sensitive nature of this compound, satisfactory elemental analysis was not possible.

Synthesis of 2 [{Ph$_2$PCHCHCMe$_2$Li(TMEDA)}$_2$]. 3,3-Dimethylallyldiphenylphosphine (**P2**) (0.2543 g, 1.00 mmol) was dissolved in dry *n*-hexane (10 mL). *n*-Butyllithium (0.69 mL, 1.6 M in hexane, 1.1 mmol) was then added dropwise at −78 °C, forming yellow solution. After warming to room temperature and stirring for a further 2 h, *N*,*N*,*N*′,*N*″-tetramethylethylenediamine (TMEDA) (0.17 mL, 1.1 mmol) was added dropwise with stirring, turning the solution orange and forming an orange precipitate. The precipitate was washed with hexane (3 × 10 mL) before the remaining solvent was removed under reduced pressure with the solid isolated in an argon box (0.311 g, 79%). Crystals suitable for X-ray diffraction were grown from a room-temperature solution of hexane where stirring was stopped upon TMEDA addition as blocks. ^{1}H NMR (C_6D_6, 400.20 MHz): δ 1.46 (s, 4H, TMEDA−CH_2), 1.66 (s, 12H, TMEDA−CH_3), 1.81 (s, 3H, −CH═CMeMe(trans)), 2.01 (s, 3H, −CH═CMeMe(cis)), 2.76 (dd, $^{3}J_{H-H}$ = 12.8 Hz, $^{2}J_{H-P}$ = 7.6 Hz, 1H, P−CH−), 6.46 (ddhept, $^{3}J_{H-H}$ = 14.9 Hz, $^{3}J_{H-H}$ = 12.8 Hz, $^{4}J_{H-H}$ = 1.0 Hz, 1H, −CH═), 7.07

https://dx.doi.org/10.1021/acs.organomet.0c00144
Organometallics 2020, 39, 2080−2090

(m, 2H, *p*-H), 7.19 (m, 4H, *m*-H), 7.84 (m, 4H, *o*-H). ^{7}Li NMR (C_6D_6, 155.53 MHz): δ −4.62. ^{13}C NMR (C_6D_6, 100.6 MHz): δ 18.76 (s, −CH═CMeMe(trans)), 26.49 (s, −CH═CMeMe(cis)), 42.20 (s, P−CH−), 45.28 (s, TMEDA−Me), 56.22 (s, TMEDA−CH_2), 91.63 (d, $^{3}J_{C-P}$ = 24.5 Hz, ═CMe_2), 126.04 (s, *p*-C), 127.74 (m, *m*-C), 132.43 (d, $^{2}J_{C-P}$ = 17.6 Hz, *o*-C), 137.58 (d, $^{2}J_{C-P}$ = 46.3 Hz, −CH═), 150.92 (d, $^{1}J_{C-P}$ = 13.4 Hz, *i*-C). ^{31}P{H} NMR (C_6D_6, 162.0 MHz): δ −1.6. $C_{46}H_{68}Li_2N_4P_2$, (752.86): calcd C 73.38, H 9.10, N 7.44. Found C 73.39, H 9.59, N 7.29. Due to the highly sensitive nature of this compound, elemental analysis within 0.4% was not attained. A difference within 0.49% in H was the closest obtained.

Synthesis of 3 (3a and 3b) [$Ph_2PCHC(Me)CH_2Li$(PMDETA)]. 2-Methylallyldiphenylphosphine (**P3**) (0.2543 g, 1.00 mmol) was dissolved in dry *n*-hexane (10 mL). *n*-Butyllithium (0.69 mL, 1.6 M in hexane, 1.1 mmol) was then added dropwise at −78 °C, forming a slightly yellow solution with a small amount of yellow precipitate. After warming to room temperature and stirring for a further 2 h, *N*,*N*,*N*′,*N*″,*N*″-pentamethyldiethylenetriamine (PMDETA) (0.23 mL, 1.1 mmol) was added dropwise with stirring, forming more precipitate and turning the solution and precipitate orange. The precipitate was washed with hexane (3 × 10 mL) before the remaining solvent was removed under reduced pressure with the solid isolated in an argon box (0.322 g, 72%). Crystals suitable for X-ray diffraction were grown from a room-temperature solution of hexane where stirring was stopped upon PMDETA addition as orange blocks (**3a**) and yellow needles (**3b**). ^{1}H NMR (C_6D_6, 400.20 MHz): δ 1.72−1.96 (m, 23H, PMDETA) 2.37 (m, $^{3}J_{H-H}$ = 1.3 Hz, 3H, −C(Me)═), 3.20 (br-s, 1H, −C(Me)═CHH), 3.38 (d, $^{2}J_{H-P}$ = 7.65 Hz, P−CH−), 3.58 (s, 1H, −C(Me)═CHH), 7.06 (m, 2H, *p*-H), 7.19 (m, 4H, *m*-H), 7.82 (m, 4H, *o*-H). ^{7}Li NMR (C_6D_6, 155.53 MHz): δ −4.28. ^{13}C NMR (C_6D_6, 100.6 MHz): δ 25.20 (s, −C(Me)═), 44.76 (s, PMDETA), 45.86 (s, PMDETA), 53.68 (s, PMDETA), 54.87 (s, P−CH−), 57.30 (s, PMDETA), 69.43 (m, ═CH_2), 126.09 (s, *p*-C), 127.72 (d, $^{3}J_{C-P}$ = 5.6 Hz, *m*-C), 132.85 (d, $^{2}J_{C-P}$ = 17.7 Hz, *o*-C), 150.21 (m, −C(Me)═), 157.59 (d, $^{1}J_{C-P}$ = 26.2 Hz, *i*-C). ^{31}P{H} NMR (C_6D_6, 162.00 MHz): δ −13.6. Due to the highly sensitive nature of this compound, satisfactory elemental analysis was not possible.

Synthesis of 4 [PhP{$CHCHCH_2Li$(TMEDA)}$_2$]. Diallylphenylphosphine (**P4**) (0.1902 g, 1.00 mmol) was dissolved in dry *n*-hexane (10 mL). *n*-Butyllithium (1.38 mL, 1.6 M in hexane, 2.2 mmol) was then added dropwise at −78 °C, forming an orange solution. After warming to room temperature and stirring for a further 2 h, TMEDA (0.33 mL, 2.2 mmol) was added dropwise with stirring, forming a dark red oil at the bottom of the flask. Solvent removal under reduced pressure formed precipitate which was isolated in an argon box (0.318 g, 73%). Crystals suitable for X-ray diffraction were grown from a concentrated solution of hexane. ^{1}H NMR (C_6D_6, 400.20 MHz): δ 1.85 (s, 8H, TMEDA−CH_2), 2.04 (s, 24H, TMEDA−CH_3), 3.16 (br-m, 4H, ═CH_2), 3.62 (br-m, 2H, P−CH−), 6.95 (br-m, 2H, −CH═), 7.09 (m, 1H, *p*-H), 7.35 (m, 2H, *m*-H), 8.08 (m, 2H, *o*-H). ^{7}Li NMR (C_6D_6, 155.53 MHz): δ −5.14. ^{13}C NMR (C_6D_6, 100.6 MHz): δ 46.12 (s, TMEDA−Me), 56.55 (s, TMEDA−CH_2), 65.02 (br-m, allyl−*C*), 73.57 (br-m, allyl−*C*), 105.72 (m, ═CH_2), 124.65 (br-s, *p*-C), 127.47 (d, $^{3}J_{C-P}$ = 3.9 Hz, *m*-C), 130.78 (br-d, $^{2}J_{C-P}$ = 12.9 Hz, *o*-C), 140.02 (br-m, −CH═), 151.31 (br-m, *i*-C). ^{31}P{H} NMR (C_6D_6, 162.0 MHz): δ −35.2. Due to the highly sensitive nature of this compound, satisfactory elemental analysis was not possible.

Synthesis of 5 [{$Ph_2P(O)CHC(Me)CH_2Li(THF)$}$_2$]. 2-Methylallyldiphenylphosphine oxide (**P3′**) (0.2563 g, 1.00 mmol) was loaded into a flask and suspended in dry THF (10 mL). *n*-Butyllithium (0.69 mL, 1.6 M in hexane, 1.1 mmol) was then added dropwise at −78 °C, immediately forming an orange solution. After warming to room temperature, the mixture was allowed to stir for a further 2 h. The majority of the solvent was removed under reduced pressure, and the solution was precipitated with hexane (10 mL) before being filtered. The product was further washed with hexane (2 × 10 mL), and all the remaining solvent was removed under reduced pressure. The orange solid was isolated in an argon box (0.226 g, 68%). Crystals suitable for X-ray diffraction were grown from a concentrated solution in THF layered with hexane at room temperature as orange needles. Mp (argon, sealed capillary): 130 °C. ^{1}H NMR (25 °C, THF-d_8, 400.20 MHz): δ 1.67 (br-s, 3H, −C(Me)═), 1.68 (m, 4H, THF), 2.33 (d, $^{3}J_{H-P}$ = 24.6 Hz, 1H, P−CH−), 3.14 (s, 1H, ═CHH), 3.39 (d, $^{2}J_{H-H}$ = 24.6 Hz, 1H, ═CHH), 3.54 (m, 4H, THF), 7.15 (m, 6H, *m* and *p*-H), 7.81 (m, 4H, *o*-H). ^{7}Li NMR (25 °C, THF-d_8, 155.53 MHz): δ −4.04, −4.50. ^{13}C NMR (25 °C, THF-d_8, 100.6 MHz): δ 26.54 (s, THF), 27.74 (d, $^{2}J_{C-P}$ = 16.8 Hz, −C(Me)═), 48.15 (d, $^{1}J_{C-P}$ = 144.0 Hz, P−CH−), 68.39 (s, THF), 82.31 (br s, ═CH_2), 128.02 (d, $^{3}J_{C-P}$ = 11.0 Hz, *m*-C), 129.40 (s, *p*-C), 133.00 (d, $^{2}J_{C-P}$ = 8.9 Hz, *o*-C), 142.30 (d, $^{1}J_{C-P}$ = 105.9 Hz, *i*-C), 149.00 (br s, −C(Me)═). ^{31}P{H} NMR (25 °C, THF-d_8, 162.0 MHz): δ 26.5, 30.7, 30.9. ^{1}H NMR (100 °C, C_7D_8, 400.20 MHz): δ 1.46 (m, 4H, THF), 1.95 (br-s, 3H, −C(Me)═), 2.72 (d, $^{3}J_{H-P}$ = 24.7 Hz, $^{4}J_{H-H}$ = 1.5 Hz, 1H, P−CH−), 3.52 (m, 4H, THF), 3.57 (s, 1H, ═CHH), 3.96 (s, 1H, ═CHH), 7.06 (m, 2H, *p*-H), 7.06 (m, 4H, *m*-H), 7.80 (m, 4H, *o*-H). ^{7}Li NMR (25 °C, C_7D_8, 155.53 MHz): δ −3.82. ^{13}C NMR (25 °C, C_7D_8, 100.6 MHz): δ 26.03 (s, THF), 28.13 (d, $^{2}J_{C-P}$ = 17.6 Hz, −C(Me)═), 45.94 (d, $^{1}J_{C-P}$ = 133.2 Hz, P−CH−), 68.37 (s, THF), 81.62 (m, ═CH_2), 128.75 (m, *p*-C), 130.75 (s, *m*-C), 132.27 (s, *o*-C), 151.78 (m, *i*-C). ^{31}P{H} NMR (25 °C, C_7D_8, 162.0 MHz): δ 36.0, 37.7. $C_{36}H_{40}Li_2O_3P_2$ (596.54): calcd (loss of one THF molecule), C 72.48, H 6.76, N 0.00. Found C 73.28, H 6.81, N 0.17. Due to the highly sensitive nature of this compound, elemental analysis within 0.4% was not attained. A difference within 0.80% in C was the closest obtained.

Synthesis of 6 [{$Ph_2P(O)CHC(Me)CH_2Li$}$_2$(TMEDA). 2-Methylallyldiphenylphosphine oxide (**P3′**) (0.2563 g, 1.00 mmol) was loaded into a flask and suspended in dry Et_2O (10 mL). *n*-Butyllithium (0.69 mL, 1.6 M in hexane, 1.1 mmol) was then added dropwise at −78 °C, immediately forming an orange solution. After warming to room temperature and stirring for a further 2 h, TMEDA (0.17 mL, 1.1 mmol) was added dropwise with stirring, turning the solution bright red. After 5 min, precipitate appeared in the mixture. The residue was extracted with hexane (10 mL) before being filtered. The solvent was removed under reduced pressure, and the dark red solid was isolated in an argon box (0.202 g, 82%). Crystals suitable for X-ray diffraction were grown from a concentrated solution in ether layered with hexane at room temperature as orange rectangular blocks. ^{1}H NMR (C_6D_6 spiked with THF-d_8, 400.20 MHz): δ 2.06 (s, 12H, TMEDA−CH_3), 2.18 (s, 4H, TMEDA−CH_2), 2.26 (s, 6H, −C(Me)═), 2.82 (d, $^{2}J_{H-P}$ = 26.5 Hz, 2H, P−CH−), 3.90 (s, 2H, −C(Me)═CHH), 4.24 (s, 2H, −C(Me)═CHH), 7.16 (m, 2H, *p*-H), 7.16 (m, 4H, *m*-H), 8.04 (m, 4H, *o*-H). ^{7}Li NMR (C_6D_6 spiked with THF-d_8, 155.53 MHz): δ −4.18. ^{13}C NMR (C_6D_6 spiked with THF-d_8, 100.6 MHz): δ 28.16 (d, $^{2}J_{C-P}$ = 17.9 Hz, −C(Me)═), 45.98 (s, TMEDA−CH_3), 46.01 (d, $^{1}J_{C-P}$ = 132.5 Hz, P−CH−), 57.84 (s, TMEDA−CH_2), 81.19 (m, ═CH_2), 128.24 (m, *p*-C), 129.91 (s, *m*-C), 132.19 (d, $^{2}J_{C-P}$ = 9.5 Hz, *o*-C), 138.91 (d, $^{2}J_{C-P}$ = 104.7 Hz, −C(Me)═), 150.86 (m, *i*-C). ^{31}P{H} NMR (C_6D_6 spiked with THF-d_8, 162.0 MHz): δ 33.3. $C_{36}H_{44}Li_2N_2O_2P_2$ (612.59): calcd C 70.59, H 7.24, N 4.57. Found C 70.76, H 7.59, N 4.13. Due to the highly sensitive nature of this compound, elemental analysis within 0.4% was not attained. A difference within 0.44% in N was the closest obtained.

Synthesis of 7 [$Ph_2P(O)CHC(Me)CH_2Li$(PMDETA)]. 2-Methylallyldiphenylphosphine oxide (**P3′**) (0.2563 g, 1.00 mmol) was loaded into a flask and suspended in dry Et_2O (10 mL). *n*-Butyllithium (0.69 mL, 1.6 M in hexane, 1.1 mmol) was then added dropwise at −78 °C, immediately forming an orange solution. After warming to room temperature and stirring for a further 2 h, PMDETA (0.23 mL, 1.1 mmol) was added dropwise with stirring, turning the solution bright red. After 5 min, precipitate appeared in the mixture. The residue was extracted with hexane (10 mL) before being filtered. The solvent was removed under reduced pressure, and the dark red solid isolated in an argon box (0.270 g, 60%). Crystals suitable for X-ray diffraction were grown from a filtered concentrated solution in ether at room temperature as red columnar crystals. Mp (argon, sealed capillary): 110 °C. ^{1}H NMR (C_6D_6, 400.20 MHz): δ 1.80−

https://dx.doi.org/10.1021/acs.organomet.0c00144
Organometallics 2020, 39, 2080−2090

2.20 (m, 23H, PMDETA), 2.36 (s, 3H, −C(Me)═), 3.05 (d, $^3J_{H-P}$ = 24.9 Hz, 1H, P−CH−), 3.96 (s, 1H, ═CHH), 4.05 (s, 1H, ═CHH), 7.13 (m, 2H, *p*-H), 7.25 (m, 4H, *m*-H), 8.32 (m, 4H, *o*-H). ^{7}Li NMR (C_6D_6, 155.53 MHz): δ −3.99. ^{13}C NMR (C_6D_6, 100.6 MHz): δ 28.31 (d, $^2J_{C-P}$ = 17.6 Hz, −C(Me)═), 44.15 (s, PMDETA), 45.58 (s, PMDETA), 48.52 (d, $^1J_{C-P}$ = 142.1 Hz, P−CH−), 53.47 (s, PMDETA), 57.20 (s, PMDETA), 81.78 (d, $^3J_{C-P}$ = 6.6 Hz, ═CH_2), 127.80 (m, *m*-C), 128.90 (s, *p*-C), 132.55 (d, $^2J_{C-P}$ = 8.7 Hz, *o*-C), 142.52 (d, $^1J_{C-P}$ = 105.0 Hz, −C(Me)═), 149.23 (d, $^2J_{C-P}$ = 7.1 Hz, *i*-C). ^{31}P{H} NMR (C_6D_6, 162.0 MHz): δ 26.1. $C_{25}H_{39}LiN_3OP$ (435.50): calcd C 68.95, H 9.03, N 9.65. Found C 68.23, H 9.00, N 9.46. Due to the highly sensitive nature of this compound, elemental analysis within 0.4% was not attained. A difference within 0.72% in C was the closest obtained.

Synthesis of 8 [$Ph_2P(O)CHCHCMe_2Li$(PMDETA)]. 3,3-Dimethylallyldiphenylphosphine oxide (**P2′**) (0.2703 g, 1.00 mmol) was loaded into a flask and suspended in dry Et2O (10 mL). *n*-Butyllithium (0.69 mL, 1.6 M in hexane, 1.1 mmol) was then added dropwise at −78 °C, forming a bright red solution. After warming to room temperature and stirring for a further 2 h, PMDETA (0.23 mL, 1.1 mmol) was added dropwise with stirring, turning the solution dark red. After 5 min, precipitate appeared in the mixture. The residue was extracted with hexane (10 mL) before being filtered. The solvent was removed under reduced pressure, and the dark red solid isolated in an argon box (0.373 g, 83%). Crystals suitable for X-ray diffraction were grown from a concentrated solution in Et_2O layered with hexane at room temperature as red needles. ^{1}H NMR (C_6D_6, 400.20 MHz): δ 1.61−2.17 (m, 23H, PMDETA), 2.17 (br-s, 6H, ═CMe_2), 3.16 (dd, $^3J_{H-P}$ = 20.0 Hz, J_{H-H} = 12.7 Hz, 1H, P−CH−), 6.24 (dd, $^3J_{H-P}$ = 13.0 Hz, J_{H-H} = 12.7 Hz, 1H, −CH═), 7.11 (m, 2H, *p*-H), 7.23 (m, 4H, *m*-H), 8.41 (m, 4H, *o*-H). ^{7}Li NMR (C_6D_6, 155.53 MHz): δ −3.94. ^{13}C NMR (C_6D_6, 100.6 MHz): δ 19.02 (s, ═CMe_2), 27.05 (s, ═CMe_2), 44.20 (s, PMDETA), 44.21 (d, $^1J_{C-P}$ = 147.2 Hz, P−CH−), 45.60 (s, PMDETA), 53.43 (s, PMDETA), 57.12 (s, PMDETA), 96.61 (d, $^3J_{C-P}$ = 21.3 Hz, ═CMe_2) 127.61 (d, $^3J_{C-P}$ = 10.6 Hz, *m*-C), 128.90 (s, *p*-C), 129.49 (d, $^2J_{C-P}$ = 9.1 Hz, −CH═), 133.41 (d, $^2J_{C-P}$ = 8.2 Hz, *o*-C), 142.90 (d, $^1J_{C-P}$ = 106.8 Hz, *i*-C). ^{31}P{H} NMR (C_6D_6, 162.0 MHz): δ 28.9. Due to the highly sensitive nature of this compound, satisfactory elemental analysis was not possible.

Synthesis of 9 [$Ph_2P(O)CHCHCH_2Li$(PMDETA)]. Allyldiphenylphosphine oxide (**P1′**) (ADPPO) (0.2423 g, 1.00 mmol) was loaded into a flask and suspended in dry Et_2O (10 mL). *n*-Butyllithium (0.69 mL, 1.6 M in hexane, 1.1 mmol) was then added dropwise at −78 °C, forming an orange solution. After warming to room temperature and stirring for a further 2 h, PMDETA (0.23 mL, 1.1 mmol) was added dropwise with stirring, turning the solution bright red. The majority of the solvent was removed under reduced pressure, and the solution was precipitated with hexane (10 mL) before being filtered. Remaining solvent was removed under reduced pressure, and the red solid isolated in an argon box (0.277 g, 66%). Crystals suitable for X-ray diffraction were grown from a concentrated solution in Et_2O layered with hexane at room temperature as red needles. ^{1}H NMR (C_6D_6, 400.20 MHz): δ 1.74−2.37 (m, 23H, PMDETA), 3.70 (dd, $^2J_{H-P}$ = 21.6 Hz, $^3J_{H-H(\beta)}$ = 12.6 Hz, 1H, P−CH−) 4.21 (dt, $^3J_{H-H(\beta)}$ = 9.85 Hz, $^3J_{H-H(trans)}$ = 3.7 Hz, 1H, −CH═CHH), 4.63 (dd, $^3J_{H-H(\beta)}$ = 15.89 Hz, $^3J_{H-H(cis)}$ = 3.3 Hz, 1H, −CH═CHH), 6.88 (tdd, $^3J_{H-H(trans)}$ = 15.89 Hz, $^3J_{H-H(\alpha)}$ = 12.63 Hz, $^3J_{H-H(cis)}$ = 9.85 Hz, 1H, −CH═CH_2), 7.11 (m, 2H, *p*-H), 7.23 (m, 4H, *m*-H), 8.36 (m, 4H, *o*-H). ^{7}Li NMR (C_6D_6, 155.53 MHz): δ −3.94. ^{13}C NMR (C_6D_6, 100.6 MHz): δ 44.05 (br s, PMDETA), 45.77 (s, PMDETA), 51.22 (d, $^1J_{C-P}$ = 146.5 Hz, P−CH−), 53.56 (s, PMDETA), 57.38 (s, PMDETA), 81.58 (d, $^3J_{C-P}$ = 21.8 Hz, ═CH_2), 127.71 (d, $^3J_{C-P}$ = 10.9 Hz, *m*-C), 129.13 (d, $^4J_{C-P}$ = 2.6 Hz, *p*-C), 133.30 (d, $^2J_{C-P}$ = 8.4 Hz, *o*-C), 141.82 (d, $^1J_{C-P}$ = 8.1 Hz, *i*-C), 142.06 (d, $^2J_{C-P}$ = 106.8 Hz, −CH═). ^{31}P{H} NMR (C_6D_6, 162.0 MHz): δ 29.2. Due to the highly sensitive nature of this compound, satisfactory elemental analysis was not possible.

Synthesis of 10 [$Ph_2PCHCHCMe_2Li$(PMDETA)]. 3,3-Dimethylallyldiphenylphosphine (**P2**) (0.2543 g, 1.00 mmol) was dissolved in dry *n*-hexane (10 mL). *n*-Butyllithium (0.69 mL, 1.6 M in hexane, 1.1 mmol) was then added dropwise at −78 °C, forming yellow solution. After warming to room temperature and stirring for a further 2 h, PMDETA (0.23 mL, 1.1 mmol) was added dropwise with stirring, turning the solution a dark orange and forming orange precipitate. The precipitate was washed with hexane (3 × 10 mL) before the remaining solvent was removed under reduced pressure with the solid isolated in an argon box (0.322 g, 72%). No crystals suitable for X-ray diffraction were acquired. ^{1}H NMR (C_6D_6, 400.20 MHz): δ 1.50−1.85 (m, 23H, PMDETA) 2.07 (m, 6H, ═CMe_2), 2.63 (dd, $^3J_{H-H}$ = 13.0 Hz, $^2J_{H-P}$ = 7.5 Hz, 1H, P−CH−), 6.37 (t, $^3J_{H-H}$ = 13.0 Hz, $^3J_{H-P}$ = 12.5 Hz, 1H, −CH═), 7.06 (m, 2H, *p*-H), 7.20 (m, 4H, *m*-H), 7.87 (m, 4H, *o*-H). ^{7}Li NMR (C_6D_6, 155.53 MHz): δ −4.50. ^{13}C NMR (C_6D_6, 100.6 MHz): δ 19.71 (d, $^4J_{C-P}$ = 3.1 Hz, ═CMeMe(trans)), 27.39 (d, $^4J_{C-P}$ = 2.6 Hz, ═CMeMe(cis)), 37.24 (br m, P−CH−), 44.55 (s, PMDETA), 45.86 (s, PMDETA), 53.48 (s, PMDETA), 57.22 (s, PMDETA), 95.94 (d, $^3J_{C-P}$ = 23.3 Hz, ═CMe_2), 125.93 (s, *p*-C), 127.69 (d, $^3J_{C-P}$ = 5.3 Hz, *m*-C), 132.87 (d, $^2J_{C-P}$ = 16.9 Hz, *o*-C), 136.79 (d, $^2J_{C-P}$ = 28.1 Hz, −CH═), 151.88 (d, $^1J_{C-P}$ = 19.7 Hz, *i*-C). ^{31}P{H} NMR (C_6D_6, 162.00 MHz): δ −2.5. $C_{26}H_{41}LiN_3P$ (433.55): calcd C 72.03, H 9.53, N 9.69. Found C 71.21, H 9.26, N 9.41. Due to the highly sensitive nature of this compound, elemental analysis within 0.4% was not attained. A difference within 0.82% in C was the closest obtained.

Synthesis of 11 [$Ph_2PCHC(Me)CH_2Li$(TMEDA)]. 2-Methylallyldiphenylphosphine (**P3**) (0.2403 g, 1.00 mmol) was dissolved in dry *n*-hexane (10 mL). *n*-Butyllithium (0.69 mL, 1.6 M in hexane, 1.1 mmol) was then added dropwise at −78 °C, forming a slightly yellow solution with a small amount of yellow precipitate. After warming to room temperature and stirring for a further 2 h, TMEDA (0.17 mL, 1.1 mmol) was added dropwise with stirring, turning the solution orange and forming yellow precipitate. The precipitate was washed with hexane (3 × 10 mL) before the remaining solvent was removed under reduced pressure with the solid isolated in an argon box (0.254 g, 70%). No crystals suitable for X-ray diffraction were acquired. ^{1}H NMR (C_6D_6, 400.20 MHz): δ 1.56 (br-s, 4H, TMEDA−CH_2), 1.73 (br-s, 12H, TMEDA−CH_3), 2.34 (br-s, 3H, −C(Me)═), 3.27 (br-s, 1H, −C(Me)═CHH), 3.34 (br-s, 1H, −C(Me)═CHH), 3.55 (br-s, 1H, P−CH−), 7.08 (m, 2H, *p*-H), 7.20 (m, 4H, *m*-H), 7.82 (m, 4H, *o*-H). ^{7}Li NMR (C_6D_6, 155.53 MHz): δ −4.47. ^{13}C NMR (C_6D_6, 100.6 MHz): δ 23.06 (br-m, −C(Me)═), 45.71 (s, TMEDA−CH_3), 55.02 (br-m, ═CH_2), 56.45 (s, TMEDA−CH_2), 67.37 (br-m, P−CH−), 126.52 (br-s, *p*-C), 128.00 (m, *m*-C), 132.66 (br-s, *o*-C), 150.01 (br-m, −C(Me)═), 157.43 (br-m, *i*-C). ^{31}P{H} NMR (C_6D_6, 162.00 MHz): δ −32.7, −27.6, −19.7. ^{1}H NMR (THF-d_8, 400.20 MHz): δ 1.93 (s, 3H, −C(Me)═), 2.15 (s, 12H, TMEDA−CH_3), 2.31 (s, 4H, TMEDA−CH_2), 2.73 (br-s, 1H, ═CHH), 2.97 (br-s, 1H, P−CH−), 3.18 (br-s, 1H═CHH), 7.00 (m, 2H, *p*-H), 7.09 (m, 4H, *m*-H), 7.36 (m, 4H, *o*-H). ^{7}Li NMR (THF-d_8, 155.53 MHz): δ −6.82. ^{13}C NMR (THF-d_8, 100.6 MHz): δ 24.55 (br-m, −C(Me)═), 46.31 (s, TMEDA−CH_3), 56.53 (br-m, P−CH−), 58.91 (s, TMEDA−CH_2), 67.13 (br-m, ═CH_2), 126.21 (s, *p*-C), 127.86 (d, $^3J_{C-P}$ = 5.6 Hz, *m*-C), 132.82 (d, $^2J_{C-P}$ = 18.0 Hz, *o*-C), 150.16 (br-m, *i*-C), 158.24 (d, $^2J_{C-P}$ = 29.1 Hz, −C(Me)═). ^{31}P{H} NMR (THF-d_8, 162.00 MHz): δ −17.4. Due to the highly sensitive nature of this compound, satisfactory elemental analysis was not possible.

Synthesis of 12 [$Ph_2P(O)CHCHCH_2Li{\cdot}Et_2O$]. Allyldiphenylphosphine oxide (**P1′**) (0.2423 g, 1.00 mmol) was loaded into a flask and suspended in dry Et_2O (10 mL). *n*-Butyllithium (0.69 mL, 1.6 M in hexane, 1.1 mmol) was then added dropwise at −78 °C, forming an orange solution. After warming to room temperature, it was allowed to stir for a further 2 h. The majority of the solvent was removed under reduced pressure, and the solution was precipitated with hexane (10 mL) before the supernatant was filtered off. Remaining solvent was removed under reduced pressure, and the red solid was isolated in an argon box (0.130 g, 42%). No crystals suitable for X-ray diffraction were acquired. ^{1}H NMR (C_6D_6, 400.20 MHz): δ 1.06 (br-t, 6H, Et_2O−CH_3), 3.22 (br-q, 4H, Et_2O−CH_2), 3.37 (dd, $^2J_{H-P}$ = 21.0 Hz,

https://dx.doi.org/10.1021/acs.organomet.0c00144
Organometallics 2020, 39, 2080−2090

$^{3}J_{H-H(\beta)}$ = 12.3 Hz, 2H, P−CH−) 3.66 (dt, $^{3}J_{H-H(\beta)}$ = 10.1 Hz, $^{3}J_{H-H(trans)}$ = 3.5 Hz, 2H, =CHH(cis)), 4.17 (dd, $^{3}J_{H-H(\beta)}$ = 16.4 Hz, $^{3}J_{H-H(cis)}$ = 2.6 Hz, 2H, =CHH(trans)), 6.63 (dddd, $^{3}J_{H-P}$= 18.1 Hz, $^{3}J_{H-H(trans)}$ = 16.5 Hz, $^{3}J_{H-H(\alpha)}$ = 12.3 Hz, $^{3}J_{H-H(cis)}$ = 10.1 Hz, 2H, −CH=), 7.03 (m, 4H, *p*-H), 7.03 (m, 2H, *p*-H), 7.03 (m, 4H, *m*-H), 7.91 (m, 4H, *o*-H). ^{7}Li NMR (C_6D_6, 155.5 MHz): δ −3.67. ^{13}C NMR (C_6D_6, 100.6 MHz): δ 15.54 (s, Et_2O-CH_3), 46.49 (br-m, P−CH−), 65.90 (s, Et_2O-CH_2), 83.66 (br-m, $=CH_2$), 128.68 (d, $^{3}J_{C-P}$ = 11.6 Hz, *m*-C), 130.84 (d, $^{4}J_{C-P}$ = 2.3 Hz, *p*-C), 133.32 (d, $^{2}J_{C-P}$ = 9.8 Hz, *o*-C), 141.82 (br m, −CH=). ^{31}P{H} NMR (C_6D_6, 162.0 MHz): δ 38.8. Due to the highly sensitive nature of this compound, satisfactory elemental analysis was not possible.

■ ASSOCIATED CONTENT

Supporting Information

The Supporting Information is available free of charge at https://pubs.acs.org/doi/10.1021/acs.organomet.0c00144.

Summary of crystallographic data for complexes **1**−**9** and **P1′**−**4′**, NMR spectroscopy data for compounds **1**−**12** (PDF)

Coordinates of **3a** and **3b** (XYZ)

Accession Codes

CCDC 1953194−1953207 contain the supplementary crystallographic data for this paper. These data can be obtained free of charge via www.ccdc.cam.ac.uk/data_request/cif, or by emailing data_request@ccdc.cam.ac.uk, or by contacting The Cambridge Crystallographic Data Centre, 12 Union Road, Cambridge CB2 1EZ, UK; fax: +44 1223 336033.

■ AUTHOR INFORMATION

Corresponding Author

Victoria L. Blair − *School of Chemistry, Monash University, Melbourne, Victoria 3800, Australia;* orcid.org/0000-0002-2984-6048; Email: Victoria.blair@monash.edu

Authors

Nimrod M. Eren − *School of Chemistry, Monash University, Melbourne, Victoria 3800, Australia*

Samantha A. Orr − *School of Chemistry, Monash University, Melbourne, Victoria 3800, Australia*

Christopher D. Thompson − *School of Chemistry, Monash University, Melbourne, Victoria 3800, Australia;* orcid.org/0000-0001-6913-9922

Emily C. Border − *School of Chemistry, Monash University, Melbourne, Victoria 3800, Australia*

Michael A. Stevens − *School of Chemistry, Monash University, Melbourne, Victoria 3800, Australia*

Complete contact information is available at: https://pubs.acs.org/10.1021/acs.organomet.0c00144

Notes

The authors declare no competing financial interest.

■ ACKNOWLEDGMENTS

We thank the Australian Research Council (DP170104722) and Monash University for financial support of this work. This research was undertaken in part using the MX1 beamline at the Australian Synchrotron, part of ANSTO. We acknowledge help provided by Dr. Craig Forsyth and Dr. Peter Nicholls of the Monash X-ray and NMR platforms.

■ REFERENCES

(1) Lappert, M.; Protchenko, A.; Power, P.; Seeber, A. *Metal Amide Chemistry*; Wiley, 2008.

(2) Wauters, I.; Debrouwer, W.; Stevens, C. V. Preparation of Phosphines through C-P Bond Formation. *Beilstein J. Org. Chem.* **2014**, *10*, 1064−1096.

(3) Arrechea, P. L.; Buchwald, S. L. Biaryl Phosphine Based Pd(II) Amido Complexes: The Effect of Ligand Structure on Reductive Elimination. *J. Am. Chem. Soc.* **2016**, *138* (38), 12486−12493.

(4) Noyori, R. Asymmetric Catalysis: Science and Opportunities (Nobel Lecture). *Angew. Chem., Int. Ed.* **2002**, *41* (12), 2008−2022.

(5) Guo, H.; Fan, Y. C.; Sun, Z.; Wu, Y.; Kwon, O. Phosphine Organocatalysis. *Chem. Rev.* **2018**, *118* (20), 10049−10293.

(6) Shameem, M. A.; Orthaber, A. Organophosphorus Compounds in Organic Electronics. *Chem. - Eur. J.* **2016**, *22* (31), 10718−10735.

(7) Demkowicz, S.; Rachon, J.; Daśko, M.; Kozak, W. Selected Organophosphorus Compounds with Biological Activity. *RSC Adv.* **2016**, *6* (9), 7101−7112.

(8) Huang, W. S.; Liu, S.; Zou, D.; Thomas, M.; Wang, Y.; Zhou, T.; Romero, J.; Kohlmann, A.; Li, F.; Qi, J.; et al. Discovery of Brigatinib (AP26113), a Phosphine Oxide-Containing, Potent, Orally Active Inhibitor of Anaplastic Lymphoma Kinase. *J. Med. Chem.* **2016**, *59* (10), 4948−4964.

(9) Stockland, R. A. Synthesis of Organophosphines, Phosphonates, and Related Compounds. *Practical Functional Group Synthesis* **2016**, 219−470.

(10) Musina, E. I.; Balueva, A. S.; Karasik, A. A. Phosphines: Preparation, Reactivity and Applications. *Organophosphorus Chem.* **2019**, *48*, 1−63.

(11) Andrews, P. C.; Blair, V. L.; Koutsaplis, M.; Thompson, C. D. Anion Rearrangements of Alkali Metal Complexes of the Chiral Amine (S)- N -α-(Methylbenzyl)Phenylallylamine: Structural and Solution Insights. *Organometallics* **2012**, *31* (23), 8135−8144.

(12) Border, E. C.; Koutsaplis, M.; Andrews, P. C. The Strange Case of Sodium (S)-N-α-(Methylbenzyl)Allylamide: Anion Rearrangement, Decomposition, and a Peculiar Propyl Addition. *Organometallics* **2016**, *35* (3), 303−305.

(13) Flynn, M. T.; Stott, R.; Blair, V. L.; Andrews, P. C. Loss of Chirality through Facile Lewis Base Mediated Aza-Enolate Formation in Na and K (S)-N-(α-Methylbenzyl)Methallylamides. *Organometallics* **2016**, *35* (16), 2707−2714.

(14) Davies, S. G.; Smith, A. D.; Price, P. D. The Conjugate Addition of Enantiomerically Pure Lithium Amides as Homochiral Ammonia Equivalents: Scope, Limitations and Synthetic Applications. *Tetrahedron: Asymmetry* **2005**, *16* (17), 2833−2891.

(15) Whisler, M. C.; Beak, P. Synthetic Applications of Lithiated N-Boc Allylic Amines as Asymmetric Homoenolate Equivalents. *J. Org. Chem.* **2003**, *68* (4), 1207−1215.

(16) Laffoon, S. D.; Wu, Z.; Hull, K. L. Rhodium-Catalyzed Asymmetric Synthesis of β-Branched Esters from Allylic Amines. *Chem. Commun.* **2018**, *54* (56), 7814−7817.

(17) Vanable, E. P.; Kennemur, J. L.; Joyce, L. A.; Ruck, R. T.; Schultz, D. M.; Hull, K. L. Rhodium-Catalyzed Asymmetric Hydroamination of Allyl Amines. *J. Am. Chem. Soc.* **2019**, *141* (2), 739−742.

(18) Skoda, E. M.; Davis, G. C.; Wipf, P. Allylic Amines as Key Building Blocks in the Synthesis of (E)-Alkene Peptide Isosteres. *Org. Process Res. Dev.* **2012**, *16*, 26−34.

(19) Stephan, D. W.; Erker, G. Frustrated Lewis Pairs: Metal-Free Hydrogen Activation and More. *Angew. Chem., Int. Ed.* **2010**, *49* (1), 46−76.

(20) Thapper, A.; Sparr, E.; Johnson, B. F. G.; Lewis, J.; Raithby, P. R.; Nordlander, E. Reversible π-Coordination of Triallylphosphine in a Trinuclear Ruthenium Carbonyl Cluster. *Inorg. Chem. Commun.* **2004**, *7* (3), 443−446.

(21) Pomogailo, S. I.; Chuev, I. I.; Dzhardimalieva, G. I.; Yarmolenko, A. V.; Makhaev, V. D.; Aldoshin, S. M.; Pomogailo, A. D. Synthesis and Reactivity of Metal-Containing Monomers 51. Synthesis and Molecular Structure of the Cluster-Containing

Complex [Rh 6 (CO) 14 (μ,η,2-$PPh_2CH_2CH{=}CH_2$)]. *Russ. Chem. Bull.* **1999**, *48* (6), 1174−1177.
(22) Appel, R.; Loos, R.; Mayr, H. Nucleophilicity Parameters for Phosphoryl-Stabilized Carbanions and Phosphorus Ylides: Implications for Wittig and Related Olefination Reactions. *J. Am. Chem. Soc.* **2009**, *131* (2), 704−714.
(23) Clayden, J.; Warren, S. Stereocontrol in Organic Synthesis Using the Diphenylphosphoryl Group. *Angew. Chem., Int. Ed. Engl.* **1996**, *35*, 241−270.
(24) Larsen, R. O.; Aksnes, G. The Effect of the Phosphoryl Substituents on the Stereochemistry of the Horner Reaction. *Phosphorus Sulfur Relat. Elem.* **1983**, *16* (3), 339−344.
(25) Grayson, J. I.; Norrish, H. K.; Warren, S. Synthesis of Phosphindoline Oxides, Tetrahydrophosphinoline Oxides, and Related Compounds by Cyclisation of Allyl- and Vinyl-Phosphine Oxides. *J. Chem. Soc., Perkin Trans. 1* **1976**, *23*, 2556−2562.
(26) Armstrong, S. K.; Warren, S.; Collington, E. W.; Naylor, A. Stereocontrolled Synthesis of Homoallylic Amines Using Phosphine Oxides and Isoxazolines. *Tetrahedron Lett.* **1991**, *32* (33), 4171−4174.
(27) Ukai, J.; Ikeda, Y.; Ikeda, N.; Yamamoto, H. Direct, Stereoselective Synthesis of Either E- or Z-1,3-Dienes. *Tetrahedron Lett.* **1983**, *24* (37), 4029−4032.
(28) Ikeda, Y.; Ukai, J.; Ikeda, N.; Yamamoto, H. Stereoselective Synthesis of (z)- and (e)-1,3-Alkadienes from Aldehydes Using Organotitanium and Lithium Reagents. *Tetrahedron* **1987**, *43* (4), 723−730.
(29) Beddoe, R. H.; Andrews, K. G.; Magné, V.; Cuthbertson, J. D.; Saska, J.; Shannon-Little, A. L.; Shanahan, S. E.; Sneddon, H. F.; Denton, R. M. Redox-Neutral Organocatalytic Mitsunobu Reactions. *Science* **2019**, *365* (6456), 910−914.
(30) Blair, V. L.; Stevens, M. A.; Thompson, C. D. The Importance of the Lewis Base in Lithium Mediated Metallation and Bond Cleavage Reaction of Allyl Amines and Allyl Phosphines. *Chem. Commun.* **2016**, *52* (52), 8111−8114.
(31) Blaurock, S.; Kühl, O.; Hey-Hawkins, E. Lithio-(Diphenylphosphino)Methane−Tetramethylethylenediamine: It's a Dimer! *Organometallics* **1997**, *16* (4), 807−808.
(32) Andrews, P. C.; Blair, V. L.; Border, E. C.; Peatt, A. C.; Maclellan, J. G.; Thompson, C. D. Alkali-Metal-Induced C-C Bond Cleavage and CH_4 Elimination in the Amido → Aza-Allyl Transformation of the (S)- N -α-(Methylbenzyl) Benzylamido Anion. *Organometallics* **2013**, *32* (24), 7509−7519.
(33) Andrews, P. C.; Koutsaplis, M.; Robertson, E. G. Thermodynamically Favored Anion Rearrangements in Li and Na Complexes of (S)-N-α-(Methylbenzyl)Allylamine. *Organometallics* **2009**, *28* (6), 1697−1704.
(34) Tang, S.; Zhang, X.; Sun, J.; Niu, D.; Chruma, J. J. 2-Azaallyl Anions, 2-Azaallyl Cations, 2-Azaallyl Radicals, and Azomethine Ylides. *Chem. Rev.* **2018**, *118* (20), 10393−10457.
(35) Frisch, M. J. G.; Trucks, W.; Schlegel, H. B.; Scuseria, G. E.; Robb, M. A.; Cheeseman, J. R.; Scalmani, G.; Barone, V.; Mennucci, B.; Petersson, G. A.; et al. *Gaussian 16, Rev. D.01*; 2016.
(36) Al-Masri, H.; Sieler, J.; Hey-Hawkins, E. Synthesis and Characterization of Novel Chelated Dimethylamino Lithium Alkoxides: Molecular Structures of [1-$LiOC(C_6H_{11})_2$-2- $NMe_2C_6H_4]_2$ and [1-$LiOCPh_2CH_2$-2- $NMe_2C_6H_4]_2$. *Appl. Organomet. Chem.* **2003**, *17* (1), 63−67.
(37) Reisinger, A.; Trapp, N.; Krossing, I. AgOC(CF3)3: Synthesis and Applications of the First Donor-Free Silver(I) Alkoxide. *Organometallics* **2007**, *26* (8), 2096−2105.
(38) Clegg, W.; Liddle, S. T.; Davies, R. P.; Dunbar, L.; Feeder, N.; Snaith, R.; Wheatley, A. E. H.; Mulvey, R. E. Lithiated Organophosphorus Enamines: A New Synthetic Approach and the First Crystal Structures. *Chem. Commun.* **1999**, *15*, 1401−1402.
(39) *US, B. A. M. V2012.2.0*; Bruker Apex. 2006.
(40) Sheldrick, G. M. *SADABS v2.30.*; Univ. Gottingen 2002.
(41) Cowieson, N. P.; Aragao, D.; Clift, M.; Ericsson, D. J.; Gee, C.; Harrop, S. J.; Mudie, N.; Panjikar, S.; Price, J. R.; Riboldi-Tunnicliffe, A.; et al. MX1: A Bending-Magnet Crystallography Beamline Serving Both Chemical and Macromolecular Crystallography Communities at the Australian Synchrotron. *J. Synchrotron Radiat.* **2015**, *22* (1), 187−190.
(42) Sheldrick, G. M. SHELXT - Integrated Space-Group and Crystal-Structure Determination. *Acta Crystallogr., Sect. A: Found. Adv.* **2015**, *71* (1), 3−8.
(43) Sheldrick, G. M. Crystal Structure Refinement with SHELXL. *Acta Crystallogr., Sect. C: Struct. Chem.* **2015**, *71*, 3−8.

https://dx.doi.org/10.1021/acs.organomet.0c00144
Organometallics 2020, 39, 2080−2090